Records of growth and weaning in fossil proboscidean tusks as tests of Pleistocene extinction mechanisms

by

Michael Dennis Cherney

A dissertation submitted in partial fulfillment
of the requirements for the degree of
Doctor of Philosophy
(Geology)
in the University of Michigan
2016

Doctoral Committee:

Professor Daniel C. Fisher, Chair
Professor Emeritus Philip D. Gingerich
Associate Professor John Kingston
Professor Kyger C. Lohmann
Adam N. Rountrey

Dedication

To my loving wife, Yarimar, and our children, Nathaniel, Gabriel, and Lydia.

Acknowledgements

The contents of this thesis to some extent represent a collective effort by the many people who provided assistance toward their development. I am particularly grateful for the insight, support, guidance, patience, and friendship of my Ph. D. adviser and mentor, Daniel Fisher. My dissertation committee, including Philip Gingerich, Kacey Lohmann, John Kingston, and Adam Rountrey, provided valuable feedback and suggestions that greatly improved my experimental approach and helped focus my efforts to collect useful data and complete projects.

Many people were involved in the procurement of study materials. These included collaborators at the Denver Museum of Nature and Science, particularly "Snowmastodon" project leaders Kirk Johnson (Smithsonian National Museum of Natural History; formerly Denver Museum of Nature and Science (DMNS)) and Ian Miller (DMNS), who included us in the scientific team studying the Ziegler Reservoir fossil site remains, invited us to participate in the excavation, and provided access to the proboscidean tusks for growth analyses. Carol Lucking (formerly DMNS) provided additional assistance with accessing the specimen database and field notes.

Toledo Zoo and Aquarium administrators, Randi Meyerson and Peter Tolson, approved my long-term project sampling hair and milk from the zoo's mother-calf pair of African elephants, while elephant manager, Ben Whitebread, generously and graciously provided extensive accommodations for my project, assistance collecting samples, and information about the elephants.

Weaning analyses for Siberian mammoths would have been impossible without the large collection of tusks acquired with the help Bernard Buigues (Saint-Jean-de-Luz, France), Dick Mol (Natural History Museum, Rotterdam, The Netherlands), and Russian colleagues, Sergey Vartanyan (Northeast Interdisciplinary Research Institute, Far Eastern Branch, Russian Academy of Sciences, Magadan, Russian Federation), Alexei Tikhonov (Zoological Institute, Russian Academy of Sciences, Saint Petersburg, Russian Federation), and Gennady Boeskorov (Geological Institute, Siberian Branch, Russian Academy of Sciences, Yakutsk, Russian Federation).

Numerous people helped with data collection in terms of sample analyses, CT scanning, access to maintained lab spaces, consultation, collaboration, tracking down resources, and accommodating tight schedules. Among these were: Lora Wingate (U-M Stable Isotopes Lab), Michelle Lynch (U-M Dental School MicroCT Core), Michael Hren (University of Connecticut Chemistry), Katarzyna, Sobczyk-Kojiro (U-M College of Pharmacy), Teera Parr (U-M Core Assay Facility – Psychology), Dyke Andreasen (UCSC

Stable Isotope Lab), Basma Khoury (U-M Medical School (UMMS)), Carol Wilke (UMMS), Brian Bagley (University of Minnesota), Jessica Durkin (UMMS), and Audrey Seasholtz (UMMS).

Staff, students, and faculty from the U-M Museum of Paleontology (UMMP) and the U-M Department of Earth and Environmental Sciences (EES) assisted with CT processing, and isotope sampling, or provided lab space, materials, and maintenance. These included Scott Beld, Ethan Shirley, Zac Calamari, Jessica Hicks, Katrina Lewandowski, Meredith Dennis, William Sanders, Selena Smith, Maria Marcano, Nathan Sheldon, James Gleason, Tim Gallagher, and Austin Boles. Anne Hudon (EES), Cindy Stauch (UMMP), Linda Garcia (UMMP), Nancy Kingsbury (EES), and Julie Haggerty (EES) provided administrative support to keep my progress smooth and uninterrupted. I received valued feedback, encouragement, and mentorship from extra-committee faculty from UMMP, EES, and U-M Ecology and Evolutionary Biology (EEB) including Jeff Wilson (UMMP, EES), Gerry Smith (EEB), Catherine Badgley (UMMP, EEB), Tom Baumiller (UMMP, EES), and Rob Van der Voo (EES). My fellow paleontology graduate students (and many others within EES not listed here) provided much appreciated support throughout the duration of my Ph. D. program. Among these peers were Emile Moacdieh, Tara Smiley, John Fronimos, Joe El Adli, Ryan Bebej, Valerie Syverson, Kris Rhodes, Takehito Ikejiri, Mike D'Emic, John Whitlock, and Iyad Zalmout.

Table of Contents

Dedication ii

Acknowledgements iii

List of Tables x

List of Figures xi

Chapter 1 Introduction 1

Previous attempts to evaluate extinction mechanisms 2

Using life-history analyses to test extinction mechanisms 7

Methods employed in this study 8

Chapter 2 summary 11

Chapter 3 summary 14

Chapter 4 summary 17

Chapter 5 summary 18

Conclusion 20

References 22

Chapter 2 Taxonomic overview and tusk growth analyses of Ziegler Reservoir proboscideans 27

Introduction 27

Materials 29

Methods 31

Specimen treatment 31

MicroCT analysis 33

Thin-section production and analysis 38

Analysis of stable isotope profiles 39

Results 42

Taxonomic overview 42

Demography 45

Taphonomy 47

MicroCT analysis 48

Thin-section analysis 49

Isotope analyses 50

Discussion 57
Conclusions 68
References 143
Chapter 3 Identifying left-right pairs in the Ziegler Reservoir mastodon mandibular tusks 148
Introduction 148
Materials 153
Methods 154
Specimen treatment 154
MicroCT scanning 155
Morphological comparisons 155
Growth feature comparisons 157
Structural comparisons 158
Stable isotope analysis 159
Results 160
Tusk comparisons 160
Discussion 170
Time averaging in ZR near-shore deposits 170
Gingival erosive features 174
Contrasting data from tusks of a single individual 175
Taphonomic and chronological implications 179
Implications for tests of 'multiple-death' hypotheses 181
Conclusion 182
References 242
Chapter 4 Stable isotope patterns in a nursing mother-calf pair of African elephants (*Loxodonta africana*) as a modern analog for interpretation of fossil tusk records 243
Introduction 243
Hair growth record 245
Hair isotopes 246
Milk composition 247
Milk isotopes 248
Nursing signature 249
Hair cortisol 250

Materials 253
Methods 253
Specimen collection and treatment 253
Milk sampling 254
Hair collection 256
Water/feed sampling 259
Isotope analyses 259
Hair sampling for cortisol analysis 264
Cortisol analysis 265
Sample timing and calculation of calf-mother offset 267
Results 267
Hair growth rates 267
Isotope records 270
Hair cortisol 277
Discussion 279
Growth rates and chronology of pre-study hair growth 279
Record alignment 281
Seasonality 282
Elephant tail hair cortisol 285
Milk isotopes 287
Isotopic signatures of birth, nursing, and weaning 289
Conclusions 294
References 325
Chapter 5 Growth patterns and weaning age estimates support hunting-induced extirpation of Siberian woolly mammoths 333
Introduction 333
Life-history analyses 334
Materials 345
Methods 347
MicroCT analyses 347
Estimating sex and ontogenetic timing of tusk records 349
Isotope sampling 352

Isotope analyses 353
AMS radiocarbon dating of tusk dentin 355
Weaning-age estimation 356
Growth rates comparisons 357
Results 358
Annual microCT features 358
MicroCT neonatal features 358
Tusk sex designations 359
Estimated growth intervals 360
AMS radiocarbon dates 362
Collagen preservation 362
δ^{15}N records 365
Weaning age estimates 367
δ^{13}C records 369
Tusk growth rates 369
Discussion 370
Aligning growth records 370
Estimating weaning age 372
Interpreting changes through time 374
Weaning age as a test of extinction hypotheses 376
δ^{13}C records 379
Conclusion 381
References 450
Chapter 6 Conclusion 460
References 464

List of Tables

Table 2.1. Increment measurements from CT scans of Ziegler Reservoir proboscidean dentition. 69
Table 2.2. Tooth measurements for Ziegler Reservoir mammoth molars. 97
Table 2.3. Mastodon tusks from Ziegler Reservoir that were used in this study. 98
Table 2.4. Isotope data from Ziegler Reservoir mastodon tusks. 99
Table 3.1. Proposed pairs in ZR mastodon mandibular tusks. 186
Table 4.1. Elephant tail hair growth measurements. 296
Table 4.2. Elephant mother tail hair isotope data. 297
Table 4.3. Elephant calf tail hair isotope data. 300
Table 4.4. Elephant milk and drinking water isotope data. 305
Table 4.5. Isotope standards cumulative data. 306
Table 4.6. Elephant mother tail hair cortisol data. 308
Table 5.1. Juvenile Siberian woolly mammoth tusks used in this study. 384
Table 5.2. Dentin collagen pretreatment data. 386
Table 5.3. Growth increments and serial isotope records for tusks used in this study. 388
Table 5.4. Results of isotope standards run with tusk analyses. 402

List of Figures

Figure 2.1. Mandible of an adult mastodon from ZR with mandibular tusks. 122
Figure 2.2. The Clay Mammoth assemblage (DMNH 60704). 124
Figure 2.3. Annual microCT growth features in a ZR mandibular tusk. 125
Figure 2.4. Protocol for measuring CT growth increments. 127
Figure 2.5. EIV growth series for ZR mandibular tusks. 129
Figure 2.6. Isotope sampling procedure for ZR tusks. 130
Figure 2.7. Mammoth molar from ZR. 131
Figure 2.8. Comparison with Great Lakes region mastodons. 132
Figure 2.9. Annual CT features in mastodon tusks from other regions. 134
Figure 2.10. Partial census of Ziegler Reservoir mastodons. 135
Figure 2.11. Deciduous tusk from ZR with neonatal line. 136
Figure 2.12. Annual periodicity of CT growth features. 137
Figure 2.13. Seasonality in stable isotopes of oxygen and nitrogen. 139
Figure 2.14. Fraction of final year (FFY) for ZR proboscideans. 140
Figure 2.15. Multiyear oxygen isotope records for ZR tusks. 141
Figure 3.1. Tusk pair 1 medial views. 188
Figure 3.2. Tusk pair 1 dorsal views. 189
Figure 3.3. Tusk pair 1 surface models from CT scans. 190
Figure 3.4. Tusk pair 1 dorsoventral digital slices through the axes of CT scans. 192
Figure 3.5. Tusk pair 1 EIV comparison. 193
Figure 3.6. Tusk pair 2 medial views. 194
Figure 3.7. Tusk pair 2 dorsal views. 195
Figure 3.8. Tusk pair 2 surface models from CT scans. 196
Figure 3.9. Tusk pair 2 dorsoventral digital slices through the axes of CT scans. 198
Figure 3.10. Tusk pair 2 EIV comparison. 199
Figure 3.11. Tusk pair 3 medial views. 200
Figure 3.12. Tusk pair 3 dorsal views. 201
Figure 3.13. Tusk pair 3 surface models from CT scans. 202
Figure 3.14. Tusk pair 3 dorsoventral digital slices through to the axes from CT scans. 204
Figure 3.15. Tusk pair 3 EIV comparison. 205
Figure 3.16. Tusk pair 3 oxygen isotope comparison. 206
Figure 3.17. Tusk pair 3 carbon isotope comparison. 207
Figure 3.18. Tusk pair 4 medial views. 208
Figure 3.19. Tusk pair 4 dorsal views. 209
Figure 3.20. Tusk pair 4 surface models from CT scans. 210
Figure 3.21. Tusk pair 4 dorsoventral digital slices through the axes of CT scans. 212
Figure 3.22. Tusk pair 4 EIV comparison. 213
Figure 3.23. Tusk pair 5 medial views. 214

Figure 3.24. Tusk pair 5 dorsal views. 215
Figure 3.25. Tusk pair 5 surface models from CT scans. 216
Figure 3.26. Tusk pair 5 mediolateral digital slices parallel to the axes from CT scans. 217
Figure 3.27. Tusk pair 5 EIV compare. 218
Figure 3.28. Tusk pair 5 oxygen isotope comparison. 219
Figure 3.29. Tusk pair 5 carbon isotope comparison. 220
Figure 3.30. Tusk pair 6 medial views. 221
Figure 3.31. Tusk pair 6 dorsoventral views. 222
Figure 3.32. Tusk pair 6 dorsoventral digital slices parallel to the axes from CT scans. 223
Figure 3.33. Tusk pair 6 EIV comparison. 224
Figure 3.34. Tusk pair 6 oxygen isotope comparison. 225
Figure 3.35. Tusk pair 6 carbon isotope comparison. 226
Figure 3.36. Tusk pair 7 medial views. 227
Figure 3.37. Tusk pair 7 dorsal views. 228
Figure 3.38. Tusk pair 7 EIV comparison. 229
Figure 3.39. Tusk pair 8 proposed medial views. 230
Figure 3.40. Tusk pair 8 proposed dorsal views. 231
Figure 3.41. Tusk pair 8 dorsoventral digital slices parallel to the axes from CT scans. 232
Figure 3.42. Tusk pair 9 proposed medial views. 233
Figure 3.43. Tusk pair 9 proposed dorsal views. 234
Figure 3.44. Tusk pair 9 dorsoventral digital slices parallel to the axes from CT scans. 235
Figure 3.45. Spatial associations of proposed mandibular tusk pairs. 236
Figure 3.46. Updated partial census of Ziegler Reservoir mastodons. 237
Figure 3.47. Updated season of death distribution for Ziegler Reservoir proboscideans. 238
Figure 3.48. Updated oxygen isotope compilation for Ziegler Reservoir proboscideans. 240
Figure 4.1. Elephant mother tail hair sampling. 310
Figure 4.2. Elephant calf tail hair sampling. 311
Figure 4.3. Sampling elephant tail hairs for serial isotopic analyses. 312
Figure 4.4. Sampling elephant tail hairs for serial cortisol analysis. 314
Figure 4.5. Tail hair growth rates. 315
Figure 4.6. Serial records of $\delta^{15}N$ from elephant tail hairs and milk. 316
Figure 4.7. Serial records of $\delta^{13}C$ from elephant tail hairs and milk. 318
Figure 4.8. Serial records of $\delta^{18}O$ from elephant tail hairs, milk water, and drinking water. 320
Figure 4.9. Serial records of δD from elephant tail hairs. 322
Figure 4.10. Serial record of elephant tail hair cortisol. 324
Figure 5.1. Regions represented by tusks used in this study. 407
Figure 5.2. Tusk CT-increment measurement protocol. 408
Figure 5.3. Tusk growth trajectories showing ontogenetic pattern and sexual divergence. 409
Figure 5.4. Sampling scheme for isotope analysis of annual growth increments. 411
Figure 5.5. Dentin collagen pretreatment test results. 412
Figure 5.6. Possible neonatal features in fully preserved tusk tips. 414
Figure 5.7. Temporal distribution of minimum $\delta^{15}N$ for each tusk analyzed. 415
Figure 5.8. TA-3 isotope and growth records. 417
Figure 5.9. 2000-245 isotope and growth records. 419
Figure 5.10. 2000-246 isotope and growth records. 421
Figure 5.11. 2000-286 isotope and growth records. 423

Figure 5.12. 2000-305 isotope and growth records. 425
Figure 5.13. 2007-002 isotope and growth records. 427
Figure 5.14. 2007-005 isotope and growth records. 429
Figure 5.15. 2009-001 isotope and growth records. 431
Figure 5.16. ZCHM-19 isotope and growth records. 433
Figure 5.17. ZCHM-20 isotope and growth records. 435
Figure 5.18. ZCHM-22 isotope and growth records. 437
Figure 5.19. ZCHM-24 isotope and growth records. 439
Figure 5.20. ZCHM-26 isotope and growth records. 441
Figure 5.21. ZCHM-51 isotope and growth records. 443
Figure 5.22. AM-6 isotope and growth records. 445
Figure 5.23. Temporal distribution of estimated weaning ages. 447
Figure 5.24. Temporal distribution of 4-year growth volumes for *males* and *females*. 449

Chapter 1

Introduction

Late Pleistocene megafaunal extinction is the focus of long-running debate and ongoing scientific investigation (Grayson, 1984). American mastodons (*Mammut americanum*) and woolly mammoths (*Mammuthus primigenius*) disappeared at about the same time as part of the mass extinction that primarily impacted megaherbivores (Gingerich, 1984; Koch and Barnosky, 2006). This drop in biodiversity overlaps with the dramatic climate change that characterized the transition from the last glacial cycle to the current interglacial period, the Holocene. Because of this overlap, some have proposed that changes to terrestrial environments brought on by the warming event caused megafaunal populations to plummet (e.g., Dreimanis, 1968; Graham and Lundelius, 1984, Guthrie, 1984; Nikolskiy et al., 2011; Willerslev et al., 2014). However, there is also overlap between regional extinctions and immigrations of human populations (Koch and Barnosky, 2006). Recognition of this overlap with human migrations in late Pleistocene records from around the globe implicates human activity as the extinction mechanism (e.g., Allentoft et al., 2014; Bartlett et al., 2015; Martin, 1973;

Martinez et al., 2012; Ripple and Van Valkenburgh, 2010; Rule et al., 2012; Sandom et al., 2014; Steadman et al., 2005; Surovell et al., 2015).

The Pleistocene Epoch ended with the onset of the Holocene a little over 10,000 years ago (Walker et al., 2009). In some ways the Holocene may be best viewed as a continuation of the Pleistocene. It is the most recent of several interglacials (relatively warm intervals with reduced glacial extent) that occurred between major glacial periods in the Pleistocene. Temperature and glacial extent during the Holocene are not unlike those of previous interglacials (Hansen et al., 2013; Müller, 2009). Nevertheless, survival of mammoths and mastodons during previous interglacial periods and extinction at the end of the Pleistocene during the transition to interglacial conditions of the Holocene show that the terminal Pleistocene was somehow significantly different from previous warming events. If it was simply a difference in intensity of certain environmental factors, we would expect populations that lived during previous warm intervals to show signs that they were somehow weathering considerable hardship.

Previous attempts to evaluate extinction mechanisms

Climate change

Environmental changes at the end of the Pleistocene provide a somewhat inadequate explanation for the extinctions. In at least one respect, the climate models are counterintuitive. We are not talking about a single extinction of a species completely

dependent on a particular ecosystem that disappeared at the end of the Pleistocene. Rather, we are considering a mass extinction event that selected against large animals distributed globally in various environments and with different ecologies (Gingerich, 1984; Koch and Barnosky, 2006). Large-bodied animals are thought to be more resilient to many forms of environmental stress because of their large home ranges, ability to migrate long distances in search of food, and capacity to weather long periods with limited food and water (Brook and Johnson, 2006; Cardillo et al., 2005; Johst and Brandl, 1997).

One challenge to establishing climate change as the cause of the extinctions is the difficulty untangling complex ecological relationships between megaherbivores and vegetation. As an extinction mechanism, climate change is thought to have driven vegetation changes that resulted in lower quality environments that were no longer able to support the high nutritional demands of large animals (e.g., Dreimanis, 1968; Graham and Lundelius, 1984, Guthrie, 1984; Nikolskiy et al., 2011; Willerslev et al., 2014). However, megaherbivores impact their environments in dramatic ways (Danell et al., 2006) and observed changes in vegetation could also be an effect of extinctions rather than a cause (Owen-Smith, 1987; Zimov, 2005; Zimov et al., 1995).

Hunting pressure

Interpreting human hunting activity as the cause of these extinctions in North America (NA) begs explanations for the rarity of definitive 'kill' sites (only 14 according to Grayson and Meltzer (2003)). If Pleistocene NA megafaunal taxa were decimated by Clovis hunters over a period of only a few thousand years, we might expect direct evidence of hunting to be common at late Pleistocene sites. Martin (1973) proposed a 'Blitzkrieg' hypothesis in which human hunters may have actually been so effective, and the annihilation so rapid, that typical site preservation rates would actually result in relatively few hunted specimens making it into the geologic record. But such an extreme proposal is unnecessary if human hunters entered NA early enough that the damage could have been done over a period of several thousand years. To explain the lack of kill sites, one could also consider processing of carcasses and meat caching (e.g., Fisher et al., 1994) that could regularly result in disassociation of recovered fossil remains of hunted individuals from actual kill sites and direct evidence of hunting (Fisher, 1996, 2001). Regardless, the current paucity of kill sites may simply reflect the immature status of the investigation. At least two new sites with direct evidence of proboscidean hunting in the Americas have been discovered in the last few years (Sanchez et al., 2014; Waters et al., 2011), and future discoveries may whittle away at this particular challenge to hypotheses that hold hunting pressure responsible for these extinctions.

Climate + hunting

Acknowledging the complexity of natural systems and the apparent temporal overlap of the extinction event with climate change as well as human migration, some researchers favor a combined model that divides responsibility between the two potential mechanisms (e.g., Braje and Erlandson, 2013; Lorenzen et al., 2011; Haynes, 2010; Brook and Barnosky, 2012). The suggestion inherent in these explanations is that the various megafauna may have been able to cope with hunting in the typical Pleistocene glacial conditions, but that population declines driven by climate change made them particularly vulnerable to pressures from human exploitation. While such an approach conveniently accommodates both of the most popular explanations, it assumes that each mechanism was in fact detrimental to populations and fails to evaluate the relative contributions of each hypothesized stressor. Even if climate and humans both had deleterious effects on megafaunal populations, it is not necessarily the case that both contributed equally or that each required the presence of the other in order to cause the extinctions.

Complications

Attempts to understand the late Pleistocene extinction event by looking at timing of potential causes and effects fail to favor one mechanism over the other. The many attempts to constrain last appearance dates and timing of human immigrations are useful for providing context, but they do not provide conclusive tests of extinction

hypotheses. Not only are they complicated by considerable uncertainty due to incompleteness of the fossil and archaeological records, as well as disagreements on what to treat as convincing evidence of human activity (e.g., Grayson and Meltzer, 2003; Holen and Holen, 2011), but dates would only bring resolution to the issue if they were to show that one mechanism or the other could not have had a causal role in the extinction. Such a breakthrough seems unlikely given the approximately simultaneous action of both mechanisms on each continent.

Evaluating the effects of hunting and climate change separately may be particularly challenging because mobility of human groups is not independent of glacial coverage, which was affected by late Pleistocene warming (Erikkson et al, 2012). Even if extinctions were linked to warming, migrating human groups buoyed by the favorable conditions may have been the primary agent directly responsible for the population stress.

Other investigations, such as those looking at shifts in body size, may not discriminate between climate and hunting explanations. Decrease in average body size is an expected consequence of nutritional limitation and has been used as an indication of climate driven stress in some species (Hill et al., 2008; Guthrie, 2003). The difficulty of using body size reduction at the end of the Pleistocene as a sign of climate-change is

that hunting pressure can produce the very same pattern (Coltman et al., 2003; Fisher, 1996; Proaktor et al., 2007).

Using life-history analyses to test extinction mechanisms

Life-history analyses have potential to end the gridlock by providing divergent predictions that can be used to test each hypothesis. Population stresses from hunting pressure and climate-related nutritional deficiency lead to very different effects on individual life histories. Nutritional stress, the direct mechanism of population pressure associated with climate shifts, is expected to make life histories slow down (e.g., Shanley and Kirkwood, 2000; Lee and Moss, 1986). This relationship is intuitive, since decreased caloric supply cannot be expected to support a sustained pace of growth and reproduction. Conversely, hunting pressure, which causes high mortality without increased energetic constraints, favors high reproductive rates and results in earlier maturation (e.g., Jennings, 1999, Proaktor et al., 2007). Life-history patterns thus provide ways to directly test opposing predictions of each hypothesis.

Life-history analyses provide direct evidence of how individuals were impacted by conditions during times of population decline leading up to regional extirpations. Previous analyses looking at tusk records from mastodons and mammoths from NA (Fisher, 1996, 2001, 2009) have provided evidence that individuals were growing faster, maturing earlier, and reproducing more quickly at the end of the Pleistocene than

during the last glacial maximum (LGM). Here I provide evidence of changes in weaning age for Siberian woolly mammoths over the interval from 40,000 to 10,000 radiocarbon years before present (^{14}C years BP) that suggest they were maturing and reproducing faster shortly before extirpation from the continent (around 10 k ^{14}C years BP) than they were during the LGM.

Analyses of proboscidean life-history data in both Siberia and North America suggest that life histories were speeding up (maturation was more rapid) in the last few thousand years of the Pleistocene. Accelerated life histories are consistent with expectations if hunting was driving down populations. Improving climate conditions could also explain such changes, but they would not lead to extinction. If deteriorating habitats brought on by changing climate were causing populations to fail, we would expect to see life histories slow down. Therefore, based on these data, hunting provides a better explanation for the extinctions.

Methods employed in this study

Tusk analyses described in following chapters rely heavily on some newly applied methods. These include X-ray computed tomography (CT) scans of tusks to measure growth increments, CT-guided serial sampling and subsampling of annual increments, collagen isotope analysis from powder samples of tusk dentin (rather than from demineralized blocks), repetitive sampling of individual elephant tail hairs for serial

analyses of hair composition, and serial analysis of cortisol in a single strand of elephant tail hair.

X-ray computed tomography (CT) was first intensively used as a tool for evaluating tusk growth records in the studies of mastodon mandibular tusks described in *Chapters 2* and *Chapter 3*. Mastodon mandibular tusks grow continuously throughout life, like their premaxillary complements, but are relatively small and compact with upwards of 30 years of growth recorded in tusks about 25 cm long. Their sizes made them ideal candidates for investigating the utility of the University of Michigan School of Dentistry's MicroCT Core facility for visualizing the 3-dimensional growth cones in tusk dentin. Analyses of small juvenile woolly mammoth tusks for assessments of weaning age (*Chapter 5*) also benefited from extensive use of local microCT facilities.

Seasonal variations in X-ray attenuation of dentin create cyclic patterns in CT scans that reveal annual growth increments. These CT increments provided the basis for *estimated increment volume* (EIV) of each year's growth (see *Chapter 2*). EIV growth series for mastodon mandibular tusks and juvenile mammoth tusks were used to determine sex, ontogenetic stage, and in some cases, specific years of life for each tusk. Year-to-year variations in EIV may have some interpretive significance, such as a decrease that often accompanies other evidence of weaning, but they may lack the precision needed to resolve multiyear growth patterns when interannual variations are

small. Even in two mandibular tusks from a single individual, year-to-year fluctuations in EIV profiles do not always match (see *Chapter 3*).

For analyses of weaning age in Siberian woolly mammoths (*Chapter 5*), I took a step back from the high-resolution isotope sampling used for looking at seasonal variations in tusks, and instead focused on annual variability. Rather than samples that represented 1-2 months of growth, I used a single bulk sample for each year of growth as identified from CT scans. These samples provided weighted-averages (with periods of faster growth weighted more heavily) of isotope compositions for each year of growth. This procedure sacrificed the ability to resolve subannual variability in order to make broad-scale analyses more feasible within time and funding constraints. Higher resolution sampling would in some ways enhance our ability to interpret records, but is unlikely to contradict results of annual-scale data. The only way such analyses could dramatically alter the results would be if they showed significant seasonal variability and inconsistent timing of annual increments, such that some samples contained more dentin from isotopically enriched seasons, while others contained more dentin from isotopically depleted seasons of growth. If this were the case, however, we would expect to see fluctuating patterns (a year of artificially high $\delta^{15}N$ would be complemented by an artificially low one either preceding it or following it). Thus, multiyear trends associated

with this phase of life history cannot be simply an artifact of inaccurate year identifications.

Most analyses of tusk dentin collagen in this study were processed from powder samples instead of dentin block samples. Powder sample pretreatment required procedural adjustments that included omission of a 'defatting' step. With very low lipid content in dentin and samples coming from unexposed, unpolished dentin surfaces cut with ethanol as a lubricant, we do not expect this to have a significant effect on results. Internal tests support this assertion.

The study of zoo elephants (*Chapter 4*) included what is to my knowledge the first-ever attempt to repeatedly clip samples from individual elephant tail hairs as they emerge from the follicle. Using this method I was able to produce serial isotope records with known timing. It also enabled me to get direct measurements of bimonthly hair growth that revealed significant seasonal variation in growth rates. This observation informed temporal reconstructions of records from the initial hair clippings, which contained growth from multiple years prior to initiation of bimonthly sampling.

Chapter 2 summary

Sites in North America (NA) from the previous interglacial (the Sangamonian – an interval for which there is currently no evidence of humans on the continent) provide comparative data for evaluating patterns observed for the end of the Pleistocene, when

human activity may have significantly impacted NA populations of megafauna. The Ziegler Reservoir (ZR) fossil site in the mountains of Colorado, preserves remains of mastodons living in a mid-latitude, high-elevation region during the Sangamon interglacial (Miller et al., 2014), when the regional climate was similar to current conditions (Anderson et al., 2014). If life-history analyses of ZR mastodons were to reveal signs of nutritional stress on Sangamonian populations, they would lend support for climate-related extinction hypotheses. In that case, even subtle differences in the most recent glacial retreat or minor pressure from limited hunting could have tipped the scale leading to catastrophic population declines.

Chapter 2 examines growth records from mandibular tusks of the ZR mastodons for signs of environmental stress. Serial stable isotope records of oxygen and nitrogen contain seasonal variation and confirm the annual periodicity of first-order radiodensity growth features present in CT scans of tusks. Measurements of CT increments show high interannual consistency represented by low mean sensitivity – a measure of variability (Douglass, 1920) shown to be higher than normal in tree ring records of specimens growing near range boundaries (Laxson, 2011). There is a shift in average oxygen isotope values of tusk dentin carbonate that appears to reflect a temperature increase during the sampled interval. This secular shift is not associated with any changes in seasonality, growth rates, or growth variability. Thus, in combination, isotope analyses

and growth measurements indicate some degree of environmental change with no apparent effect on individual growth records.

Multiyear records of growth in ZR mastodon mandibular tusks provide an indication of nutritional condition in these individuals. Even though we currently lack other datasets for mandibular tusks, which are markedly smaller than premaxillary tusks and cannot be directly compared in terms of absolute growth, we can look at variation within and between individual records from ZR specimens to search for patterns in year-to-year variability that might indicate environmental stress. Analyses of tusk growth records for these mastodons show no evidence that populations were stressed by interglacial conditions. Rather, they suggest that individuals were thriving in this environment. It is possible that this montane setting provided a refugium for populations when interglacial conditions were unfavorable for mastodons at lower elevations. However, even if range contraction associated with this shift resulted in diminished regional populations, other pine and spruce forests at higher latitudes would have provided additional potential range for mastodons at the time. Mastodon remains in Alaska and the Yukon demonstrate range extensions far northward during deglaciated periods (Harington and Clulow, 1973; Zazula et al., 2014).

In addition to characterizing growth patterns in mastodon mandibular tusks, *Chapter 2* provides preliminary notes on ZR taphonomy, specifically in terms of

generating mechanisms for the mass death assemblage of mastodons in the lake-margin deposits, and regarding the presence of multiple isolated mammoth specimens in upper lake-center units. Investigations are ongoing regarding the enigmatic association of partial mammoth carcasses with small boulders. Meanwhile, comparisons of intra-annual timing of death and multiyear isotope patterns failed to confirm hypotheses involving catastrophic genesis of the lake-margin mastodon assemblage. Some limited support from tusk records for potential multiple-death events was weakened by subsequent discoveries reported in *Chapter 3*.

Chapter 3 summary

Mandibular and deciduous tusks from Ziegler Reservoir (ZR) mastodons were considered in *Chapter 2* to represent 26 individuals. Recognition of several likely left-right pairs required revision of this count. Tusk pairings decrease the number of mastodons analyzed from 17, support consolidation of certain stratigraphic intervals previously treated as discrete, and suggest some time-averaging in the ZR mastodon near-shore assemblage.

The site census in *Chapter 2* was in part based on stratigraphic associations. Tusks had been compared within stratigraphic units in order to identify left-right complements and prevent treatment of two tusks from one individual as independent records. However, due to time constraints and a simple working model of site formation

that did not sufficiently accommodate potential for mixing between layers, we treated stratigraphic units as representing distinct time slices. As a consequence, we did not at first thoroughly entertain the possibility of matching pairs among tusks sourced from different units.

Similarities in overall morphologies, surface patterns, CT features, growth increment series, and isotope records support the existence of 9 previously unidentified pairs in the assemblage of 27 mandibular and deciduous tusks, bringing the number of individuals represented by the tusks down from 26 to 17 (two of the 27 were previously known to be from a single individual). In most cases, pairs combine tusks from different stratigraphic units, which in each case means either that stratigraphy was misidentified for at least one tusk, or that remains of a single individual were spread over multiple depositional units.

This new information undermines some interpretations discussed in *Chapter 2*. As an effect of eliminating duplicate records for paired tusks, season of death estimates become more evenly distributed throughout the year and more consistent among stratigraphic intervals. In addition, the new analysis reveals a match between two tusks that were previously considered some of the strongest evidence of simultaneous death at the site.

Other inferences presented in *Chapter 2* are either unaffected or reinforced by the new understanding of the data. Chronological revisions do not refute the original claim that mean sensitivity (a measure of variability in serial measurements; Douglass, 1920) remained fairly consistent through time. Meanwhile, the secular trend in average $\delta^{18}O$ becomes slightly clearer with the adjustments.

Recognizing tusk pairs among specimens initially treated as independent provides an opportunity to determine limits of certain methods for comparing growth records. *Estimated increment volumes* (EIV; a calculation based on a triad of orthogonal linear measurements for each annual CT growth increment; *Chapter 2*) and fractions of final year (FFY; a proxy for season of death; *Chapter 2*) are both only somewhat consistent in matched tusks. Since contemporaneous growth records cannot be expected to correspond better than those from each tusk of a single individual, we may not be able to identify contemporaneous individuals through comparison of EIV records. That is, EIVs measured from CT data appear to lack the precision necessary to make such comparisons. This also means that disparity between any two EIV records does not demonstrate that the individuals were living at different times. In contrast, isotope data match closely for paired tusks, except where diagenetic processes have apparently altered records. Further improvements in EIV accuracy and direct measurements of increment volumes could both enhance inter-tusk comparisons of CT growth records. In

the meantime, efforts should focus on oxygen isotope records and FFYs as data that could detect multiple-death events represented in the tusk assemblage.

In summary, *Chapter 3* documents the discovery of left-right pairs in the ZR mandibular tusk assemblage reported in *Chapter 2*. This provides evidence of time-averaging in the ZR near-shore deposits, additional support for a secular trend toward warmer temperatures in the interval represented by mastodon remains, and maximum expectations for congruence in contemporaneous tusk records.

Chapter 4 summary

Chapter 4 documents results from a multiyear continuous study monitoring stable isotopes in water, milk, and hair for a mother-calf pair of African elephants (*Loxodonta africana*) at the Toledo Zoo and Aquarium in Toledo, Ohio. An isotopic signature of nursing documented in various mammals (e.g., Fogel et al., 1989, Fuller et al., 2006; Jenkins et al., 2001) supported interpretations of nursing in tusk records from juvenile woolly mammoths and a single African elephant (Rountrey, 2009; Rountrey et al., 2007), but the isotopic relationships between a mother and her nursing calf had not been previously observed in elephants. This project provides a framework to support interpretations of nursing and weaning in records from fossil juvenile tusks and corroborates previous interpretations of a nursing effect in isotope records from

proboscidean tusks and teeth (Metcalfe et al., 2010; Rountrey, 2009; Rountrey et al., 2007).

Data from this ongoing study demonstrate a pattern of enrichment in nitrogen stable isotope content of the nursing calf's hair, relative to its mother's hair grown during the same interval. This enrichment is highest shortly after birth and then decreases over the remaining years of the analysis, during which time nursing decreases significantly but does not stop. Other isotope systems display significant enrichment in calf values compared to those of its mother, but none shows as clearly the convergence between calf and mother records that coincides with decreased milk consumption.

In addition to documenting effects of nursing on hair isotopes in the calf and mother, study results show a $\delta^{18}O$ fractionation between drinking water and hair, a strong seasonal effect on tail hair growth rates, and suitability of elephant tail hairs for assessing changes in multi-week average systemic cortisol level over multiple years prior to sampling.

Chapter 5 summary

Growth records and serial isotope analyses of juvenile Siberian woolly mammoth tusks suggest that populations were not stressed by climate changes during the interval of warming that immediately preceded their extirpation from the continent. Evidence of a shift to earlier weaning age during this time is inconsistent with expectations of

climate-driven extinction hypotheses. A general increase in female juvenile growth rates during this time is also contrary to the idea that warming conditions were detrimental to woolly mammoth populations. Most observed patterns appear to track climate changes, but not in ways that support climate-driven extinction hypotheses. In fact, evidence from weaning age is consistent with warming ushering in more favorable environments. Hunting pressure provides a mechanism consistent with these observed trends that could explain the continental extirpation.

Although sample sizes are too small to strongly support any trends in growth rates, the data suggest that male growth rates may be in decline just as female rates are increasing. Further tests are required to verify this pattern, but if corroborated, it would be difficult to explain with climate change alone, but could be consistent with hunting, especially if Pleistocene hunters selected against large tusked males.

Weaning ages can be interpreted from nitrogen stable isotope (δ^{15}N) records of juvenile woolly mammoth tusks. δ^{15}N profiles for the first years of life consistently show a pattern that appears to represent the gradual decrease in nursing and subsequent weaning that characterize early life histories in mammals. Analyses of annual average δ^{15}N over several years of life were used to investigate weaning age in 15 woolly mammoth tusks. Records for 12 of these tusks have a sufficient span of years that weaning age could be estimated based on δ^{15}N patterns.

Weaning age estimates compiled from tusks distributed over the last 30 ka of the Pleistocene provide evidence that woolly mammoths were nursing longer during the last glacial maximum (LGM) than during the warmer periods that preceded and followed it. The decrease in weaning age following the LGM and leading up to the end of the Pleistocene when mammoths were extirpated from continental Siberia is inconsistent with the hypothesis that vegetational responses to climate change resulted in population decline. Instead, it supports hunting pressure as the deleterious force behind the extirpation. Both hunting stress and improving nutritional conditions could explain a shift to earlier weaning, but only one of these would also explain the failure of populations to maintain viable levels. Whether hunting or nutrition is behind the reduction in weaning age, the absence of a well-supported alternative extinction mechanism leaves hunting stress as the most likely cause for this event.

Trends in weaning age and growth rates support hunting-induced extirpation of continental Siberian woolly mammoths at the end of the Pleistocene. Although these results are currently limited to Siberia, the implication is that human hunting activity played a significant role in the end-Pleistocene megafaunal extinctions.

Conclusion

These studies contribute to two discussions that enhance our understanding of the late Pleistocene megafauna extinctions: (1) Characterization of megafauna

populations during previous interglacial periods, and (2) life-history responses to extinction pressures at the end of the Pleistocene. Analyses of tusks from the ZR assemblage tell us something about how mastodons fared during a previous interglacial period with conditions similar to the Holocene. Analyses of juvenile woolly mammoth tusks contradict climate as the cause of extirpation from continental Siberia.

The study of weaning in zoo elephants provides the first documentation of the isotopic relationship between a lactating elephant and her nursing calf, the first direct bimonthly measurements of elephant tail hair growth rates, and the first long-term serial record of hair cortisol in an elephant. Observed isotopic patterns support interpretations of weaning in fossil tusk records described in *Chapter 5* and will provide context for future studies. Measurements of hair growth rates and seasonal variability will inform reconstruction of long-term serial hair records for elephants and guide development of other sampling procedures to analyze elephant tail hair records. Hair cortisol is increasingly being used as a measure of long-term well-being in mammals. Our detection of cortisol throughout the full length of an elephant tail hair representing multiple years of growth provides evidence that it could be useful as an indicator of mental and physical condition in previous years.

Projects documented herein contribute meaningful data to discussions of the late Pleistocene megafaunal extinctions. Perhaps most importantly, they chart a possible way

forward that circumvents obstacles presented by the fact that the timing of late Pleistocene extinctions is fairly well correlated both with dramatic climate change and with human activity. Life-history reconstructions provide tests of proposed extinction mechanisms that offer clear conclusions.

References

Allentoft, M. E., Heller, R., Oskam, C. L., Lorenzen, E. D., Hale, M. L., Gilbert, M. T. P., Jacomb, C., Holdaway, R. N., Bunce, M. 2014. Extinct New Zealand megafauna were not in decline before human colonization. Proceedings of the National Academy of Sciences 111(13):4922–4927.

Anderson, R. S., Jiménez-Moreno, G., Ager, T., Porinchu, D. F. 2014. High-elevation paleoenvironmental change during MIS 6–4 in the central Rockies of Colorado as determined from pollen analysis. Quaternary Research 82(3):542–552.

Bartlett, L. J., Williams, D. R., Prescott, G. W., Balmford, A., Green, R. E., Eriksson, A., Valdes, P. J., Singarayer, J. S., Manica, A., 2015. Robustness despite uncertainty: regional climate data reveal the dominant role of humans in explaining global extinctions of Late Quaternary megafauna. Ecography 38:1–10.

Braje, T. J., Erlandson, J. M. 2013. Human acceleration of animal and plant extinctions: a late Pleistocene, Holocene, and Anthropocene continuum. Anthropocene 4:14–23.

Brook, B. W., Barnosky, A. D. 2012. Quaternary extinctions and their link to climate change. In: Hannah, L. (Ed.), Saving a Million Species. Island Press/Center for Resource Economics, pp. 179–198.

Coltman, D. W., O'Donoghue, P., Jorgenson, J. T., Hogg, J. T., Strobeck, C., Festa-Bianchet, M. 2003. Undesirable evolutionary consequences of trophy hunting. Nature 426(6967): 655–658.

Danell, K., Bergström, R., Duncan, P., Pastor, J. (Eds.). 2006. Large herbivore ecology, ecosystem dynamics and conservation (Vol. 11). Cambridge University Press.

Dreimanis, A. 1968. Extinction of mastodons in eastern North America: testing a new climatic-environmental hypothesis. Ohio Journal of Science 68(6):257–272.

Douglass, A.E., 1920. Evidence of climatic effects in the annual rings of trees. Ecology 1, 24–32.

Eriksson, A., Betti, L., Friend, A. D., Lycett, S. J., Singarayer, J. S., von Cramon-Taubadel, N., Valdes, P. J., Balloux, F., Manica, A. 2012. Late Pleistocene climate change and the

global expansion of anatomically modern humans. Proceedings of the National Academy of Sciences 109(40):16089–16094.
Fisher, D. C. 1996. Extinction of proboscideans in North America. In: Shoshani, J., Tassy, P. (Eds.), The Proboscidea: Evolution and Palaeoecology of Elephants and Their Relatives. Oxford University Press, Oxford, pp. 296–315.
Fisher, D. C. 2001. Season of death, growth rates, and life history of North American mammoths. In: West, D. (Ed.), Proceedings of the First International Conference on Mammoth Site Studies: 11-13 March 1998 (pp. 121–135).
Fisher, D. C., 2009. Paleobiology and extinction of proboscideans in the Great Lakes region of North America. In: Haynes, G. (Ed.), American Megafaunal Extinctions at the End of the Pleistocene. Springer, Dordrecht, pp. 55–75.
Fisher, D. C., Lepper, B. T., Hooge, P. E., 1994. Evidence for butchery of the Burning Tree mastodon. In Dancy, W. S. (Ed.), The First Discovery of America: Archaeological Evidence of the Early Inhabitants of the Ohio Area, Ohio Archaeological Council, Columbus, pp.43–57.
Fogel, M. L., Tuross, N., Owsley, D. W. 1989. Nitrogen isotope tracers of human lactation in modern and archaeological populations. Carnegie Institution of Washington Yearbook 1989:111–117.
Fuller, B. T., Fuller, J. L., Harris, D. A., Hedges, R. E. M. 2006. Detection of breastfeeding and weaning in modern human infants with carbon and nitrogen stable isotope ratios. American Journal of Physical Anthropology 129:279–293.
Gingerich, P. D. 1984. Pleistocene extinctions in the context of origination-extinction equilibria in Cenozoic mammals. In: Martin, P. S., Klein, R. G. (Eds.), Quaternary extinctions: a prehistoric revolution. The University of Arizona Press, Tucson, Arizona, pp. 211–222.
Graham, R. W., Lundelius, E. L. 1984. Coevolutionary disequilibrium and Pleistocene extinctions. In: Martin, P. S., Klein, R. G. (Eds.), Quaternary extinctions: a prehistoric revolution. The University of Arizona Press, Tucson, Arizona, pp. 223–249.
Grayson, D. K. 1984. Nineteenth century explanations of Pleistocene extinctions: A review and analysis. In: Martin, P. S., Klein, R. G. (Eds.), Quaternary extinctions: a prehistoric revolution. The University of Arizona Press, Tucson, Arizona, pp. 5-39.
Grayson, D. K., Meltzer, D. J. 2003. A requiem for North American overkill. Journal of Archaeological Science 30(5):585-593.
Guthrie, R. D. 1984. Mosaics, allelochemics and nutrients. In: Martin, P. S., Klein, R. G. (Eds.), Quaternary extinctions: a prehistoric revolution. The University of Arizona Press, Tucson, Arizona, pp. 259-298.
Guthrie, R. D. 2003. Rapid body size decline in Alaskan Pleistocene horses before extinction. Nature 426(6963):169-171.

Harington, C. R., Clulow, F. V. 1973. Pleistocene mammals from Gold Run Creek, Yukon Territory. Canadian Journal of Earth Sciences 10(5):697-759.
Haynes, G. 2002. The catastrophic extinction of North American mammoths and mastodonts. World Archaeology 33(3):391-416.
Hill, M. E., Hill, M. G., Widga, C. C. 2008. Late Quaternary Bison diminution on the Great Plains of North America: evaluating the role of human hunting versus climate change. Quaternary Science Reviews 27(17):1752-1771.
Holen, S. R., Holen, K. A. 2011. Evidence for a human occupation of the North American Great Plains during the Last Glacial Maximum. In: Jiménez-López, J. C. J., Serrano-Sánchez, C., González-González, A., Aguilar-Arellano, F. J. (Eds.), SIV Simposio Internacional El Hombre Temprano en América, pp. 85-105.
Jenkins, S. G., Partridge, S. T., Stephenson, T. R., Farley, S. D., Robbins, C. T. 2001. Nitrogen and carbon isotope fractionation between mothers, neonates, and nursing offspring. Oecologia 129:336-341.
Jennings, S., Greenstreet, S., Reynolds, J. 1999. Structural change in an exploited fish community: a consequence of differential fishing effects on species with contrasting life histories. Journal of Animal Ecology 68(3):617-627.
Johst, K., Brandl, R. 1997. Body size and extinction risk in a stochastic environment. Oikos 78(3):612-617.
Koch, P. L., Barnosky, A. D. 2006. Late Quaternary extinctions: state of the debate. Annual Review of Ecology, Evolution, and Systematics 37:215-250.
Laxson, T.A., 2011. Geospatial analysis of mean sensitivity in *Pinus strobus*. M.A. dissertation. The University of North Carolina at Greensboro, 121 pp.
Lee, P. C., Moss, C. J. 1986. Early maternal investment in male and female African elephant calves. Behavioral Ecology and Sociobiology 18(5):353-361.
Lorenzen, E. D., Nogués-Bravo, D., Orlando, L., Weinstock, J., Binladen, J., Marske, K. A., ..., Cooper, A. 2011. Species-specific responses of Late Quaternary megafauna to climate and humans. Nature 479(7373):359-364.
Martin, P. S. 1973. The discovery of America. Science 179(4077):969-974.
Martínez, G., Gutiérrez, M. A., Tonni, E. P. 2013. Paleoenvironments and faunal extinctions: Analysis of the archaeological assemblages at the Paso Otero locality (Argentina) during the Late Pleistocene–Early Holocene. Quaternary International 299:53-63.
McNeil, P., Hills, L. V., Kooyman, B., Tolman, S. M. 2005. Mammoth tracks indicate a declining Late Pleistocene population in southwestern Alberta, Canada. Quaternary Science Reviews 24(10):1253-1259.
Metcalfe, J. Z., Longstaffe, F. J., Zazula, G. D. 2010. Nursing, weaning, and tooth development in woolly mammoths from Old Crow, Yukon, Canada: implications

for Pleistocene extinctions. Palaeogeography, Palaeoclimatology Palaeoecology, 298(3):257-270.

Miller, I.M., Pigati, J. S., Anderson, R. S., Johnson, K. R., Mahan, S. A., Ager, T. A., … Wilson, J. 2014. A high-elevation, multi-proxy biotic and environmental record of MIS 6–4 from the Ziegler Reservoir fossil site, Snowmass Village, Colorado, USA. Quaternary Research 82(3):618-634.

Müller, U.C., 2009. Eemian (Sangamonian) Interglacial. In Encyclopedia of Paleoclimatology and Ancient Environments, Springer, Netherlands, pp. 302-307.

Nikolskiy, P. A., Sulerzhitsky, L. D., Pitulko, V. V. 2011. Last straw versus Blitzkrieg overkill: climate-driven changes in the Arctic Siberian mammoth population and the Late Pleistocene extinction problem. Quaternary Science Reviews 30(17):2309-2328.

Owen-Smith, N. 1987. Pleistocene extinctions: the pivotal role of megaherbivores. Paleobiology 13(3):351-362.

Proaktor, G., Coulson, T., Milner-Gulland, E. J. 2007. Evolutionary responses to harvesting in ungulates. Journal of Animal Ecology 76(4):669-678.

Ripple, W. J., Van Valkenburgh, B. 2010. Linking top-down forces to the Pleistocene megafaunal extinctions. BioScience 60(7):516-526.

Rountrey, A.N., Fisher, D.C., Vartanyan, S., Fox, D.L., 2007. Carbon and nitrogen isotope analyses of a juvenile woolly mammoth tusk: Evidence of weaning. Quaternary International 169-170, 166–173.

Rule, S., Brook, B. W., Haberle, S. G., Turney, C. S., Kershaw, A. P., Johnson, C. N. 2012. The aftermath of megafaunal extinction: ecosystem transformation in Pleistocene Australia. Science 335(6075):1483-1486.

Sanchez, G., Holliday, V. T., Gaines, E. P., Arroyo-Cabrales, J., Martinez-Tagüeña, N., Kowler, A., Lange, T., Hodgins, G. W., Mentzer, S. M., Sanchez-Morales, I. 2014. Human (Clovis)–gomphotheres (*Cuvieronius* sp.) association ~13,390 calibrated yBP in Sonora, Mexico. Proceedings of the National Academy of Sciences 111(30):10972-10977.

Sandom, C., Faurby, S., Sandel, B., Svenning, J. C. 2014. Global late Quaternary megafauna extinctions linked to humans, not climate change. Proceedings of the Royal Society of London B: Biological Sciences 281(1787):20133254.

Shanley, D. P., Kirkwood, T. B. 2000. Calorie restriction and aging: a life-history analysis. Evolution 54(3):740-750.

Steadman, D. W., Martin, P. S., MacPhee, R. D., Jull, A. J. T., McDonald, H. G., Woods, C. A., Iturralde-Vinent, M., Hodgins, G. W., 2005. Asynchronous extinction of late Quaternary sloths on continents and islands. Proceedings of the National Academy of Sciences of the United States of America 102(33):11763-11768.

Surovell, T. A., Pelton, S. R., Anderson-Sprecher, R., Myers, A. D. 2015. Test of Martin's overkill hypothesis using radiocarbon dates on extinct megafauna. Proceedings of the National Academy of Sciences p. 201504020.

Walker, M., Johnsen, S., Rasmussen, S. O., Popp, T., Steffensen, J. P., Gibbard, P., Hoek, W., Lowe, J., Andrews, J., Björck, S., Cwynar, L. C. 2009. Formal definition and dating of the GSSP (Global Stratotype Section and Point) for the base of the Holocene using the Greenland NGRIP ice core, and selected auxiliary records. Journal of Quaternary Science 24(1):3-17.

Waters, M. R., Stafford, T. W., McDonald, H. G., Gustafson, C., Rasmussen, M., Cappellini, E., Olsen, J. V., Szklarczyk, D., Jensen, L. J., Gilbert, M. T. P., Willerslev, E. 2011. Pre-Clovis mastodon hunting 13,800 years ago at the Manis site, Washington. Science 334(6054): 351-353.

Willerslev, E., Davison, J., Moora, M., Zobel, M., Coissac, E., Edwards, M.E., Lorenzen, E.D., Vestergård, M., Gussarova, G., Haile, J. Craine, J., …, Taberlet, P. 2014. Fifty thousand years of Arctic vegetation and megafaunal diet. Nature 506(7486):47-51.Zimov, S. A. 2005. Pleistocene park: return of the mammoth's ecosystem. Science 308(5723):796-798.

Zimov, S. A., Chuprynin, V. I., Oreshko, A. P., Chapin III, F. S., Reynolds, J. F., Chapin, M. C. 1995. Steppe-tundra transition: a herbivore-driven biome shift at the end of the Pleistocene. American Naturalist 146(5):765-794.

Chapter 2

Taxonomic overview and tusk growth analyses of Ziegler Reservoir proboscideans

Introduction

The Ziegler Reservoir (ZR) fossil site just outside Snowmass Village, Colorado provides a remarkable opportunity to follow a high-altitude biota associated with an alpine lake/marsh environment through about 85,000 years of the Pleistocene (Pigati et al., 2014; Mahan et al., 2014). Its most numerous macroscopically identifiable remains are of proboscideans, both mammoths and mastodons. Three partial mammoth skeletons, additional mammoth molars, and disarticulated (mostly unassociated) bones and tusks representing about 35 mastodons constitute about 80% of more than 5000 macro-vertebrate specimens recovered during fall 2010 and summer 2011 excavations. In this report, we discuss both the mammoths and the mastodons found at the site, but the bones of each taxon are associated with different depositional settings. All mammoth remains were found in bog or marsh deposits near the top of the section, in what are effectively lake-center locations. In contrast, mastodon remains were mostly

lower in the section, near the lake margin, in diamictic slump deposits derived from the moraine that formed the lake margin or in silty layers below and between these deposits.

For this assessment of ZR proboscidean material, we focus on provisional taxonomic assignment and extraction of paleobiologically and paleoclimatically relevant data from the tusk record. ZR mammoths present intriguing taphonomic questions, touched on below, but they are not yet thoroughly extracted from matrix and do not present a sample large enough to support comparative analysis. In contrast, the number and preservational quality of ZR mastodon specimens offer diverse opportunities for comparison. Our main source of insight into the lives and environments of these animals is analysis of the structure and composition of their tusks. Proboscidean tusks are ever-growing incisors composed primarily of dentin that grows through continuous apposition along a conical pulp cavity surface at the tusk's proximal end. Previous studies of proboscidean tusk growth records have featured premaxillary (upper) tusks (e.g., Fisher, 1996, 2009), and although multiple premaxillary tusks were found at the ZR site, most required jacketing for safe removal and transport and are not yet opened, stabilized, and available for study. Mastodon mandibular (lower) tusks are smaller and more compact than upper tusks and did not require jacketing. Mandibular tusks typically experience extreme attrition at their distal end, removing the record of early

years of life, but they can still yield data on growth rates and compositional changes reflective of diet, nutritional status, life history, and climate during the years recorded in tusks (Figure 2.1). They provide clues (if not dislodged during life) to the timing of death and conditions leading up to it. Most isolated but intact mandibular tusks probably slid out of their alveoli (near the mandibular symphysis) after death (and decomposition of their periodontal ligament). They thus provide a means of monitoring the lives of ZR mastodons over intervals ranging from years to decades.

Materials

The first mammoth found, nicknamed "Snowy" in honor of the local village, was a young adult, represented by a large portion of a skeleton (DMNH 60676; numbers in this format are accession numbers for the Denver Museum of Nature and Science, DMNS) in Unit 15 of Pigati et al. (2014). This specimen was damaged by bulldozer strikes before it was recognized. It also experienced significant desiccation-induced fracturing (from shrinkage stresses produced by drying).

Another mammoth, nicknamed the "Clay Mammoth" (DMNH 60704) for the clayey silt in which it was found (Unit 17, Pigati et al., 2014), was stratigraphically above Snowy and near the lake center. The Clay Mammoth was notable for its association with a concentration of rocks (most were locally derived Maroon Sandstone) in the cobble to

boulder size range. The southern margin of the assemblage was hit by a bulldozer, damaging the right tusk, but the entire assemblage constitutes less than half the skeleton. A third set of even less complete mammoth remains, "Cody's Mammoth" (Loc. 87; numbers in this format are one style of field number), was encountered, also in Unit 17, as the excavation was closing. Like the Clay Mammoth, it was associated with rocks, but these were smaller and less numerous. Finally, several isolated mammoth molars were recovered as float or in place in Unit 17. Three of these were recovered as a single association (CCN 42-44; another style of field number).

ZR mastodon remains were found near the southeast corner of the site, along the margin of the former alpine lake. They are distributed from the clay at the base of the lake-center sequence (Unit 3, extending locally below the Basement Red Pebble unit of the lake margin) up to the Beach Silt, although the uppermost specimens do not include mandibular tusks. Our analysis of tusks for the environmental data they provide focuses on the units where mastodons are most abundant, from the Basement Silt up through the Primary Debris Flow (Pigati et al., 2014). The ZR assemblage is remarkable not only in the number of specimens and individuals but also in that it represents a time, region, and environment that has not been well documented for mastodons (Miller et al., 2014). It provides an opportunity to investigate mastodon paleobiology prior to human contact and through a significant span of time.

Methods

Specimen treatment

Specimens such as the three partial mammoth skeletons were exposed (using non-metallic tools), mapped, and photographed in situ (Figure 2.2A). The Clay Mammoth was also documented by three LiDAR scans. We took this step because observations made during exposure of this specimen suggested it warranted closer study. We therefore jacketed the entire assemblage with burlap and plaster, supporting it from below with beams that were then joined into a solid framework, allowing the entire mass – bones, boulders, and surrounding sediment – to be lifted and transported to DMNS. The LiDAR scans were "insurance", in case the block's integrity was compromised during transport, but it arrived safely and has now been partly exposed, documented by total station readings on individual bones and rocks prior to their removal from the jacket, rejacketed from above, flipped, and exposed from below (Figure 2.2B). Additional documentation and analysis is planned.

Fossils preserved at ZR were typically saturated with ground water and thus required efforts to mitigate the damaging effects of rapid desiccation. Large elements were jacketed and moved to DMNS facilities, where they could be cleaned and slowly dried. Smaller elements were removed from sediment and wrapped in plastic or placed

in sealed plastic bags, after which they were washed and photographed and then returned to plastic bags to begin a slow process of controlled drying that continued at DMNS.

Isolated remains were logged into a whole-site coordinate system prior to removal. Each specimen was located by distance, azimuth, and vertical displacement relative to one of a series of staked total station points around the site. Field numbers in the format "30.076" refer to the 76th specimen located in the vicinity of stake 30. Azimuth and plunge of the long axis of each element and a measure of rotational orientation about this axis (inadvertently omitted for some elements) were also taken before removal, along with photos of many bones. Bones were identified to the stratigraphic unit in which they were found; some extended across unit boundaries and were attributed to the unit containing most of their mass. Specimens from spoil piles and any removed prior to measurement were marked as "float."

Cheek teeth and mandibular tusk diameters were measured with calipers, and tusk circumferences and lengths (along the outside curve), with a flexible tape measure. Measurements (except enamel thickness) were to the nearest millimeter. Identifications of teeth were based on measures of crown size, on published descriptions (e.g., Saunders, 1977; Green and Hurlbert, 2005), and on associations in intact dentaries and maxillae. Premaxillary tusks not associated with cheek teeth were identified as

mammoth/mastodon from the Schreger pattern, best seen in transverse section (Trapani and Fisher, 2003). Mandibular tusks, with their shallow pulp cavities and cylindrical form, are unknown for mammoths.

To document morphology prior to any sectioning, each specimen was molded using a tin-based silicone rubber, supported by fiberglass mother molds, and then cast using pigmented polyester resin and fiberglass. Molds and first casts of each tusk will be accessioned into DMNS collections. 3D surface models of many specimens were also produced.

MicroCT analysis

Computed tomography (CT) was used to document variation in density (x-ray attenuation) of tusk dentin, revealing patterns that are interpreted below as demarcating annual increments of tusk growth. CT scans used to analyze ZR specimens were produced by the MicroCT Core facility in the University of Michigan School of Dentistry on a SCANCO Medical µCT100 operating at 90kV, 78µA, and 500 ms, yielding uniform cubic voxels 40–60 µm on a side. Some tusks had to be sectioned to fit the chamber, scanned in multiple parts, and then reassembled virtually. In these cases we used a thin saw blade to minimize kerf loss, stopped the cut prior to completion, and fractured the last connection, allowing us to reassemble the pieces with accurate spacing. CT scans were processed in Amira 5.4.1. Volumetric measurements were

acquired using Amira, but linear measurements were taken from 2D virtual slices (extracted from the CT data) that were imported into ImageJ and Adobe Photoshop. To maximize consistency between growth series in different tusks, dorsoventral slices following the long axis of the tusk were used whenever feasible (Figure 2.3).

Patterns interpreted as annual variation in x-ray attenuation in most specimens consisted of a gradient from low values to high. Zones characterized in this fashion were usually followed by a relatively abrupt return to low values marking the start of the next cycle (Figure 2.3). These CT features are relatively distinct but somewhat variable in clarity and always require careful inspection to determine optimal placement of boundaries. Multi-year growth trends, average growth rates, annual variability, and approximate fraction of a year that was realized at the end of life all appear to reflect meaningful variation.

Several measurement protocols were used to quantify annual increments in mandibular tusks using CT data. Data on increment thickness required a special convention because annual increments taper from the central axis of the tusk toward the cementum-dentin junction, or CDJ. Thus, no thickness measure can be exactly perpendicular to both proximal and distal increment boundaries, nor is there any point along increment boundaries at which a stable thickness value is attained. As a compromise, we located a reference point along each increment boundary, halfway

between the tusk axis and the CDJ. From each such point, we constructed a line perpendicular to the increment boundary that projected toward the preceding (next-distal) increment boundary. The distance along this perpendicular from the originating boundary to the preceding boundary was used as the thickness for that increment (Figure 2.4D, E). In CT data, increment boundaries are usually easier to trace midway between the axis and CDJ than along either the axis or the CDJ, so this convention could be implemented for most specimens.

Although thickness is one standard measure of increment magnitude, volumes represent an interesting alternative. With full CT scans, increment volumes can be measured directly, by digitally segmenting increments, essentially isolating and counting voxels inside the CDJ and between proximal and distal boundaries of a given annual increment. Increment volumes provide the most dimensionally comprehensive quantification of the magnitude of annual increments. However, complete segmentation is time-consuming and requires radiodensity transitions that are sharp over their entire extent. We treated some tusks in this fashion to document the relationship between increment thickness and volume, but we subsequently developed a proxy for volume that we call "estimated increment volume" (EIV).

EIV recognizes that mandibular tusks usually have an elliptical transverse cross section with a major (dorsoventral) diameter and a minor (mediolateral) diameter. EIV

uses major and minor half-diameters (radii) and increment lengths (*L* in Figure 2.3D, the proximodistal distance between successive originating points for thickness measures) to estimate the volume of a growth increment – approximated as the volume of a cylinder equivalent to the volume bounded by two cones separated by *L* (see also Figure 2.4D, upper half of tusk). Comparisons using two tusks (60.057 and 76.085) demonstrated close agreement between EIVs and actual volumes measured from 3D CT data (Table 2.1; Figure 2.5).

To compare variability in growth increment series, we used a metric called mean sensitivity (MS), developed to compare variability in tree ring series (Douglass, 1920; Fritts, 1976; Laxson, 2011). MS is an index that reflects the average proportional change from one increment to the next within a series. It is calculated using the following equation, where *x* is the measure of increment magnitude (we used increment thickness), *t* indicates the position of this increment within the series, and *n* is the number of increments in the series:

$$MS_{tusk} = \frac{1}{n-1}\sum_{t=1}^{t=n-1}\left|\frac{2(x_{t+1}-x_t)}{x_{t+1}+x_t}\right|$$

By its formulation, MS ranges between 0 and 2, with higher values representing greater disparity in consecutive increment measures. Prior to calculating mean sensitivity, the series were individually detrended by dividing each by a cubic smoothing spline with a

50% frequency response cutoff (Cook and Peters, 1981) of 20 years using the dplR package for R (Bunn, 2008), version 1.6.0. This method of removing ontogenetic trends was chosen over modeling and removing the expected trend because ages of individuals could not be determined with sufficient precision to allow alignment of growth increments by age, and normal growth trajectories are not yet well documented. When averaging MS values, we ignored series with fewer than five years.

The last year of life recorded in CT data begins with an abrupt transition in x-ray attenuation like any other year in the tusk record, but the end of this year may be different from prior year-ends, because this increment terminates when the animal dies, and that may or may not coincide with the transition in x-ray attenuation used to trace whole years in the earlier record of tusk growth. Once the typical season of transitions in x-ray attenuation has been determined, the fraction of the final year through which an animal survived gives a means of estimating season of death (SOD), but until then, we refer to this determination in more neutral terms, as "fraction (of expected growth in) final year" (FFY). FFY is a ratio of some measure observed for the final year over the corresponding measure expected for a full year. The measure of growth could be an increment thickness or length, increment area along a plane following the tusk axis, or increment volume; for most of our analyses, we used EIV. We estimated expected annual growth in three ways, distinguished in terms of how many years we used as the basis for

the estimate: 1) only the last complete year, 2) the average for the last two complete years, and 3) a linear projection of the trend shown by logged values over the last five complete years.

Thin-section production and analysis

Thin-section production followed procedures used previously (Fisher, 1988); section thickness ranged from 0.25 to 0.38 mm. Slides were viewed at 40x magnification using a Leitz Laborlux Pol petrographic microscope. Small amounts of kerosene were sometimes added to a slide to enhance light transmission and clarify growth increments. Digital photographs taken with a camera mounted on the microscope were analyzed using an ImageJ measurement utility (IncMeas 1.3c; Rountrey, 2009).

Proboscidean tusk dentin contains three scales of growth features, two of which require thin-sections for precise analysis. First-order features are often visible without magnification and represent annual growth increments. Third-order features represent daily dentin apposition and are sometimes seen in thin-sections under magnification, but are rarely clear enough to permit serial growth measurements. Second-order features, also best seen in thin-section, are strongly developed third-order features that occur with fairly consistent periodicity. The periodicity of second-order features can differ between taxa and dental elements. In mastodon premaxillary tusks, second-order features have a periodicity of approximately two weeks (Fisher, 1987, 1996), but

periodicity of these features has not been analyzed previously in mastodon mandibular tusks. Growth analyses of thin-section data focus on variations in thickness of second-order increments.

Analysis of stable isotope profiles

After 3D digitizing, molding, and casting, mandibular tusks being prepared for isotope sampling were sectioned longitudinally parallel to, but about 2 mm to one side of the axis. The larger half, including the axis, was then polished in preparation for sampling (usually without removing a 5-mm slab). We then milled samples of dentin 1-2 mm deep across this longitudinal surface without significant time-averaging. When we sample isotope profiles from premaxillary tusks, we usually mill samples by following second-order increments on polished transverse sections (often on a slab 5 mm thick). The angle at the apex of dentin cones in premaxillary tusks is so small that a bit penetrating perpendicular to a transverse surface produces little unintended time-averaging. In mastodon mandibular tusks, the angle at the apex of dentin cones is much greater (ca. 60°). In this case, time-averaging is minimized by sampling from longitudinal surfaces.

Second-order growth lines visible in images of the specimen surface (acquired by flatbed scanner and digitally enhanced to accentuate features) and traceable under magnification guided design of a series of mill-paths sampling dentin formed during

consecutive, non-overlapping intervals of time. Where growth lines were difficult to follow, macroscopically visible first-order features and boundaries transferred from microCT results also assisted in sample planning. For the first tusks studied (two adult premaxillary tusks and two mandibular tusks), sample plans were mapped on a magnified image of the polished surface, printed at actual size on acetate sheets, and then transferred to the tusk, followed by hand-milling under a stereomicroscope (Rountrey, 2009). For subsequent studies, we increased accuracy and precision (critical for the relatively thin years of mandibular tusks) by programming mill-paths (Figure 2.6) into the computer-controlled Merchantek MicroMill in the University of Michigan Stable Isotope Lab (UMSIL).

Samples were milled using either a 0.5-mm round carbide burr or a 1-mm diamond cylindrical bit. To acquire samples narrower than one bit-width, milling proceeded via shallow passes initiated from the open pulp cavity and progressed inward toward earlier growth markers.

Analyses of structural carbonate in dentin were performed on powder samples pretreated using the procedure documented by Rountrey (2009), and collagen preparation methods were based on those outlined by Rountrey et al. (2007). Collagen analyses were performed on blocks of dentin (ranging from 7 to 15 mg) that were demineralized in 10 ml 0.5 N HCl at 4 °C until translucent and flexible (approximately 2-3

days; procedure documented thoroughly by Rountrey et al., 2007). We then thoroughly rinsed the samples and treated them with a 2:1 chloroform-methanol mixture (10 ml) at room temperature in a sonicator for 30 minutes to remove any oils introduced during the sampling process. After final rinsing and lyophilization, we wrapped subsamples of 583 to 600 µg (adjusted to match sample and standard peak voltages to the degree possible within individual runs) in tin capsules for analysis of $\delta^{15}N$ and $\delta^{13}C$ on a Costech Elemental Analyzer attached to a Finnigan Delta V+ mass spectrometer in UMSIL. Collagen and carbonate samples reported here correspond directly, with each collagen sample having a carbonate sample complement that was milled from the same growth interval.

For dentin carbonate pretreatment, we soaked powder samples in 30% H_2O_2 (for dentin, we used 0.08 ml per mg of sample; for enamel we followed UCSC stable isotope lab protocol (http://es.ucsc.edu/~silab/di.apatite_SOP.php last accessed 07/10/2014) and used 0.1 ml per mg) for 24 hours at room temperature to remove organics. Next, we rinsed samples in ultrapure water and treated them with 1M acetic acid-calcium acetate buffer solution (0.08 ml per mg of sample for both dentin and enamel) at room temperature for an additional 24 hours to remove secondarily deposited carbonate. Following another rinsing and subsequent lyophilization, we weighed 800 to 1000 µg aliquots into stainless steel boats for analysis of $\delta^{18}O$ and $\delta^{13}C$ on a MAT Kiel IV

preparation device coupled to a Finnigan MAT 253 mass spectrometer in UMSIL. Prior to analysis, samples were roasted at 200 °C for 1 hour under vacuum. In unpublished tests prior to this work, changes were observed in oxygen isotope values of pretreated dentin powders that sat for extended periods of time. We therefore scheduled sampling to limit time between pretreatment and analysis to no more than two days. Results for carbonate and collagen analyses are reported in delta notation relative to VSMOW ($\delta^{18}O$), VPDB ($\delta^{13}C$), and air-N_2 ($\delta^{15}N$).

Results

Taxonomic overview

Most proboscidean taxonomic discrimination focuses on the morphology of third molars (Maglio, 1973; these are the largest teeth, with the longest functional life and the greatest likelihood of recovery). A partial right lower third molar (m3; DMNH 60704.008) with 16 lophs, 9 of which are exposed on the occlusal surface, was dislodged by the bulldozer that grazed the southern edge of the Clay Mammoth assemblage (Figure 2.7). Two molar fragments found with Cody's Mammoth represent a left m3 (Loc. 87-44; differences in stage of tooth wear and duplication of seventh cervical vertebrae and right first ribs between these two occurrences preclude interpreting them as a single individual) similar to that of the Clay Mammoth (Table 2.2). Three first and second

molars were recovered for Snowy (DMNH 60676, Table 2.2), a younger individual, and another three first and second molars (CCN 42-44, Table 2.2) were recovered in an association separate from the three partial skeletal assemblages.

Molar form for the Clay mammoth and Cody's mammoth, and for the isolated teeth (not treated here, but to be described elsewhere) is entirely consistent with *Mammuthus columbi* (Falconer, 1857), for which comparative data are given in Saunders (1970), Graham (1986), and Agenbroad (1994). Snowy's molars are likewise readily accommodated within this taxon, although her enamel is thinner than expected. The only observations that complicate this simple picture are the relatively narrow crowns, the high lamellar frequencies, and the relatively thin enamel of CCN 42-44 (Table 2.2), traits that are at least suggestive of *M. primigenius*. Plate number for these molars is still within expected range for *M. columbi*, but this mosaic of traits raises the possibility that we are seeing morphological evidence for introgression between *M. columbi* and *M. primigenius*, as has been proposed on the basis of mtDNA evidence (Enk et al., 2011).

Measurements of a subset of cheek teeth of ZR mastodons are presented in Table 2.2, and natural logarithms of molar lengths and widths are plotted over comparable data for *M. americanum* from the Great Lakes region in Figure 2.8. We could of course use larger sample sizes on both sides of this comparison (and more are available for a more comprehensive analysis), but ZR mastodons shown here present no

clear metric differences from other well-documented North American occurrences of the genus. Likewise, finer details of tooth form correspond closely to material attributed to the American mastodon (e.g., Saunders, 1977). On this basis, we provisionally refer ZR mastodons to *Mammut americanum* (Kerr, 1792).

Nonetheless, we have noticed differences between ZR mastodons and populations from elsewhere in North America. For example, premaxillary tusks of male mastodons in the Great Lakes region show a helical component to their curvature that is notable, but visually subordinate to the arcuate curvature conspicuous in lateral view. In contrast, the best preserved ZR mastodon premaxillary tusk shows a much more pronounced helical curvature. In addition, the surface of Great Lakes region mastodon tusks is relatively smooth, with only subtle longitudinal ridges and grooves, whereas ZR mastodon premaxillary tusks, both male and female, show a pattern of longitudinal fluting expressed most strongly at the cementum-dentin junction (although it carries through to the external surface of the cementum). This pattern consists of centimeter-scale grooves separated by narrow ridges that twist (dextrally on left tusks, in concert with their overall helical form; sinistrally on right tusks) around the structural axis of the tusk. These differences and others, such as the common occurrence of mandibular tusks in ZR female mastodons, as well as males (see below) have raised the possibility that ZR mastodons could represent a new species. However, many ZR specimens remain

unprepared, and quantitative morphologic studies have barely begun. In view of the abundance of material that should be considered, recognition of a new species at this time would be premature.

Demography

The Clay Mammoth molar examined above suggests a Laws' Age Class of XX-XXII, equivalent to an African elephant age of 34-39 (Laws, 1966). Tusk circumference and length of this individual (48 cm, 195 cm – estimated) indicate a male, based on sexual size dimorphism, which is especially clear in tusks (Fisher, 2008; Smith and Fisher, 2011). Patterns of epiphysis fusion are consistent with an adult male almost, but not yet, fully grown (Haynes, 1991). Cody's Mammoth suggests a Laws' Age Class of XVIII (ca. 30±2) but currently offers no clear evidence of sex. Snowy suggests a Laws' Age Class of XII (ca. 18±1), and with a tusk circumference and length of ca. 35.9 and 60 cm, must be a sub-adult female.

Mastodon dentitions can also be age-ranked using Laws' Age Classes, as shown by Saunders (1977), though stages of eruption and wear in mastodons do not precisely correspond to those seen in elephants and mammoths, and implied ages are even less likely to match elephant ages (Fisher, 1996). Figure 2.10 is a first attempt to census ZR mastodons, based on elements of the mandibular dentition (Table 2.3). Our general approach was to use Laws' Age Class (where available), stratigraphic provenience, and

left-right identity to attempt to rule out double-counting of individuals. For isolated mandibular tusks (offering no basis for assigning Law's Age Class), we supplement stratigraphic provenience and left-right identity by checking for matching overall lateral profile, maximum circumference, and lateral profile of dorsal and ventral wear facets at the distal ends of tusks, all of which show strong similarities in left-right pairs present within the collection (e.g., field no. 44.035). Similar comparisons make it unlikely that any of the isolated tusks come from empty alveoli in mandibles with lower dentitions. The smallest tusks are clearly deciduous (with closing pulp cavities, and some with initial stages of proximal resorption). Some of these could be premaxillary rather than mandibular, but this would not affect the count by more than a few. Some other mandibular specimens are unprepared, and many isolated cheek teeth have not yet been assigned to individuals, so the ~35 specimens in this plot (39 are shown, but we conservatively discount a few) are probably an undercount for the whole site (broken tusk tips and expectorated cheek teeth were excluded because they could represent antemortem events).

Attribution of sex to the larger mandibular tusks is based on the evident size-dimorphism in tusks. Scanning the bivariate portion of Figure 2.10, for specimens with a Laws' Age Class >XV (a stage at which an African elephant would be 24±2, and sexual dimorphism would already be well developed), there is a separation in maximum tusk

circumference between one specimen identified as an adult female and five identified as adult males. Projecting down to the histogram below the bivariate plot, three isolated mandibular tusks with circumferences of about 13 cm are identified as adult females, and four tusks with circumferences of 16-17 cm are identified as adult males. The three tusks in between, with circumferences of 14-14.5 cm were identified on the basis of EIV trends discussed below. In short, we see here a pattern that parallels the well-documented dimorphism in premaxillary tusks (Smith and Fisher, 2011).

Taphonomy

Most taphonomic issues beyond season of death will be treated in subsequent papers. However, a few taphonomic observations emerged in the course of research performed to meet the explicit goals of this paper and are of general interest. Among these, several features of the Clay Mammoth are notable. The Clay Mammoth includes some articulated remains (e.g., a series of thoracic and lumbar vertebrae), but most bones are disarticulated, although in some cases in approximate relative anatomical positions. Some of the assemblage remains unexcavated, so the inventory of bones is incomplete. Parts of both fore and hind limbs are present, as well as parts of the axial skeleton, and yet less than half the skeleton is present. During initial excavation, we encountered a small rib fragment completely surrounded by peat and with transversely oriented marks that we initially considered as possible cut marks. At the time, we knew

little about the age of the specimen and decided to err on the side of caution in considering explanations for this assemblage. The most unusual aspect of the assemblage was the suite of boulders, which were both above and below bones; no simple statement of precedence applies consistently to these categories of material. Subsequent analysis of these boulders has identified several refits on non-adjacent fragments, requiring a more complex history than was evident at first. During excavation of the entire expanse of Units 16 and 17, few if any other rocks of comparable size were encountered, and none in this type of concentration. The only hint of a similar pattern is the smaller set of smaller rocks found with Cody's mammoth.

MicroCT analysis

MicroCT scans of ZR proboscidean tusks show variability in x-ray attenuation of dentin paralleling growth increments, indicating that changes in dentin radiodensity occurred during growth. This phenomenon is not unique to ZR tusks, but patterns of variation differ among tusks from different regions (Figure 2.9; also see *Chapter 5* and El Adli et al., 2015). As described under Methods, the typical pattern of variation is a gradient from lower to higher values (in the direction of apposition), followed by a relatively abrupt drop to lower values initiating the next cycle. This high-to-low drop is the only density-feature well-defined enough in most specimens to use for serial

measurements of radiodensity increments. In addition to the repetition of this pattern, its spatial scale is relatively constant within and between ZR mandibular tusks.

Recognizing increments as annual does not identify the season of any given part of the cycle, but striving toward this goal, we have followed the high-to-low density drop along second-order increments, in thin section and on thick, polished sections, tracing it to the CDJ. In tusks where the CDJ shows a series of topographic features known as periradicular bands (common in adult males, as in Figure 2.1B–D, and variable in expression, from broad undulations to quite discrete topographic anomalies), density drops are closely aligned with periradicular bands. This association will figure in our discussion of the seasonal significance of radiodensity features.

MicroCT records for six small deciduous tusks (17.1/60696; 44.146; 68.032; 68.050; 71.092; 77.099) contain a brief density decrease that can be traced from the crown into the root. This density anomaly presents as a dark line on polished sections in reflected light (Figure 2.11). We interpret it as a neonatal line, marking the time of birth. Most ZR tusks in this size range lack clear annual radiodensity features, either because these animals were too young to show more than part of a year or because, as nursing juveniles, they were buffered from seasonal variability.

Thin-section analysis

To explore the relationship between radiodensity variation and rate of dentin apposition, we examined transverse thin-sections of the final years of growth in two premaxillary tusks of ZR mastodons, one adult male and one adult female (based on tusk diameters; Loc. 8 and 70.018, respectively). Figure 2.12 shows results for the male, where drops in x-ray attenuation are preceded by thin second-order increments (slow growth) and followed by thicker second-order increments (more rapid apposition), supporting the hypothesis that density drops are associated with winter-spring boundaries. Results for the female premaxillary tusk were similar. Thin-sections from two mandibular tusks (58.360, 45.015) were more difficult to analyze, with less distinct second-order features.

Isotope analyses

$\delta^{18}O_{[carbonate]}$

Oxygen isotope values from serial sampling of ZR mastodon tusks show remarkable consistency between specimens (all isotope values are reported in Table 2.4). Most were sampled over a succession of annual increments that would have formed over an interval of 3-4 years. Profiles generally contain one oscillation per year, with some smaller-scale fluctuations and an amplitude of about 3‰ (Figures 2.12C, 2.13, 2.15). Peak values are associated with the low-density dentin that we provisionally designated as spring in our interpretation of CT data. The annual oscillations conform

well to expectation, but peaks occur earlier in the year than in Great Lakes region specimens (Koch et al. 1989). Annual amplitudes are lower than we often see (Koch et al. 1989) but comparable to other cases (Fisher and Fox, 2003); we expect both hydrological and physiological processes exert a damping effect on annual amplitude.

Average $\delta^{18}O$ values for ZR tusks generally increase up-section (i.e., tusks from younger strata tend to have more enriched oxygen isotope ratios). This is probably not a diagenetic effect because the tusks in question come from a similar set of lithologies, and few show unexpected shifts in isotopic values near specimen surfaces, where exposure to pore fluids would have been greatest. We suspect the up-section increase in oxygen values represents regional climate change during the period of mastodon occupation.

Fine-scale sampling in two of the six deciduous tusks with neonatal lines (17.1/60696; 68.050) yields $\delta^{18}O$ records that exhibit an oscillatory pattern consistent with data from other tusks. This is expected, as both fetal and newborn values should track the mother's oxygen values. Because these tusks have no clear annual features, the temporal scale of this variation is currently unclear. However, using apparent second-order features visible in each record and comparative growth rate data from other proboscidean deciduous tusks, we should be able to compare timing of the neonatal line to the seasonal oxygen pattern to deduce the season of birth.

$\delta^{13}C_{[carbonate]}$

Carbon isotope results from structural carbonate in samples of dentin powder for ZR tusks range from -3.16 to 4.27 ‰ (individual tusk averages). The highest of these values are unexpected for any mammalian herbivore, even committed C_4 feeders (Koch et al., 1994). This, in combination with the high level of variation among individuals, is suggestive of diagenetic alteration of dentin carbonate. Dentin carbonate is known to be more susceptible to alteration than enamel carbonate – Koch et al. (1997) observed high variation and many elevated $\delta^{13}C$ values for dentin carbonate of Great Lakes region mastodons (range -13.1 to +0.4 ‰), while enamel carbonate and collagen carbonate showed consistent values expected of C_3 browsers and much less variability in each (standard deviations of 1.0 and 1.3‰, respectively). Many ZR tusk individual time series showed little variation, and some had more enriched $\delta^{13}C$ carbonate values near the exposed pulp cavity surface, additional evidence of diagenetic alteration.

To further evaluate this finding, we isolated a bulk sample of enamel from 68.050, a deciduous tusk with enamel present distally (Figure 2.11). Given its coarser crystal size and lower permeability, we would expect this tissue to be less susceptible to alteration, and indeed, the mean $\delta^{13}C$ (three analyses) of its structural carbonate was -7.79 ‰ (s.d. = 0.11; Table 2.4).

$\delta^{15}N_{[collagen]}$

Collagen samples for two mandibular tusks (45.015; 58.360) exhibit clear and consistent nitrogen isotope patterns that correlate closely with CT density features (Figure 2.13). One way of assessing collagen preservation is to be suspect of samples with carbon-nitrogen molar ratios below 2.9 or above 3.6, a range determined empirically from measurements of modern bone (DeNiro, 1985). One tusk (45.015) has C/N ratios between 3.25 and 3.46 – high, but within acceptable values. C/N for samples from 58.360 falls mostly between 3.50 and 3.63 with two higher values up to 3.89. If preservation is questionable here and not in 45.015, degradation does not appear to have affected the nitrogen values, because $\delta^{15}N$ series from both tusks display similar patterns with similar ranges (58.360 values in Figure 2.13).

Nitrogen isotope series for both mandibular tusks sampled exhibit annually repeated oscillations with amplitudes of about 2‰. Just as in carbonate oxygen results, peak values correspond to samples from the low-density phase of annual CT cycles.

Collagen samples from two mastodon premaxillary tusks (Loc. 8 and 70.018) included samples with C/N ratios that were farther outside the accepted range. In these tusks, samples frequently broke up during demineralization and remaining collagen was visibly degraded – sometimes leading to complete sample loss. Serial samples for Loc. 8 were not analyzed, and with multiple lost samples in 70.018, it is unclear whether the

$\delta^{15}N$ pattern is similar to those observed in mandibular tusks, but values fall within the same 2 ‰ range.

$$\delta^{13}C_{[collagen]}$$

Carbon isotope ratios in all collagen samples matched expectations for C_3 browsers and displayed no cues suggesting alteration. They are therefore likely more reliable than values from dentin carbonate powder samples but are not useful for seasonal determination because they lack any clear pattern of intra-annual variation (Table 2.4: 45.015, 58.360, 70.018).

Fraction (of expected growth in) Final Year

CT scans of dentin from the anterior root of the right m3 (DMNH 60704.008) of the Clay Mammoth showed density variation indicative of annual increments for the final 3-4 years of life. This series was not long enough to establish trends or meaningful variation but did allow us to establish FFY (using linear measurements, not EIVs), the fraction of expected growth in the final year. The Clay Mammoth died about 60% of the way into its final year (Figure 2.14). We leave the seasonal interpretation of this fraction to the *Discussion* section. Scans of blocks cut from two adult mastodon premaxillary tusks (Loc. 8 and 70.018) also did not contain enough information to evaluate variation in growth but again provided FFY determinations (based on linear measurements, not EIVs; Figure 2.14).

Scans of six deciduous tusks (17.1/60696; 44.146; 68.032; 68.050; 71.092; 77.099) contain only one distinct feature, a brief density drop identified above as a neonatal line. These are different from all other radiodensity features observed in this study, but without annual increments, the CT record yielded no FFY. However, one juvenile (but permanent) premaxillary tusk (56.266) contained parts of three annual density cycles but no neonatal line, despite being essentially complete, implying that it initiated formation following birth. Like other tusks with short annual series, this scan was useful *only* for FFY (based on thicknesses; Figure 2.14).

Twenty-one mastodon permanent mandibular tusks containing multiple years were analyzed by microCT. As noted above, these are interpreted as derived from different individuals (with the exception of one pair: 49.594 and 49.595), and they span five stratigraphic units (Basement Silt through Primary Debris Flow). Based on circumference and growth measurements, they appear to include nine adult males, six adult females, three adolescent males, and two sexually indeterminate juveniles (Figure 2.5). EIVs (estimated increment volumes) were calculated for all these tusks, and all display breakage and/or wear at their tips, indicating that the record of the earliest years of life has been lost. Increment series for adult tusks suggest a bimodal distribution, with most increments plotting either in the upper or lower range of logEIV values indicated on the right border of Figure 2.5. In addition, one adult from the Main Silt (MS) has

proximal increments within the female range but a circumference (on a part of the tusk not scanned) that suggests it is a male. Its declining EIVs suggest it may be senescent.

Some other specimens display a decreasing EIV trend over the final years of growth. Most of these tusks are also decreasing in circumference as death approaches, and they have shallow pulp cavities, characteristics typical of older individuals. However, a few exhibit decreasing increment trends with increasing circumferences and relatively deep pulp cavities. This could indicate that slowed increment growth precedes the reduction in tusk circumference that occurs in older individuals.

FFY evaluations were impossible for five tusks with missing proximal ends. For the remaining specimens, FFY for ten falls near the completion of the final cycle (Figure 2.14. One tusk's final increment measures 111% of expected volume, meaning either that the final year was unusually productive or that the final increment boundary is unclear, and growth actually persisted into the beginning of a subsequent, undetected cycle. Likewise, some that appear to have stopped short of a full year, could have been growing more slowly at the end of life and completed more of their final year than is evident by this calculation.

One additional mandibular tusk (44.035) was found within the alveolus of an adult mandible (probably female) and was measured for EIVs through most of its length,

up to its last three years, at which point root bifurcation complicated calculation of EIV. FFY was estimated for this tusk using increment length measurements alone.

Comparing EIVs among individuals and stratigraphic units does not reveal any trends in growth rates correlated with time (Figure 2.5), and growth variability, quantified as mean sensitivity, also shows little change through time. Two adult and one sub-adult record from the lowest layer sampled (Basement Silt) average 0.07. The average of three tusks from the uppermost layer sampled (Primary Debris Flow) is 0.08, and 12 tusks from intermediate layers (Main Floor, Main Floor Red Pebble, and Main Silt) have an average value of 0.08.

Discussion

New sites frequently raise taxonomic issues, and the ZR mammoths are no exception. We were interested in seeing whether there would be morphologic evidence of the introgression between *M. columbi* and *M. primigenius* that left its mark in the mitogenome (Enk et al. 2011). Like the mammoths that yielded the first ancient DNA evidence of this relationship, the first ZR mammoths we focused on (Snowy, Clay, and the isolated teeth not discussed here) showed a more or less normal *M. columbi* phenotype. However, the three associated molars recovered late in the excavation (CCN 42-44) show definite hints of *M. primigenius* influence. However, these specimens do

not include the more definitive third molars, and they still display a few features that are more consistent with *M. columbi*. We therefore formally recognize only this species as occurring at this site, but with additional material in the future, local influence of *M. primigenius* may be placed on firmer ground.

The species-level identity of ZR mastodons is also an intriguing problem but one whose resolution will require additional comparative treatment. The tusk configuration of ZR mastodons is distinctive but needs to be documented in more individuals and ideally replicated elsewhere. Another characteristic trait of ZR mastodons is the presence of mandibular tusks in both sexes (based on tusk diameters and growth measurements; Figure 2.5). It was initially surprising to find so many mandibular tusks, because in late Pleistocene mastodons from the Midwest and Great Lakes region, they are usually present only in males and are typically lost before adulthood, although retention of mandibular tusks by adult males is known (e.g., Hay, 1914; Barbour, 1931; Skeels, 1962; Saunders, 1977). Retention in both sexes is likely the primitive condition for this lineage, but when and why did this change? Green (2006) indicated the presence of mandibular tusks in all (11) Irvingtonian *M. americanum* mandibles from Florida in his study, but mandibular tusks were only present in 27% of his Rancholabrean sample (22). Time binning limits the ability to track the pattern of reduced mandibular tusk occurrence through time in detail based on the Florida data. However, at the ZR site, we now have

considerable evidence that mandibular tusks were present in both sexes in the 138–113 ka interval in this region. Pinsof (1992) also noted that all mastodon mandibles from the American Falls site (Idaho, Sangamonian Stage) have mandibular tusks or alveoli.

The demographic profile of the ZR site as a whole is notable for the abundance of young individuals and prime-age adults. Any site with this many individuals is likely to incorporate some remains derived from attritional mortality, and the partitioning of mastodon remains among and between several debris flows means that there were probably at least as many mortality events as there are stratigraphic associations. Nevertheless, the site-level demographic profile, the only data on demography we had before stratigraphic associations were sorted out, well into this research, looks more catastrophic than attritional (Klein and Cruz-Uribe, 1984; with an abundance of juveniles, adolescents, and prime-age adults). This was the initial impetus for entertaining the possibility that some distinctive entrapment mechanism might have operated at the site (Cherney et al. 2012). With stratigraphic data now in hand, individual stratigraphic units show patterns similar to the whole-site pattern, with an abundance of juveniles and few or no very old individuals (Laws' Age Class >XXV). We consider briefly below how some of the evidence obtained from this site might be used to test a hypothesis of simultaneity of death for multiple individuals, but we have mostly deferred considering

causes of death in favor of learning about the lives of ZR proboscideans and what they can tell us about their response to their environment.

Another taphonomic issue not fully resolved here is the origin of the Clay Mammoth bone/boulder association. When Units 16 and 17 were being deposited (post-Bull Lake and pre-Pinedale glaciation; Pigati et al., 2014), no glacial mechanism was available to account for postmortem transport of this assemblage. In addition, water depth at this stage in the history of the lake is unlikely to have been great enough to transport the entire assemblage in one ice-rafting event, and transport of individual boulders as dropstones fails to account for the number and concentration of carcass parts and boulders, especially against the backdrop of boulder scarcity in the broad expanse of Units 16 and 17. The basin had no fluvial activity competent to displace this material, nor was there sufficient local relief to explain these elements as having slid from a higher source, even on an ice-covered surface, to the center of the basin. At present, we have no satisfactory explanation for this assemblage, but until a complete inventory and 3D model is complete, any summary statement is premature.

The most important and thoroughly investigated of the periodic features of ZR mastodon tusks are the radiodensity features analyzed here by microCT and recognized as marking annual increments of dentin apposition. We suspect these are a widespread feature of tusk development that has only begun to see its full range of application. The

annual nature of patterns of variation in radiodensity seems clear, and the correspondence of abrupt drops in radiodensity with periradicular bands is evidence for associating these drops with points in the annual cycle interpreted elsewhere (based on second-order increment profiles; Fisher, 1987) as winter-spring boundaries. Our thin-section studies support this interpretation, but to acquire data on more years in more individuals, our emphasis for this study has shifted from thin sections to microCT data.

Our isotopic studies were designed both as tests of the seasonal interpretation of radiodensity variation and as sources of paleobiological data in their own right. Frankly, our carbonate oxygen results were initially surprising. If radiodensity drops occur near winter-spring boundaries, tusk $\delta^{18}O$ is highest in spring and lowest during fall. This is different from expectations based on Great Lakes region mastodons, which record high values during summer and low values during winter, in agreement with regional precipitation records (e.g., Koch et al., 1989; Fisher, 2008).

However, seasonal variation in $\delta^{18}O$ of drinking water high in the Colorado Rockies might differ from expectations based on low-altitude Great Lakes locations, and relatively high $\delta^{18}O$ during winter has been documented for Colorado River discharge (Dettman et al., 2003). Possible explanations for the seasonal pattern in ZR tusks include seasonal migration, but we suspect that the relatively heavy oxygen values were obtained near the site because $\delta^{18}O$ series from many ZR tusks terminate at high values

in a cycle. Moreover, our FFY results (Figure 2.14) indicate that some mastodons were present in each season.

One potential cause for high winter $\delta^{18}O$ that does not require migration is ingestion of sublimated surface snowpack or meltwater derived from it. If snow provided the primary water source for ZR mastodons during winter, the $\delta^{18}O$ of ingested water could increase progressively as surface-snow became enriched by sublimation (Lechler and Niemi, 2011). Snowmelt during spring would initially feed runoff with enriched $\delta^{18}O$ from sublimated surface snow, but would gradually begin supplying more light oxygen as the bulk of deeper snow melted into the watershed. If summer drinking sources were fed from snowmelt and relatively light, high-altitude precipitation, heavier $\delta^{18}O$ values might return only when sublimation effects returned the next winter.

Carbonate $\delta^{13}C$ values unfortunately show evidence of diagenetic alteration, in part because they diverge from expectation for C_3 browsers, a dietary habitus documented for mastodons elsewhere (Koch et al., 1998) and corroborated here by collagen $\delta^{13}C$ values of multiple individuals and enamel carbonate $\delta^{13}C$ for one juvenile. How an oxygen isotope pattern can remain intact despite alteration of carbonate carbon isotopic composition is a question that requires additional investigation, but this is a pattern we frequently observe (e.g., Fisher and Fox, 2006). One possible explanation for the results is that these specimens, preserved in fine-grained, clay-rich sediments, may

have had opportunities for isotopic exchange with only a limited volume of water in which carbonate was particularly enriched in ^{13}C, possibly as a result of methane production in the organic-rich lake basin (personal communication, K.C. Lohman, 2014). In this context, it is interesting that the record of $\delta^{13}C$ from ostracode calcite also shows evidence of enrichment and possible methane production (Sharpe and Bright, 2014).

The cause of nitrogen isotope variation in ZR tusks could be seasonal changes in diet, as different plants fractionate nitrogen differently (Bocherens, 2003), but it would be difficult to predict such changes a priori. Another approach is to explain the pattern in terms of a general feature of seasonal environments. The same nitrogen isotope fractionation that elevates predator $\delta^{15}N$ by about 3‰ over tissues of their prey (Gaebler et al., 1966; DeNiro and Epstein, 1981) operates in nutritionally stressed herbivores that catabolize their own proteins in times of food shortage (Hobson et al., 1993). This results in elevated $\delta^{15}N$ for tissues produced during times of stress, such as winter (in a seasonal context, of course, stress is transient), and lower $\delta^{15}N$ in spring or early summer when new plant growth increases access to dietary protein. Seasonal climates in continental interiors might thus elicit patterns of nitrogen isotope variation like those observed in ZR mastodons, although ZR maxima (spring) and minima (fall) appear later in the year than expected, suggesting there could be a dietary component as well. In any case, we do not observe nitrogen values that rise above the apparent

seasonal norm or that are associated with any dramatic reduction in tusk growth rate, suggesting that the animals tested did not experience severe nutritional stress prior to death.

Our collagen $\delta^{13}C$ values for ZR mastodons are entirely consistent with the widely held understanding that this species was a predominantly C_3 feeder. These values were only "inconvenient" in that they did not vary enough on a seasonal scale to assist with our identification of seasons in the tusk record. Although our isotope analyses did not include ZR mammoths, we did note with interest that Pigati et al. (2014) report a $\delta^{13}C$ value of -18.9 ‰ (measured in conjunction with an AMS radiocarbon age estimate) for the Clay mammoth. This value suggests that this mammoth was also consuming mostly C_3 vegetation. Although mammoths are generally thought of as grazers, and frequently did consume C_4 vegetation, it may be that in this ecosystem, plants engaging in C_4 photosynthesis were rare.

Our report of results for the fraction of expected growth in the final year of life hinted at the seasonal identity of the radiodensity features used to discriminate years, but we return to this question now. We consider the association of abrupt radiodensity drops with periradicular bands and with a shift from thin to thicker second-order dentin increments as sufficient evidence that these features mark an approximate winter-spring boundary. We have considered our isotope results in this light, and this interpretation is

not yet refuted. There is of course room for refinement of this picture, but we will proceed under this model (assignments at top of Figure 2.14).

Season of death determinations were originally undertaken as a first step in evaluating the hypothesis that some entrapment mechanism might have operated at ZR, explaining aspects of the demographic profile. One such mechanism is seismically-induced substrate liquefaction, which has the interesting property of relating site demography and stratigraphy (the sequence of debris flows) to a common cause, acknowledging that entrapment and dispersal of disarticulated remains imply some temporal separation of events. That is, it is clear that final deposition of ZR mastodon remains occurred well after death, so if one event was responsible for death, that same event could not also have figured in final transport and burial of those same remains. We have no prior expectation for how the probability of entrapment by this mechanism might relate to season, and we realize that a similar season of death does not demonstrate simultaneity of death. We nonetheless note that especially in the Main Silt and Main Floor Red Pebble units, a number of deaths occurred near the end of an annual CT increment. Perhaps this is only a reflection of higher probability of death from various causes at this time of year (Fisher, 1987), but it invites further reflection.

A better check on simultaneity of death would be serial isotope records of multiple individuals that show, or fail to show, the degree of correspondence expected

for individuals that occupied the same landscape and whose last years of life were *the same years.* Figure 2.15 shows three such series from mandibular tusks (45.015, 48.530, 56.015) from the Main Silt and adjacent Main Floor Red Pebble layer. Although these units can be distinguished descriptively, it is less clear that they are genetically distinct. These oxygen isotope series overlap for at least the last three years of life and show remarkable consistency in overall pattern, peak values, low values, and multi-year trends. Resolving this issue is not currently our highest priority, but there are intriguing patterns that might yield to further analysis.

Whatever modes of death and postmortem transport and modification are represented at Ziegler Reservoir, the mastodon mandibular tusks preserved there are valuable archives of environmental data. They span five stratigraphic units that have been dated roughly 138ka to 113ka based on OSL (optically stimulated luminescence) dates on correlated sediments in lake-center deposits (Mahan et al., 2014) and the local glacial record (Pigati et al., 2014). This places these strata within MIS 5e and d, an interglacial warm period following Bull Lake alpine glaciation. Over this interval, we see a slight rise (~2 ‰) in average $\delta^{18}O$ values (Figure 2.15A). Other things being equal, this could imply a mean annual temperature increase of 3-4ºC (Dansgaard, 1964; Rozanski et al., 1993; Kohn and Welker, 2005). However, changes in precipitation and/or vapor source regions could also account for some of this difference (Koch, 1998).

Values for mean sensitivity calculated from tusk growth series change little over the MIS 5e–d interval, and are so low overall that we doubt these mastodons were seriously stressed by interannual environmental variations. To our knowledge, mean sensitivity has not been calculated for other mammalian accretionary growth structures, so the published values with which we can make comparisons are limited. For tree-ring data, there is a conventional threshold (0.30) for distinguishing "complacent" and "sensitive" responses (Creber, 1977). Black (2009) reported mean sensitivities of 0.15 to 0.20 for fish otolith growth series and 0.22 to 0.29 for growth series from geoduck valves that appeared responsive to environmental variations. Additionally, Butler et al. (2013) gave a value of 0.499 for shell growth series of *Arctica islandica*, a relatively sensitive bivalve species often used for marine climate reconstructions. The average for all adult ZR tusk series (0.08) is low in comparison to values from growth structures in these ectotherms, but it is also lower than values we calculated for two mastodon premaxillary tusks from late Pleistocene sites in New York (Fisher, 2008; Fisher et al., 2008; Table 2.1). That ZR mastodons were not facing significant stress is further supported by the relatively low $\delta^{15}N$ values we measured. Higher in the section, mastodons are replaced by mammoths, implying that the change to MIS 4 eventually elicited a range shift, requiring us to pick up the mastodon story at some other site. We originally hoped to be able to track more of the history of environmental change at this one site, and we

have a few options (including specimens in the Beach Silt, not represented by mandibular tusks) for extending our analyses both up- and down-section, but a longer-term perspective may require broader geographic as well as stratigraphic integration.

Conclusions

The Ziegler Reservoir fossil site is noteworthy in producing a large number of well-preserved mandibular tusks of late Pleistocene mastodons. This study represents a first attempt to use American mastodon mandibular tusks to assess individual life histories and environmental change at a single site. Given the time range sampled, this site provides more than the usual "snapshot" of an ancient ecosystem, but we still only get a series of snapshots, or a short "video clip," of the response to longer-term patterns of climate change. The most promising results are that mandibular tusks offer a compact record extending sometimes through decades of life, and microCT analyses represent an effective means of gathering data on tusk growth rates that should act as sensitive indicators of environmental conditions. Mastodons inhabiting alpine regions of central Colorado 140–110ka appear to have thrived within a highly seasonal interglacial environment. Some of our methods for studying their paleobiology may translate effectively to studies of mastodon response to even later changes in the Pleistocene, closer to the time of their extinction.

Table 2.1. Increment measurements from CT scans of Ziegler Reservoir proboscidean dentition.

Increment – numbered from earliest growth (distal) to latest growth (proximal); final increments marked "P. C." represent the pulp cavity surface.

L – increment length measured half-way between axis and CDJ.

r_{maj} – half the major diameter (usually dorsoventral) of the tusk at location of increment length measurement.

r_{min} – half the minor diameter (usually mediolateral) of the tusk at location of increment length measurement.

EIV – estimated increment volume calculated from $EIV = L * r_{maj} * r_{min} * \pi$

MS – mean sensitivity calculated from detrended sequence of thicknesses for complete increments (final increment is assumed to be incomplete and is excluded from mean sensitivity calculation).

FFY (1-3) – fraction of final year - the final increment (EIV where available, otherwise thickness) expressed as a percentage of annual increment volume expected for a complete year (1 – measurement of last complete increment; 2 – average of last 2 complete measurements; 3 – projected measurement based on a linear trend of logged values for the last 5 complete years).

Measurements in parentheses are estimates of internal features based on exterior measurements except where otherwise noted.

Specimen		Increment	Measurements				
Field ID	DMNS #	numbered toward pulp cavity (marked P. C. where preserved)	L (mm)	r_{maj} (mm)	r_{min} (mm)	EIV (cm^3)	Thickness (cm)
30.017	-	1	4.9	18.6	*(18.6)*	5.34	4.53
		2	4.7	18.6	*(18.6)*	5.11	4.41
		3	4.8	18.7	*(18.7)*	5.28	4.88
		4	4.7	19.0	*(19.0)*	5.36	4.41
		5	5.5	19.3	*(19.3)*	6.36	4.46
		6	5.0	19.4	*(19.4)*	5.91	4.24
		7	4.8	19.5	*(19.5)*	5.75	4.61
		8	4.9	19.6	*(19.6)*	5.91	4.49
		9	4.8	18.9	*(18.9)*	5.37	5.74
		10	4.8	18.2	*(18.2)*	4.95	4.66
		11	7.0	18.6	*(17.9)*	7.30	4.41
		12	7.1	19.1	*(18.3)*	7.84	3.55
		13	5.9	20.3	*(19.8)*	7.49	3.77
		14	7.5	21.0	*(20.5)*	10.14	3.85
		15	7.0	21.6	*(20.7)*	9.83	3.68
		16	7.7	21.8	*(20.9)*	11.03	4.39
		17 (P. C.)	3.5	21.8	*(21.1)*	5.09	1.99

Average	6.81	4.38
Std Dev	1.96	0.52

17 (P. C.) not included

MS	0.09
FFY 1	46%
FFY 2	49%
FFY 3	42%

Table 2.1 (cont.)

Specimen		Increment	Measurements				
Field ID	DMNS #	numbered toward pulp cavity (marked P. C. where preserved)	L (mm)	r_{maj} (mm)	r_{min} (mm)	EIV (cm^3)	Thickness (cm)
30.076	-	1	11.5	17.5	*(16.1)*	10.72	4.14
		2	12.1	17.7	*(16.2)*	11.60	4.04
		3	12.0	17.5	*(16.1)*	11.23	4.07
		4	10.6	17.2	*(16.5)*	10.33	3.70
		5	10.1	17.1	*(16.4)*	9.68	3.73
		6	9.8	16.9	*(16.2)*	9.45	3.59
		7	10.0	16.7	*(16.0)*	9.40	3.58
		8	10.5	16.5	*(16.9)*	10.59	3.88
		9	10.7	16.1	*(16.5)*	10.45	3.86
		10	10.5	15.9	*(16.3)*	9.90	3.73
		11	9.3	15.7	*(16.0)*	8.65	3.62
		12	9.2	15.4	*(14.9)*	8.13	3.65
		13	8.2	15.3	*(14.8)*	7.10	3.30
		14	8.8	15.0	*(14.5)*	7.31	3.55
		15	8.6	14.8	*(14.3)*	6.80	3.42
		16	8.1	14.7	*(13.9)*	6.11	3.28
		17	8.7	14.3	*(13.5)*	6.45	3.58
		18	7.4	14.1	*(13.3)*	5.29	3.18
		19	7.3	13.6	*(12.9)*	4.96	3.27
		20 (P. C.)	7.2	13.4	*(12.3)*	4.61	3.00

Average	8.64	3.64
Std Dev	2.07	0.28

20 (P. C.) not included

MS	0.04
FFY 1	93%
FFY 2	90%
FFY 3	99%

Table 2.1 (cont.)

Specimen		Increment	Measurements				
Field ID	DMNS #	numbered toward pulp cavity (marked P. C. where preserved)	L (mm)	r_{maj} (mm)	r_{min} (mm)	EIV (cm^3)	Thickness (cm)
30.130	-	1	8.1	20.4	*(15.9)*	8.23	3.81
		2	8.7	20.3	*(15.9)*	8.82	4.22
		3	8.7	20.1	*(15.9)*	8.72	4.35
		4	7.6	19.9	*(15.7)*	7.47	3.90
		5	8.5	19.7	*(15.4)*	8.08	4.53
		6	7.0	19.2	*(15.1)*	6.37	3.97
		7	7.2	19.1	*(15.5)*	6.70	4.10
		8 (P. C.)	6.2	19.1	*(15.5)*	5.73	3.46

Average	7.77	4.12
Std Dev	0.96	0.26

8 (P. C.) not included

MS	0.09
FFY 1	86%
FFY 2	88%
FFY 3	95%

Table 2.1 (cont.)

Specimen		Increment	Measurements				
Field ID	DMNS #	numbered toward pulp cavity (marked P. C. where preserved)	L (mm)	r_{maj} (mm)	r_{min} (mm)	EIV (cm^3)	Thickness (cm)
33.238	-	1	6.8	19.3	*(14.8)*	6.12	4.34
		2	6.4	19.5	*(14.9)*	5.88	3.92
		3	6.9	19.8	*(15.3)*	6.51	3.87
		4	7.5	20.2	*(15.6)*	7.48	3.85
		5	6.5	20	*(15.5)*	6.28	3.42
		6	6.1	20	*(15.2)*	5.87	3.37
		7	5	19.8	*(15.0)*	4.71	3.23
		8	6.4	19.7	*(14.9)*	5.90	4.03
		9	4.9	19.7	*(15.3)*	4.60	3.21
		10	4.8	20	*(15.5)*	4.72	3.48
		11	5.3	19.2	*(15.0)*	4.78	4.01
		12	4.6	18.8	*(13.9)*	3.77	3.54
		13	5.1	18.9	*(14.0)*	4.27	3.97
		14 (P. C.)	3.3	19.9	*(14.7)*	2.99	2.31

Average	5.45	3.71
Std Dev	1.06	0.35

14 (P. C.) not included

MS	0.10
FFY 1	70%
FFY 2	74%
FFY 3	76%

Table 2.1 (cont.)

Specimen		Increment	Measurements				
Field ID	DMNS #	numbered toward pulp cavity (marked P. C. where preserved)	L (mm)	r_{maj} (mm)	r_{min} (mm)	EIV (cm^3)	Thickness (cm)
44.035	-	1	9.9	*(19.2)*	*(16.6)*	9.89	3.52
		2	10.7	*(18.2)*	*(15.8)*	9.69	3.58
		3	10.6	*(18.2)*	*(15.7)*	9.50	3.99
		4	9.8	17.7	15.4	8.41	3.79
		5	9.2	18.0	15.1	7.90	4.03
		6	10.6	17.7	15.0	8.83	4.04
		7	9.2	17.2	14.1	7.05	3.85
		8	7.7	16.5	13.5	5.36	3.25
		9	8.4	16.6	13.0	5.70	3.32
		10	9.8	16.6	12.9	6.59	3.47
		11	9.9	16.5	12.5	6.41	3.34
		12	9.4	16.5	12.2	5.96	3.36
		13	9.8	15.9	12.3	6.06	3.16
		14	7.7	15.5	12.0	4.51	2.87
		15	9.1	15.4	11.9	5.25	3.04
		16	10.0	15.0	11.2	5.31	2.83
		17	10.1	14.6	10.8	4.98	3.09
		18	10.0	14.5	10.7	4.90	2.75
		19	8.6	14.5	10.2	4.01	2.63
		20	9.7	14.2	10.1	4.37	2.54
		21	7.0	14.7	9.8	3.14	2.31
		22	8.6	14.3	9.4	3.60	2.68
		23	7.5	14.3	9.0	3.05	2.17
		24	8.5	14.7	8.3	3.28	2.48
		25	8.3	14.7	7.6	2.92	2.42
		26	*(8.3)*	-	-	-	-
		27	*(7.9)*	-	-	-	-
		28 (P. C.)	*(4.9)*	-	-	-	-

Average	5.87	3.14
Std Dev	2.16	0.56

Table 2.1 (cont.)

[44.035 cont.]

MS	0.07
FFY 1*	62%
FFY 2*	61%
FFY 3*	62%

*based on lengths

Specimen		Increment	Measurements				
Field ID	DMNS #	numbered toward pulp cavity (marked P. C. where preserved)	L (mm)	r_{maj} (mm)	r_{min} (mm)	EIV (cm^3)	Thickness (cm)
45.015	-	1	11.3	22.5	*(21.8)*	17.42	3.58
		2	12.2	22.4	*(21.7)*	18.73	3.70
		3	12.0	22.7	*(23.2)*	19.81	3.58
		4	13.7	22.8	*(23.2)*	22.71	4.40
		5	11.4	22.7	*(23.1)*	18.72	3.84
		6	10.1	22.4	*(24.1)*	17.07	3.57
		7	12.6	22.2	*(23.9)*	20.90	4.27
		8	10.1	22.0	*(23.6)*	16.37	3.65
		9	9.3	21.9	*(24.8)*	15.80	3.60
		10	10.4	21.5	*(24.3)*	17.12	4.25
		11 (P. C.)	9.0	21.6	*(24.4)*	14.91	3.56

Average	18.47	3.84
Std Dev	2.17	0.33

11 (P. C.) not included

MS	0.11
FFY 1	87%
FFY 2	91%
FFY 3	93%

Table 2.1 (cont.)

Specimen		Increment	Measurements				
Field ID	DMNS #	numbered toward pulp cavity (marked P. C. where preserved)	L (mm)	r_{maj} (mm)	r_{min} (mm)	EIV (cm^3)	Thickness (cm)
48.530	-	1	13.4	19.6	*(18.2)*	14.96	4.22
		2	11.8	20.1	*(18.7)*	13.93	3.83
		3	15.5	20.8	*(19.4)*	19.58	4.44
		4	12.7	21.3	*(20.4)*	17.26	4.13
		5	15.4	22.3	*(21.3)*	22.99	4.44
		6	12.9	23.0	*(22.0)*	20.52	4.01
		7	12.9	23.4	*(21.8)*	20.58	4.38
		8	14.2	23.8	*(22.2)*	23.47	4.06
		9	12.5	24.0	*(22.4)*	21.03	4.16
		10	11.6	24.4	*(23.0)*	20.33	3.89
		11	11.4	24.3	*(22.9)*	19.92	3.90
		12	13.3	23.9	*(22.5)*	22.34	3.98
		13	11.7	23.7	*(22.8)*	19.77	4.21
		14	9.6	23.3	*(22.4)*	15.82	3.75
		15	9.2	23.3	*(22.5)*	15.14	3.68
		16	11.1	23.1	*(22.4)*	18.04	4.53
		17	8.5	22.9	*(22.2)*	13.51	3.95
		18 (P. C.)	8.5	22.4	*(21.7)*	12.99	3.84

Average	18.78	4.09
Std Dev	3.16	0.25

18 (P. C.) not included

MS	0.08
FFY 1	96%
FFY 2	82%
FFY 3	96%

Table 2.1 (cont.)

Specimen		Increment	Measurements				
Field ID	DMNS #	numbered toward pulp cavity (marked P. C. where preserved)	L (mm)	r_{maj} (mm)	r_{min} (mm)	EIV (cm^3)	Thickness (cm)
48.594	-	1	13.0	18.8	*(15.0)*	11.51	*(3.7)*
		2	10.0	19.4	15.5	9.43	*(3.3)*
		3	12.6	19.7	15.5	12.10	*(4.2)*
		4	14.7	19.8	16.4	14.91	4.25
		5	11.8	20.7	16.5	12.63	3.59
		6	13.8	21.2	17.5	16.13	4.21
		7	11.9	22.0	17.8	14.63	3.59
		8	12.2	22.4	18.2	15.64	4.03
		9	12.1	22.7	18.7	16.05	3.87
		10	11.7	23.1	19.1	16.25	3.96
		11	11.322	23.5	19.5	16.33	3.96
		12	10.127	23.7	19.9	15.02	3.55
		13	12.926	23.8	20.5	19.85	4.53
		14 (P. C.)	10.819	24.3	21.1	17.39	3.90

Average	14.65	3.91
Std Dev	2.67	0.35

14 (P. C.) not included

MS	0.11
FFY 1	88%
FFY 2	100%
FFY 3	94%

Table 2.1 (cont.)

Specimen		Increment	Measurements				
Field ID	DMNS #	numbered toward pulp cavity (marked P. C. where preserved)	L (mm)	r_{maj} (mm)	r_{min} (mm)	EIV (cm^3)	Thickness (cm)
48.595	-	1	13.6	14.8	12.7	8.05	3.65
		2	13.4	14.9	13.4	8.46	3.53
		3	12.3	15.5	13.7	8.18	3.28
		4	13.3	16.4	14.0	9.61	3.63
		5	10.2	17.3	14.6	8.11	3.24
		6	10.8	17.9	15.0	9.13	3.30
		7	12.5	18.4	15.9	11.54	3.88
		8	12.8	19.3	16.7	12.95	3.76
		9	11.8	20.0	17.0	12.54	3.63
		10	11.7	20.5	17.5	13.13	3.76

Average	10.17	3.57
Std Dev	2.13	0.22

MS	0.07
FFY 1	-
FFY 2	-
FFY 3	-

Table 2.1 (cont.)

Specimen		Increment	Measurements				
Field ID	DMNS #	numbered toward pulp cavity (marked P. C. where preserved)	L (mm)	r_{maj} (mm)	r_{min} (mm)	EIV (cm^3)	Thickness (cm)
56.015	-	1	4.3	15.4	*(11.5)*	2.39	3.29
		2	5.6	15.6	*(11.7)*	3.19	4.37
		3	5.9	16.0	*(11.9)*	3.54	4.53
		4	5.8	16.0	*(12.0)*	3.47	4.41
		5	6.0	16.6	*(12.4)*	3.88	4.43
		6	6.5	16.9	*(12.6)*	4.38	4.52
		7	7.1	17.3	*(13.0)*	5.02	4.76
		8	5.6	17.3	*(13.0)*	3.94	3.89
		9	5.7	17.6	*(13.2)*	4.18	3.63
		10	7.0	17.5	*(13.2)*	5.07	3.98
		11	6.7	17.4	*(13.1)*	4.80	3.93
		12	7.2	17.6	*(13.2)*	5.24	4.32
		13	7.1	17.4	*(13.6)*	5.30	4.38
		14	6.2	17.2	*(13.5)*	4.51	4.04
		15	6.2	16.8	*(13.2)*	4.29	3.90
		16	6.5	16.7	*(13.1)*	4.47	3.80
		17	6.0	16.8	*(13.2)*	4.19	3.33
		18	6.7	16.9	*(13.3)*	4.69	3.66
		19	7.4	16.9	*(13.3)*	5.21	4.02
		20	6.8	16.9	*(13.2)*	4.76	4.05
		21	6.3	17.0	*(13.3)*	4.48	3.78
		22	7.4	16.9	*(13.2)*	5.15	4.32
		23	5.7	16.9	*(13.3)*	4.02	3.78
		24	5.4	16.8	*(13.1)*	3.76	3.62
		25	5.4	16.6	*(13.8)*	3.86	3.74
		26	5.2	16.6	*(13.8)*	3.74	3.78
		27	5.7	16.3	*(13.6)*	3.98	3.84
		28	5.1	16.0	*(13.3)*	3.39	3.48
		29 (P. C.)	5.7	15.8	*(13.2)*	3.70	3.92

Average	4.25	3.98
Std Dev	0.71	0.38

29 (P. C.) not included

Table 2.1 (cont.)

[56.015 cont.]

MS	0.07
FFY 1	109%
FFY 2	101%
FFY 3	104%

Specimen		Increment	Measurements				
Field ID	DMNS #	numbered toward pulp cavity (marked P. C. where preserved)	L (mm)	r_{maj} (mm)	r_{min} (mm)	EIV (cm^3)	Thickness (cm)
56.127	-	1	-	-	-	-	2.81
		2	29.8	8.5	*(7.6)*	6.03	6.14
		3	21.0	9.3	*(7.8)*	4.75	5.70
		4	17.8	10.4	*(9.2)*	5.35	4.88
		5 (P. C.)	12.7	10.4	*(8.9)*	3.68	3.63

Average	5.37	5.57
Std Dev	0.64	0.64

5 (P. C.) not included

MS	0.36
FFY 1	69%
FFY 2	73%
FFY 3	77%

Table 2.1 (cont.)

Specimen		Increment	Measurements				
Field ID	DMNS #	numbered toward pulp cavity (marked P. C. where preserved)	L (mm)	r_{maj} (mm)	r_{min} (mm)	EIV (cm^3)	Thickness (cm)
56.266	-	1	-	15.0	-	-	5.97
		2	-	17.1	-	-	5.29
		3 (P. C.)	-	17.3	-	-	0.87

Average	-	5.63
Std Dev	-	0.48

3 (P. C.) not included

MS	-
FFY 1	16%
FFY 2	15%
FFY 3	-

Table 2.1 (cont.)

Specimen		Increment	Measurements				
Field ID	DMNS #	numbered toward pulp cavity (marked P. C. where preserved)	L (mm)	r_{maj} (mm)	r_{min} (mm)	EIV (cm^3)	Thickness (cm)
58.025	-	1	13.4	18.6	*(16.2)*	12.69	4.55
		2	13.5	19.3	*(16.9)*	13.80	4.64
		3	11.8	19.8	*(16.9)*	12.42	4.15
		4	13.4	20.4	*(17.4)*	14.92	4.85
		5	10.0	20.9	*(17.8)*	11.73	3.86
		6	11.7	21.4	*(19.3)*	15.19	4.40
		7	9.7	22.0	*(19.8)*	13.16	4.05
		8	10.6	22.2	*(20.0)*	14.79	4.42
		9	11.4	22.5	*(20.5)*	16.53	4.69
		10	10.3	22.7	*(20.7)*	15.19	4.59
		11	10.9	22.8	*(20.8)*	16.15	4.83
		12	10.9	23.1	*(21.8)*	17.24	4.01
		13	9.9	23.2	*(21.9)*	15.80	4.76
		14	8.5	23.4	*(22.1)*	13.84	4.25
		15	8.6	23.3	*(22.7)*	14.30	3.82
		16	9.0	23.3	*(22.7)*	14.91	4.69
		17	9.4	23.4	*(22.8)*	15.73	4.31
		18	8.4	23.3	*(22.8)*	13.98	4.20
		19	8.4	23.3	*(22.8)*	14.02	4.24
		20	9.5	23.3	*(22.8)*	15.88	4.56
		21	8.8	23.1	*(22.6)*	14.41	4.29
		22	7.9	23.0	*(22.5)*	12.80	4.22
		23 (P. C.)	8.8	22.9	*(22.3)*	14.16	4.52

Average	14.52	4.38
Std Dev	1.42	0.30

23 (P. C.) not included

MS	0.09
FFY 1	111%
FFY 2	104%
FFY 3	104%

Table 2.1 (cont.)

Specimen		Increment	Measurements				
Field ID	DMNS #	numbered toward pulp cavity (marked P. C. where preserved)	L (mm)	r_{maj} (mm)	r_{min} (mm)	EIV (cm^3)	Thickness (cm)
58.032	-	1	-	-	-	-	3.97
		2	-	-	-	-	4.24
		3	14.4	19.3	18.0	15.73	4.22
		4	12.9	19.6	18.0	14.29	4.50
		5	13.6	19.9	17.9	15.16	3.91
		6	11.3	20.2	18.2	13.06	3.85
		7	10.7	20.9	18.7	13.11	4.18
		8	11.7	21.0	18.9	14.60	4.54
		9	11.8	21.8	19.2	15.50	4.34
		10	11.1	22.2	19.9	15.35	4.30
		11	10.5	22.5	20.5	15.19	4.62
		12	11.0	22.9	20.8	16.39	4.83
		13	10.9	23.2	21.5	17.11	4.67
		14	10.1	23.6	22.1	16.48	5.18

Average	15.16	4.38
Std Dev	1.25	0.37

MS	0.06
FFY 1	-
FFY 2	-
FFY 3	-

Table 2.1 (cont.)

Specimen		Increment	Measurements				
Field ID	DMNS #	numbered toward pulp cavity (marked P. C. where preserved)	L (mm)	r_{maj} (mm)	r_{min} (mm)	EIV (cm^3)	Thickness (cm)
58.360	-	1	14.7	*(13.2)*	*(12.2)*	7.46	4.17
		2	15.2	*(14.1)*	*(13.1)*	8.81	5.02
		3	12.4	*(15.4)*	*(13.8)*	8.30	4.39
		4	13.8	*(16.4)*	*(14.6)*	10.36	4.55
		5	13.4	*(17.4)*	*(15.8)*	11.53	4.47
		6	14.0	*(17.8)*	*(16.3)*	12.75	4.24
		7	13.7	*(18.5)*	*(16.9)*	13.45	4.29
		8	14.3	*(19.3)*	*(17.8)*	15.38	4.45
		9	13.3	*(20.2)*	*(18.5)*	15.60	4.32
		10	13.3	*(20.5)*	*(19.0)*	16.23	4.35
		11	12.2	*(21.0)*	*(19.6)*	15.65	4.13
		12	12.6	*(21.3)*	*(19.8)*	16.74	4.37
		13	11.8	*(21.6)*	*(20.2)*	16.09	4.05
		14 (P. C.)	10.8	*(21.5)*	*(20.0)*	14.59	4.24

Average	12.95	4.37
Std Dev	3.33	0.24

14 (P. C.) not included

MS	0.05
FFY 1	91%
FFY 2	89%
FFY 3	88%

Table 2.1 (cont.)

Specimen		Increment	Measurements				
Field ID	DMNS #	numbered toward pulp cavity (marked P. C. where preserved)	L (mm)	r_{maj} (mm)	r_{min} (mm)	EIV (cm^3)	Thickness (cm)
60.057	-	1	6.8	19.0	*(15.2)*	6.17	4.28
		2	6.8	19.4	*(15.5)*	6.39	4.14
		3	6.6	19.5	*(15.0)*	6.08	4.10
		4	6.5	19.8	*(15.2)*	6.11	3.75
		5	6.6	19.7	*(14.7)*	5.97	4.05
		6	6.5	19.7	*(14.7)*	5.89	4.08
		7	6.3	19.8	*(14.9)*	5.86	4.07
		8	6.5	20.0	*(14.6)*	5.94	4.31
		9	5.5	20.3	*(14.8)*	5.17	3.82
		10 (P. C.)	3.9	20.2	*(14.7)*	3.60	2.62

Average	5.95	4.07
Std Dev	0.34	0.18

10 (P. C.) not included

MS	0.05
FFY 1	70%
FFY 2	65%
FFY 3	68%

Table 2.1 (cont.)

[60.057 cont.]

	Volumes measured directly from CT (cm^3)
3	6.16
4	5.49
5	5.98
6	5.60
7	5.29
8	5.58
9	5.11
10 (P. C.)	3.22

Average	5.60
Std Dev	0.37

10 (P. C.) not included

MS	-
FFY 1	63%
FFY 2	60%
FFY 3	64%

Table 2.1 (cont.)

Specimen		Increment	Measurements				
Field ID	DMNS #	numbered toward pulp cavity (marked P. C. where preserved)	L (mm)	r_{maj} (mm)	r_{min} (mm)	EIV (cm^3)	Thickness (cm)
63.125	-	1	*(10.9)*	*(16.1)*	*(14.1)*	7.75	-
		2	*(8.2)*	*(16.6)*	*(14.8)*	6.27	-
		3	*(5.4)*	*(16.0)*	*(14.0)*	3.77	-
		4	*(6.3)*	*(15.7)*	*(13.8)*	4.25	-
		5	*(6.3)*	*(15.7)*	*(14.4)*	4.42	-
		6	*(6.1)*	*(15.8)*	*(14.5)*	4.38	-
		7	*(9.7)*	*(16.0)*	*(14.8)*	7.20	-
		8	*(9.7)*	*(16.0)*	*(15.5)*	7.58	-
		9	*(7.8)*	*(15.4)*	*(14.9)*	5.58	-
		10	*(7.2)*	*(15.1)*	*(15.5)*	5.29	-
		11	*(6.2)*	*(15.1)*	*(15.6)*	4.59	-
		12	*(5.0)*	*(15.1)*	*(15.2)*	3.58	-
		13 (P. C.)	*(4.6)*	*(15.0)*	*(15.6)*	3.36	-

Features not clear

Average	5.39	-
Std Dev	1.49	-

13 (P. C.) not included

MS	-
FFY 1	94%
FFY 2	82%
FFY 3	108%

Table 2.1 (cont.)

Specimen		Increment	Measurements				
Field ID	DMNS #	numbered toward pulp cavity (marked P. C. where preserved)	L (mm)	r_{maj} (mm)	r_{min} (mm)	EIV (cm^3)	Thickness (cm)
63.170	-	1	15.2	18.6	15.7	13.86	3.90
		2	13.1	18.8	15.9	12.34	3.63
		3	14.2	19.1	16.2	13.78	4.31
		4	15.7	19.5	16.7	16.10	5.48
		5	13.1	19.9	17.2	14.10	5.21
		6	13.9	20.8	17.7	16.07	5.94

Average	14.37	4.74
Std Dev	1.46	0.93

MS	0.12
FFY 1	-
FFY 2	-
FFY 3	-

Table 2.1 (cont.)

Specimen		Increment	Measurements				
Field ID	DMNS #	numbered toward pulp cavity (marked P. C. where preserved)	L (mm)	r_{maj} (mm)	r_{min} (mm)	EIV (cm^3)	Thickness (cm)
64.013	-	1	15.4	20.5	*(17.6)*	17.36	4.24
		2	15.7	20.8	*(17.9)*	18.38	4.72
		3	12.3	21.7	18.6	15.53	4.61
		4	13.5	22.0	19.1	17.89	5.14
		5	12.2	22.6	19.3	16.80	4.46
		6	11.4	22.8	19.8	16.12	4.30
		7	11.0	23.3	20.0	16.09	4.11
		8	12.3	23.5	20.5	18.60	4.30
		9	12.5	24.0	20.6	19.39	4.16
		10	12.3	24.4	21.0	19.74	4.91

Average	17.59	4.49
Std Dev	1.45	0.34

MS	0.08
FFY 1	-
FFY 2	-
FFY 3	-

Table 2.1 (cont.)

Specimen		Increment	Measurements				
Field ID	DMNS #	numbered toward pulp cavity (marked P. C. where preserved)	L (mm)	r_{maj} (mm)	r_{min} (mm)	EIV (cm^3)	Thickness (*)
70.018	-	1	-	-	-	-	82
		2	-	-	-	-	82
		3	-	-	-	-	87
		4	-	-	-	-	95
		5	-	-	-	-	90
		6 (P. C.)	-	-	-	-	28

* pixels - unscaled

Average	-	87.10
Std Dev	-	5.38

6 (P. C.) not included

MS	0.05
FFY 1	31%
FFY 2	30%
FFY 3	29%

Table 2.1 (cont.)

Specimen		Increment	Measurements				
Field ID	DMNS #	numbered toward pulp cavity (marked P. C. where preserved)	L (mm)	r_{maj} (mm)	r_{min} (mm)	EIV (cm^3)	Thickness (cm)
76.064	-	1	14.3	18.3	14.5	11.87	4.87
		2	13.1	18.9	15.5	12.05	4.46
		3	13.2	19.5	16.0	12.90	4.44
		4	11.6	20.0	16.6	12.05	3.97
		5	12.1	20.6	17.5	13.73	4.25
		6	13.4	20.8	18.0	15.73	4.78
		7	12.2	21.1	18.4	14.82	4.61
		8	11.7	21.6	19.0	15.12	4.44
		9	12.8	21.7	19.2	16.68	4.26
		10	14.6	21.9	19.6	19.63	4.67
		11	14.8	21.9	19.6	19.86	4.24
		12	16.6	22.2	19.3	22.18	4.42

Average	15.55	4.45
Std Dev	3.43	0.25

MS	0.07
FFY 1	-
FFY 2	-
FFY 3	-

Table 2.1 (cont.)

Specimen		Increment	Measurements				
Field ID	DMNS #	numbered toward pulp cavity (marked P. C. where preserved)	L (mm)	r_{maj} (mm)	r_{min} (mm)	EIV (cm^3)	Thickness (cm)
76.085	-	1	33.9	7.7	*(6.9)*	5.60	4.91
		2	18.8	8.4	*(8.1)*	4.00	4.32
		3	20.7	9.2	*(8.8)*	5.25	4.58
		4	22.8	9.7	*(9.4)*	6.51	4.35
		5	18.4	10.3	*(10.4)*	6.17	4.14
		6	18.4	10.8	*(10.9)*	6.82	4.07
		7 (P. C.)	8.9	11.5	*(11.9)*	3.82	2.89

Average	5.73	4.40
Std Dev	1.02	0.31

7 (P. C.) not included

MS	0.05
FFY 1	56%
FFY 2	59%
FFY 3	47%

	Volumes measured directly from CT (cm^3)
2	4.25
3	5.44
4	6.07
5	5.58
6	5.14
7 (P. C.)	3.04

Average	5.30
Std Dev	0.67

7 (P. C.) not included

Table 2.1 (cont.)

[76.085 cont.]

MS	-
FFY 1	59%
FFY 2	57%
FFY 3	51%

Specimen		Increment	Measurements				
Field ID	DMNS #	numbered toward pulp cavity (marked P. C. where preserved)	L (mm)	r_{maj} (mm)	r_{min} (mm)	EIV (cm^3)	Thickness (cm)
82.179	-	1	13.2	13.6	13.4	7.74	4.32
		2	15.3	14.2	13.7	9.42	4.24
		3	14.1	14.7	14.2	9.35	4.06
		4	13.7	15.3	14.9	10.03	4.20
		5	12.8	15.8	15.4	10.01	3.95
		6	14.0	16.5	16.0	11.70	4.39
		7	13.4	17.2	16.5	12.07	4.23
		8	14.6	17.6	17.3	14.11	4.50
		9	13.1	18.0	17.6	13.26	4.31
		10	12.8	18.6	18.5	13.88	4.34
		11	12.2	19.0	18.9	13.87	4.33
		12	11.6	19.5	19.5	13.92	4.37
		13	11.5	19.7	19.9	14.14	4.47
		14 (P. C.)	11.5	19.9	20.3	14.54	4.53

Average	11.81	4.29
Std Dev	2.25	0.15

14 (P. C.) not included

MS	0.04
FFY 1	103%
FFY 2	104%
FFY 3	101%

Table 2.1 (cont.)

Specimen		Increment	Measurements				
Field ID	DMNS #	numbered toward pulp cavity (marked P. C. where preserved)	L (mm)	r_{maj} (mm)	r_{min} (mm)	EIV (cm^3)	Thickness (*)
Loc. 8	-	1	-	-	-	-	160
		2	-	-	-	-	166
		3	-	-	-	-	169
		4 (P. C.)	-	-	-	-	27

* pixels - unscaled

Average	-	165.08
Std Dev	-	4.61

4 (P. C.) not included

MS	-
FFY 1	16%
FFY 2	16%
FFY 3*	15%

* based on 3 years

Table 2.1 (cont.)

Specimen		Increment	Measurements				
Field ID	DMNS #	numbered toward pulp cavity (marked P. C. where preserved)	L (mm)	r_{maj} (mm)	r_{min} (mm)	EIV (cm^3)	Thickness (*)
"Clay"	60704	1	-	-	-	-	63
		2	-	-	-	-	62
		3 (P. C.)	-	-	-	-	36

* pixels - unscaled

Average	-	62.22
Std Dev	-	0.79

3 (P. C.) not included

MS	-
FFY 1	58%
FFY 2	58%
FFY 3	-

Hyde Park mastodon	
Increment	Thickness (cm)
1	2.84
2	2.72
3	3.54
4	3.61
5	3.74
6	4.36
7	4.55
8	4.41
9	4.37
10	4.59
11	4.52
12	2.80
13	4.94
14	5.29
15	4.32

North Java mastodon	
Increment	Thickness (cm)
1	2.83
2	4.21
3	4.31
4	5.32
5	5.66
6	4.16
7	4.14
8	4.55
9	3.71
10	3.76
11	4.12
12	4.92
13	3.81
14	3.75
15	3.83

Table 2.1 (cont.)

Hyde Park mastodon	
16	4.32
17	4.88
18	4.85
19	4.20
20	5.82
21	5.07
22	3.46
23	4.55
24	3.68
25	4.66
26	3.87
27	4.40
28	4.28
29	3.96
30	4.71
31	3.91
32	4.29

Average	4.23
Std Dev	0.70
MS	0.15

North Java mastodon	
16	3.41
17	3.46
18	4.64
19	3.44
20	3.73
21	3.68
22	3.00
23	3.88
24	3.91
25	4.02
26	4.04
27	3.18
28	3.29
29	3.60
30	3.80
31	2.89
32	3.63
33	3.54
34	3.79

Average	3.88
Std Dev	0.62
MS	0.13

Table 2.2. Tooth measurements for Ziegler Reservoir mammoth molars.
The presence of a superscript 'e' identifies and estimated measurement.

Specimen	Tooth	L (cm)	P	Pocc	W (cm)	H (cm)	LF	E (mm)
Clay Mammoth								
60704.008	Rm3	>33.4	16+	9	8.7^{3}	15.9	7.0	2.0
Cody's Mamm.								
Loc. 87-44	Lm3	>29.5	15+	1	9.5^{2}	17.5	6.0	2.2
Snowy								
60676.001	Lm1	16.4	11	11	7.1^{6}	in jaw	7.0	1.5
60676.194	LM1	17.0	11	11	7.8^{5}	in max.	7.0	1.5
60676.007	RM1	16.5	11	11	8.0^{6}	in max.	7.5	2.0
Assoc. molars								
CCN 44	Lm1	12.2^{e}	10	10	6.0^{5}	>7.0	8.5	2.0
CCN 42	Rm2	>16.1	11+	2	6.5^{2}	13.0	9.0	1.5
CCN 43	LM2	>17.8	14+	1	5.1^{3}	14.0	8.5	1.0

Table 2.3. Mastodon tusks from Ziegler Reservoir that were used in this study.

Field #	Sex[1]	Side[2]	Max ext. circ. (mm)[3]	Greatest length (outside curve) (mm)[3]	Medio-lateral diam. (mm)	Dorso-ventral diam. (mm)	Condition of distal end	Condition of pulp cavity	Strat[4]	µCT (# of parts)	Isotope analysis		Thin-section analysis
											Carb	Coll	
Adult mandibular tusks													
30.076	F	R	137	[215]	42	44	missing - unworn break	preserved	PDF (5d)	2	X		
30.130	F	?[5]	?[5]	?[5]	?[5]	?[5]	?[5]	preserved	MS (5d)	1			
33.238	F	?	128	117	35	44	missing - partially worn	preserved	PDF (5d)	1			
44.035	F	L	[115]	242	31	38	worn smooth - intact	preserved	MS (5d)	3			
45.015	M	?	167	[255]	53	52	broken - unworn	preserved	MS (5d)	4	X	X	
48.530	M	R	163	298	51	52	heavily spalled - unworn	preserved	MFRP (5d)	3	X		
48.594	M	L	155	[227]	43	54	unworn break	preserved	MFRP (5d)	3			
48.595	M	R	155	[167]	45	50	worn smooth - fresh spall	missing	MFRP (5d)	2			
56.015	F	R	129	215	34	44	worn smooth	preserved	MS (5d)	3	X		
58.025	M	R	161	282	49	51	worn smooth - intact	preserved	MS (5d)	3			
58.032	M	L	162	185	47	53	worn smooth - intact	missing	MS (5d)	2			
60.057	F	?	117	79	32	41	missing - unworn break	preserved	MF (5d)	1	X		
63.125	F	L	128	[220]	36	44	worn smooth - intact	preserved	MFRP (5d)	3	X		
63.170	M	L	163	[130]	47	58	worn smooth - fresh spall	missing	MFRP (5d)	2			
64.013	M	R	174	[150]	49	60	worn smooth - intact	missing	BS (5e)	2	X		
76.064	M	?	>133*	[165]	39	43	missing	missing	BS (5e)	2			
Subadult permanent mandibular tusk													
30.017	M	L?	139	152	41	46	worn - mostly smooth	preserved	PDF (5d)	2			
58.360	M	L	139	217	43	45	broken - light wear	preserved	BS (5e)	2	X	X	X
82.179	M	R	136	212	41	44	worn - mostly smooth	preserved	MS (5d)	2			
Juvenile permanent mandibular tusks													
56.127	J	R?	69	[117]	20	23	worn smooth - intact	preserved	MS (5d)	1	X		
76.085	J	R?	80	160	25	25	worn smooth - intact	preserved	BS (5e)	2	X		
Deciduous tusks													
17.1	J	L?	50	105	15	17	enamel present - worn tip	closed	PDF (5d)?	1	X		
44.146	J	L?	56	80	14	18	enamel present - worn tip	preserved	MS (5d)	1			
68.032	J	?	55	92	15	18	enamel present - worn tip	preserved	Unit 3 (5e)	1			
68.050	J	R?	64	105	17	20	enamel present - worn tip	preserved	BS (5e)	1	X		
71.092	J	?	60	[90]	18	20	enamel present - worn tip	preserved	MF (5d)	1			
77.099	J	L?	55	125	15	17	enamel present - spalled	closed	BS (5e)	1			
Adult premaxillary tusks													
Loc. 8	M	R	610	1730	210	170	missing	preserved	PDF (5d)	1	X		X
70.018	F	L	[260]	[520]	[82]	84	broken tip - lightly worn	preserved	MFRP (5d)	2	X	X	X
Juvenile permanent premaxillary tusk													
56.266	J	L?	126	247	38	41	worn - mostly smooth	preserved	MFRP (5d)	3	X		

[1] Sex determinations based on estimated increment volumes (Fig. 11); when not available, maximum circumference was used (Fig. 5).

[2] Side determinations based on general morphology and presence of attritional features often found on the medial surface.

[3] Bracketed entries in measurement columns are estimates.

[4] Stratigraphy refers to lithologic units described in Pigati et al. (in this volume) for lake-margin deposits: Unit 3; BS, Basement Silt; MF, Main Floor; MFRP, Main Floor Red Pebble; MS, Main Silt; PDF, Primary Debris Flow. Abbreviati
Primary Debris Flow. Abbreviations in parentheses follow biozone designations from Miller et al. (in this volume).

[5] Specimen is on secondary loan.

* 76.064 is the distal tip of a large (likely male) tusk. Near the broken proximal end, its circumference is increasing, so the maximum exterior circumference must be >133 mm.

Table 2.4. Isotope data from Ziegler Reservoir mastodon tusks.

Specimen		Sample	Dentin carbonate		Dentin collagen		
Field ID	DMNS #	numbered toward pulp cavity (marked P. C. where preserved)	$\delta^{18}O$ (VSMOW)	$\delta^{13}C$ (VPDB)	$\delta^{15}N$ (air N_2)	$\delta^{13}C$ (VPDB)	C:N
17.1	60696	1	24.42‰	3.36‰	-	-	-
		2	23.78‰	2.75‰	-	-	-
		3	24.06‰	2.96‰	-	-	-
		4	24.20‰	3.23‰	-	-	-
		5	23.37‰	3.49‰	-	-	-
		6	22.97‰	2.66‰	-	-	-
		7	23.30‰	2.97‰	-	-	-
		8	23.45‰	3.35‰	-	-	-
		9	23.95‰	3.21‰	-	-	-
		10	24.29‰	3.47‰	-	-	-
		11	25.69‰	4.03‰	-	-	-
		12	25.26‰	4.62‰	-	-	-
		13	25.63‰	5.00‰	-	-	-
		14	25.50‰	5.17‰	-	-	-
		Average	24.28‰	3.59‰			
		Std Dev	0.91‰	0.81‰			

Standards (Dentin carbonate)		$\delta^{18}O$ (VPDB)	$\delta^{13}C$ (VPDB)
NBS 19	Average	1.97‰	-2.17‰
Meas. = 5	Std Dev	0.02‰	0.08‰

Table 2.4 (cont.)

Specimen		Sample	Dentin carbonate		Dentin collagen		
Field ID	DMNS #	numbered toward pulp cavity (marked P. C. where preserved)	$\delta^{18}O$ (VSMOW)	$\delta^{13}C$ (VPDB)	$\delta^{15}N$ (air N_2)	$\delta^{13}C$ (VPDB)	C:N
30.017	-	1	20.97‰	0.68‰	-	-	-
		2	21.93‰	1.04‰	-	-	-
		3	21.70‰	0.48‰	-	-	-
		4	20.87‰	0.16‰	-	-	-
		5	24.08‰	0.57‰	-	-	-
		6	23.69‰	0.89‰	-	-	-
		7	22.07‰	0.90‰	-	-	-
		8	21.10‰	0.57‰	-	-	-
		9	21.85‰	1.02‰	-	-	-
		10	21.78‰	1.46‰	-	-	-
		11	23.91‰	2.11‰	-	-	-
		12	24.43‰	2.09‰	-	-	-
		13	24.28‰	2.30‰	-	-	-
		14	23.22‰	2.52‰	-	-	-
		15	22.26‰	2.66‰	-	-	-
		16	22.57‰	2.66‰	-	-	-
		17	22.46‰	2.66‰	-	-	-
		18	24.29‰	3.20‰	-	-	-
		19	24.95‰	4.20‰	-	-	-
		20	25.19‰	4.34‰	-	-	-
		21	25.80‰	4.49‰	-	-	-
		22 (P. C.)	25.69‰	3.57‰	-	-	-
		Average	23.14‰	2.03‰			
		Std Dev	1.56‰	1.35‰			

Standards (Dentin carbonate)		$\delta^{18}O$ (VPDB)	$\delta^{13}C$ (VPDB)
NBS 19	Average	1.98‰	-2.20‰
Meas. = 6	Std Dev	0.06‰	0.04‰

Table 2.4 (cont.)

Specimen		Sample	Dentin carbonate		Dentin collagen		
Field ID	DMNS #	numbered toward pulp cavity (marked P. C. where preserved)	$\delta^{18}O$ (VSMOW)	$\delta^{13}C$ (VPDB)	$\delta^{15}N$ (air N_2)	$\delta^{13}C$ (VPDB)	C:N
30.076	-	1	23.48‰	-0.34‰	-	-	-
		2	-	-	-	-	-
		3	23.82‰	-0.35‰	-	-	-
		4	23.68‰	-0.03‰	-	-	-
		5	24.19‰	-0.54‰	-	-	-
		6	25.28‰	0.01‰	-	-	-
		7	25.03‰	0.35‰	-	-	-
		8	23.94‰	0.75‰	-	-	-
		9	24.02‰	0.53‰	-	-	-
		10	22.61‰	0.04‰	-	-	-
		11	23.88‰	0.59‰	-	-	-
		12	23.99‰	1.01‰	-	-	-
		13	23.63‰	0.33‰	-	-	-
		14	24.08‰	1.45‰	-	-	-
		15	24.09‰	0.81‰	-	-	-
		16	24.14‰	1.41‰	-	-	-
		17	24.32‰	1.35‰	-	-	-
		18	23.35‰	0.96‰	-	-	-
		19	25.34‰	1.50‰	-	-	-
		20	23.02‰	1.60‰	-	-	-
		21	25.33‰	1.97‰	-	-	-
		22 (P. C.)	23.90‰	1.49‰	-	-	-
		Average	24.05‰	0.71‰			
		Std Dev	0.72‰	0.74‰			

Standards (Dentin carbonate)		$\delta^{18}O$ (VPDB)	$\delta^{13}C$ (VPDB)
NBS 19	Average	1.95‰	-2.16‰
Meas. = 5	Std Dev	0.04‰	0.07‰

Table 2.4 (cont.)

Specimen		Sample	Dentin carbonate		Dentin collagen		
Field ID	DMNS #	numbered toward pulp cavity (marked P. C. where preserved)	$\delta^{18}O$ (VSMOW)	$\delta^{13}C$ (VPDB)	$\delta^{15}N$ (air N_2)	$\delta^{13}C$ (VPDB)	C:N
45.015	-	1	22.94‰	-4.27‰	-	-	-
		2	23.07‰	-4.54‰	-	-	-
		3	21.66‰	-3.80‰	-	-	-
		4	~~-0.45‰~~	~~-7.45‰~~	-	-	-
		5	22.10‰	-2.85‰	-	-	-
		6	24.13‰	-3.75‰	5.37‰	-19.48‰	3.42
		7	24.07‰	-2.17‰	4.78‰	-18.88‰	3.27
		8	21.31‰	-3.44‰	3.96‰	-18.75‰	3.28
		9	22.75‰	-1.74‰	3.89‰	-18.82‰	3.25
		10	23.97‰	-2.92‰	5.47‰	-18.71‰	3.26
		11	23.05‰	-1.53‰	4.89‰	-18.55‰	3.32
		12	~~-4.56‰~~	~~-15.13‰~~	3.78‰	-18.28‰	3.34
		13	21.99‰	-1.03‰	3.90‰	-18.13‰	3.32
		14	24.08‰	-1.80‰	4.35‰	-18.45‰	3.32
		15	24.37‰	-0.69‰	5.11‰	-19.17‰	3.28
		16	25.61‰	-1.25‰	5.65‰	-19.21‰	3.29
		17	22.21‰	-0.76‰	4.43‰	-18.92‰	3.29
		18	22.25‰	-1.54‰	4.04‰	-19.20‰	3.31
		19	21.87‰	-0.65‰	4.03‰	-19.22‰	3.40
		20 (P. C.)	24.10‰	-1.85‰	4.30‰	-19.40‰	3.46
		Average	23.09‰	-2.25‰	4.53‰	-18.88‰	3.32
		Std Dev	1.17‰	1.27‰	0.64‰	-0.41‰	0.06

Strikethroughs indicate samples with low CO_2 yield

Standards (Dentin carbonate)		$\delta^{18}O$ (VPDB)	$\delta^{13}C$ (VPDB)
NBS 19	Average	1.96‰	-2.19‰
Meas. = 3	Std Dev	0.01‰	0.04‰

Table 2.4 (cont.)

[45.015 cont.]

Standards (Dentin collagen)		$\delta^{15}N$ (air N_2)	$\delta^{13}C$ (VPDB)
IAEA 600 Caffeine	Average	-	-27.77‰
Measurements = 3	Std Dev	-	0.06‰
IAEA-CH-6 Sucrose	Average	-	-10.45‰
Measurements = 3	Std Dev	-	0.04‰
USGS 25	Average	-30.40‰	-
Measurements = 3	Std Dev	0.12‰	-
IAEA N2	Average	20.30‰	-
Measurements = 3	Std Dev	0.14‰	-

Table 2.4 (cont.)

Specimen		Sample	Dentin carbonate		Dentin collagen		
Field ID	DMNS #	numbered toward pulp cavity (marked P. C. where preserved)	$\delta^{18}O$ (VSMOW)	$\delta^{13}C$ (VPDB)	$\delta^{15}N$ (air N_2)	$\delta^{13}C$ (VPDB)	C:N
48.530	-	1	23.76‰	0.89‰	-	-	-
		2	23.35‰	0.88‰	-	-	-
		3	22.84‰	0.32‰	-	-	-
		4	21.85‰	0.10‰	-	-	-
		5	21.78‰	0.13‰	-	-	-
		6	21.66‰	0.22‰	-	-	-
		7	22.95‰	0.03‰	-	-	-
		8	23.03‰	-0.18‰	-	-	-
		9	23.72‰	0.07‰	-	-	-
		10	22.85‰	0.07‰	-	-	-
		11	22.33‰	-0.21‰	-	-	-
		12	21.53‰	0.17‰	-	-	-
		13	21.83‰	0.23‰	-	-	-
		14	21.45‰	0.59‰	-	-	-
		15	22.89‰	0.27‰	-	-	-
		16	24.29‰	0.28‰	-	-	-
		17	25.10‰	0.42‰	-	-	-
		18	24.91‰	0.29‰	-	-	-
		19	22.56‰	-0.02‰	-	-	-
		20	22.08‰	-0.32‰	-	-	-
		21	22.77‰	-0.23‰	-	-	-
		22	23.21‰	-0.15‰	-	-	-
		23 (P. C.)	24.81‰	-1.28‰	-	-	-
		Average	22.94‰	0.11‰			
		Std Dev	1.09‰	0.44‰			

Samples 1-22 Standards (Dentin carbonate)		$\delta^{18}O$ (VPDB)	$\delta^{13}C$ (VPDB)
NBS 19	Average	1.98‰	-2.17‰
Meas. = 6	Std Dev	0.04‰	0.08‰

Table 2.4 (cont.)

[48.530 cont.]

Samples 17-23 Standards (Dentin carbonate)		$\delta^{18}O$ (VPDB)	$\delta^{13}C$ (VPDB)
NBS 19	Average	1.98‰	-2.19‰
Meas. = 4	Std Dev	0.05‰	0.05‰

Table 2.4 (cont.)

Specimen		Sample	Dentin carbonate		Dentin collagen		
Field ID	DMNS #	numbered toward pulp cavity (marked P. C. where preserved)	$\delta^{18}O$ (VSMOW)	$\delta^{13}C$ (VPDB)	$\delta^{15}N$ (air N_2)	$\delta^{13}C$ (VPDB)	C:N
56.015	-	1	21.54‰	1.30‰	-	-	-
		2	21.12‰	1.14‰	-	-	-
		3	22.48‰	1.24‰	-	-	-
		4	23.65‰	1.40‰	-	-	-
		5	23.75‰	1.22‰	-	-	-
		6	23.28‰	1.16‰	-	-	-
		7	21.74‰	1.48‰	-	-	-
		8	20.95‰	1.12‰	-	-	-
		9	21.17‰	1.18‰	-	-	-
		10	21.27‰	0.94‰	-	-	-
		11	23.50‰	1.03‰	-	-	-
		12	23.92‰	0.98‰	-	-	-
		13	24.10‰	1.17‰	-	-	-
		14	23.79‰	1.35‰	-	-	-
		15	22.69‰	1.48‰	-	-	-
		16	21.40‰	1.42‰	-	-	-
		17	21.27‰	1.21‰	-	-	-
		18	21.32‰	1.40‰	-	-	-
		19	23.37‰	2.17‰	-	-	-
		20	25.47‰	3.00‰	-	-	-
		21	25.51‰	3.39‰	-	-	-
		22	24.38‰	3.01‰	-	-	-
		23	22.76‰	3.32‰	-	-	-
		24	21.98‰	3.59‰	-	-	-
		25	22.58‰	3.38‰	-	-	-
		26 (P. C.)	24.49‰	3.35‰	-	-	-
		Average	22.83‰	1.83‰			
		Std Dev	1.38‰	0.94‰			

Table 2.4 (cont.)

[56.015 cont.]

Samples 1-5, 7-26 Standards (Dentin carbonate)		$\delta^{18}O$ (VPDB)	$\delta^{13}C$ (VPDB)
NBS 19	Average	1.88‰	-2.23‰
Meas. = 5	Std Dev	0.02‰	0.05‰

Sample 6 (rerun for low yield) Standards (Dentin carbonate)		$\delta^{18}O$ (VPDB)	$\delta^{13}C$ (VPDB)
NBS 19	Average	1.98‰	-2.19‰
Meas. = 4	Std Dev	0.05‰	0.05‰

Table 2.4 (cont.)

Specimen		Sample	Dentin carbonate		Dentin collagen		
Field ID	DMNS #	numbered toward pulp cavity (marked P. C. where preserved)	$\delta^{18}O$ (VSMOW)	$\delta^{13}C$ (VPDB)	$\delta^{15}N$ (air N_2)	$\delta^{13}C$ (VPDB)	C:N
56.127	-	1	24.30‰	0.75‰	-	-	-
		2	24.41‰	0.92‰	-	-	-
		3	23.55‰	0.89‰	-	-	-
		4	22.91‰	1.02‰	-	-	-
		5	21.51‰	0.82‰	-	-	-
		6	22.04‰	0.66‰	-	-	-
		7	21.55‰	0.70‰	-	-	-
		8	23.69‰	0.99‰	-	-	-
		9	23.64‰	1.14‰	-	-	-
		10	23.86‰	1.05‰	-	-	-
		11	23.71‰	1.27‰	-	-	-
		12	23.07‰	1.26‰	-	-	-
		13	21.68‰	0.72‰	-	-	-
		14	21.92‰	0.37‰	-	-	-
		15	22.12‰	0.14‰	-	-	-
		16	24.09‰	0.10‰	-	-	-
		17	23.69‰	0.11‰	-	-	-
		18	23.50‰	0.33‰	-	-	-
		19	22.35‰	-0.09‰	-	-	-
		20	21.49‰	-0.37‰	-	-	-
		21	21.24‰	-0.58‰	-	-	-
		22 (P. C.)	22.11‰	-0.32‰	-	-	-
		Average	22.84‰	0.54‰			
		Std Dev	1.05‰	0.55‰			

Standards (Dentin carbonate)		$\delta^{18}O$ (VPDB)	$\delta^{13}C$ (VPDB)
NBS 19	Average	1.97‰	-2.17‰
Meas. = 6	Std Dev	0.02‰	0.08‰

Table 2.4 (cont.)

Specimen		Sample	Dentin carbonate		Dentin collagen		
Field ID	DMNS #	numbered toward pulp cavity (marked P. C. where preserved)	$\delta^{18}O$ (VSMOW)	$\delta^{13}C$ (VPDB)	$\delta^{15}N$ (air N_2)	$\delta^{13}C$ (VPDB)	C:N
56.266	-	1	22.22‰	1.92‰	-	-	-
		2	23.26‰	2.62‰	-	-	-
		3	22.94‰	2.70‰	-	-	-
		4	23.74‰	2.87‰	-	-	-
		5	24.54‰	3.28‰	-	-	-
		6	24.65‰	4.14‰	-	-	-
		7	23.97‰	4.11‰	-	-	-
		8	25.27‰	4.44‰	-	-	-
		9	23.35‰	4.57‰	-	-	-
		10	22.99‰	4.39‰	-	-	-
		11	22.31‰	4.10‰	-	-	-
		12	22.55‰	4.37‰	-	-	-
		13	21.47‰	4.22‰	-	-	-
		14	22.66‰	4.24‰	-	-	-
		15	23.25‰	2.42‰	-	-	-
		16	25.20‰	3.90‰	-	-	-
		17 (P. C.)	24.78‰	3.51‰	-	-	-
		Average	23.48‰	3.64‰			
		Std Dev	1.11‰	0.84‰			

Samples 1-5 Standards (Dentin carbonate)		$\delta^{18}O$ (VPDB)	$\delta^{13}C$ (VPDB)
NBS 19	Average	1.97‰	-2.17‰
Meas. = 6	Std Dev	0.02‰	0.08‰

Samples 6-17 Standards (Dentin carbonate)		$\delta^{18}O$ (VPDB)	$\delta^{13}C$ (VPDB)
NBS 19	Average	1.98‰	-2.17‰
Meas. = 6	Std Dev	0.04‰	0.08‰

Table 2.4 (cont.)

Specimen		Sample	Dentin carbonate		Dentin collagen		
Field ID	DMNS #	numbered toward pulp cavity (marked P. C. where preserved)	$\delta^{18}O$ (VSMOW)	$\delta^{13}C$ (VPDB)	$\delta^{15}N$ (air N_2)	$\delta^{13}C$ (VPDB)	C:N
58.360	-	1	20.35‰	-3.52‰	-	-	-
		2	21.67‰	-3.79‰	-	-	-
		3	22.04‰	-3.99‰	4.74‰	-19.28‰	3.51
		4	21.33‰	-3.14‰	3.42‰	-18.90‰	3.61
		5	20.75‰	-3.43‰	2.94‰	-18.72‰	3.60
		6	20.72‰	-3.41‰	2.84‰	-19.24‰	3.50
		7	22.78‰	-3.59‰	4.58‰	-18.66‰	3.59
		8	23.98‰	-2.97‰	4.57‰	-19.16‰	3.62
		9	20.11‰	-3.07‰	3.60‰	-18.69‰	3.67
		10	20.74‰	-2.78‰	2.96‰	-18.83‰	3.56
		11	20.12‰	-3.03‰	3.00‰	-18.78‰	3.54
		12	20.99‰	-3.13‰	3.54‰	-18.72‰	3.50
		13	22.81‰	-2.67‰	4.82‰	-18.76‰	3.50
		14	22.56‰	-3.00‰	3.94‰	-19.09‰	3.59
		15	20.84‰	-3.00‰	3.42‰	-18.95‰	3.62
		16	20.78‰	-2.69‰	2.88‰	-18.97‰	3.50
		17	20.03‰	-2.88‰	3.09‰	-18.88‰	3.63
		18	20.81‰	-2.64‰	2.93‰	-19.05‰	3.63
		19 (P. C.)	23.10‰	-3.33‰	4.55‰	-19.19‰	3.89
		Average	21.40‰	-3.16‰	3.64‰	-18.93‰	3.59
		Std Dev	1.16‰	0.38‰	0.74‰	0.20‰	0.10

Standards (Dentin carbonate)		$\delta^{18}O$ (VPDB)	$\delta^{13}C$ (VPDB)
NBS 19	Average	1.92‰	-2.21‰
Meas. = 6	Std Dev	0.08‰	0.08‰

Table 2.4 (cont.)

[58.360 cont.]

Standards (Dentin collagen)		$\delta^{15}N$ (air N_2)	$\delta^{13}C$ (VPDB)
IAEA 600 Caffeine	Average	-	-27.77‰
Measurements = 3	Std Dev	-	0.06‰
IAEA-CH-6 Sucrose	Average	-	-10.45‰
Measurements = 3	Std Dev	-	0.04‰
USGS 25	Average	-30.40‰	-
Measurements = 3	Std Dev	0.12‰	-
IAEA N2	Average	20.30‰	-
Measurements = 3	Std Dev	0.14‰	-

Table 2.4 (cont.)

Specimen		Sample	Dentin carbonate		Dentin collagen		
Field ID	DMNS #	numbered toward pulp cavity (marked P. C. where preserved)	$\delta^{18}O$ (VSMOW)	$\delta^{13}C$ (VPDB)	$\delta^{15}N$ (air N_2)	$\delta^{13}C$ (VPDB)	C:N
60.057	-	1	22.12‰	0.54‰	-	-	-
		2	22.96‰	0.11‰	-	-	-
		3	22.81‰	0.66‰	-	-	-
		4	24.57‰	0.99‰	-	-	-
		5	24.28‰	0.65‰	-	-	-
		6	24.48‰	1.50‰	-	-	-
		7	22.73‰	0.26‰	-	-	-
		8	22.14‰	0.65‰	-	-	-
		9	21.49‰	0.43‰	-	-	-
		10	21.83‰	-0.53‰	-	-	-
		11	22.33‰	-0.01‰	-	-	-
		12	24.10‰	0.48‰	-	-	-
		13	23.44‰	0.09‰	-	-	-
		14	24.37‰	0.74‰	-	-	-
		15	22.72‰	0.03‰	-	-	-
		16	23.16‰	0.33‰	-	-	-
		17	21.84‰	-0.04‰	-	-	-
		18	22.60‰	-0.27‰	-	-	-
		19	22.12‰	-0.48‰	-	-	-
		20	24.57‰	0.02‰	-	-	-
		21	23.80‰	-0.34‰	-	-	-
		22	23.80‰	-0.32‰	-	-	-
		23	22.54‰	-0.32‰	-	-	-
		24	22.51‰	0.20‰	-	-	-
		25 (P. C.)	22.17‰	-0.92‰	-	-	-
		Average	23.02‰	0.18‰			
		Std Dev	0.97‰	0.54‰			

Standards (Dentin carbonate)		$\delta^{18}O$ (VPDB)	$\delta^{13}C$ (VPDB)
NBS 19	Average	1.96‰	-2.18‰
Meas. = 5	Std Dev	0.06‰	0.07‰

Table 2.4 (cont.)

Specimen		Sample	Dentin carbonate		Dentin collagen		
Field ID	DMNS #	numbered toward pulp cavity (marked P. C. where preserved)	$\delta^{18}O$ (VSMOW)	$\delta^{13}C$ (VPDB)	$\delta^{15}N$ (air N_2)	$\delta^{13}C$ (VPDB)	C:N
63.125	-	1	20.90‰	-0.35‰	-	-	-
		2	20.71‰	0.30‰	-	-	-
		3	21.98‰	0.06‰	-	-	-
		4	23.31‰	0.27‰	-	-	-
		5	23.33‰	-0.13‰	-	-	-
		6	23.20‰	0.20‰	-	-	-
		7	21.83‰	0.37‰	-	-	-
		8	21.57‰	0.20‰	-	-	-
		9	20.37‰	-0.21‰	-	-	-
		10	20.62‰	-0.29‰	-	-	-
		11	22.81‰	0.07‰	-	-	-
		12	23.30‰	-0.75‰	-	-	-
		13	23.41‰	-0.44‰	-	-	-
		14	23.46‰	-0.52‰	-	-	-
		15	21.36‰	-0.03‰	-	-	-
		16	21.75‰	0.20‰	-	-	-
		17	20.94‰	-0.32‰	-	-	-
		18	20.74‰	-0.32‰	-	-	-
		19	21.84‰	0.16‰	-	-	-
		20	23.42‰	0.41‰	-	-	-
		21	24.12‰	0.96‰	-	-	-
		22	23.72‰	1.02‰	-	-	-
		23	22.78‰	1.04‰	-	-	-
		24	21.69‰	1.22‰	-	-	-
		25	22.13‰	1.68‰	-	-	-
		26 (P. C.)	23.31‰	0.95‰	-	-	-
		Average	22.25‰	0.22‰			
		Std Dev	1.14‰	0.60‰			

Table 2.4 (cont.)

[63.125 cont.]

Samples 1-22 Standards (Dentin carbonate)		$\delta^{18}O$ (VPDB)	$\delta^{13}C$ (VPDB)
NBS 19	Average	1.98‰	-2.19‰
Meas. = 4	Std Dev	0.05‰	0.05‰

Samples 23-26 Standards (Dentin carbonate)		$\delta^{18}O$ (VPDB)	$\delta^{13}C$ (VPDB)
NBS 19	Average	1.88‰	-2.23‰
Meas. = 5	Std Dev	0.02‰	0.05‰

Samples 2, 15 (rerun for low yields) Standards (Dentin carbonate)		$\delta^{18}O$ (VPDB)	$\delta^{13}C$ (VPDB)
NBS 19	Average	1.98‰	-2.17‰
Meas. = 6	Std Dev	0.04‰	0.08‰

Table 2.4 (cont.)

Specimen		Sample	Dentin carbonate		Dentin collagen		
Field ID	DMNS #	numbered toward pulp cavity (marked P. C. where preserved)	$\delta^{18}O$ (VSMOW)	$\delta^{13}C$ (VPDB)	$\delta^{15}N$ (air N_2)	$\delta^{13}C$ (VPDB)	C:N
64.013	-	1	23.10‰	1.50‰	-	-	-
		2	24.16‰	1.75‰	-	-	-
		3	22.68‰	1.61‰	-	-	-
		4	22.33‰	1.08‰	-	-	-
		5	20.39‰	1.14‰	-	-	-
		6	21.76‰	1.16‰	-	-	-
		7	21.24‰	1.63‰	-	-	-
		8	24.23‰	1.94‰	-	-	-
		9	20.82‰	1.60‰	-	-	-
		10	21.63‰	1.75‰	-	-	-
		11	20.52‰	1.46‰	-	-	-
		12	21.91‰	2.18‰	-	-	-
		13	22.14‰	2.20‰	-	-	-
		14	24.28‰	2.81‰	-	-	-
		Average	22.23‰	1.70‰			
		Std Dev	1.33‰	0.47‰			

Standards (Dentin carbonate)		$\delta^{18}O$ (VPDB)	$\delta^{13}C$ (VPDB)
NBS 19	Average	1.96‰	-2.14‰
Meas. = 4	Std Dev	0.03‰	0.04‰

Table 2.4 (cont.)

Specimen		Sample	Dentin carbonate		Dentin collagen		
Field ID	DMNS #	numbered toward pulp cavity (marked P. C. where preserved)	$\delta^{18}O$ (VSMOW)	$\delta^{13}C$ (VPDB)	$\delta^{15}N$ (air N_2)	$\delta^{13}C$ (VPDB)	C:N
68.050	-	1	24.03‰	4.29‰	-	-	-
		2	24.32‰	4.31‰	-	-	-
		3	23.78‰	4.20‰	-	-	-
		4	23.44‰	4.54‰	-	-	-
		5	22.46‰	4.23‰	-	-	-
		6	22.18‰	4.39‰	-	-	-
		7	22.33‰	3.77‰	-	-	-
		8	23.13‰	3.64‰	-	-	-
		9	23.45‰	4.10‰	-	-	-
		10	24.36‰	4.14‰	-	-	-
		11 (P. C.)	25.98‰	5.37‰	-	-	-
		Average	23.59‰	4.27‰			
		Std Dev	1.10‰	0.45‰			

Standards (Dentin carbonate)		$\delta^{18}O$ (VPDB)	$\delta^{13}C$ (VPDB)
NBS 19	Average	1.97‰	-2.17‰
Meas. = 5	Std Dev	0.02‰	0.08‰

Sample	Enamel carbonate	
Bulk sample run 3X	$\delta^{18}O$ (VSMOW)	$\delta^{13}C$ (VPDB)
1	19.10‰	-7.70‰
1	19.14‰	-7.76‰
1	18.59‰	-7.92‰
Average	18.94‰	-7.79‰
Std Dev	0.31‰	0.11‰

Table 2.4 (cont.)

[68.050 cont.]

Standards (Enamel carbonate)		$\delta^{18}O$ (VPDB)	$\delta^{13}C$ (VPDB)
NBS 19	Average	1.88‰	-2.23‰
Meas. = 2	Std Dev	0.03‰	0.01‰

Specimen		Sample	Dentin carbonate		Dentin collagen		
Field ID	DMNS #	numbered toward pulp cavity (marked P. C. where preserved)	$\delta^{18}O$ (VSMOW)	$\delta^{13}C$ (VPDB)	$\delta^{15}N$ (air N_2)	$\delta^{13}C$ (VPDB)	C:N
70.018	-	1	23.03‰	0.08‰	-	-	-
		2	22.53‰	-0.23‰	-	-	-
		3	21.89‰	-0.43‰	-	-	-
		4	22.95‰	0.15‰	-	-	-
		5	20.94‰	-0.50‰	-	-	-
		6	22.16‰	-0.70‰	-	-	-
		7	23.44‰	0.27‰	-	-	-
		8	24.29‰	0.41‰	-	-	-
		9	24.73‰	0.48‰	-	-	-
		10	23.60‰	-0.08‰	-	-	-
		11	21.95‰	-0.24‰	-	-	-
		12	22.57‰	0.32‰	-	-	-
		13	21.40‰	-0.02‰	-	-	-
		14	21.41‰	-0.11‰	-	-	-
		15	22.29‰	-0.39‰	-	-	-
		16	24.11‰	0.91‰	-	-	-
		17	24.01‰	0.64‰	-	-	-
		18	24.24‰	0.64‰	-	-	-
		19	23.06‰	0.99‰	~~2.21‰~~	~~-24.60‰~~	7.09
		20	22.98‰	0.07‰	3.59‰	-19.59‰	4.05
		21	22.03‰	0.18‰	3.64‰	-19.62‰	3.97
		22	22.14‰	0.25‰	3.45‰	-19.51‰	3.29
		23	21.64‰	0.08‰	3.72‰	-19.52‰	3.57
		24	22.39‰	0.36‰	4.35‰	-19.54‰	3.83
		25	24.05‰	0.61‰	5.13‰	-19.46‰	3.84

Table 2.4 (cont.)

[70.018 cont.]

26	24.35‰	1.06‰	5.01‰	-19.57‰	4.10
27	26.66‰	1.91‰	~~4.72‰~~	~~-20.42‰~~	4.22
28	23.93‰	0.80‰	~~3.94‰~~	~~-22.74‰~~	5.55
29	22.79‰	0.15‰	4.41‰	-19.47‰	3.98
30	23.22‰	0.37‰	3.87‰	-19.33‰	3.84
31	22.62‰	0.49‰	4.09‰	-19.24‰	3.90
32	22.45‰	0.42‰	4.05‰	-19.16‰	4.07
33	22.42‰	0.17‰	3.74‰	-19.59‰	3.50
34	24.37‰	0.73‰	4.33‰	-19.43‰	3.91
35	24.70‰	1.77‰	4.38‰	-19.58‰	4.18
36	25.12‰	2.36‰	~~-4.55‰~~	~~-23.90‰~~	8.28
37 (P. C.)	25.05‰	6.75‰	~~-5.27‰~~	~~-28.40‰~~	24.42
Average	23.18‰	0.56‰	4.13‰	-19.47‰	3.86
Std Dev	1.25‰	1.23‰	0.51‰	0.14‰	0.25

Strikethroughs indicate samples with epoxy contamination, which is reflected in higher C:N ratios

Standards (Dentin carbonate)		$\delta^{18}O$ (VPDB)	$\delta^{13}C$ (VPDB)
NBS 19	Average	1.98‰	-2.17‰
Meas. = 9	Std Dev	0.03‰	0.04‰

Standards (Dentin collagen)		$\delta^{15}N$ (air N_2)	$\delta^{13}C$ (VPDB)
IAEA 600 Caffeine	Average	-	-27.77‰
Measurements = 3	Std Dev	-	0.02‰
IAEA-CH-6 Sucrose	Average	-	-10.45‰
Measurements = 3	Std Dev	-	0.01‰
USGS 25	Average	-30.40‰	-
Measurements = 3	Std Dev	0.07‰	-
IAEA N2	Average	20.30‰	-
Measurements = 3	Std Dev	0.09‰	-

Table 2.4 (cont.)

Specimen		Sample	Dentin carbonate		Dentin collagen		
Field ID	DMNS #	numbered toward pulp cavity (marked P. C. where preserved)	$\delta^{18}O$ (VSMOW)	$\delta^{13}C$ (VPDB)	$\delta^{15}N$ (air N_2)	$\delta^{13}C$ (VPDB)	C:N
76.085	-	1	23.64‰	1.16‰	-	-	-
		2	23.14‰	1.43‰	-	-	-
		3	23.33‰	1.21‰	-	-	-
		4	23.50‰	1.50‰	-	-	-
		5	21.08‰	0.95‰	-	-	-
		6	21.83‰	0.91‰	-	-	-
		7	21.11‰	0.66‰	-	-	-
		8	22.29‰	0.98‰	-	-	-
		9	23.65‰	1.59‰	-	-	-
		10	24.49‰	1.20‰	-	-	-
		11	24.19‰	1.20‰	-	-	-
		12	23.16‰	1.08‰	-	-	-
		13	21.97‰	1.04‰	-	-	-
		14	21.26‰	0.53‰	-	-	-
		15	22.03‰	0.56‰	-	-	-
		16	22.45‰	0.61‰	-	-	-
		17	24.09‰	1.33‰	-	-	-
		18	23.98‰	1.35‰	-	-	-
		19	23.90‰	1.38‰	-	-	-
		20	22.67‰	1.69‰	-	-	-
		21 (P. C.)	22.32‰	1.70‰	-	-	-
		Average	22.86‰	1.15‰			
		Std Dev	1.06‰	0.36‰			

Standards (Dentin carbonate)		$\delta^{18}O$ (VPDB)	$\delta^{13}C$ (VPDB)
NBS 19	Average	1.95‰	-2.18‰
Meas. = 5	Std Dev	0.04‰	0.04‰

Table 2.4 (cont.)

Specimen		Sample	Dentin carbonate		Dentin collagen		
Field ID	DMNS #	numbered toward pulp cavity (marked P. C. where preserved)	$\delta^{18}O$ (VSMOW)	$\delta^{13}C$ (VPDB)	$\delta^{15}N$ (air N_2)	$\delta^{13}C$ (VPDB)	C:N
82.179	-	1	23.24‰	-2.64‰	-	-	-
		2	20.68‰	-2.53‰	-	-	-
		3	19.96‰	-2.77‰	-	-	-
		4	20.64‰	-2.56‰	-	-	-
		5	21.31‰	-2.67‰	-	-	-
		6	23.26‰	-2.35‰	-	-	-
		7	21.00‰	-3.15‰	-	-	-
		8	22.12‰	-2.58‰	-	-	-
		9	22.09‰	-2.52‰	-	-	-
		10	21.59‰	-2.42‰	-	-	-
		11	23.62‰	-2.01‰	-	-	-
		12 (P. C.)	24.89‰	-1.62‰	-	-	-
		Average	22.03‰	-2.49‰			
		Std Dev	1.46‰	0.38‰			

Standards (Dentin carbonate)		$\delta^{18}O$ (VPDB)	$\delta^{13}C$ (VPDB)
NBS 19	Average	1.96‰	-2.14‰
Meas. = 6	Std Dev	0.03‰	0.04‰

Table 2.4 (cont.)

Specimen		Sample	Dentin carbonate		Dentin collagen		
Field ID	DMNS #	numbered toward pulp cavity (marked P. C. where preserved)	$\delta^{18}O$ (VSMOW)	$\delta^{13}C$ (VPDB)	$\delta^{15}N$ (air N_2)	$\delta^{13}C$ (VPDB)	C:N
Loc. 8	-	1	23.37‰	1.43‰	-	-	-
		2	23.60‰	2.08‰	-	-	-
		3	24.31‰	2.21‰	-	-	-
		4	25.89‰	3.37‰	-	-	-
		5	25.42‰	3.83‰	-	-	-
		6	25.03‰	3.86‰	-	-	-
		7	25.80‰	4.16‰	-	-	-
		8	24.95‰	3.93‰	-	-	-
		9	25.13‰	3.77‰	-	-	-
		10	25.26‰	3.84‰	-	-	-
		11	25.71‰	4.18‰	-	-	-
		12	26.56‰	4.79‰	-	-	-
		13	25.73‰	4.49‰	-	-	-
		14	24.37‰	3.68‰	-	-	-
		15	23.77‰	3.54‰	-	-	-
		16	24.99‰	3.99‰	-	-	-
		17	24.56‰	3.49‰	-	-	-
		18	25.09‰	4.27‰	-	-	-
		19	25.70‰	4.77‰	-	-	-
		20	25.81‰	4.76‰	-	-	-
		21	24.34‰	4.04‰	-	-	-
		22	24.37‰	4.09‰	-	-	-
		23	24.59‰	4.17‰	-	-	-
		24	25.78‰	3.52‰	-	-	-
		25 (P. C.)	28.23‰	5.28‰	-	-	-
		Average	25.13‰	3.82‰			
		Std Dev	1.02‰	0.86‰			

Standards (Dentin carbonate)		$\delta^{18}O$ (VPDB)	$\delta^{13}C$ (VPDB)
NBS 19	Average	1.99‰	-2.19‰
Measurements = 6	Std Dev	0.03‰	0.05‰

Figure 2.1. Mandible of an adult mastodon from ZR with mandibular tusks.
(A) Field no. 44.035 (DMNH) - Mandible of an adult mastodon (likely female, based on molar dimensions) displaying prominent tusks. (B)–(D) Field no. 58.025 (DMNH), right mandibular tusk of an adult male (based on maximum circumference and growth increment volumes estimated from microCT scans). (B) Medial view; irregular topography on medial surface of the distal two-thirds of the tusk is antemortem interdental resorption or chemical erosion along the contact with the left mandibular tusk. Circumferential ridges ('periradicular bands') near the proximal end of the tusk are annually repeating deflections of the cementum-dentin junction. (C) Lateral view. (D) Composite microCT image along tusk axis, showing annual increments and periradicular features. Linear white features above and below (and approximately parallel to) the tusk axis are a "cylindrical artifact" produced during volume reconstruction.

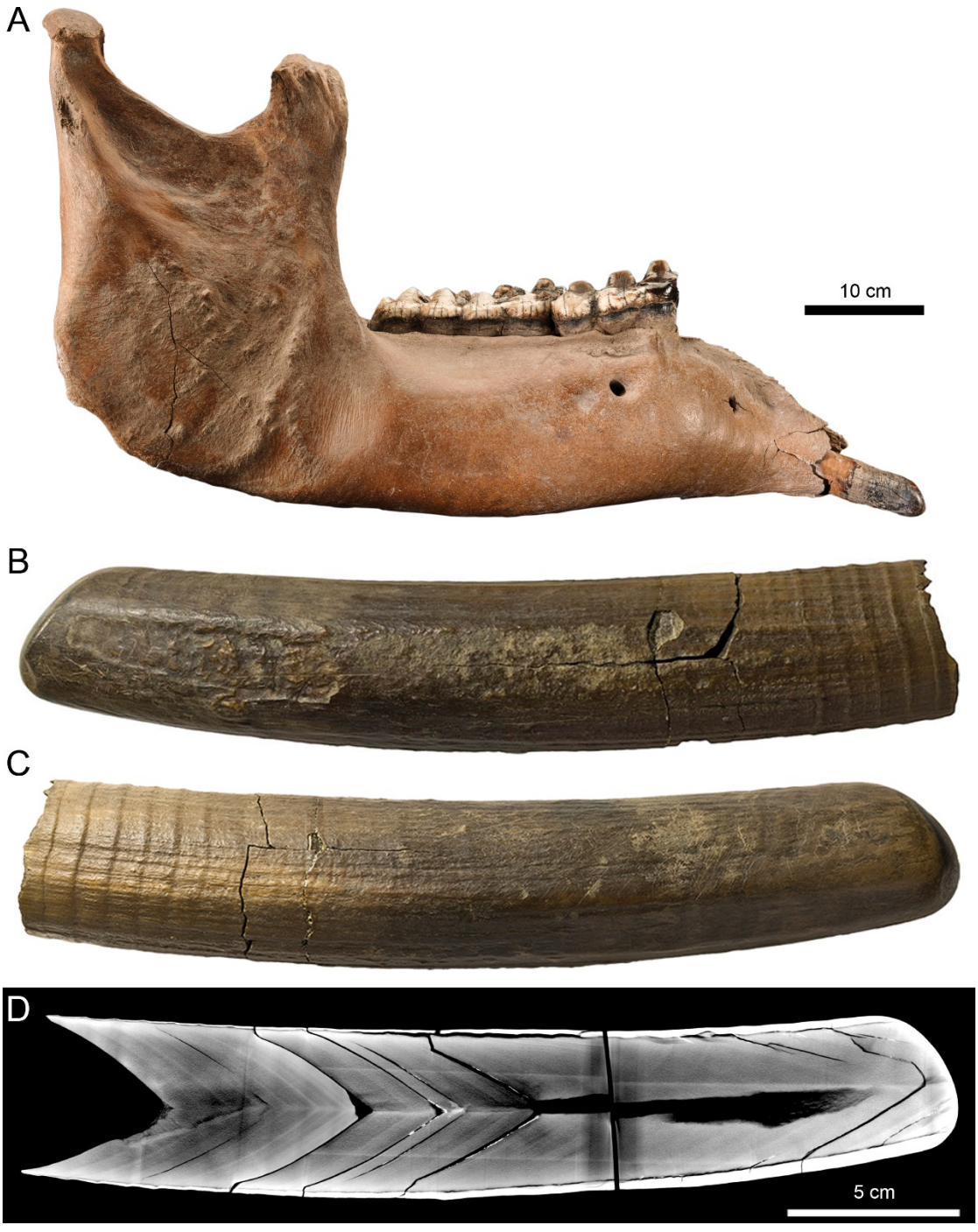
A
10 cm
B
C
D
5 cm

Figure 2.2. The Clay Mammoth assemblage (DMNH 60704).
(A) In situ field exposure, from above (north arrow at bottom-left). Numerous boulders (only some indicated) associated with the specimen are visible near the right end of the assemblage. (B) Lab preparation of the underside of the assemblage revealed additional boulders beneath skull (string grid on 1-m scale).

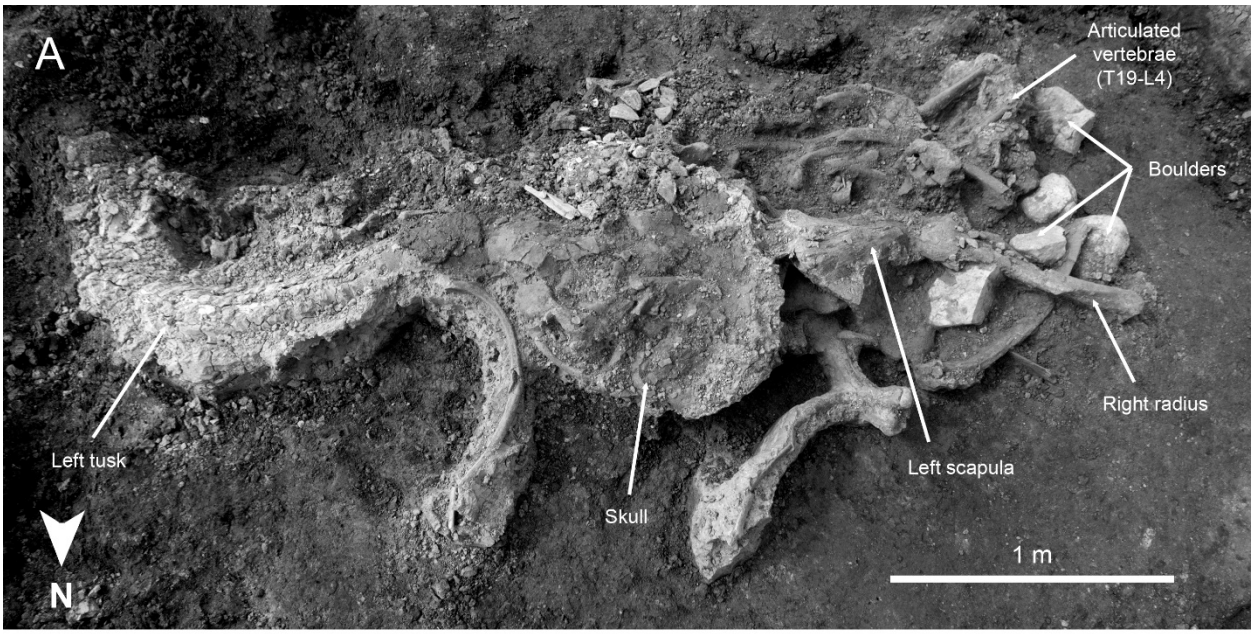

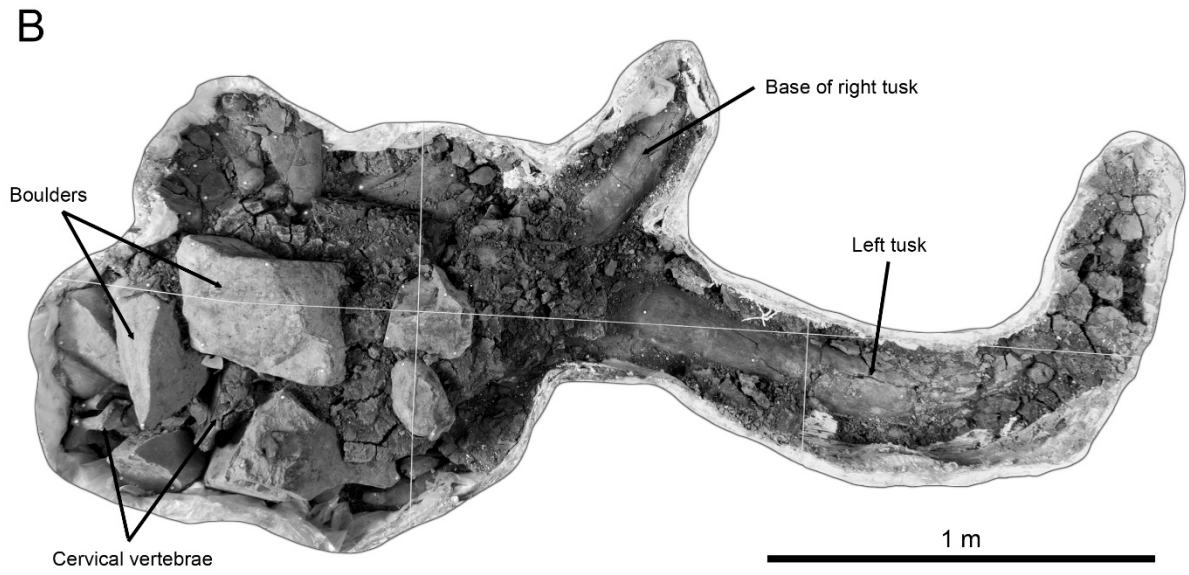

Figure 2.3. Annual microCT growth features in a ZR mandibular tusk.
(A)–(D) Field no. 60.057 (DMNH). (A) Mandibular tusk cut longitudinally along axis; surface polished for isotope sampling. Schreger pattern (displayed here as tightly packed, discontinuous "tiger" stripes) obscures growth lines at this magnification. (B) Virtual 2D slice of microCT data shows radiodensity variation. Each gradual transition from dark (low radiodensity) to light (high radiodensity) producing a zonation that parallels the pulp cavity surface represents a year of growth. (C) Segmentation of microCT data enables direct volumetric measurement of annual growth increments (years distinguished by color/grayscale value). (D) Linear measurements taken from 2D projections of CT data provide a close approximation of increment volumes; L, increment length measured along a line half-way between axis and CDJ, r_{maj}, half the major diameter (usually dorsoventral) of the tusk at location of increment length measurement, r_{min}, half the minor diameter (usually mediolateral) of the tusk at location of increment length measurement. Estimated and measured volumes are compared in Figure 2.5B.

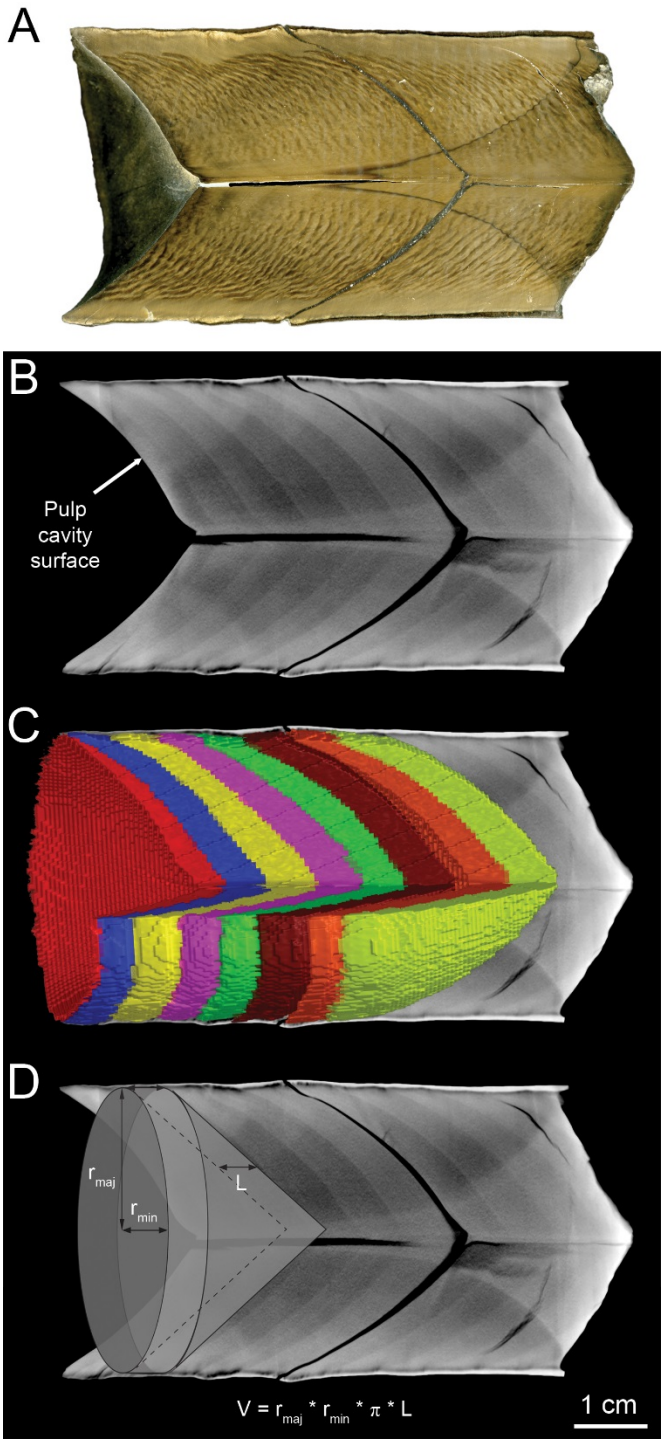
A
B
Pulp
cavity
surface
C
D
r maj
r min
L
V = r maj * r min * π * L
1 cm

Figure 2.4. Protocol for measuring CT growth increments.
(A)–(E) demonstrate the sequence of steps for obtaining growth increment length measurements from a microCT scan of an adult male mandibular tusk (48.530). (A) CT scans processed in multiple pieces are reassembled, and a 2D dorsoventral slice passing along the tusk axis is exported as an image file. CT "ring" artifact near tip of tusk is produced during volume reconstruction and is equivalent to the "cylindrical artifact" in Figure 2.1. (B) CT features are identified and traced. (C) Lines are drawn midway between the CDJ and the tusk axis. (D)–(E) Increment lengths are measured along this line from one CT feature to the next. Whenever possible, lengths, shown here in the dorsal half of these slices, are calculated by averaging values obtained in the dorsal and ventral halves. Measures of increment thickness are shown here in the ventral half.

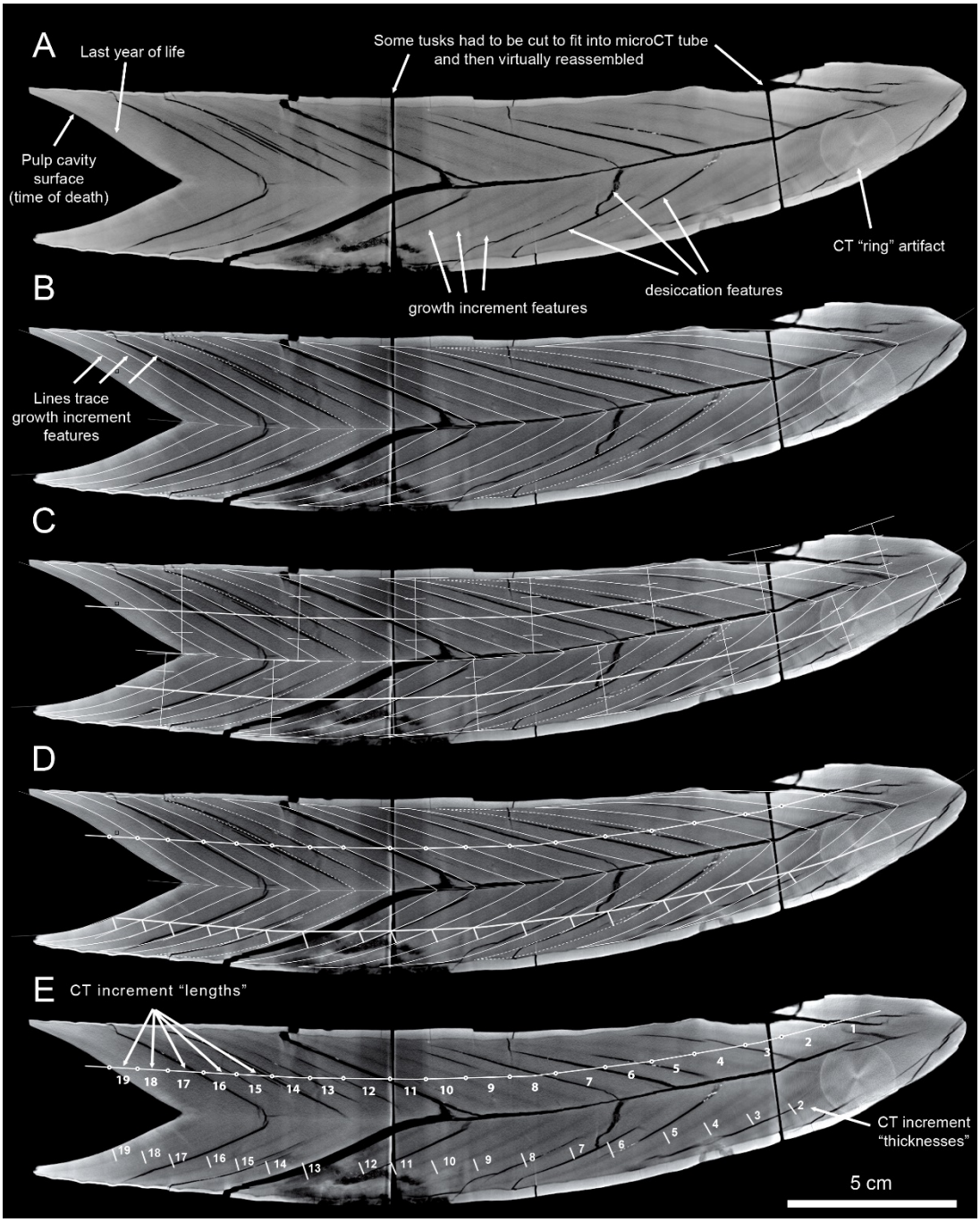
A
Last year of life
Some tusks had to be cut to fit into microCT tube and then virtually reassembled
Pulp cavity surface (time of death)
CT "ring" artifact
desiccation features
growth increment features
B
Lines trace growth increment features
C
D
E
CT increment "lengths"
19 18 17 16 15 14 13 12 11 10 9 8 7 6 5 4 3 2 1
CT increment "thicknesses"
5 cm

Figure 2.5. EIV growth series for ZR mandibular tusks.
The final (incomplete) annual increment has been dropped for each series. (A) Growth series display bimodality (log scale; EIV has units of cm^3) among adult tusks indicative of sexual dimorphism. Ranges for juveniles and adult females vs. adult males are identified along right margin. Asterisks mark EIV plots for four specimens (shifted to left side of graph) missing their proximal end (time of death). (B) Specimens 60.057 and 76.085 show EIVs (see Figure 2.3) and measured CT volumes for comparison.

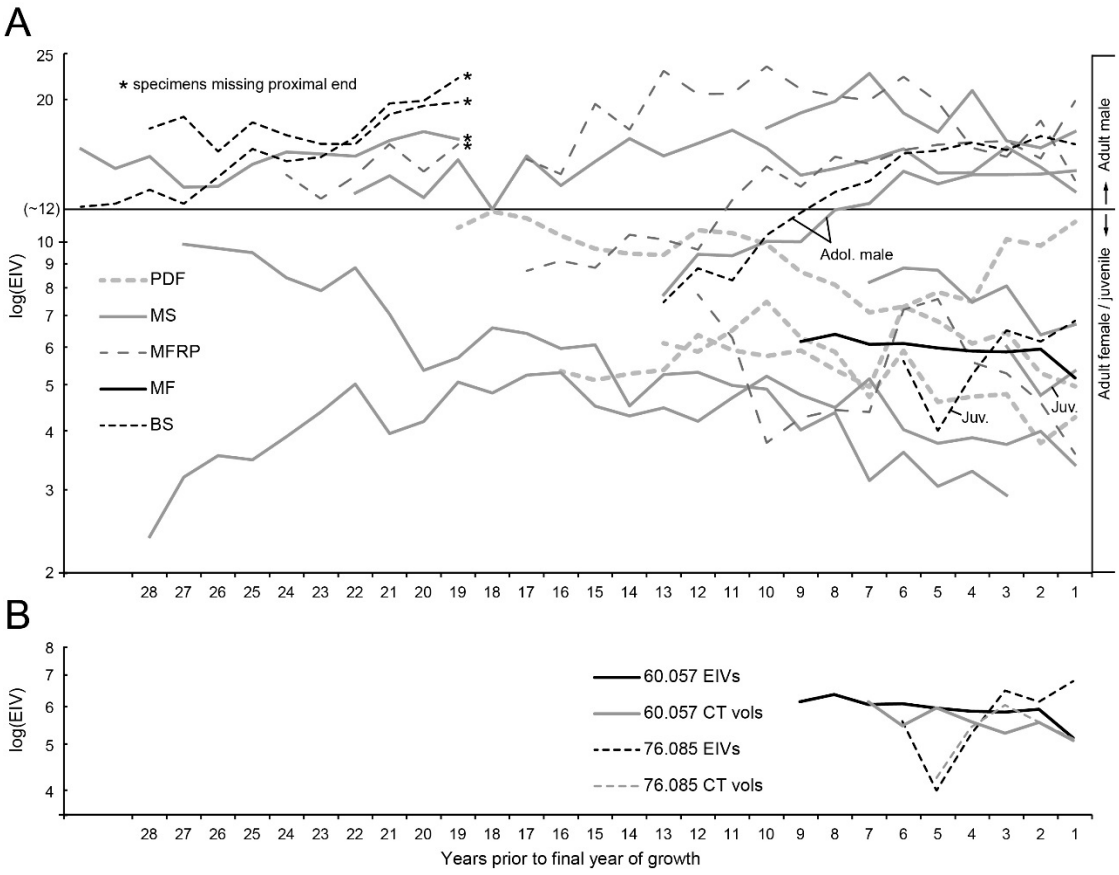

Figure 2.6. Isotope sampling procedure for ZR tusks.
(A) Plan for isotope sampling of an adult female mandibular tusk (60.057) overlaid on a microCT slice. Fine white lines paralleling pulp surface demarcate sample paths. Thicker white lines parallel to tusk axis mark the location of planned "truncation grooves" explained in C. (B) Sampling plan overlaid on scan of polished sampling surface; a computer-controlled milling machine enabled precise sampling of planned increments. (C) Tusk after isotope sampling of last four years of life from lower half of polished longitudinal surface; deep "truncation grooves" (t. g.) parallel to tusk axis and CDJ were cut first, allowing serial sampling paths to start and end without contacting dentin formed before or after targeted interval of time.

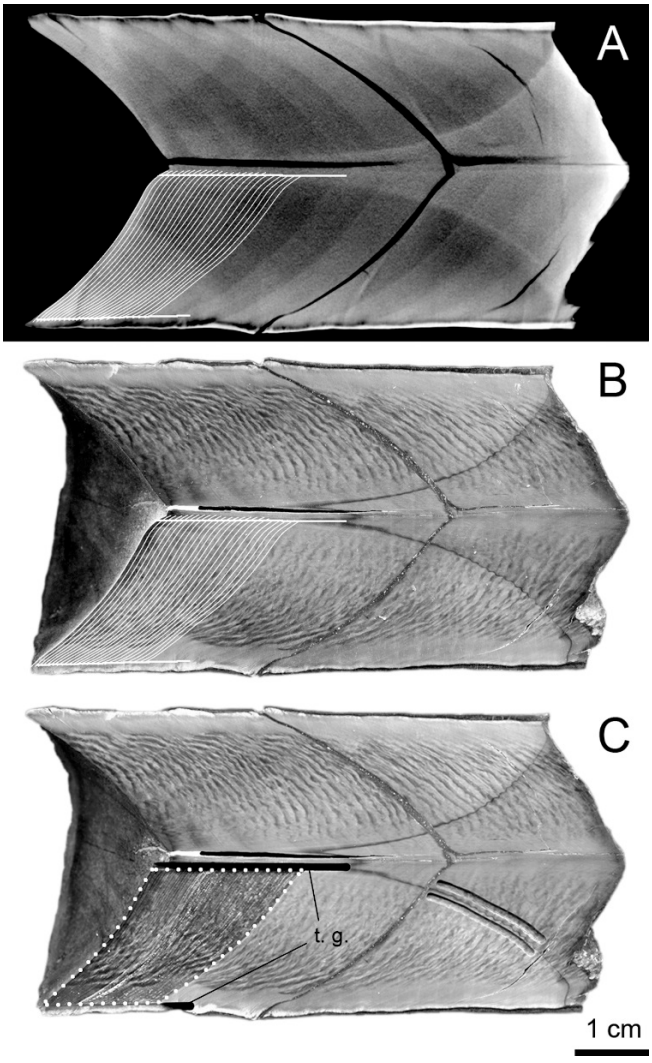

Figure 2.7. Mammoth molar from ZR.
(A) Buccal and (B) occlusal views of lower right third molar (DMNH 60704.008) from the Clay Mammoth.

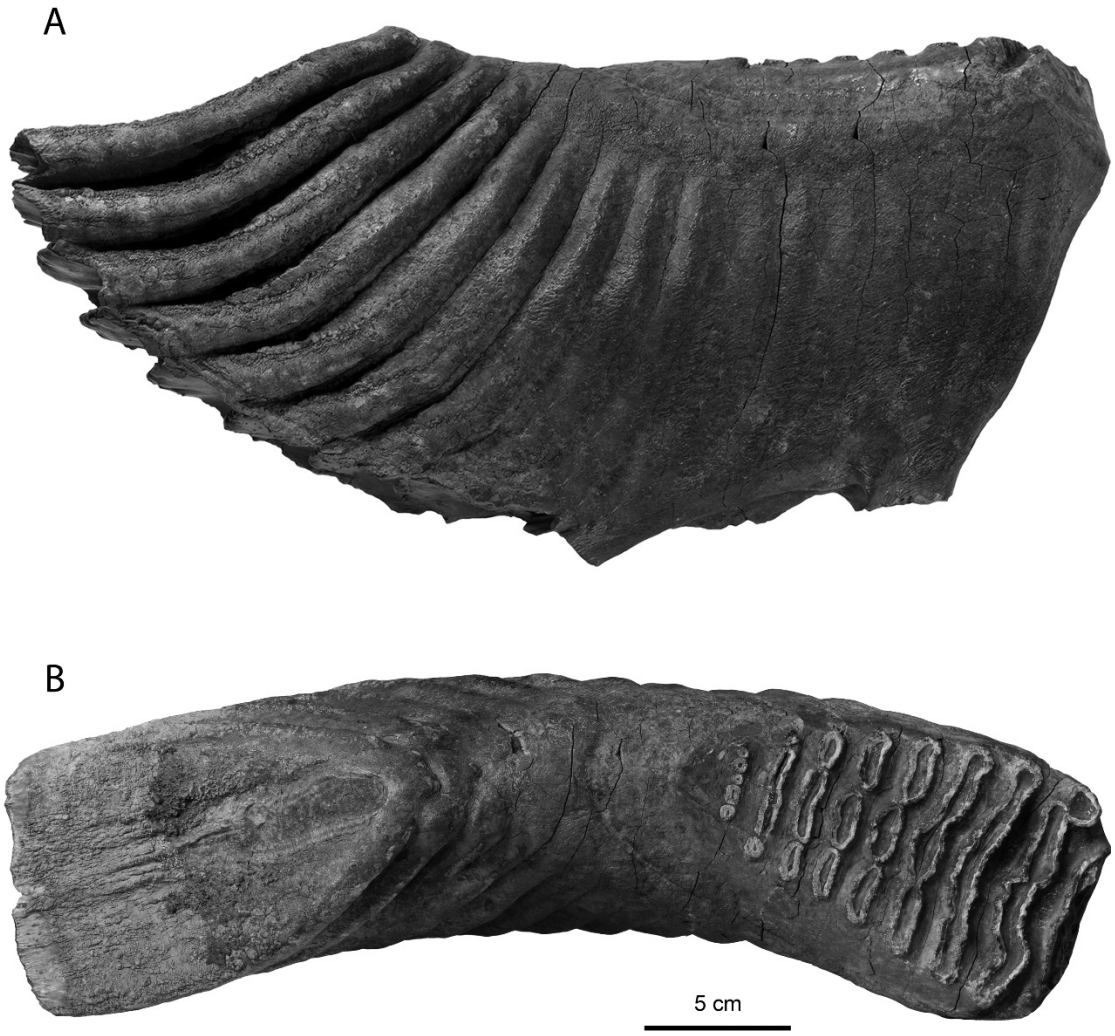

Figure 2.8. Comparison with Great Lakes region mastodons.
Bivariate plots of natural logarithms of cheek tooth lengths and widths for ZR mastodons (red symbols, sexes not distinguished), superimposed on distributions for mastodons from the Great Lakes region (black symbols, males and females distinguished as in legends). (A) Maxillary (upper) dentition. (B) Mandibular (lower) dentition.

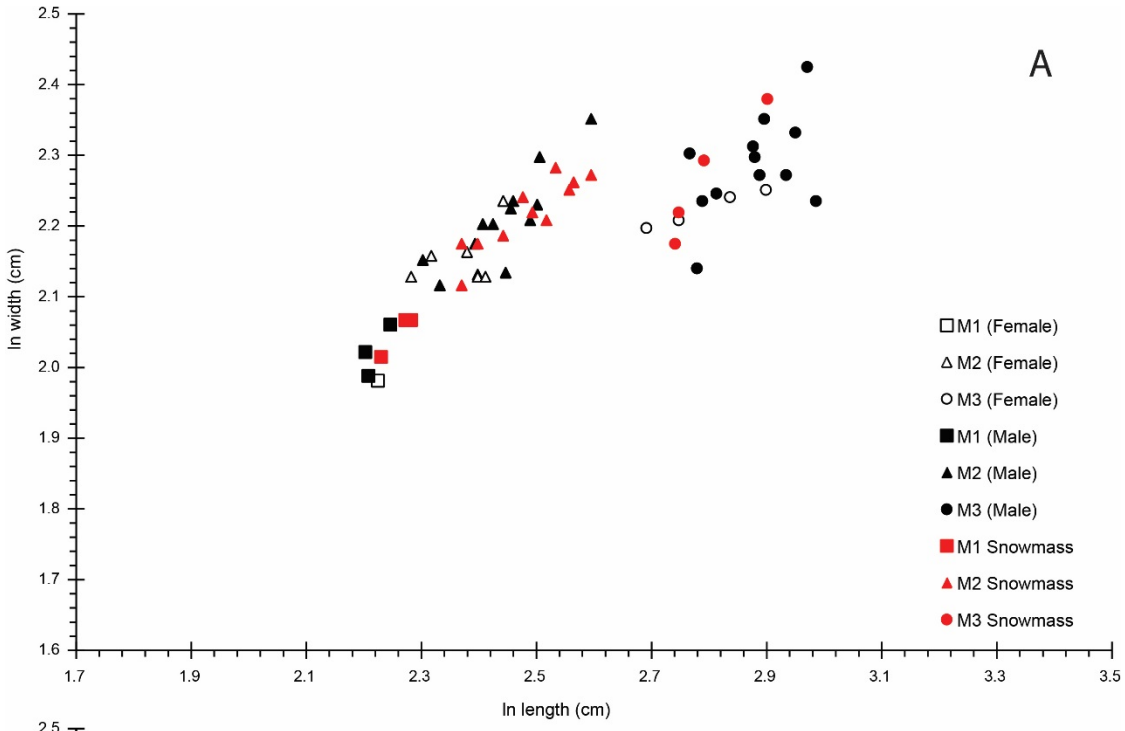
A
ln width (cm)
ln length (cm)
2.5
2.4
2.3
2.2
2.1
2.0
1.9
1.8
1.7
1.6
1.7
1.9
2.1
2.3
2.5
2.7
2.9
3.1
3.3
3.5
M1 (Female)
M2 (Female)
M3 (Female)
M1 (Male)
M2 (Male)
M3 (Male)
M1 Snowmass
M2 Snowmass
M3 Snowmass

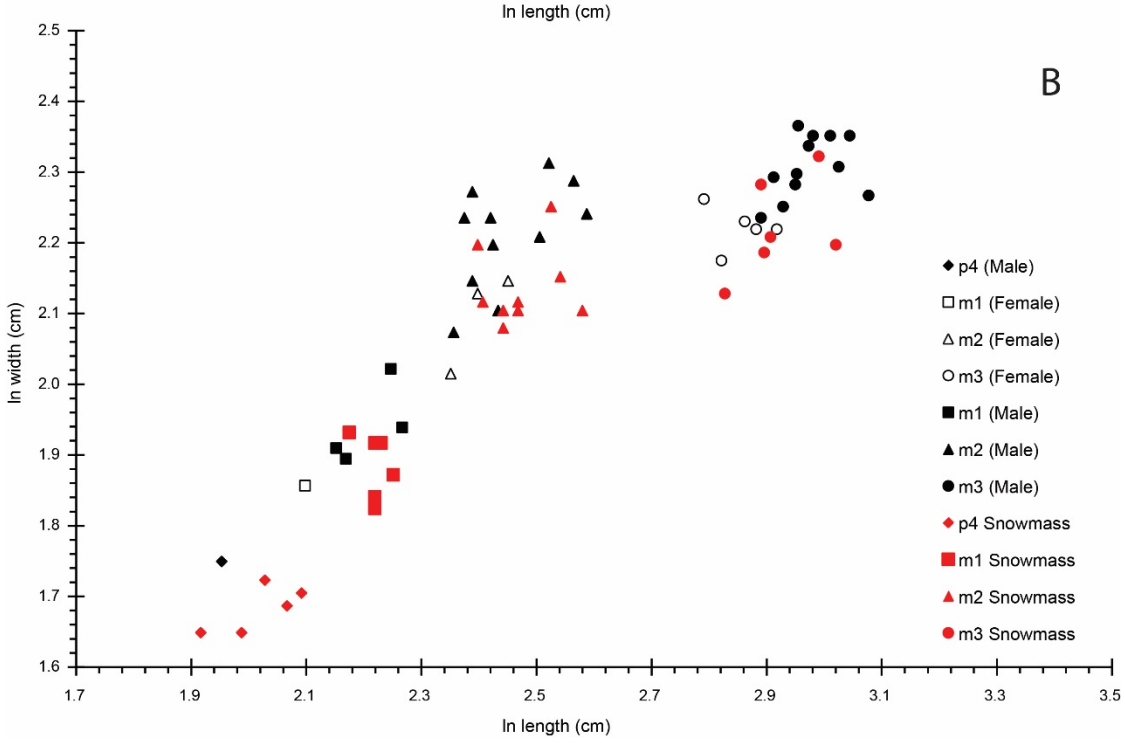
B
ln width (cm)
ln length (cm)
2.5
2.4
2.3
2.2
2.1
2.0
1.9
1.8
1.7
1.6
1.7
1.9
2.1
2.3
2.5
2.7
2.9
3.1
3.3
3.5
p4 (Male)
m1 (Female)
m2 (Female)
m3 (Female)
m1 (Male)
m2 (Male)
m3 (Male)
p4 Snowmass
m1 Snowmass
m2 Snowmass
m3 Snowmass

Figure 2.9. Annual CT features in mastodon tusks from other regions.
MicroCT scans of tusk samples from near the end of life for mastodons from eastern North America. (A) Hyde Park mastodon (Paleontological Research Institution 49820, Ithaca, NY). White lines superimposed on CT image mark approximate locations of thin second-order increments immediately preceding winter-spring boundaries, an interpretation consistent with other data from the tusk. Correlation of second-order increment analysis with CT scan is based on text-Figure 5 in Fisher (2008). (B) Mastodon from Aucilla River, Florida (UF 150701). White lines superimposed on CT image mark second-order increment thickness minima (not explicitly identified as winter-spring because of low-latitude setting, but recognized as bounding annual increments) documented in Figure 12.4 of Fisher and Fox (2006).

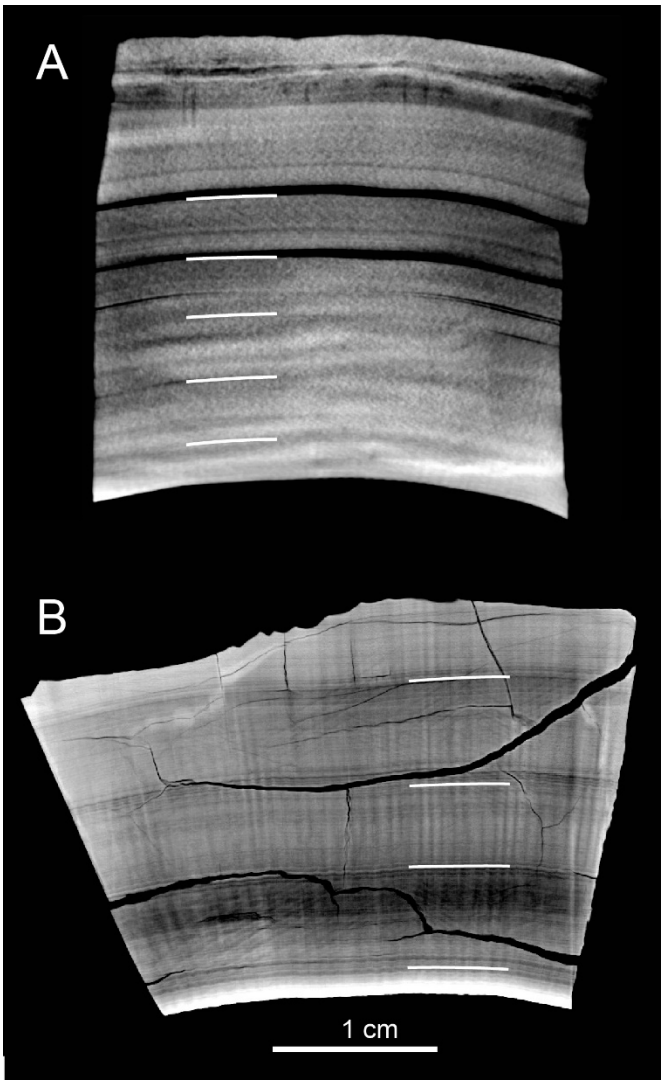

Figure 2.10. Partial census of Ziegler Reservoir mastodons.
This plot uses mandibular tusk circumferences and stage of cheek tooth eruption and wear to determine relative ages of individuals. Main area of figure is a bivariate plot of Laws' Age Class determinations (Laws, 1966) vs. maximum circumference of mandibular tusks for specimens for which both can be assessed. At left is a histogram of additional specimens (mandibles without tusks) for which maximum tusk circumference cannot be assessed. Below is a histogram of additional specimens (isolated tusks) for which no Laws' Age Class is available (maximum tusk circumference rounded to nearest 0.5 mm).

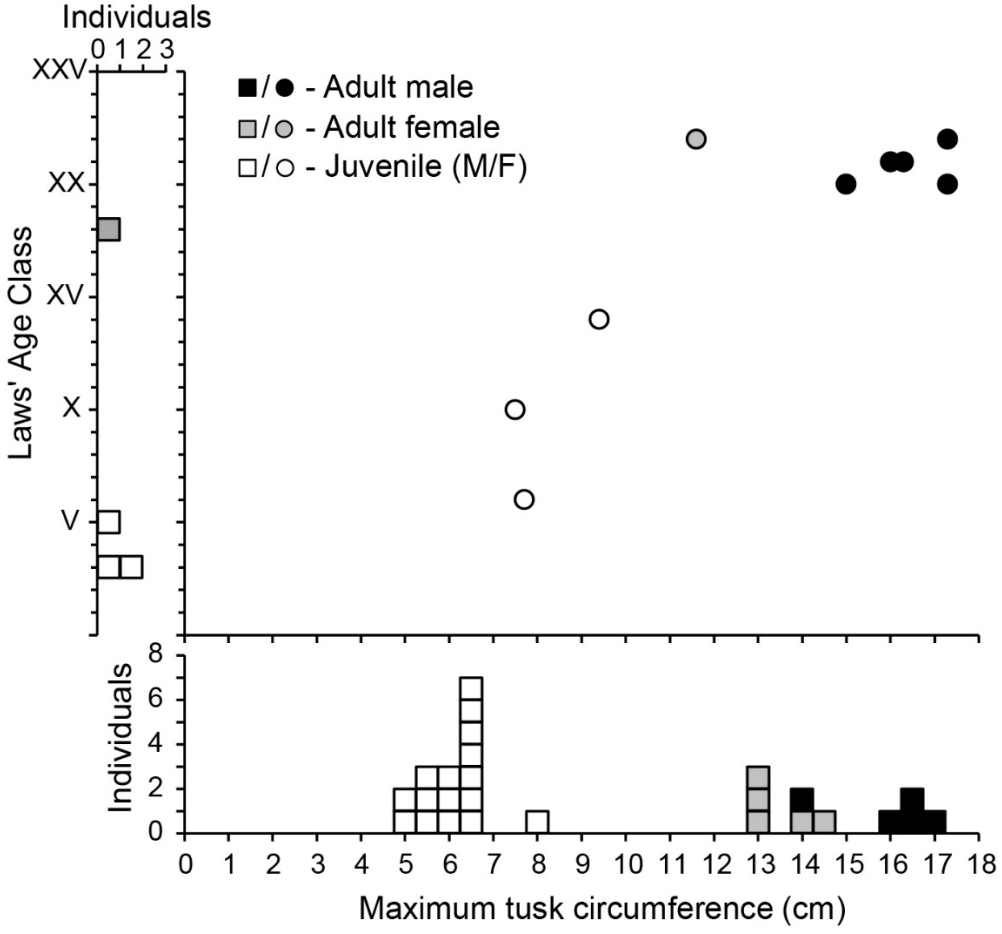

Figure 2.11. Deciduous tusk from ZR with neonatal line.
Field no. 68.050 (DMNH). (A) and (B) Two exterior views (orthogonal to each other but with uncertain anatomical orientation) of a deciduous mastodon tusk. Enamel crown is intact. Color/grayscale boundary on cementum surface at gingival margin (approximately 1/3 distance from distal end) and smoothly worn crown indicate tusk had erupted. (C) Tusk cut longitudinally along axis (polished in preparation for isotope sampling; some enamel spalled during polishing) displays a deep pulp cavity and distinct feature recognized as a neonatal line. (D) Virtual longitudinal slice through microCT data (enamel is bright white) displays a radiodensity manifestation of the neonatal line. This feature is present in approximately the same location in all ZR deciduous tusks analyzed.

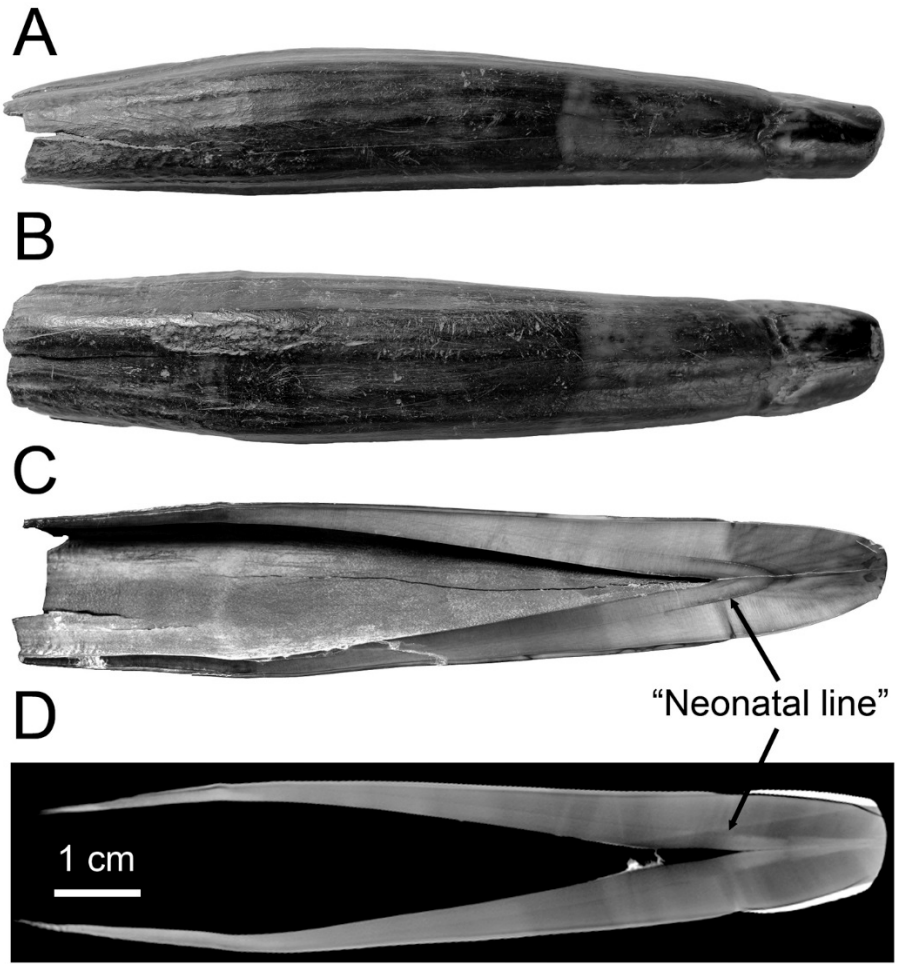

Figure 2.12. Annual periodicity of CT growth features.
Locality 8 (DMNH). (A) Digital skull and tusks at top show source of tusk sample (microCT inset; white dashed lines frame cropped CT image (CDJ to pulp cavity, PC) enlarged below. (B) Extracted region of interest in A, from CDJ at left to PC at right. Below this (y-axis label on right) is a plot of luminance (gray values measured on a scale of 0 [black, lower density] to 255 [white, higher density] measured in ImageJ) along a transect from CDJ to PC and a graph of second-order increment thicknesses along the same transect, from a thin section of the same dentin sequence (x-axis records distance from pulp cavity). Black dashed lines mark drops in radiodensity. (C) Oxygen isotope values from the same specimen cover the last three-plus years of life. Second-order profile and oxygen isotope results suggest a final winter-spring boundary not visible in CT data.

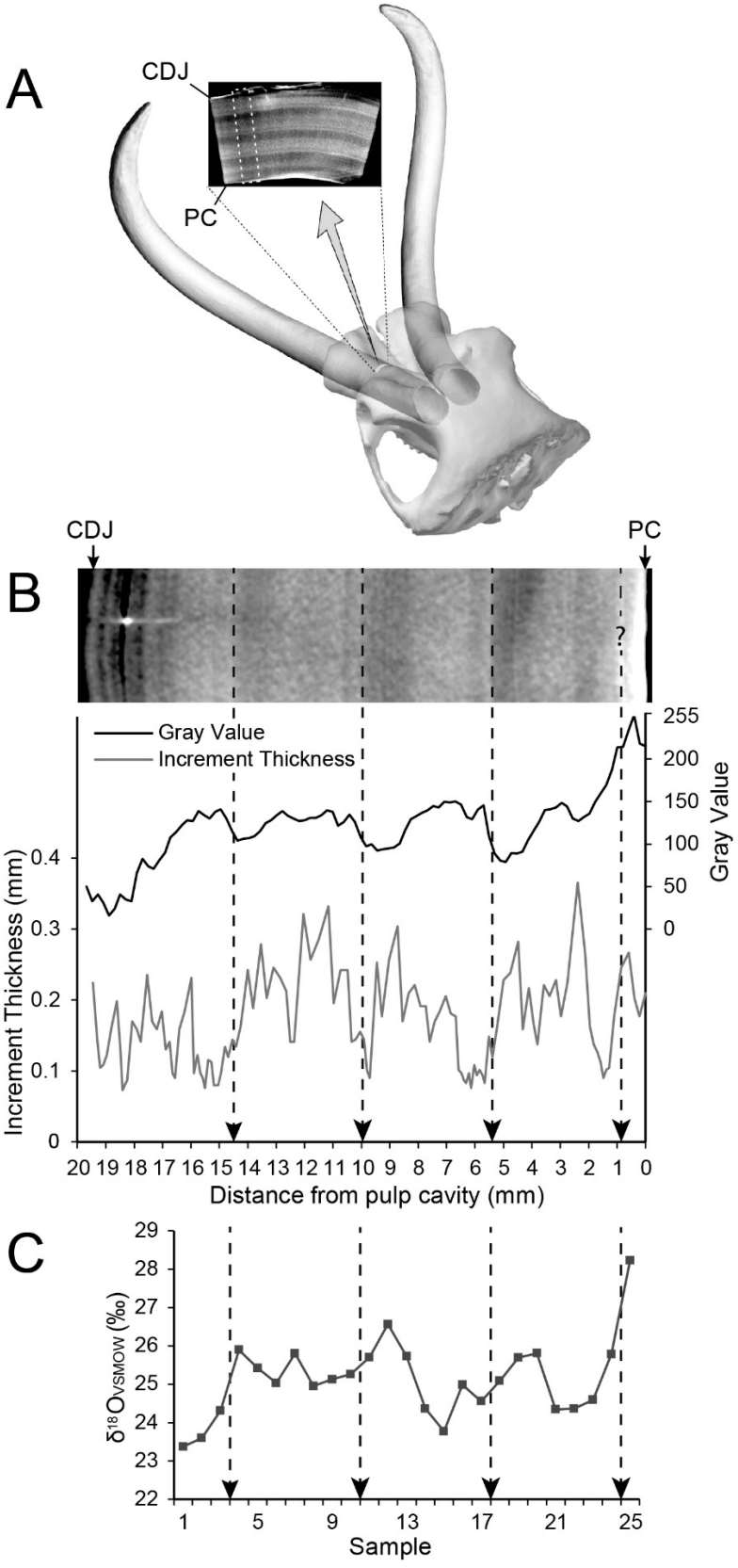
A
CDJ
PC
B
CDJ
PC
?
Gray Value
Increment Thickness
Increment Thickness (mm)
Gray Value
0
0.1
0.2
0.3
0.4
0
50
100
150
200
255
20 19 18 17 16 15 14 13 12 11 10 9 8 7 6 5 4 3 2 1 0
Distance from pulp cavity (mm)
C
δ18OVSMOW (‰)
22
23
24
25
26
27
28
29
1 5 9 13 17 21 25
Sample

Figure 2.13. Seasonality in stable isotopes of oxygen and nitrogen.
Serial measurements of $\delta^{18}O$ and $\delta^{15}N$ for adult male mastodon mandibular tusk (Field no. 58.360). Vertical dashed lines indicate locations of annual CT features in image below graph (abrupt transition from high to low density). Nitrogen record is in phase with oxygen profile.

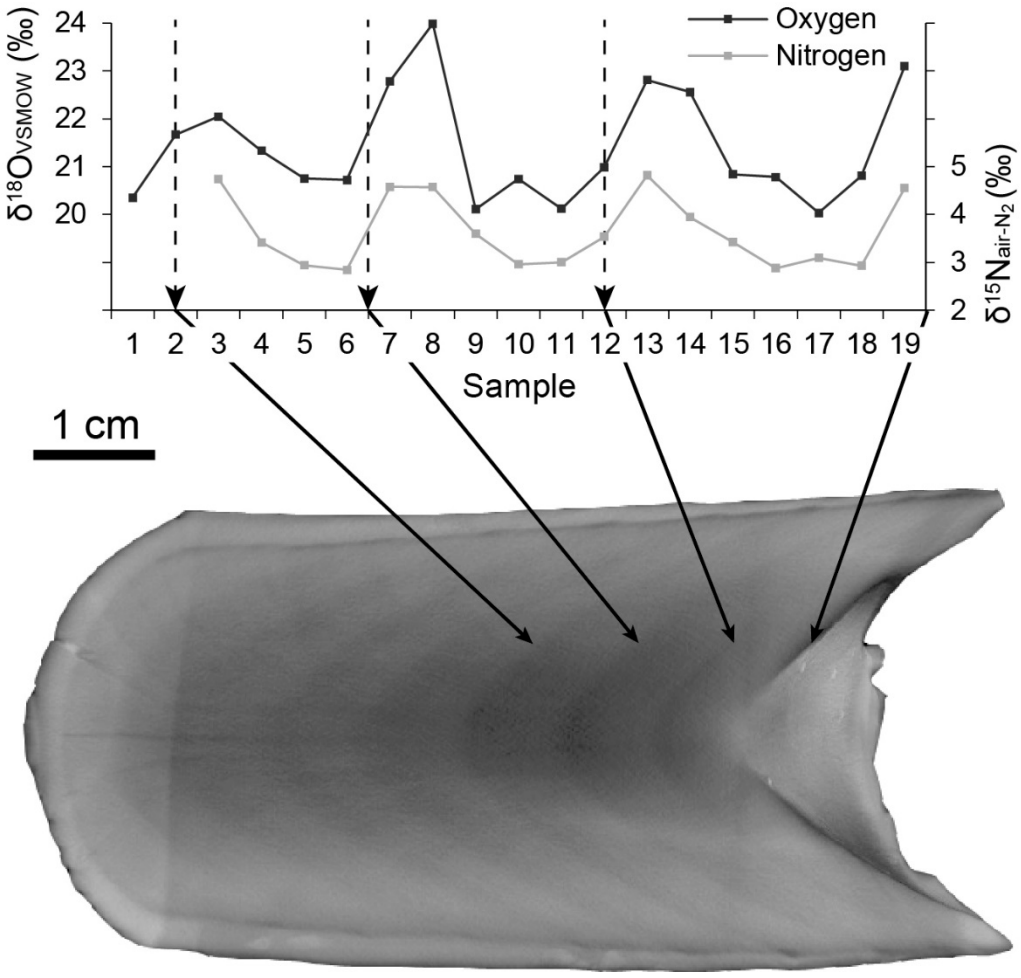

Figure 2.14. Fraction of final year (FFY) for ZR proboscideans.
Calculations are grouped by association with stratigraphic units from Pigati et al. (2014): [Lake-margin] BS, Basement Silt; MF, Main Floor; MFRP, Main Floor Red Pebble; MS, Main Silt; PDF, Primary Debris Flow; [Lake-center] 16/17, boundary between Unit 16 (peat) and 17 (clayey silt). Units arranged in succession with youngest at top; order of specimens within units is by field number. Each estimate expresses the final increment volume as a percentage of annual increment volume expected for a complete year. For solid circles, expected volume = EIV for the last complete year; for open diamonds, expected volume = average EIV for the last two complete years; for open squares, expected volume is projected from a 5-yr linear trend (except for 56.127 and Loc 8 in which only three previous years are available) of logged EIVs. Data for Loc 8, Clay, 44.035, 70.018, and 56.266 are based on linear measurements rather than EIVs. Symbols beyond 100 % (e.g., 56.015) reflect either an uncharacteristically productive year or failure to recognize an obscure final feature. Numerous individuals from the Main Floor Red Pebble and Main Silt display a season of death near the end of an annual CT density cycle. Provisional seasonal designations (based on evidence presented in *Discussion*) for each quarter of an expected year's growth are listed in parentheses along the top of the graph.

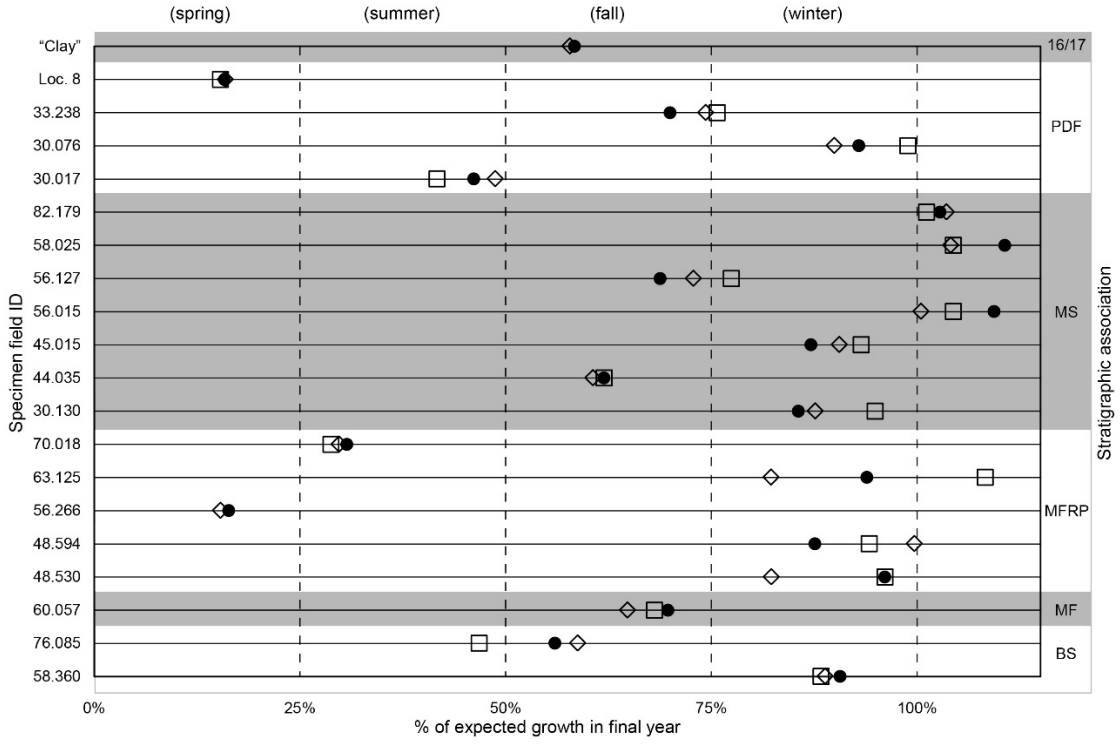

Figure 2.15. Multiyear oxygen isotope records for ZR tusks.
(A) Comparison of multi-year oxygen isotope series for mastodon tusks from different stratigraphic units. Vertical lines represent locations of annual CT features (abrupt transition from high to low density); fraction of final year is plotted as a percentage of expected growth for a complete year (see Figure 2.14). Because different tusks and different years within the same tusk may have different numbers of samples per year, sample intervals are spaced variably along the x-axis and aligned to annual CT features. Tusk isotope records from the oldest unit sampled (BS, Basement Silt) produced average $\delta^{18}O$ values ~2.1 ‰ lower than those of specimens obtained from the highest unit sampled (PDF, Primary Debris Flow). Tusks from intermediate units (MF, Main Floor; MFRP, Main Floor Red Pebble; MS, Main Silt) consistently show $\delta^{18}O$ values between the two extremes. Horizontal lines mark average $\delta^{18}O$ values over all specimens sampled from each unit (BS – 3 spec., MF – 1 spec., MFRP – 4 spec., MS – 3 spec., PDF – 3 spec.). (B) Two mandibular tusks from Main Silt (MS) and one from the subjacent (and potentially genetically related) Main Floor Red Pebble (MFRP) have similar seasons of death and similar $\delta^{18}O$ series.

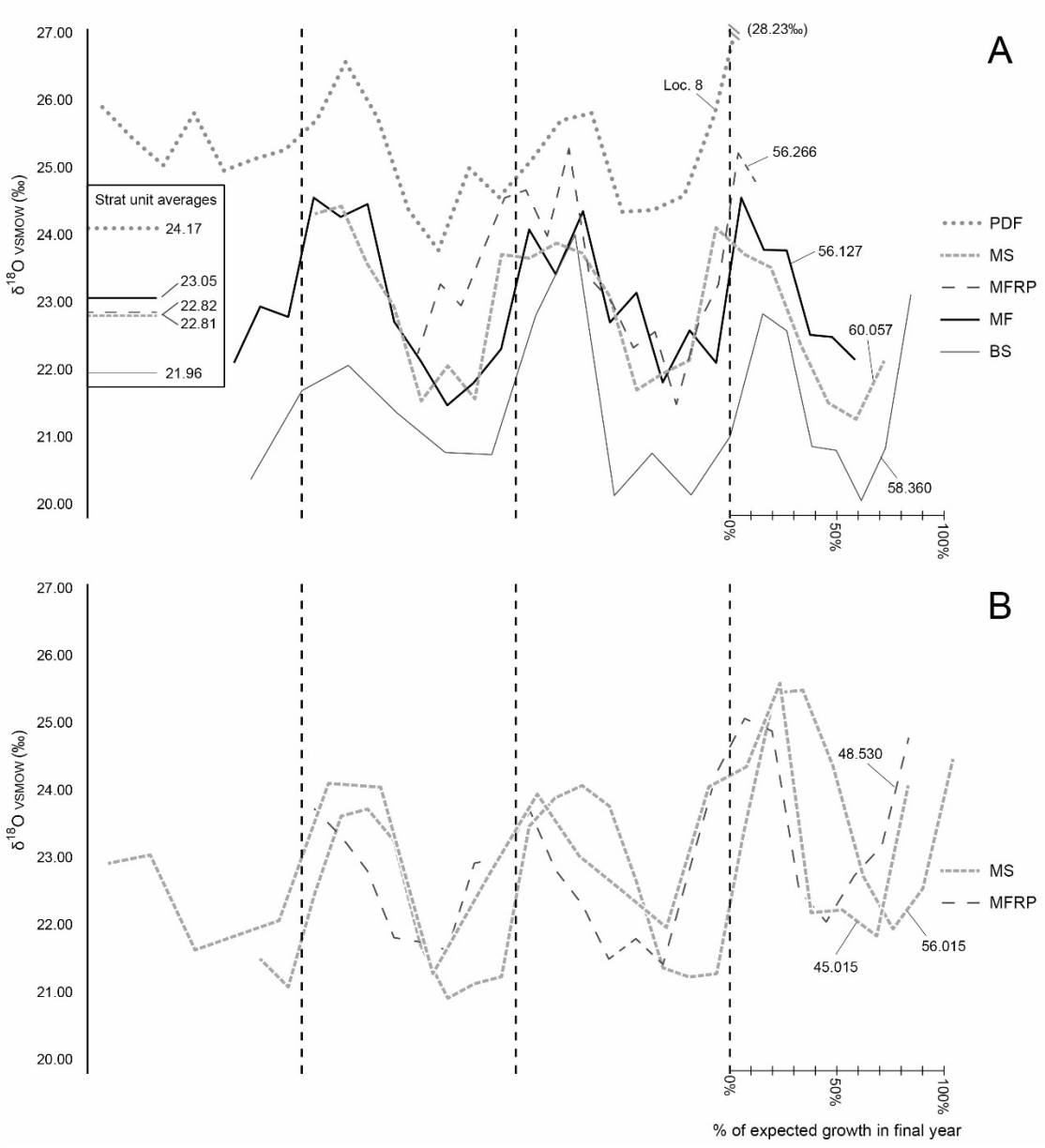
A
B
27.00
26.00
25.00
24.00
23.00
22.00
21.00
20.00
δ18O VSMOW (‰)
Strat unit averages
24.17
23.05
22.82
22.81
21.96
(28.23‰)
Loc. 8
56.266
56.127
60.057
58.360
48.530
45.015
56.015
PDF
MS
MFRP
MF
BS
0%
50%
100%
% of expected growth in final year

References

Agenbroad, L. D. 1994. Taxonomy of North American *Mammuthus* and biometrics of the Hot Springs mammoths. In: Agenbroad, L. D., Mead, J. I. (Eds.), The Hot Springs Mammoth Site. The Mammoth Site, Hot Springs, South Dakota, pp. 158–207.

Barbour, E. H. 1931. The American mastodon with mandibular tusks. Nebraska State Museum Bulletin 19(1), 163–170.

Bocherens, H. 2003. Isotopic biogeochemistry and the paleoecology of the mammoth steppe fauna. In: Reumer, J. W. F., de Vos, J., Mol, D. (Eds.), Advances in Mammoth Research, Deinsea 9, 57–76.

Black, B. A. 2009. Climate-driven synchrony across tree, bivalve, and rockfish growth-increment chronologies of the northeast Pacific. Marine Ecology Progress Series 378, 37–46.

Bunn, A. G. 2008. A dendrochronology program library in R (dplR). Dendrochronologia 26, 115–124.

Butler, P. G., Wanamaker, A. D., Scourse, J. D., Richardson, C. A., Reynolds, D. J. 2013. Variability of marine climate on the North Icelandic Shelf in a 1357-year proxy archive based on growth increments in the bivalve *Arctica islandica*. Palaeogeography, Palaeoclimatology, Palaeoecology 373, 141–151.

Cherney, M. D., Fisher, D. C., Rountrey, A. N., Calamari, Z. T. 2012. Isotope analyses support use of CT scans for identifying annual increments in Snowmass mastodon mandibular tusks. Journal of Vertebrate Paleontology, Supplement, 72nd Annual Meeting, Program and Abstracts, 77.

Cook, E. R., Peters, K. 1981. The smoothing spline: a new approach to standardizing forest interior tree-ring width series for dendroclimatic studies. Tree-ring Bulletin 41, 45–53.

Creber, G. T. 1977. Tree rings: a natural data-storage system. Biological Reviews 52, 349–383.

Dansgaard, W. 1964. Stable isotopes in precipitation. Tellus 16, 436–468.

DeNiro, M. J. 1985. Postmortem preservation and alteration of in vivo bone collagen isotope ratios in relation to palaeodietary reconstruction. Nature 317, 806–809.

DeNiro, M.J., Epstein, S. 1981. Influence of diet on the distribution of nitrogen isotopes in animals. Geochimica et Cosmochimica Acta 45, 341–351.

Dettman, D. L., Flessa, K. W., Roopnarine, P. D. Schöne, B. R., Goodwin, D. H. 2003. The use of oxygen isotope variation in shells of estuarine mollusks as a quantitative record of seasonal and annual Colorado River discharge. Geochimica et Cosmochimica Acta 69, 1253–1263.

Douglass, A.E. 1920. Evidence of climatic effects in the annual rings of trees. Ecology 1, 24–32.

El Adli, J. J., Cherney, M. D., Fisher, D. C., Harris, J. M., Farrell, A. B. and Cox, S. M. 2015. Last years of life and season of death of a Columbian mammoth from Rancho La Brea. In: Harris, J. M. (Ed.), La Brea and beyond: The paleontology of asphalt-preserved biotas, Natural History Museum of Los Angeles County, Science Series 42, pp. 65-80.

Enk, J., Debruyne, R., Devault, A., King, C. E., Treangen, T., O'Rourke, D., Slazberg, S. L., Fisher, D., MacPhee, R., Poinar, H. 2011. Complete Columbian mammoth mitogenome suggests interbreeding with woolly mammoths. Genome Biology 12, R51, 1–8, doi:10.1186/gb-2011-12-5-r51.

Falconer, H. 1857. On the species of mastodon and elephant occurring in the fossil state in Great Britain. Part 1. *Mastodon*. Quarterly Journal of the Geological Society of London 13, 307–360.

Fisher, D. C. 1987. Mastodont procurement by Paleoindians of the Great Lakes region: hunting or scavenging? In: Nitecki, M.H., Nitecki, D. V. (Eds.), The Evolution of Human Hunting. Plenum Press, New York, pp. 309–421.

Fisher, D. C. 1988. Season of death of the Hiscock mastodonts. In: Laub, R. S., Miller, N. G., Steadman, D. W. (Eds.), Late Pleistocene and Early Holocene Paleoecology and Archaeology of the Eastern Great Lakes Region. Bulletin of the Buffalo Society of Natural Sciences 33, 115–125.

Fisher, D. C. 1996. Extinction of proboscideans in North America. In: Shoshani, J., Tassy, P. (Eds.), The Proboscidea: Evolution and Palaeoecology of Elephants and Their Relatives. Oxford University Press, Oxford, pp. 296–315.

Fisher, D. C. 2008. Taphonomy and paleobiology of the Hyde Park mastodon. In: Allmon, W.D., Nester, P.L. (Eds.), Mastodon Paleobiology, Taphonomy, and Paleoenvironment in the Late Pleistocene of New York State: Studies on the Hyde Park, Chemung, and North Java Sites. Palaeontographica Americana 61, 197–290.

Fisher, D. C. 2009. Paleobiology and extinction of proboscideans in the Great Lakes region of North America. In: Haynes, G. (Ed.), American Megafaunal Extinctions at the End of the Pleistocene. Springer, Dordrecht, pp. 55–75.

Fisher, D. C., Beld, S. G., Rountrey, A. N. 2008. Tusk record of the North Java mastodon. In: Allmon, W. D., Nester, P. L. (Eds.), Mastodon Paleobiology, Taphonomy, and Paleoenvironment in the Late Pleistocene of New York State: Studies on the Hyde Park, Chemung, and North Java Sites. Palaeontographica Americana 61, 417–463.

Fisher, D. C., Fox, D. L. 2003. Season of death and terminal growth histories of Hiscock mastodons. In: Laub, R. S. (Ed.), The Hiscock Site: Late Pleistocene and Holocene

Paleoecology and Archaeology of Western New York State. Bulletin of the Buffalo Society of Natural Sciences 37, 83–101.

Fisher, D. C., Fox, D. L. 2006. Five years in the life of an Aucilla River mastodon. In: Webb, S. D. (Ed.), First Floridians and Last Mastodons: The Page-Ladson Site in the Aucilla River. Springer, Dordrecht, pp. 343–377.

Fisher, D. C., Fox, D. L., Agenbroad L. D. 2003. Tusk growth rate and Season of death of *Mammuthus columbi* from Hot Springs, South Dakota, USA. In: Reumer, J.W.F., De Vos, J., Mol, D. (Eds.), Advances in Mammoth Research (Proceedings of the Second International Mammoth Conference, Rotterdam, May 16-20 1999). Deinsea 9, 117–133.

Fritts, H. C. 1976. Tree Rings and Climate. Academic Press, New York, 567 pp.

Gaebler, O. H., Vitti, T. G., Vukmirovich, R. 1966. Isotope effects in metabolism of ^{14}N and ^{15}N from unlabeled dietary proteins. Canadian Journal of Biochemistry 44, 1249–1257.

Graham, R. 1986. Descriptions of the dentitions and stylohyoids of *Mammuthus columbi* from the Colby Site. In: Frison, G. C., Todd, L. C. (Eds.), The Colby Mammoth Site: Taphonomy and Archaeology of a Clovis Kill in Northern Wyoming. University of New Mexico Press, Albuquerque, pp. 171–190.

Green, J. L., Hulbert, R. C., Jr. 2005. The deciduous premolars of *Mammut americanum* (Mammalia, Proboscidea). Journal of Vertebrate Paleontology 25, 702–715.

Hay, O. P. 1914. The Pleistocene mammals of Iowa. Iowa Geological Survey Annual Reports 23, 1–662.

Haynes, G. 1991. Mammoths, Mastodonts, and Elephants. Cambridge University Press, Cambridge, 413 pp.

Hobson, K. A., Alisauskas, R. T., Clark, R. G. 1993. Stable-nitrogen isotope enrichment in avian tissues due to fasting and nutritional stress: implications for isotopic analysis of diet. The Condor 95, 388–394.

Kerr, R. 1792. The animal kingdom or zoological system, of the celebrated Sir Charles Linnaeus …, London [complete citation, together with C. Linnaeus and J.F. Gmelin, in Osborn, H.F., 1936. Proboscidea. The American Museum Press, New York, p. 782].

Klein, R. G., Cruz-Uribe, K. 1984. The Analysis of Animal Bones from Archaeological Sites. The University of Chicago Press, Chicago, xii+266 pp.

Koch, P. L. 1998. Isotopic reconstruction of past continental environments. Annual Review of Earth and Planetary Sciences 26, 573–613.

Koch, P. L., Fisher, D. C., Dettman, D. 1989. Oxygen isotope variation in the tusks of extinct proboscideans: A measure of season of death and seasonality. Geology 17, 515–519.

Koch, P. L., Fogel, M. L., Tuross, N. 1994. Tracing the diets of fossil animals using stable isotopes. In: Lajtha, K., Michener, B. (Eds.). Stable Isotopes in Ecology and Environmental Science. Blackwell Scientific Publications, Oxford, pp. 63–92.

Koch, P. L, Tuross, N., Fogel, M. L. 1997. The effects of sample treatment and diagenesis on the isotopic integrity of carbonate in biogenic hydroxylapatite. Journal of Archaeological Science 24, 417–429.

Koch, P. L., Hoppe, K. A., Webb, S. D. 1998. The isotopic ecology of late Pleistocene mammals in North America, Part 1. Florida. Chemical Geology 152, 119–138.

Kohn, M. J., Welker, J. M. 2005. On the temperature correlation of $\delta^{18}O$ in modern precipitation. Earth and Planetary Science Letters 231, 87–96.

Laws, R. M. 1966. Age criteria for the African elephant, *Loxodonta a. africana*. East African Wildlife Journal 4, 1–37.

Laxson, T. A. 2011. Geospatial analysis of mean sensitivity in *Pinus strobus*. M.A. dissertation. The University of North Carolina at Greensboro, 121 pp.

Lechler, A. R., Niemi, N. A. 2011. The influence of snow sublimation on the isotopic composition of spring and surface waters in the southwestern United States: Implications for stable isotope-based paleoaltimetry and hydrologic studies. Geological Society of America Bulletin, published on-line September 30, 2011 as doi:http://dx.doi.org/10.1130/B30467.1

Maglio, V. J., 1973. Origin and evolution of the Elephantidae. Transactions of the American Philosophical Society, New Series, 63, 1–149.

Mahan, S. A., Gray, H. J., Pigati, J. S., Wilson, J., Lifton, N.A., Paces, J., Blaauw, M. 2014. A geochronologic framework for the Ziegler Reservoir fossil site, Snowmass Village, Colorado. Quaternary Research 82(3):490-503.

Miller, I. M., Pigati, J. S., Anderson, R. S., Johnson, K. R., Mahan, S. A., Ager, T. A., … Wilson, J. 2014. A high-elevation, multi-proxy biotic and environmental record of MIS 6–4 from the Ziegler Reservoir fossil site, Snowmass Village, Colorado, USA. Quaternary Research 82(3):618-634.

Pigati, J. S., Miller, I. M., Johnson, K. R., Honke, J. S., Carrara, P. E., Muhs, D. R., Skipp, G., Bryant, B. 2014. Geologic setting and stratigraphy of the Ziegler Reservoir fossil site, Snowmass Village, Colorado. Quaternary Research 82(3):477-489.

Pinsof, J. D. 1992. The late Pleistocene vertebrate fauna from the American Falls area, southeastern Idaho. Ph.D. dissertation. Idaho State University, 399 pp.

Rozanski, K., Araguás-Araguás, L., Gonfiantini, R. 1993. Isotopic patterns in modern global precipitation. In: Swart, J. P., Lohmann, K. C., McKenzie, J., Savin, S. (Eds.), Climate Change in Continental Isotopic Records. American Geophysical Union, Geophysical Monograph 78, 1–36.

Rountrey, A. N. 2009. Life Histories of Juvenile Woolly Mammoths from Siberia: Stable Isotope and Elemental Analyses of Tooth Dentin. Unpublished dissertation, University of Michigan, xiii+331 pp.

Rountrey, A. N., Fisher, D. C., Vartanyan, S., Fox, D. L. 2007. Carbon and nitrogen isotope analyses of a juvenile woolly mammoth tusk: Evidence of weaning. Quaternary International 169-170, 166–173.

Rountrey, A. N., Fisher, D. C., Tikhonov, A. N., Kosintsev, P. A., Lazarev, P. A., Boeskorov, G., Buigues, B. 2012. Early tooth development, gestation, and season of birth in mammoths. Quaternary International 255, 196–205.

Saunders, J. J. 1970. The distribution and taxonomy of *Mammuthus* in Arizona. Unpublished M.S. thesis, University of Arizona, 115 pp.

Saunders, J. J. 1977. Late Pleistocene vertebrates of the western Ozark Highland, Missouri. Illinois State Museum Reports of Investigations 33, 1–118.

Sharpe, S. E., Bright, J. 2014. A high-elevation MIS 5 hydrologic record using mollusks and ostracodes from Snowmass Village, Colorado, USA. Quaternary Research 82(3):604-617.

Skeels, M. A., 1962. The mastodons and mammoths of Michigan. Michigan Academy of Science, Arts, and Letters, Papers 47, 101–133.

Smith, K. M., Fisher, D. C. 2011. Sexual dimorphism of structures showing indeterminate growth: tusks of American mastodons (*Mammut americanum*). Paleobiology 37, 175–194.

Trapani, J. Fisher, D. C. 2003. Discriminating proboscidean taxa using features of the Schreger pattern in tusk dentin. Journal of Archaeological Science 30, 429–438.

Chapter 3

Identifying left-right pairs in the Ziegler Reservoir mastodon mandibular tusks

Introduction

The Ziegler Reservoir fossil site (ZR) was a small, moraine-bounded, high-elevation, lake in the late Pleistocene Colorado Rockies (Miller et al., 2014, Pigati et al., 2014). American mastodons (*Mammut americanum*) from the ZR represent populations that lived during the Sangamon interglacial (*Chapter 2* – Fisher et al., 2014; Mahan et al., 2014 Miller et al., 2014). Their remains include 27 mandibular and deciduous tusks described previously that were mostly from the lake margin, in and between diamictic slump deposits derived from the surrounding moraine (Pigati et al., 2014). Initial analyses treated these as representing 26 different individuals (2 of the 27, 48.594 and 48.595, were extracted from the same mandible).

In *Chapter 2* – Fisher et al. (2014) proboscidean remains from each of a series of stacked deposits ("Unit 3", Basement Silt (BS), Main Floor (MF), Main Floor Red Pebble (MFRP), Main Silt (MS), Primary Debris Flow (PDF) (Miller et al., 2014)) were thought to

represent a sequential record of regional populations through time. As a consequence, stratigraphic provenance was one of the primary criteria used when counting individuals (i.e. bones found in different sedimentary units were considered to be from different individuals). That interpretation was based on a preliminary taphonomic understanding of site formation that had, at the time, not been thoroughly tested. Early findings were published as a contribution to the Quaternary Research special volume dedicated to the Ziegler Reservoir fossil site (ZR), a high-elevation, late Pleistocene lake/marsh discovered in 2010. Excavation of the reservoir produced over 5,000 macrofossil specimens representing dozens of mastodons, several mammoths, and representatives of a variety of other Pleistocene megafauna. Subsequent identification of 9 possible left-right pairs (7 of which involve tusks associated with different stratigraphic units) demonstrate time-averaging in the assemblage. This new evidence does not negate the idea that bones from higher layers are in general more recent, but it does complicate the chronology of ZR lake-margin remains. Here we present support for 9 left-right tusk pairings, reevaluate previously observed temporal patterns, and amend the census of individuals represented by ZR mastodon remains.

Proboscidean tusks (those both in the premaxilla and mandible) are ever-growing incisors composed primarily of dentin that grows through continuous apposition. Growth increment and serial isotope measurements from tusk dentin provide data for

mastodon life-history analyses (e.g., Fisher, 2008; Fisher et al., 2008). Mastodon mandibular (lower) tusks are more compact than premaxillary (upper) tusks and do not typically contain as many years of growth, since much of the tip is lost through abrasion and breakage during an animal's life. Analyses of ZR mastodons focused on these mandibular tusks, which could be more quickly cleaned, dried, and transported than the large upper tusks that were not immediately available for study. Most adult mandibular tusks from ZR retain a record of the final 1-3 decades of life. Because permanent tusks grow throughout life, the final layers of growth preserve information that pertains to circumstances and timing of death.

X-ray computed tomography (CT) of ZR mandibular tusks reveals cyclic patterns of variability in dentin radiodensity that represent annual growth increments (Cherney et al., 2012, 2014; *Chapter 2* – Fisher et al., 2014). Serial linear and volumetric measurements of these CT growth increments were used to determine growth rates, ontogenetic stages, sex, and season of death for many of the ZR tusks. Comparisons of multiyear patterns of growth provided a possible way to test the hypothesis that remains represent simultaneous deaths of multiple individuals, since individuals living in the same environment through the same years are expected to display similar profiles. However, this test depends on measurement precision being greater than annual variability. Comparing records from the two tusks of one individual provides a way to

determine if measurement precision is up to the task. Since two tusks from the same individual are likely to record more similar growth patterns than two tusks from different individuals, we cannot expect measurements of patterns to match for two individuals living at the same time in the same place any better than they do in the two tusks of a single individual.

Stable isotope profiles of oxygen ($\delta^{18}O$) reported for ZR mastodon mandibular tusks displayed consistent seasonal variation (*Chapter 2* – Fisher et al., 2014). Meanwhile, average values and detailed multiyear patterns were sometimes significantly different for different tusks. Based on the assumption that mastodon remains from stratigraphically higher layers represented individuals that died more recently, *Chapter 2* – Fisher et al. (2014) suggested that an up-section increase in average tusk dentin carbonate $\delta^{18}O$ was a reflection of changing regional climate through time. Similarity in multiyear records of three tusks was cited as possible evidence of simultaneous deaths that would support catastrophic death scenarios that had been proposed to explain the mass assemblage.

Left-right tusk pair identifications below are supported by similarities in size, shape, wear, surface erosion characteristics, CT features, growth profiles, locations of desiccation fractures, and stable isotope records. Pairs were designated on the basis of how closely they matched relative to the total range for the assemblage. Most

comparisons were both obvious enough in light of other supporting data and sufficiently complex that quantitative statistical approaches seemed unnecessary and impractical. Some details, such as isotope ratios, start as quantified data, and might therefore seem ideal for statistical comparison. However, differences in sampling schemes for some paired tusks (different numbers of samples per year) and apparent presence of differential diagenetic effects in different tusks make even these comparisons complicated to process statistically. This appears to be a situation where displaying the actual specimens side-by-side provides a more intelligible and comprehensive comparison than statistical approaches that focus on only some components of the data. Statistical models could enhance results, but only with substantial effort for little gain.

In two cases, the proposed pair involves tusks from the same stratigraphic unit. Morphological anomalies confounded recognition of one of these pairs. In the second case, independent selection of each tusk for a different type of analyses led to them being mistakenly treated as different individuals when substantial evidence points to their shared genetic origin. The remaining 7 pairs combine tusks from different stratigraphic units. Strength of evidence for pairing is variable, but in all cases involving permanent mandibular tusks (7), we consider it fairly conclusive.

Two sets of deciduous tusks are supported only by general morphology, stage of growth, and extent of wear. Both pairs combine tusks that were found widely separated in the assemblage and in different stratigraphic units. We treat these as possible pairs, but the evidence is inconclusive. Five confidently identified left-right pairs linking different stratigraphic units impel us to reconsider the temporal integrity of ZR stratigraphy and stratigraphic identifications of specimens in question. Three pairs sourced from adjacent units merely reinforce the previous suggestion that at least some adjacent units might not be as temporally and stratigraphically distinct from each other as originally treated. Two pairs were identified among specimens from distant stratigraphic units and provide evidence of more extreme time-averaging across distinct layers.

Materials

The ZR proboscidean assemblage is described in more detail elsewhere (*Chapter 2* – Fisher et al., 2014). Here we revisit discussion of the mastodon mandibular tusks with a focus on 18 tusks previously considered to belong to 18 different individuals (30.017, 30.076, 30.130, 33.238, 44.146, 45.015, 48.530, 56.015, 58.025, 58.032, 58.360, 63.125, 63.170, 64.013, 68.032, 68.050, 71.092, 82.179) that instead represent left-right pairs for as few as 9 individuals (Table 3.1). All 18 tusks considered here were found

separated from their source mandibles. Seven of the tusks (33.238, 58.032, 58.360, 64.013, 68.032, 68.050, and 71.092) were not recovered *in situ* and lack precise coordinates, but were confidently assigned a stratigraphic association in the field. Five of these (33.238, 58.032, 58.360, 68.050, and 71.092) were marked as "float" indicating that they were either recovered from nearby spoil piles or as the backhoe was assisting with removal of overburden. The other two (64.013 and 68.032) were not marked as "float" and were therefore reportedly found *in situ* but not measured in place prior to collection.

This report and direct implications of it are limited to basal through middle lake-margin units represented by mastodon mandibular tusks; most ZR mastodon remains came from these deposits.

Methods

Specimen treatment

Detailed description of field documentation was reported previously (*Chapter 2* – Fisher et al., 2014). The number preceding the decimal in field numbers refers to the reference stake used for measuring site coordinates. Thus, specimens with the same number or numbered for adjacent stakes were found in the same general area. Specimens spotted in spoil piles or when heavy machinery was being used to move

large volumes of sediment were marked "float" and collected without logging precise field position. Stratigraphic associations for float specimens were recorded only when a confident association could be made (pers. comm., Carol Lucking).

In the field, small elements such as mandibular tusks were promptly removed from the sediment (after recording location) and placed into sealed plastic bags to prevent desiccation prior to cleaning. At an offsite facility, they were washed and photographed before being returned to plastic bags to begin a slow process of controlled drying.

MicroCT scanning

CT methods are detailed more thoroughly in *Chapter 2* – Fisher et al. (2014). Briefly, CT scans used to analyze ZR specimens were produced by the MicroCT Core facility in the University of Michigan School of Dentistry on a SCANCO Medical µCT100 operating at 90kV, 78µA, and 500 ms, yielding uniform cubic voxels 40–60 µm on a side. Most tusks had to be scanned in multiple parts and then reassembled virtually. CT scans were processed in Amira 5.4.1. Volumetric measurements were acquired using Amira, but linear measurements were taken from 2D projections of virtual slices (extracted from the CT data) in ImageJ using IncMeas 1.3c (Rountrey, 2009).

Morphological comparisons

Tusks were compared based on complementarity of overall size and shape, as well as wear patterns and fine-scale surface features. Abrasion from use determines the morphology of the distal ends of mandibular tusks. Since these lower tusks are closely spaced (often abutting medially) they act to some extent in tandem as a "dental battery" that forms a continuous wear facet across the anterior surfaces of each tusk. When distal ends are present, paired tusks should have complementary wear facets. The primary wear facet is expected to face anterodorsally as displayed in 44.035 (see *Chapter 2*, Figure 2.1)

Another characteristic of the distal portion of tusks is referred to here a "gingival furrow" (GF). GFs are shallow channels in the cementum oriented transversely with a slight angle so that the medial side of each groove is located more distally than the lateral side. They are most prominent on the dorsal and ventral surfaces of a tusk, just anterior to where the tusk erupts from the gingiva. GFs are apparently an effect of chemical abrasion of cementum at or near the gingival margin. The grooves are the low points in topographical undulations that appear to result from either differential rates of chemical dissolution (perhaps due to seasonal dietary changes) or from more or less constant rates of dissolutions at the margin with varying rates of eruption that result in more thorough erosion when eruption rates are slower. GFs in ZR mandibular tusks are only present within a few centimeters distal to the gingival margin; they fade out more

distally due to smoothing from surface polish. When clearly expressed, GFs combined with tusk curvature and/or tip-wear angles (both of which can indicate a tusk's dorsoventral orientation – see *Chapter 2*, Figure 2.1) provide a clear indication of tusk side.

A second erosive feature provides a minor corroboration of many tusk-pair identifications is cavitation that consistently occurs on the medial surfaces of tusks, where they meet the opposing tusk from the other side of the mandible. The origin of these features is not perfectly clear, but they appear to be a common pattern of chemical erosion in these tusks. Combined with either curvature or tip wear, medial dissolution features can help identify tusk side when GFs are not present. Medial dissolution features could occur in the same locations on matching tusks if due to a common erosive source, but they are not features that are expected to match perfectly in paired tusks.

Growth feature comparisons

Three linear measurements from each annual radiodensity increment provide a measure of growth we call "estimated increment volume" (EIV), which closely approximates actual increment volume in ZR mandibular tusks (*Chapter 2* – Fisher et al., 2014). The final increment is assumed to represent only a fraction of the final year (FFY) of growth. FFY is a seasonally neutral approximation of the time of year the animal died

(*Chapter 2* – Fisher et al., 2014). FFYs reported here refer to the 3rd of the approximation methods described in *Chapter 2* – Fisher et al. (2014) (Table 2.1) that uses a 5-year trend in EIVs to establish expected growth in the final year.

Periradicular features (El Adli et al., 2015) are the surface manifestation of deflections along the cementum-dentin junction that occur on different scales, but are most prominent as annual annuli on the outer surface near the base of a tusk root. These features parallel other variations in annual growth, but reflect a particular unique combination of growth variables, possibly resulting from the interaction of dentin apposition rate and tusk eruption rate, and thus contain growth information not recorded in other features. Periradicular features formed in different tusks and during different years are not identical. The pattern contained in series of these topographical features provides a tusk characteristic related to an individual's growth history that can contribute to pair identifications.

Structural comparisons

Qualitative features of tusk structure provide some additional data for tusk comparisons. Though the expression of annual increments in microCT scans is fairly consistent in ZR mandibular tusks, variations do exist, between tusks and between individual years within each tusk. Similar qualities in different tusks, such as indistinct features or matching patterns of lower and higher density years of dentin growth,

provide a line of support for tusk pairings. Also visible in CT scans are cementum thickness over the entire tusk length, deflections at the cementum-dentin junction (CDJ) associated with periradicular features, and locations of internal desiccation cracks. Each of these enable detailed qualitative comparisons that in some cases provide overwhelming evidence of genetic equivalence. Although pulp cavities can be assessed externally, 2D longitudinal slices from CT scans provide a way to easily compare the shape and depth of pulp cavities at the time of death as well as earlier in an individual's life, since annual growth features display the shape of the pulp cavity surface during previous years of growth.

Stable isotope analysis

All isotope data referenced here are also documented in *Chapter 2* – Fisher et al. (2014). Methods for isotope analysis are described in that paper. Anticipating the possibility that one tusk pair ([58.360, 82.179]) belonged to the same individual, we replicated the sampling process used for the final two years in 58.360 when analyzing 82.179. In both cases, the penultimate year was divided into 5 approximately equal parts and the final year into 7 parts. Powder samples were collected from both tusks using a manually-controlled milling station with a 0.5 mm carbide burr and were pretreated for carbonate analysis following methods described in Rountrey (2009). Samples from these

two years in each tusk are "equivalent" to the precision this sampling method provides. Isotope results are reported in delta notation relative to VSMOW ($\delta^{18}O$) and VPDB ($\delta^{13}C$).

Results

Tusk comparisons

I identify 7 left-right pairs in the assortment of 21 permanent mandibular tusks and 2 additional potential pairs in the 6 deciduous tusks described in the initial report on ZR mastodons (*Chapter 2* – Fisher et al., 2014). One damaged permanent tusk (45.015), 2 pathological tusks (30.017, 33.238), and all 4 deciduous tusks (44.146, 68.032, 68.050, 71.092) lacked features needed to determine left-right identity. The two pathological specimens were identified as a pair. Each of the other tusks was matched with one previously and independently identified as being from the opposite side. Combinations consist of specimens that for the most part have very similar external morphologies, consistent growth patterns, and matching internal structures. Overlapping growth increment (EIV) series for matched tusks do not display exactly the same year-to-year patterns of variation (though in some cases they are close), but for the most part have similar averages and general trends. Two proposed left-right pairs link tusks that in our initial report had significantly different EIV series. In the first of these pairs ([30.017, 33.238]), trauma-induced anomalies appear to have altered growth

in different ways for each tusk. Discrepancies in the second pair ([63.125, 56.015]) are likely due to relatively indistinct annual CT features in those tusks, which are confidently matched here based on other data. Where carbonate isotope profiles are available for comparison ([58.360, 82.179], [63.125, 56.015], and [45.015, 48.530]), paired series are remarkably consistent for overlapping years, especially in terms of oxygen values. Each attribute used for comparison showed a significant range of variability in the assemblage.

[30.017, 33.238].

This tusk pair consists of tusks that did not previously have secure side identifications. The side represented by each tusk is here based on an interpretation of dorsally-concave curvature in lateral profile, combined with the presence of matching erosion on medial surfaces. Both were associated in the field with the Main Silt (MS) unit, even though the precise location of 33.238 was not recorded. Tusks have similar dimensions and both specimens exhibit wear postdating traumatic fractures that removed their distal ends. Nonconical growth features are evidence of additional trauma affecting the dental pulp earlier in growth record (Figure 3.1-4). 30.017 has an abrupt bend about halfway along its total length consistent with the tusk at some point being partially dislodged from its alveolus and subsequently resuming growth in a slightly different orientation. Both had nonconical (deformed) pulp cavity surfaces throughout

much of their recent growth (as visible in CT – Figure 3.4), which were probably deformities due to trauma. The pulp cavity of 30.017 reestablished a more conical shape close to the time of death. Both tusks have a conspicuous constriction occurring in their 3rd to last full year of growth. For the first part of overlapping EIV growth series, tusk records are similar (Figure 3.5). About half way through the sequence of years represented in 30.017, its EIVs increase dramatically as it gradually establishes a more conical pulp cavity, while the same years trend slightly downward at the end of the 33.238 record. Different FFYs reported previously (*Chapter 2* – Fisher et al., 2014) resulted from difficulty pinpointing the final feature in 33.238. Upon further inspection, it is clear that both tusks have indistinguishable FFYs around 40-50 %. The extent of damage in 30.017 as well as its growth series approaching adult male range for the last portion of its record (the only part of either record seemingly unaffected by pathological growth) are consistent with this representing an adolescent male (as described in *Chapter 2* – Fisher et al. (2014)) with a particularly violent history. 33.238 was previously thought to represent an adult (possibly senescent) female, but is now recognized as an adolescent male with severe traumatic pathologies.

[30.130, 30.076].

Tusks were both found and mapped *in situ* and were associated with adjacent stratigraphic units (Main Silt and Primary Debris Flow (PDF)) in the field. Both tusks have

features that were used to assign them to a side prior to their recognition as a pair. The left tusk, 30.130, has the typically upturned dorsoventral curvature with clear GFs (see *Methods: Morphological comparisons* for description of this feature), and cavitation on its medial surface that mirrors the pattern of medial cavitation in the right tusk, 30.076. Specimen 30.076 is curved similarly to 30.130, but is missing its distal portion where GFs would be located. Overall morphology is very similar, differing moderately only in transverse-section shape, with 30.076 being approximately round and 30.130 being somewhat mediolaterally compressed (Figures 3.6, 3.7). Density features and other attributes visible in CT scans are highly congruent. Even fractures occur mostly in similar locations, which suggests they have the same 'weak' spots due to compositional changes during growth (Figure 3.8). Patterns of periradicular features at the proximal ends of the tusks are essentially identical (Figure 3.9). EIV series match closely (Figure 3.10) and FFYs for both indicate death near the end of an annual cycle (Table 3.1).

[45.015, 48.530]

Tusks were both found and mapped *in situ* and were associated with adjacent stratigraphic units (MS and Main Floor Red Pebble (MFRP)) in the field. Specimen 48.530 can be independently identified as a right tusk, based on the characteristically upturned dorsoventral curvature with significant cavitation as is typical for the medial surface. Its tip is too damaged to assess orientation of GFs. The opposite tusk, 45.015 has no

evident dorsoventral curvature and is also missing the tip along with any sign of GFs. It is identified as a left tusk based on the determination that it is the complement to 48.530. The medial erosion pattern in 45.015 mirrors that present on 48.530 and both have similar circumferences (Table 3.1). Both tusks are very circular in transverse cross-section with 45.015 becoming slightly dorsoventrally compressed at the proximal end (Figures 3.11, 3.12). Patterns of periradicular topographic features on the exterior surface of the proximal ends are highly consistent (Figure 3.13). CT scans of each tusk have relatively obscure annual density features but also numerous desiccation fractures corresponding to low density portions each year. Other features visible in CT including cementum thickness and annually occurring deflections at the cementum dentin junction (CDJ) are also consistent (Figure 3.14). Interannual variations in tusk EIV profiles do not match precisely, but general EIV range and trends are almost identical for overlapping years (Figure 3.15). Differences in patterns of year-to-year fluctuations probably result from difficulty in precisely identifying year boundaries in this pair of tusks. Carbonate oxygen isotope profiles for the last 3 years of each tusk record are nearly identical – so similar that they were previously considered to represent possibly contemporaneous individuals based on this alone (Figure 3.16). Carbonate carbon isotopes are much less consistent (in fact, the least consistent between proposed pairs with isotope data), but show signs of significant diagenetic alteration as is common for

ZR remains (Figure 3.17). FFY for each indicates death most of the way into an annual cycle (Table 3.1).

[58.032, 58.025]

Although 58.032 was marked as "float," and therefore not found *in situ*, both tusks were field associated with the MS stratigraphic unit. Based on slightly upturned dorsoventral curvatures, significant medial erosion features, anterodorsally oriented primary wear facets at the tips, and normally-angled GFs, tusks can be confidently assigned to their respective sides. The distal portions of the tusks are near mirror images of each other with the same angle of tip wear, curvature, diameter, pattern of GFs, and medial erosion pattern (Figures 3.18, 3.19, 3.20). CT scans of both tusks reveal similar cementum thicknesses, expressions of annual density features, and locations of desiccation fractures (Figure 3.21). Overlapping portions of EIV records match in terms of general range and trends but not in terms of interannual patterns of variation (Figure 3.22). Isotope data are not available from both tusks for comparison.

[58.360, 82.179]

The left tusk, 58.360, was marked as "float," and therefore not found *in situ*, but was confidently associated with the Basement Silt (BS) stratigraphic unit based on field observations. Its right-side complement, 82.179, was mapped in the field as being from MS, a unit separated from BS by a diamictic slump deposit, which consists of the Main

Floor (MF) and overlying MFRP. Neither tusk has significant dorsoventral curvature, but their side identifications are reasonably well established based on the presence of erosion on medial surfaces and anterodorsal orientation of the primary wear facet. Both tusks have almost identical morphologies including some medially oriented curvature not seen in any of the other ZR mandibular tusks. The distal end of each tusk is partly worn smooth, though not as polished as on many of the others, suggesting both tips were broken not long before the animal's death. The tip of each tusk has a similar wear pattern with a small ventral facet and larger anterodorsal facet. (Figures 3.23, 3.24). Periradicular topographic features are only subtly expressed in both tusks, but GFs clear in both match closely (Figure 3.25). CT scans of each are also nearly identical. They show the same number of annual density features, which are conspicuous for the final 5-6 years of growth and less clear in the earlier record of each tusk. Compared at equivalent distances from the pulp cavity surface, growth-line angles in each tusk are equivalent. In both tusks, annually occurring deflections at the CDJ are more pronounced for the final three repetitions than all earlier occurrences. Of those final three, the middle one is most pronounced in both tusks (Figure 3.26). The EIV series is consistently slightly higher in 58.360 than 82.179, but profiles follow similar increasing trajectories and appear to represent equivalent ontogenetic intervals (Figure 3.27). FFYs for both tusks are close to 100 % indicating death late in an annual cycle (Table 3.1). Carbonate $\delta^{18}O$ profiles for

58.360 and 82.179 are approximately equivalent where they overlap in the final two years. The earliest 6 samples in each record are nearly identical. For the final portion of each series, where sampling was close to the exposed pulp cavity surface, $\delta^{18}O$ values for 82.179 follow an increasing trend while corresponding measurements for 58.360 do not (Figure 3.28). Carbonate $\delta^{13}C$ records for 58.360 and 82.179 are fairly congruent considering the amount of variation in ZR mandibular tusk $\delta^{13}C$. For the overlapping interval (excluding each final sample, which represents the exposed surface of the pulp cavity), the record for 82.179 is consistently enriched compared to that of 58.360 (Figure 3.29).

[63.125, 56.015]

Both tusks were found and mapped *in situ*. The left tusk, 63.125, was associated with the Main Floor Red Pebble unit, while the right tusk, 56.015, was associated with the Main Silt. With considerable erosion that formed significant GFs, clear erosion on the medial surface, and intact anterodorsally oriented primary wear facets, the side of each tusk had been confidently determined. Both tusks have the same dimensions, are nearly straight, and taper proximally with shallow pulp cavities that indicate a late stage of growth (Figures 3.30, 3.31, 3.32). CT scans did not include the axis of either tusk, which made annual features difficult to measure and compare. However, pattern of desiccation fractures, expression of annual density features, and thickness of cementum are all

nearly equivalent (Figure 3.32). EIVs only match in terms of general averages, but measurements for multiannual patterns of both tusks were hampered by obscure year boundaries in CT (Figure 3.33). Dentin carbonate $\delta^{18}O$ profiles for the last three years of growth in both tusks are almost identical for two years and then diverge slightly for the third (Figure 3.34). Carbonate $\delta^{13}C$ profiles display very similar patterns with values for 56.015 consistently enriched by about 1-1.5 ‰ compared to those for 63.125 (Figure 3.35).

[63.170, 64.013]

Although both tusks were apparently found *in situ* and associated with different stratigraphic units (63.170 – MFRP; 64.013 – BS) separated by one of the major diamictic slump deposits (MF), a precise location was not recorded in the field for 64.013. Each specimen consists only of the distal tip but contains enough of the GFs and primary wear facet to determine which side it came from. They have nearly the same circumference, shape in transverse cross-section, and angle of the distal wear facet (Table 3.1; Figures 3.36, 3.37). CT scans are not particularly clear for either tusk, but measured EIVs have similar year-to-year variations, general ranges, and trends (Figure 3.38).

[68.032, 44.146]

Both deciduous tusks were reportedly found *in situ,* but 68.032 was not mapped in the field. They were field-associated with stratigraphic units more widely separated than for any other pair described here (68.032 – 'Unit 3'; 44.146 – MS). Left and right designations for ZR deciduous tusks are uncertain, but 68.032 and 44.146 appear to be from opposite sides. Each tusk is a near identical mirror image of the other in overall morphology (Figures 3.39, 3.40). The same amount of growth after the neonatal line feature in CT scans and congruent wear at the distal tip together indicate the same age of death for each tusk (Figure 3.41).

[68.050, 71.092]

Both deciduous tusks were marked as "float" indicating that they were not found *in situ*. They were field-associated with adjacent stratigraphic units (68.050 –BS; 71.092 – MF). Left and right designations for ZR deciduous tusks are uncertain, but 68.050 and 71.092 appear to be from opposite sides. Each tusk is a nearly identical mirror image of the other in overall morphology for the overlapping portions present. Both tusks also have one periradicular feature the same distance from its distal tip that is associated with its neonatal line. (Figures 3.42, 3.43). The same amount of growth after the neonatal line feature in CT scans and congruent wear at the distal tip together indicate the same age of death for each tusk (Figure 3.44).

Discussion

Morphological and compositional similarities provide convincing evidence of 7 left-right pairs of permanent mandibular tusks and some support for two pairings of deciduous tusks in the mastodon assemblage reported in *Chapter 2* – Fisher et al. (2014). In 7 of these 9 instances, the pair consists of tusks that were each associated with a different depositional unit in the near-shore stratigraphy of ZR. These stratigraphic units represent independent slump events and intervening sedimentation through time (Pigati et al., 2014). Association with one of these events via incorporation into its resulting deposit was initially considered ample justification for considering a tusk genetically distinct from any tusk found in a different unit (*Chapter 2* – Fisher et al., 2014). However, detailed consideration of external morphologies, CT scans, and isotopic compositions provide enough verification of proposed combinations to override the stratigraphic evidence for the independence of at least some of these proposed pairs.

Time averaging in ZR near-shore deposits

Rather than accept this evidence of time-averaging as sufficient cause to abandon the possibility of observing change through time in the stratigraphic sequence, we propose a less well constrained chronological succession for specimens from ZR nearshore deposits. With a few exceptions, left-right associations described here link tusks found near each other, either in the same stratigraphic unit or in adjacent units

(Figure 3.45). Such pairs have already been accommodated by the assertion in *Chapter 2* – Fisher et al. (2014) that not all of the units are necessarily as distinct as original treatments suggested. Even in the early stages, we entertained the idea that the three "Main" units might be genetically linked as three parts of one normally-graded flow deposit. Other strata above and below could also be lumped in the same way to yield as few as three genetically distinct units ("Basement," "Main," and "Primary") containing the bulk of mastodon bones. So although these combinations modify census data and affect statistical treatments in important ways (see Figures 3.46, 3.47, 3.48), it is really only pairs linking more distant units that provide a substantive challenge to the integrity of chronologies based on stratigraphic association.

Only 3 of the pairs link non-adjacent units from clearly distinct deposits, and 1 of these is a marginally confident grouping of deciduous tusks. Each of the other 2 includes 1 specimen that was not assigned map coordinates in the field. Field measurements were typically not taken when specimens were found in spoil piles or when they became inadvertently dislodged from the matrix while digging with imprecise implements such that they could not be replaced *in situ* for measurement (this procedural description is based on personal experience during participation in the dig). There is a temptation to discredit stratigraphic associations for unmapped specimens. After all, in one of the cases where permanent tusk combinations link specimens from

separated stratigraphic units, one unmapped specimen is even marked as "float" indicating that it was not found *in situ*, but instead was either discovered in a spoil pile or when heavy machinery was being used to remove overburden.

Tusk pairs proposed here indicate either that some stratigraphic identifications were in error, or that ZR near-shore deposits contain some time-averaging. Acknowledging that both options are defensible, I take the conservative approach of accepting field associations made by dig supervisors who assigned stratigraphic associations to "float" specimens only when it could be done confidently, and then modifying interpretations only as necessary to accommodate specific instances of apparent stratigraphic inconsistency. Though they may be a sign of more extensive time averaging in near-shore deposits, the only adjustments necessarily required if we choose to trust reported stratigraphic associations for 58.360 [Basement Silt] and 64.013 [Basement Silt] are reassignment of their complements (82.179 [Main Silt] and 63.170 [Main Floor Red Pebble] respectively) to the Basement Silt. Accepting deciduous tusks 68.032 and 44.146 as a pair, we further have to reassign 44.146 from the Main Silt to Unit 3, but since deciduous tusks lack much growth information, they were excluded from most analyses anyway.

Although putative pairs do not provide rationale for completely abandoning chronological interpretations of site stratigraphy, they do alter the census (Figure 3.46),

season of death pattern (Figure 3.47), and oxygen isotope trends (Figure 3.48) to various extents. The preliminary count in *Chapter 2* – Fisher et al. (2014) was merely to provide a first approximation of the magnitude of the assemblage, and a sense of demographic representation. With most of 5000+ macrofossil remains being from mastodons (many of which are still in field jackets), a comprehensive census has not yet been completed. Pairs determined here have only a minor impact on the previously reported census. The most remarkable attribute of this census, the abundance of juveniles, remains intact.

The season of death analysis based on FFYs for specimens from each stratigraphic unit is affected moderately when accommodating pairs. Whereas the previous interpretation displayed a FFY distribution heavily weighted around 100 %, the modified plot has just equal numbers of individuals in the 50-75 % and 75-100 % ranges. The new pattern that stands out is a predominance of deaths in the second half of the annual cycle with 12 of 16 FFYs greater than 50 %. Rather than supporting a common cause for many of the mastodon deaths at ZR, the new interpretation could simply reflect seasonal use of this high-elevation site.

The reported trend in average annual oxygen isotope values is mostly unaffected by reevaluated chronologies (Figure 3.48). Six of the 17 tusks analyzed for dentin carbonate $\delta^{18}O$ are here combined as 3 pairs. This change lowers the number of individual records to 14 and shifts data for 2 specimens to their newly referred

stratigraphic positions. As long as we consider stratigraphic association to be generally indicative of temporal placement, there remains a considerable up-section enrichment in $\delta^{18}O$. However, recognizing significant diagenetic alteration of some isotope data, differential diagenetic impact according to stratigraphic environment cannot be ruled out as a potential source of the oxygen pattern.

Accepting a time-averaging effect does not necessarily require that we treat the phenomenon as having broad implications for treatment of stratigraphic succession, but it does imply certain properties of the assemblage. The vast majority of ZR mastodon remains are associated with diamictic deposits and were transported some distance downslope along with other debris. If the original resting place for remains was up on shore (whether exposed or buried), displacement of rock, mud, and other debris from the margin of the basin could have incorporated some of the remains, but left the rest on shore where they would have been available for subsequent transport with a later deposit. With additional remains accumulating at the rim of the basin over time, successive flow units would be primarily populated by more recent remains, but could incorporate elements left behind by previous landslides as well.

Gingival erosive features

Most of the ZR mastodon mandibular tusks have a series of about equally spaced shallow transverse grooves near their distal ends. These features appear to be caused by

erosion along the gingival line that had a periodic component, likely being more intense during a particular season. Spacing of gingival line features is therefore apparently determined by growth rate and presents similarly in left-right tusk pairs.

Medial surfaces of most adult ZR mandibular tusks have a sizeable patch of erosion, apparently resulting from chemical dissolution, where they came into close contact with the opposite tusk. These erosive features tend to align and match in severity on the surfaces of left-right pairs. Since matching medial patterns evidence a unique fit between tusk pairs, they in some cases may provide some of the most convincing support for left-right associations. Unlike some other compared parameters, which conceivably could match in individuals of similar size and age living simultaneously in the same environment, this characteristic provides a direct link between tusks that were once positioned adjacent to one another in the same mandible.

Contrasting data from tusks of a single individual

Comparisons between two tusks from the same individual help establish maximum expectation of congruence in the various qualities described for tusks. We cannot expect any two tusks from different individuals to match in morphology, growth records, and composition better than the highly symmetrical left and right permanent mandibular tusks of a single mastodon. In *Chapter 2* – Fisher et al. (2014), similarity of oxygen isotope records was suggested as evidence of different individuals living

contemporaneously. In order for variance between records to be meaningful, differences at least must be greater than those present in left-right pairs. In this way analyses of paired tusks provide a comprehensive range of variation to consider when comparing tusks characteristics.

Differences in interannual variability and FFY between tusk pairs may be due to tusk-specific growth histories. We cannot rule out *a priori* that growth in each tusk could have its own cycle or otherwise be partially independent of systemic control of growth rates (e.g., compensatory growth due to tusk breakage (Fisher, 2008)). If so, one tusk could be growing faster than normal when the other is not. In that case, we would not expect perfect congruence between interannual variability in growth and composition profiles. It is also possible, and perhaps more likely given no direct evidence for asynchronous growth in paired tusks, that differences between reported tusk records are entirely attributable to analytical and measurement error. Whatever the source of inconsistencies reported above, it is clear that interannual variations in EIV measurements for any one ZR mandibular tusk do not necessarily reflect annual-scale changes in the regional environment (even if actual growth variation does).

Since FFYs are based on a prediction, rather than an exact expectation, of growth in the final year, they are necessarily treated as rough estimates. However, they should be similar in tusk pairs since the prediction for growth in the final year is based on the

growth trend in the final years of life that is mostly consistent within pairs. Differences between FFYs of matched tusks (ranging from 0.03 – 0.04 years in revised records; Table 3.1) are within *a priori* expectations for congruent records (in *Chapter 2* – Fisher et al. (2014) FFYs all considered to be "near the completion of the final cycle" ranged from 0.88 – 1.08). Thus, they provide useful comparisons when evaluating seasons of death for the assemblage. However, two significant differences between FFYs of paired tusks motivated a second look at FFY calculations for those tusks. Upon re-evaluation, it was evident that the discrepancies resulted from errors in FFY measurements for one tusk of each pair. The two clearly inaccurate FFYs have been abandoned in this analysis. These mismeasurements highlight the importance of consistently using on-axis measurements and the pitfall of sometimes inconspicuous CT features.

Despite measurement error and the effects of it described above, growth increment (EIV) profiles have some interpretive value. Intra-pair similarity of trends and multiyear averages demonstrates that growth patterns have meaningful variation related to ontogenetic and sexual differences.

Oxygen isotope records are more consistent between left-right pairs than EIV profiles are. Differences may reflect a combination of sampling error, analytical error, and differential diagenetic alteration between tusks. Despite these possible confounding factors, precise serial sampling along growth lines (in most cases with assistance from a

computer-controlled milling station) provided high equivalence between paired profiles for two of the three left-right sets in which each tusk had been analyzed. Prior to identification as a pair, [45.015, 48.530] had been flagged as likely contemporaneous based on similarity of $\delta^{18}O$ profiles. However, differences between records in [58.360, 82.179] show the potential for diagenetic effects to obscure comparisons.

Carbon isotope profiles for paired tusks preserve similarities (Figures 3.29, 3.35) even though they display evidence of substantial diagenetic alteration (*Chapter 2* – Fisher et al., 2014). This suggests that some remnant of the original isotope pattern of variation in carbon isotope values is preserved. Nevertheless, carbon patterns in paired ZR tusks are more different than oxygen data. This variation in $\delta^{13}C$ between genetically linked tusks is consistent with prior conclusions that these records are too altered to be used for meaningful interpretation.

If different stratigraphic units were characterized by different diagenetic regimes, contrasting profiles for paired tusks would corroborate field determinations that link them to different stratigraphic units. Two nearly identical tusks with the same starting compositions exposed to the same depositional environments might be expected to show consistent diagenetic alteration, but those same tusks placed in different depositional environments, possibly at different times (as expected if each unit is a secondary deposit of the remains), would likely display different diagenetic effects.

Taphonomic and chronological implications

One potential impact that these discoveries have on our understanding of the ZR assemblage would be that we cannot treat the interval containing the vast majority of mastodon remains as necessarily containing an ordered chronological record of mastodons occupying the site through the interval of deposition. At a coarse level, most remains from the highest layers may be more recent than those in the lowest layers, but there appears to be some mixing in the series of units that contained mastodon mandibular tusks. This time-averaging must be considered when using the assemblage to investigate changes through time.

Although temporal mixing was not previously detected, it is not particularly surprising. Mastodon remains in the near-shore sediments (particularly those in the stratigraphic interval represented by mandibular tusks) are associated with slump deposits sourced from material that was originally further up on shore (*Chapter 2* – Fisher et al., 2014; Miller et al., 2014; Pigati et al., 2014). Remains associated with a single deposit onshore could transform into a seemingly chronological stack of specimens downslope from the original location if portions of the remains had been moved in multiple events. In that case, portions of a single individual that were moved later could be higher stratigraphically in the secondary deposit than portions that were moved earlier. Allowing for extended time between transport events, during which new

skeletons could accumulate, the sequence could still generally preserve a sampling of populations through time with some 'mixing' between units.

Evidence of time-averaging in these remains means that stratigraphic succession will not necessarily reveal changes (or lack of them) through time. However, we can still consider the possibility that apparent trends represent real temporal patterns that are robust enough to show despite the complications produced by mixing. All that is necessarily required in any further consideration of such hypotheses is that known pairs are treated as both representing the same stratigraphic unit. When field associations for members of a pair are different, both tusks should be attributed to the unit that occurs lower stratigraphically. Doing this with currently available data only reinforces the up-section $\delta^{18}O$ trend by reassigning the unexpectedly low record for 82.179 down to BS and records for 56.015 and 45.015 (both of which bring down the average for MS) down to MFRP (Figure 3.48).

The alternative approach of throwing out all stratigraphic distinctions within the interval is also an option. Taken to its extreme, evidence of time-averaging might be considered to confound all attempts to tie an interpretation to any specific chronology. However, treatment of stratigraphic association in this interval as meaningless would require a new hypothesis to explain the shift in $\delta^{18}O$ values reported in *Chapter 2* – Fisher et al. (2014).

Implications for tests of 'multiple-death' hypotheses

The demographics (sample weighted toward juveniles and prime adults) and depositional features (association with flow deposits) invite consideration of 'catastrophic' multiple-death scenarios to explain at least some ZR mastodon remains (Cherney et al., 2012; *Chapter 2* – Fisher et al., 2014). To some extent evidence of time-averaging in the remains disrupts this narrative by presenting a challenge to the common-cause hypothesis for death (seismically-induced liquefaction resulting in entrapment (*Chapter 2* – Fisher et al. (2014)) and deposition into discreet flow units (seismically-induced slope failure and subsequent transport). If proposed pairs and stratigraphic identifications are correct, then at least some of the remains in the higher "Main" units belonged to animals that died at or before deposition of the lower Basement Silt. This does not by itself falsify catastrophic hypotheses, but the implied complicated taphonomic model will probably make them difficult to test.

Empirically determined measurement error factors must be considered while evaluating multiple-death scenarios. As extended records of interannual variation, tusk growth series (such as EIV records) provide potential for detecting contemporaneous growth between multiple individuals. Büntgen et al. (2014) detected a climate-related response in annual growth of ibex horns. Their data were based on 8043 males with known temporal provenances. Tusks provide an analogous growth system that likely

responds similarly to climate and resource fluctuations. Although the ibex study demonstrated that environment can have a measurable effect on annual growth in certain systems, it is not clear that this effect is consistent enough between individuals that a small sample of tusk records with low interannual growth variability (*Chapter 2* – Fisher et al., 2014) would reveal contemporaneity, even without the confounding effects of diagenesis and analytical error.

Analytical precision of isotope analyses demonstrated through comparisons of $\delta^{18}O$ and $\delta^{13}C$ profiles for paired tusks suggests that we might be able to see similarities between $\delta^{18}O$ records of contemporaneous individuals (possibly even from the same social group) who were utilizing the same water sources over the same years. Perhaps the best chance of detecting simultaneous death is from multi-year isotope records (particularly $\delta^{18}O$) combined with FFY estimates for tusks of different individuals. Based on this, at least one occurrence of simultaneous death involving [63.125, 56.015] and [45.015, 48.530] remains, since specimens 45.015, 48.530, and 56.015 are all identified as having nearly congruent FFY and $\delta^{18}O$ records in Figure 2.15 (*Chapter 2*).

Conclusion

Morphological features, isotope profiles, and growth records support identification of 9 left-right pairs in mandibular tusks previously thought to represent 18

different individuals in the ZR mastodon assemblage. In 7 of the 9 cases, paired specimens each had a different stratigraphic association. These instances of an individual skeleton occurring in multiple, sometimes distant, sedimentary units show that the stratigraphic sequence of mastodon remains is not as chronologically ordered as originally assumed. In spite of this, stratigraphic reassignment of the higher-occurring tusk in each pair to the unit from which the lower-occurring specimen was derived does not diminish the up-section trend toward higher average annual dentin carbonate $\delta^{18}O$ values or the explanation for it proposed in *Chapter 2* – Fisher et al. (2014). Combination of FFY estimates for paired tusks reduces the number of yearend deaths (FFY: 90 – 110 %) from 10 to 6 (Figure 3.47). FFY is still heavily weighted in the second half of the annual cycle across the assemblage in general, but there no longer appears to be a predominance of end-year deaths in the Main Silt. Tusk pairings have a minimal effect on the preliminary census reported in *Chapter 2* – Fisher et al. (2014).

With the discovery that [45.015, 48.530] represents a left-right pair, current support for the occurrence of catastrophic death events at ZR has decreased, since similar isotope profiles from each tusk had been considered the best evidence of two individuals living and dying contemporaneously at the site (*Chapter 2* – Fisher et al., 2014). However, a general consequence of this being a time-averaged assemblage is

that we should now consider all groupings to be possible candidates for simultaneous death instead of limiting such attention to individuals that co-occur stratigraphically.

Comparisons of records separately obtained from left-right pairs provide an upper limit for expected congruence between records from tusks of contemporaneous individuals. Close agreement between isotope profiles of tusks from a single individual demonstrates that sampling and analytical methods used provide adequate precision and accuracy for detecting similar isotope profiles, such as might be expected from mastodons that concurrently occupied the same region. On the other hand, inconsistent EIV patterns from left and right tusks of the same individual suggest that growth increment measurements from CT projections lack the necessary precision and accuracy for comparing fine-scale multiyear fluctuations. EIV series do appear useful for sex determination, analysis of ontogenetic growth sequences, and season of death estimates, but differences between serial patterns do not necessarily indicate noncontemporaneous growth records.

Taphonomic reconstructions for ZR lake-margin assemblage formation should incorporate a mechanistic explanation for secondary deposition capable of spreading an individual's remains into multiple flow deposits. Further use of the ZR mastodon record to investigate changes through the Sangamonian interglacial must consider the

possibility that study specimens are not all chronologically ordered according to stratigraphic succession.

Table 3.1. Proposed pairs in ZR mastodon mandibular tusks.
Here 18 tusks previously treated as genetically distinct are grouped into 9 pairs. Bold type identifies additions and modifications to data reported in *Chapter 2* – Fisher et al. (2014). Bracketed figures represent adjustments made based on pair identifications. "*Tusk pair numbers*" – identifications referenced in the text and other figures. "*Specimen #*" – field numbers using the system described in methods of *Chapter 2* – Fisher et al. (2014). "*Side*" – L/R identification in most cases remains unchanged from *Chapter 2* – Fisher et al. (2014). Even when considered as pairs, juvenile deciduous tusks lack unambiguous side-identifying morphologies. "*Chrono (strat)*" – stratigraphic units ("Unit 3"; BS – "Basement Silt"; MF – "Main Floor"; MFRP – "Main Floor Red Pebble"; MS – "Main Silt"; PDF – "Primary Debris Flow") are identified in Pigati et al. (2014). Stratigraphic reinterpretations support evaluation of chronological patterns, but do not revise actual field associations for specimens. Adjusted chronologies were set to the lower unit represented by the pair. "*Ontog. + sex*" – sex and ontogeny identifications are not independent and were combined in this table. Sex was apparently misidentified in 33.238 due to pathological growth affecting morphology and annual growth volumes. " "*Circ. (mm)*" – greatest circumference measured with a flexible tape around the outside surface of a tusk includes thickness of cementum. "*FFY*" – fraction of final year is an uncalibrated metric for season of death and is described more thoroughly in *Chapter 2* – Fisher et al. (2014). Two FFYs were disregarded and set to match their paired complement based on reevaluation of final CT increments (33.238) and preference for on-axis measurements (58.360 was measured along a plane displaced from the tusk axis).

Tusk pairs	Specimen #	Side	Chrono (strat)	Ontog.+ sex	Circ. (mm)	FFY
1	30.017	**[L]**	PDF (5d)	Adol. M	139	0.42
	33.238	**[R]**	PDF (5d)	**[Adol. M]**	128	**[0.42]**
2	30.130	**L**	MS (5d)	Senesc. F	**142**	0.95
	30.076	R	**[MS (5d)]**	Senesc. F	137	0.99
3	45.015	**[L]**	**[MFRP (5d)]**	Adult M	167	0.93
	48.530	R	MFRP (5d)	Adult M	163	0.96
4	58.032	L	MS (5d)	Adult M	162	-
	58.025	R	MS (5d)	Adult M	161	1.04
5	58.360	L	BS (5e)	Adol. M	139	**[1.01]**
	82.179	R	**[BS (5e)]**	Adol. M	136	1.01
6	63.125	L	MFRP (5d)	Senesc. F	128	1.08
	56.015	R	**[MFRP (5d)]**	Senesc. F	129	1.04
7	63.170	L	**[BS (5e)]**	Adult M	163	-
	64.013	R	BS (5e)	Adult M	174	-
8	68.032	L?	Unit 3 (5e)	Juvenile	55	-
	44.146	**[R?]**	**[Unit 3 (5e)]**	Juvenile	56	-
9	68.050	**[L?]**	BS (5e)	Juvenile	64	-
	71.092	R?	**[BS (5e)]**	Juvenile	60	-

Figure 3.1. Tusk pair 1 medial views.
(A) field no. 33.238 (DMNH), right mandibular tusk, and (B) field no. 30.017 (DMNH), left mandibular tusk. Photos display general morphological similarities in dorsoventral diameter and wear at the distal ends, which show partial smoothing of surfaces fractured prior to death. Matching erosion patterns occur 7 – 8 cm from proximal ends (right).

Figure 3.2. Tusk pair 1 dorsal views.
(A) field no. 33.238 (DMNH), right mandibular tusk, and (B) field no. 30.017 (DMNH), left mandibular tusk. Photos display general morphological similarities in mediolateral diameter and wear at the distal ends which show partial smoothing of surfaces fractured prior to death. Both tusks have an abrupt constriction about 2 cm from the proximal end (right).

Figure 3.3. Tusk pair 1 surface models from CT scans.
Medial surfaces for proximal ends of (A) field no. 33.238 (DMNH), right mandibular tusk, and (B) field no. 30.017 (DMNH), left mandibular tusk. Surface models from CT scans clearly display the distinct abrupt constriction in each tusk occurring about the same distance (~2 cm) from the proximal end (right).

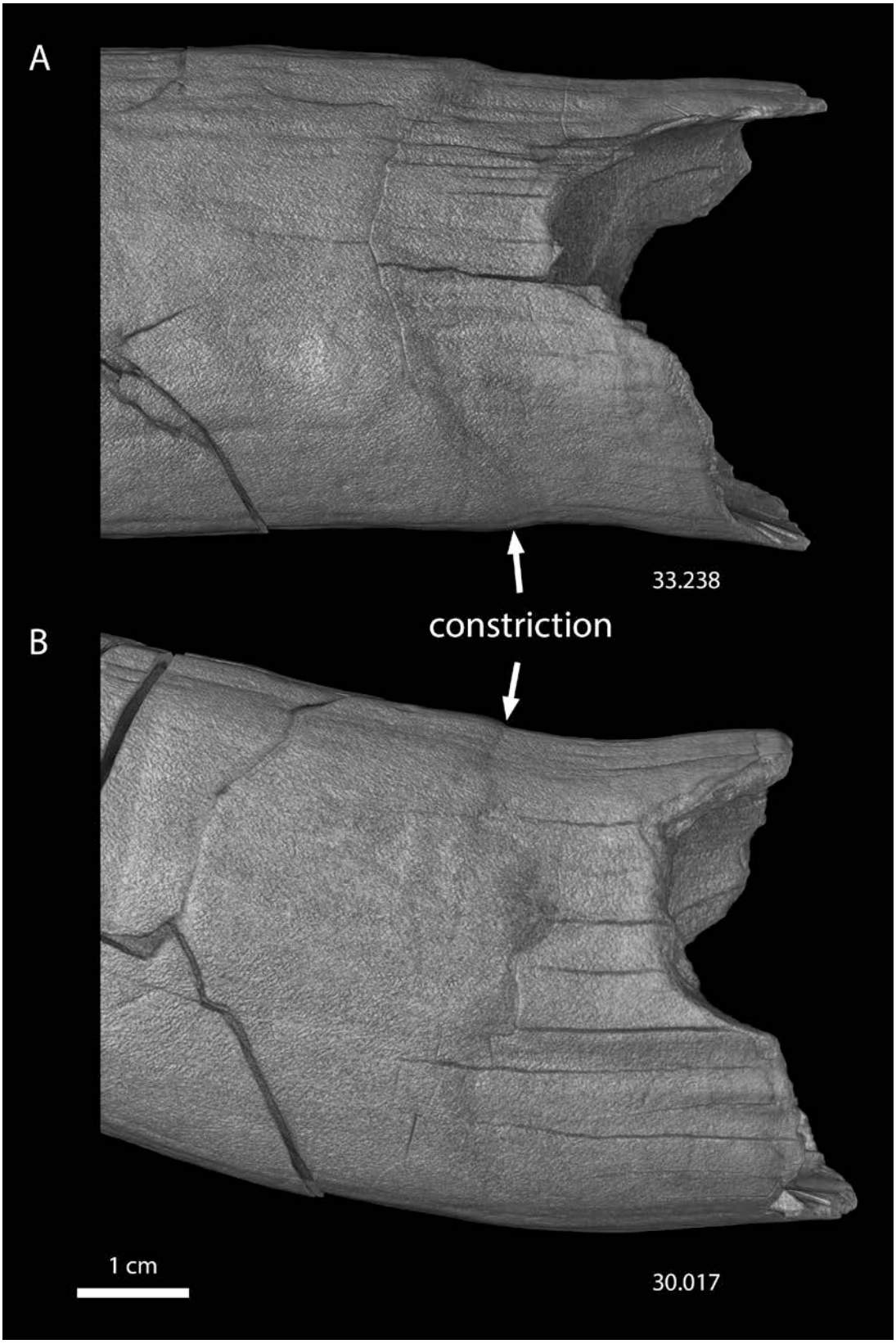
A
33.238
constriction
B
1 cm
30.017

Figure 3.4. Tusk pair 1 dorsoventral digital slices through the axes of CT scans. (A) field no. 33.238 (DMNH), right mandibular tusk, and (B) field no. 30.017 (DMNH), left mandibular tusk. CT images display similarities in expression of annual growth increments, cementum thicknesses, deflections at the cementum-dentin junction (one particularly prominent one marked "constriction" in image), and locations of desiccation cracks. Proximal ends on the right show pulp cavity surfaces at time of death. Growth lines in the tusk show the shape of the pulp cavity in previous years. One growth line in each tusk (traced with dotted lines) show how the pulp cavity has changed shaped through life. This is presumably a result of trauma in both tusks.

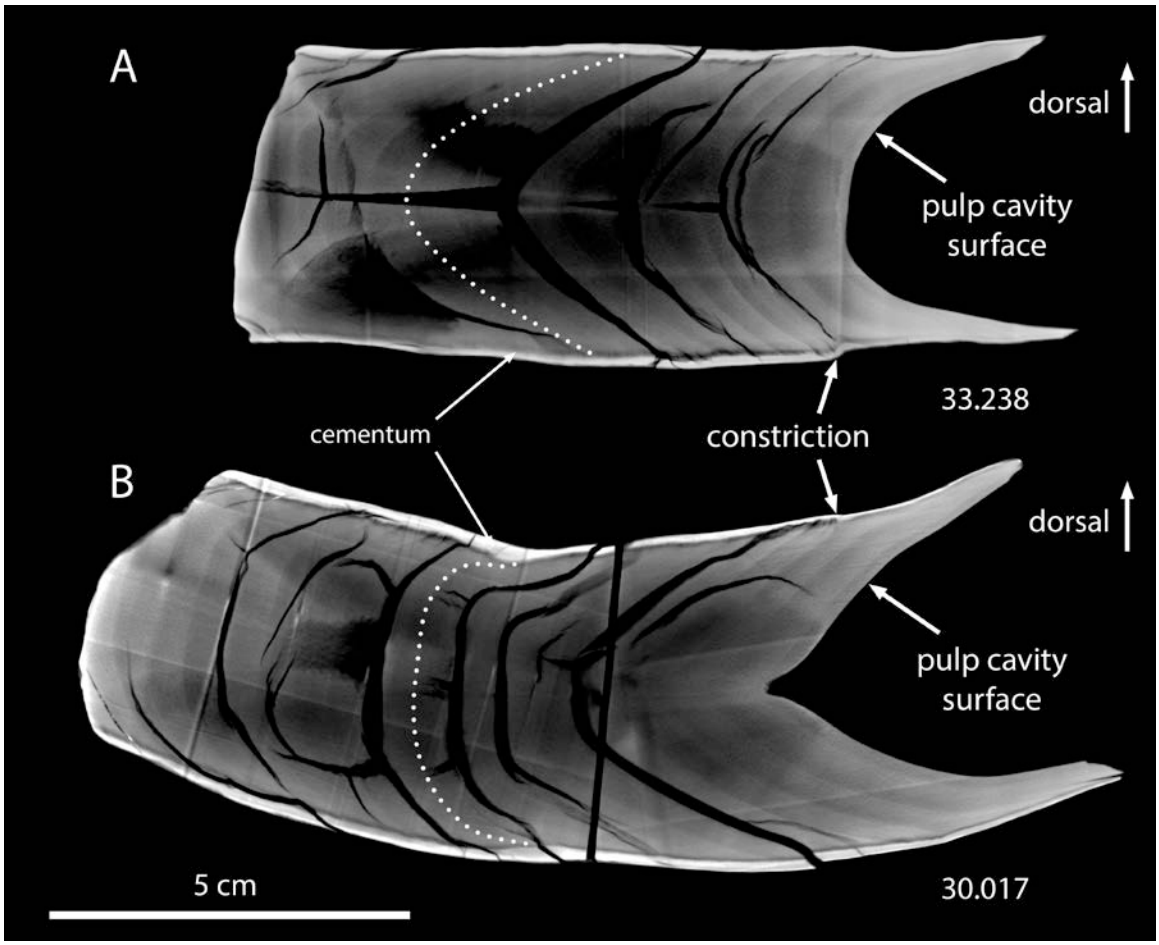

Figure 3.5. Tusk pair 1 EIV comparison.
EIV profiles for all ZR mandibular tusks scanned display considerable variation, apparent sexual dimorphism, and ontogenetic patterns. In this plot, partial growth records for tusks now identified as a left-right complement to another measured tusk have been aligned to the matching record. Annual growth profiles of EIV measurements taken from CT scans of field nos. 30.017 and 33.238 are highlighted. They occupy the same general range and display some overlap in multiyear patterns. Divergence follows an abrupt bend (likely a traumatic pathology) in 30.017 after which point, its EIVs increase dramatically as its pulp cavity reestablishes a typical conical morphology. (modified from *Chapter 2* – Fisher et al., 2014).

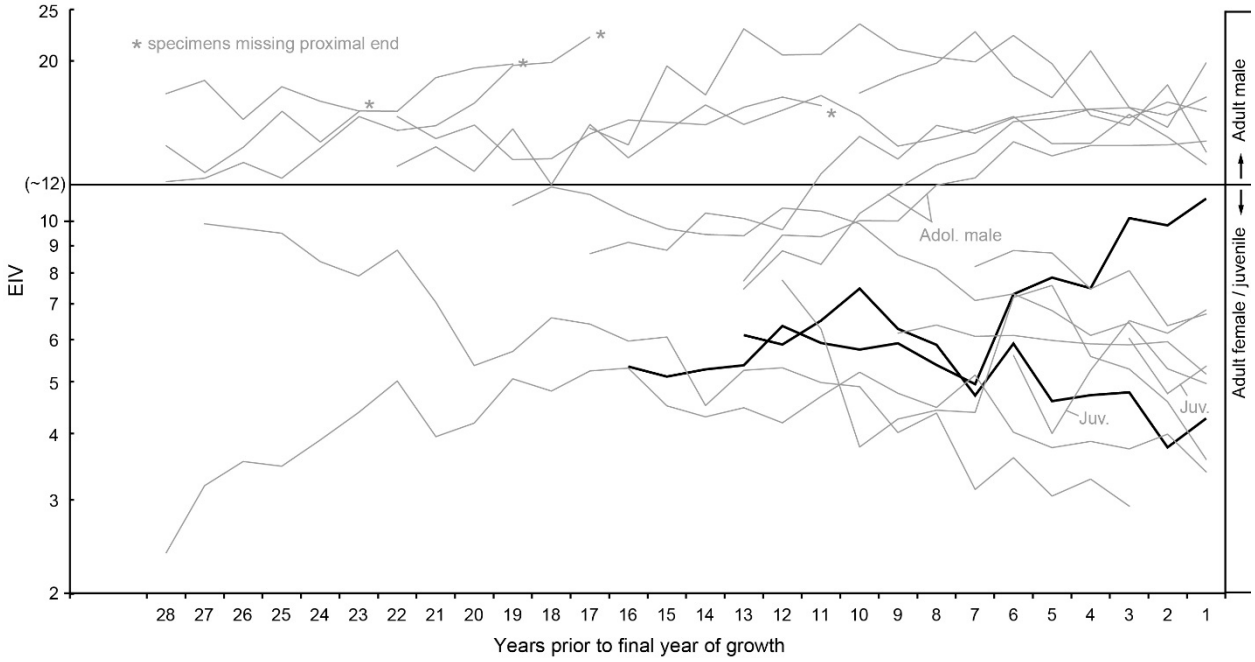

Figure 3.6. Tusk pair 2 medial views.
(A) field no. 30.076 (DMNH), right mandibular tusk, and (B) field no. 30.130 (DMNH), left mandibular tusk. Photos display general morphological similarities in dorsoventral diameter and curvature. Both tusks are fractured ~20 cm from the proximal end. The distal portion of 30.130 was recovered and reattached. Matching subtle erosion patterns are present on the medial surface of each tusk about 18 – 20 cm from proximal ends (right).

Figure 3.7. Tusk pair 2 dorsal views.
(A) field no. 30.076 (DMNH), right mandibular tusk, and (B) field no. 30.130 (DMNH), left mandibular tusk. Photos display general morphological similarities in mediolateral diameter and curvature. Both tusks are fractured ~20 cm from the proximal end (right). The distal portion of 30.130 was recovered and reattached.

Figure 3.8. Tusk pair 2 surface models from CT scans.
Medial surfaces for proximal ends of (A) field no. 30.076 (DMNH), right mandibular tusk, and (B) field no. 30.130 (DMNH), left mandibular tusk. Surface models from CT scans clearly display matching patterns of topographical periradicular features (marked with arrows) on the proximal ends of the tusks (right).

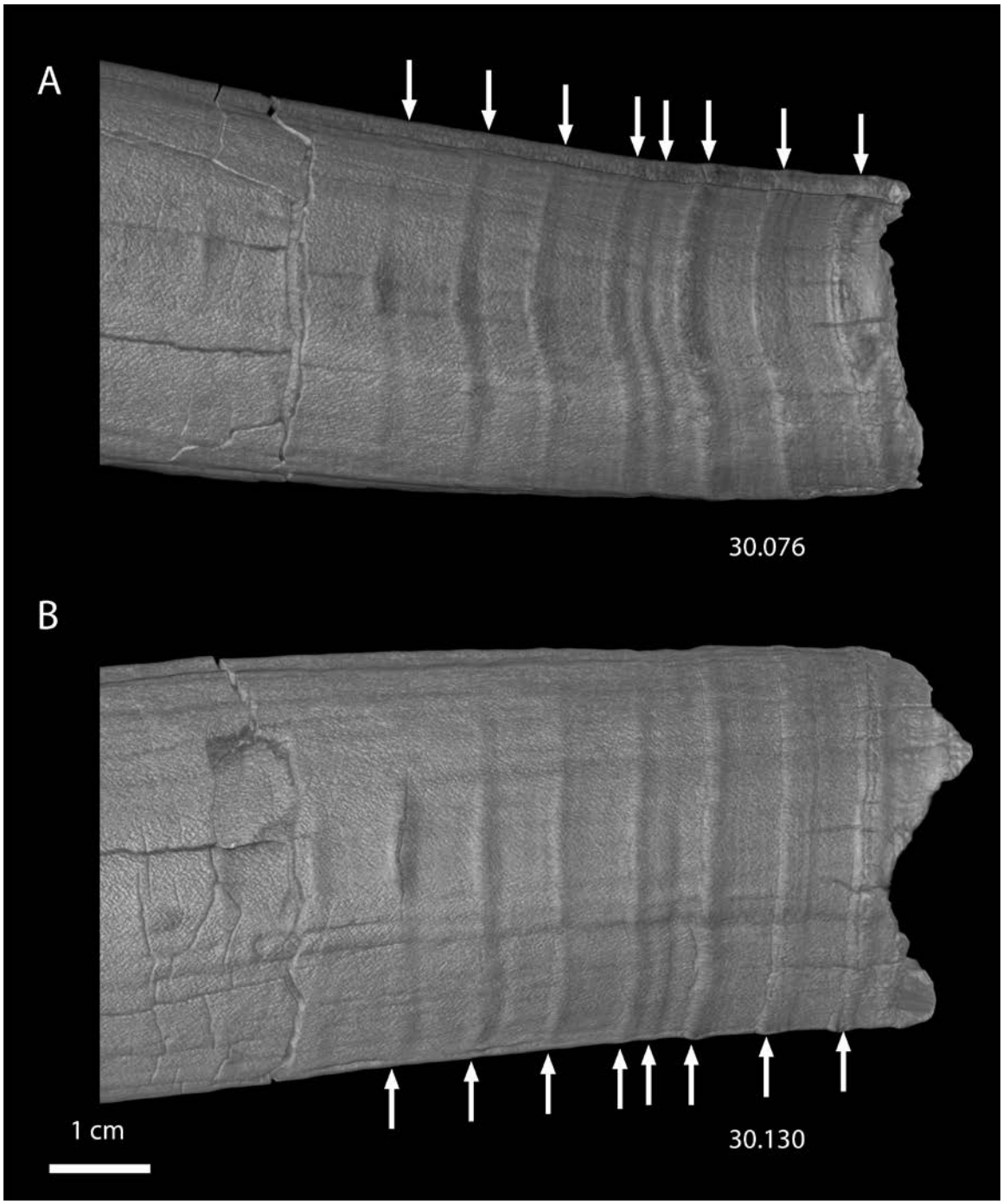
A
30.076
B
1 cm
30.130

Figure 3.9. Tusk pair 2 dorsoventral digital slices through the axes of CT scans. (A) field no. 30.076 (DMNH), right mandibular tusk, and (B) field no. 30.130 (DMNH), left mandibular tusk. CT images display similarities in depth and angle of the pulp cavity, expression of annual growth increments, cementum thicknesses, deflections at the cementum-dentin junction, and locations of desiccation cracks. The proximal ends (right) contain intact pulp cavity surfaces that represent growth at the time of death.

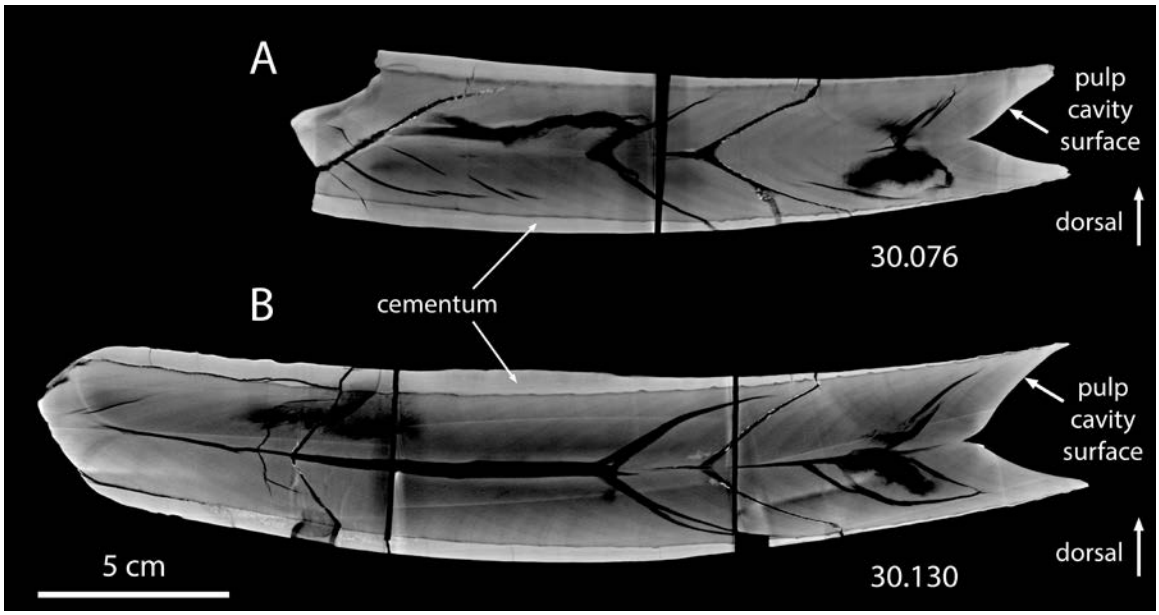

Figure 3.10. Tusk pair 2 EIV comparison.
EIV profiles for all ZR mandibular tusks scanned display considerable variation, apparent sexual dimorphism, and ontogenetic patterns. In this plot, partial growth records for tusks now identified as a left-right complement to another measured tusk have been aligned to the matching record. Annual growth profiles of EIV measurements taken from CT scans of field nos. 30.076 and 30.130 are highlighted. They occupy the same general range and contain some overlap of year-to-year variation. Higher average EIVs for 30.076 are likely due to mediolateral constriction at the proximal end of 30.130 and imprecision of EIVs for estimating volume of the resulting irregular growth cones. (modified from *Chapter 2* – Fisher et al., 2014).

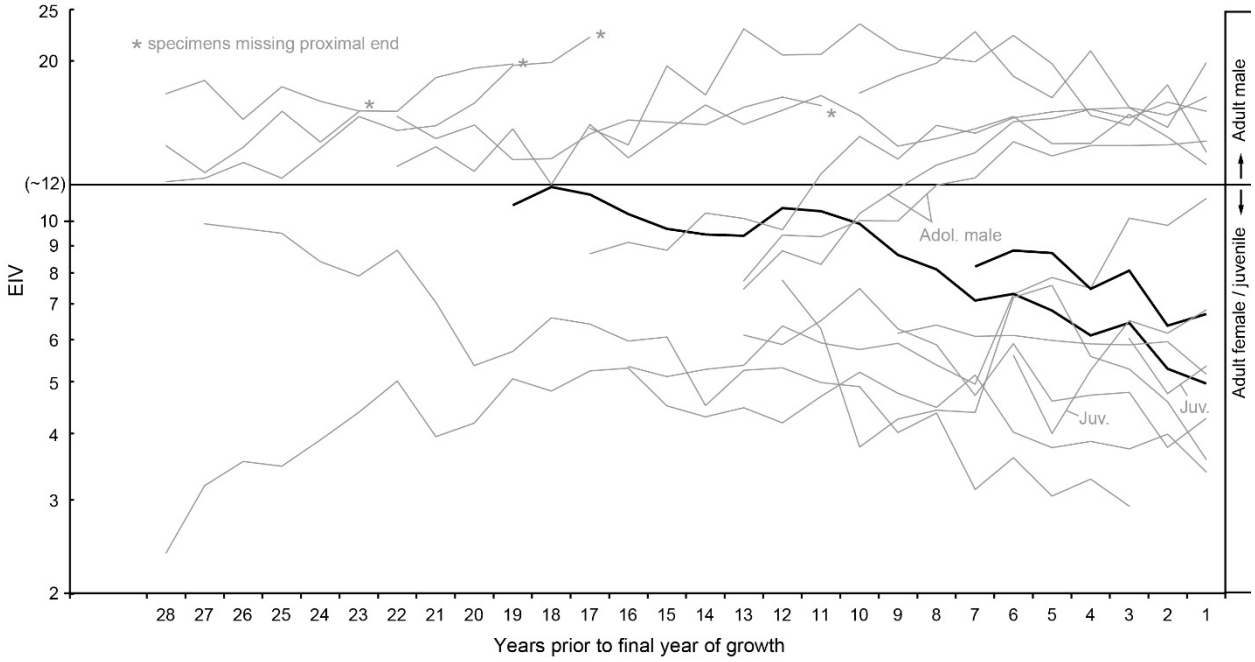

Figure 3.11. Tusk pair 3 medial views.
(A) field no. 48.530 (DMNH), right mandibular tusk, and its likely left complement, (B) field no. 45.015 (DMNH). Photos display general similarities in dorsoventral diameter, expression of periradicular features (more clearly displayed in Figure 3.13) at the proximal ends (right), and medial erosion. Extensive damage at the distal ends (left) prevents comparison of lengths, overall curvatures, and wear patterns.

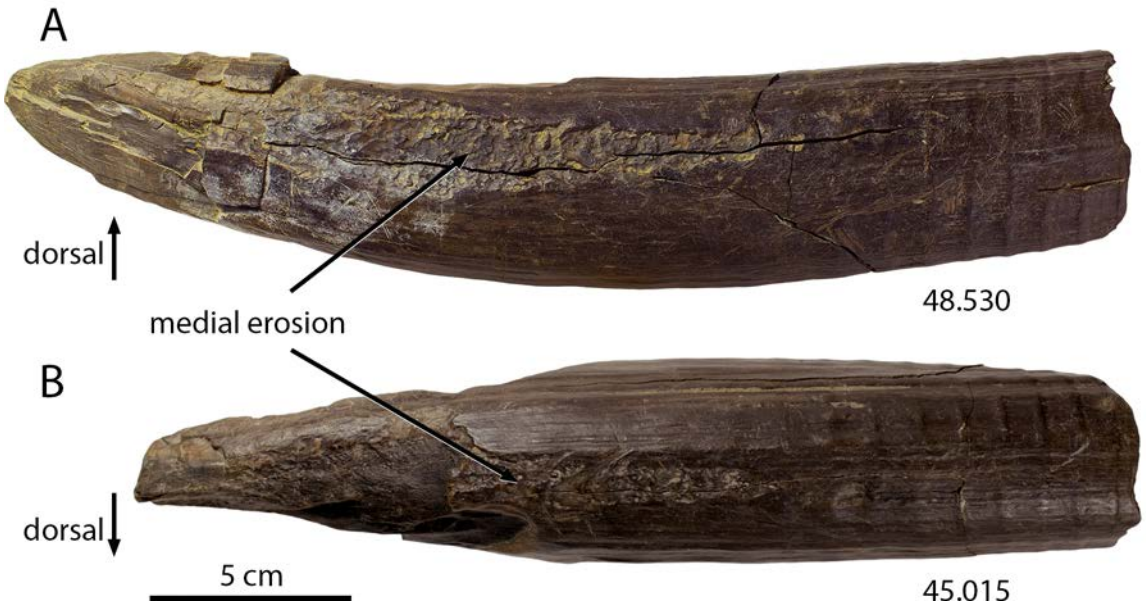

Figure 3.12. Tusk pair 3 dorsal views.
(A) field no. 48.530 (DMNH), right mandibular tusk, and its likely left complement, (B) field no. 45.015 (DMNH). Photos display general similarities in mediolateral diameter, expression of periradicular features (more clearly displayed in Figure 3.13) at the proximal ends (right), and medial erosion. Extensive damage at the distal ends (left) prevents comparison of lengths and gingival topographic features.

Figure 3.13. Tusk pair 3 surface models from CT scans.
Medial surfaces for proximal ends of (A) field no. 48.530 (DMNH), right mandibular tusk, and its likely left complement, (B) field no. 45.015 (DMNH). Surface models from CT scans clearly display matching patterns of topographical periradicular features (marked with arrows) on the proximal ends of the tusks (proximal ends on right).

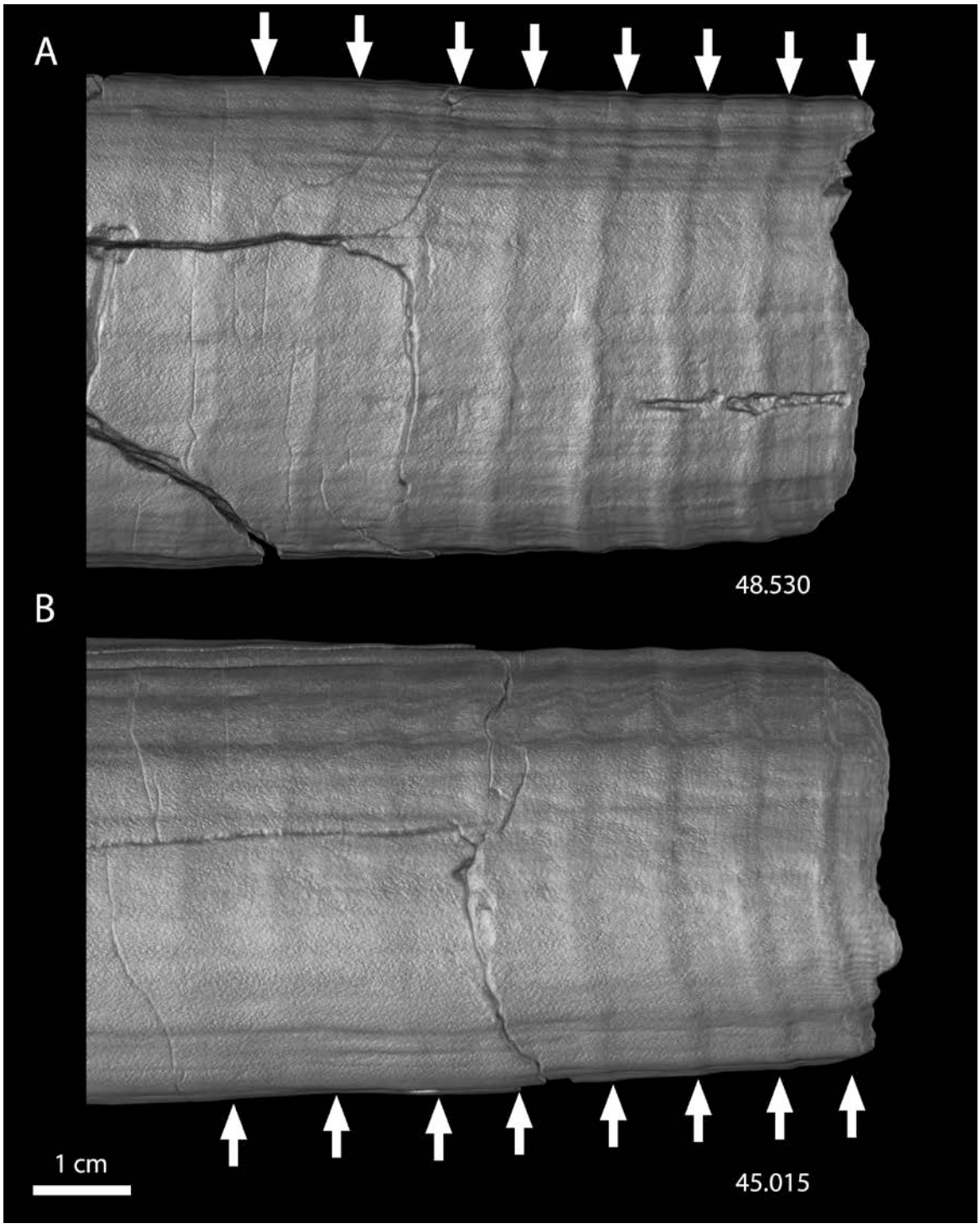
A
48.530
B
1 cm
45.015

Figure 3.14. Tusk pair 3 dorsoventral digital slices through to the axes from CT scans. (A) field no. 48.530 (DMNH), right mandibular tusk, and its likely left complement, (B) field no. 45.015 (DMNH). CT images display similarities in depth and angle of the pulp cavity, expression of annual growth increments, cementum thicknesses, deflections at the cementum-dentin junction, and locations of desiccation cracks. The proximal ends (right) contain intact pulp cavity surfaces that represent growth at the time of death. The 'ring' at the tip (left) of (A) is a CT artifact and not a density feature in the tusk.

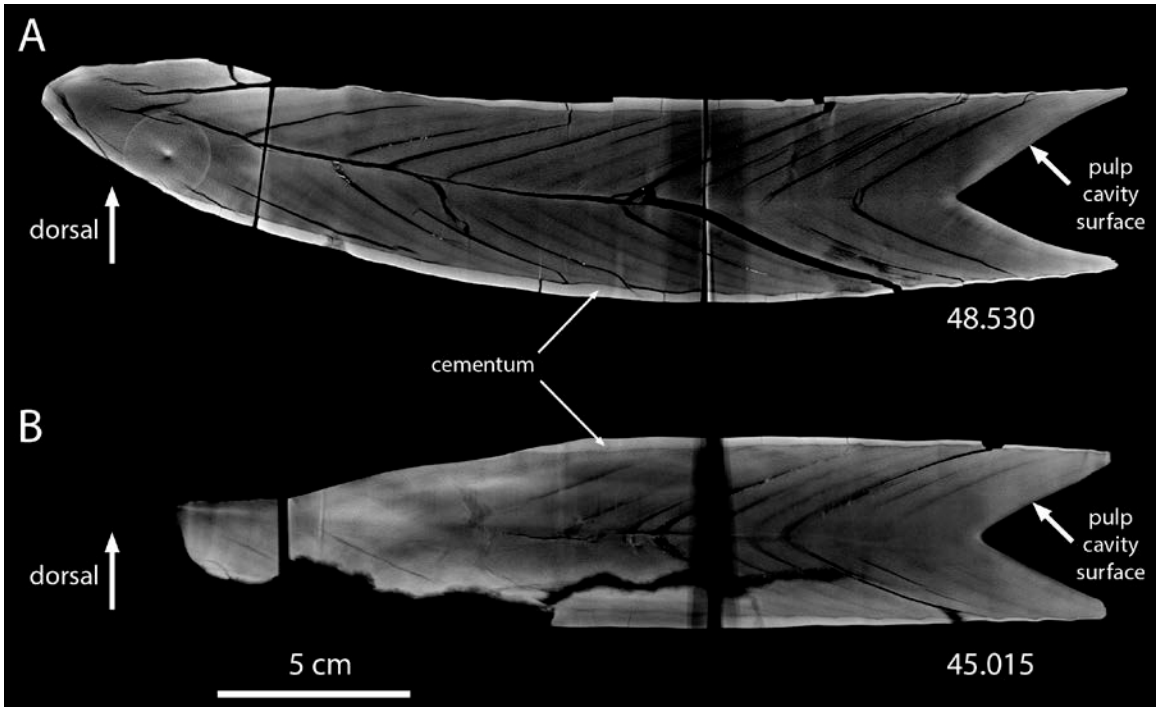

Figure 3.15. Tusk pair 3 EIV comparison.
EIV profiles for all ZR mandibular tusks scanned display considerable variation, apparent sexual dimorphism, and ontogenetic patterns. In this plot, partial growth records for tusks now identified as a left-right complement to another measured tusk have been aligned to the matching record. Annual growth profiles of EIV measurements taken from CT scans of field nos. 48.530 and 45.015 are highlighted. They occupy the same range and although interannual patterns do not match, the general trends in the overlapping portion of the records are highly consistent. (modified from *Chapter 2* – Fisher et al., 2014).

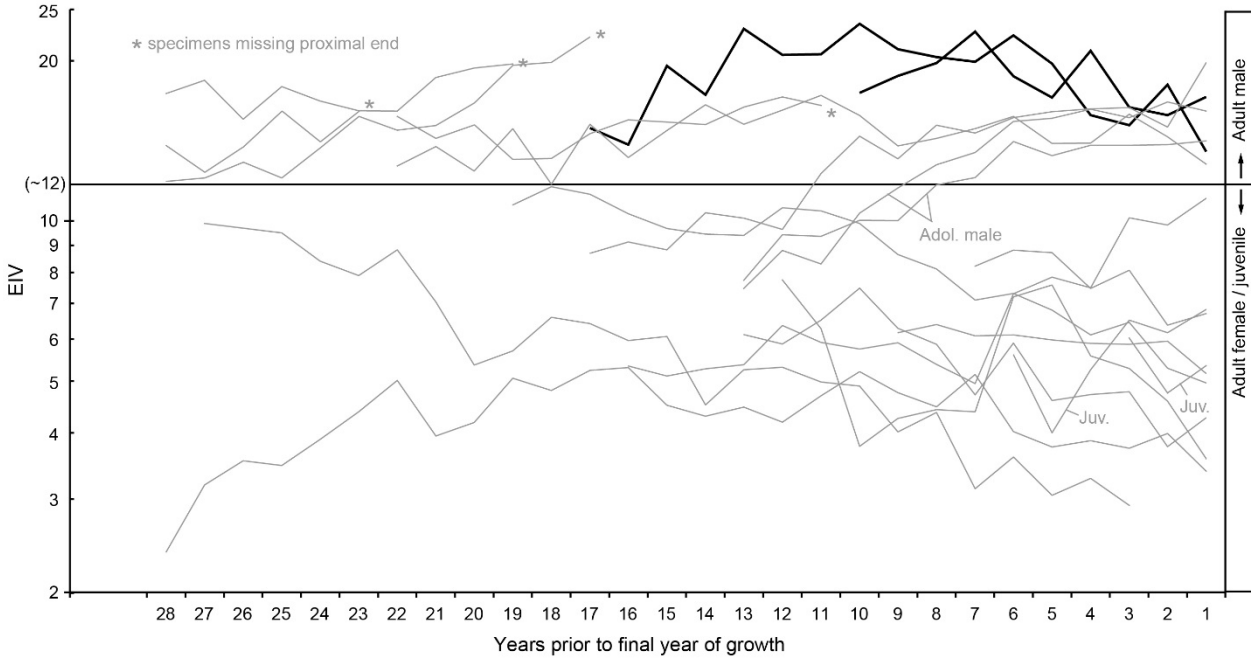

Figure 3.16. Tusk pair 3 oxygen isotope comparison.
Carbonate $\delta^{18}O$ records for ZR tusks have highly consistent seasonal variation, but average annual values vary by up to ~4 ‰. Vertical lines represent locations of annual CT features (abrupt transition from high to low density); fraction of final year is plotted as a percentage of expected growth for a complete year (see Figure 2.14). Because different tusks and different years within the same tusk may have different numbers of samples per year, sample intervals are spaced variably along the x-axis and aligned to annual CT features. Serial records for field nos. 48.530 and 45.015 are highlighted against the backdrop of all other ZR records obtained. General multiyear patterns, seasonal fluctuations, and annual averages are highly consistent between the two tusks. Small differences in the isotope profiles are expected due to different sampling schemes. Prior to recognition as a left-right pair, 48.530 and 45.015 were candidates for individuals living contemporaneously based on their highly congruent $\delta^{18}O$ profiles and early acknowledgement that identification to adjacent stratigraphic units "Main Silt" and "Main Floor Red Pebble" (Pigati et al., 2014) might not indicate chronological separation (*Chapter 2* – Fisher et al., 2014; figure modified from *Chapter 2* – Fisher et al., 2014).

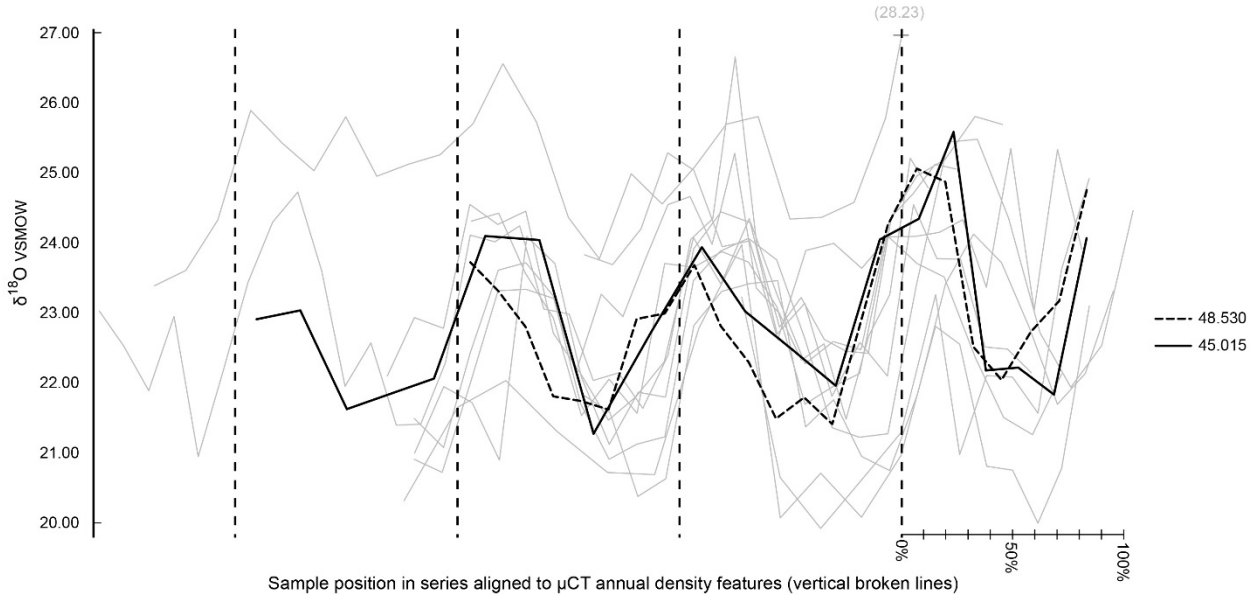

Figure 3.17. Tusk pair 3 carbon isotope comparison.
Carbonate $\delta^{13}C$ records for ZR tusks are highly variable and show signs of significant diagenetic effects (*Chapter 2* – Fisher et al., 2014). Data points are plotted in series with measurements from earlier growth on the left and $\delta^{13}C$ of later growth on the right. All records are right-justified so that the end of each series (representing the time of death) is aligned, but records in this plot do not have equivalent timing (sampling resolution varied between 5 – 8 samples per annual increment). Tick marks along the x-axis are unlabeled to highlight that data points for a particular abscissa are not equivalent. Serial records for field nos. 48.530 and 45.015 are highlighted against the backdrop of all other ZR records obtained. Variations in carbon isotope profiles may reflect taphonomic history more than original compositions. Differences between $\delta^{13}C$ records are more extreme than in other proposed left-right pairs and apparently indicate significantly different taphonomic conditions for each tusk.

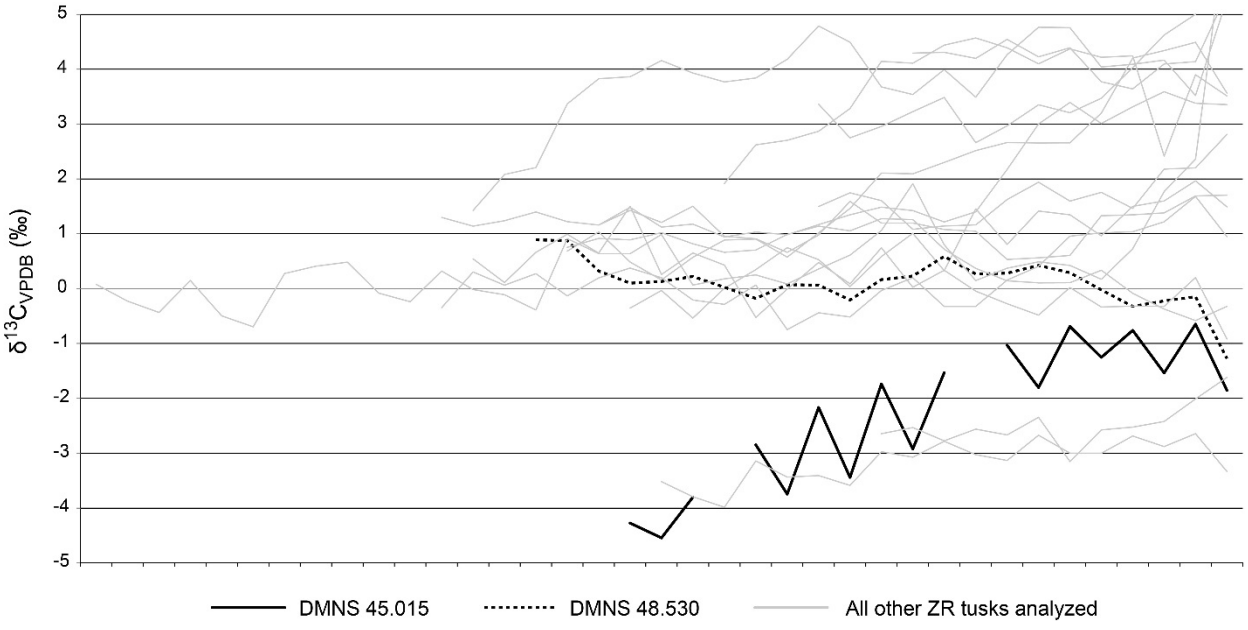

Figure 3.18. Tusk pair 4 medial views.
(A) field no. 58.025 (DMNH), right mandibular tusk, and (B) field no. 58.032 (DMNH), left mandibular tusk. Photos display general morphological similarities in dorsoventral diameter, curvature, and angles of wear facets at the distal ends. Similar prominent erosion patterns are present along much of the medial surface of each tusk. Distal ends are on the left. Only 58.025 retains its proximal end (right).

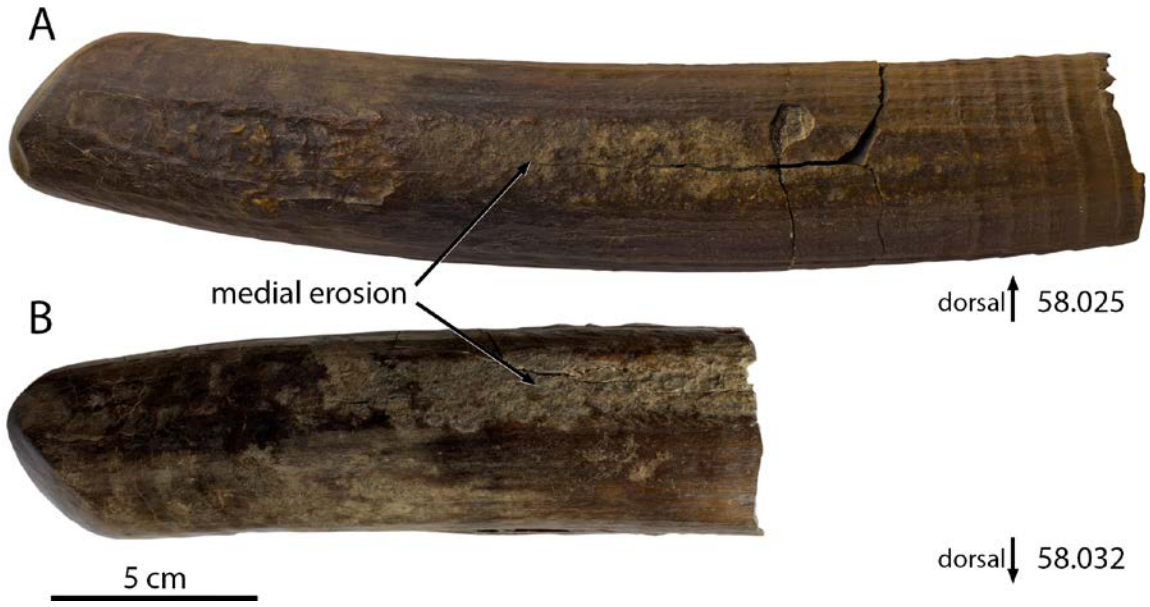

Figure 3.19. Tusk pair 4 dorsal views.
(A) field no. 58.025 (DMNH), right mandibular tusk, and (B) field no. 58.032 (DMNH), left mandibular tusk. Photos display general morphological similarities in mediolateral diameter and curvature. Three distinct GFs (see *Methods*) present at the distal end of each tusk have the same spacing, depth, longitudinal location, and lateromedial angle to the tusk axis. The exterior surface on the proximal end (right) contains pronounced periradicular ridges in 58.025. The proximal end of 58.032 is missing.

Figure 3.20. Tusk pair 4 surface models from CT scans.
Medial surfaces from the dorsal view of the distal ends of (A) field no. 58.025 (DMNH), right mandibular tusk, and (B) field no. 58.032 (DMNH), left mandibular tusk. GFs (see *Methods*) at the distal end (left) have a nearly identical topographic manifestation in the two tusks. GFs are marked here with arrows.

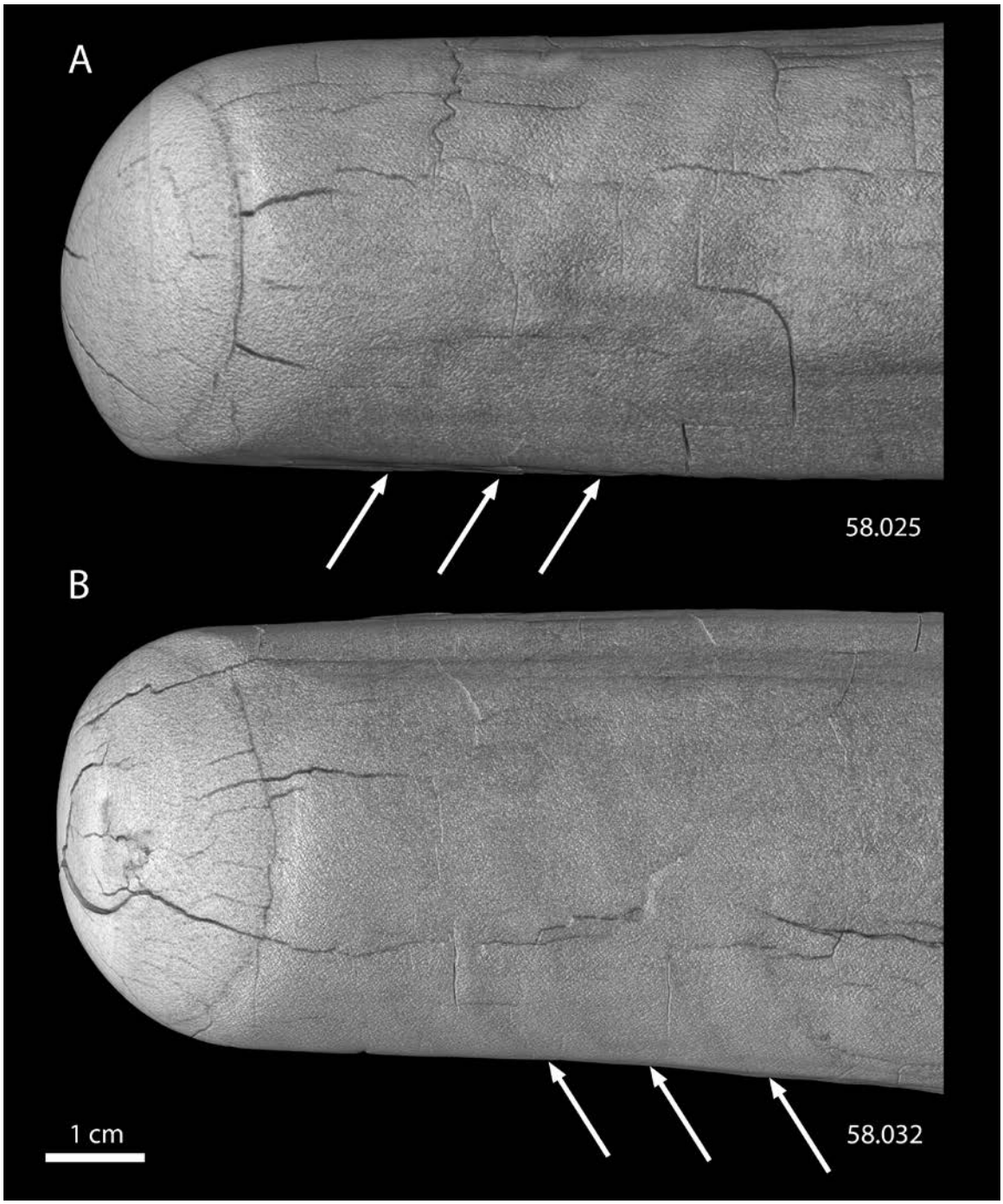
A
58.025
B
1 cm
58.032

Figure 3.21. Tusk pair 4 dorsoventral digital slices through the axes of CT scans. (A) field no. 58.025 (DMNH), right mandibular tusk, and (B) field no. 58.032 (DMNH), left mandibular tusk. CT images display similarities in angle of growth lines (which represents depth of pulp cavity at the time of dentin formation), expression of annual growth increments, cementum thicknesses, deflections at the cementum-dentin junction, and locations of desiccation cracks. The proximal end (right) of 58.025 contains the pulp cavity surface that formed just prior to death. The pulp cavity of 58.032 is missing.

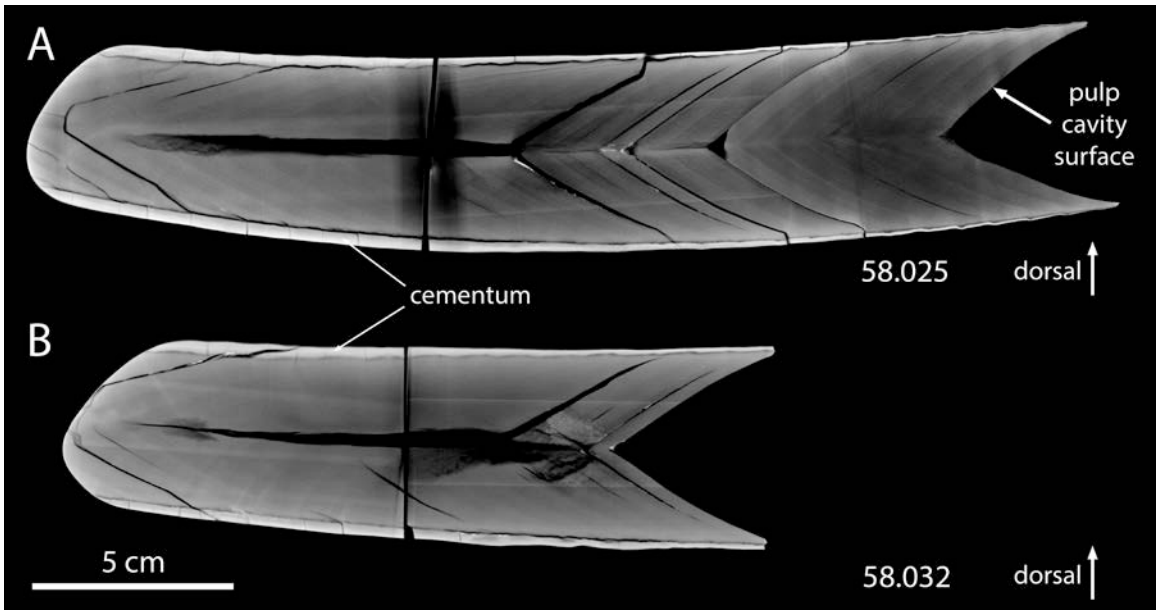

Figure 3.22. Tusk pair 4 EIV comparison.
EIV profiles for all ZR mandibular tusks scanned display considerable variation, apparent sexual dimorphism, and ontogenetic patterns. In this plot, partial growth records for tusks now identified as a left-right complement to another measured tusk have been aligned to the matching record. Annual growth profiles of EIV measurements taken from CT scans of field nos. 58.025 and 58.032 are highlighted. They occupy the same range and display some overlap in multiyear patterns. Although their year-to-year variations do not match, the general trends in the overlapping portion of the records are highly consistent. (modified from *Chapter 2* – Fisher et al., 2014).

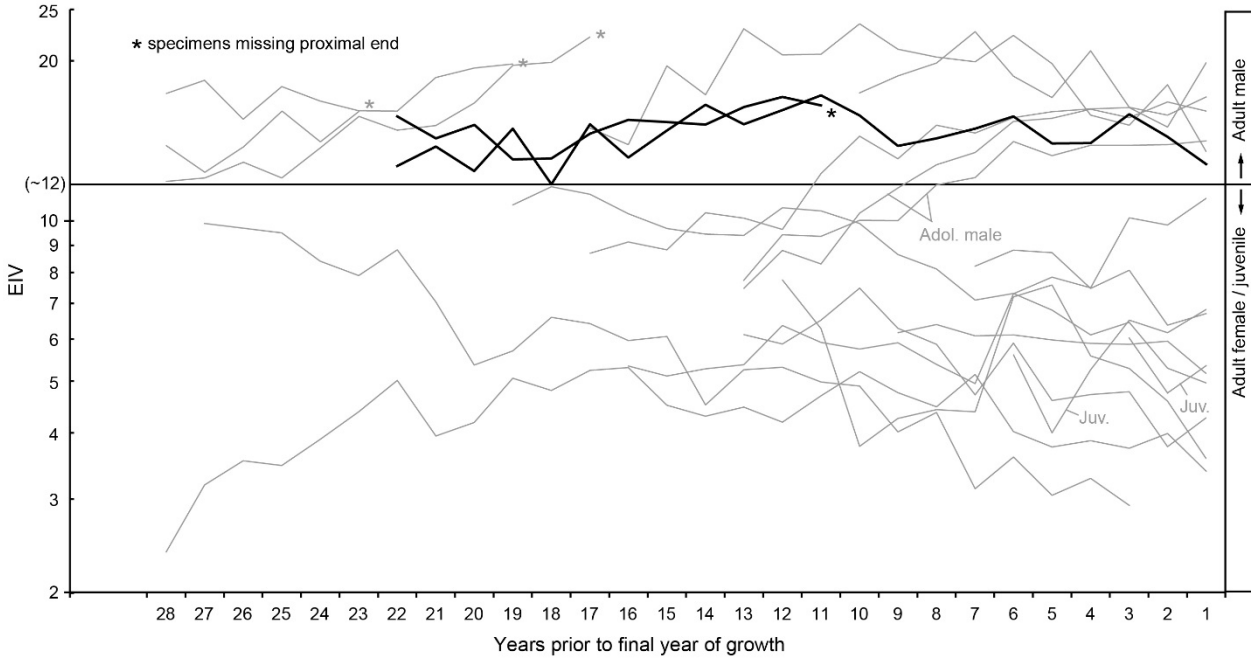

Figure 3.23. Tusk pair 5 medial views.
(A) field no. 82.179 (DMNH), right mandibular tusk, and (B) field no. 58.360 (DMNH), left mandibular tusk. Photos display general similarities in dorsoventral diameter and curvature, as well as overall length, expression of periradicular features, and distal wear. Both tusks were partially worn smooth at the distal ends (left) following traumatic fractures during life and have similarly angled wear facets. Both tusks have only very subtle erosion patterns on their medial surfaces.

Figure 3.24. Tusk pair 5 dorsal views.
(A) field no. 82.179 (DMNH), right mandibular tusk, and (B) field no. 58.360 (DMNH), left mandibular tusk. Photos display general similarities in mediolateral diameter and curvature, as well as overall length and expression of topographic GFs (see *Methods*) near the distal end. Both tusks were partially worn smooth at the distal ends (left) following traumatic fractures during life and have similarly angled wear facets. Different staining corroborates their associations with separate stratigraphic units and the implication of divergent taphonomic histories.

Figure 3.25. Tusk pair 5 surface models from CT scans.
Ventral surfaces for (A) field no. 82.179 (DMNH), left mandibular tusk, and (B) field no. 58.360 (DMNH), right mandibular tusk. Surface models from CT scans clearly display matching patterns of topographical GFs (see *Methods*) near the distal ends (left) of the tusks, and similar expression of periradicular features near the proximal end (right).

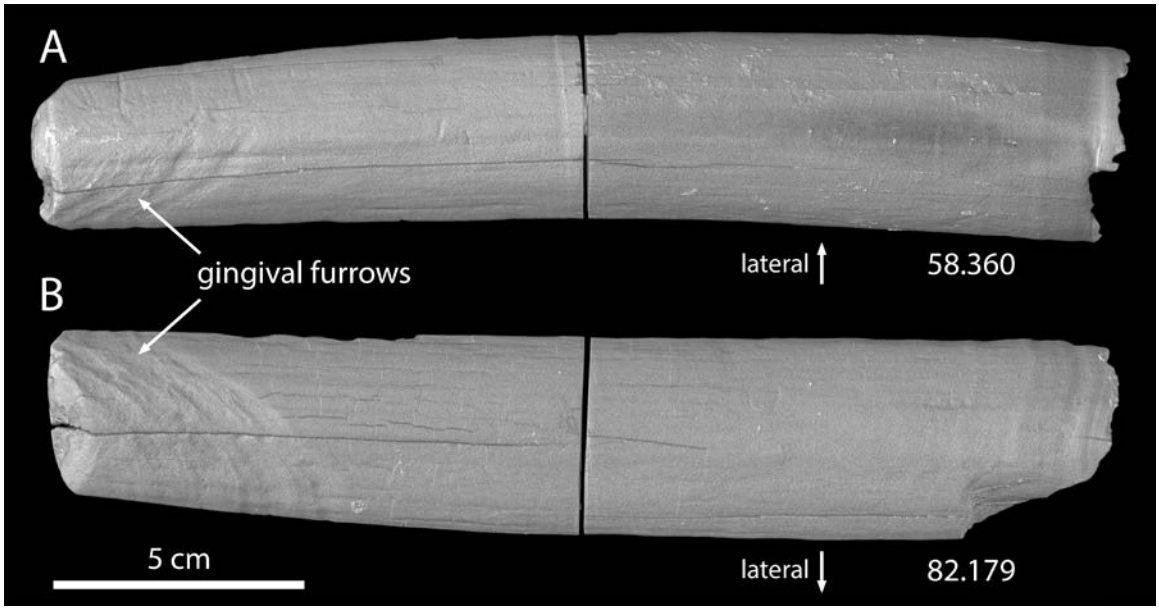

Figure 3.26. Tusk pair 5 mediolateral digital slices parallel to the axes from CT scans. (A) field no. 82.179 (DMNH), right mandibular tusk, and (B) field no. 58.360 (DMNH), left mandibular tusk. CT images display similarities in depth and angle of the pulp cavity, expression of annual growth increments, cementum thicknesses, and deflections at the cementum-dentin junction. Proximal ends (right) of both tusks contain the pulp cavity surface which preserves growth from the time of death.

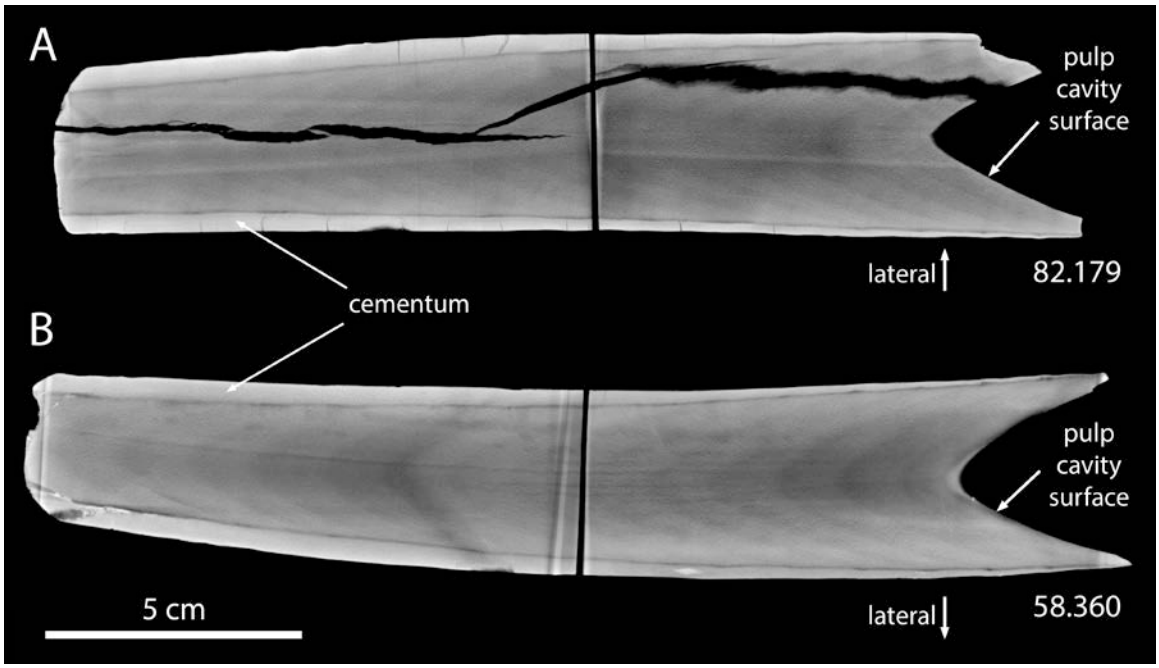

Figure 3.27. Tusk pair 5 EIV compare.
EIV profiles for all ZR mandibular tusks scanned display considerable variation, apparent sexual dimorphism, and ontogenetic patterns. In this plot, partial growth records for tusks now identified as a left-right complement to another measured tusk have been aligned to the matching record. Annual growth profiles of EIV measurements taken from CT scans of field nos. 82.179 and 58.360 are highlighted. They occupy the same range, have the same number of years, and have some overlap in multiyear patterns. Although interannual patterns do not match perfectly, the general trends in the records are highly consistent. EIV records for both tusks begin in the adult female/juvenile range and increase into the adult male range (modified from *Chapter 2* – Fisher et al., 2014)

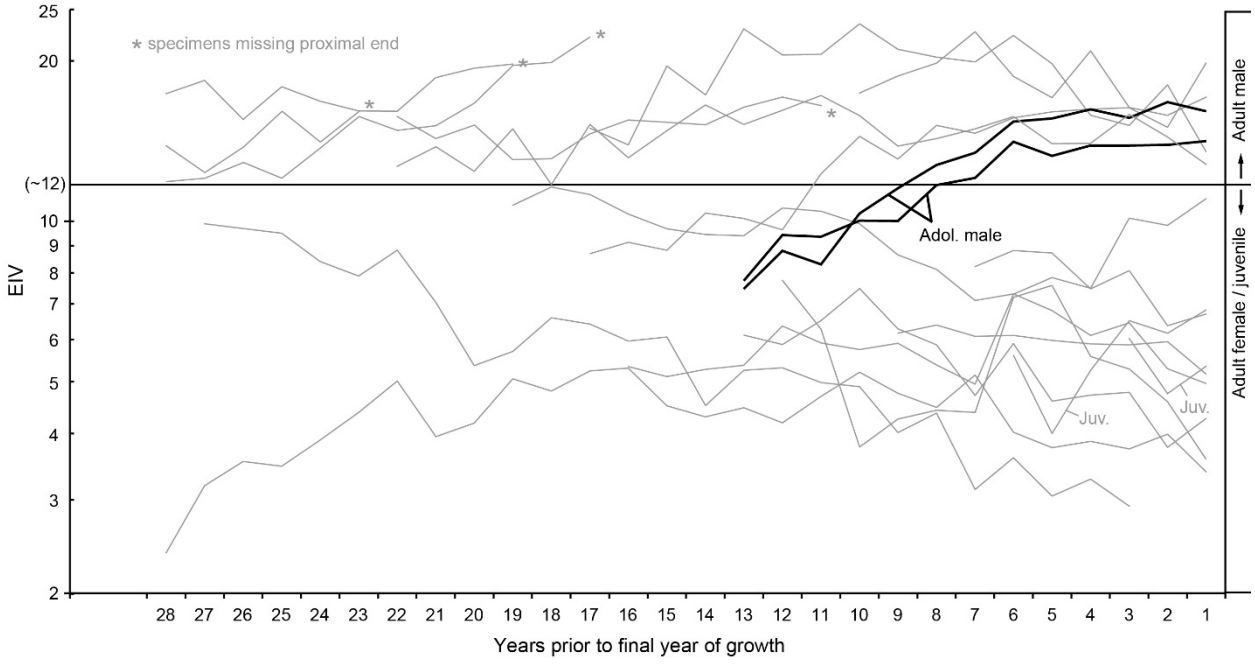

Figure 3.28. Tusk pair 5 oxygen isotope comparison.
Carbonate $\delta^{18}O$ records for ZR tusks have highly consistent seasonal variation, but average annual values vary by up to ~4 ‰. Vertical lines represent locations of annual CT features (abrupt transition from high to low density); fraction of final year is plotted as a percentage of expected growth for a complete year (see Figure 2.14). Because different tusks and different years within the same tusk may have different numbers of samples per year, sample intervals are spaced variably along the x-axis and aligned to annual CT features. Serial records for field nos. 82.179 and 58.360 are highlighted against the backdrop of all other ZR records obtained. General multiyear patterns, seasonal fluctuations, and annual averages are fairly consistent between the two tusks which contain the two most depleted records. Sampling was planned to be as consistent as possible between the tusks. Small differences in the isotope profiles are expected due to different sampling schemes. Divergence at the end of the records occurs where samples were taken from near exposed pulp cavity surfaces and is consistent with different diagenetic effects related with their distant stratigraphic associations (modified from *Chapter 2* – Fisher et al., 2014).

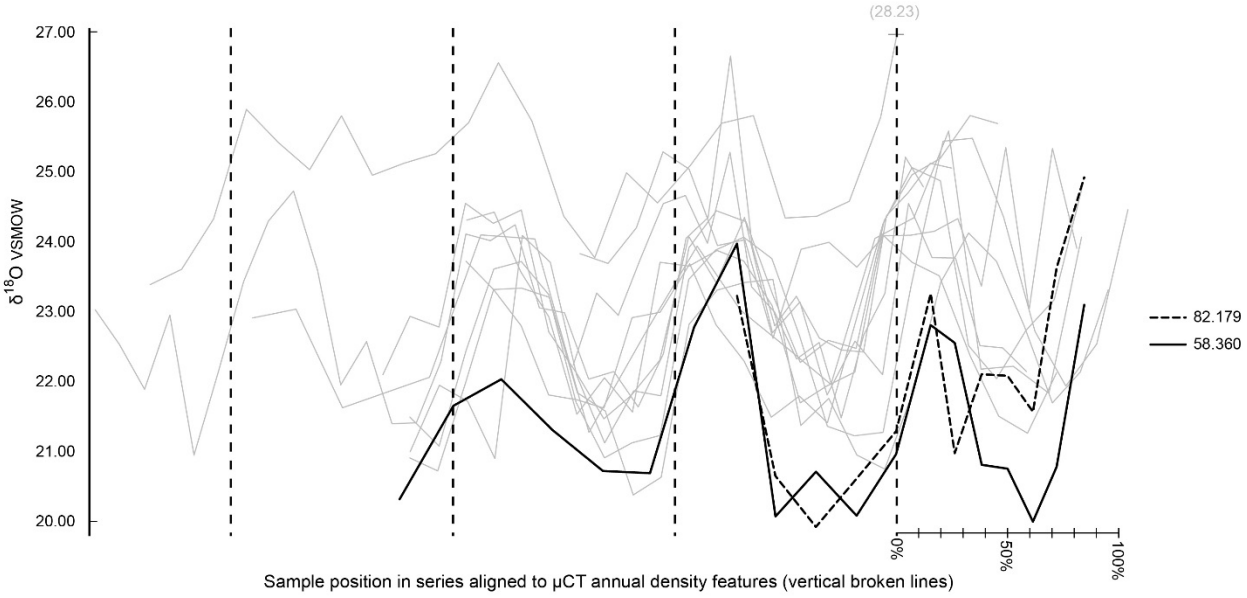

Figure 3.29. Tusk pair 5 carbon isotope comparison.
Carbonate $\delta^{13}C$ records for ZR tusks are highly variable and show signs of significant diagenetic effects (*Chapter 2* – Fisher et al., 2014). Data points are plotted in series with measurements from earlier growth on the left and $\delta^{13}C$ of later growth on the right. All records are right-justified so that the end of each series (representing the time of death) is aligned, but records in this plot do not have equivalent timing (sampling resolution varied between 5 – 8 samples per annual increment). Tick marks along the x-axis are unlabeled to highlight that data points for a particular abscissa are not equivalent. Serial records for field nos. 82.179 and 58.360 are highlighted against the backdrop of all other ZR records obtained. Variations in carbon isotope profiles may reflect taphonomic history more than original compositions. The records are remarkably consistent considering the apparent diagenetic effects and different stratigraphic associations of the tusks. Carbon isotope series nearly overlap at the low end of the range for ZR tusks.

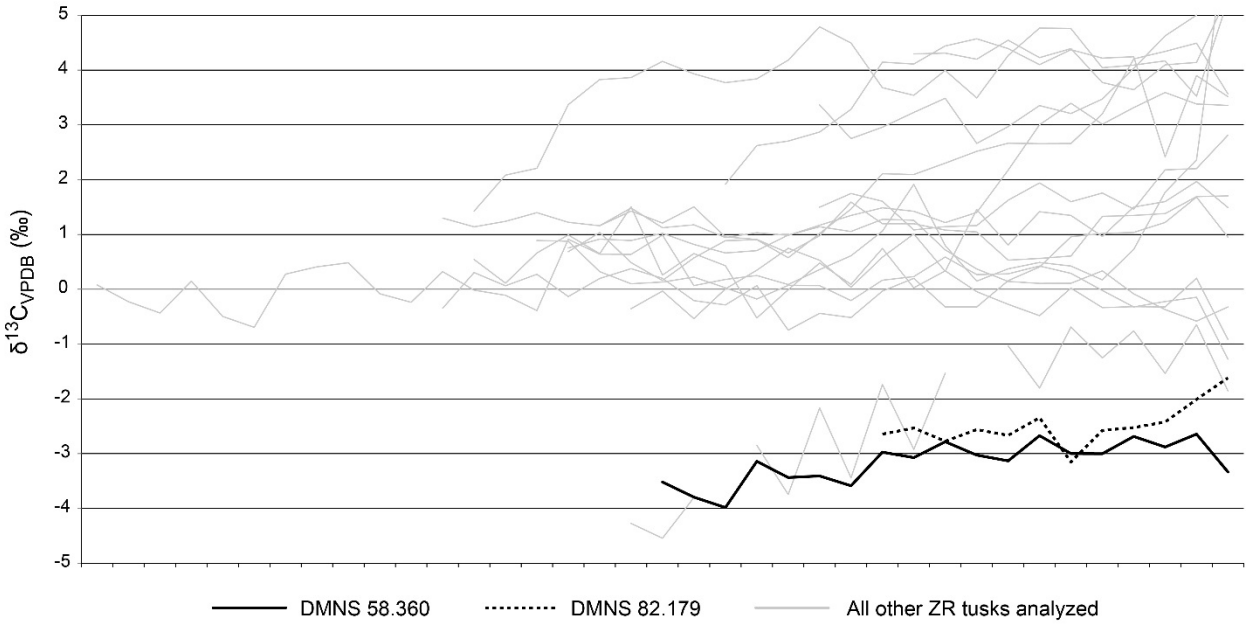

Figure 3.30. Tusk pair 6 medial views.
(A) field no. 56.015 (DMNH), right mandibular tusk, and (B) field no. 63.125 (DMNH), left mandibular tusk. Photos display general similarities in dorsoventral diameter and curvature, as well as overall length, subtle expression of periradicular features, and distal wear. Both tusks are worn smooth at the distal ends (left) and have identically angled wear facets. Only 63.125 has significant cavitation on its medial surface. A small pit of erosion is present on 56.015 opposite a cavitation on 63.125. Both tusks have two pronounced constrictions ~9 cm and ~4 cm from the proximal ends (right).

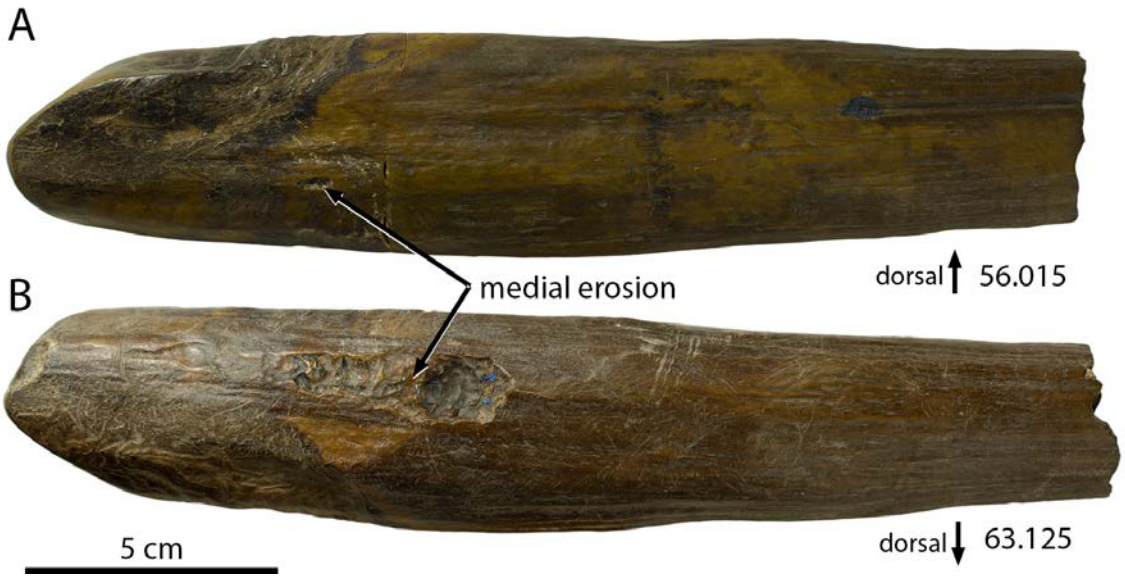

Figure 3.31. Tusk pair 6 dorsoventral views.
(A) field no. 56.015 (DMNH), right mandibular tusk, and (B) field no. 63.125 (DMNH), left mandibular tusk. Photos display general similarities in mediolateral diameter and curvature, as well as overall length, distal wear, and topographical GFs (see *Methods*). Both tusks are worn smooth at the distal ends (left), have identically angled wear facets, and have significant loss of cementum distal to the gingival line.

Figure 3.32. Tusk pair 6 dorsoventral digital slices parallel to the axes from CT scans. (A) field no. 56.015 (DMNH), right mandibular tusk, and (B) field no. 63.125 (DMNH), left mandibular tusk. CT images display similarities in depth, angle, and shape of the pulp cavity, expression of annual growth increments, cementum thicknesses, deflections at the cementum-dentin junction, and locations of desiccation cracks. Proximal ends (right) of both tusks contain the pulp cavity surface which preserves growth from the time of death.

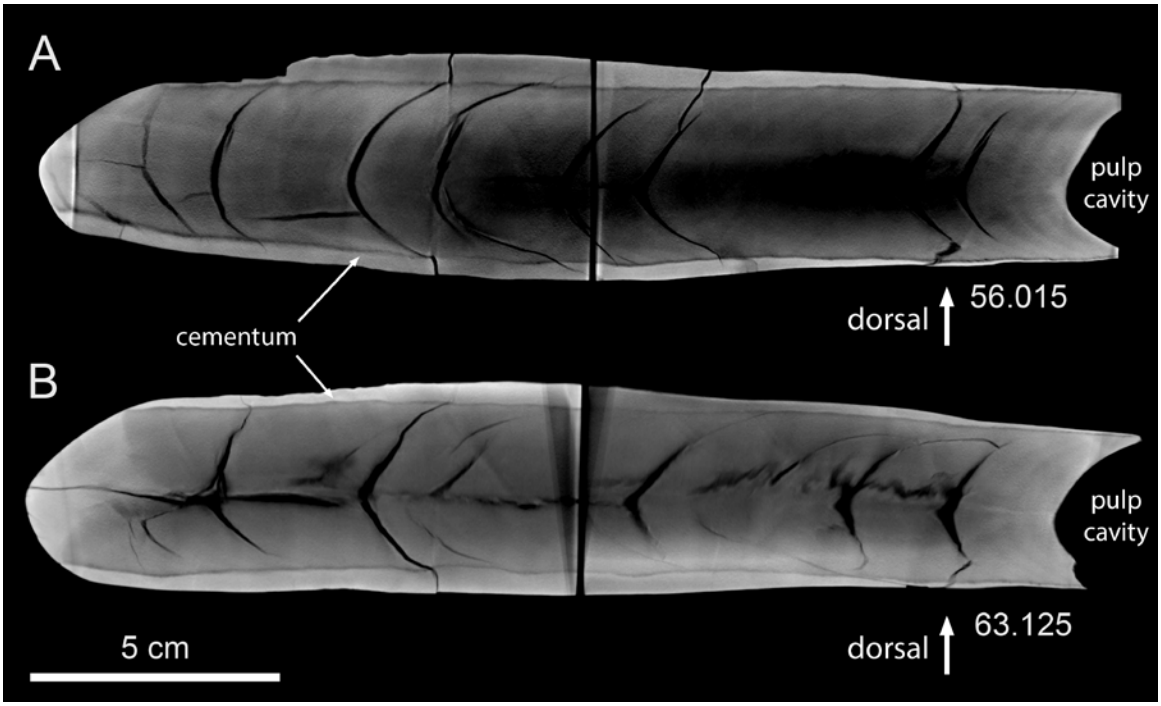

Figure 3.33. Tusk pair 6 EIV comparison.
EIV profiles for all ZR mandibular tusks scanned display considerable variation, apparent sexual dimorphism, and ontogenetic patterns. In this plot, partial growth records for tusks now identified as a left-right complement to another measured tusk have been aligned to the matching record. Annual growth profiles of EIV measurements taken from CT scans of field nos. 56.015 and 63.125 are highlighted. The overlapping portions of the records occupy the same general range but have significantly different multiyear patterns. CT features were obscure for both tusks, so different patterns of interannual variation do not reject pairing these two specimens. (modified from *Chapter 2* – Fisher et al., 2014).

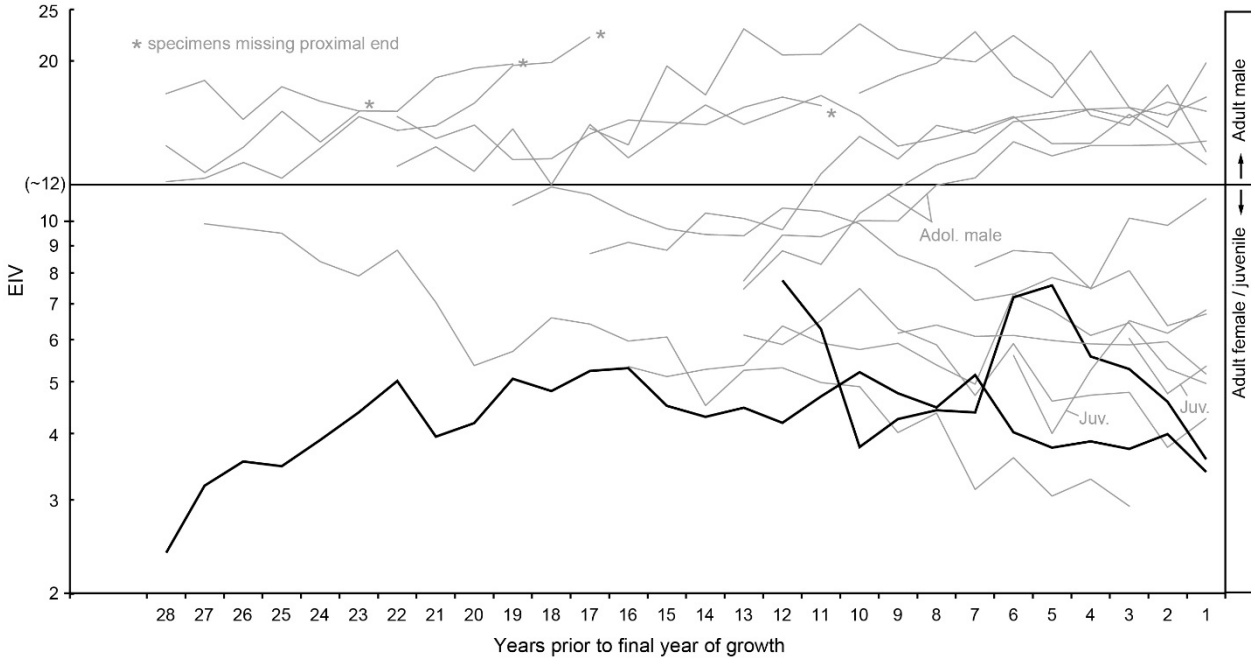

Figure 3.34. Tusk pair 6 oxygen isotope comparison.
Carbonate $\delta^{18}O$ records for ZR tusks have highly consistent seasonal variation, but average annual values vary by up to ~4 ‰. Vertical lines represent locations of annual CT features (abrupt transition from high to low density); fraction of final year is plotted as a percentage of expected growth for a complete year (see Figure 2.14). Because different tusks and different years within the same tusk may have different numbers of samples per year, sample intervals are spaced variably along the x-axis and aligned to annual CT features. Serial records for field nos. 56.015 and 63.125 are highlighted against the backdrop of all other ZR records obtained. General multiyear patterns, seasonal fluctuations, and annual averages are highly consistent between the two tusks. Small differences in the isotope profiles are an expected limit of sampling precision. Potentially different diagenetic effects associated with their different stratigraphic placements ("Main Silt" and "Main Floor Red Pebble" (Pigati et al., 2014)) could also produce differences such as the general enrichment in 56.015 that becomes more pronounced as samples approach the exposed pulp cavity surface. (modified from *Chapter 2* – Fisher et al., 2014).

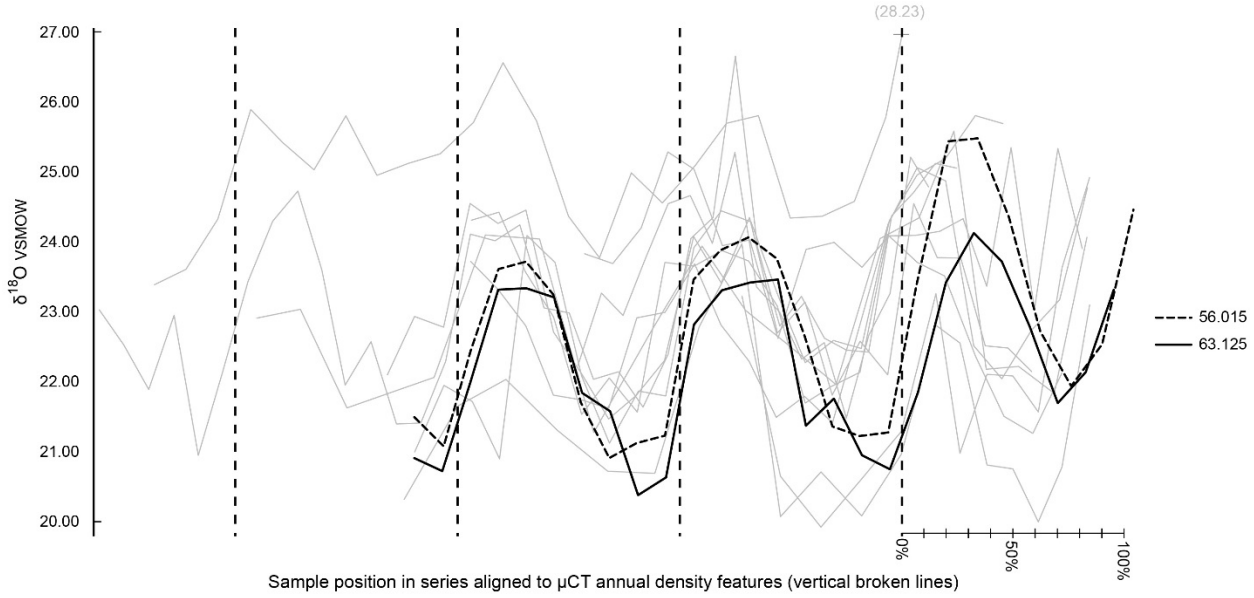

Figure 3.35. Tusk pair 6 carbon isotope comparison.
Carbonate $\delta^{13}C$ records for ZR tusks are highly variable and show signs of significant diagenetic effects (*Chapter 2* – Fisher et al., 2014). Data points are plotted in series with measurements from earlier growth on the left and $\delta^{13}C$ of later growth on the right. All records are right-justified so that the end of each series (representing the time of death) is aligned, but records in this plot do not have equivalent timing (sampling resolution varied between 5 – 8 samples per annual increment). Tick marks along the x-axis are unlabeled to highlight that data points for a particular abscissa are not equivalent. Serial records for field nos. 56.015 and 63.125 are highlighted against the backdrop of all other ZR records obtained. Variations in carbon isotope profiles may reflect taphonomic history more than original compositions. The records are remarkably consistent considering the apparent diagenetic effects and different stratigraphic associations of the tusks. Carbon isotope patterns are largely parallel with 56.015 consistently enriched compared to 63.125.

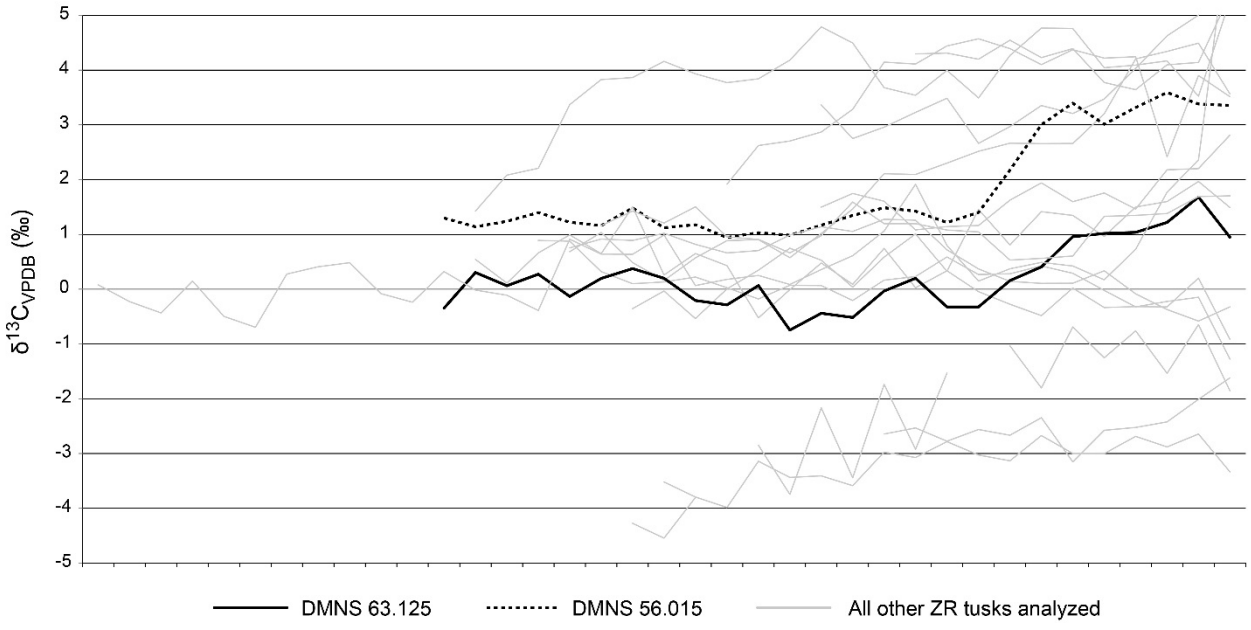

Figure 3.36. Tusk pair 7 medial views.
(A) field no. 64.013 (DMNH), right mandibular tusk, and (B) field no. 63.170 (DMNH), left mandibular tusk. Photos display general similarities in dorsoventral diameter, curvature, and distal wear. Both tusks are worn smooth at the distal ends (left) and have identically-angled wear facets.

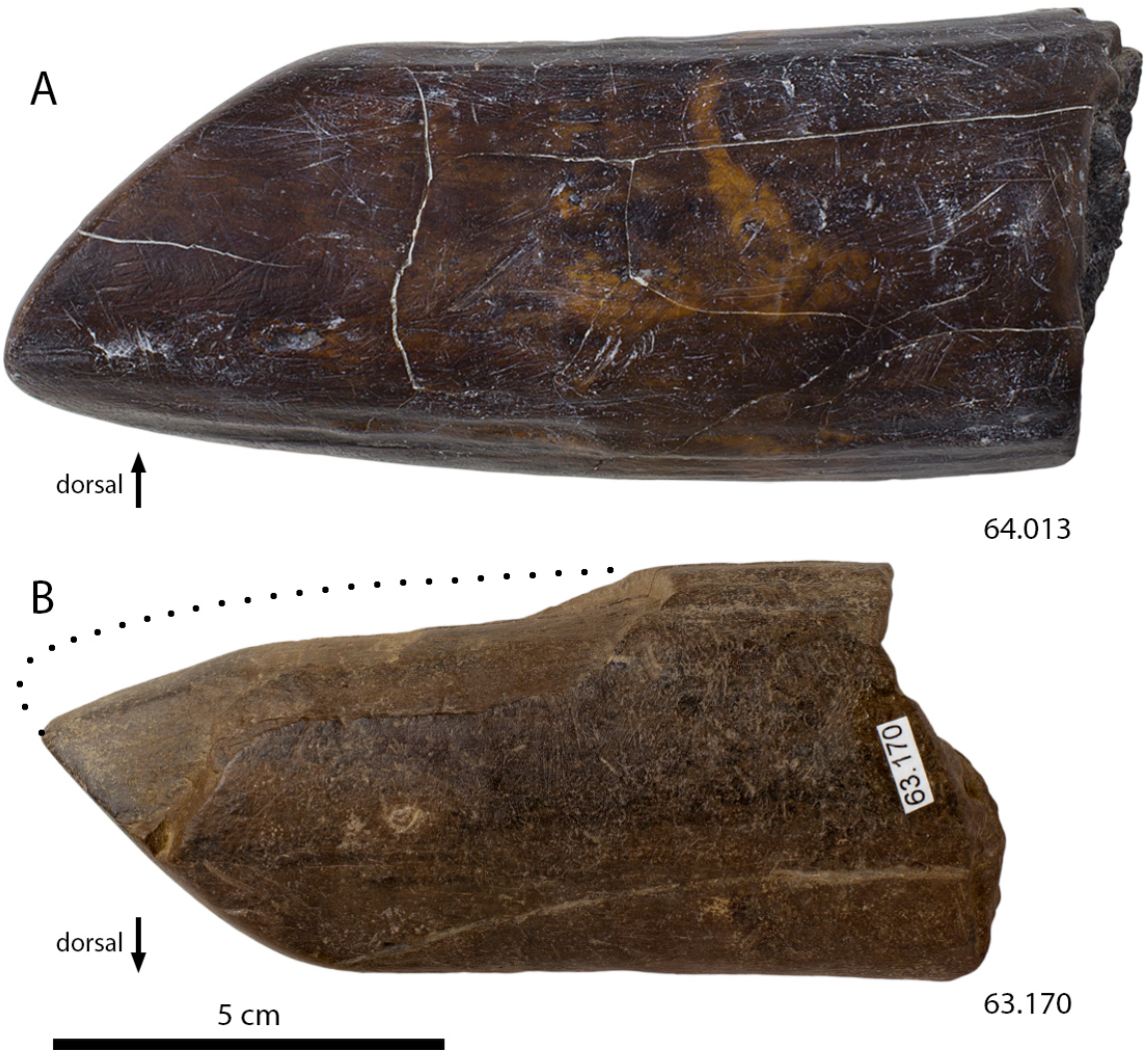

Figure 3.37. Tusk pair 7 dorsal views.
(A) field no. 64.013 (DMNH), right mandibular tusk, and (B) field no. 63.170 (DMNH), left mandibular tusk. Photos display general similarities in mediolateral diameter, curvature, distal wear, and gingival erosion features. Both tusks are worn smooth at the distal ends (left) and have identically-angled wear facets.

Figure 3.38. Tusk pair 7 EIV comparison.
EIV profiles for all ZR mandibular tusks scanned display considerable variation, apparent sexual dimorphism, and ontogenetic patterns. In this plot, partial growth records for tusks now identified as a left-right complement to another measured tusk have been aligned to the matching record. Annual growth profiles of EIV measurements taken from CT scans of field nos. 64.013 and 63.170 are highlighted. The overlapping portions of the records occupy the same general range and partially matching interannual variations. CT features were obscure for both tusks, so different patterns of interannual variation do not reject pairing these two specimens. (modified from *Chapter 2* – Fisher et al., 2014).

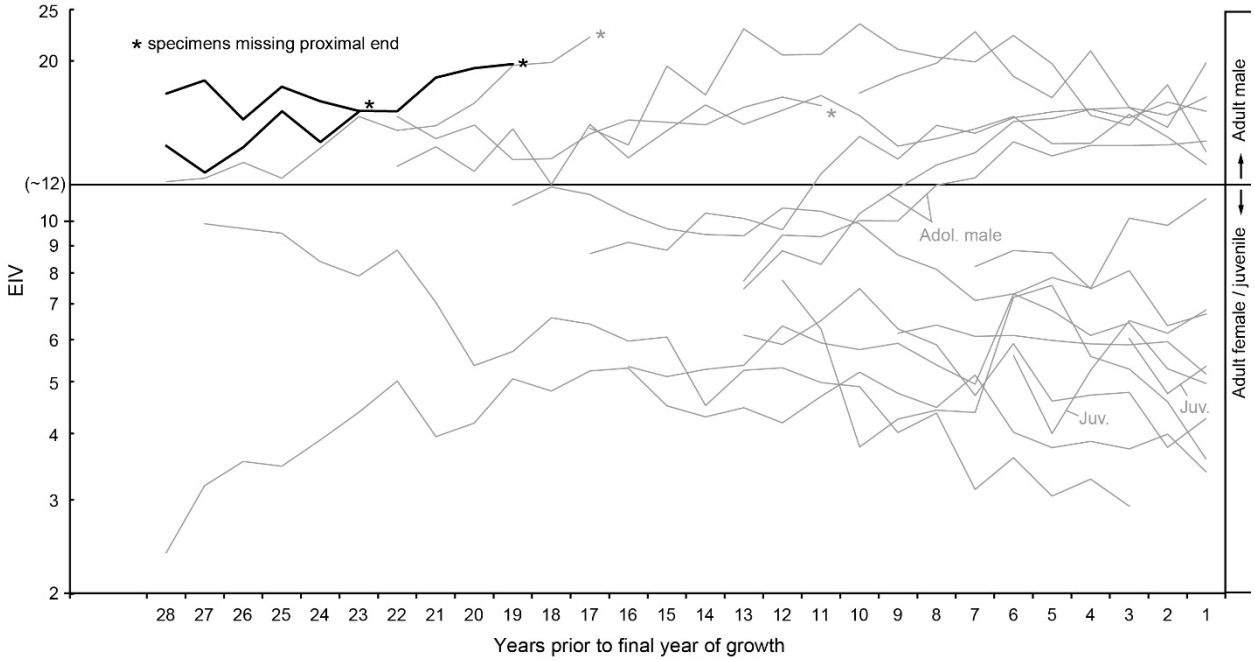

Figure 3.39. Tusk pair 8 proposed medial views.
(A) field no. 44.146 (DMNH), identified tentatively as a deciduous right mandibular tusk, and its possible complement (B) field no. 68.032 (DMNH). Photos display general similarities in dorsoventral diameter, curvature, crown size and shape, overall length, and distal wear. Both tusks are worn smooth at the distal ends such that about half the enamel crown remains. The proximal end (right) of 44.146 is missing, but most of the pulp cavity surface is preserved (see Figure 3.41).

Figure 3.40. Tusk pair 8 proposed dorsal views.
(A) field no. 44.146 (DMNH), identified tentatively as a deciduous right mandibular tusk, and its possible complement (B) field no. 68.032 (DMNH). Photos display general similarities in mediolateral diameter, curvature, crown size and shape, overall length, and distal wear. Both tusks are worn smooth at the distal ends such that about half the enamel crown remains. The proximal end (right) of 44.146 is missing, but most of the pulp cavity surface is preserved (see Figure 3.41).

Figure 3.41. Tusk pair 8 dorsoventral digital slices parallel to the axes from CT scans. (A) field no. 44.146 (DMNH), identified tentatively as a deciduous right mandibular tusk, and its possible complement (B) field no. 68.032 (DMNH). CT images display similarities in radiodensity expression of the feature identified as the neonatal line (*Chapter 2*; Fisher et al., 2014), depth and angle of the pulp cavity, enamel coverage and thickness, and cementum thickness. Termination of growth occurs simultaneously (in terms of growth after the neonatal line) in both tusks. The proximal end (right) of 44.146 is missing.

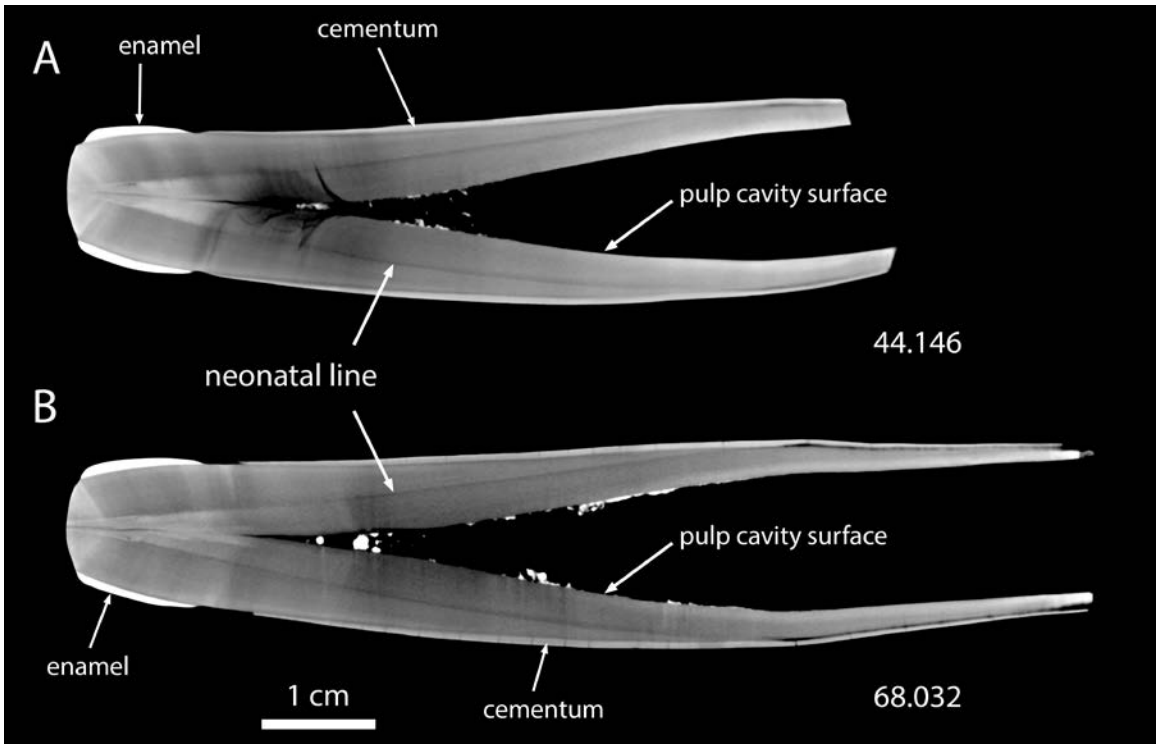

Figure 3.42. Tusk pair 9 proposed medial views.
(A) field no. 71.092 (DMNH), identified tentatively as a deciduous right mandibular tusk, and its possible complement (B) field no. 68.050 (DMNH). Photos display general similarities in dorsoventral diameter, curvature, crown size and shape, overall length, and distal wear. Both tusks are worn smooth at the distal ends such that about three-quarters of the enamel crown remains. The proximal end (right) of 71.092 is missing.

Figure 3.43. Tusk pair 9 proposed dorsal views.
(A) field no. 71.092 (DMNH), identified tentatively as a deciduous right mandibular tusk, and its possible complement (B) field no. 68.050 (DMNH). Photos display general similarities in mediolateral diameter, curvature, crown size and shape, overall length, and distal wear. Both tusks are worn smooth at the distal ends such that about three-quarters of the enamel crown remains. The proximal end (right) of 71.092 is missing.

Figure 3.44. Tusk pair 9 dorsoventral digital slices parallel to the axes from CT scans. (A) field no. 71.092 (DMNH), identified tentatively as a deciduous right mandibular tusk, and its possible complement (B) field no. 68.050 (DMNH). CT images display similarities in radiodensity expression of the feature identified as the neonatal line (*Chapter 2*; Fisher et al., 2014), depth and angle of the pulp cavity, enamel coverage and thickness, and cementum thickness. Termination of growth occurs simultaneously (in terms of growth after the neonatal line) in both tusks. The proximal end (right) of 71.092 is missing.

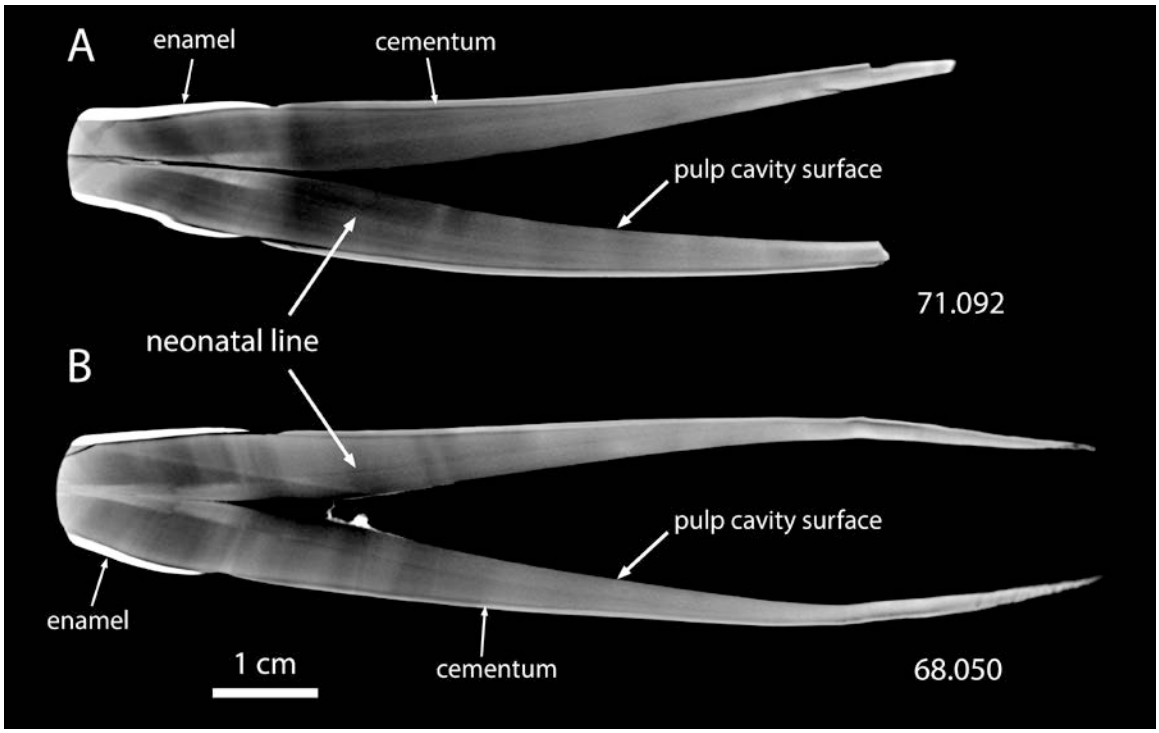

Figure 3.45. Spatial associations of proposed mandibular tusk pairs.
Aerial photograph of site with enlarged window showing portion of the "bone cloud" (Miller et al., 2014) where paired mandibular tusk specimens were found. Photograph from Google Earth was taken on 9/22/2011. Circles color-coded for stratigraphic association indicate locations of discovery for specimens proposed to be left-right pairs. Asterisks identify specimens not found in situ, for which stratigraphic association was confidently determined but original location not well-constrained. For those specimens, location plotted is that of the nearest stake. Dark gray broken lines connect pairs of permanent mandibular tusks and light gray broken lines connect potential pairs of deciduous tusks. Stratigraphic units refer to named near-shore units (Pigati et al., 2014) with the exception of "Unit 3," which refers to an unnamed clay layer at the base of the section that is correlated with Unit 3 in the lake-center stratigraphy. PDF – Primary Debris Flow; MS – Main Silt; MFRP – Main Floor Red Pebble; MF – Main Floor; BS – Basement Silt; BRP – Basement Red Pebble.

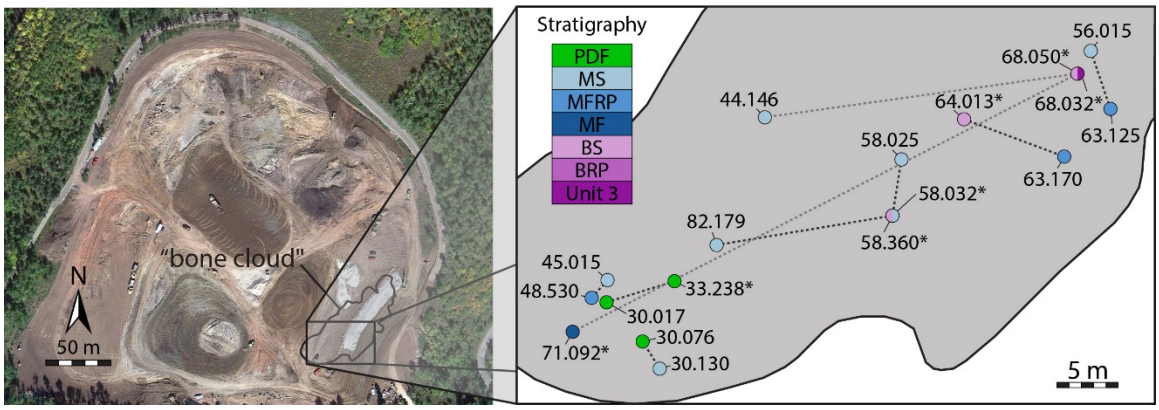

Figure 3.46. Updated partial census of Ziegler Reservoir mastodons.
Mandibular tusk circumferences and stage of cheek tooth eruption and wear determine relative ages of individuals. Main area of figure is a bivariate plot of Laws' Age Class determinations (Laws, 1966) vs. maximum circumference of mandibular tusks for specimens for which both can be assessed. At left is a histogram of additional specimens (mandibles without tusks) for which maximum tusk circumference cannot be assessed. Below is a histogram of additional specimens (isolated tusks) for which no Laws' Age Class is available (maximum tusk circumference rounded to nearest 0.5 mm). Updated from *Chapter 2* – Fisher et al. (2014).

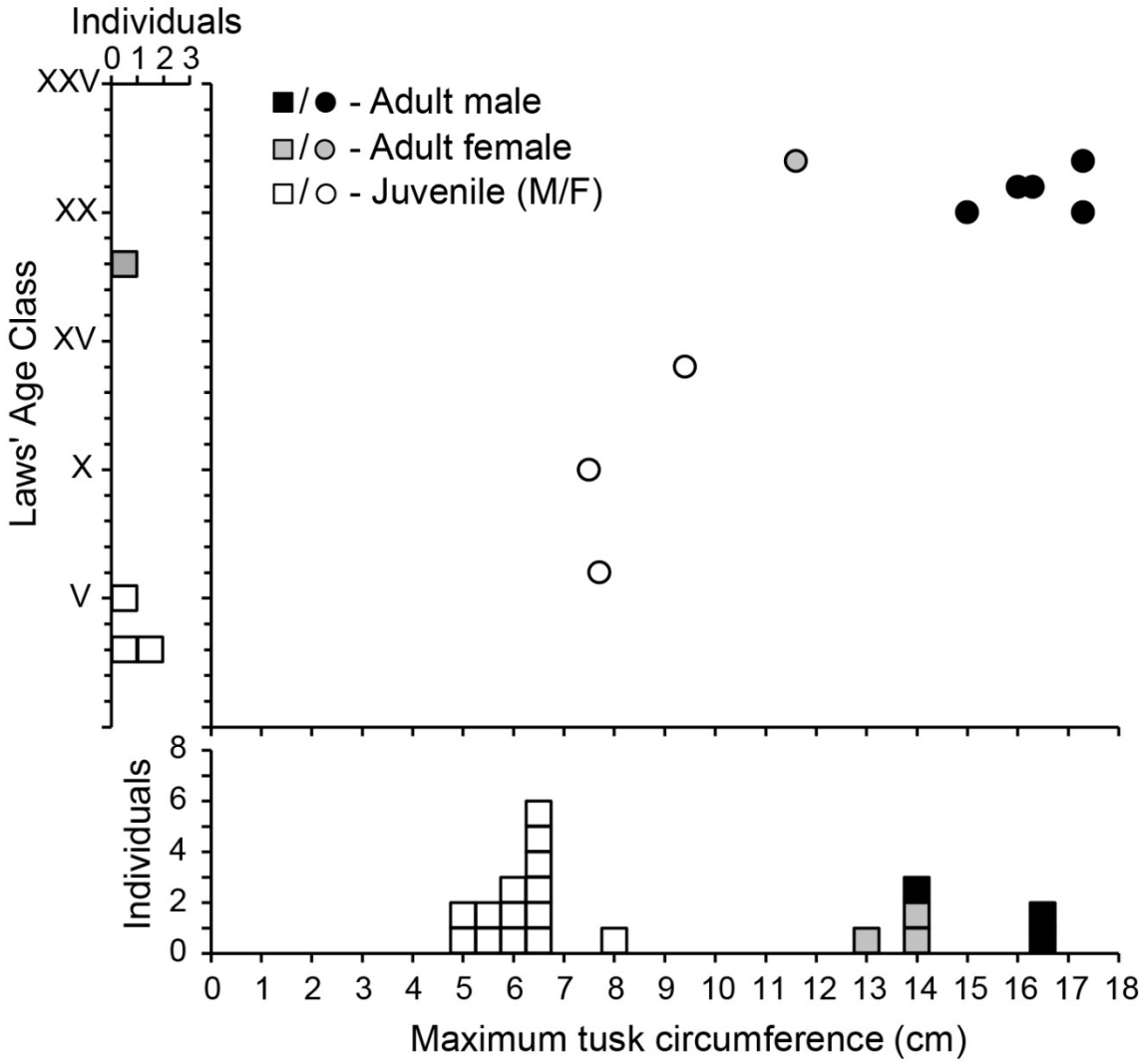

Figure 3.47. Updated season of death distribution for Ziegler Reservoir proboscideans. Calculations are grouped by association with stratigraphic units from Pigati et al. (2014): [Lake-margin] BS, Basement Silt; MF, Main Floor; MFRP, Main Floor Red Pebble; MS, Main Silt; PDF, Primary Debris Flow; [Lake-center] 16/17, boundary between Unit 16 (peat) and 17 (clayey silt). Units arranged in succession with youngest at top; order of specimens within units is by field number. Each estimate expresses the final increment volume as a percentage of annual increment volume expected for a complete year. For solid circles, expected volume = EIV for the last complete year; for open diamonds, expected volume = average EIV for the last two complete years; for open squares, expected volume is projected from a 5-yr linear trend (except for 56.127 and Loc 8 in which only three previous years are available) of logged EIVs. This last formulation of FFY is the one referred to in *Chapter 3* text. Data for Loc 8, Clay, 44.035, 70.018, and 56.266 are based on linear measurements rather than EIVs. Symbols beyond 100 % (e.g., 56.015) reflect either an uncharacteristically productive year or failure to recognize an obscure final feature. Provisional seasonal designations (based on evidence presented in *Discussion*) for each quarter of an expected year's growth are listed in parentheses along the top of the graph. Combining fraction of final year (FFY) measurements for identified left-right pairs and assigning both specimens to the lower stratigraphic unit represented has a significant impact on the season of death pattern for the ZR fossil site. Specimens reassigned to a lower stratigraphic unit are marked in gray. (*) Asterisk identifies FFYs that were abandoned, either due to an obscure penultimate feature better resolved upon re-inspection (33.238) or off-axis measurements that confounded FFY accuracy (58.360). For those specimens, FFYs are reassigned to calculations obtained for their matching specimen (see Table 3.1) In all but one proposed pair, FFYs were in the 4th quadrant (75-100+ %). Combining pairs thus reduces the number of year-end deaths by 4 and produces a slightly more scattered FFY distribution. Deaths are still concentrated in the second half of the annual cycle with only a quarter of individuals dying in the first half. Updated from *Chapter 2* – Fisher et al. (2014).

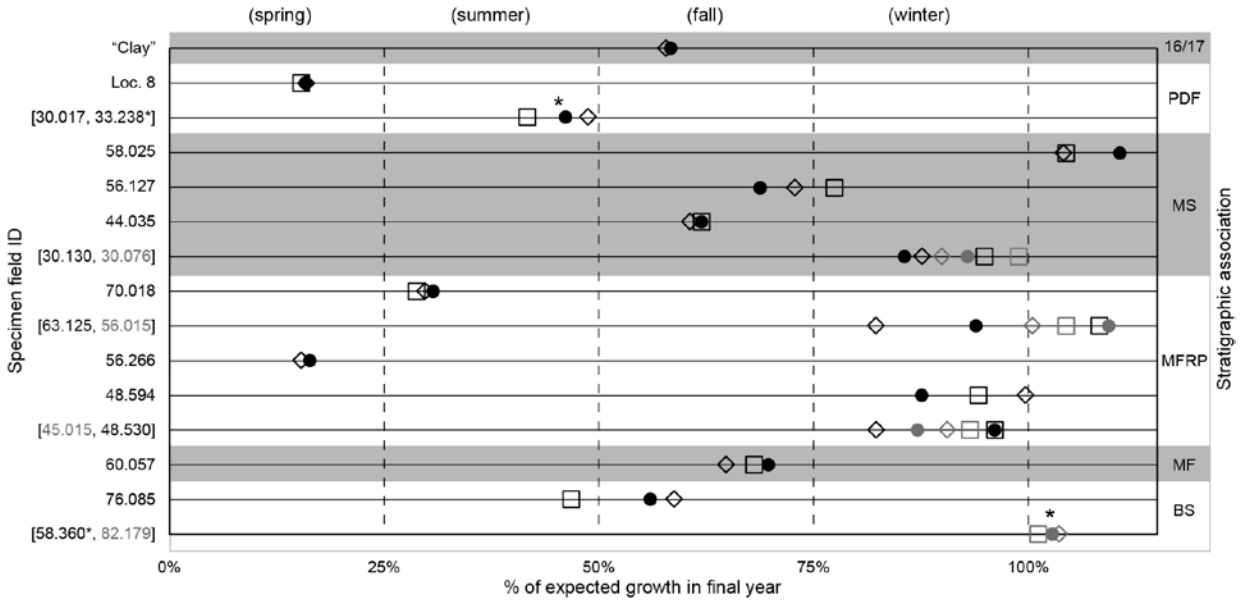
(spring)
(summer)
(fall)
(winter)
"Clay"
Loc. 8
[30.017, 33.238*]
58.025
56.127
44.035
[30.130, 30.076]
70.018
[63.125, 56.015]
56.266
48.594
[45.015, 48.530]
60.057
76.085
[58.360*, 82.179]
Specimen field ID
16/17
PDF
MS
MFRP
MF
BS
Stratigraphic association
0%
25%
50%
75%
100%
% of expected growth in final year

Figure 3.48. Updated oxygen isotope compilation for Ziegler Reservoir proboscideans. Comparison of multi-year oxygen isotope series for mastodon tusks from different stratigraphic units. Vertical lines represent locations of annual CT features (abrupt transition from high to low density); fraction of final year is plotted as a percentage of expected growth for a complete year (see Figure 2.14). Because different tusks and different years within the same tusk may have different numbers of samples per year, sample intervals are spaced variably along the x-axis and aligned to annual CT features. Tusk isotope records from the oldest unit sampled (BS, Basement Silt) produced average $\delta^{18}O$ values ~2.1 ‰ lower than those of specimens obtained from the highest unit sampled (PDF, Primary Debris Flow). Tusks from intermediate units (MF, Main Floor; MFRP, Main Floor Red Pebble; MS, Main Silt) consistently show $\delta^{18}O$ values between the two extremes. Horizontal lines mark average $\delta^{18}O$ values over all specimens sampled from each unit (BS – 3 spec., MF – 1 spec., MFRP – 4 spec., MS – 3 spec., PDF – 3 spec.). (B) Two mandibular tusks from Main Silt (MS) and one from the subjacent (and potentially genetically related) Main Floor Red Pebble (MFRP) have similar seasons of death and similar $\delta^{18}O$ series. Figure is a modified version of Figure 2.15. Notice that reassigning isotope records for each specimen paired with another from a lower stratigraphic unit has minimal impact on the up-section enrichment in $\delta^{18}O$ (compare to Figure 2.15). Averages for stratigraphic units change slightly, but the overall pattern remains intact with a ~2 ‰ enrichment between Basement Silt and Primary Debris Flow and the 'Main' units (Main Floor, Main Floor Red Pebble, and Main Silt) all overlapping about half way between. Stratigraphic unit names refer to those described in Pigati et al. (2014).

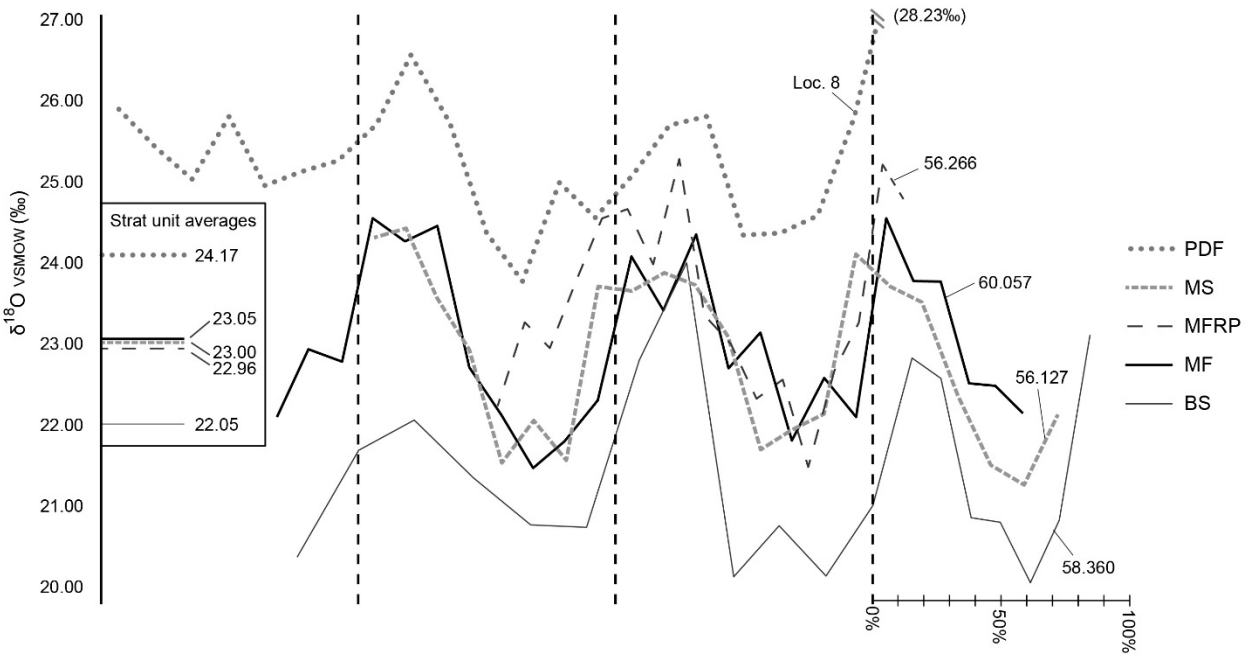
27.00
26.00
25.00
24.00
23.00
22.00
21.00
20.00
δ18O VSMOW (‰)
Strat unit averages
24.17
23.05
23.00
22.96
22.05
(28.23‰)
Loc. 8
56.266
60.057
56.127
58.360
0%
50%
100%
PDF
MS
MFRP
MF
BS

References

Büntgen, U., Liebhold, A., Jenny, H., Mysterud, A., Egli, S., Nievergelt, D., Stenseth, N. C., Bollmann, K. 2014. European springtime temperature synchronises ibex horn growth across the eastern Swiss Alps. Ecology letters 17(3):303-313.

Cherney, M. D., Fisher, D. C., Rountrey, A. N., Calamari, Z. T., 2012. Isotope analyses support use of CT scans for identifying annual increments in Snowmass mastodon mandibular tusks. Journal of Vertebrate Paleontology, Supplement, 72nd Annual Meeting, Program and Abstracts, p. 77.

Cherney, M. D., Fisher, D. C., Rountrey, A. N. 2014. X-ray computed tomography as a tool for analyzing life history information in proboscidean tusks. Abstracts of the VIth International Conference on Mammoths and Their Relatives, Scientific Annals of the School of Geology, Aristotle University of Thessaloniki, Special Volume 102, p. 41.

El Adli, J., Fisher, D., Cherney, M., Labarca, R., Lacombat, F. 2015. First analysis of tusk growth rate and season of death of a South American gomphothere. Journal of Vertebrate Paleontology, Program and Abstracts, 2014, p. 120.

Fisher, D. C., 2008. Taphonomy and paleobiology of the Hyde Park mastodon. In: Allmon, W. D., Nester, P.L. (Eds.), Mastodon Paleobiology, Taphonomy, and Paleoenvironment in the Late Pleistocene of New York State: Studies on the Hyde Park, Chemung, and North Java Sites. Palaeontographica Americana 61, 197–290.

Fisher, D. C., Beld, S. G., Rountrey, A. N., 2008. Tusk record of the North Java mastodon. In: Allmon, W. D., Nester, P.L. (Eds.), Mastodon Paleobiology, Taphonomy, and Paleoenvironment in the Late Pleistocene of New York State: Studies on the Hyde Park, Chemung, and North Java Sites. Palaeontographica Americana 61, 417–463.

Mahan, S. A., Gray, H. J., Pigati, J. S., Wilson, J., Lifton, N. A., Paces, J., Blaauw, M. 2014. A geochronologic framework for the Ziegler Reservoir fossil site, Snowmass Village, Colorado. Quaternary Research 82(3):490-503.

Miller, I. M., Pigati, J. S., Anderson, R. S., Johnson, K. R., Mahan, S. A., Ager, T. A., … Wilson, J. 2014. A high-elevation, multi-proxy biotic and environmental record of MIS 6–4 from the Ziegler Reservoir fossil site, Snowmass Village, Colorado, USA. Quaternary Research 82(3):618-634.

Pigati, J. S., Miller, I. M., Johnson, K. R., Honke, J. S., Carrara, P. E., Muhs, D. R., Skipp, G., Bryant, B. 2014. Geologic setting and stratigraphy of the Ziegler Reservoir fossil site, Snowmass Village, Colorado. Quaternary Research 82(3):477-489.

Chapter 4

Stable isotope patterns in a nursing mother-calf pair of African elephants (*Loxodonta africana*) as a modern analog for interpretation of fossil tusk records

Introduction

Nursing extends a direct nutritional connection between mother and offspring beyond parturition and affects stable isotope body chemistry of both suckling young and lactating mothers (Fuller et al., 2004, 2006). Weaning is the process of eliminating this mother-offspring interaction and forces juveniles to begin living without supplementation from their mother's milk.

We can investigate nursing and weaning retrospectively using stable isotope compositions of tissues produced during lactation in mothers and nursing in offspring. Isotope ratios preserved in archaeological (Dupras et al., 2001; Fogel et al., 1989; Richards et al., 2002) and paleontological remains (Liden and Angerbjorn, 1999; Nelson et al., 1998) including fossil proboscideans (Metcalfe et al., 2010; Rountrey et al., 2007,

Rountrey, 2009) make it possible to look at nursing and weaning even in long-dead individuals, including extinct organisms that cannot be observed directly. Studies investigating the stable isotope signatures of lactation in records from reproductive-age females are less common than those looking at nursing in juveniles, but in at least one case, stable isotope patterns recorded in the growth layers of mastodon tusks were proposed to reflect lactation (Fisher and Fox, 2003).

Interpretations of lactation, nursing, and weaning in fossil proboscideans have been based on a general understanding of how nursing affects the stable isotope compositions of a newborn's tissues (e.g., Dalerum et al., 2007; Fogel et al., 1989; Fuller et al., 2006; Hobson and Sease, 1998; Hobson et al., 2000; Jenkins et al., 2001; Polischuk et al., 2001; Richards et al., 2002). Previous analyses of the tusk of a deceased African elephant calf corroborated expectations regarding compositional patterns during the first few years of life (Rountrey, 2009), but the isotopic relationship between mother and calf had not previous been investigated in proboscideans. Differences in isotope patterns associated with nursing and weaning in different species (Jenkins et al., 2001) and variations from theoretical expectations (Dalerum et al., 2007) highlight the need for close analogs when looking for signatures of weaning. This report describes observed effects of nursing and weaning on stable isotope records (nitrogen – $\delta^{15}N$, carbon – $\delta^{13}C$, oxygen – $\delta^{18}O$, and hydrogen – δD) of a mother-calf pair of captive African

elephants (*Loxodonta africana*) as a reference for interpretation of isotope records from fossil proboscideans. Two years of bimonthly sampling of hair and milk, observations during sampling episodes, and attempts to align records for hair grown prior to initial sampling all resulted in additional discoveries pertaining to elephant hair growth, milk composition, and hair cortisol measurements that are also reported below.

Hair growth record

Hair has been used extensively in biology as a continuous recorder of an individual's stable isotope chemistry spanning the interval of formation (e.g., Cerling et al., 2004, 2006, 2009; Darimont and Reimchen, 2002; Ehleringer et al., 2008; O'Connell and Hedges, 1999; Valenzuela et al., 2011). Because it is often composed of very fine strands, typical analyses use sampled derived from multiple hairs, each of which may be in anagen (the growing phase of a hair follicle) or catagen (a period when the hair stops growing prior to telogen when the follicle becomes temporarily hairless) and could be growing at a different rate than others. Human hair growth is enhanced during pregnancy when the number of follicles in anagen increases and the number in telogen decreases (Lynfield, 1960). It also shows seasonal variation with increases in anagen hairs accompanied by increases in growth rate (Randall and Ebling, 1991). In some special cases, such as an elephant's tail tuft, each hair is massive enough to individually provide material for serial compositional analyses. A single hair can grow for multiple years and

thus provide a potential tool for looking at past long-term patterns of variation with high fidelity. Elephant tail hairs have been analyzed as recorders of past diet and behavior over extended periods (Cerling et al., 2004, 2006, 2009; Wittemyer et al., 2009) and provide data comparable to proboscidean tusk records (Uno, 2012). Unlike tusks, which contain features that provide independent constraints on timing of dentin apposition, tail hairs have no clear incremental features. As such, hair chronologies have to be reconstructed using growth rate and variability estimates to constrain alignment of temporal 'landmarks' shared by records from individual hairs. Previous authors have back-calculated growth rates and variability by comparing profiles from overlapping records of multiple hairs from a single individual (Cerling et al., 2004, 2006, 2009; Wittemyer et al., 2009). In this study, we monitored individual hair growth rates (as well as average growth rates) on a bimonthly basis over two years and used observed parameters to inform reconstruction of hair record chronologies for preceding years.

Hair isotopes

Hair $\delta^{13}C$ and $\delta^{15}N$ reflect diet (O'Connell and Hedges, 1999; Osorio et al., 2011; Sponheimer et al., 2003A, 2003B), but due to different fractionation factors for amino acids in hair keratin, isotope values are offset from those in bone (and tusk) collagen (Ambrose and Norr, 1995; Deniro and Epstein, 1978; Nakagawa et al., 1985; O'Connell et al., 2001). $\delta^{18}O$ and δD of hair partially reflect drinking water (Podlesak et al., 2008) and

as a result are imprinted with information that can inform geographic interpretations based on regional variability in water isotopes (Ehleringer et al., 2008; Thompson et al., 2010).

Milk composition

Milk is usually composed primarily of water, with protein, fat, sugar, and mineral components. Milk proteins can be divided into caseins, most of which precipitate at pH 4.6 (Whitney, 1988), and whey proteins that remain soluble. Milk fats consist mostly of triacylglycerols with small amounts of sterols and phospholipids (Jensen and Clark, 1988). The primary carbohydrate in milk is lactose (Jenness, 1988; Jenness et al., 1964). Milk composition differs among mammal species (Holt and Jenness, 1984; Jenness et al., 1964; Jenness and Sloan, 1970; Jenness, 1974; McCullagh and Widdowson, 1970) significantly in relative amounts of each component. Its composition also changes from beginning to end of lactation (Rook, 1961) and may even display seasonal changes (Nickerson, 1960). Species can have different patterns of variation in milk composition over the course of lactation. Cow and elephant milk increases in fat and protein later in lactation (McCullagh and Widdowson, 1970; Rook, 1961), whereas protein decreases in horse and zebra milk over time (Oftedal and Jenness, 1988). On a minute scale, composition changes during suckling with foremilk containing less fat than hindmilk (Atwood and Hartmann, 1992).

In terms of percent contributions of fat, protein, and lactose, elephant milk most closely resembles pig and giraffe milk (McCullagh and Widdowson, 1970). Elephant milk is expected to have more fat and whey proteins (11.6%, 3.0%) than both cow (3.7%, 0.6%) and human (3.8%, 0.6%) milk, caseins (1.9%) intermediate between cow (2.8%) and human (0.4%) milk, and about the same amount of lactose (4.7%) as cow (4.8%) compared to higher concentrations in human milk (7.0%) (Jenness, 1974).

Milk isotopes

Stable isotope fractionation in carbon and nitrogen varies in milks of different species. This can be explained at least in part by different compositions (described above). For example, milks with high fat contents would be expected to have lower $\delta^{13}C$ values due to the preferential incorporation of light carbon during lipid synthesis (Deniro and Epstein, 1977). Oxygen in milk water is typically enriched compared to drinking water by 2 – 6 ‰ (Kornexl et al., 1997; Lin et al., 2003), and a simple linear relationship with milk-water oxygen as a function of drinking-water oxygen may explain much of the variation in enrichment between about 1 and 4 ‰ (Chesson et al., 2010). Feeding regimen may also affect this relationship. In a study by Renou et al. (2004) water oxygen in milk from grazing cows was enriched by 3 – 6 ‰, while from hay-fed cows it was only enriched by 1 ‰.

Nursing signature

Nursing and weaning produce characteristic patterns in $\delta^{13}C$ and $\delta^{15}N$ of mother and offspring. Typically, nursing young are enriched in $\delta^{15}N$ and $\delta^{13}C$ compared to their mothers (Dalerum et al., 2007; Fogel et al., 1989; Fuller et al., 2006; Hobson and Sease, 1998; Hobson et al., 2000) due to what is effectively trophic-level enrichment as they feed on their mothers' milk. Jenkins et al. (2001) recorded variations in this pattern across different species. They detected little enrichment in $\delta^{13}C$ and sometimes not much more enrichment in $\delta^{15}N$. According to that analysis, trophic enrichment is offset by milk being depleted in both $\delta^{13}C$ and $\delta^{15}N$ compared to the lactating female's plasma. There is also some suggestion from a comparison of juveniles and adult mammoth fossil isotope records of a nursing enrichment in oxygen (Metcalfe et al., 2010), but we found no study documenting this in a modern species.

High-resolution serial records documenting changes in $\delta^{13}C$ and $\delta^{15}N$ throughout nursing and weaning in fingernail samples from several human mother-baby pairs (Fuller et al., 2006) in some cases showed a decrease in infant $\delta^{13}C$ immediately after birth, followed by enrichment and then another depletion relative to its mother shortly after weaning was initiated. Peak enrichment in both $\delta^{13}C$ and $\delta^{15}N$ occurred around 20-30 weeks and was typically earlier in $\delta^{13}C$ than $\delta^{15}N$. Although weaning in this study was associated with some convergence in parent-offspring isotope records, baby values

remained elevated compared to mother values in these studies even after final weaning. This could be due to dietary differences between mothers and their recently weaned infants. Alternatively, it could also indicate the baby catabolizing stored proteins to compensate for the removal of breast milk from its diet, since recycling proteins would also enrich the baby's systemic $\delta^{15}N$ (Hobson et al., 1993).

Hair cortisol

Cortisol is commonly known as the "stress hormone" in mammals. It is a glucocorticoid (a steroid that regulates glucose metabolism) produced by the adrenal cortex as a physiological response to stress that increases blood sugar and aids in metabolism. Cortisol levels in blood serum and saliva can change significantly from one hour to the next. Cyclic diurnal patterns show cortisol levels highest around waking time and then dropping throughout the day (e.g., in humans: Aardal and Holm, 1995; Weitzman et al., 1971; in horses: Aurich et al., 2015; in elephants: Menargues et al., 2012). Systemic cortisol levels can also change abruptly in direct response to stressors (Young et al., 2004). Because of consistent circadian cycling, long-term analyses of serum and saliva cortisol require collections to be at the same time every day of sampling. However, by point-sampling an isolated moment of each day during an interval, these analyses cannot detect long-term changes that are only expressed during

unsampled portions of the day. For example, an increase in evening cortisol might go undetected with a consistent regimen of morning sampling.

Cortisol measurements from hair samples representing days, weeks, months, or years of growth are claimed to reflect long-term averages of systemic cortisol levels (Dettenborn et al., 2010; Skoluda et al., 2012; Stalder et al., 2012; Van Uum et al., 2008). An isolated stressful event would not be likely to make a significant contribution to the hair cortisol record. Meanwhile, increases in frequency of stressful events are indistinguishable in the hair record from persistent elevated levels. Hair cortisol analyses also have the benefit of providing records of past cortisol levels, whereas blood serum and saliva only offer a momentary present snapshot of a system in constant flux.

There are a few challenges to interpreting hair cortisol records as accurate representations of average systemic values over time. Local production of cortisol in the hair follicle (Ito et al., 2005; Slominski et al., 2007) could produce patterns that do not reflect systemic cortisol variation (Sharpley et al., 2009, 2010), and although most cortisol in hair likely originates directly from blood as hair cells form, additional cortisol may come from sweat and sebum after hair emerges from the follicle (Henderson, 1993; Stalder and Kirschbaum, 2012). There is also evidence of a "washout" effect with cortisol only being preserved in hair close to the scalp (Hamel et al., 2011; Kirschbaum et al.,

2009). However, not all studies display patterns consistent with this, and Manenschijn et al. (2011) suggest it may actually be an effect of sample cleaning having a more pronounced effect on older hair more damaged by exposure.

Despite challenges, hair cortisol is being used increasingly as a tool for looking at long-term patterns in humans and other mammals. Some effort has even been made to measure and interpret cortisol levels in preserved archaeological hair samples (Webb et al., 2010, 2015), but the extremely high concentrations detected in those studies cast some doubt on the integrity of the results.

Analyses of cortisol in elephant blood serum and saliva show seasonal variability (Marcilla et al., 2012) and provide a measure of well-being in captive individuals (Mason and Veasey, 2010). Although average levels may be relatively low in pregnant elephants (Oliviera et al., 2008) we expect cortisol to increase during late pregnancy (Kajaysri and Nokkaew, 2013; Sandman et al., 2006) and for at least a short period following birth (pers. comm. with Sharon Glaeser, Oregon Zoo). Elephant hair cortisol levels have been documented previously (Berkvens, 2012), but to our knowledge the analysis described here is the first long-term serial analysis of elephant tail hair and demonstrates the technique's potential as a tool for assessing multiyear patterns of stress in elephants.

Materials

Lucas is a male African elephant (*Loxodonta africana*) born at the Toledo Zoo (Toledo, OH) on June 1, 2011 following a normal ~22 month gestation after his mother, Renee, was artificially inseminated in September of 2009 when she was 30 years old. With extensive cooperation from zoo staff and administrators, we started on November 1, 2012 collecting Renee's milk, Lucas' and Renee's tail hair, and water from the elephant drink tank. Twice during the study period, we also collected samples of a variety of foods that were regularly incorporated into the animals' diets. These included hay (that provides the bulk of their diet) as well as various fruits, vegetables, tubers, and other roughage.

Methods

Specimen collection and treatment

Zoo handlers collected milk and tail hair samples bimonthly over a period of just over two years (11/2012 through 01/2015 – this represents the time period reported here; at time of writing, sampling was ongoing). I monitored and assisted each sampling episode and hand-carried all samples back to facilities at the University of Michigan Museum of Paleontology for processing and preparation for stable isotope and cortisol

analyses. The live animal testing was sanctioned by the University of Michigan, and procedures were approved and implemented by zoo staff under the authority of the Toledo Zoo. To limit impact on the elephants, we planned sampling to correspond with daily physical inspection routines. Tail hairs were clipped during routine tail inspection, but milk collection was an add-on to normal procedure. Following voice commands, elephants presented their appendages through an open gate that permitted access through the safety barrier.

Milk sampling

Toledo Zoo elephant handlers expressed milk manually from one or both of the mother elephant's nipples into a clean stainless steel pan and promptly transferred it to 2 mL plastic screw-top vials using a bulb pipette. To prevent atmospheric isotope exchange, vials were filled to the top, thus limiting the amount of air included with the milk sample. We wrapped closed screw-top vials with Parafilm® laboratory film to seal them thoroughly. A small bubble of air in the sealed vial provided room for expansion during freezing. Samples were transported to the museum in an insulated bag with a cold pack and then immediately placed in a freezer and stored at –28°C. Total transport time was variable (between 2 and 5 hours) but in all cases, we were able to keep the sample cold throughout transport.

We attempted to collect two vials during each sampling episode. Milk flow was different in each breast and during each sampling episode, but we detected no long-term trends in production during the sampling interval. Usually we collected one full vial without much difficulty, but we only successfully collected two vials on some occasions. This variability could have been related to timing of her calf's suckling, which was not consistently monitored. Typical collection involved milk from both breasts.

Prior to analysis, frozen milk samples were thawed overnight in a refrigerator at 8 °C. We first removed 0.5 mL of each sample for analysis of milk-water $\delta^{18}O$. The remaining milk was centrifuged to isolate fats and skim milk for separate analyses. 1 – 1.5 mL of each sample was pipetted into a 1.5 mL microcentrifuge tube for separation. We separated and collected milk fat via multiple rounds of centrifugation (10 min. at 7000 rpm – ~3000 g) skimming fat from the surface after each round and depositing it into a separate microcentrifuge tube. The supernatant from the first tube (skim milk) was pipetted into a third tube, and the remaining debris (mostly leukocytes) was set aside. We attempted to isolate casein from elephant milk via acidification-induced coagulation (following procedures for bovine milk documented in Kornexl et al. (1997) that used 0.5 M HCl for acidification to pH 4.3), but at pH 4.3, no curdling occurred. Instead, the entire volume thickened evenly to the consistency of thin yogurt. In contrast, control samples (bovine milk (pasteurized and homogenized) and human milk (raw) that had been

frozen along with the elephant milk samples) produced the expected curds that readily separated from the whey following centrifugation at 7000 rpm (~3000 g) for 5 minutes. Since the elephant milk (which also had a higher starting pH than both the bovine and human milk and thus required more HCl to get to pH 4.3) did not curdle, we lyophilized the entire thickened skim milk mass for collective analysis of casein, whey proteins, and lactose.

Three tubes for each milk sample (1 – debris, 2 – lipids, 3 – skim milk) were lyophilized. For all milk samples, debris in tube 1 produced insufficient mass for analysis, lipids in tube 2 resulted in a mixture of clear oil (liquid at room temperature) and solid fats that separated during lyophilization, and skim milk in tube 3 turned into an apparently homogenous dry powder. We analyzed dehydrated skim milk for both nitrogen ($\delta^{15}N$) and carbon ($\delta^{13}C$) separately, and processed liquid oil and solid fat components each for $\delta^{13}C$.

Hair collection

Three hairs from the ventral side of Renee's tail (where most of the long hairs reside) were repeatedly clipped and monitored for extended periods during the study period. To obtain definitively serial records for Renee's hairs, we repeatedly targeted individual hairs (Figure 4.1), in most cases sampling only the previous two months of

growth each time. At the time of cutting, the distal tip of each hair (which had sharp edges when it was cut two months prior) was sometimes worn smooth (particularly during summer and fall sampling when insects would have been more abundant) from two months of use, but there was never any indication of breakage on these growing hairs, and the amount of hair lost due to gradual wear appears to have been very small. After one year of repeatedly sampling the same two hairs (A_{mother} – more proximal, closer to the base of the tail; B_{mother} – more distal, closer to the tip of the tail), the more proximally located hair (A_{mother}) could no longer be positively identified due to thinning and breakage in the proximal portion of the hair tuft. At this point, we started sampling a new hair (C_{mother}) distal to hair B_{mother} and well within the region of the tuft containing the longest hairs. For the second year of sampling, hair B_{mother} was the more proximal hair. Initial samples of hairs A_{mother} and B_{mother} were long hairs representing many months of growth. The initial sample of hair C_{mother} was short and likely contained approximately 1 month of growth. Samples taken during winter and spring could frequently be verified by matching the cut on the lightly worn distal end to the cut on the proximal end of the previous sample. The distal ends of samples taken during summer and fall were worn smooth, and cut surfaces could not be matched. For these samples, photo documentation of sampling provided some confidence that we were in fact collecting new growth from the same two hairs. Complicating photographic

documentation was the continuously changing pattern of dermal furrows on the tail surface, which makes it difficult to align photographs taken even just months apart. With the exception of the time hair A_{mother} could not be identified and was lost, two hairs in the same location, with the same spatial relationship to each other, and with similar amounts of new growth stood out prominently against the other long hairs during each sampling episode. These hairs were usually quickly and confidently identified as the two target hairs.

Several different hairs were sampled from Lucas' tail and monitored with varying degrees of success over the duration of the study period. During the first sampling episode, we only cut one long hair (A_{calf}). In our next sampling visit to the zoo, we found what we thought was the same hair, but being uncertain, we cut an additional previously uncut long hair (B_{calf}). Lucas' individual tail hairs were substantially thinner than his mother's throughout the sampling period. It was more difficult to find previously cut hairs, and hairs were more likely to be broken and lost. Besides being less robust, the reasons for this are not all clear, but a witnessed incident of Renee biting Lucas' tail provides one possible explanation. For these reasons, it became clear that it would be difficult to serially clip individual hairs, as was possible for Renee. Instead, we repeatedly cut a single clump of six hairs (C_{calf}) that stood out from surrounding hair when cut (Figure 4.2). Additional breakage of nearby hair made it difficult to find this clump after

a few repeated samplings. When we felt that we could no longer positively identify the hair clump, we clipped a new 8-hair clump (F_{calf}) located more distally, where surrounding hairs were more substantial and less likely to suffer breakage. This clump has been easily identified and clipped in subsequent sampling episodes and has provided a reliable average growth rate for the hair clump over a 4-month period. We do not know how F_{calf} rates compare to those of hair grown earlier in life, but other less reliable estimates from earlier samples were lower. Growth rate analyses are discussed in detail in *Results* below.

Water/feed sampling

Drinking water was collected during several visits to the zoo by submerging vials in the reservoir and capping them underwater to avoid inclusion of air in the sealed vials. We wrapped closed screw-top vials with Parafilm® laboratory film for an extra seal and transported them to the museum in an insulated bag with a cold pack. Back at the museum, we placed them in a refrigerator at 8 °C where they remained (up to 18 months) before being analyzed for $\delta^{18}O$. All feed samples were packed in separate sealed plastic bags and were placed in a freezer at –28 °C. These have not yet been analyzed.

Isotope analyses

To sample for isotope analyses of Renee's hair, we removed small (2 – 3 mm) wedges from one side of the hair shaft, leaving the length of the hair intact (Figure 4.3A). Each bimonthly clipping was sampled once at its proximal end close to the base. The longer of the two hairs initially cut from Renee (B_{mother}) was sampled every 20 mm starting from the base to roughly approximate a monthly periodicity of analyses (see *Results* for growth rate estimates) that represented time prior to initial sampling. Each wedge removed from the hair was divided into a larger portion for $\delta^{13}C$ and $\delta^{15}N$ analysis and a smaller one that was analyzed for $\delta^{18}O$ and hydrogen (δD).

We sectioned the first hair sampled from Lucas (A_{calf}) into twenty-six segments (3.5 – 8 mm long depending on hair thickness where the sample was taken) cut to meet the target mass for joint $\delta^{13}C$ and $\delta^{15}N$ analysis. (Figure 4.3B). Since sample mass was a limiting factor for Lucas' hairs, this strategy provided the highest temporal resolution we could achieve. For 11 samples of hair grown during the study period, we trimmed the sample mass required for $\delta^{13}C$ and $\delta^{15}N$ analysis from the proximal ends of cut hairs. A distally adjacent smaller sample of each hair (or tuft of hairs) collected after November 2012 was analyzed for $\delta^{18}O$ and δD. However, because hair A_{calf} had been exhausted for carbon and nitrogen analysis, reconstruction of $\delta^{18}O$ and δD records for the period prior to initial sampling required the use of a second hair ($C[1]_{calf}$) that was cut into 5 mm

segments (this time attempting to approximate monthly growth), from which subsamples were analyzed.

Prior to sampling, all hairs were wiped with acetone to remove surface oil and debris. Samples weighing 622 ± 10 µg (the target mass determined to match sample and standard peak voltages for both nitrogen and carbon) were wrapped in tin capsules for joint analysis of $\delta^{13}C$ and $\delta^{15}N$. For joint analysis of $\delta^{18}O$ and δD, samples weighing 150 ± 10 µg were wrapped in silver capsules.

Milk oil and solid milk fat were analyzed for $\delta^{13}C$ only. Oil samples were weighed to 425 ± 10 µg using 1.0 µl Drummond Microcaps® pipettes and folded into tin capsules taking care to prevent leaks. Solid fat samples were weighed into tin capsules to 460 ± 10 µg. Sample masses for both fat components were selected based on a target peak voltage of 7 kV for carbon.

Nonfat milk solids (containing casein, lactose, and whey proteins) were analyzed for $\delta^{13}C$ and $\delta^{15}N$ separately. Samples for $\delta^{13}C$ analysis were weighed to 613 ± 10 µg to target peak voltage 7 kV for carbon. For $\delta^{15}N$ analysis, additional portions of each lyophilized sample were weighed to 1200 ± 10 µg to get a peak voltage of 6.5 kV for nitrogen. Samples were wrapped in tin capsules for analysis of $\delta^{13}C$ and $\delta^{15}N$.

All $\delta^{13}C$ and $\delta^{15}N$ analyses of hair and milk solids were performed in the University of Michigan Stable Isotope Laboratory on a Costech ECS 4010 elemental analyzer coupled to the inlet of a Finnigan Delta V Plus mass spectrometer in continuous flow mode. Internationally calibrated standards were used to normalize on a per-run basis, and accuracy and precision of $\delta^{13}C$ and $\delta^{15}N$ was maintained at better than ± 0.12 ‰.

Adsorbed atmospheric water and isotopic exchange can substantially affect the measured δD and $\delta^{18}O$ composition of keratin. To address this source of isotopic uncertainty, we followed procedures outlined by Coplen et al. (2012) for hair isotope analysis. All samples and standards were allowed to equilibrate in the laboratory for 5 days prior to preparation. Following this period, approximately 150 µg of sample and reference materials were weighed into 3 X 5 mm silver capsules (Costech Analytic) and crimped using solvent-washed tweezers. Sample and standard materials were then placed into a vacuum dryer for five days. Hair samples and keratin standards were placed in a sealed, dry equilibration chamber along with non-keratin hydrogen isotope reference materials NBS 22, PEF-1, and a laboratory clay standard, for a period of seven days. Following equilibration in the dry chamber, all samples were immediately loaded into a Costech Zero-blank autosampler attached to a Thermo Scientific Temperature Conversion Elemental Analyzer (TC/EA). Samples were allowed to further dry for a period

of 2 hours in the dry He-stream of the autosampler in an effort to remove any potential water sorbed during sample transfer. Samples were then pyrolyzed at 1400°C, and the resultant H_2 and CO_2 were carried in a continuous stream of UHP He to a Thermo Scientific Conflo IV coupled to a Thermo Scientific Delta V Plus IRMS.

Sample δD and $\delta^{18}O$ were normalized using standard hair reference materials (USGS 42 and 43) for which the δD and δ18O of non-exchangeable H and O have been determined, and a series of non-keratin hydrogen isotope standards that do not contain any exchangeable hydrogen. δD and $\delta^{18}O$ values of hair samples are reported relative to the VSMOW-VSLAP scale, and on this scale the δD and $\delta^{18}O$ values of USGS42 and USGS 43 are -78.5, 8.56, -50.3 and 14.11 ‰ respectively (Coplen et al., 2012). Hair samples were sampled along the growth axis of individual hairs; thus, it was not possible to produce duplicate measurements of any single sample, requiring the peak jumping protocol for analysis of H_2 and CO_2. Scale and drift corrections were applied to the data, and multiple analyses of standard materials show reproducibility on the order of $<\pm 2$‰ for δD and $<\pm 0.7$‰ for $\delta^{18}O$.

A 0.5-mL aliquot of each milk and water sample was injected into pre-evacuated Labco exetainers for measurement of $\delta^{18}O$ in the University of Michigan Stable Isotope Laboratory using continuous flow via a Thermo Finnigan Gas Bench II coupled to the

inlet of a Thermo Finnigan Delta V Plus mass spectrometer. For that analysis, a CTC Analytics PAL Autosampler flushed the samples with a 0.3% CO_2 in Helium mixture for 8 minutes each, and samples were then allowed to equilibrate for two days at 30 °C (Epstein and Mayeda, 1953). Samples were then flushed with pure (UHP grade) Helium for 8 minutes. The sample gas, carried via helium flow and cleaned of water via the Gas Bench water traps, was fed through a GC column maintained at 70 °C. The CO_2 was then admitted through a capillary to the inlet of the mass spectrometer where multiple sample peaks were measured against the CO_2 reference gas peaks. Data are normalized and reported relative to the VSMOW/VSLAP scale, and accuracy and precision are ± 0.1 ‰.

All isotope data are presented in delta notation using VPDB as the reference standard for $\delta^{13}C$, N_2-air for $\delta^{15}N$, and VSMOW for $\delta^{18}O$ and δD.

Hair sampling for cortisol analysis

After removing wedges from the initial cut of B_{mother} for stable isotope analysis, we performed a serial analysis of its cortisol content. Each 20 mm segment between notches removed for isotopes was milled into a fine powder using a 1 mm carbide bit at low speed with the hair clamped tightly to an aluminum plate (Figure 4.4). C_{mother}

samples collected bimonthly from 12/27/2013 through 12/30/2014 were treated in the same manner to produce a single powder sample from each.

Cortisol analysis

Cortisol was extracted from hair powder and analyzed following improvised procedures based on Van Uum et al. (2008), Webb et al. (2010, 2015), and Meyer et al. (2014). We placed 10 – 60 mg (depending on mass of segment) of each finely ground hair sample into a 1.5 mL polypropylene microcentrifuge tube with 1.0 mL HPLC grade methanol. After 24 hours with shaking (400 rpm) at 50 °C, samples were centrifuged for 3 minutes at 14000 rpm (~15000 g). We then transferred 0.6 mL of the supernatant from each tube to a 3.0 mL glass scintillation vial and evaporated the methanol at 40 °C under nitrogen stream. Sample residues were reconstituted with 0.2 mL Salimetrics® Assay Diluent (PN 8005), which was transferred to clean microcentrifuge tubes for analysis in the University of Michigan Core Assay Facility using a Salimetrics® salivary cortisol assay EIA kit that has been verified for human hair cortisol analyses (Meyer et al., 2014). Each sample was analyzed in duplicate using 25 µL aliquots. Some analyses had to be rerun due to high variance between duplicates and were processed the second time using 50 µL. All of the 50 µL reruns had low coefficients of variation (<10), indicating that the larger sample size was beneficial given low cortisol concentrations.

Cortisol content in hair is reported in ng/mg, and sensitivity of the assay kit is listed as 0.007 µg/dL. Raw results were measured in micrograms of cortisol per deciliter of assay diluent (µg/dL) and were converted to nanograms cortisol per gram of hair (ng/g) using the following unit conversion for comparison with results from other studies:

$$\frac{\boldsymbol{x}\ \mu\mathrm{g}[cort.]}{\mathrm{dL}[ass.dil.]} \times \frac{1\ \mathrm{dL}}{100\ \mathrm{mL}} \times \frac{1000\ \mathrm{ng}}{1\ \mu\mathrm{g}} \times \frac{0.2\ \mathrm{mL}[ass.dil.]}{0.6\ \mathrm{mL}[meth.]} \times \frac{1\ \mathrm{mL}[meth.]}{\boldsymbol{y}\ \mathrm{mg}[hair]} \times \frac{1000\ \mathrm{mg}}{1\ \mathrm{g}} = \frac{\boldsymbol{z}\ \mathrm{ng}[cort.]}{\mathrm{g}[hair]}$$

Four blank samples (empty vials treated as samples during extraction and analysis) processed to control for 'background' values, consistently tested 'positive' for cortisol with an average of 0.015 µg/dL (σ = 0.0023). The source of these results is unknown, but something in the blank samples either actively bound to cortisol-binding antibodies in the kit (e.g., cortisol contamination – possibly in the methanol) or otherwise interfered in analytical reactions (horseradish peroxidase binding, tetramethylbenzidine-peroxidase reaction, or sulfuric acid stop reaction). If apparent presence of cortisol is due to some kind of interference, adjusting results for samples that actually contain cortisol could be more complicated than simply accommodating background contamination from methanol or sample vials. As a conservative approach, we assumed systematic contamination that impacted all results consistently and subtracted the average blank analysis from raw measurements to calibrate the data.

Furthermore, samples within three standard deviations of the background average were considered indistinguishable from background noise –they are included in figures (and noted) but excluded from reported ranges and averages.

Sample timing and calculation of calf-mother offset

To estimate time of hair sample formation, we used growth rate measurements (Table 4.1; Figure 4.5) and alignment of prominent landmarks in isotope records of both individuals to reconstruct a long-term chronology (Figures 4.6 – 4.9). For samples cut during the study, hair shaft formation is estimated to occur approximately 5 mm (Lucas) and 8 mm (Renee) proximal to where hairs were clipped just above the surface of the skin. To calculate offset between Lucas and Renee samples that did not have the same chronological divisions, we first used linear interpolation to create comparable records with points representing the first day of each month. 'Lucas-Renee' curves represent comparisons between these interpolated records.

Results

Hair growth rates

Initial clippings of Renee's two tail hairs cut on November 1, 2012 were 357 mm long for the more proximal hair (A_{mother}) and 723 mm long for the more distal hair

(B_{mother}). Each hair had an average diameter of 1.3 mm (approximately the same as a 16 gauge wire) at its base. In the first year of analysis (11/1/2012 – 11/6/2013), A_{mother} and B_{mother} were monitored simultaneously between 11/1/2012 and 11/6/2013, with A_{mother} displaying faster growth (A_{mother}: 0.54 – 0.88 mm/day, mean = 0.71, σ = 0.13; B_{mother}: 0.36 – 0.83 mm/day, mean = 0.60, σ = 0.16). After the first year of sampling A_{mother} was lost, and we began repeated sampling of a third hair, C_{mother}. For the second year (12/30/2013 – 12/29/2014) B_{mother} and C_{mother} were monitored with C_{mother} outgrowing B_{mother} for most of the interval (B_{mother}: 0.29 – 0.72 mm/day, mean = 0.51, σ = 0.16; C_{mother}: 0.27 – 0.81 mm/day, mean = 0.61, σ = 0.20). B_{mother}'s growth was fairly consistent throughout the two years, but both A_{mother} and C_{mother} had downward trends in growth rate starting each year with significantly higher rates than B_{mother} but ending with rates close to those of B_{mother}. Average growth rates during each two-month interval were highly variable for all hairs, and growth measurements for simultaneously monitored hairs were in phase with each other, suggesting systemic processes dominated control of rates (Table 4.1; Figure 4.5).

Lucas' tail hairs clipped throughout the duration of the two-year study were significantly less robust. The diameter at the base of hairs clipped in the first three sampling episodes averaged 0.35 mm. The last samples (E_{calf}, 12/29/2014) were more substantial, but at 0.6 mm they were still significantly more gracile than Renee's hairs.

Difficulty identifying previously cut hairs along with hair breakage and loss throughout the study period complicated growth rate estimates for Lucas' hair. Initial attempts to determine rates by repeatedly cutting the same individual hairs resulted in a growth rate estimate of 0.17 mm/day. Average growth rate for individual hairs in the first clump (C_{calf}) sampled repeatedly over 14 months (3/4/2013 – 4/30/14) was only 0.09 mm/day, but this process sampled multiple hairs that were at any given time at different stages in the follicular life cycle and in a few sampling episodes displayed very little growth between all hairs. C_{calf} initially contained only two hairs, but over the next four sampling episodes, hairs increased to six. At final sampling C_{calf} contained only five hairs. Thus, it appeared that throughout the 14 months new hairs in anagen joined the clump while old hairs in telogen were shed, but there was some uncertainty that the same hair clump had been sampled in each episode. A new hair clump (E_{calf}) monitored only in the last two sampling episodes displayed an average growth rate of 0.31 mm/day (σ = 0.09) – almost 70% the amount of growth in B_{mother} and C_{mother} sampled synchronously. Near the beginning of the study period four hairs containing significant prior growth (A_{calf} – 169 mm, B_{calf} – 166 mm , $C[1]_{calf}$ – 182 mm, $C[2]_{calf}$ – 145 mm) were cut. A_{calf} likely records the earliest growth (including growth in utero – see *Discussion* section for interpretation of growth records) of all hairs sampled from Lucas' tail (Table 4.1; Figure 4.5).

Isotope records

Comparisons of isotopic compositions of water, milk, and tail hairs are based on chronological calibration of each individual's long-term serial record. The calibrations used were based on observed growth rates (Table 4.1; Figure 4.5), alignment of features and profiles of records from each individual, and perturbations in the hair record that we think indicate timing of birth (see *Discussion: Growth rates and chronology*).

At the time of writing, when Lucas was about 3.5 years old, zoo handlers were witnessing Lucas suckle only a few times a day for very brief intervals. I observed the elephants continuously for 2 hours the morning of 10/8/2014 and recorded Lucas nursing twice for ~3-5 minutes each time. Persistent enrichment of $\delta^{15}N$ and $\delta^{13}C$ in Lucas' hair compared to Renee's hair suggests that Lucas may have been nursing significant amounts while unobserved at night.

According to the elephant management staff, Renee and Lucas had all throughout Lucas' first 3.5 years been eating from the same supplies to the extent that Lucas was eating solids at any given time. Renee did receive a vitamin E supplement that Lucas did not have. Both had different preferences when it came to fruits, vegetables, browse, and other treats, but the bulk of both their diets came from the same hay.

Hair $\delta^{15}N$ and $\delta^{13}C$

Nitrogen and carbon results for both Renee and Lucas span the interval from 12/2010 to 8/2014 in the hair record chronology proposed below, from approximately 5 months prior to Lucas' birth until he was almost 3.5 years old. The record is represented by 37 samples of Lucas' hair and 35 samples of Renee's (Tables 4.2, 4.3; Figures 4.6, 4.7).

Hair samples from Lucas had an average $\delta^{15}N$ measurement of 6.09 ‰ (σ = 0.39). Average in utero value was 6.11 ‰ (σ = 0.16), and averages for the first three years of his life after birth were 6.29 ‰ (σ = 0.27), 6.20 ‰ (σ = 0.25), and 5.68 ‰ (σ = 0.22) consecutively. Samples from Renee averaged 4.54 ‰ (σ = 0.38). Averages for the final stage of pregnancy and the subsequent three years were 5.05 ‰ (σ = 0.04), 4.45 ‰ (σ = 0.36), 4.52 ‰ (σ = 0.27), and 4.41 ‰ (σ = 0.20).

The pre-birth record contained in Renee's and Lucas' tail hairs has a consistent offset in $\delta^{15}N$ with Lucas' values ~1 ‰ higher than Renee's. The records diverge sharply at the time of birth, with Renee's becoming more depleted and Lucas' becoming enriched, reaching a peak separation of ~2.5 ‰ at 6 months. After that the records converge gradually with some fluctuations over the next ~3 years returning to the original ~1 ‰ separation. Nitrogen isotope profiles for the elephants did not fully converge during the period of study (Figure 4.6).

Lucas' hair samples analyzed for $\delta^{13}C$ averaged -23.53 ‰ (σ = 0.53). Renee's hair carbon was moderately depleted compared to Lucas' with an average of -24.35 ‰ (σ = 0.53). Splitting records into pre-birth and first, second, and third years following birth, averages for each interval are as follows: Lucas – -23.33 ‰ (σ = 0.21), -23.90 ‰ (σ = 0.41), -23.21 ‰ (σ = 0.59), -23.64 ‰ (σ = 0.09); Renee – -24.25 ‰ (σ = 0.41), -24.61 ‰ (σ = 0.53), -24.16 ‰ (σ = 0.68), -24.16 ‰ (σ = 0.34).

Hair $\delta^{13}C$ serial records for Renee and Lucas are somewhat erratic but maintain a fairly consistent relationship through most of the nearly 4-year span covered (including while Lucas was in utero) with Lucas' hair enriched by 0.5 – 1.5 ‰ compared to Renee's through most of the interval. Notable departures from this pattern occur in the calibrated records: immediately following birth, the only time Lucas' hair was depleted compared to Renee's; eight months after birth, when we see peak offset (Lucas – Renee = 1.9 ‰); and during a 5-month period (7/13 – 11/13) when both records are nearly equivalent. During the sampling period, when sample timing is well constrained, Lucas' values track Renee's with an average relative enrichment of 0.85 ‰ (σ = 0.47) (Figure 4.7).

Hair $\delta^{18}O$ and δD

Results for oxygen and deuterium from Renee's tail hair were obtained from 23 samples adjacent to those taken from B_{mother} that span the growth interval from 11/2010 to 10/2012 (Table 4.2). The most distal sample along the hair shaft (earliest in the growth record) did not return a dependable $\delta^{18}O$ measurement. Since nitrogen and carbon analyses exhausted material from A_{calf}, oxygen isotope and deuterium results for growth prior to initial sampling (11/2011 – 11/2012) were obtained for 36 contiguous segments of $C[1]_{calf}$ (Table 4.3). The most distal three of these samples did not produce reliable results for oxygen. Five additional samples of calf hair (C_{calf} and $C[1]_{calf}$) from the study period (11/2012 – 8/2013) were cut immediately distal to samples of that had been analyzed for $\delta^{15}N$ and $\delta^{13}C$ for that same interval. The overlapping portion of the mother and calf hair records of oxygen isotopes and deuterium (11/2011 – 10/2012) thus extends over one year that does not span birth.

Measurements of $\delta^{18}O$ in Lucas' hair varied between 9.11 and 14.98 ‰ (μ = 12.16 ‰, σ = 1.22). Renee's hair $\delta^{18}O$ values occupied almost the same total range, between 8.83 and 14.35 ‰ (μ = 11.31 ‰, σ = 1.44). Where the two records overlap, Lucas' record is consistently enriched compared to Renee's by about 2 ‰. Lucas' average $\delta^{18}O$ is 2.0 ‰ higher than Renee's (Figure 4.8).

Deuterium measurements from Lucas' hair were between -93.65 and -82.91 (μ = -88.08 ‰, σ = 2.78), while Renee's were shifted lower, from -97.56 and -85.24 (μ = -91.97 ‰, σ = 3.43). For the interval where the two records overlap, Lucas' record goes from being somewhat enriched compared to Renee's at the beginning (~9 ‰) to being approximately equivalent to Renee's at the end (Figure 4.9). In samples representing that interval Lucas' average δD is 4.1 ‰ higher than Renee's.

Milk and drinking water $\delta^{18}O$

Six samples of drinking water collected along with hair and milk during zoo visits were analyzed for $\delta^{18}O$. Samples represented different times throughout the year (mostly from 2014) and values ranged from -11.70 ‰ up to -5.84 ‰ (μ = -8.98, σ = 1.60). Water $\delta^{18}O$ results were also obtained for 10 milk samples collected from Renee bimonthly between 11/2012 and 7/2014. One sample from this period failed to yield a reliable measurement. Milk values ranged -11.96 ‰ up to -4.40 ‰ (μ = -8.03, σ = 1.39) (Table 4.4).

Considerable scatter in results of repeated analyses (each duplicate sample was analyzed 9 times in sequence) challenges the integrity of milk water (H_2O_{milk}) and drinking water (H_2O_{drink}) oxygen results in this study. The causes of discrepant

measurements are unclear but may be related to loading raw milk samples. One possibility is that contaminants from the milk became incorporated into the CO_2 during equilibration and somehow made it through the multiple water traps to interfere with measurements. Water standards run with milk samples were also affected (Table 4.5), while the system had demonstrated reliable results prior to milk analyses and returned to proper function following cleaning procedures. However, ignoring extreme outliers that clearly resulted from machine malfunction, H_2O_{milk} and H_2O_{drink} values for samples collected at the same time have a consistent relationship. Contrary to our initial expectation of a roughly 4 ‰ enrichment in oxygen of H_2O_{milk} compared to H_2O_{drink} (Lin et al., 2003; also present in human milk and drinking water samples used as controls for our analyses), we observed an average $H_2O_{milk} - H_2O_{drink}$ enrichment of only 0.48 ‰. This is more consistent with results from Chesson et al. (2010) and Renou et al. (2004), who report enrichment as low as 1 ‰ in some tests. H_2O_{milk}, drink $\delta^{18}O$ records display apparently seasonal variation with high values in summer and low values in winter. Results display an approximately 5 ‰ difference between late winter lows and late summer highs (Figure 4.8).

Milk $\delta^{15}N$

Thirteen samples of lyophilized skim milk from bimonthly sampling from 11/1/2012 through 10/30/2014 had an average $\delta^{15}N$ of 5.22 ‰ (σ = 0.39). During this

interval, milk $\delta^{15}N$ was enriched by about 1.0 ‰ relative to Renee's hair $\delta^{15}N$ (μ = 4.28 ‰, σ = 0.29) and depleted by about 0.5 ‰ relative to Lucas' hair $\delta^{15}N$ (μ = 5.71, σ = 0.39) (Table 4.4).

For the entire first year of the series, Lucas' hair $\delta^{15}N$ values are enriched compared to milk $\delta^{15}N$ (μ = 0.89 ‰). At the beginning of the second year when Lucas was about 2.5 years old, milk and Lucas' hair values converge and occupy the same overlapping range (μ = 0.00 ‰) for the remainder of the study period. Simultaneous to convergence in Lucas and milk records, milk $\delta^{15}N$ diverges from Renee's hair $\delta^{15}N$ going from average enrichment of 0.72 ‰ in the first year to 1.19 ‰ in the second year (Figure 4.6)

Milk $\delta^{13}C$

Skim milk solids, solid milk fat, and milk oil were separately analyzed for $\delta^{13}C$ for each of the 13 milk samples (where present; two samples of milk did not yield measureable amounts of oil). Milk $\delta^{13}C$ ranged from -27.69 to -25.41 ‰ (μ = -26.78, σ = 0.69) for skim milk solids, -28.80 to -27.15 ‰ (μ = -28.07, σ = 0.49) for solid milk fat, and -28.96 to -27.38 ‰ (μ = -28.26, σ = 0.45) for milk oil (Table 4.4).

The three records track each other consistently with skim solids being most enriched, solid fat being depleted an average 1.29 ‰ (σ = 0.29) relative to those, and oil

$\delta^{13}C$ being 0.27 ‰ (σ = 0.12) lower still. All records display a dramatic drop in the first 5 samples and then gradually increase over the remaining 8. Relative to both hair records, which have a fairly consistent relationship during this time (see *Hair $\delta^{13}C$* above) milk carbon is less depleted at the ends of the record (11/1/2012 – 12/27/2012, 7/1/2014 – 10/30/2014) and more depleted in the middle of the sampling period (3/3/2014 – 4/30/2014) when offset between Renee's hair and milk $\delta^{13}C$ (averaged over the three components) reaches 4.21 ‰ in summer 2013 (Figure 4.7).

Hair cortisol

After sampling for analysis of $\delta^{15}N$, $\delta^{13}C$, $\delta^{18}O$, and δD, B_{mother} was sampled for cortisol analysis. Twenty-two cortisol measurements represented a continuous record of growth between 1/2011 and 10/2012 (Table 4.6). These results include late pregnancy and the first year after Lucas' birth. Excluding one result that was indistinguishable from 'background' levels, the average for this period was 4.56 ng/g (σ = 1.21), and the range was 3.01 – 7.13 ng/g. Eight additional samples of hair grown between 11/2013 and 11/2014 (parts of the third and fourth year after Lucas' birth) had an average cortisol concentration of 3.67 ng/g (σ = 0.79) and spanned from 2.73 to 4.58 ng/g. Raw analytical results for measurement of extracted cortisol from hair samples were from 0.022 to 0.057 µg/dL (μ = 0.039, σ = 0.008), and concentrations did not correlate with sample mass.

With some results showing concentrations close to the analytical lower limit of detection for the salivary assay kit used, this approximately monthly resolution from a single hair tests the limits of the procedure described above. Modification of the method to further concentrate extracted cortisol in the assay diluent prior to analysis would improve the analysis.

Average cortisol concentrations are higher during late pregnancy through the first 6 months after Lucas' birth (4.98 ng/g) than those synchronous with the end of Lucas' first year and beginning of his second (3.72 ng/g) and higher than average concentrations during the most recent year of the record from C_{mother} (3.76 ng/g). Minimum levels are fairly consistent between both B_{mother} and C_{mother} records, with higher averages in the early part of the series reflecting higher maximum values. Highest levels correlate with the position in the B_{mother} record estimated to be winter of the first year after Lucas' birth, but these are only a little higher than measurements from those representing the same months in the previous year. Lack of a long-term trend toward lower levels in distal portions of hair (in fact, more distal samples produced the highest concentrations on average) suggests cortisol is preserved in elephant hair that has been exposed to the elements for multiple years. In the bimonthly average analysis of C_{mother} from 10/2013 to 10/2014, higher concentrations are associated with times of faster hair growth in late winter/early spring and late summer/early fall. According to calendar-date

calibration from isotope and growth rate analyses, we see the same two-peak annual pattern in B_{mother} samples from 1/2011 to 10/2012 (Figure 4.10).

Discussion

Growth rates and chronology of pre-study hair growth

Previous estimates of tail hair growth rates for female African elephants range from about 0.7 – 1.0 mm/day (Cerling et al., 2003, 2005, 2009). These growth rates were estimated by aligning overlapping portions of isotope chronologies from different hairs as described in Wittemyer et al. (2009). To our knowledge, this study is the first to document growth rates of individual hairs resampled at regular intervals. Whereas Cerling et al. (2005, 2009) concluded that growth rate for an individual hair did not show significant variation, even during times of stress, our analysis demonstrated that growth rate of individual hairs in a captive female varied significantly in bimonthly growth during the second and third years postpartum. A_{mother} varied from 0.54 – 0.88 mm/day (calculated from bimonthly clippings), while B_{mother} varied from 0.29 – 0.83 mm/day and C_{mother} varied from 0.27 – 0.81 mm/day. In all hairs, individual growth rates oscillated in phase with fastest growth occurring during late summer and a lower peak in early spring. Overlying the seasonal variation was a cycle that was independent to each hair and resulted in A_{mother} and C_{mother} growing faster than B_{mother} during most of their

sampled growth and then slowing to B_{mother} rates. Average rate for B_{mother} was nearly constant over two years with only a slight decline. This likely reflects the cycle stage of each follicle, with A_{mother} and C_{mother} in waning anagen (approaching catagen) and B_{mother} in prime anagen with lower production than both A_{mother} and C_{mother} had when they were in the middle of anagen (Table 4.1; Figure 4.5).

Based on this average growth rate calculated for B_{mother}, we estimate that the initial clipping represents about three years of growth. This estimate doesn't accommodate systemic changes in hair growth associated with pregnancy, which have been documented in humans (Lynfield, 1960), or changes associated with position in the follicles' growth cycle, but it provides a useful starting estimate for calibrating the hair record to calendar dates. Calculating growth rate for Lucas' hair was complicated both by difficulty in repeat-sampling of individual hairs (see *Methods* for further explanation) and by chance selection of an entire clump of hair that apparently grew very little over several months and was likely growing much more slowly than other hair clumps at the same time. However, early rate calculations from the sampled clump suggested an average growth rate of approximately 5 mm/mo. Coincidentally, ~5 mm segments of A_{calf} provided the target 622 µg sample required for joint analysis of $\delta^{13}C$ and $\delta^{15}N$. At first approximation, this sampling regime provides monthly values for A_{calf}. Approximate correlation between conspicuous $\delta^{15}N$ peaks in calendar-calibrated records and

agreement between divergence of the two $\delta^{15}N$ profiles and Lucas' date of birth support the use of measured growth rate averages to estimate growth in previous years.

Record alignment

Final alignment of pre-study (before 11/2012) records involved integration of hair growth rate data (including seasonal variability) and isotope records from mother and calf, as well as the cortisol pattern for B_{mother}. Measured growth rates provided an initial calibration for each hair record and guided sampling strategies (see *Methods: Hair sampling*). Observed seasonal variability in growth rates were used to refine the mother's hair chronology. They also justified secondary adjustments in the calf hair chronology to improve alignment with the mother's record, and established reasonable limits for such adjustments. There were multiple clear $\delta^{15}N$ and $\delta^{13}C$ landmarks shared between records of both individuals that guided adjustments to match the record of A_{calf} to that of B_{mother}, which was fixed at the initial, seasonally-calibrated record established from growth rate patterns observed over the duration of the study (Figures 4.6, 4.7). Comparison of mother and calf profiles informed alignment of $C[1]_{calf}$ $\delta^{18}O$ and δD to the fixed B_{mother} records (Figures 4.8, 4.9). Nitrogen and carbon records contain a perturbation in the relationship between mother and calf that corresponds to Lucas' birth in the calibrated chronologies, but oxygen and deuterium records for the calf are less complete than were carbon and nitrogen records and apparently do not extend

back to the time of birth in $C[1]_{calf}$. In $\delta^{15}N$ this is manifested as a sudden divergence between values. In $\delta^{13}C$ the same time frame is marked by a convergence. Divergence in $\delta^{15}N$ is presumably due to a trophic enrichment effect that occurs when Lucas metabolizes proteins in Renee's milk. Convergence in $\delta^{13}C$ seems to reflect high fat content with isotopically light carbon (Deniro and Epstein, 1977) in early milk. Although fat content of milk typically increases through the duration of lactation (Oftedal and Jenness, 1988; Rook, 1961), colostrum is typically higher in fat than milk (Jenness, 1988). Cortisol results are consistent with the proposed chronology, showing seasonal correlation of high and low values equivalent to the pattern detected in C_{mother} with known timing.

Seasonality

Much of the variation in mother and calf records appears to be related to pregnancy, birth, nursing, and weaning. Underlying that variability are unrelated dietary changes (such as the shift to non-local hay due to poor local growing conditions in 2013) and recurring seasonal patterns. Despite stability of their controlled environment we detect seasonal patterns over multiple years in milk and drinking water oxygen, hair growth rates, hair wear patterns, hair nitrogen, and hair cortisol levels.

Seasonal variation in both milk water and drinking water oxygen matches meteoric water patterns for the region (Dutton et al., 2005) with higher $\delta^{18}O$ in the warm summer (peaking in late summer due to biological and environmental reservoir effects) and lower $\delta^{18}O$ in the cool winter. The difference between winter and summer values is approximately 5 ‰ (Figure 4.8).

Over two years of sampling, hair growth for both Lucas and Renee was consistently fastest in late summer and slowest in mid-winter. Growth rates also briefly increased in late winter of both years (Table 4.1; Figure 4.5). Thus seasonal variations persist in captive elephants living in a mostly controlled environment with a consistent well-rounded diet. Toledo Zoo handlers carefully regulate how much their elephants eat and provide a consistent quantity year-round. It is possible that hair growth rate could be an aspect of physiological responses to changes in amount of daylight throughout the year, but an alternate explanation is that although energetic requirements of maintaining body temperature change throughout the year, nutrition remains more or less constant. During warm periods the elephants would be able to devote the most energy to growth, and during moderately cold periods when elephants are still spending most of their time outdoors, we might expect slowest growth. The uptick in growth during late winter months (the coldest time of year in the region) would seem contradictory in this model if not for the increased amount of time the animals spent

indoors to escape the cold. Even though the natural range of African elephants does not have such extreme seasonal temperatures, it seems reasonable to expect at least a similar degree of seasonal growth rate variation in wild populations more directly affected by climate. These data may also provide comparison for seasonal fluctuations in tusk growth rate, since that is, at least in part, also a consequence of protein synthesis.

In addition to growth, severity of wear also varied by season with tips of freshly cut hairs wearing smooth more quickly during warm months, and most quickly in early fall. A simple explanation for this is increased use of the tail to swat flies and other insects when populations swelled during warm months. For much of the year identifying sample hairs was facilitated by an observation that the distal tip had clearly been recently cut. In many cases, the base of the previous sample fit perfectly against this mildly worn cut end. When sampling in late summer and fall, distal ends of sample hairs were rounded smooth and showed no evidence of previous sampling. More frequent sampling during this time of year when growth rates are high anyway should be considered.

Hair nitrogen profiles do not display an overt seasonal pattern, but it is worth noting that end-winter values are consistently elevated. In tusk records we sometimes associate seasonal increases in $\delta^{15}N$ with nutritional stress (e.g., *Chapter 2* – Fisher et al.,

2014) when autophagy produces a trophic level enrichment from the animal's own tissue values (Hobson et al., 1993). We do not expect to see a signal of 'nutritional stress' in zoo elephants, but there is still a possibility that they would catabolize some of their own proteins to keep warm while relatively inactive in the cold, dark winters of Toledo.

The serial record of hair cortisol for B_{mother} displays seasonal variation with highest levels corresponding to times of fastest hair growth during late winter/early spring and late summer/early fall (Figure 4.10). This pattern is similar to results of long-term analyses of salivary cortisol for eight captive Asian elephants in Spain (Marcilla et al., 2012). Differences may be a consequence of different implications of short-term salivary values and long-term averages in hair cortisol values. In any case, our analyses show hair cortisol correlating directly with hair growth rates, suggesting a common season-related cause for both.

Elephant tail hair cortisol

This analysis suggests that tail hairs could be used to monitor prior cortisol levels in elephants. In serial samples of a single strand of hair representing about 2 years of growth, we detected concentrations in the lower end of the normal range documented for human hair and consistent with other measurements from elephant hair (Berkvens,

2012). This is consistent with comparison between typical serum and saliva concentrations in elephants (Kajaysri and Nokkaew, 2013; Oliviera et al., 2008; Marcilla et al., 2012; Menargues et al., 2012) and humans (Aardal and Holm, 1995; Hellhammer et al., 2009). Intact seasonal variation and elevated levels associated with pregnancy and postnatal stress in hair grown through two years prior to first sampling on 11/1/2012 suggest that cortisol is preserved in distal portions of hair that has been exposed to the elements for multiple years. Some studies indicate that cortisol is not well preserved in hair more than about 6 centimeters from the scalp in humans (Kirschbaum et al., 2009), but at least two factors make elephant hair more likely than human hair to retain a signal long after hair formation. The first is that elephant hair, even in zoo specimens, does not experience as intense shampooing as most human hair. The second is that at over 1 mm diameter, elephant tail hair has a much lower surface area to volume ratio than human hair. If washout only affects keratin near the exposed outer surface, a higher proportion of a powder sample of elephant tail hair will be unaffected by environmental factors. This assumes that cortisol is contained more or less evenly throughout the hair cuticle and cortex. Theoretically, if cortisol were concentrated near the hair surface, such as might occur if sweat and sebum were its primary source, then finer hair would contain higher relative amounts per unit mass and washout may impact fine and coarse hair equally. Assuming absorbed cortisol would not permeate all the way into the hair

shaft, another consequence of sorption-sourcing would be that elephant hair would contain far less cortisol per unit mass due to its low surface-volume ratio. With no sign of washout and cortisol levels comparable to those found in human hair (adjusting some for lower levels detected generally in proboscideans), our results do not support significant incorporation of cortisol via sorption after keratin synthesis.

Late pregnancy and early postnatal elevation in hair cortisol provides a signal of birthing that could be detected in an unknown female elephant hair sample. Although this will not likely provide a direct tool for investigating calving cycles in fossil specimens, results of exploratory analyses suggest that cortisol is present in tusk dentin and may even be preserved in some fossil specimens. If so, this pattern in hair cortisol could provide a signal of pregnancy that could be detected in fossil tusk records.

Milk isotopes

According to work by Jenkins et al. (2001), milk is depleted compared to a lactating female's plasma in both $\delta^{15}N$ and $\delta^{13}C$ for various species. If this is the case for elephant milk, we should not expect to see a full trophic shift between maternal and calf hair values. Assuming consistent fractionation from plasma to hair $\delta^{15}N$ and $\delta^{13}C$ in both individuals, the hair isotope relationships would reflect trophic level shifts offset by the difference between mother's plasma and milk. Our data are consistent with this model.

Peak calf-mother hair difference (~2.5 ‰) is less than the expected trophic-level shift of 3 ‰. It is also less in $\delta^{13}C$ than $\delta^{15}N$, which is consistent with the greater depletion in milk $\delta^{13}C$ than $\delta^{15}N$, but probably also reflects the less extreme trophic shift in carbon (Schoeninger and DeNiro, 1984).

We did not sample blood serum as part of this study, but assuming fairly consistent relationships between serum and milk carbon and nitrogen, such as those documented in Jenkins et al. (2001), we can estimate the fractionation between serum $\delta^{15}N$ and $\delta^{13}C$ and hair in elephants. Milk $\delta^{15}N$ is about 0.5 – 1 ‰ higher than hair $\delta^{15}N$ in temporally proximate samples of Renee's milk and hair. If serum nitrogen is enriched by another 1 ‰, it should be about 1.5 – 2 ‰ heavier than hair values. For those same samples, milk carbon is lighter than hair carbon by about 2.5 – 4 ‰. If milk is depleted by 1.5 ‰, serum $\delta^{13}C$ should be 1 – 2.5 ‰ lower than values measured in hair.

Our results do not include precise measurements of relative compositions of milk components. Most data presented here are consistent with previous analyses of elephant milk (Jenness, 1974; McCullagh and Widdowson, 1970), but at least three observations (milk pH, failure to separate caseins, significant presence of milk oil) were unexpected. In methods described above, we document difficulty insolubilizing and separating caseins using the procedure described in Kornexl et al. (1997). Starting pH of

elephant milk was higher than control samples (bovine and human) (Table 4.3) and acidification to pH 4.3 required significantly more HCl. Whether this contributed to the lack of expected coagulation is beyond the scope of this study. However, since caseins coagulated in human milk reference samples which were expected to have a smaller casein component than elephant milk samples (Jenness and Sloan, 1970; Jenness, 1974), we do not think lack of curd production reflected absence of caseins. General congealing of all elephant samples at pH 4.3 indicates that some form of coagulation did occur, but that it was different than what we observed in cow and human milk.

Isotopic signatures of birth, nursing, and weaning

The isotope system that provides the clearest signal of nursing and weaning in proboscidean calves is δ^{15}N. Immediately after birth when the elephant calf starts to nurse, nitrogen in its hair starts to become enriched. Following a period of increasing offset from the mother's hair values, calf hair δ^{15}N declines slowly and steadily as milk is gradually replaced by the adult diet shared with its mother. At the time of writing, the calf is not yet fully weaned and his hair is still recording elevated δ^{15}N levels compared to his mother's despite reports that he now nurses very little. There have been no attempts to monitor activity at night, and we suspect more frequent nighttime nursing as has been documented in zoo elephants during the first few months of life (Andrews et al., 2005) may explain the apparent discrepancy. We expect calf and mother δ^{15}N to

match after final weaning. Differences that persist after weaning in humans (Fuller et al., 2006) are likely due to differences between adult and infant/toddler diets in humans. When Lucas is fully weaned, his diet should closely approximate that of Renee.

The delayed peak δ^{15}N offset from mother's hair values presents a bit of an enigma. Six months seems too long to be solely due to a reservoir effect, but a similar extended buildup to peak difference is recorded in humans (Fuller et al., 2006). It is possible that 6 months is not an accurate estimate of the actual delay, since it is based on average growth rate being constant; actual growth rates during the first few months after Lucas' birth might stray significantly from the average. However, adjustment for growth rate differences is unlikely to bring the delay into the reasonable range for a reservoir effect, since a growth rate about 10 X the average would be required to change the 6 month delay to a few weeks. One possibility is that colostrum and preliminary milk are more depleted in δ^{15}N compared to mother's serum than later milk, but to our knowledge no one has looked at serum-milk δ^{15}N variation throughout lactation. Another perhaps less likely explanation would be that newborn metabolism of proteins or keratin synthesis is sufficiently different from normal that it results in either less enrichment of calf serum compared to milk protein or more depletion of calf hair compared to calf serum. Lastly, the pattern could reflect particularly rapid growth in the calf during the first few months after birth. Fuller et al. (2004) document a δ^{15}N

depletion during pregnancy-related weight gain that they attributed to a positive nitrogen balance associated with tissue synthesis that results in lower than usual urea production. A similar effect could explain the gradual increase during the first six months of nursing. Though the phenomenon is not yet clearly understood, depletion due to a positive nitrogen balance in the rapidly growing neonate could offset the trophic-level increase due to milk consumption. In that model, as volumetric growth rate decreased, the nursing-related enrichment would overpower the growth-related depletion.

In this study, the relationship between mother and calf hair carbon isotopes shows very little change throughout almost 4 years that includes late pregnancy, birth, and more than 3 years of nursing, during which time milk composition and nursing intensity change significantly. In the two years of active sampling for milk and hair, the relationship between $\delta^{13}C$ of each milk component (dry solids, solid fat, and oil) remains remarkably static. Whole milk values would be averages of the different components weighted according to relative abundance of each. Consequently, the pattern of $\delta^{13}C$ in milk consumed by the calf might look a little different than the profiles we document. However, we expected to see a consistent relationship between each milk component and the mother's hair. Since the dry solids contained various proteins and lactose, their values reflect weighted contributions of the various components, but consistent

relationships between $\delta^{13}C$ of dry solids and both lipids suggests minimal effects from variation in proportions of different dry-solid constituents. Contrary to expectations, the relationship between Renee's hair $\delta^{13}C$ and each milk-component $\delta^{13}C$ was variable over the two years of sampling. Changes in serum to milk fractionation during lactation may account for absence of a consistent pattern in the relationship between mother and calf hair $\delta^{13}C$.

Two notable details in the mother-calf hair $\delta^{13}C$ relationship are the overlapping calf and mother hair $\delta^{13}C$ values immediately following birth and peak separation between the two records approximately synchronous with peak separation in $\delta^{15}N$. Except for a brief period after birth when calf and mother hair $\delta^{13}C$ records converge, calf carbon is enriched compared to that of its mother. Lower relative $\delta^{13}C$ in the neonate could be accounted for by the high content of light-carbon fat in colostrum and preliminary milk. Coincident timing of peak offset between the carbon and nitrogen records supports existence of a nursing pattern in $\delta^{13}C$ similar to that observed in $\delta^{15}N$.

All isotope systems evaluated show a general pattern of enrichment in calf hair compared to the mother's hair. We are not aware of any documentation of trophic level enrichment in $\delta^{18}O$, but evidence of higher $\delta^{18}O$ values in juvenile mammoth tooth enamel (Metcalfe et al., 2010) suggests our observations are not anomalous. Rather than

a trophic level effect, the scenario for oxygen and hydrogen could be unique to nursing and due to fractionation during milk production. Milk water is typically enriched compared to drinking water, but to our knowledge the relationship between milk water and the lactating female's body water has not been directly measured.

The average growth rate for $C[1]_{calf}$ (the hair used for calf $\delta^{18}O$ and δD) was apparently significantly higher than the originally estimated 6 mm/month that provided a good first-order estimate for the A_{calf} records of $\delta^{15}N$ and $\delta^{13}C$. As a result, oxygen isotope and deuterium records did not extend back prior to birth as originally anticipated. Although the overlapping portions of Lucas' and Renee's $\delta^{18}O$ and δD records does not elucidate mother-calf relationships at the time of birth, they do provide a look at the relationships between mother and calf deuterium and oxygen isotopes spanning a year of nursing near the beginning of the calf's transition to consuming solid food. In that year, there is little change in $\Delta^{18}O_{calf\text{-}mother}$, which stays around 2 ‰ (Figure 4.8). During that same interval, in samples that were jointly analyzed for $\delta^{18}O$ and δD, the deuterium record of the calf converges completely on that of the mother, from an initial displacement ($\Delta D_{calf\text{-}mother}$) of about 8 ‰ (Figure 4.9). These data suggest enrichment in both $\delta^{18}O$ and δD due to nursing, but reveal differences in how each isotope system responds to the reduction in nursing during the second year postnatal.

Conclusions

This study details an isotopic signature that characterizes protein synthesis during nursing and weaning in modern African elephants. Our analyses did not reveal any clear patterns in the Renee's hair isotopes that would indicate pregnancy, birth, lactation, or weaning in a fossil female tusk record, but mother-calf relationships in stable isotope systems documented here facilitate more informed interpretations of isotopic patterns observed in female tusk records. On the other hand, isotope profiles of calf hair, even in the absence of a record for the mother, display clear signals of birth, nursing, and characteristics of weaning, such as duration and rate of decrease in dietary contribution from milk. Patterns in hair keratin isotopes provide an analog for patterns detected in tusk collagen of fossil proboscideans.

Results presented here demonstrate that elephant tail hairs can be used to investigate cortisol levels for at least 2 years prior to sampling. Since inter-hair growth rates are variable, analyses using multiple hairs have limited precision. Single hair records, which are possible only for animals with very robust hairs, provide very precise long-term records.

Elephant tail hair growth rates measured bimonthly over two years exhibit significantly more variability than previously predicted. This discovery has implications for interpretation of future elephant tail hair analyses.

Table 4.1. Elephant tail hair growth measurements.

Throughout the study, we monitored individual hairs in the mother (A_{mother}, B_{mother}, C_{mother}), and recorded the amount of new growth at 2 month intervals. After losing track of A_{mother} (its growth rate had been decreasing and the thought was that it perhaps had been shed), we started monitoring a new hair (C_{mother}) to continue monitoring 2 hairs simultaneously. Calf hairs were finer and more difficult to track from one sampling interval to the next. After failing to monitor individual hairs (A_{calf}), we started clipping a single 2-hair clump that apparently grew very little throughout an entire year (C_{calf}). Still unsure that we were successfully monitoring bimonthly growth in the same hairs we began sampling an entire tuft (F_{calf}) containing between 7-9 hairs, that was easily re-identified during each sampling episode. The only reliable calf tail hair growth rates are for the interval represented by F_{calf}. However, even with minimal bimonthly growth being recorded for C_{calf}, variations in its growth rate follow the same seasonal pattern displayed in the mother's hair growth. This suggests we were successfully identifying the same hair clump each time and that these particular hairs were growing relatively slowly. Growth of individual hairs in F_{calf} varied significantly, with some hairs growing more than twice as fast as others.

Hair growth	Mother			Calf		
Sample date	**A_{mother}** (mm)	**B_{mother}** (mm)	**C_{mother}** (mm)	**A_{calf}** (mm)	**C_{calf}**[1] (mm)	**F_{calf}**[1] (mm)
11/1/2012	-	-	-	-	-	-
12/27/2012	40.0	32.0	-	13.0	-	-
3/4/2013	45.5	39.0	-	9.0	-	-
5/1/2013	35.0	21.0	-	-	2.8	-
7/1/2013	50.0	43.0	-	-	2.0	-
8/29/2013	52.0	49.0	-	-	8.4	-
11/6/2013	37.0	37.0	-	-	7.8	-
12/30/2013	-	18.9	33.1	-	2.3	-
3/4/2014	-	39.0	52.0	-	4.6	-
4/30/2014	-	27.0	37.0	-	6.6	-
7/1/2014	-	40.0	44.5	-	-	-
8/28/2014	-	42.0	46.0	-	-	-
10/30/2014	-	30.0	28.0	-	-	19.6
12/29/2014	-	17.1	16.4	-	-	9.4
3/3/2015	-	29.0	29.0	-	-	13.2
5/4/2015	-	26.0	35.0	-	-	8.6
Avg daily growth	**0.70**	**0.54**	**0.59**	**0.18**	**0.08**	**0.20**
Std Dev	**0.13**	**0.15**	**0.18**	**0.07**	**0.04**	**0.08**

[1] Each value is average of all hairs in clump

Table 4.2. Elephant mother tail hair isotope data.
Results of analyses of samples taken from two hairs. The initial clipping of B_{mother} contained was nearly ¾ meter long and contained multiple years of growth. Sampling along the B_{mother} hair shaft was used to reconstruct a record for a portion of pregnancy and the first 1.5 years after parturition prior to the first sampling episode. Subsequent growth from B_{mother} was sampled over the first year of sampling. After that, C_{mother} provided the ongoing isotope record. Date of growth estimates for growth prior to initial sampling on 11/01/2012 are based on backward projection of the seasonal pattern of growth rates observed over the period of repeat-sampling from the same individual tail hairs. Estimates for samples excised from near the proximal end of hair segments collected during the sampling period are based on average observed bimonthly growth rate since the previous sampling episode. All estimates accommodate 8 mm of hair remaining in the follicle, since hair at the surface of the skin represents growth from some amount of time earlier. We have not yet been able to verify our estimate of length of hair inside the follicle.

Mother		Distance							
Sample ID:	**B_{mother}**	from prox	Date of	$\delta^{15}N$	$\delta^{13}C$	$\delta^{18}O$	δD		*Date of growth*
Description:	Single tail hair	end (cm)	analysis	$‰_{air\text{-}N2}$	$‰_{VPDB}$	$‰_{VSMOW}$	$‰_{VSMOW}$	C:N	*(estimate)*
Sample date:	11/1/2012	44.0	11/18/2013	5.00	-23.92	-	-86.93	3.53	*11/28/2010*
Length (cm):	72.3	42.0	11/18/2013	5.08	-24.61	12.99	-88.97	3.62	*1/1/2011*
		40.0	11/18/2013	5.11	-24.38	14.35	-91.43	3.71	*1/30/2011*
		38.0	11/18/2013	5.06	-24.80	12.26	-91.80	3.74	*2/27/2011*
		36.0	11/18/2013	5.03	-24.06	12.85	-92.36	3.72	*4/7/2011*
		34.0	11/18/2013	5.05	-23.74	10.46	-94.05	3.77	*5/12/2011*
		32.0	11/18/2013	4.68	-24.21	13.24	-96.15	3.77	*6/9/2011*
		30.0	11/18/2013	4.75	-23.64	12.52	-90.71	3.76	*7/7/2011*
		28.0	11/18/2013	4.64	-24.22	11.11	-89.95	3.74	*7/31/2011*
		26.0	11/18/2013	4.66	-24.32	11.86	-89.12	3.67	*8/25/2011*
		24.0	11/18/2013	4.38	-24.44	12.60	-88.30	3.69	*9/30/2011*
		22.0	11/18/2013	3.71	-24.94	11.17	-96.36	3.56	*11/8/2011*
		20.0	3/24/2014	3.99	-24.93	11.63	-94.21	3.70	*12/12/2011*
		18.0	3/24/2014	4.01	-25.80	12.21	-89.37	3.82	*1/13/2012*
		16.0	3/24/2014	4.84	-24.69	10.58	-93.22	3.61	*2/11/2012*
		14.0	3/24/2014	4.51	-24.91	9.63	-97.56	3.77	*3/14/2012*
		12.0	3/24/2014	4.63	-24.75	8.83	-97.27	3.80	*4/22/2012*
		10.0	3/24/2014	4.64	-24.52	9.51	-96.58	3.83	*5/23/2012*
		8.0	3/24/2014	4.65	-25.01	10.08	-94.25	3.63	*6/20/2012*
		6.0	3/24/2014	4.66	-24.89	10.28	-92.30	3.48	*7/16/2012*
		4.0	3/24/2014	4.61	-24.20	9.94	-89.69	3.75	*8/10/2012*
		2.0	3/24/2014	4.88	-23.92	10.52	-89.56	3.52	*9/5/2012*
		0.3	3/24/2014	4.43	-24.93	10.09	-85.24	3.72	*10/15/2012*
Sample date:	12/27/2012	2.4	3/24/2014	4.67	-24.16	-	-	3.79	*11/1/2012*
Length (cm):	3.2	0.3	4/14/2014	3.92	-23.41	-	-	3.57	*12/7/2012*
Sample date:	3/4/2013	0.3	4/14/2014	4.52	-23.12	-	-	3.61	*2/13/2013*
Length (cm):	3.9								
Sample date:	5/1/2013	0.3	4/14/2014	4.34	-23.85	-	-	3.50	*3/31/2013*
Length (cm):	2.1								
Sample date:	7/1/2013	0.3	4/14/2014	4.35	-23.69	-	-	3.45	*6/15/2013*
Length (cm):	4.3								
Sample date:	8/29/2013	0.3	4/14/2014	4.27	-24.03	-	-	3.65	*8/15/2013*
Length (cm):	4.9								
Sample date:	11/6/2013	0.3	4/14/2014	4.55	-23.93	-	-	3.63	*10/16/2013*
Length (cm):	3.7								
Sample date:	12/30/2013	0.3	4/14/2014	4.54	-24.42	-	-	3.59	*12/12/2013*
Length (cm):	1.9								

Table 4.2 (cont.)

Sample ID:	C_{mother}	Distance from prox end (cm)	Date of analysis	$\delta^{15}N$ ‰$_{air\text{-}N2}$	$\delta^{13}C$ ‰$_{VPDB}$	$\delta^{18}O$ ‰$_{VSMOW}$	δD ‰$_{VSMOW}$	C:N	*Date of growth (estimate)*
Description:	Single tail hair								
Sample date:	3/4/2014	0.3	4/14/2014	4.64	-24.29	-	-	3.50	*2/18/2014*
Length (cm):	3.9								
Sample date:	4/30/2014	0.3	12/18/2014	4.13	-	-	-	-	*4/13/2014*
Length (cm):	2.7	0.3	12/19/2014	-	-24.59	-	-	-	*4/13/2014*
Sample date:	7/1/2014	0.3	12/18/2014	3.72	-	-	-	-	*6/15/2014*
Length (cm):	4.0	0.3	12/19/2014	-	-24.63	-	-	-	*6/15/2014*
Sample date:	8/28/2014	0.3	12/18/2014	4.15	-	-	-	-	*8/14/2014*
Length (cm):	4.2	0.3	12/19/2014	-	-24.42	-	-	-	*8/14/2014*
			Average	**4.54**	**-24.35**	**11.31**	**-91.97**	**3.66**	
			Std Dev	**0.38**	**0.53**	**1.44**	**3.43**	**0.1**	

Table 4.3. Elephant calf tail hair isotope data.
Results of analyses of samples taken from calf tail hairs. A single hair (A_{calf}) was segmented to reconstruct $\delta^{13}C$ and $\delta^{15}N$ over a period stretching back to prenatal growth. A second individual hair ($C[1]_{calf}$) was similarly segmented for analysis of $\delta^{18}O$ and δD after A_{calf} was exhausted by the first analysis. Hair analyses for growth that occurred during the study period were based on clumps of hair (C_{calf}, D_{calf}, E_{calf}, and F_{calf}), which were easier to resample in the calf, whose hairs were much finer than his mother's. It was not until late in the sampling period reported here that we began sampling an entire tuft of hair (F_{calf}) that we were able to reliably resample from the same hairs over subsequent episodes. Date of growth estimates for growth prior to initial sampling on 11/01/2012 are based alignment of prominent isotope landmarks with the mother's record (see Figures 4.6, 4.7, 4.8, 4.9). Estimates for samples excised from near the proximal end of hair segments collected during the sampling period are based on average observed bimonthly growth rate since the previous sampling episode. All estimates accommodate 5 mm of hair remaining in the follicle, since hair at the surface of the skin represents growth from some amount of time earlier. We have not yet been able to verify our estimate of length of hair inside the follicle.

Calf		Distance							
Sample ID:	**A_{calf}**	from prox	Date of	$\delta^{15}N$	$\delta^{13}C$	$\delta^{18}O$	δD		*Date of growth*
Description:	Single tail hair	end (cm)	analysis	‰$_{air\text{-}N2}$	‰$_{VPDB}$	‰$_{VSMOW}$	‰$_{VSMOW}$	C:N	*(estimate)*
Sample date:	11/1/2012	13.3	11/18/2013	5.89	-23.38	-	-	3.50	*2/27/2011*
Length (cm):	16.9	12.5	11/18/2013	6.24	-23.03	-	-	3.52	*3/24/2011*
		11.8	11/18/2013	6.10	-23.39	-	-	3.59	*4/19/2011*
		11.0	11/18/2013	6.20	-23.51	-	-	3.68	*5/14/2011*
		10.3	11/18/2013	5.73	-23.51	-	-	3.60	*6/9/2011*
		9.6	11/18/2013	6.02	-23.55	-	-	3.54	*7/4/2011*
		8.9	11/18/2013	6.03	-24.52	-	-	3.52	*7/29/2011*
		8.2	11/18/2013	6.20	-23.85	-	-	3.50	*8/24/2011*
		7.5	11/18/2013	6.34	-24.39	-	-	3.51	*9/18/2011*
		6.8	11/18/2013	6.42	-23.61	-	-	3.57	*10/13/2011*
		6.2	11/18/2013	6.17	-23.68	-	-	3.52	*11/8/2011*
		5.6	11/18/2013	6.35	-23.72	-	-	3.48	*11/30/2011*
		5.1	3/24/2014	6.63	-23.67	-	-	3.57	*12/22/2011*
		4.6	3/24/2014	6.66	-24.71	-	-	3.61	*1/13/2012*
		4.2	3/24/2014	6.44	-23.90	-	-	3.58	*2/28/2012*
		3.8	3/24/2014	6.45	-23.74	-	-	3.77	*4/14/2012*
		3.4	3/24/2014	6.44	-23.69	-	-	3.76	*5/30/2012*
		2.9	3/24/2014	6.38	-24.62	-	-	3.51	*7/16/2012*
		2.4	3/24/2014	6.34	-23.27	-	-	3.58	*8/8/2012*
		2.0	3/24/2014	6.43	-23.34	-	-	3.56	*9/1/2012*
		1.7	3/24/2014	6.57	-24.22	-	-	3.68	*9/25/2012*
		1.3	3/24/2014	6.38	-23.11	-	-	3.37	*10/2/2012*
		1.0	3/24/2014	6.36	-23.04	-	-	3.78	*10/9/2012*
		0.6	3/24/2014	5.94	-22.91	-	-	3.57	*10/16/2012*
		0.2	3/24/2014	5.83	-22.87	-	-	3.58	*10/24/2012*
Sample date:	12/27/2012[1]	1.1	3/24/2014	5.90	-22.93	-	-	3.56	*11/4/2012*
Length (cm):	1.3	0.2	4/14/2014	5.89	-22.79	-	-	3.57	*12/2/2012*
Sample date:	3/4/2013[1]	0.2	4/14/2014	5.95	-22.84	-	-	3.61	*2/7/2013*
Length (cm):	0.9								

		Distance							
Sample ID:	**C_{calf}**	from prox	Date of	$\delta^{15}N$	$\delta^{13}C$	$\delta^{18}O$	δD		*Date of growth*
Description:	Hair tuft	end (cm)	analysis	‰$_{air\text{-}N2}$	‰$_{VPDB}$	‰$_{VSMOW}$	‰$_{VSMOW}$	C:N	*(estimate)*
Sample date:	5/1/2013	0.2	4/14/2014	6.23	-22.55	-	-	3.50	*4/1/2013*
Length (cm):	0.3								
Sample date:	7/1/2013	0.2	4/14/2014	6.18	-22.71	-	-	3.45	*6/8/2013*
Length (cm):	0.3								
Sample date:	8/29/2013	0.1	4/14/2014	5.82	-23.58	-	-	3.65	*8/11/2013*
Length (cm):	1.1								
Sample date:	11/6/2013	0.1	4/14/2014	5.55	-23.75	-	-	3.63	*10/19/2013*
Length (cm):	1.0								

Table 4.3 (cont.)

Sample date:	12/30/2013	0.1	4/14/2014	5.78	-23.73	-	-	3.59	*12/6/2013*
Length (cm):	0.3								
Sample date:	3/4/2014	0.1	4/14/2014	5.90	-23.59	-	-	3.50	*1/28/2014*
Length (cm):	0.5								
Sample date:	4/30/2014	0.1	12/18/2014	5.38	-	-	-	-	*4/6/2014*
Length (cm):	0.8	0.1	12/19/2014	-	-23.56	-	-	-	*4/6/2014*

Sample ID:	**D_{calf}**	Distance from prox end (cm)	Date of analysis	$\delta^{15}N$ ‰$_{air\text{-}N2}$	$\delta^{13}C$ ‰$_{VPDB}$	$\delta^{18}O$ ‰$_{VSMOW}$	δD ‰$_{VSMOW}$	C:N	*Date of growth (estimate)*
Description:	Single tail hair								
Sample date:	7/1/2014	0.2	12/18/2014	5.00	-	-	-	-	*6/8/2014*
Length (cm):	14.4								

Sample ID:	**E_{calf}**	Distance from prox end (cm)	Date of analysis	$\delta^{15}N$ ‰$_{air\text{-}N2}$	$\delta^{13}C$ ‰$_{VPDB}$	$\delta^{18}O$ ‰$_{VSMOW}$	δD ‰$_{VSMOW}$	C:N	*Date of growth (estimate)*
Description:	Single tail hair								
Sample date:	7/2/2014	0.2	12/19/2014	-	-23.88	-	-	-	*6/8/2014*
Length (cm):	26.5								

Sample ID:	**F_{calf}**	Distance from prox end (cm)	Date of analysis	$\delta^{15}N$ ‰$_{air\text{-}N2}$	$\delta^{13}C$ ‰$_{VPDB}$	$\delta^{18}O$ ‰$_{VSMOW}$	δD ‰$_{VSMOW}$	C:N	*Date of growth (estimate)*
Description:	Hair tuft								
Sample date:	8/28/2014	0.2	12/18/2014	5.09	-	-	-	-	*8/13/2014*
Length (cm):	21.1	0.2	12/19/2014	-	-23.63	-	-	-	*8/13/2014*
			Average	**6.09**	**-23.53**	**-**	**-**	**3.57**	
			Std Dev	**0.39**	**0.53**	**-**	**-**	**0.1**	

[1] uncertain association with previously cut hair

Table 4.3 (cont.)

Calf		Distance							
Sample ID:	**C[1]$_{calf}$**[2]	from prox	Date of	$\delta^{15}N$	$\delta^{13}C$	$\delta^{18}O$	δD		*Date of growth*
Description:	Single tail hair	end (cm)	analysis	‰$_{air\text{-}N2}$	‰$_{VPDB}$	‰$_{VSMOW}$	‰$_{VSMOW}$	C:N	*(estimate)*
Sample date:	3/4/2013	175.5	9/30/2014[4]	-	-	-	-88.45	-	*11/1/2011*
Length (cm):	18.2	170.5	9/30/2014[4]	-	-	-	-87.57	-	*11/16/2011*
		165.5	9/30/2014[4]	-	-	-	-83.89	-	*12/1/2011*
		160.5	9/30/2014[4]	-	-	14.65	-83.98	-	*12/16/2011*
		155.5	9/30/2014[4]	-	-	14.29	-86.37	-	*12/31/2011*
		150.5	9/30/2014[4]	-	-	14.98	-83.27	-	*1/15/2012*
		145.5	9/30/2014[4]	-	-	14.19[3]	-84.83[3]	-	*1/27/2012*
		140.5	9/30/2014[4]	-	-	13.40	-86.38	-	*2/8/2012*
		135.5	9/30/2014[4]	-	-	12.88[3]	-85.97[3]	-	*2/16/2012*
		130.5	9/30/2014[4]	-	-	12.37[3]	-85.56[3]	-	*2/24/2012*
		125.5	9/30/2014[4]	-	-	11.85	-85.15	-	*3/3/2012*
		120.5	9/30/2014[4]	-	-	11.41	-91.69	-	*3/11/2012*
		115.5	9/30/2014[4]	-	-	11.56	-91.38	-	*3/19/2012*
		110.5	9/30/2014[4]	-	-	12.33	-93.65	-	*3/29/2012*
		105.5	9/30/2014[4]	-	-	11.44	-93.46	-	*4/8/2012*
		100.5	9/30/2014[4]	-	-	11.66	-92.96	-	*4/23/2012*
		95.5	9/30/2014[4]	-	-	10.98	-90.87	-	*5/8/2012*
		90.5	9/30/2014[4]	-	-	10.68	-90.94	-	*5/23/2012*
		85.5	9/30/2014[4]	-	-	11.60	-89.12	-	*6/7/2012*
		80.5	9/30/2014[4]	-	-	10.92	-89.83	-	*6/17/2012*
		75.5	9/30/2014[4]	-	-	13.12	-89.59	-	*6/27/2012*
		70.5	9/30/2014[4]	-	-	12.34	-88.55	-	*7/7/2012*
		65.5	9/30/2014[4]	-	-	13.00	-88.05	-	*7/17/2012*
		60.5	9/30/2014[4]	-	-	13.16	-90.16	-	*7/27/2012*
		55.5	9/30/2014[4]	-	-	11.66	-88.93	-	*8/6/2012*
		50.5	9/30/2014[4]	-	-	13.21	-89.04	-	*8/16/2012*
		45.5	9/30/2014[4]	-	-	12.66	-86.91	-	*8/26/2012*
		40.5	9/30/2014[4]	-	-	12.54	-88.03	-	*9/10/2012*
		35.5	9/30/2014[4]	-	-	12.28	-87.45	-	*9/25/2012*
		30.5	9/30/2014[4]	-	-	11.55	-88.29	-	*10/10/2012*
		25.5	9/30/2014[4]	-	-	12.32	-89.11	-	*10/30/2012*
		20.5	9/30/2014[4]	-	-	11.91	-87.42	-	*11/19/2012*
		15.5	9/30/2014[4]	-	-	12.29	-89.52	-	*12/9/2012*[5]
		10.5	9/30/2014[4]	-	-	11.61	-90.50	-	*1/3/2013*[5]
		5.5	9/30/2014[4]	-	-	12.15	-89.93	-	*1/28/2013*[5]
		0.5	9/30/2014[4]	-	-	12.07[3]	-82.91	-	*2/17/2013*[5]
Sample date:	12/27/2012[1]	0.3	9/30/2014[4]	-	-	11.99	-90.25	-	*11/27/2012*[5]
Length (cm):	1.3								
Sample date:	3/4/2013[1]	0.3	9/30/2014[4]	-	-	10.32	-85.56	-	*1/18/2013*[5]
Length (cm):	0.9								

Table 4.3 (cont.)

Sample ID:	C_{calf}	Distance from prox	Date of	$\delta^{15}N$	$\delta^{13}C$	$\delta^{18}O$	δD		*Date of growth*
Description:	Hair tuft	end (cm)	analysis	$‰_{air\text{-}N2}$	$‰_{VPDB}$	$‰_{VSMOW}$	$‰_{VSMOW}$	C:N	*(estimate)*
Sample date:	5/1/2013	0.2	9/30/2014[4]	-	-	9.86	-86.33	-	*3/12/2013*
Length (cm):	0.3								
Sample date:	7/1/2013	0.3	9/30/2014[4]	-	-	9.11	-85.17	-	*5/24/2013*
Length (cm):	0.3								
Sample date:	8/29/2013	0.2	9/30/2014[4]	-	-	11.89	-84.16	-	*8/6/2013*
Length (cm):	1.1								
			Average	**-**	**-**	**12.08**	**-88.29**	**-**	
			Std Dev	**-**	**-**	**1.24**	**2.78**	**-**	

[1] Uncertain association with previously cut hair

[2] Data presented is from the longest hair from the initial clipping (3/4/2013) of the C_{Lucas} hair tuft

[3] Suspect due to analytical error

[4] Date file received

[5] Estimated date of growth overlaps with other samples

Table 4.4. Elephant milk and drinking water isotope data.

Samples of elephant drinking water were collected throughout most of the study for oxygen isotope analysis. One extra sample was collected during a 3-day Toledo water ban in August 2014, when elephant drinking water was brought in from outside Toledo. Milk was collected during every sampling episode. After setting aside a portion of whole milk for analysis of milk-water oxygen, the remainder was separated into milk fats and nonfat solids for isolated analyses. $\delta^{13}C$ and $\delta^{15}N$ were measured for nonfat solids and $\delta^{13}C$ was measured separately for solid 'butter fat' and liquid oil. Small amounts of suspended debris consolidated in the base of tubes during centrifugation to isolate fats, and was weighed but not analyzed. Milk pH was measured only in samples that had enough remaining after processing for isotope analyses.

Milk/	**Zoo H_2O**	**Whole milk**		**Milk 'debris'**	**Milk nonfat solids**			**Milk fats**		
Water	$\delta^{18}O$		Water $\delta^{18}O$	Isolated	Isolated	$\delta^{15}N$	$\delta^{13}C$	Isolated	Solids $\delta^{13}C$	Oil $\delta^{13}C$
Sample date	$‰_{VSMOW}$	pH	$‰_{VSMOW}$	mass (mg/l)	mass (mg/l)	$‰_{air\text{-}N2}$	$‰_{VPDB}$	mass (mg/l)	$‰_{VPDB}$	$‰_{VPDB}$
11/1/2012	-	8.43	-6.09	1.89	120.3	5.32	-25.43	91.47	-27.15	-27.38
12/27/2012	-	8.385	-8.27	1.71	123.3	5.47	-25.41	108.39	-27.40	-27.98
3/4/2013	-	-	-8.33	1.96	125.4	5.22	-26.80	89.43	-27.84	-28.11
5/1/2013	-7.58	8.52	-7.22	4.58	114.8	4.65	-26.76	92.79	-27.93	-28.11
7/1/2013	-	-	-7.55	5.06	99.1	4.88	-27.69	47.94	-28.80	-
8/29/2013	-	-	-5.95	3.19	125.6	4.79	-27.39	101.99	-28.36	-28.47
11/6/2013	-	-	-	3.41	131.2	5.02	-27.28	112.72	-28.65	-28.96
12/30/2013	-9.45	-	-8.95	2.41	103.2	6.06	-27.23	192.50	-28.51	-28.80
3/4/2014	-11.38	-	-10.62	5.03	118.6	5.38	-27.20	114.68	-28.30	-28.52
4/30/2014	-10.12	-	-8.65	3.90	101.1	5.38	-26.96	149.62	-28.23	-28.51
7/1/2014	-7.96	-	-8.62	2.53	130.2	5.11	-26.93	40.70	-28.20	-
8/4/2014[1]	-7.39	-	-	-	-	-	-	-	-	-
8/28/2014	-	8.03	-	2.79	103.6	5.68	-26.48	118.07	-27.93	-28.14
10/30/2014	-	-	-	3.15	86.4	4.96	-26.58	148.18	-27.62	-27.89
Average	**-8.98**	**8.34**	**-8.03**	**3.20**	**114.06**	**5.22**	**-26.78**	**108.35**	**-28.07**	**-28.26**
Std Dev	**1.60**	**0.21**	**1.39**	**1.16**	**13.99**	**0.39**	**0.69**	**40.49**	**0.49**	**0.45**

[1] Sample was taken during the Toledo, OH water ban due to high algal bloom in Lake Erie - alternate water source

Table 4.5. Isotope standards cumulative data.
Isotope standards run with $\delta^{13}C$ and $\delta^{15}N$ analyses of milk solids and fat were all highly consistent. Oxygen standards frequently failed to produce results due to machine issues, but when they did, results were in the expected range. Treatment of water-$\delta^{18}O$ results is discussed in the text (see *Results: Milk and drinking water $\delta^{18}O$*).

Isotope Standards		# of	Avg $\delta^{13}C$	Std
Carbon	Date	tests	$‰_{VPDB}$	Dev
IAEA 600 Caffeine	11/18/2013	3	-27.77	0.07
	3/24/2014	3	-27.77	0.08
	4/14/2014	3	-27.77	0.10
	1/27/2015	3	-27.77	0.02
	1/28/2015	3	-27.77	0.08
IAEA-CH-6 Sucrose	11/18/2013	3	-10.45	0.09
	3/24/2014	3	-10.45	0.01
	4/14/2014	3	-10.45	0.06
	1/27/2015	3	-10.45	0.04
	1/28/2015	3	-10.45	0.05

		# of	Avg $\delta^{15}N$	Std
Nitrogen	Date	tests	$‰_{air\text{-}N2}$	Dev
IAEA N2	11/18/2013	3	20.30	0.09
	3/24/2014	3	20.30	0.09
	4/14/2014	3	20.30	0.10
	1/20/2015	3	20.30	0.16
USGS 25	11/18/2013	3	-30.40	0.16
	3/24/2014	3	-30.40	0.15
	4/14/2014	3	-30.40	0.08
	1/20/2015	3	-30.40	0.09

		# of	Avg $\delta^{18}O$	Std
Oxygen (water)	Date	tests[1]	$‰_{VSMOW}$	Dev
MDIW#3	12/8/2014	9	-8.92	0.04
	12/8/2014	9	-9.11	0.05
	12/8/2014	3	-9.17	0.06
	12/8/2014	2	-9.07	0.18
	12/12/1914	7	-9.17	0.05
AAS	12/8/2014	9	-22.09	0.07
	12/8/2014	9	-22.02	0.04
	12/8/2014	9	-21.97	0.07
	12/8/2014	1	-22.19	-
	12/12/1914	6	-21.99	0.07
	12/13/2014	3	-22.15	0.49
Evaporated	12/8/2014	9	7.12	0.05
	12/8/2014	9	7.08	0.06
	12/8/2014	6	6.86	0.07
	12/8/2014	3	7.02	0.26
	12/12/1914	8	7.11	0.07

[1] Not all 9 attempts always produced measurements

Table 4.6. Elephant mother tail hair cortisol data.
After samples were excised every 20 mm to reconstruct hair $\delta^{13}C$ and $\delta^{15}N$ records over multiple years prior to the beginning of sampling, the remainder of B_{mother} was milled into fine powder samples (1 sample for every 20 mm length, RHC1-RHC22) for cortisol extraction. Each measurement represents the bulk cortisol over an approximately 3 – 5 week interval. Estimated timing for the reconstructed interval is derived from the reconstructed chronology for $\delta^{13}C$ and $\delta^{15}N$ records, which was established from measured growth rates. Two month samples collected between the end of 2013 and the end of 2014 were each milled along their entire length for a single bulk cortisol measurement. Timing of analyses for hair segments collected during the study was based on dates of sampling with an accommodation for an estimated 8 mm of hair remaining in the follicle.

Hair cortisol - B_{mother}				
	Hair	Cortisol content		
Sample ID	Mass (mg)	(µg/dL)	(ng/g)	Growth interval (est.)
RHC22	19.28	0.036	3.82	*11/28/2010-1/1/2011*
RHC21	18.39	0.043	5.40	*1/1/2011-1/30/2011*
RHC20	20.15	0.051	6.32	*1/30/2011-2/27/2011*
RHC19	18.75	0.044	5.46	*2/27/2011-4/7/2011*
RHC18	14.47	0.028	3.01	*4/7/2011-5/12/2011*
RHC17	15.30	0.034	4.38	*5/12/2011-6/9/2011*
RHC16	19.19	0.044	5.24	*6/9/2011-7/7/2011*
RHC15	19.04	0.041	4.81	*7/7/2011-7/31/2011*
RHC14	14.86	0.037	5.09	*7/31/2011-8/25/2011*
RHC13	16.56	0.031	3.36	*8/25/2011-9/30/2011*
RHC12	15.15	0.030	3.48	*9/30-2011-11/8/2011*
RHC11	13.65	0.038	5.74	*11/8/2011-12/12/2011*
RHC10	15.70	0.047	7.13	*12/12/2011-1/13/2012*
RHC9	11.28	0.036	6.47	*1/13/2012-2/11/2012*
RHC8	13.94	0.022	1.66	*2/11/2012-3/14/2012*
RHC7	18.32	0.040	4.85	*3/14/2012-4/22/2012*
RHC6	16.32	0.031	3.44	*4/22/2012-5/23/2012*
RHC5	17.71	0.034	3.74	*5/23/2012-6/20/2012*
RHC4	22.67	0.037	3.39	*6/20/2012-7/16/2012*
RHC3	23.73	0.039	3.52	*7/16/2012-8/10/2012*
RHC2	29.92	0.045	3.52	*8/10/2012-9/5/2012*
RHC1	23.93	0.040	3.57	*9/5/2012-10/15/2012*
RHC12-30-13	25.41	0.038	3.09	*10/16/2013-12/12/2013*
RHC3-4-14	27.53	0.043	3.56	*12/12/2013-2/18/2014*
RHC4-30-14	22.49	0.044	4.50	*2/18/2014-4/13/2014*
RHC7-1-14	61.52	0.057	2.91	*4/13/2014-6/15/2014*
RHC8-28-14	22.95	0.045	4.58	*6/15/2014-8/14/2014*
RHC10-30-14	28.22	0.050	4.31	*8/14/2014-10/5/2014*
RHC12-29-14	21.78	0.032	2.73	*10/5/2014-11/18/2014*
Average	**20.97**	**0.039**	**4.24**	
Std Dev	**9.10**	**0.008**	**1.25**	
Blank1	-	0.012		
Blank2	-	0.016		
Blank3	-	0.017		
Blank4	-	0.017		
	Average	**0.015**		
	Std Dev	**0.002**		

Figure 4.1. Elephant mother tail hair sampling.
The mother elephant's tail hairs were robust enough that we were able to resample individual hairs at bimonthly intervals. Photos taken during each sampling event were used to help re-identify target hairs and verify that the same two hairs had been continuously monitored. Furrow patterns in the skin helped monitor hair locations, but gradually changed over time.

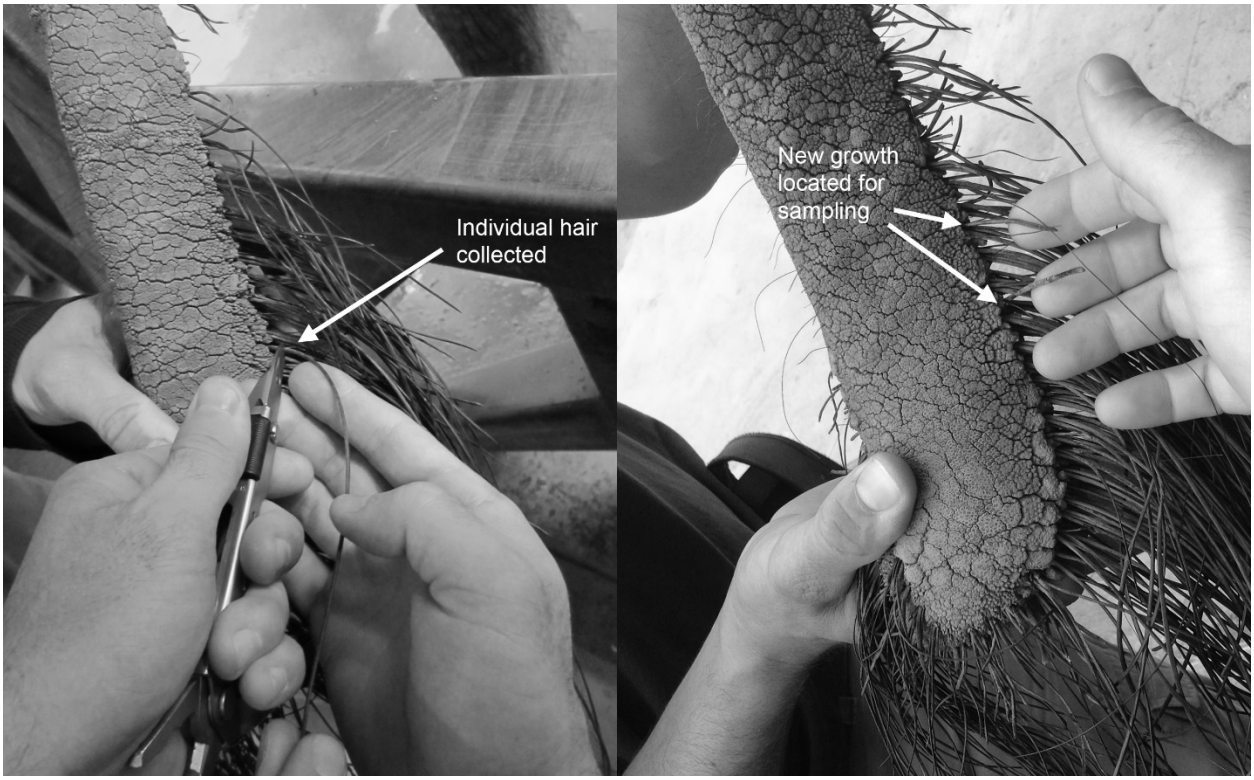

Figure 4.2. Elephant calf tail hair sampling.

The only procedure that resulted in confident resampling of the same calf tail hairs was to clip an entire tuft of hair. Photos taken at each sampling were used to verify that the same hairs had been repeatedly sampled, but were not required during sampling as the previously cut tuft was easily identified after 2 months of growth. Epidermal furrow patterns and hair counts appeared to change at a more rapid pace in the growing calf's tail than in the mother's tail, which, along with the finer scale of calf hairs, made calf tail hairs more difficult to track.

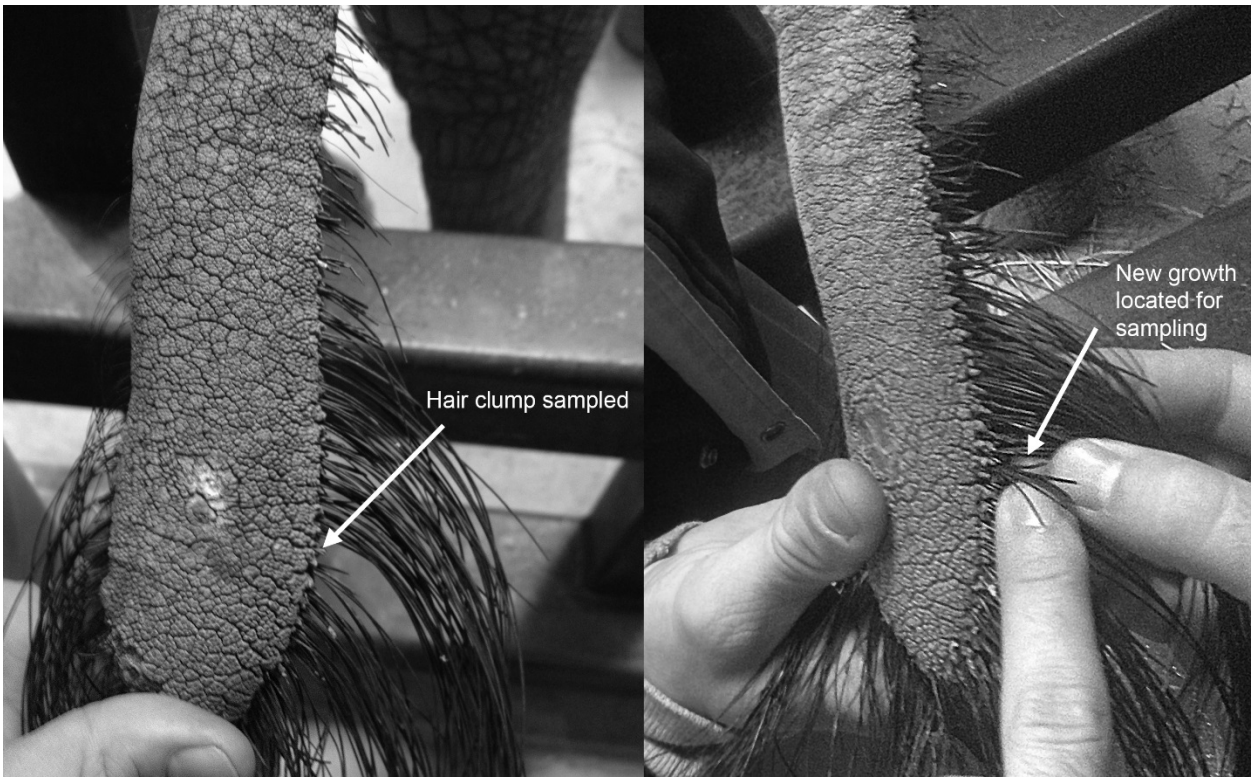

Figure 4.3. Sampling elephant tail hairs for serial isotopic analyses.
(A) The procedure for sampling the mother's tail hair for isotope analysis involved excising small wedges at measured distances from the location of hair generation (estimated to be 8 mm beneath the surface of the skin), while leaving the length of the hair intact. (B) The procedure for sampling calf tail hairs for isotope analysis differed because of the difference in scale. Rather than remove wedges of hair, we clipped the hair into ~5 mm segments that appear to represent approximately monthly growth for the early portion of the growth record. For analysis of hair segments collected at bimonthly intervals, we removed a single small wedge (mother) or clipped the required length (calf) from the proximal end.

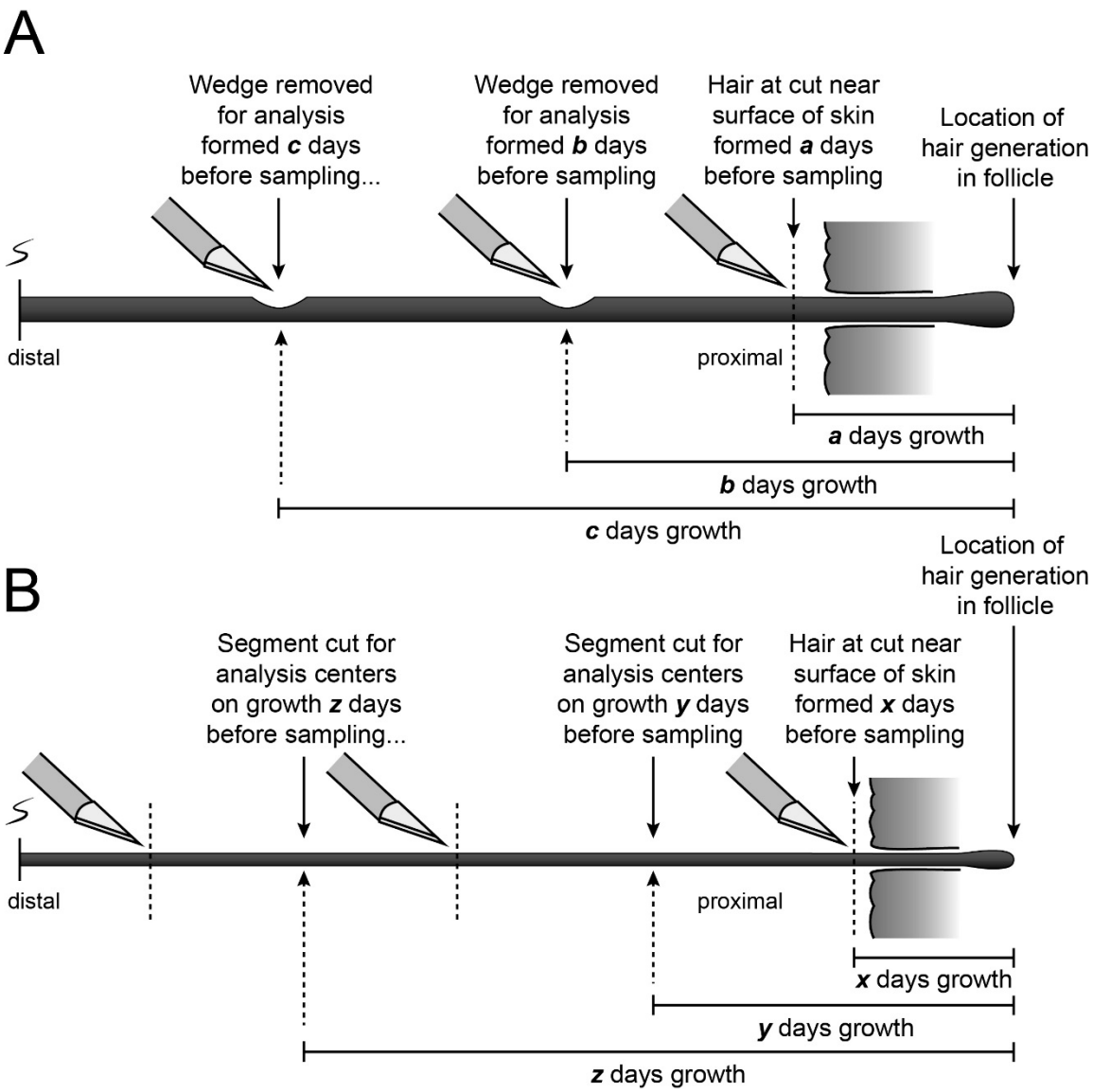
A
Wedge removed for analysis formed c days before sampling...
Wedge removed for analysis formed b days before sampling
Hair at cut near surface of skin formed a days before sampling
Location of hair generation in follicle
distal
proximal
a days growth
b days growth
c days growth
B
Location of hair generation in follicle
Segment cut for analysis centers on growth z days before sampling...
Segment cut for analysis centers on growth y days before sampling
Hair at cut near surface of skin formed x days before sampling
distal
proximal
x days growth
y days growth
z days growth

Figure 4.4. Sampling elephant tail hairs for serial cortisol analysis.
To produce samples for cortisol extraction, we clamped individual tail hairs flat on an aluminum base and milled part of the way through the hair by manipulating the sample under microscope on a moveable stage under a fixed-position dental drill. Samples were milled at low speed using a 1 mm carbide bit to prevent heating the sample. This procedure produced fine powder samples ideal for methanol extraction of cortisol and left a portion of the hair shaft intact for potential future analyses.

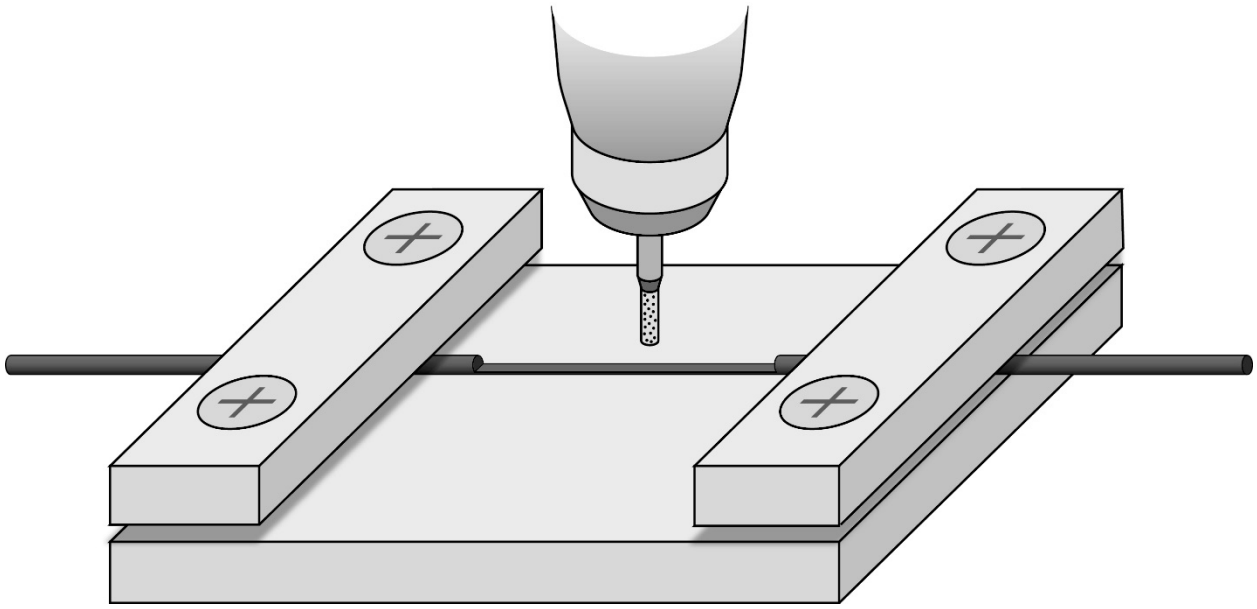

Figure 4.5. Tail hair growth rates.
New hair growth was measured for hairs repeatedly sampled bimonthly. Bimonthly average growth rates varied seasonally with fastest growth in a single tail hair being about two times as great as the slowest growth. Average growth rates for all hairs from both mother and calf were fastest in the summer and slowest in the winter. The mother's growth rates also show a spike in the coldest months which likely results from increased time spent indoors during that time. Growth rates displayed for hairs from the mother are all based on repeated sampling of individual hairs. A_{calf} is also the record from an individual hair, but with questionable identification though multiple samplings. C_{calf} and F_{calf} values plotted represent the average growth for multiple hairs sampled simultaneously.

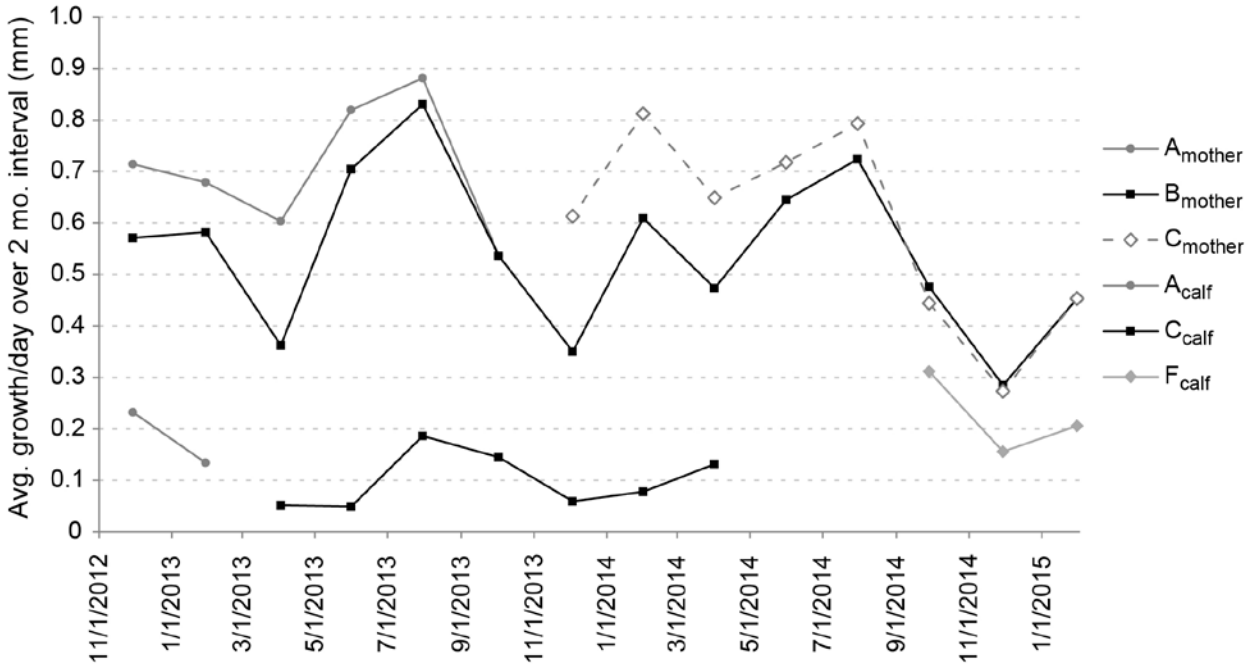

Figure 4.6. Serial records of $\delta^{15}N$ from elephant tail hairs and milk.
(A) Serial records of tail hair $\delta^{15}N$ for mother and calf. Nitrogen isotope records for milk nonfat solids are also plotted. Estimated chronology of the isotope records for the mother's hair is based on direct bimonthly measurements of growth in that same individual hair over a more than 2-year period. In this plot, the corresponding calf hair chronology is reconstructed using an average growth rate of 6 mm/month, based on measurements made early in the study. (B) Calf hair chronology has been adjusted to align prominent landmarks in its $\delta^{15}N$ and $\delta^{13}C$ records with apparently related features in its mother's $\delta^{15}N$ and $\delta^{13}C$ records (see Figure 4.7 for $\delta^{13}C$). (C) Monthly estimates were interpolated onto the nitrogen profiles of both mother and calf to produce records that could be compared directly. (D) Plotting the difference between corresponding interpolated values in calf and mother shows calf values enriched by about 1 – 2.5 ‰ compared to those of its mother throughout the entire sampled interval. $\Delta^{15}N_{calf\text{-}mother}$ is highest about 6 months after birth and then gradually declines over the subsequent ~ 3 years of nursing.

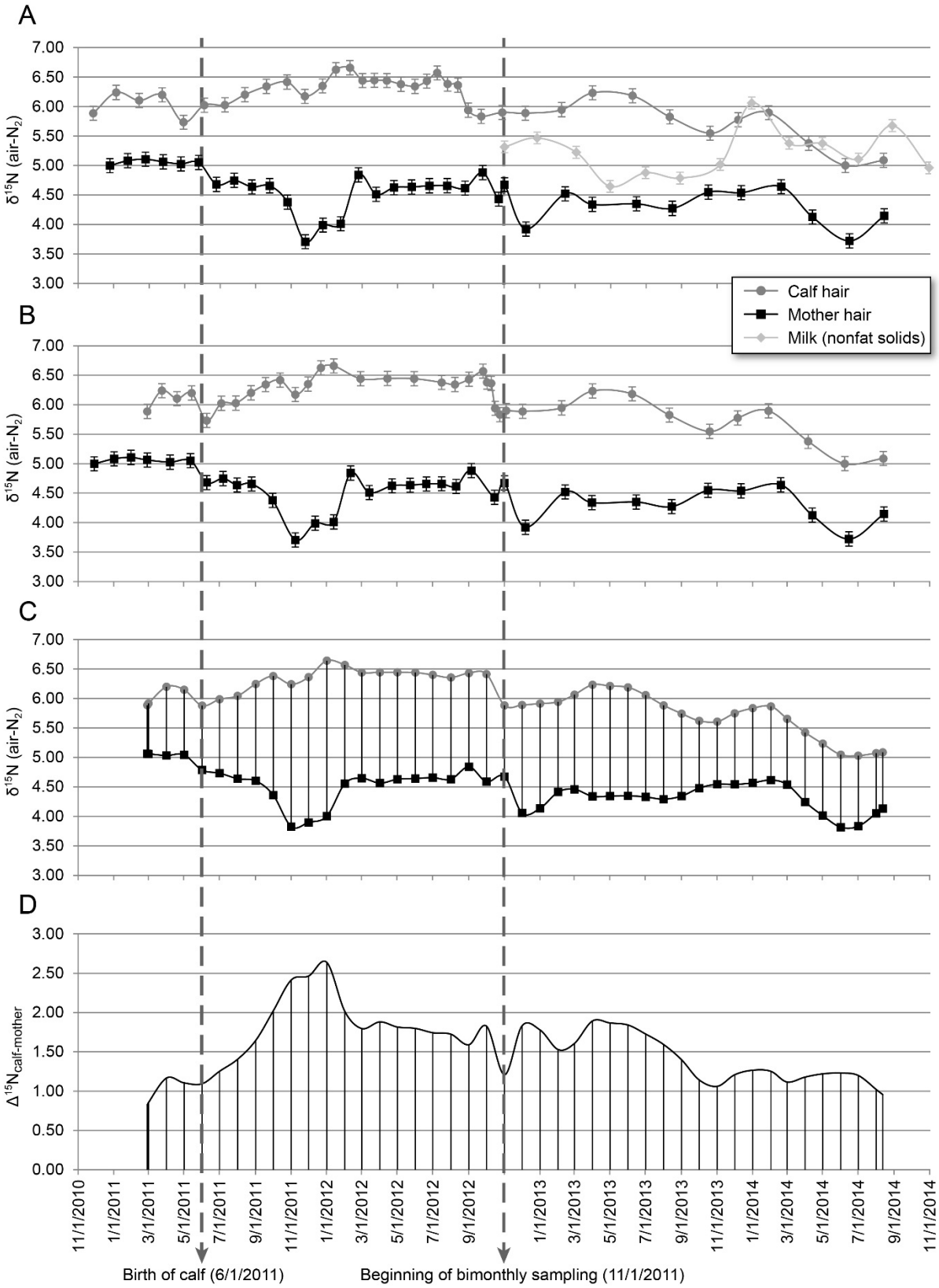
A
B
C
D
δ15N (air-N2)
Δ15Ncalf-mother
Calf hair
Mother hair
Milk (nonfat solids)
Birth of calf (6/1/2011)
Beginning of bimonthly sampling (11/1/2011)

Figure 4.7. Serial records of $\delta^{13}C$ from elephant tail hairs and milk.
(A) Serial records of tail hair $\delta^{13}C$ for mother and calf. Carbon isotope records for milk nonfat solids, milk fat, and milk oil are also plotted. Estimated chronology of the isotope records for the mother's hair is based on direct bimonthly measurements of growth in that same individual hair over a more than 2 year period. In this plot, the corresponding calf hair chronology is reconstructed using an average growth rate of 6 mm/month, based on measurements made early in the study. (B) Calf hair chronology has been adjusted to align prominent landmarks in its $\delta^{15}N$ and $\delta^{13}C$ records with apparently related features in its mother's $\delta^{15}N$ and $\delta^{13}C$ records (see Figure 4.6 for $\delta^{15}N$). (C) Monthly estimates were interpolated onto the carbon profiles of both mother and calf to produce records that could be compared directly. (D) Plotting the difference between corresponding interpolated values in calf and mother shows calf values enriched by about 1 ‰ compared to those of its mother throughout most of the interval. $\Delta^{13}C_{calf\text{-}mother}$ is negative immediately after birth and then increases to its postnatal peak of about 1.4 ‰ at about 6-7 months after birth. It then displays a very gradual decline with significant fluctuations over the subsequent ~ 3 years of nursing.

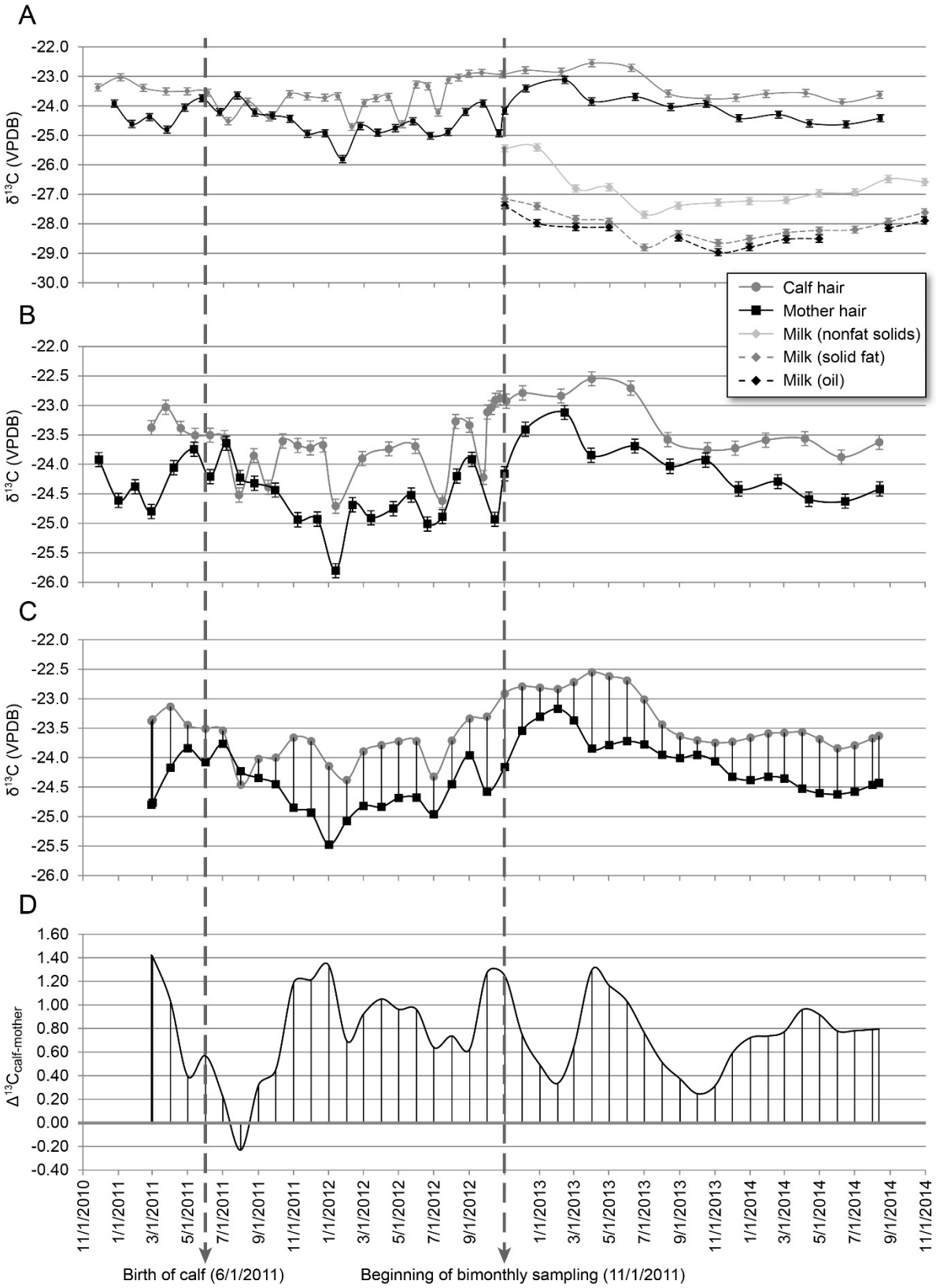
A
B
C
D
δ13C (VPDB)
Δ13Ccalf-mother
Calf hair
Mother hair
Milk (nonfat solids)
Milk (solid fat)
Milk (oil)
Birth of calf (6/1/2011)
Beginning of bimonthly sampling (11/1/2011)

Figure 4.8. Serial records of $\delta^{18}O$ from elephant tail hairs, milk water, and drinking water. (A) Serial records of tail hair $\delta^{18}O$ for mother and calf. Oxygen records for elephant drinking water and milk water are also plotted. Estimated chronology of the isotope records for the mother's hair is based on direct bimonthly measurements of growth in that same individual hair over a more than 2 year period. In this plot, the corresponding calf hair chronology is reconstructed using an average growth rate of 6 mm/month, based on measurements made early in the study. Although 6 mm/month appears to provide a close approximate chronology for the hair used for nitrogen and carbon analyses, it does not seem to provide a reasonable chronology for this separate hair analyzed for $\delta^{18}O$ and δD. (B) Calf hair chronology has been adjusted to align the pattern present in $\delta^{18}O$ and δD to apparently related fluctuations in its mother's $\delta^{18}O$ and δD. (see Figure 4.9 for δD). Using this alignment infers significantly faster growth in this calf hair than in the one analyzed for $\delta^{15}N$ and $\delta^{13}C$. It also means the duration represented by the calf oxygen record is an interval of less than one year that begins 6 – 7 months after birth. (C) Monthly estimates were interpolated onto the oxygen profiles of both mother and calf to produce records that could be compared directly. (D) Plotting the difference between corresponding interpolated values in calf and mother shows the calf record consistently enriched by about 2 ‰ compared to that of the mother. $\Delta^{18}O_{calf\text{-}mother}$ is positive throughout the entire overlapping interval and shows a moderate decreasing trend during that time.

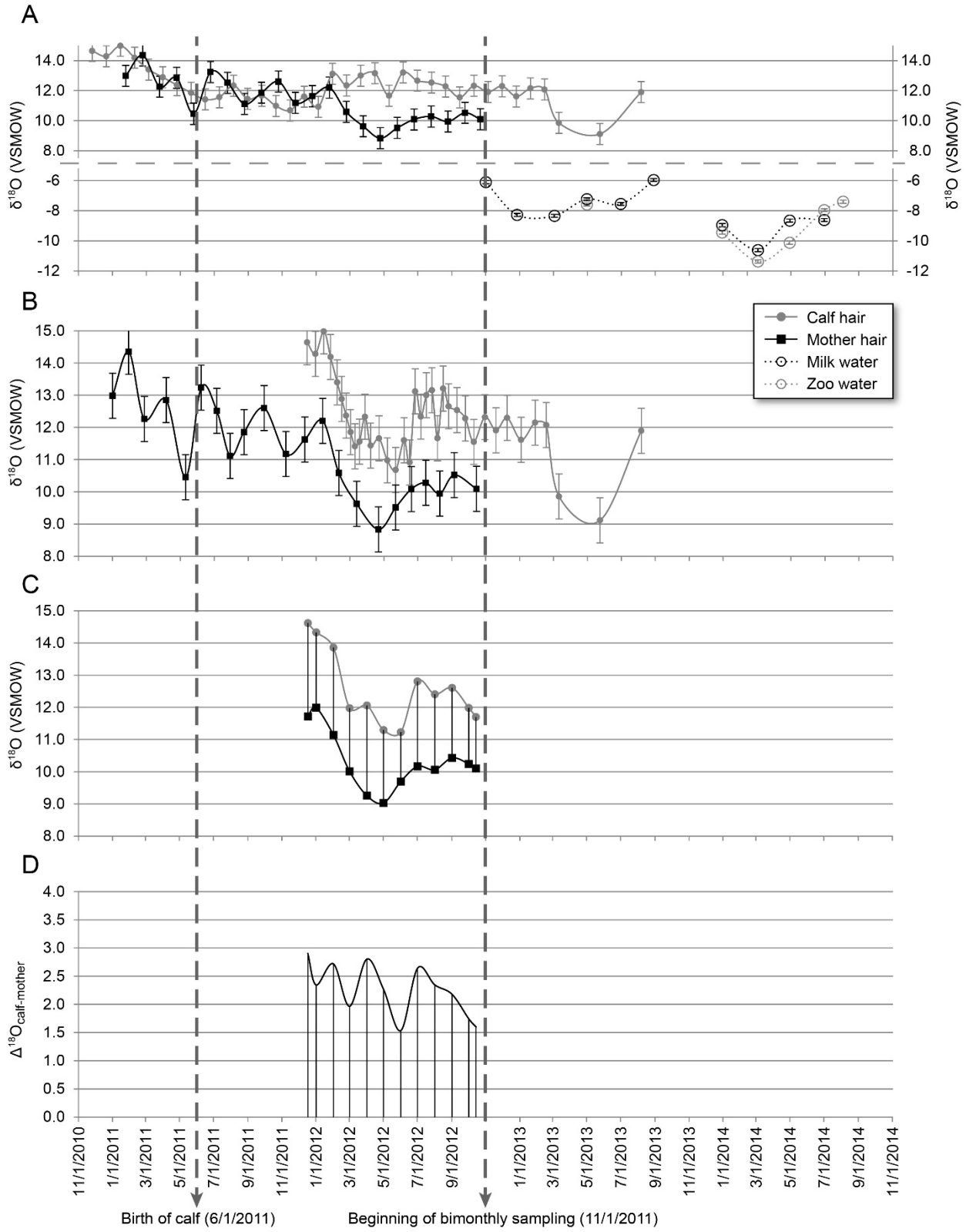
A
B
C
D
δ18O (VSMOW)
Δ18Ocalf-mother
Calf hair
Mother hair
Milk water
Zoo water
Birth of calf (6/1/2011)
Beginning of bimonthly sampling (11/1/2011)

Figure 4.9. Serial records of δD from elephant tail hairs.
(A) Serial records of tail hair δD for mother and calf. Estimated chronology of the isotope records for the mother's hair is based on direct bimonthly measurements of growth in that same individual hair over a more than 2 year period. In this plot, the corresponding calf hair chronology is reconstructed using an average growth rate of 6 mm/month, based on measurements made early in the study. Although 6 mm/month appears to provide a close approximate chronology for the hair used for nitrogen and carbon analyses, it does not seem to provide a reasonable chronology for this separate hair analyzed for $\delta^{18}O$ and δD. (B) Calf hair chronology has been adjusted to align the pattern present in $\delta^{18}O$ and δD to apparently related fluctuations in its mother's $\delta^{18}O$ and δD. (see Figure 4.8 for $\delta^{18}O$). Using this alignment infers significantly faster growth in this calf hair than in the one analyzed for $\delta^{15}N$ and $\delta^{13}C$. It also means the duration represented by the calf deuterium record is less than one year beginning 6 – 7 months after birth. (C) Monthly estimates were interpolated onto the deuterium profiles of both mother and calf to produce records that could be compared directly. (D) Plotting the difference between corresponding interpolated values in calf and mother shows the calf record enriched (0 – 11 ‰) compared to that of the mother until the very end of the overlapping records when calf δD dips below the mother's record. $\Delta D_{calf\text{-}mother}$ is generally positive throughout the entire overlapping interval and shows a moderate decreasing trend during that time.

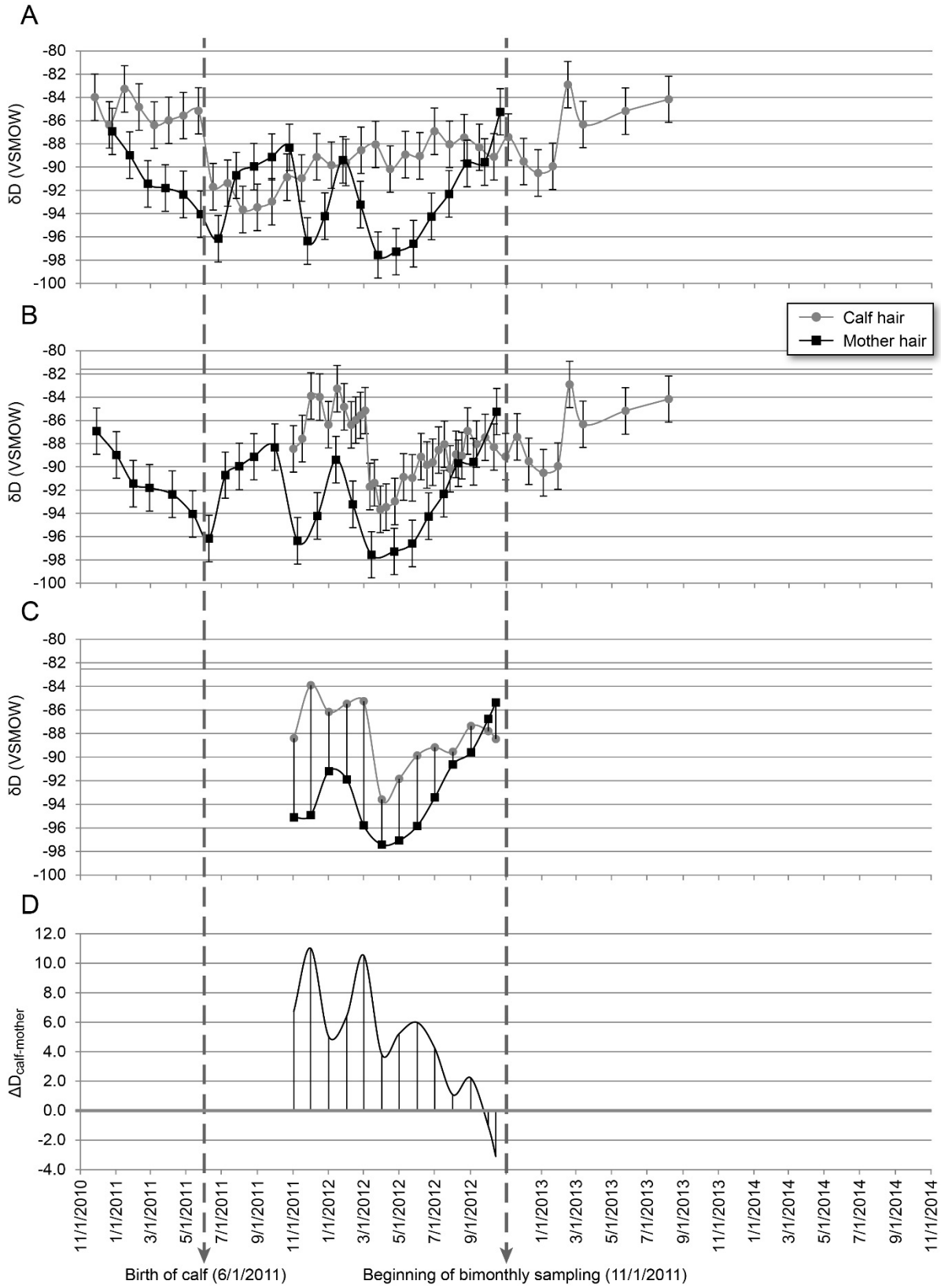
A
B
C
D
δD (VSMOW)
ΔDcalf-mother
Calf hair
Mother hair
Birth of calf (6/1/2011)
Beginning of bimonthly sampling (11/1/2011)

Figure 4.10. Serial record of elephant tail hair cortisol.
The same tail hair used to reconstruct the mother's isotope records (B_{mother}) was subsequently processed for hair cortisol analysis. Based on the chronology established from measured growth rates in the same hair over 2 years, the highest cortisol levels correspond with pregnancy and the first 8 months after parturition in the pre-study growth record. Seven bimonthly hair segments representing growth during the study period were had generally lower concentrations than detected in hair grown in the two years prior to first sampling. These bimonthly segments had well-constrained chronologies and show a double-peak annual profile that can also be observed in the earlier record.

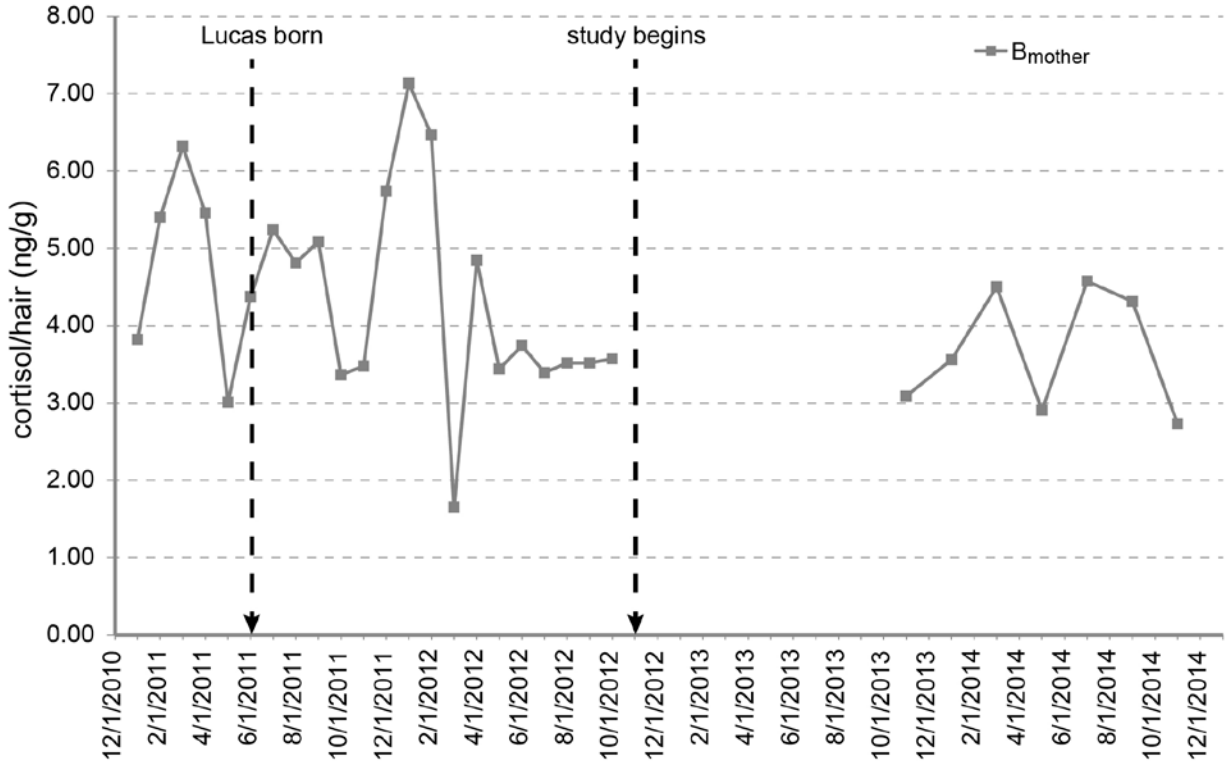

References

Aardal, E., Holm, A. 1995. Cortisol in saliva – references ranges and relation to cortisol in serum. European Journal of Clinical Chemistry and Clinical Biochemistry 33:927-932.

Ambrose, S. H., Norr, L. 1995. Experimental evidence for the relationship of the carbon isotope ratios of whole diet and dietary protein to those of bone collagen and carbonate. In: Lambert, J. B., Grupe, G. (Eds.), Prehistoric human bone: Archaeology at the molecular level. Springer-Verlag, Berlin, pp. 1-37.

Andrews, J., Mecklenborg, A., Bercovitch, F. B., 2005. Milk intake and development in a newborn captive African elephant (*Loxodonta africana*). Zoo Biology 24:275-281.

Atwood, C. S., Hartmann, P. E. 1992. Collection of fore and hind milk from the sow and the changes in milk composition during suckling. Journal of Dairy Research 59:287-298.

Aurich, J., Wulf, M., Ille, N., Erber, R., von Lewinski, M., Palme, R. 2015. Effects of season, age, sex, and housing on salivary cortisol concentrations in horses. Domestic Animal Endocrinology 52:11-16.

Berkvens, C. N. 2012. Keratin glucocorticoid analysis by enzyme immunoassay in mammals, birds, and reptiles. Unpublished dissertation, University of Guelph, Ontario, Canada, (xxv + 241 pp.)

Cerling, T. E., Passey, B. H., Ayliffe, L. K., Cook, C. S., Ehleringer, J. R., Harris, J. M., Dhidha, M. B., Kasiki, S. M. 2004. Orphans' tales: seasonal dietary changes in elephants from Tsavo National Park, Kenya. Palaeogeography, Palaeoclimatology, Palaeoecology 206(3):367-376.

Cerling, T. E., Wittemyer, G., Rasmussen, H. B., Vollrath, F., Cerling, C. E., Robinson, T. J., Douglas-Hamilton, I. 2006. Stable isotopes in elephant hair document migration patterns and diet changes. Proceedings of the National Academy of Sciences 103(2):371-373.

Cerling, T. E., Wittemyer, G., Ehleringer, J. R., Remien, C. H., Douglas-Hamilton, I. 2009. History of Animals using Isotope Records (HAIR): A 6-year dietary history of one family of African elephants. Proceedings of the National Academy of Sciences 106(20):8093-8100.

Chesson, L. A., Valenzuela, L. O., O'Grady, S. P., Cerling, T. E., Ehleringer, J. R. 2010. Journal of Agricultural and Food Chemistry 58:2358-2363.

Coplen, T. B., Qi, H. 2012. USGS42 and USGS43: Human-hair stable hydrogen and oxygen isotopic reference materials and analytical methods for forensic science

and implications for published measurement results. Forensic science international 214(1):135-141.

Dalerum, F., Bennett, N. C., Clutton-Brock, T. H., 2007. Longitudinal differences in ^{15}N between mothers and offspring during and after weaning in a small cooperative mammal, the meerkat (*Suricata suricatta*). Rapid Communications in Mass Spectrometry 21:1889-1892.

Darimont, C. T., Reimchen, T. E. 2002. Intra-hair stable isotope analysis implies seasonal shift to salmon in gray wolf diet. Canadian Journal of Zoology 80(9):1638-1642.

DeNiro, M. J., Epstein, S. 1977. Mechanism of carbon isotope fractionation associated with lipid synthesis. Science 197(4300):261-263.

DeNiro, M. J., Epstein, S. 1978. Influence of diet on the distribution of carbon isotopes in animals. Geochimica et Cosmochimica Acta 42:495-506.

Dettenborn, L., Tietze, A., Bruckner, F., Kirschbaum, C. 2010. Higher cortisol content in hair among long-term unemployed individuals compared to controls. Psychoneuroendocrinology 35:1404-1409.

Dupras, T. L., Schwarcz, H. P., Fairgrieve, S. I., 2001. Infant feeding and weaning practices in Roman Egypt. American Journal of Physical Anthropology 115:204-212.

Dutton, A., Wilkinson, B. H., Welker, J. M., Bowen, G. J., and Lohmann, K. C. 2005. Spatial distribution and seasonal variation in $^{18}O/^{16}O$ of modern precipitation and river water across the conterminous USA.

Ehleringer, J. R., Bowen, G. J., Chesson, L. A., West, A. G., Podlesak, D. W., Cerling, T. E. 2008. Hydrogen and oxygen isotope ratios in human hair are related to geography. Proceedings of the National Academy of Sciences 105(8):2788-2793.

Epstein, S., Mayeda, T. 1953. Variation of O^{18} content of waters from natural sources. Geochimica et Cosmochimica Acta 4:213-224.

Fisher, D. C., Fox, D. L. 2003. Season of death and terminal growth histories of Hiscock mastodons. In: Laub, R. S. (Ed.), The Hiscock site: late Pleistocene and Holocene Paleoecology an Archaeology of Western New York State. Bulletin of the Buffalo Society of Natural Sciences 37, pp. 83-101.

Fisher, D. C., Cherney, M. D., Newton, C., Rountrey, A. N., Calamari, Z. T., Stucky, R. K., Lucking, C., Petrie, L. 2014. Taxonomic overview and tusk growth analyses of Ziegler Reservoir proboscideans. Quaternary Research 82:518-532.

Fogel, M. L., Tuross, N., Owsley, D. W. 1989. Nitrogen isotope tracers of human lactation in modern and archaeological populations. Carnegie Institution of Washington Yearbook 1989:111-117.

Fuller, B. T., Fuller, J. L., Sage, N. E., Harris, D. A., O'Connell, T. C., Hedges, R. E. M. 2004. Nitrogen balance and $\delta^{15}N$: why you're not what you eat during pregnancy. Rapid Communications in Mass Spectrometry 18:2889-2896.

Fuller, B. T., Fuller, J. L., Harris, D. A., Hedges, R. E. M. 2006. Detection of breastfeeding and weaning in modern human infants with carbon and nitrogen stable isotope ratios. American Journal of Physical Anthropology 129:279-293.

Hamel, A. F., Meyer, J. S., Henchey, E., Dettmer, A. M., Suomi, S. J., Novak, M. A. 2011. Effects of shampoo and water washing on hair cortisol concentrations. Clinica Chimica Acta 412:382-385.

Hellhammer, D. H., Wüst, S., Kudielka, B. M. 2009. Salivary cortisol as a biomarker in stress research. Psychoneuroendocrinology 34:163-171.

Henderson, G. L. 1993. Mechanisms of drug incorporation into hair. Forensic Science International 63:19-29.

Hobson, K. A., Alisauskas, R. T., Clark, R. G. 1993. Stable-nitrogen isotope enrichment in avian tissues due to fasting and nutritional stress: implications for isotopic analysis of diet. The Condor 95(2):388-394.

Hobson, K., Sease, J. 1998. Stable isotope analyses of tooth annuli reveal temporal dietary records: an example using stellar sea lions. Marine Mammal Science 14(1):116-129.

Hobson, K. A., McLellan, B. N., Woods, J. G. 2000. Using stable carbon ($\delta^{13}C$) and nitrogen ($\delta^{15}N$) isotopes to infer trophic relationships among black and grizzly bears in the upper Columbia River basin, British Columbia. Canadian Journal of Zoology 78:1332-1339.

Holt, C., Jenness, R. 1984. Interrelationships of constituents and partition of salts in milk samples from eight species. Comparative Biochemistry and Physiology 77A(2):275-282.

Ito, N., Ito, T., Kromminga, A., Bettermann, A., Takigawa, M., Kees, F., Straub, R. H., Paus, R. 2005. Human hair follicles display a functional equivalent of the hypothalamic-pituitary-adrenal axis and synthesize cortisol. FASEB 19:1332-1334.

Jenkins, S. G., Partridge, S. T., Stephenson, T. R., Farley, S. D., Robbins, C. T. 2001. Nitrogen and carbon isotope fractionation between mothers, neonates, and nursing offspring. Oecologia 129:336-341.

Jenness, R. 1988. Composition of milk. In: Wong, N. P., Jenness, R., Keeney, M., Marth, E. H. (Eds.), Fundamentals of dairy chemistry. Van Nostrand Reinhold Company, New York, USA, pp 1-38.

Jenness, R., Regehr, E. A., Sloan, R. E. 1964. Comparative biochemical studies of milks—II. Dialyzable carbohydrates. Comparative biochemistry and physiology 13(4):339-352.

Jenness, R., Sloan, R. E. 1970. The composition of milks of various species: a review. In: Dairy Science Abstracts 32(10):599-612.

Jenness, R. 1974. Biosynthesis and composition of milk. The Journal of Investigative Dermatology 63:109-118.

Jensen, R. G., Clark, R. W., 1988. Lipid composition and properties. In: Wong, N. P., Jenness, R., Keeney, M., Marth, E. H. (Eds.), Fundamentals of dairy chemistry. Van Nostrand Reinhold Company, New York, USA, pp 171-213.

Kajaysri, J., Nokkaew, W. 2013. Assessment of pregnancy status in Asian elephants (*Elephas maximus*) by measurement of progestogen and glucocorticoid and their metabolite concentrations in serum and feces, using Enzyme Immunoassay (EIA). Journal of Veterinary Medical Science 76(3):363-368.

Kirschbaum, C., Tietze, A., Skoluda, N., Dettenborn, L. 2009. Hair as a retrospective calendar of cortisol production – Increased cortisol incorporation into hair in the third trimester of pregnancy. Psychoneuroendocrinology 34:32-37.

Kornexl, B. E., Werner, T., Roßmann, A., Schmidt, H. 1997. Measurement of stable isotope abundances in milk and milk ingredients – a possible tool for origin assignment and quality control. Zeitschrift für Lebensmittel-Untersuchung und –Forschung A 205:19-24.

Lin, G. P., Rau, Y. H., Chou, C. C., Fu, W. G. 2003. Measurements of δD and δ^{18}O stable isotope ratios in milk. Food Chemistry and Toxicology 68(7):2192-2195.

Lidén, K., Angerbjörn, A. 1999. Dietary change and stable isotopes: A model of growth and dormancy in cave bears. Proceedings of the Royal Society of London B 266:1779-1783.

Lynfield, Y. L. 1960. Effect of pregnancy on the human hair cycle. The Journal of Investigative Dermatology. 35(6).323-327.

Manenschijn, L., Koper, J. W., Lamberts, W. J., van Rossum, E. F. C. 2011. Evaluation of a method to measure long term cortisol levels. Steroids 76:1032-1036.

Marcilla, A. M., Urios, V., Limiñana, R. 2012. Seasonal rhythms of salivary cortisol secretion in captive Asian elephants (*Elephas maximus*). General and Comparative Endocrinology 176:259-264.

Mason, G. J., Veasey, J. S. 2010. How should the psychological well-being of zoo elephants be objectively investigated? Zoo Biology 29:237-255.

McCullagh, K. G., Widdowson, E. M. 1970. The milk of the African elephant. British Journal of Nutrition 24(1):109-117.

Menargues, A., Urios, V., Limiñana, R., Mauri, M. 2012. Circadian rhythm of salivary cortisol in Asian elephants (*Elephas maximus*): A factor to consider during welfare assessment. Journal of Animal Welfare Science 15:383-390.

Metcalfe, J. Z., Longstaffe, F. J., Zazula, G. D. 2010. Nursing, weaning, and tooth development in woolly mammoths from Old Crow, Yukon, Canada: Implications for Pleistocene extinctions. Paleogeography, Paleoclimatology, Paleoecology 298:257-270.

Meyer, J., Novak, M., Hamel, A., Rosenberg, K. 2014. Extraction and Analysis of Cortisol from Human and Monkey Hair. Journal of Visualized Experiments (83), e50882, doi:10.3791/50882.

Nakagawa, A., Kitagawa, A., Asami, M., Nakamura, K. 1985. Evaluation of isotope ratio (IR) mass spectrometry for the study of drug metabolism. Biomedical mass spectrometry 12(9):502-506.

Nelson, D. E., Angerbjörn, A., Lidén, K., Turk, L. 1998. Stable isotopes and the metabolism of the European cave bear. Oecologia 116:177-181.

Nickerson, T. A. 1960. Chemical composition of milk. Journal of Dairy Science 43(5):598-606.

O'Connell, T. C., Hedges, R. E. M. 1999. Investigations into the effect of diet on modern human hair isotopic values. American Journal of Physical Anthropology 108:409-425.

O'Connell, T. C., Hedges, R. E. M., Healey, M. A., Simpson, A. H. R. W. 2001. Isotopic comparison of hair, nail and bone: Modern analyses. Journal of Archaeological Science 28:1247-1255.

Oftedal, O. T., Jenness, R. 1988. Interspecies variation in milk composition among horses, zebras, and asses (*Perissodactyla: Equidae*). Journal of Dairy Research 55:57-66.

Oliveira, C. A., Felippe, E. C. G., Chelini, M. O. M. 2008. Serum cortisol and progestin concentrations in pregnant and non-pregnant Asian elephants (*Elephas maximus*). Research in Veterinary Science 84:361-363.

Osorio, M. T., Moloney, A. P., Schmidt, O., Monahan, F. J. 2011. Beef authentication and retrospective dietary verification using stable isotope ratio analysis of bovine muscle and tail hair. Journal of Agricultural and Food Chemistry 59:3295-3305.

Podlesak, D. W., Torregrossa, A., Ehleringer, J. R., Dearing, M. D., Passey, B. H., Cerling, T. E. 2008. Turnover of oxygen and hydrogen isotopes in the body water, CO_2, hair, and enamel of a small mammal. Geochimica et Cosmochimica Acta 72:19-35.

Polischuk, S. C., Hobson, K. A., Ramsay, M. A. 2001. Use of stable-carbon and –nitrogen isotopes to assess weaning and fasting in female polar bears and their cubs. Canadian Journal of Zoology 79:599-511.

Randall, V. A., Ebling, F. J. G. 1991. Seasonal changes in human hair growth. British Journal of Dermatology 124:146-151.

Renou, J., Deponge, C., Gachon, P. Bonnefoy, J., Coulon, J., Garel, J., Vérité, R., Ritz, P. 2004. Characterization of animal products according to geographic origin and feeding diet using nuclear magnetic resonance and isotope ratio mass spectrometry: cow milk. Food Chemistry 85:63-66.

Richards, M. P., Mays, S., Fuller, B. T. 2002. Stable carbon and nitrogen isotope values of bone and teeth reflect weaning age at the medieval Wharram Percy site, Yorkshire, UK. American Journal of Physical Anthropology 119:205-210.

Rook, J. A. F. 1961. Variations in the chemical composition of the milk of the cow. Dairy Science Abstracts 23:251-258, 303-308.

Rountrey, A. N., Fisher, D. C., Vartanyan, S., Fox, D. L. 2007. Carbon and nitrogen isotope analyses of a juvenile woolly mammoth tusk: Evidence of weaning. Quaternary International 169-170:166-173.

Sandman, C. A., Glynn, S., Schetter, C. D., Wadhwa, P., Garite, T., Chicz-DeMet, A., Hobel, C. 2006. Elevated maternal cortisol early in pregnancy predicts third trimester levels of placental corticotropin releasing hormone (CRH): Priming the placental clock. Peptides 27:1457-1463.

Sharpley, C. F., Kauter, K. G., McFarlane, J. R. 2009. An initial exploration of in vivo hair cortisol responses to a brief pain stressor: Latency, localization and independence effects. Physiological Research 58:757-761.

Sharpley, C. F., Kauter, K. G., McFarlane, J. R. 2010. Hair cortisol concentration differs across site and person: Localization and consistency of responses to a brief pain stressor. Physiological Research 59:979-983.

Schoeninger, M. J., DeNiro, M. J. 1984. Nitrogen and carbon isotopic composition of bone collagen from marine and terrestrial animals. Geochimica et Cosmochimica Acta 48:625-639.

Skoluda, N., Dettenborn, L., Stalder, T., Kirschbaum, C. 2012. Elevated hair cortisol concentrations in endurance athletes. Psychoneuroendocrinology 37:611-617.

Slominski, A., Wortsman, J., Tuckey, R. C., Paus, R. 2007. Differential expression of HPA axis homolog in the skin. Molecular and Cellular Endocrinology 265-266:143-149.

Sponheimer, M., Robinson, T., Ayliffe, L., Passey, B., Roeder, B., Shipley, L., Lopez, E., Cerling, T., Dearing, D., Ehleringer, J. 2003A. An experimental study of carbon-isotope fractionation between diet, hair, and feces of mammalian herbivores. Canadian Journal of Zoology 81:871-876.

Sponheimer, M., Robinson, T., Ayliffe, L., Roeder, B., Hammer, J., Passey, B., West, A., Cerling, T., Dearing, D., Ehleringer, J. 2003B. Nitrogen isotopes in mammalian

herbivores: hair δ^{15}N values from a controlled feeding study. International Journal of Osteoarchaeology 13(1-2):80-87.

Stalder, T., Steudte, S., Miller, R., Skoluda, N., Detternborn, L., Kirschbaum, C. 2012. Intraindividual stability of hair cortisol concentrations. Psychoneuroendocrinology 37:602-610.

Stalder, T., Kirschbaum, C. 2012. Analysis of cortisol in hair – State of the art and future directions. Brain, Behavior, and Immunity 26:1019-1029.

Thompson, A. H., Chesson, L. A., Podlesak, D. W., Bowen, G. J., Cerling, T. E., Ehleringer, J. R. 2010. Stable isotope analysis of modern human hair collected from Asia (China, India, Mongolia, and Pakistan). American Journal of Physical Anthropology 141:440-451.

Uno, K. T. 2012. Advances in terrestrial paleoecology from intratooth stable isotope profiles in tooth enamel and tusk dentin. Unpublished dissertation, University of Utah, x+307 pp.

Valenzuela, L. O., Chesson, L. A., O'Grady, S. P., Cerling, T. E., Ehleringer, J. R. 2011. Spatial distributions of carbon, nitrogen and sulfur isotope ratios in human hair across the central United States. Rapid Communications in Mass Spectrometry 25(7):861-868.

Van Uum, S. H. M., Sauvé, B., Fraser, L. A., Morley-Forster, P., Paul, T. L., Koren, G. 2008. Elevated content of cortisol in hair of patients with severe chronic pain: A novel biomarker for stress. Stress 11(6):483-488.

Webb, E., Thomson, S., Nelson, A., White, C., Koren, G., Rieder, M., Van Uum, S. 2010. Assessing individual systemic stress through cortisol analysis of archaeological hair. Journal of Archaeological Science 37:807-812.

Webb, E. C., White, C. D., Van Uum, S., Longstaffe, F. J. 2015. Integrating cortisol and isotopic analyses of archaeological hair: Elucidating juvenile ante-mortem stress and behavior. International Journal of Paleopathology 9:28-37.

Weitzman, E. D., Fukushima, D., Nogeire, C., Roffwarg, H., Gallagher, T. F., Hellman, L. 1971. Twenty-four hour pattern of the episodic secretion of cortisol in normal subjects. The Journal of Clinical Endocrinology & Metabolism 33(1):14-22.

Whitney, R. M. 1988. Proteins of milk. In: Wong, N. P., Jenness, R., Keeney, M., Marth, E. H. (Eds.), Fundamentals of dairy chemistry. Van Nostrand Reinhold Company, New York, USA, pp 81-169.

Wittemyer, G., Cerling, T. E., Douglas-Hamilton, I. 2009. Establishing chronologies from isotopic profiles in serially collected animal tissues: An example using tail hairs from African elephants. Chemical Geology 267:3-11.

Young, E. A., Abelson, J., Lightman, S. L. 2004. Cortisol pulsatility and its role in stress regulation and health. Frontiers in Neuroendocrinology 25:69-76.

Chapter 5

Growth patterns and weaning age estimates support hunting-induced extirpation of Siberian woolly mammoths

Introduction

Secular changes in weaning age and juvenile growth patterns hold promise for resolving the cause of the end Pleistocene megafaunal extinctions. Current investigations and debate focus mainly on two possible mechanisms for causing these extinctions, (1) climate change (e.g., Breslawski and Byers, 2014; Cooper et al., 2015; Dreimanis, 1968; Faith, 2011, 2013; Graham and Lundelius, 1984; Grayson and Meltzer, 2003; Leshchinskiy, 2009; Lister and Sher, 1995; Palkopaoulou et al., 2013; Schweger et al., 2011; Wroe et al., 2013) and (2) hunting (e.g., Allentoft et al., 2014; Alroy, 2001; Brook and Bowman, 2004; Fisher, 2001; Grund et al., 2012; Johnson, 2013; Johnson et al., 2013; Koch and Barnosky, 2006; Martin, 1973; Martínez et al., 2013; Mosimann and Martin, 1975; Ripple and van Valkenburgh, 2010; Sandom et al., 2014; Steadman et al., 2005). Considering that generations of scientists have failed to establish a consensus on this issue (Grayson, 1984a), it is tempting to think it might be a question will never really

have a clear answer. The impasse results, at least in part, from approaches that generally lack the capacity to falsify either hypothesis (Grayson, 1984b). Much effort has been devoted to establishing chronologies for extirpations, population bottlenecks, and proposed mechanisms in order to evaluate cause-effect relationships (e.g., Cooper et al., 2015; Allentoft et al., 2014; Burney and Flannery, 2005; Johnson et al., 2013; Jones et al., 2007; Lima-Ribeiro and Diniz-Filho, 2013, Lister and Sher, 1995; Lopes dos Santos et al., 2013; Prescott et al., 2012; Wroe and Field, 2006), but temporal and spatial overlap between all three factors (climate changes, human activity, and extinctions) complicate these efforts. Population demographics (e.g., Hill et al., 2008; Lyman, 1987) and life-history patterns (e.g., Fisher, 1996, 2001, 2009), parameters that would be differently affected by climate stress and over-hunting, provide alternative approaches to determining the pressures that triggered extinction. Here I present results of weaning-age analyses as a way to directly test each of these extinction models. All other things (such as average body size) being constant, a shift to earlier weaning would provide exclusive support for excessive hunting, while an extension of nursing would only be consistent with predictions of climate-driven extinction.

Life-history analyses

Proboscidean tusks grow throughout life and contain records of dentin apposition that extend from the earliest increment of growth preserved at the distal

end, to the dentin formed immediately prior to death at the proximal end. Tusks of African elephants are already growing in the first year of life (Raubenheimer, 2000; Raubenheimer et al., 1995; Sikes, 1971) and may begin forming *in utero* in male woolly mammoths (Rountrey et al., 2012), but because abrasion and breakage at the tip progressively remove the earliest portion of each growth record, the only tusks that contain a record of the beginning of life are from individuals that died very young. Tusk tips that broke off before the early portion of the record was eliminated can also provide information about the first years of life.

Incremental growth features in tusk dentin can be used to analyze growth rate variations and guide serial analyses of tusk composition through life (e.g., Fisher, 1996; Koch et al., 1989). In addition, predictable patterns in individual growth records can indicate occurrence and timing of life events, such as weaning (Rountrey et al., 2007), maturation (Fisher, 1996), calving (Fisher, 1996), and musth (El Adli et al., 2015; Fisher, 2008). Compiled for many specimens, these data can reveal patterns and trends through time and space.

Malnutrition and hunting differently influence growth and timing of life-history events (Fisher 1996, 2009), with poor nutrition having a general effect of slowing down the process (Bengtson and Laws, 1985; Lee and Moss, 1986; Little et al., 1983; Geist,

1989) and hunting having the reverse effect (Carrick et al., 1962; Geist, 1989; Jennings et al., 1999; Proaktor et al., 2007; Wheeler et al., 2009). Although at least some individual life-history and growth changes could be explained by both mechanisms, the two hypotheses predict mutually exclusive combinations of life-history and growth parameters (Fisher, 1996, 2001, 2009). For example, diminution could be caused by both hunting (Jennings et al., 1999; Proaktor et al., 2007) and nutritional stress (Guthrie, 2003; Hill et al., 2008; Sheridan and Bickford, 2011; Walker et al., 2006), but each process would be distinguished by associated changes. Nutrition-driven diminution would likely be associated with slowed growth, whereas diminution caused by high mortality due to something other than starvation (e.g., hunting) would likely be accompanied by stable or increased growth rates (Fisher, 1996, 2001, 2009; Migliano, 2007; Walker et al., 2006).

Energy constraints due to poor nutrition limit capacity for growth and reproduction. Accordingly, growth, maturation, and reproduction rates (Geist, 1989; Shanley and Kirkwood, 2000), as well as adult body sizes (Bateson et al., 2004; Geist, 1989), are expected to decrease as a plastic compensatory response in phenotypes of malnourished individuals. There can also be an adaptive genetic effect over longer time spans, due to relative success of genotypes associated with low caloric demand (Guthrie, 2003; Hill et al., 2008; Sheridan and Bickford, 2011).

Even with a limited energy budget, selective pressures could encourage fast growth, rapid reproduction, or large body size, but not all at the same time. Faced with relatively poor nutrition, Turkana pastoralists that were studied in the early 1980s had adult stature in the average range of U. S. adults of the time, but with slower growth and later maturation (Little et al., 1983). There are clear benefits to large body size in terms of antipredation, energetic efficiency (Johnson, 2013; Langman et al., 1995; Taylor et al., 1970; Tucker, 1970), and ability to endure fluctuations in food availability (Lindstedt and Boyce, 1985), among other things. There are also potential costs associated with delayed maturation. Reduced stature in some "pygmy" populations appears to have been an adaptive response to selective pressure for rapid maturation at the expense of adult body size, to accommodate high juvenile and adult female mortality that was not directly related to malnutrition (Migliano, 2007; Walker et al., 2006). If there had been significant selective pressure for large body size in this population, as there apparently was for the Turkana pastoralists, accelerated maturation could have been accomplished without the diminution, but it would have required sufficient nutrition to support faster growth rates in juveniles. There is some limited evidence for diminution in mammoths from continental Siberia at the very end of the Pleistocene (Tikhonov and Vartanyan, 2001), but there is also conflicting data suggesting size stasis in Eurasian mammoths (Ouden et al., 2012). In any case, there likely was not the dramatic diminution that would

have been necessary to accommodate stable or accelerated maturation in a situation where nutritional limitations were causing populations to decline. Therefore, if populations failed as a result of vegetational changes in response to climate change, then we expect to see, at the end of the Pleistocene, slower growth and later maturation in woolly mammoths, which would have enabled them to maintain body size with reduced energetic resources.

In contrast to the effects of nutritional stress, overhunting has been observed to accelerate maturation. In exploited fish populations, size and age at maturation decrease under pressure from selective harvest of large individuals (e.g., Jennings et al., 1999; Wheeler et al., 2009). Similar effects have also been documented for large mammals due to targeting of large males (Carrick et al., 1962; Coltman et al., 2003). Population modeling predicts that hunting will decrease average age of maturation and adult body size in red deer, even if harvest is nonselective (Proaktor et al., 2007). Accelerated maturation and body-size reduction in these situations may in part be genetic adaptations to environments of high mortality, where genotypes associated with earlier and more frequent reproduction would be advantageous (Wheeler et al., 2009), but earlier maturation would also be expected as a plastic response to reduced intraspecies resource competition (Bengtson and Laws, 1985).

The particular suite of responses in a stressed population is a function of its complete selective regime, in which the primary stressor is only one of the contributing factors. As mentioned above, high mortality rates promote early maturation in human "pygmy" populations (Migliano, 2007; Walker et al., 2006), but also lead to diminution. In fact, earlier maturation (which means a shorter time devoted exclusively to growth) and shorter birth spacing (which requires calves to reach minimum weaning size more quickly) are less energetically costly if they are accompanied by diminution. If there is strong selection for large body size, accelerated maturation has to be accompanied by increased growth rates, at least early in life. Since faster growth implies increased nutrition, the occurrence of accelerated life histories simultaneous with stasis (or increase) in body size in woolly mammoths would strongly favor hypotheses that attribute the extinction to hunting pressure over those that attribute it to nutritional deficiency brought on by a changing climate.

Weaning age results from a complex interaction between mother and offspring (e.g., Gomendio, 1991; Lee et al., 1991; Lee and Moss, 1986; McDade, 2000; Trivers, 1974), with each member in the pair having overlapping but not entirely equivalent interests, especially as the calf grows. Intensive nursing prolongs postpartum amenorrhea (Howie and McNeilly, 1982; Lee, 1987; McNeilly, 1994, 1997; Usmani et al., 1990), which reduces a female's lifetime reproductive output. On the other hand, a calf

has long-term benefits from extended nursing (Lee et al., 2013), and insufficient maternal supplementation as a consequence of early weaning may result in a calf's immediate death or reduced lifespan (Lee et al., 2013; Lee and Moss, 1986).

In elephants, the ultimate determinant of weaning age can be calf size, but the mediating factor is more typically the birth of a sibling (Lee and Moss, 1986). Both of these may be indirectly affected by maternal diet. The first of these relationships is straight-forward; nutritional conditions affect quality and quantity of milk produced by a lactating female (Delgado et al., 1982; Delvoye et al., 1980; Hennart and Vis, 1980; Lee an Moss, 1986), which, to the extent that offspring benefit from milk, boosts the calf's growth rate, reducing the age at which it reaches ideal weaning size (Lee et al., 1991). The relationship between maternal diet and birth spacing is probably at least partially mediated through feedback from a calf's nursing behavior, which is related to its nutritional status and growth rate. Poor milk quality necessitates more intense and frequent suckling (Delgado et al., 1982; Konner and Worthman, 1980; Loudon et al., 1983) that triggers high levels of maternal prolactin (Konner and Worthman, 1980; Kurz et al., 1993; Usmani et al., 1990), a hormone that promotes milk production and suppresses estrous. As a result, birth spacing is greater in malnourished populations (Ciccioli et al., 2003; Konner and Worthman, 1980; Lee and Moss, 1986; Rutter and Randel, 1984).

At least one study seems to contradict the conclusion that poor nutrition leads to later weaning. Smith (1991) showed that restricting maternal food supply led to earlier weaning in hooded rats. However, this study has limited relevance for understanding natural systems, because in that study, only the mother's food was limited. Pups were apparently free to feed on demand from solid food, which may have eliminated any feedback effect from intensification of suckling, since they could consume solid food to make up for low quality milk being produced by their undernourished mother. In fact, in that case, poor milk quality may have led to them abandoning nursing earlier than normal in favor of solid food. This would not be an option for a baby mammoth in deteriorating environmental conditions.

In addition to prolonged lactation amenorrhea, there is a possibility that poor maternal nutrition directly impacts female fertility (Ciccioli et al., 2003; Delgado et al., 1978; Kurz et al., 1993; Van der Spuy, 1985), but some efforts to understand this dynamic have failed to find any correlation (e.g., Chowdhury, 1978; Lee, 1987). In any case, later weaning in wild African elephant (*Loxodonta africana*) populations during drought periods (at an average of 5.6 years) compared to wet intervals (at 3.5 years) (Lee and Moss, 1986) provides an empirical observation of the effect of nutritional stress on weaning age in proboscideans. A shift of this magnitude should be detectable in records from mammoth tusks.

One way that mammalian nursing can be characterized is with respect to isotopic fractionations that occur during lactation by mothers and consumption of milk by their offspring. In terms of stable isotope chemistry, nursing is essentially equivalent to matriphagy. This makes a neonate one trophic level above its mother (Fogel et al., 1989; Fuller et al., 2006). As a calf increasingly incorporates solid food into its diet, this trophic relationship gradually disappears. This trophic effect could impact carbon ($\delta^{13}C$), nitrogen ($\delta^{15}N$), oxygen ($\delta^{18}O$), and deuterium (δD) of both individuals, but only $\delta^{15}N$ showed a clear signal of nursing in our study of African elephants (see *Chapter 3*). Since isotopic signatures of nursing exist primarily as a relationship between maternal and calf values, only the most consistent and dramatic patterns are likely to be detected in the calf's record alone. Serial analyses of tusks reported by Rountrey et al. (2007) and Rountrey (2009), as well as additional tusks described below, almost universally display a pattern of declining $\delta^{15}N$ over the first few years of life. This pattern appears to reflect an approximately 3.0 ‰ trophic enrichment (DeNiro and Epstein, 1981; Fogel et al., 1989; Minagawa and Wada, 1984; Schoeninger and DeNiro, 1984) during an initial period of exclusive nursing, with subsequent decreases in the trophic effect associated with gradual reduction of nursing and transition to an adult diet.

Tusks analyzed previously were from individuals that all died very young (Rountrey, 2009). The only one that contained a record possibly extending beyond final

weaning displayed a consistent decrease in average annual $\delta^{15}N$ values through the first four years of the record followed by a partial fifth year that had values similar to, if slightly higher than, the same interval in the previous year (Rountrey et al., 2007; Rountrey, 2009). Ignoring other factors and assuming a diet of solid foods that is fairly consistent interannually, we would expect final weaning to be marked by interruption of the decreasing trend, and the beginning of generally stable annual $\delta^{15}N$ values. However, isotope records that span final weaning in other taxa do not show a 'leveling off' as expected under this simple model. In a study of breastfeeding in humans, fully weaned babies remained slightly enriched in $\delta^{15}N$ compared to their mothers and display a fairly consistent increase immediately following weaning (Fuller et al., 2006). Evidence of nursing and weaning in $\delta^{15}N$ records of archaeological settings also show an initial decline in the first few years, followed by an increase around the time of expected weaning (Dupras et al., 2001; Richards et al., 2002). In these human examples, the continued difference between baby and mother could be caused by differences in the diets of mothers and their recently weaned babies. However, a similar post-weaning spike in $\delta^{15}N$ for sea lions probably reflects catabolization of stored resources, to supplement pups as they learn to hunt for themselves (Hobson and Sease, 1998).

In summary, we expect climate-related nutritional stress, especially in the absence of reduced body size, to be associated with a drawn out immature phase during which

limited energy is budgeted for growth, and maturation is delayed. In concert with this we expect to see a shift to later weaning in tusk records spanning the late Pleistocene, if climate was responsible for extirpation of woolly mammoths from mainland Siberia. Modern African elephants stressed by multi-year droughts wean about two years later than when they are not facing such hardship (Lee and Moss, 1986). Based on this, a shift to later weaning would be consistent with climate-driven extinction, but not with population stress from exploitation, which would favor faster maturation and more frequent reproduction. Conversely, a decrease in weaning age without an even more substantive decrease in body size would be inconsistent with energy constraints inflicted by depleted resources, but would be an expected result of hunting pressure.

It is not necessarily the case that all of the Pleistocene megafaunal extinctions had the same cause or that any mechanism was solely responsible, but the similar timing of extinctions on several land masses and selection against megafauna across the globe (e.g., Koch and Barnosky, 2006; Lyons et al., 2004; Roberts et al., 2001; Webb, 1984) suggest that there may be an elegant and unifying explanation. Results from this study have immediate implications only for continental populations in north-central and northeastern Siberia, but may impact interpretations pertaining to regional late Pleistocene megafaunal extinctions around the globe.

Materials

Tusk growth records analyzed here were based on University of Michigan Museum of Paleontology (UMMP) specimens from northern Siberia. These 29 tusks were collected over several years by my adviser, Daniel Fisher, with help from colleagues in Russia, France, and the Netherlands. Fifteen of the tusks retain their distal tip that preserves the first years of growth. Maximum diameters for all tusks are less than 55 mm, which is considerably smaller than adult woolly mammoth tusks for both sexes. Twelve tusks include the pulp cavity surface at their proximal end. These are from individuals that died young and they contain information about circumstances, seasons, and ages of death. Each of the other 17 is a cut or broken tip separated from the rest of the tusk. Because an unknown amount of growth occurred subsequent to years represented in these records, these tusk tips do not tell us anything about death but can contain information about the early years of growth for an individual that lived much longer. Specimens range from 21 cm to 77 cm along the outside curve and contain between 4 and 12 years of growth (Table 5.1).

Tusks used for this study do not yet have, but will be assigned accession numbers in the University of Michigan Museum of Paleontology (UMMP). Field numbers all have

different formats, but they identify the general region where they were collected. Tusks with the label “ZCHM” are from Chukotka, while “AM” and “MMY” reference localities in Yakutia. Numbers with no alphabetic identifiers identify tusks collected in various field seasons in the Taimyr region.

As permafrost specimens, most of the tusks have exceptional preservation, retaining the color and consistency of fresh ivory. Five tusks (AM-7, ZCHM-46, ZCHM-52, ZCHM-53, and MMY) have moderate to significant staining, evidence of taphonomic histories that could have compromised isotopic integrity. Most tusks have some splitting, cracking, or fracturing due to desiccation, and some required consolidation with epoxy prior to cutting and sampling. All tusks were thoroughly documented photographically from at least six angles. Specimens with good surficial and structural integrity were molded, and cast in fiberglass with polyester resin. In addition to physical casts, photo-realistic 3D surface models are being produced, using a combination of photogrammetry, CT scans, 3D ‘point clouds’ (produced more than a decade ago using a 3D point digitizer), and specimen photos. Specimens and casts are conserved in the UMMP collections. Digital models will be maintained in the University of Michigan Online Repository for Fossils (UMORF; http://umorf.ummp.lsa.umich.edu/).

Tusks included in this study have a broad but disjointed geographic distribution representing different regions of northern Siberia. Ten from the Taimyr region are the most western specimens included, while 8 from northern Yakutia and 11 from Chukotka extend the represented range eastward to the northeastern corner of Siberia. Fifteen of the tusks were sampled for isotope analyses in attempts to estimate weaning age (Figure 5.1).

Methods

MicroCT scans of each tusk were used to analyze annual growth features that reflect seasonal variation in radiodensity of dentin formed (see *Chapter 2* – Fisher et al., 2014a). Serial measurements of annual growth increments visible in CT scans provided records of increasing diameter and estimated increment volume (EIV; *Chapter 2* – Fisher et al., 2014a). Models were constructed from growth trajectories of tusks with the first year of growth present. These provided data for estimating years of growth represented in tusks missing the first year(s), which therefore contained no independent indication of the years of growth represented. AMS radiocarbon dates were processed for all tusks reported here.

MicroCT analyses

Variable attenuation of X-rays projected through a tusk provides raw data for computed tomography (CT) that produces a 3D representation of density variation throughout the volume of a tusk. Cyclic seasonal patterns in dentin radiodensity reveal annual increments of growth in CT scans (*Chapter 2* – Fisher et al., 2014a). Thus, data provided by microCT scans enable 3D measurements of annual growth increments. Increment diameters presented below represent the average of the major and minor diameter of the tusk in a transverse cross-section near the proximal end of a growth cone (Figure 5.2). Estimated Increment Volume (EIV; *Chapter 2* – Fisher et al., 2014a) utilizes linear measurements in three orthogonal directions to capture a rough estimate of actual volume of a growth increment. EIV can provide a close approximation of actual volume (*Chapter 2* – Fisher et al., 2014a), but might not do so for irregularly-shaped growth cones. Nevertheless, in each case it provides a measurement that condenses increment length, radial size, and transverse cross-sectional shape of a growth cone into a single quantity.

CT data were produced by the University of Michigan School of Dentistry MicroCT Core facility (UMDCT) using a SCANCO Medical µCT100 operating at 90 kV, 78 µA, and 500ms, yielding uniform cubic voxels 60 µm on each side. To accommodate the small maximum scan volume (a 12 cm long cylinder with 5 cm radius), tusks had to be sectioned into approximately 11 cm lengths. To avoid cylindrical ring-artifacts in the CT

scans that could obscure conical growth features, tusk sections were scanned with their axes off-center in the chamber when possible. Tusk scan data were processed using Amira 5.4.2. Virtual planar projections that represent either average, minimum, or maximum luminosity (selecting the projection that most clearly displayed annual features) over a 'slice thickness' (*z*-dimension) of 0.5 – 1.5 mm were used to inspect and measure annual increments. EIVs and tusk diameters measured for each year of growth were used to compare growth trends from each tusk. All measurements focused on the dentin core of the tusk, ignoring the contribution to size made by the cementum outer layer.

Estimating sex and ontogenetic timing of tusk records

Using tusk growth records to interpret ontogenetic timing of life-history milestones requires accurate estimation of the years of life represented in each record. Since ontogenetic timing of tusk development and rate of growth are to some extent sexually determined, year-of-life estimates are dependent on sex identifications for tusks. Although adult tusks display dramatic sexual dimorphism, juvenile tusks cannot be sexed based on external dimensions alone; a juvenile male tusk can be well within the size range of a typical female tusk.

Ancient DNA (aDNA) from tusk dentin can provide an independent determination of sex that would enhance year-of-life estimates. Efforts to use aDNA to determine sex of the tusks included in this study are ongoing, but results were not yet available at the time of writing, and will have to be incorporated in subsequent treatments of these data. Here, I interpret sex from multi-year growth rates, which show evidence of a sex-based difference even at this early stage of life. Serial EIV records and serial diameter records clump into two divergent trajectories (Figure 5.3). Based on clear sexual dimorphism in adult tusks of modern elephants and evidence that another proboscidean, the American mastodon (*Mammut americanum*) displayed adult sexual dimorphism as well as different growth trajectories for males and females (Fisher, 2008, 2009; Smith and Fisher, 2011), I interpret tusks with faster growth rates as *males* and those with slower growth rates as *females*.

Evidence from three woolly mammoth mummies suggests that tusks may have begun to mineralize earlier in males than females. One individual that died when it was around 7 months old, had a permanent tusk already forming and a neonatal line indicating that initial mineralization had begun prior to birth (Rountrey et al., 2012). Genetic analysis identified this specimen as a male (unpublished data, personal communication with D. C. Fisher). A second individual (this time a confirmed female, approximately 1 month old at the time of death) had not yet begun mineralizing its

permanent tusks (Rountrey et al., 2012). A third individual (also a female, but close to 2 months old when it died) also had not yet begun to mineralize its permanent tusks (Fisher et al., 2014b). Therefore, based on available evidence, it looks like tusks of males may have begun forming prior to birth, whereas tusks of females started forming sometime after the first couple months following birth. In this study, I treat the first complete year of growth as the first year after birth in *male* tusks and as the second year in *female* tusks.

To estimate specific years of growth represented in tusks that are missing their tips, I compared their growth sequences to those from tusks that preserved the first years of growth, and had well-constrained timing. Intervals for tusks with unknown starting points were determined to be the years that most closely matched predictions for each annual increment provided by Generalized Additive Mixed Models (GAMMs) constructed from tusk records with known timing. GAMMs were produced separately for *male* tusks and for *female* tusks, to accommodate apparent differences in growth trajectories. Model predictions were calculated using the gamm4 package for R (Wood, 2006) version 0.2-3. In models used for year-of-growth estimation, tusk ID was defined as a random effect, while increment *diameter* and *diameter increase* (from the previous increment in series) were each used as fixed effects.

Unknown records were submitted to both GAMMs for year-of-growth estimations. Estimates of each model were evaluated in terms of how well they represented a contiguous sequence of real years. Preferred fit of model predictions was the sequence of estimates that resulted in the lowest average difference between year-of-growth predictions (decimal approximations) and a corresponding sequence of *real* years (whole numbers). Using this method, the predicted sequence (2.3, 3.5, 4.7, 5.9) is most consistent with years 3, 4, 5, and 6, which results in an average difference between predicted and real years of 0.4. The alternative sequence of *real* years rejected in this case (2, 3, 4, 5) would produce a higher average difference between each prediction and its corresponding year in the sequence (0.6). Diameter growth trajectories, best approximated with log trend lines, were used to assess GAMM predictions. Average standard error of predictions produced with GAMM results was also considered but did not differ significantly between estimates of competing models.

Isotope sampling

Isotope sampling was performed on interior surfaces exposed by cutting tusk sections longitudinally through the axis. For each tusk segment, serial samples were planned according to locations of annual features that were visible in a virtual CT slice oriented to match the plane of the cut surface. Sample outlines were drawn in Adobe Photoshop and Adobe Illustrator onto a flatbed scan of the tusk's exposed internal

surface. These were guided by growth features visible in the superimposed corresponding CT image. These milling boundaries were then transferred onto tusk surfaces using a needle to trace lines printed on acetate transparencies and viewed at 25X under a Wild M5 stereomicroscope, through to the tusk surface as described in Rountrey (2009). Non-overlapping serial samples from each tusk were milled by hand using a free-standing stage beneath a fixed-position dental drill with a 1.0 mm carbide bit on a medium-low speed setting to avoid overheating the dentin. Each sample represented a complete year of growth from one annual boundary to the next (Figure 5.4). Homogenized powder samples each provided a bulk analysis for an annual increment of growth.

Isotope analyses

To isolate collagen from each powder dentin sample, we weighed 20 mg of powder into a 1.5 ml polypropylene microcentrifuge tube and added 1.5 ml of 0.5 M HCl that had been chilled in a refrigerator for 30 minutes prior to use. After vortexing the sample for 5 seconds, we allowed samples to react at room temperature for 10 minutes. After this brief treatment, the sample was centrifuged at 8 krpm (approximately 5000 *g*) for 5 minutes. Following centrifugation, supernatant was immediately removed with a faucet aspirator, and the demineralized sample was rinsed by adding 1.0 ml ultrapure water. The tube was then vortexed until the sample was suspended in the water, and

then centrifuged at 8 krpm for 5 minutes. The rinsing process was repeated 5 times. After the final rinse and removal of supernatant, the sample was placed in a freezer for 1 hour and then lyophilized. Because the polypropylene microcentrifuge tubes used are slightly soluble in typical defatting agents, we opted not to perform the defatting step that is often included in pretreatment for bone collagen analysis. Internal tests showed that this adjustment to the process did not significantly affect $\delta^{15}N$ values (Table 5.2; Figure 5.5). Samples were taken from clean unpolished internal surfaces of dentin cut using a band saw with no lubricants. Dry pretreated samples were typically 20 – 25 % of the original powder mass, but some less well-preserved samples yielded only 10 – 15 % in pretreated mass. Lyophilized collagen formed foam pellets that were easily subsampled with a scalpel for analysis.

Sample analysis was split between the University of Michigan Stable Isotope Lab (UMSIL) and the Stable Isotope Laboratory at University of California, Santa Cruz (UCSCSIL). For UMSIL analyses, 500 ± 10 µg subsamples of collagen foam blocks were wrapped in tin capsules for measurement of $\delta^{15}N$ on a Costech Elemental Analyzer attached to a Finnigan Delta V+ mass spectrometer. Separate 650 µg subsamples for one tusk were analyzed for $\delta^{13}C$. Specifications for the UMSIL instrument are listed in *Chapter 2* and *Chapter 4*. Samples weighing 380 ± 10 µg were sent to UCSCSIL for combined measurement of $\delta^{15}N$ and $\delta^{13}C$. In the UCSC lab carbon and nitrogen isotopic

and elemental compositions were determined by Dumas combustion using a Carlo Erba 1108 elemental analyzer coupled to a ThermoFinnigan Delta Plus XP isotope ratio mass spectrometer. Analytical precision of internationally calibrated in-house standards is better than 0.2 ‰ for both $\delta^{13}C$ and $\delta^{15}N$. Sample isotopic values are corrected for size, drift and source stretching effects. Carbon and nitrogen elemental composition is estimated based on standards with known elemental compositions. Precision of these known compounds is determined to better than 1 %.

Ratios of carbon to nitrogen in collagen samples are often used to assess effects of diagenesis. Where reported in this study, C:N refers to atomic ratio (C:N = [X μg_{carbon}/12.0107]/[Y $\mu g_{nitrogen}$/14.0067]]). Stable isotope values are expressed in standard delta notation relative to air-N_2 for nitrogen and VPDB for carbon.

AMS radiocarbon dating of tusk dentin

All specimens were sampled for radiocarbon (^{14}C) dating. Specimens with too little ^{14}C remaining for reliable analysis were assigned "infinite" geologic ages. When available, radiocarbon dates and growth interval estimates helped with the selection of tusks that were sampled for stable isotope analyses ($\delta^{15}N$, and sometimes $\delta^{13}C$) of tusk collagen. Tusks without specific ^{14}C dates and those that did not include significant portions of the first decade of growth were considered unsuitable for the analysis of

secular changes in weaning age, and were mostly excluded from sampling efforts. Unsampled tusks do contribute to tusk growth models and other auxiliary analyses where appropriate.

AMS radiocarbon dates were processed by Beta Analytic on ~1.5 g blocks of dentin removed from solid areas of tusk free of cracks and staining (except in a few cases where dentin was stained throughout the tusk). Blocks were handled with gloves and were cut in so that all exterior faces were newly exposed surfaces. Immediately prior to packing aluminum-wrapped blocks for shipment to Beta Analytic, we sanded each exposed surface with clean 120 grit sandpaper as an extra safeguard against contamination. Dates based on collagen extractions are reported in uncalibrated radiocarbon years before present (^{14}C years BP).

Weaning-age estimation

Estimation of weaning age from nitrogen isotope analyses of tusk growth records is discussed below, and is supported by ongoing work looking at isotopic patterns in a mother-calf pair of African elephants as a modern analog (*Chapter 4*). Evidence suggests that weaning is typically marked by an increase in δ^{15}N, following a multiyear decline associated with the gradual reduction of milk in a calf's diet. In this study, we treat an increase in annual bulk δ^{15}N (greater than measurement error – ± 0.12 ‰ (UMSIL) and

± 0.2 ‰ (UCSCSIL)) following a sustained decline from the first year of life as a clear signal that the individual has been weaned. The year of life displaying this increase is identified as the individual's weaning age. Most records do not contain a complete record from age 1 to weaning, however. For incomplete records, I consider the first significant δ^{15}N increase in a record beginning in the 2nd, 3rd, or 4th year of life as compelling evidence of weaning. For records that begin with the 5th or 6th year or life, a significant increase at or before age 10 that is preceded by at least 2 years of stable or gradually decreasing δ^{15}N is treated here as only moderate evidence for weaning. Some poorly constrained estimates are included in results but identified as having limited reliability.

Growth rates comparisons

Inter-tusk comparisons of growth rates were based on estimated volume of dentin formed during a set span of years. Females and males were considered separately. In male tusks, the interval shared by the most tusk records was years 3 – 6. In females, it was years 5 – 8. Summed EIVs throughout the compared interval provided an estimate of total volumetric growth over a 4-year period that could be compared with estimates from other same-sex individuals.

Results

Annual microCT features

Annual growth increments were easily discernible in microCT scans of most Siberian woolly mammoth tusks analyzed for this study. However, instead of showing gradual density transitions across seasons, as have been described for mastodon mandibular tusks from Colorado (*Chapter 2* – Fisher et al., 2014a), increments were in most cases characterized by general homogeneity throughout most of a year with a narrow, higher-density band of dentin demarcating each year boundary (Figure 5.4). Some years did not display the brief interval of higher density growth we used to mark year boundaries. In these cases, some other density perturbation (such as an abrupt change to lower density growth) occurring in the approximate expected location of an annual feature (based on the normal size of annual growth increments clearly expressed elsewhere in the same tusk) was instead used to mark the year boundary.

MicroCT neonatal features

Five tusks with initial growth represented in their well-preserved distal tips have perturbations visible in microCT that may be neonatal features in dentin. These features consist of a small number of closely spaced low-density features that are spread over a short interval (on the order of days or weeks rather than months) of growth (Figure 5.6). Although we did not detect these features in CT scans of all *male* tusks with preserved

tips, they are most prominent in tusks identified as male based on growth trajectories. One of the tusks with a possible neonatal CT feature in its distal tip has a *female* growth trajectory. Thin-section analyses should be able to verify or refute the identification of these features as representing time of birth.

Tusk sex designations

Annual diameters of tusks used in this analysis displayed continuous increases throughout their records at rates between approximately 1.5 – 4.5 mm/yr (Table 5.3). Intra-tusk series of annual diameter measurements are almost perfectly predicted by log trends in all records (R-squared values range from 0.9198 – 0.9997 with median = 0.9846) with higher rates of increase in the earliest years of growth. Annual diametric growth series cluster into two divergent trajectories that are interpreted here as representing 14 *male* and 15 *female* tusks (Figure 5.3). Differences between diametric growth trajectories primarily result from different lengths, and as a result, volumes, of dentin produced each year. Higher rates of diameter increase *per year* do not necessarily correspond to higher rates of diameter increase *per unit length* along the tusk. In fact, expansion per unit length is fairly consistent between all tusks. Female and male juvenile tusks cannot be distinguished by external dimensions or shapes, but apparently do have different rates of dentin apposition (volume/time and diameter/time) even at this early stage of life. All *female* tusks included in this study

have nearly parallel growth trajectories, while *males* display a bit more variability in our sample.

Estimated growth intervals

Based on the presence of tusk-tip features, such as presence of enamel, cusplets (along the distal aspect of the tusk crown), and highly elliptical transverse cross-sections, 15 of the 29 tusks analyzed here begin with the first year of growth (Table 5.1). When the first year is present, it anchors the entire sequence giving a high degree of confidence in the specific interval of growth represented in the record. There is still the question of which years of *life* are represented. Ten of the tusks with first year of growth preserved are interpreted as female tusks based on their growth trajectories (Figure 5.3). The first year of growth in these tusks is considered to represent the second year of life.

Of the 14 *unknown* tusks that do not have the first year of dentin growth represented at their distal tip and have no independent indication of specific years contained in their records, GAMM models predict intervals of growth beginning as early as year 2 and as late as year 6 (Table 5.1). Growth intervals for known and calibrated tusk records are concentrated in the first few years of life with only a few stretching past year 10.

A diameter-based GAMM fit to growth records for 10 *female* tusks with well-constrained ontogenetic intervals (based on growth records that extend back to year 1) provided the best estimates of ontogenetic intervals represented in 5 tusks with uncertain ontogenetic timing. We categorized these as *female* tusks and assigned years-of-life based on predictions provided by the *female* GAMM. A diameter-based GAMM fit to growth sequences of 5 *male* tusks, whose records were anchored in the first year of growth, provided better estimates for the other 9 *unknown* records. Sex and ontogenetic timing of increments were assigned accordingly.

Diameter-based GAMMs provided estimates with lower standard errors that better predicted a real sequence of years than EIV-based GAMMs in all cases. However, for four tusks (TA-3, ZCHM-25, ZCHM-26, and ZCHM-51), log trends for the data using diameter-based GAMM alignments did not display the expected trajectory (based on tusks containing the 1st year) for the first years of growth that were missing from each record. For TA-3 and ZCHM-25, EIV-based GAMM predictions (with EIVs used in place of diameters) that produced reasonable growth trajectories were used instead, even though they resulted in higher average differences between predictions and corresponding years (see Table 5.3 and Methods: Estimating sex and ontogenetic timing of tusk records). For ZCHM-26, two alignments of diameter-based *female* GAMM estimates were equally well supported and better than the preferred *male* GAMM

estimate. However, only the earlier ontogenetic alignment resulted in a log trend that fit expectations for the missing early portion of the record. Finally, *female* GAMMs produced estimates that better represented a real sequence of years for ZCHM-51, but the predicted years of growth were later in life than the interval actually represented in source data for building the *female* GAMM. In that case, estimates from the male GAMMs provided a log trend that was more consistent with the pattern displayed in the more complete records.

AMS radiocarbon dates

AMS radiocarbon analyses produced definite dates for 15 of the 29 tusks (Table 5.1). The other 14 produced minimum ages only. These tusks, too old for radiocarbon dating methods, may be datable using other approaches, but at present they provide information only about the overall range of weaning age prior to about 40 ka. Since they could not help resolve temporal patterns leading up to the end of the Pleistocene, tusks without reliable dates were generally rejected for isotope analysis. Twelve of the reliable AMS ^{14}C dates were from before and during the LGM (19 – 26 k ^{14}C years BP; Clark et al., 2009). Only 3 returned post-LGM dates. Confidence intervals were mostly less than ± 250.

Collagen preservation

As is typical for Siberian permafrost tusks, dentin collagen was apparently well preserved. Most tusks had creamy-white hard dentin resembling modern ivory. Acid demineralized powder samples averaged 22.42 % (σ = 4.72 %, median = 22.22) of the total powder sample mass. Many C:N results were outside of the usually accepted range for well-preserved collagen (Table 5.3). Inconsistent peak jumping on the mass spectrometer in UMSIL necessitated separate analyses for $\delta^{15}N$ and $\delta^{13}C$ results. In four separate runs of sample analyses, nitrogen weight percent was highly consistent in all runs (μ = 16.0, σ = 1.08, n = 141). This level of compositional consistency is typical of permafrost tusks that have been analyzed in our lab. Although carbon weight percent was fairly consistent *within* each run (average standard deviation = 3.0), it varied significantly *between* runs (batch 1: μ = 44.4 %, σ = 1.32; batch 2: μ = 47.9 %, σ = 3.90; batch 3: μ = 56.0 %, σ = 2.36; batch 4: μ = 54.5 %, σ = 5.85; batch 5: μ = 45.1 %, σ= 1.6). The first two batches were separate single-gas analyses for $\delta^{15}N$ (batch 1) and $\delta^{13}C$ (batch 2) of subsamples (500 µg for $\delta^{15}N$, 650 µg for $\delta^{13}C$) taken from the same homogenized and pretreated collagen samples of a single tusk. Batch 3 and batch 4 were both multi-tusk runs (32 analyses and 4 – 5 tusks each; 500 µg samples prepared for analysis) that included specimens from distant regions in northern Siberia (Taimyr and Chukotka). Batches 3 and 4 were run in sequence over a couple days. C:N for batches 1 and 2 were substantially different from each other due to the discrepancy in

carbon weight percent, but were both within the 2.9 – 3.6 range documented for well-preserved collagen (Deniro, 1985). However, C:N calculations for batches 3 and 4 were between 3.6 – 5.1, values typically considered evidence of diagenetic alteration. Identically treated samples for 6 additional tusks (also permafrost specimens from northern Siberia – Taimyr, Chukotka, and Yakutia) processed for joint analysis of $\delta^{15}N$ and $\delta^{13}C$ in UCSCSIL showed highly consistent C:N (μ =3.26, σ = 0.27), with nitrogen at 16.2 % (σ = 0.8) of sample mass and carbon 45.1 % (σ = 1.6). These results from UCSCSIL are consistent with past analyses of Siberian permafrost tusks (e.g., Rountrey et al., 2007; Rountrey, 2009). Standards for elemental analysis (acetanilide) and nitrogen (USGS 25 and IAEA N_2) produced normal results in all runs that returned improbable carbon weight percent (Table 5.4). There is no systematic difference between $\delta^{15}N$ results for tusks analyzed in UMSIL and tusks analyzed in UCSCSIL and all values fall within the normal range for Siberian mammoth tusks (Gohman, 2009; Gohman et al., 2010; Iacumin et al., 2000). Considering all available evidence, it seems reasonable that although EA error prevents meaningful C:N calculations for tusks analyzed in UMSIL, $\delta^{15}N$ results from these analyses are reliable. There were a few samples with considerably higher C:N than other samples in their respective batches. These samples likely included traces of epoxy that was used to fill cracks in some tusks. Although

analyses for epoxy-contaminated samples would inaccurately represent collagen $\delta^{13}C$ values, $\delta^{15}N$ analyses should not be affected.

$\delta^{15}N$ records

Each annual $\delta^{15}N$ value represents an average for a complete year of growth (weighted toward values representing times of faster apposition that make greater relative contributions to annual growth). Nitrogen values for all annual samples in this study display a significant range (7.83 – 14.55 ‰, μ = 10.35 ‰, σ = 1.50; Table 5.3). The most an individual tusk record varies is 2.2 ‰ from highest and lowest annual values, so most of the total variation in analyses is accommodated by inter-tusk differences. The observed range of serial annual values for a tusk does not constrain subannual variability, which could display a greater range. Monthly to bimonthly values typically reveal 2 – 3 ‰ seasonal variations in Siberian mammoth tusks (Gohman, 2009).

Apparent temporal patterns in tusk-minimum $\delta^{15}N$ (a 'baseline' value for each tusk that eliminates some of the impact from nursing enrichment in early years that aren't represented in every tusk) (Figure 5.7) are not statistically supported either by linear or rank-order correlations. Correlations are slightly stronger if we recognize the possibility of opposing trends leading into and out of the LGM, but are still not statistically significant. Further divided by region, samples have too few individuals to

process meaningful statistical analyses, but appear to show difference between Chukotka and Taimyr. Minimum $\delta^{15}N$ in Taimyr tusks shows a general decrease through time with the lowest point being for the one LGM tusk from the region. In contrast, minimum $\delta^{15}N$ in LGM tusks from Chukotka are about 2 ‰ higher than the 2 pre-LGM tusks and 2.5 ‰ higher than the single post-LGM tusk. The lone isotope record from Yakutia is an LGM specimen with minimum $\delta^{15}N$ falling in the range of pre- and post-LGM tusks from Chukotka and Taimyr (Figure 5.7).

Nitrogen records contain region-specific variation. In the 8 specimens sampled from Taimyr, minimum $\delta^{15}N$ was lower (range = 8.07 – 10.76 ‰, μ = 9.22 ‰, σ = 0.88 ‰, median = 9.14 ‰) than in 6 tusks from Chukotka (range = 9.78 – 13.18 ‰, μ = 11.42 ‰, σ = 1.36 ‰, median = 11.29 ‰). The one tusk sampled for Yakutia had a minimum (9.82 ‰) within the range of variation for both Taimyr and Chukotka. Three anomalously high records from the LGM and shortly before in Chukotka are primarily responsible for this regional difference, but do not account for it completely. The other 3 Chukotka specimens have minimum $\delta^{15}N$ values that are either higher than contemporary specimens from Taimyr or otherwise near the top of the total range for Taimyr minima.

Serial records of annual measurements from tusks of 15 juveniles display early-life $\delta^{15}N$ patterns for Siberian woolly mammoths (Figures 5.8 – 5.22). The interval from year 1 to year 3 shows a decrease in $\delta^{15}N$ from one year to the next, across all analyses of tusks that contained these early years of growth (n = 8 tusks; average annual change = -0.3 ‰).

Weaning age estimates

In 11 of 15 tusks, the first significant increase occurring in years 4 – 8 is interpreted as an indication of weaning. Of the other 4, one tusk represents an individual that died at age 4, likely before it had been weaned (Figure 5.17). Another is a tusk whose growth record contains years 5 – 11 but does not display an increase until year 10 (Figure 5.20). The third is currently missing year 5 from its isotope record, but displays only declining $\delta^{15}N$ across 4 complete increments between years 3 – 7 (Figure 5.19). The last one had a dramatic increase in year 8, but the result was discarded due to high nitrogen and carbon yields (26.3 % N, 80.8 % C) (Figure 5.15). Reanalyses of these last two are in progress.

Weaning age estimates (Figures 4.7-4.22) for 12 tusks range from 4 – 10 (μ = 6.83, σ = 1.8) and show a temporal pattern with two apparent opposing trends: one during the period of cooling leading into the LGM and one during the period of

warming from the LGM up until the end of the Pleistocene (Figure 5.23). One estimate is from a tusk that was too old for AMS ^{14}C dating. This weaning estimate was included for general understanding of weaning age in Siberian woolly mammoths through time, but it was not considered in analyses of late Pleistocene trends.

During the interval of cooling leading into the LGM, there is a strong and significant correlation between weaning age and ^{14}C years BP (Linear correlation: R = -0.919, p = 0.01; Spearman's rank-order correlation: R = -0.986, p = 0.00; n = 6). In the interval of general warming from the LGM to the end of the Pleistocene there is a moderate correlation between weaning age and time (Linear correlation: R = 0.550, p = 0.05; Spearman's rank order correlation: R = 0.564, p = 0.32; n = 5). Both trends involve small numbers of specimens. Strength of correlations and their statistical significances can be greatly affected by addition or removal of even one key data point. An alternative treatment that includes all the weaning age estimates but recognizes the presence of two separate trends leading into and out of the LGM, is to look at weaning age with respect to the time before or after the LGM (t = |^{14}C date – 22,500|). In this rather crude formulation, the rank-correlation is only moderate but significant (Spearman's rank order correlation: R = -0.675, p = 0.03; n = 11). No significant correlations were detected between weaning age and sex, growth rates, average δ^{15}N, or region.

$\delta^{13}C$ records

For 7 of the 15 tusks sampled for nitrogen stable isotope analyses, carbon isotope results ($\delta^{13}C$) were also obtained. Annual carbon values display less overall variation (range = -22.52 – -20.72 ‰, μ = -21.72, σ = 0.39 ‰, median = -21.72 ‰) and lower intra-tusk variation (maximum range = 1.07 ‰) than nitrogen. This pattern of $\delta^{13}C$ being more conserved than $\delta^{15}N$ is not unusual in Siberian mammoth tusks, and is also expressed in lower seasonal variabilities of around 1 – 2 ‰ (Gohman, 2009; Gohman et al., 2010). Carbon isotope profiles display no clear patterns that help constrain weaning age. In 2 specimens, an increase coincident with the weaning 'spike' in $\delta^{15}N$ could be seen as a corroboration of weaning, since subtraction of carbon-light milkfat from the diet could lead to increased values. In the small sample of $\delta^{13}C$ records reported here, there is no significant variation correlated with region or time.

Tusk growth rates

Five *female* tusks with finite ^{14}C dates contained a record of the growth interval from year 5 to year 8. Average total estimated growth volume (summed EIVs) for this overlapping period of growth was 184.6 cm^3 (σ = 15.9). Values display a moderate increase through time, but it is not statistically significant, and the sample lacks the resolution to address the possibility of multiple trends (Figure 5.24A). Five ^{14}C-dated *male* tusks had records that contained years 3 – 6. Average estimated dentin volume for

that interval was 265.4 cm^3 (σ = 56.1). *Male* values show no clear trend through the 30 ka interval, but two post-LGM records have a lower average (260.5 cm^3) than two early LGM records (305.6 cm^3)(Figure 5.24B).

Discussion

Aligning growth records

Determining the years of growth represented in individual tusk records requires a few reasonable assumptions. One is that we know when tusk formation begins. Precise timing of tusk formation in woolly mammoths may vary to some extent even in contemporary individuals. Evidence suggests initiation before birth in male woolly mammoths and after birth in females. Based on this observation, we treat female records as lagging behind male records by 1 year (i.e. year x in female tusks is ontogenetically equivalent to year x+1 in male tusks). We accommodate this discrepancy by assigning weaning age for female tusks as one year later than the year-of-growth containing the $\delta^{15}N$ weaning signature (Table 5.1, Figure 5.22).

Another assumption is that age at initial tusk mineralization did not change over the sampled interval. We don't yet have enough data to evaluate this possibility, but in order for it to completely confound results presented here, timing would have to vary by 3-4 years, which seems unlikely. In modern African elephants, permanent tusks start

forming prior to eruption, which occurs at about one year after birth in both sexes (Raubenheimer, 2000; Raubenheimer et al., 1995; Sikes, 1971).

The use of GAMM models to estimate years of life based on records of growth in other tusks takes for granted that tusk diameters and growth increment volumes for different individuals conform to sex-specific growth trajectories. Sex determinations from aDNA analyses that are in progress will test the interpretation of sexual differences in growth rates and may improve year-of-life estimates reported here.

Initial attempts to determine years of life for records with unknown starting points involved visual alignment of diameter and EIV growth trajectories. This relied heavily on recognition of trends, and then backward projection of trends to the first years of growth, where they were expected to approximately match records from tusks that did contain the first years in their preserved distal tips. GAMM predictions were generally consistent with visual alignments, but in some cases, GAMM estimates provided estimates that were untenable when overall trends were considered. That is, when the timing of growth records was established by GAMMs, sometimes the backward projection of growth trajectories (based on a log trend) implied that growth initiated sometime after the first year of growth. Part of the reason for this failure may be that GAMMs were constructed from small numbers of incomplete records that were

concentrated in the first few years of growth. Perturbations in each growth trajectory had potential to significantly impact the model. Another complication was that for years after 5, the *male* GAMM was fit to only 1 tusk, meaning that portion of the model fit to later growth didn't accommodate as much inter-tusk variability.

Despite shortcomings of GAMMs (some estimates were rejected as unrealistic) they did in some cases result in reconsidered visual alignments of growth records and minor changes to year estimates. The most significant contributions were to provide a way to quantitatively compare various potential competing alignments that could not be resolved visually (cases in which more than one different alignment seemed to fit the record equally well). They also provided a way to quantify and compare 'fit' of proposed alignments.

Estimating weaning age

Nitrogen isotope enrichment following weaning has been observed in other animals (Dupras et al., 2001; Fuller et al., 2006; Hobson and Sease, 1998; Nelson et al., 1998). In sea lions, this increase appears to reflect catabolization of proteins stored during nursing to help them survive the interval after being weaned when they are not yet proficient at hunting for their own food (Hobson and Sease, 1998). By the time they are fully weaned, elephant calves have already become competent at acquiring their

own food, but the loss of a backup supplement in the form of mother's milk could still cause them to utilize energy stores. If weaning resulted in a sustained period of nutritional difficulty for calves, we might expect to see a dip in growth that accompanies the enrichment in nitrogen. In some tusks, $\delta^{15}N$ increases interpreted as the result of weaning are accompanied by lower EIV than expected based on the overall trend, but this is not consistent enough that EIV records could themselves be used to confidently estimate weaning.

We interpret a spike in $\delta^{15}N$ following a gradual depletion sustained over multiple years in a juvenile tusk as a clear indicator of weaning age. For records missing the earliest years of life but containing at least some of the interval during which we expect weaning to occur (ages 3 – 8, based on modern elephants (Douglas-Hamilton and Douglas-Hamilton, 1975; Lee and Moss, 1986)), we interpret the first increase in $\delta^{15}N$ as an indicator of weaning. This is based on the expectation that average annual $\delta^{15}N$ will decrease throughout nursing, an assertion supported by data from modern elephants (*Chapter 4*) and by the most complete records reported here that show consistent year-to-year decreases leading up the abrupt increase interpreted as a signal of weaning. Taken alone, records missing the earliest years may only provide weak evidence of weaning age, but when considered as part of the larger picture, they provide data that can help characterize patterns through time.

Interpreting changes through time

Whether or not observed trends in weaning age are statistically supported depends in part on how the data are separated into groups. Treated as one group, data do not display any significant trend. Splitting data into two groups (pre-LGM through mid-LGM, and mid-LGM through post-LGM) provides two sets of data with moderate to strong trends. Further splitting could be used to improve trends even more, but with such a small sample to begin with, divisions quickly make sample sizes inconsequentially small. When dealing with small sample sizes, the addition or removal of even a couple points can greatly affect the statistical relevance of a trend. For instance, starting the more recent interval at 30 ka instead of 26.5 ka adds 2 estimates of late weaning to the early part of the interval and improves the strength of the trend greatly. Removal of just one estimate from the end of the Pleistocene could be similarly impactful but with the opposite effect. The most obvious dividing point was the beginning of the LGM (26.5 ka), although climate conditions of the LGM may have developed prior to full glacial extent in some regions. In any case, a sample this size does not provide adequate data for resolving fine details of complex patterns, but regardless what statistical model best describes the secular trends in weaning age, what the data most clearly demonstrate is earlier weaning during less glacial intervals before and after the LGM, and generally later

weaning in both Taimyr and Chukotka during the LGM. A lone data point from Yakutia shows "early" weaning during the LGM.

Variation in $\delta^{15}N$ by region has been noted before (Gohman, 2009; Iacumin et al., 2000). Secular trends in average $\delta^{15}N$ through time have also been observed (Iacumin et al., 2000) and warrant further investigation and discussion. Higher $\delta^{15}N$ during the LGM than in periods both preceding and following it could reflect a vegetational response in a cooler, dryer climate (Heaton et al., 1986), lower-quality protein sources (Robbins et al., 2005), increased urea recycling (Gannes et al., 1998), or greater seasonal reliance on catabolism of stored proteins (Hobson et al., 1993) during more glacial periods, just to name a few possibilities. Without being able to link changes in $\delta^{15}N$ to changes in nutritional status, this pattern contributes little to the current conversation. In any case, even though both baseline $\delta^{15}N$ and weaning age display some higher values during the LGM, they are actually not correlated with each other.

Tusk growth rates play an important role in determining the cause of a shift in weaning age. Considered in isolation, the shift to significantly earlier weaning proposed here could be interpreted as a genetic response to consistently poor nutrition, *if* conditions also provided a considerable selective pressure for higher reproductive rates. Such a regime would favor a population that matured more quickly on a reduced energy

budget. This implies not only considerable reduction in adult (mature) body size, but also slowed growth rates underlying body size reduction. Merely acknowledging that the degree of body size reduction that is suggested by some Siberian records is fairly moderate might be enough to rule out climate change as a potential cause of the estimated decrease in weaning age, but it could be even more informative to look at growth rates during early ontogeny.

The suggestion of lower total growth volume from year 3 – 6 in late Pleistocene *males* compared to LGM males is based on only 4 individuals. A slightly more significant shift to greater tusk growth rate is observed in EIVs of years 5 – 8 for five *female* tusks. Due to the paucity of comparable data, growth rates do not contribute much to interpretations proposed here. The most that can be said is that they display no clear evidence of the dramatic reduction in growth rate that would be necessary to accommodate early weaning in a situation of reduced habitat quality.

Weaning age as a test of extinction hypotheses

The test proposed here does not by itself exclusively support any one hypothesis as the explanation for extirpation of Siberian woolly mammoths. As a test of climate change hypotheses, it refutes the assertion of heightened mortality due to general reduction in food supply or quality. Hunting is not the only mechanism that would

provide selective pressure to wean earlier, but it is one that could reasonably have had the long-term sustained impact necessary to simultaneously drive this shift and lead to extinction. Climate could explain the shift if conditions were actually improving at the end of the Pleistocene, but that would require something else (like hunting) to explain the extinction. Climate changes that increased mortality without sustained nutritional deficiency could also delay weaning and maturation and might explain population declines. Frequent droughts punctuating otherwise highly productive environments could increase juvenile mortality, while permitting faster attainment of large body sizes. In such conditions, earlier weaning could accompany the faster juvenile growth rates being selected by high juvenile mortality. However, this model requires finely tuned environmental parameters that would need to be consistent over long intervals to explain the counterintuitive effects. It would also be expected to result in growth records with high interannual variability (see *Chapter 2* – Fisher et al. (2014a) for discussion of mean sensitivity in tusk growth records). Extended maternal investment would seem the most likely population response to environments that threatened calf survival. In the absence of direct evidence for improbable environmental conditions that were simultaneously hyper-productive and difficult for young individuals to endure, we should be able to discount such suggestions. In general, the types of habitat changes that might create long-term sustained stress on a population (range reduction,

ecological collapse, shifts to lower quality vegetation regimes) would predict slower growth, later weaning, and later maturation.

There are certainly other possibilities, but none that currently provides a convincing alternative to hunting. Parasites and disease could increase mortality without general resource limitations, and such proposals are in some ways preferable to the assertion that climate was somehow both really good and catastrophically bad. However, at this point they are mere speculation. In contrast, there is extensive evidence that Pleistocene humans hunted mammoths. How frequently they hunted them and whether that rate provides a sufficient explanation for the extinctions is currently an open question. Nevertheless, hunting currently provides the best-supported extinction mechanism that would be expected to result in a substantial decrease in weaning age without a considerable reduction in body size.

Early weaning age during an interval of relatively warm conditions before the LGM may share a common cause with early weaning at the end of the Pleistocene. One way would be the aforementioned suggestion that conditions were actually more favorable for woolly mammoths during warmer periods, making late weaning during the LGM the stress-related exception rather than the rule for favorable conditions. Alternatively, hunting could explain both periods of reduced weaning age if hunting

intensity was higher from 40 – 30 ka than during the LGM, when cold conditions may have provided a time-limited reprieve from human activity.

$\delta^{13}C$ records

Previous studies have detected evidence of nursing and weaning in $\delta^{13}C$ records as well as $\delta^{15}N$. Similar to how a trophic-level fractionation in $\delta^{15}N$ produces higher values in a nursing calf than those of its mother, a smaller trophic level increase (~ 1.0 ‰) could result in elevated calf $\delta^{13}C$ due to nursing. Throughout most of the first 3 years after birth, elephant calf hair was consistently enriched by about 1.0 ‰ compared to hair from its mother (*Chapter 4*). During that time nursing continued but decreased. As a result, the difference between calf and mother hair $\delta^{13}C$ decreased slightly.

There is also the potential for depletion in the calf due to a *lipid effect* when the calf feeds on milk with high fat content. Since lipids are depleted in ^{13}C, milkfat can offset the trophic effect, and result in $\delta^{13}C$ being lower in nursing young than in the mother. This is clearly displayed in human analyses (Fuller et al., 2006) and seems to have been detected in a high resolution serial $\delta^{13}C$ analysis from a woolly mammoth calf (Rountrey et al., 2007). Absence of a clear lipid effect in the zoo elephant calf hair (except possibly immediately after birth) despite there being significant amounts of low $\delta^{13}C$ lipids in its mother's milk even after 3 years of nursing suggests that other factors

might obscure this effect in proboscideans. Considering the results of the zoo study, it is actually surprising that the previously analyzed mammoth tusk displayed increasing $\delta^{13}C$ in the first two years as an apparent reflection of decreasing dietary contribution from milk.

Seasonal variation in $\delta^{13}C$ of the Rountrey et al. (2007) record may help explain the lack of clear patterns in annual $\delta^{13}C$ values reported in this study. First, in that record there only appears to be a significant change in the first two years of life. Along with results from the zoo elephants and other tusk analyses (Rountrey, 2009), this suggests that the lipid effect may only be detectable at the beginning of nursing. Many records from this study are missing the first couple years of growth. Second, the previously published record shows significant seasonal variation in calf $\delta^{13}C$. Whether this is due to seasonal changes in milk composition or consumption, interannual differences in the calf $\delta^{13}C$ seasonality could result in unintelligible patterns at the resolution of annual samples. Third, $\delta^{15}N$ continues to decline long after lipid effect on $\delta^{13}C$ disappears in both the high-resolution woolly mammoth analysis and the zoo record. Although it looks like $\delta^{15}N$ records display a clear response to weaning, it could be that the only detectable shift in $\delta^{13}C$ occurs relatively early in nursing and marks a change in milk composition rather than a change in nursing intensity. Finally, there may be other factors in the mother's diet and physiology that complicate the pattern. Although the

high-resolution mammoth analysis shows remarkably consistent inter- and intra-annual patterns, the unintelligible zoo calf $\delta^{13}C$ record tracks the highly variable pattern displayed in his mother's hair. Other serial records of adult mammoths from continental Siberia display somewhat variable interannual $\delta^{13}C$ patterns (Gohman, 2009) that might be behind some of the variation in this study's calf records.

Because milk composition and life-history strategies vary dramatically between distantly related taxa, isotopic signatures of milk consumption and the trauma of weaning should also be different. This thinking was behind the zoo elephant analysis reported in *Chapter 4*. In elephants and woolly mammoths, nursing clearly affects calf $\delta^{13}C$ during nursing, but the effect appears to change substantially and may also not be significant enough to avoid being drowned out by normal interannual variations in the vegetation consumed by both the mother and calf. For the purposes of this study, serial records of annual $\delta^{13}C$ did not help constrain weaning age. Though reported when available, carbon records did not contribute to the findings of this study.

Conclusion

Serial analyses of $\delta^{15}N$ for juvenile Siberian woolly mammoth tusk records consistently display a sustained decline in the first years of life. This pattern had been

detected previously in tusk records from a modern African elephant and multiple woolly mammoths (Rountrey, 2009; Rountrey et al., 2007). The negative $\delta^{15}N$ trend appears to reflect the decreasing amount of milk in a juvenile's diet as it transitions to solid food. This pattern in $\delta^{15}N$ records of nursing offspring is fairly well established. A jump in $\delta^{15}N$ marks the end of this decreasing trend in most of the tusks analyzed, and is thought to represent the end of nursing, when the calf was weaned by its mother. The increase may be an effect of nutritional stress and protein catabolism in the newly independent weanling. This pattern provides estimates of weaning age from fossil tusk records.

Weaning age estimates for 11 tusks distributed over the final 30 ka of the Pleistocene show a shift from weaning at about 8 years of age in specimens dating to the period leading up to and including the last glacial maximum (30 – 19 ka BP), to weaning at about 5 years in the most recent specimens, which represent individuals who lived between 15 and 10 ka BP, shortly before the species became extinct in continental settings. An earlier interval of relatively warmer conditions from 40 – 35 ka BP is also characterized by younger weaning age (~ 6 years old). This suggests the possibility of a general correlation between lower weaning age and less glacial conditions. The total range of weaning age estimates in this study is 4 – 10, which is not unlike the range of weaning ages observed in modern African elephants.

Data presented here refute climate-based hypotheses for the late Pleistocene extinctions. Explaining a shift to earlier weaning under poor environmental conditions would be difficult and require appeal to creative speculation. In contrast, results of this study are consistent with expectations if hunting was responsible for declining populations prior to extinction. There are other possible explanations for a decrease in weaning age, but none that seem likely to have made late Pleistocene conditions catastrophically detrimental to continental populations of Siberian woolly mammoths. Therefore, the broad implication of refuting climate-based hypotheses is that humans were the primary cause of these extinctions.

Additional juvenile tusks are needed in order to flesh out regional patterns of weaning and growth rates for northern Siberia. The strategies used here in principle could be applied to other species and regions, but require a large number of well-preserved juvenile tusks that might not be currently available. Further analyses could also extend the procedure to accommodate tooth rows of deciduous dentitions that record growth from the first years of life, and in doing so, would enable weaning age analyses for other Pleistocene mammals that lack the remarkable records provided by proboscidean tusks.

Table 5.1. Juvenile Siberian woolly mammoth tusks used in this study.
Tusks represent three regions of northern Siberia (TMR – Taimyr, YAK – Yakutia, CHK – Chukotka). Sex identifications not italicized here are based on growth trajectories, which apparently display sexual differences at this early stage of life (see *Figure 5.3*). Italicized sex identifications are based on whether the male or female GAMM provided a better growth interval prediction (see *Methods: Estimating sex and ontogenetic timing of tusk records*). *Years of growth* estimates are listed. *Years of life* estimates require some assumption about when growth initiated ontogenetically. In this study, the first full year of growth is equivalent to the first year of life for male tusks, but is considered the second year of life in female tusks. Consequently, estimated weaning *ages* listed are the same as the weaning year of *growth* for males, but a year after the weaning year of *growth* for females. Year '0' identifies growth prior to the first full year. In males this might be prenatal growth. In females, this might be growth that initiated during the first year of life. Minimum $\delta^{15}N$ was used to compare nitrogen values through time.

Tusk ID	Region	Sex	AMS date (^{14}C years BP)	Years included	Weaning age	Minimum δ^{15}N (‰)
TA-3	TMR	*Female*	10,480 ± 100	3 - 17	6	8.40
2000/245	TMR	Female	29,900 ± 1000	1 - 9	9	9.04
2000/246	TMR	Female	35,800 ± 2100	1 - 9	6	10.02
2000/286	TMR	Male	10,150 ± 100	0 - 8	4	9.23
2000/305	TMR	*Female*	24,070 ± 500	2 - 9	8	8.07
2001/411	TMR	Female	> 43,500	1 - 9	-	-
2003/857	TMR	Male	34,970 ± 190	0 - 4	-	-
2007/002	TMR	Female	39,320 ± 340	1 - 7	5	9.54
2007/005	TMR	*Male*	34,280 ± 250	2 - 12	8	8.68
2009/001	TMR	*Female*	34,300 ± 240	3 - 9	7	10.76
ZCHM-19	CHK	*Female*	> 41,100	6 - 14	?	10.51
ZCHM-20	CHK	Female	> 37,200	1 - 12	8	10.42
ZCHM-22	CHK	Male	20,050 ± 60	0 - 5	?	12.07
ZCHM-24	CHK	*Male*	14,850 ± 170	2 - 9	6	9.78
ZCHM-25	CHK	*Male*	> 43,500	3 - 6	-	-
ZCHM-26	CHK	*Male*	25,960 ± 570	2 - 8	?	13.18
ZCHM-42	CHK	*Female*	> 43,500	6 - 17	-	-
ZCHM-46	CHK	*Male*	> 43,500	3 - 13	-	-
ZCHM-51	CHK	*Male*	28,480 ± 100	5 - 11	10	12.54
ZCHM-52	CHK	*Male*	> 43,500	2 - 6	-	-
ZCHM-53	CHK	Female	> 43,500	1 - 5	-	-
AM-1	YAK	Female	> 43,500	1 - 5	-	-
AM-2	YAK	Female	> 43,500	0 - 4	-	-
AM-3	YAK	Female	> 43,500	1 - 5	-	-
AM-4	YAK	Female	> 43,500	1 - 5	-	-
AM-5	YAK	Male	40,490 ± 360	0 - 3	-	-
AM-6	YAK	*Male*	25,850 ± 90	2 - 7	5	9.82
AM-7	YAK	*Male*	> 43,500	3 - 6	-	-
MMY	YAK	Male	> 43,500	0 - 5	-	-

Table 5.2. Dentin collagen pretreatment data.
A block sample of dentin from a mastodon premaxillary tusk ("Loc. 8") from the Ziegler Reservoir fossil site assemblage was split into two pieces that each represent approximately equivalent growth intervals. After demineralization with 0.5 M HCl, one was treated with chloroform-methanol (C:M = 2:1) to remove lipids (see *Chapter 2* – Fisher et al., 2014: *Methods*) and the other was not. A powder sample approximately representing the same growth interval as the block samples was divided into six subsamples. Three of these were for demineralized using the procedure described above (*Methods: Isotope analyses*) that does not include a 'defatting' step. The other three were treated with C:M for 5 minutes and rinsed 5 times with ultrapure (double-deionized) water prior to demineralization. Isotope values are reported in reference to international standards (air-N_2 for $\delta^{15}N$ and VPDB for $\delta^{13}C$). Relative abundance of carbon and nitrogen in samples are reported in percent of total sample mass ("N wt%" and "C wt%"), as well as atomic ratio (C:N). The original powder sample and two block samples are equivalent to the precision afforded by the sampling method (see *Chapter 2* – Fisher et al., 2014; Rountrey et al., 2009). The powder sample was mixed thoroughly (sample was suspended in ultrapure water and vortexed for 1 minute) prior to being divided into six equal samples to ensure sample consistency. Higher average C:N in samples not treated with C:M likely reflects the presence of a small amount of lipids in the dentin samples. This is corroborated by lower $\delta^{13}C$ in samples that were not 'defatted.' On average, defatted samples are higher in $\delta^{13}C$ by 0.11 ‰ and lower in $\delta^{15}N$ by 0.05 ‰. Samples were analyzed in the University of Michigan Stable Isotope Lab where machine precision for both carbon and nitrogen is maintained at ± 0.12 ‰ (see *Chapter 2* – Fisher et al., 2014). For a graphical representation of this data, see Figure 5.5.

	N wt%	$\delta^{15}N$	C wt%	$\delta^{13}C$	C:N
Block w/ C:M	15.19	4.91	45.44	-19.37	3.49
Block w/ C:M	15.42	4.95	45.58	-19.34	3.45
Block w/ C:M	14.81	4.77	45.14	-19.34	3.55
Average	**15.14**	**4.88**	**45.39**	**-19.35**	**3.50**
Std Dev	**0.30**	**0.09**	**0.23**	**0.02**	**0.05**
Powder w/ C:M	15.42	5.10	46.10	-19.43	3.49
Powder w/ C:M	15.14	4.97	45.07	-19.39	3.47
Powder w/ C:M*	12.36*	4.50	36.31*	-19.23	3.44*
Average	**14.31**	**4.86**	**42.49**	**-19.35**	**3.47**
Std Dev	**1.69**	**0.31**	**5.38**	**0.11**	**0.03**
Block w/o C:M	15.64	4.90	46.28	-19.39	3.46
Block w/o C:M	14.82	4.88	45.43	-19.40	3.59
Block w/o C:M	14.55	4.89	45.19	-19.71	3.63
Average	**15.00**	**4.89**	**45.63**	**-19.50**	**3.56**
Std Dev	**0.57**	**0.01**	**0.57**	**0.18**	**0.09**
Powder w/o C:M	14.87	4.98	44.90	-19.41	3.52
Powder w/o C:M	14.88	4.87	44.48	-19.41	3.47
Powder w/o C:M	15.10	5.03	44.85	-19.44	3.45
Average	**14.95**	**4.96**	**44.74**	**-19.42**	**3.48**
Std Dev	**0.13**	**0.08**	**0.23**	**0.01**	**0.04**
w/ C:M (total)					
Average	**14.72**	**4.87**	**43.94**	**-19.35**	**3.48**
Std Dev	**1.18**	**0.21**	**3.76**	**0.07**	**0.04**
w/o C:M (total)					
Average	**14.97**	**4.92**	**45.19**	**-19.46**	**3.52**
Std Dev	**0.37**	**0.06**	**0.62**	**0.12**	**0.07**
*low concentrations of carbon and nitrogen					

Table 5.3. Growth increments and serial isotope records for tusks used in this study. *Year of growth* lists the sequence that best matches GAMM predictions shown in the second to last column. The best fit alignment was the one that minimized the average difference between GAMM predictions and corresponding years in sequence (see */pred-yr/* column on right). Diameter increase refers to proportional increase from the previous year ($diam_{yr\ x}/diam_{yr\ x-1}$). Nitrogen isotope values are reported relative to air-N_2, and carbon is reported relative VPDB. Reported *Range* for isotope data is the difference between highest and lowest annual measurement. *C:N* lists atomic ratio of carbon to nitrogen measured from each sample. High C:N values (>3.6, based on Deniro, 1985) in many of the specimens are likely due to equipment malfunction rather than poor preservation of organics (see *Methods: Collagen preservation*). When C:N deviated significantly from within-batch average due to high detection of carbon but normal detection of nitrogen, only $\delta^{13}C$ for that sample was considered unreliable (2000-245, years 1 and 4). $\delta^{15}N$ was discarded for one sample (ZCHM-19, year 8) that had normal C:N, but high percentages of both nitrogen and carbon. The final year in some sequences represents an incomplete annual increment. Discarded isotope values and those for partial years were excluded from calculations of average, range, and standard deviation. Analyses were split between the University of Michigan Stable Isotope Lab (UMSIL) and the University of California Santa Cruz Stable Isotope Lab (UCSCSIL).

Tusk ID - **TA-3**	Year of growth	Diam (mm)	EIV (cm^3)	Diam increase	$\delta^{15}N$ (‰)	$\delta^{13}C$ (‰)	C:N	GAMM pred.	|pred-yr|
Batch 3	3	-	-	-	8.41	-	4.58	-	-
UMSIL	4	28.35	-	-	8.40	-	4.00	-	-
	5	31.24	39.46	1.10	9.36	-	4.02	5.31	0.31
	6	32.63	46.34	1.04	9.04	-	4.07	7.40	1.40
	7	34.25	52.82	1.05	8.71	-	4.03	7.99	0.99
	8	36.65	62.15	1.07	8.59	-	4.09	8.54	0.54
	9	37.82	60.27	1.03	8.77	-	4.05	9.35	0.35
	10	39.10	74.86	1.03	8.78	-	4.05	10.96	0.96
	11	40.31	81.86	1.03	-	-	-	11.84	0.84
	12	41.74	66.33	1.04	-	-	-	9.94	2.06
	13	43.74	81.05	1.05	-	-	-	11.27	1.73
	14	45.24	90.64	1.03	-	-	-	12.74	1.26
				Average	8.76	-	4.11	Average	1.04
				Range	0.97	-	0.58		
				St. Dev.	0.32	-	0.19		

Table 5.3 (cont.)

Tusk ID - **2000-245**	Year of growth	Diam (mm)	EIV (cm^3)	Diam increase	$\delta^{15}N$ (‰)	$\delta^{13}C$ (‰)	C:N	GAMM pred.	|pred-yr|
Batch 5	1	19.45	-	-	9.39	~~-24.41~~	5.03	-	-
UCSCSIL	2	21.35	16.44	1.10	10.54	-21.77	3.23	-	-
	3	23.64	24.34	1.11	10.35	-21.51	3.25	-	-
	4	26.30	30.53	1.11	10.18	~~-22.45~~	3.57	-	-
	5	29.52	40.76	1.12	9.45	-21.54	3.24	-	-
	6	31.25	50.30	1.06	9.33	-21.42	3.22	-	-
	7	33.77	55.49	1.08	9.04	-21.49	3.22	-	-
	8	35.07	54.78	1.04	9.79	-21.65	3.20	-	-
	9	35.60	58.12	1.01	9.32	-22.32	3.26	-	-
	Rejected data not included			Average	9.75	-21.67	3.27	Average	-
	in Avg., Range, St. Dev.			Range	1.50	0.90	0.37		
				St. Dev.	0.55	0.31	0.12		

Tusk ID - **2000-246**	Year of growth	Diam (mm)	EIV (cm^3)	Diam increase	$\delta^{15}N$ (‰)	$\delta^{13}C$ (‰)	C:N	GAMM pred.	|pred-yr|
Batch 4	1	17.50	-	-	-	-	-	-	-
UMSIL	2	20.00	17.43	1.14	10.27	-	3.86	-	-
	3	22.08	23.62	1.10	10.34	-	3.90	-	-
	4	24.10	32.10	1.09	10.37	-	3.90	-	-
	5	26.50	35.89	1.10	10.59	-	3.84	-	-
	6	28.55	43.35	1.08	10.30	-	3.98	-	-
	7	31.40	49.85	1.10	10.02	-	3.89	-	-
	8	31.73	47.87	1.01	10.41	-	3.87	-	-
	9 (part.)	32.35	28.15	1.02	-	-	-	-	-
	Partial years not included			Average	10.33	-	3.89	Average	-
	in Avg., Range, St. Dev.			Range	0.56	-	0.15		
				St. Dev.	0.17	-	0.05		

Table 5.3 (cont.)

Tusk ID - **2000-286**	Year of growth	Diam (mm)	EIV (cm^3)	Diam increase	$\delta^{15}N$ (‰)	$\delta^{13}C$ (‰)	C:N	GAMM pred.	|pred-yr|
Batch 4	1	18.10	-	-	-	-	-	-	-
UMSIL	2	23.55	24.56	1.30	10.13	-	3.89	-	-
	3	26.35	33.26	1.12	9.94	-	3.80	-	-
	4	29.00	48.29	1.10	10.09	-	3.91	-	-
	5	33.00	60.38	1.14	10.03	-	3.85	-	-
	6	36.40	88.03	1.10	9.73	-	3.91	-	-
	7	36.95	78.58	1.02	9.83	-	3.86	-	-
	8 (part.)	39.40	56.10	1.07	9.23	-	5.08	-	-
	Partial years not included			Average	9.96	-	3.87	Average	-
	in Avg., Range, St. Dev.			Range	0.40	-	0.11		
				St. Dev.	0.15	-	0.04		

Tusk ID - **2000-305**	Year of growth	Diam (mm)	EIV (cm^3)	Diam increase	$\delta^{15}N$ (‰)	$\delta^{13}C$ (‰)	C:N	GAMM pred.	|pred-yr|
Batch 1	2	20.36	-	-	-	-	-	-	-
UMSIL	3	23.49	26.26	1.15	9.14	-	3.80	2.98	0.02
($\delta^{15}N$ only)	4	26.63	32.14	1.13	8.58	-	3.40	4.33	0.33
	5	27.39	34.66	1.03	8.35	-	3.59	5.41	0.41
	6	30.14	40.00	1.10	8.28	-	3.41	6.15	0.15
	7	32.22	42.72	1.07	8.71	-	3.37	7.44	0.44
	8	35.05	61.14	1.09	8.07	-	3.41	8.76	0.76
	9	-	-	-	8.43	-	3.53	-	-
				Average	8.51	-	3.50	Average	0.35
				Range	1.08	-	0.43		
				St. Dev.	0.35		0.15		

Table 5.3 (cont.)

Tusk ID - **2000-305**	Year of growth	Diam (mm)	EIV (cm^3)	Diam increase	$\delta^{15}N$ (‰)	$\delta^{13}C$ (‰)	C:N	GAMM pred.	|pred-yr|
Batch 2	2	20.36	-	-	-	-	-	-	-
UMSIL	3	23.49	26.26	1.15	-	-22.04	3.30	2.98	0.02
Analysis	4	26.63	32.14	1.13	-	-21.73	3.24	4.33	0.33
($\delta^{13}C$ only)	5	27.39	34.66	1.03	-	-22.09	3.20	5.41	0.41
	6	30.14	40.00	1.10	-	-22.25	3.26	6.15	0.15
	7	32.22	42.72	1.07	-	-21.85	3.24	7.44	0.44
	8	35.05	61.14	1.09	-	-22.17	3.30	8.76	0.76
	9	-	-	-	-	-22.35	3.73	-	-
				Average	-	-22.07	3.32	Average	0.35
				Range	-	0.62	0.53		
				St. Dev.		0.22	0.18		

Tusk ID - **2001-411**	Year of growth	Diam (mm)	EIV (cm^3)	Diam increase	$\delta^{15}N$ (‰)	$\delta^{13}C$ (‰)	C:N	GAMM pred.	|pred-yr|
	1	20.48	-	-	-	-	-	-	-
	2	22.59	23.34	1.10	-	-	-	-	-
	3	24.76	21.94	1.10	-	-	-	-	-
	4	25.97	13.18	1.05	-	-	-	-	-
	5	27.61	15.16	1.06	-	-	-	-	-
	6	29.70	30.09	1.08	-	-	-	-	-
	7	30.78	30.53	1.04	-	-	-	-	-
	8	31.57	34.84	1.03	-	-	-	-	-
	9	33.50	35.33	1.06	-	-	-	-	-

Tusk ID - **2003-857**	Year of growth	Diam (mm)	EIV (cm^3)	Diam increase	$\delta^{15}N$ (‰)	$\delta^{13}C$ (‰)	C:N	GAMM pred.	|pred-yr|
	1	17.55	-	-	-	-	-	-	-
	2	24.48	26.80	1.39	-	-	-	-	-
	3	30.06	41.55	1.23	-	-	-	-	-

Table 5.3 (cont.)

Tusk ID - **2007-002**	Year of growth	Diam (mm)	EIV (cm^3)	Diam increase	$\delta^{15}N$ (‰)	$\delta^{13}C$ (‰)	C:N	GAMM pred.	|pred-yr|
Batch 3	1	14.39	-	-	11.26	-	4.07	-	-
UMSIL	2	19.48	20.09	1.35	10.22	-	5.05	-	-
	3	22.66	25.99	1.16	9.68	-	4.15	-	-
	4	24.21	24.74	1.07	10.09	-	4.13	-	-
	5	27.25	33.10	1.13	9.94	-	4.08	-	-
	6	28.75	31.22	1.06	9.54	-	4.13	-	-
	7 (part.)	30.00	19.82	1.24	9.58	-	4.15	-	-
	Partial years not included			Average	10.12	-	4.27	Average	-
	in Avg., Range, St. Dev.			Range	1.72	-	0.97		
				St. Dev.	0.61	-	0.38		

Tusk ID - **2007-005**	Year of growth	Diam (mm)	EIV (cm^3)	Diam increase	$\delta^{15}N$ (‰)	$\delta^{13}C$ (‰)	C:N	GAMM pred.	|pred-yr|
Batch 5	2	24.17	27.32	-	10.64	-21.73	3.23	-	-
UCSCSIL	3	27.49	38.67	1.14	10.54	-21.71	3.20	2.89	0.11
	4	30.29	43.15	1.10	10.30	-21.72	3.18	3.67	0.33
	5	32.50	53.02	1.07	10.21	-21.88	3.22	4.43	0.57
	6	34.76	59.96	1.07	10.05	-21.61	3.20	5.23	0.77
	7	38.60	84.80	1.11	9.78	-21.48	3.20	6.56	0.44
	8	41.20	78.66	1.07	10.15	-21.53	3.22	7.72	0.28
	9	45.06	101.80	1.09	9.36	-21.60	3.21	9.13	0.13
	10	48.26	105.84	1.07	9.03	-21.66	3.21	10.46	0.46
	11	49.73	112.69	1.03	9.12	-21.94	3.22	11.17	0.17
	12 (part.)	50.68	70.36	1.02	8.68	-21.97	3.23	-	-
	Partial years not included			Average	9.92	-21.69	3.21	Average	0.36
	in Avg., Range, St. Dev.			Range	1.61	0.46	0.05		
				St. Dev.	0.57	0.14	0.02		

Table 5.3 (cont.)

Tusk ID - **2009-001**	Year of growth	Diam (mm)	EIV (cm^3)	Diam increase	$\delta^{15}N$ (‰)	$\delta^{13}C$ (‰)	C:N	GAMM pred.	|pred-yr|
Batch 3	3	22.00	-	-	-	-	-	-	-
UMSIL	4	25.37	26.68	1.15	11.49	-	4.00	3.73	0.27
	5	27.81	32.31	1.10	10.99	-	4.07	5.03	0.03
	6	30.02	38.67	1.08	11.28	-	4.09	6.22	0.22
	7	31.59	45.05	1.05	11.96	-	4.08	7.25	0.25
	8	33.93	49.32	1.07	11.36	-	4.22	8.28	0.28
	9	-	-	-	10.76	-	4.11	-	-
				Average	11.31	-	4.10	Average	0.21
				Range	1.20	-	0.22		
				St. Dev.	0.42	-	0.07		

Tusk ID - **ZCHM-19**	Year of growth	Diam (mm)	EIV (cm^3)	Diam increase	$\delta^{15}N$ (‰)	$\delta^{13}C$ (‰)	C:N	GAMM pred.	|pred-yr|
Batch 4	6	30.45	54.70	-	11.48	-	4.04	-	-
UMSIL	7	31.32	57.81	1.03	11.60	-	3.86	7.36	0.36
	8	34.50	62.98	1.10	~~12.54~~	-	3.59	8.41	0.41
	9	36.80	72.25	1.07	10.51	-	4.70	9.82	0.82
	10	38.00	64.79	1.03	10.96	-	3.89	10.78	0.78
	11	39.10	60.41	1.03	11.33	-	3.85	11.39	0.39
	12	41.25	84.21	1.05	12.17	-	3.87	12.23	0.23
	13	42.88	74.97	1.04	11.85	-	3.83	13.23	0.23
	14 (part.)	44.20	68.45	1.03	-	-	-	-	-
	Partial years not included			Average	11.41	-	3.95	Average	0.46
	in Avg., Range, St. Dev.			Range	1.66	-	1.11		
				St. Dev.	0.55	-	0.33		

Table 5.3 (cont.)

Tusk ID - **ZCHM-20**	Year of growth	Diam (mm)	EIV (cm^3)	Diam increase	$\delta^{15}N$ (‰)	$\delta^{13}C$ (‰)	C:N	GAMM pred.	|pred-yr|
Batch 4	1	15.47	-	-	-	-	-	-	-
UMSIL	2	20.48	18.26	1.32	11.18	-	4.72	-	-
	3	23.48	24.06	1.15	10.64	-	3.98	-	-
	4	25.25	30.76	1.08	10.42	-	3.90	-	-
	5	26.50	33.51	1.05	10.47	-	3.86	-	-
	6	29.20	28.99	1.10	10.55	-	3.90	-	-
	7	30.65	49.68	1.05	11.87	-	3.81	-	-
	8	32.45	50.80	1.06	12.62	-	3.93	-	-
	9	35.23	62.79	1.09	11.86	-	3.91	-	-
	10	36.50	68.77	1.04	11.64	-	3.87	-	-
	11	36.30	54.96	0.99	12.41	-	3.89	-	-
	12 (part.)	37.50	28.78	1.03	-	-	-	-	-
	Partial years not included			Average	11.37	-	3.98	Average	-
	in Avg., Range, St. Dev.			Range	2.20	-	0.91		
				St. Dev.	0.83	-	0.27		

Tusk ID - **ZCHM-22**	Year of growth	Diam (mm)	EIV (cm^3)	Diam increase	$\delta^{15}N$ (‰)	$\delta^{13}C$ (‰)	C:N	GAMM pred.	|pred-yr|
Batch 3	Prenatal	7.40	-	-		-	-	-	-
UMSIL	1	18.35	15.80	2.48	13.85	-	4.20	-	-
	2	24.10	27.67	1.31	13.30	-	4.07	-	-
	3	30.17	47.17	1.25	13.39	-	4.10	-	-
	4	33.50	58.62	1.11	12.07	-	4.10	-	-
	5 (part.)	36.63	62.04	1.09		-	-	-	-
	Partial years not included			Average	13.15	-	4.12	Average	-
	in Avg., Range, St. Dev.			Range	1.78	-	0.13		
				St. Dev.	0.76	-	0.06		

Table 5.3 (cont.)

Tusk ID - **ZCHM-24**	Year of growth	Diam (mm)	EIV (cm^3)	Diam increase	$\delta^{15}N$ (‰)	$\delta^{13}C$ (‰)	C:N	GAMM pred.	|pred-yr|
Batch 5	2	25.45	-	-	-	-	-	-	-
UCSCSIL	3	30.37	56.88	1.19	9.78	-21.08	3.20	3.42	0.42
	4	32.42	49.96	1.07	10.11	-20.88	3.21	4.42	0.42
	5	34.91	88.88	1.08	10.00	-21.32	3.21	5.26	0.26
	6	37.48	95.32	1.07	10.85	-21.28	3.20	6.26	0.26
	7	39.84	86.66	1.06	10.46	-21.24	3.22	7.21	0.21
	8	41.91	96.39	1.05	11.05	-21.19	3.22	8.06	0.06
	9 (part.)	42.54	99.44	1.01	10.11	-21.95	3.25	-	-
	Partial years not included			Average	10.37	-21.16	3.21	Average	0.27
	in Avg., Range, St. Dev.			Range	1.28	0.44	0.02		
				St. Dev.	0.50	0.16	0.01		

Tusk ID - **ZCHM-25**	Year of growth	Diam (mm)	EIV (cm^3)	Diam increase	$\delta^{15}N$ (‰)	$\delta^{13}C$ (‰)	C:N	GAMM pred.	|pred-yr|
Batch 5	3	25.76	22.56	-	-	-	-	-	-
UCSCSIL	4	34.14	51.96	1.33	-	-	-	3.29	0.71
	5	38.88	67.60	1.14	-	-	-	4.67	0.33
	6	39.37	55.16	1.01	-	-	-	5.04	0.96
				Average	-	-	-	Average	0.66
				Range	-	-	-		
				St. Dev.	-	-	-		

Table 5.3 (cont.)

Tusk ID - **ZCHM-26**	Year of growth	Diam (mm)	EIV (cm^3)	Diam increase	$\delta^{15}N$ (‰)	$\delta^{13}C$ (‰)	C:N	GAMM pred.	|pred-yr|
Batch 5	2	22.25	-	-	-	-	-	-	-
UCSCSIL	3	26.94	38.16	1.21	14.55	-22.15	3.19	2.57	0.43
	4	32.24	80.00	1.20	13.80	-22.52	3.21	3.96	0.04
	5	36.00	95.04	1.12	-	-	-	5.53	0.53
	6	40.66	127.47	1.13	13.35	-22.15	3.20	7.30	1.30
	7	43.55	123.16	1.07	13.18	-22.01	3.19	8.62	1.62
	8 (part.)	45.07	121.30	1.03	13.33	-22.02	3.30	-	-
	Partial years not included			Average	13.72	-22.21	3.20	Average	0.79
	in Avg., Range, St. Dev.			Range	1.37	0.51	0.03		
				St. Dev.	0.61	0.21	0.01		

Tusk ID - **ZCHM-42**	Year of growth	Diam (mm)	EIV (cm^3)	Diam increase	$\delta^{15}N$ (‰)	$\delta^{13}C$ (‰)	C:N	GAMM pred.	|pred-yr|
Batch 4	6	33.68	-	-	-	-	-	-	-
UMSIL	7	34.32	46.06	1.02	-	-	-	9.03	2.03
	8	35.27	45.32	1.03	-	-	-	9.42	1.42
	9	36.02	70.56	1.02	-	-	-	9.88	0.88
	10	37.36	68.99	1.04	-	-	-	10.39	0.39
	11	39.60	67.65	1.06	-	-	-	11.33	0.33
	12	40.29	58.10	1.02	-	-	-	12.14	0.14
	13	41.88	42.63	1.04	-	-	-	12.71	0.29
	14	42.24	50.22	1.01	-	-	-	13.25	0.75
	15	43.04	55.27	1.02	-	-	-	13.54	1.46
	16	43.39	74.95	1.01	-	-	-	13.85	2.15
	17	45.79	77.64	1.06	-	-	-	14.58	2.42
				Average	-	-	-	Average	1.11
				Range	-	-	-		
				St. Dev.	-	-	-		

Table 5.3 (cont.)

Tusk ID - **ZCHM-46**	Year of growth	Diam (mm)	EIV (cm^3)	Diam increase	$\delta^{15}N$ (‰)	$\delta^{13}C$ (‰)	C:N	GAMM pred.	|pred-yr|
Batch 4	3	23.88	-	-	-	-	-	-	-
UMSIL	4	31.58	27.46	1.32	-	-	-	3.51	0.49
	5	33.59	35.44	1.06	-	-	-	4.83	0.17
	6	38.23	59.03	1.14	-	-	-	6.33	0.33
	7	41.57	67.02	1.09	-	-	-	7.80	0.80
	8	43.22	55.86	1.04	-	-	-	8.61	0.61
	9	44.92	84.05	1.04	-	-	-	9.27	0.27
	10	46.96	85.28	1.05	-	-	-	10.04	0.04
	11	48.37	105.18	1.03	-	-	-	10.65	0.35
	12	51.72	156.08	1.07	-	-	-	11.80	0.20
	13	53.39	145.07	1.03	-	-	-	12.59	0.41
				Average	-	-	-	Average	0.37
				Range	-	-	-		
				St. Dev.	-	-	-		

Tusk ID - **ZCHM-51**	Year of growth	Diam (mm)	EIV (cm^3)	Diam increase	$\delta^{15}N$ (‰)	$\delta^{13}C$ (‰)	C:N	GAMM pred.	|pred-yr|
Batch 5	5	-	-	-	12.60	-21.07	3.22	-	-
UCSCSIL	6	37.32	68.46		12.70	-20.72	3.18	-	-
	7	39.85	77.77	1.07	12.54	-21.06	3.20	7.20	0.20
	8	40.20	60.59	1.01	12.65	-21.73	3.19	7.55	0.45
	9	42.24	67.64	1.05	12.56	-21.70	3.20	8.19	0.81
	10	46.05	85.36	1.09	13.17	-21.64	3.19	9.53	0.47
	11	48.00	90.61	1.04	13.72	-21.48	3.23	10.46	0.54
				Average	12.70	-21.32	3.20	Average	0.49
				Range	1.18	1.01	0.05		
				St. Dev.	0.44	0.39	0.02		

Table 5.3 (cont.)

Tusk ID - **ZCHM-52**	Year of growth	Diam (mm)	EIV (cm^3)	Diam increase	$\delta^{15}N$ (‰)	$\delta^{13}C$ (‰)	C:N	GAMM pred.	|pred-yr|
	2	22.99	-	-	-	-	-	-	-
	3	26.95	27.48	1.17	-	-	-	2.68	0.32
	4	29.66	39.26	1.10	-	-	-	3.51	0.49
	5	33.05	57.82	1.11	-	-	-	4.47	0.53
	6	35.20	51.17	1.07	-	-	-	5.41	0.59
				Average	-	-	-	Average	0.49
				Range	-	-	-		
				St. Dev.	-	-	-		

Tusk ID - **ZCHM-53**	Year of growth	Diam (mm)	EIV (cm^3)	Diam increase	$\delta^{15}N$ (‰)	$\delta^{13}C$ (‰)	C:N	GAMM pred.	|pred-yr|
	1	15.97	-	-	-	-	-	-	-
	2	21.47	-	1.34	-	-	-	-	-
	3	24.01	29.18	1.12	-	-	-	-	-
	4	25.78	39.03	1.07	-	-	-	-	-
	5	27.75	39.86	1.08	-	-	-	-	-

Tusk ID - **AM-1**	Year of growth	Diam (mm)	EIV (cm^3)	Diam increase	$\delta^{15}N$ (‰)	$\delta^{13}C$ (‰)	C:N	GAMM pred.	|pred-yr|
	1	17.90	-	-	-	-	-	-	-
	2	20.75	16.30	1.16	-	-	-	-	-
	3	23.85	20.00	1.15	-	-	-	-	-
	4	26.32	22.11	1.10	-	-	-	-	-
	5	27.89	23.05	1.06	-	-	-	-	-

Table 5.3 (cont.)

Tusk ID - **AM-2**	Year of growth	Diam (mm)	EIV (cm^3)	Diam increase	$\delta^{15}N$ (‰)	$\delta^{13}C$ (‰)	C:N	GAMM pred.	|pred-yr|
	1	14.67	-	-	-	-	-	-	-
	2	18.56	13.08	1.27	-	-	-	-	-
	3	21.49	18.81	1.16	-	-	-	-	-
	4	23.76	18.99	1.11	-	-	-	-	-

Tusk ID - **AM-3**	Year of growth	Diam (mm)	EIV (cm^3)	Diam increase	$\delta^{15}N$ (‰)	$\delta^{13}C$ (‰)	C:N	GAMM pred.	|pred-yr|
	1	16.36	-	-	-	-	-	-	-
	2	18.20	-	1.11	-	-	-	-	-
	3	22.28	25.70	1.22	-	-	-	-	-
	4	24.33	31.36	1.09	-	-	-	-	-
	5	26.19	35.27	1.08	-	-	-	-	-

Tusk ID - **AM-4**	Year of growth	Diam (mm)	EIV (cm^3)	Diam increase	$\delta^{15}N$ (‰)	$\delta^{13}C$ (‰)	C:N	GAMM pred.	|pred-yr|
	1	15.63	-	-	-	-	-	-	-
	2	22.46	14.25	1.44	-	-	-	-	-
	3	25.11	23.12	1.12	-	-	-	-	-
	4	27.85	36.48	1.11	-	-	-	-	-
	5	29.89	38.44	1.07	-	-	-	-	-

Tusk ID - **AM-5**	Year of growth	Diam (mm)	EIV (cm^3)	Diam increase	$\delta^{15}N$ (‰)	$\delta^{13}C$ (‰)	C:N	GAMM pred.	|pred-yr|
	1	16.06	-	-	-	-	-	-	-
	2	21.66	21.13	1.35	-	-	-	-	-
	3	25.65	30.10	1.18	-	-	-	-	-
	4	31.46	59.78	1.23	-	-	-	-	-

Table 5.3 (cont.)

Tusk ID - **AM-6**	Year of growth	Diam (mm)	EIV (cm^3)	Diam increase	$\delta^{15}N$ (‰)	$\delta^{13}C$ (‰)	C:N	GAMM pred.	|pred-yr|
Batch 5	2	21.91	-	-	10.40	-21.39	3.22	-	-
UCSCSIL	3	29.04	53.16	1.33	10.26	-21.99	3.22	2.82	0.18
	4	33.07	61.21	1.14	9.82	-22.12	3.22	4.40	0.40
	5	35.95	83.11	1.09	10.26	-21.49	3.21	5.62	0.62
	6	37.98	73.12	1.06	10.57	-21.97	3.23	6.51	0.51
	7	-	-	-	10.67	-21.81	3.21	-	-
				Average	10.32	-21.87	3.22	Average	0.43
				Range	0.86	0.73	0.02		
				St. Dev.	0.30	0.29	0.01		

Tusk ID - **AM-7**	Year of growth	Diam (mm)	EIV (cm^3)	Diam increase	$\delta^{15}N$ (‰)	$\delta^{13}C$ (‰)	C:N	GAMM pred.	|pred-yr|
	3	26.09	-	-	-	-	-	-	-
	4	33.84	76.40	1.30	-	-	-	4.29	0.29
	5	34.91	87.13	1.03	-	-	-	5.42	0.42
	6	37.16	80.68	1.06	-	-	-	6.17	0.17
				Average	-	-	-	Average	0.29
				Range	-	-	-		
				St. Dev.	-	-	-		

Tusk ID - **MMY**	Year of growth	Diam (mm)	EIV (cm^3)	Diam increase	$\delta^{15}N$ (‰)	$\delta^{13}C$ (‰)	C:N	GAMM pred.	|pred-yr|
	0	8.23	-	-	-	-	-	-	-
	1	17.10	5.42	2.08	-	-	-	-	-
	2	24.69	20.90	1.44	-	-	-	-	-
	3	26.81	33.58	1.09	-	-	-	-	-
	4	30.71	52.51	1.15	-	-	-	-	-
	5	32.81	54.60	1.07	-	-	-	-	-

Table 5.4. Results of isotope standards run with tusk analyses.
Results for relevant standards run with each batch of analyses are reported separately. Analyses were divided between the University of Michigan Stable Isotope Lab (UMSIL) and the University of California Santa Cruz Stable Isotope Lab (UCSCSIL). Results of UCSCSIL internal calibrated standards were all within expected ranges and are not listed.

	Assoc.		sample	N mass	$\delta^{15}N$	C mass	$\delta^{13}C$	
Batch 1	analyses	Standard	mass (mg)	(mg)	(‰)	(mg)	(‰)	C:N
UMSIL	2000-305	Acetanilide	0.19	0.02	-	-	-	-
12/22/2014	($\delta^{13}N$ only)	Acetanilide	0.40	0.04	-	0.29	-	8.05
		Acetanilide	0.61	0.06	-	0.44	-	8.04
		Acetanilide	0.89	0.09	-	0.61	-	7.86
		Acetanilide	1.19	0.12	-	0.86	-	8.11
		Acetanilide	0.88	0.09	-	0.62	-	7.88
			Average	0.07	-	0.56	-	7.99
			St. Dev.	0.04	-	0.21	-	0.11
		IAEA N2	0.45	0.09	20.30	-	-	-
		IAEA N2	0.47	0.10	20.40	-	-	-
		IAEA N2	0.47	0.10	20.21	-	-	-
			Average	0.10	20.30	-	-	-
			St. Dev.	0.00	0.09	-	-	-
		USGS 25	0.45	0.09	-30.55	-	-	-
		USGS 25	0.47	0.10	-30.36	-	-	-
		USGS 25	0.46		-30.29	-	-	-
			Average	0.10	-30.40	-	-	-
			St. Dev.	0.00	0.14	-	-	-

Table 5.4 (cont.)

	Assoc.		sample	N mass	$\delta^{15}N$	C mass	$\delta^{13}C$	
Batch 2	analyses	Standard	mass (mg)	(mg)	(‰)	(mg)	(‰)	C:N
UMSIL	2000-305	Acetanilide	0.19	0.02	-	0.13	-33.72	7.76
1/5/2015	($\delta^{13}C$ only)	Acetanilide	0.41	0.04	-	0.29	-33.76	8.11
		Acetanilide	0.60	0.06	-	0.43	-33.88	7.94
		Acetanilide	0.80	0.08	-	0.56	-33.84	8.02
		Acetanilide	1.19	0.12	-	0.85	-33.75	8.02
		Acetanilide	0.88	0.09	-	0.63	-33.84	8.02
		Acetanilide	0.89	0.09	-	0.63	-33.77	8.02
		Acetanilide	0.89	0.09	-	0.69	-33.84	9.12
			Average	0.08	-	0.53	-	8.13
			St. Dev.	0.03	-	0.23	-	0.41
	IAEA 600 Caffeine		0.69	28.58	-	0.34	-27.77	0.01
	IAEA 600 Caffeine		0.68	28.51	-	0.34	-27.76	0.01
	IAEA 600 Caffeine		0.69	28.45	-	0.38	-27.78	0.02
			Average	28.51	-	-	-	-
			St. Dev.	0.06	-	-	-	-
	IAEA-CH-6 Sucrose		0.78	-	-	0.31	-10.42	-
	IAEA-CH-6 Sucrose		0.77	-	-	0.32	-10.43	-
	IAEA-CH-6 Sucrose		0.79	-	-	0.35	-10.51	-
			Average	-	-	-	-	-
			St. Dev.	-	-	-	-	-

Table 5.4 (cont.)

	Assoc.		sample	N mass	δ^{15}N	C mass	δ^{13}C	
Batch 3	analyses	Standard	mass (mg)	(mg)	(‰)	(mg)	(‰)	C:N
UMSIL	TA-3	Acetanilide	0.20	0.02	-	0.14	-	7.72
2/6/2015	2007-002	Acetanilide	0.40	0.04	-	0.28	-	8.05
	ZCHM-22	Acetanilide	0.60	0.06	-	0.43	-	7.96
	2009-001	Acetanilide	0.80	0.08	-	0.57	-	7.94
	(δ^{15}N only)	Acetanilide	0.89	0.09	-	0.64	-	8.34
		Acetanilide	0.89	0.09	-	0.64	-	8.15
		Acetanilide	0.89	0.09	-	0.65	-	8.36
		Acetanilide	1.20	0.12	-	0.85	-	8.03
			Average	0.08	-	0.53	-	8.07
			St. Dev.	0.03	-	0.23	-	0.21
		IAEA N2	0.40	0.08	20.56	-	-	-
		IAEA N2	0.40	0.08	20.26	-	-	-
		IAEA N2	0.41	0.08	20.07	-	-	-
			Average	0.08	20.30	-	-	-
			St. Dev.	0.00	0.25	-	-	-
		USGS 25	0.40	0.08	-30.37	-	-	-
		USGS 25	0.40	0.08	-30.57	-	-	-
		USGS 25	0.41	0.08	-30.26	-	-	-
			Average	0.08	-30.40	-	-	-
			St. Dev.	0.00	0.16	-	-	-

Table 5.4 (cont.)

	Assoc.		sample	N mass	δ^{15}N	C mass	δ^{13}C	
Batch 4	analyses	Standard	mass (mg)	(mg)	(‰)	(mg)	(‰)	C:N
UMSIL	2000-246	Acetanilide	0.40	0.04	-	0.28	-	8.05
2/10/2015	2000-286	Acetanilide	0.60	0.06	-	0.42	-	7.94
	ZCHM-19	Acetanilide	0.80	0.08	-	0.57	-	7.99
	ZCHM-20	Acetanilide	1.20	0.12	-	0.85	-	7.99
	(δ^{15}N only)	Acetanilide	0.20	0.02	-	-	-	-
		Acetanilide	0.88	0.09	-	0.64	-	8.19
		Acetanilide	0.88	0.09	-	0.65	-	8.38
		Acetanilide	0.89	0.09	-	0.65	-	8.30
			Average	0.08	-	0.58	-	8.12
			St. Dev.	0.03	-	0.18	-	0.17
		IAEA N2	0.40	0.08	20.33	-	-	-
		IAEA N2	0.40	0.08	20.32	-	-	-
		IAEA N2	0.40	0.08	20.25	-	-	-
			Average	0.08	20.30	-	-	-
			St. Dev.	0.00	0.04	-	-	-
		USGS 25	0.40	0.08	-30.43	-	-	-
		USGS 25	0.39	0.08	-30.60	-	-	-
		USGS 25	0.39	0.08	-30.17	-	-	-
			Average	0.08	-30.40	-	-	-
			St. Dev.	0.00	0.22	-	-	-

Table 5.4 (cont.)

	Assoc.		sample	N mass	$\delta^{15}N$	C mass	$\delta^{13}C$	
Batch 5	analyses	Standard	mass (mg)	(mg)	(‰)	(mg)	(‰)	C:N
UCSCSIL	2000-245	Acetanilide	0.57	0.06	1.00	0.41	-29.57	8.06
9/30/2015	ZCHM-51	Acetanilide	0.58	0.06	1.17	0.41	-29.60	8.03
	ZCHM-26	Acetanilide	0.60	0.06	1.08	0.43	-29.64	8.05
	ZCHM-24	Acetanilide	0.22	0.02	1.22	0.15	-29.36	7.84
	AM-6		Average	0.05	-	0.35	-	8.00
	2007-005		St. Dev.	0.02	-	0.13	-	0.10

Figure 5.1. Regions represented by tusks used in this study.
All tusks used in this study come from high latitude sites in Taimyr, Yakutia, and Chukotka in northcentral and northeastern Siberia. Precise locations may be available for some of the specimens but are not reported here.

Figure 5.2. Tusk CT-increment measurement protocol.
MicroCT data for tusk ZCHM-22 scanned in 4 sections and reassembled virtually. (A) Projection of a longitudinal slice through tusk axis averaged over 1 mm thickness in *z*-dimension. (B) Projection of transverse slice orthogonal to tusk axis.
Diameter reported for each year of growth is the average of major (d_{maj}) and minor diameter (d_{min}) measured from a transverse slice (B) at the proximal end of an annual increment's length measurement (*L*) excluding the cementum outer layer. When full diameter of a tusk was not present, diameters were estimated by doubling radial measurements. Annual estimated increment volume (EIV) was calculated using d_{maj}, d_{min}, and *L*, which is the average distance from one year boundary to next measured along two lines midway between the tusk axis (traced in (A) with a black line) and the cementum dentin junction (*CDJ*, traced in (A) with a black line). (see *Chapter 2* for further explanation of increment length). Displayed measurement scheme for the increment between the 1st and 2nd year boundaries corresponds to year 2 of growth.

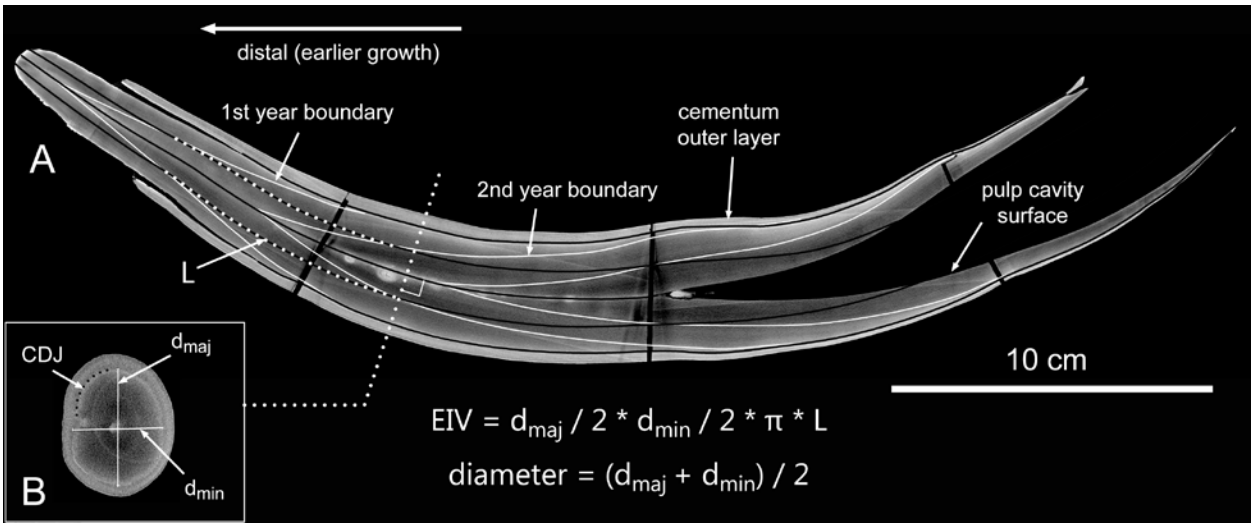

Figure 5.3. Tusk growth trajectories showing ontogenetic pattern and sexual divergence. Growth series for all 29 juvenile woolly mammoth tusks used in this study. (A) shows annual diameters (see Figure 5.2) and (B) shows annual EIVs (see Figures 5.2, 2.3) for the record contained in each tusk. Both increment measurements are plotted on logged axes. Records for tusks with distal tip preserved are anchored at year 1 (1st year of growth represented). Anchored records can be separated into 2 groups with generally different trajectories. Identification as *male* and *female* in these plots is based on whether they are part of the high or low trajectory group and has not yet been confirmed by other data. Male and female GAMMs used to estimate timing of growth records for 14 tusks missing their distal ends were based on these 15 tusks. Timing of the 14 *unknown* records are plotted here according to results of GAMM predictions. Sex determinations for *unknown* records (listed in Table 5.1) are based whether the male or female GAMM provided a better growth interval prediction (see *Methods: Estimating sex and ontogenetic timing of tusk records*).

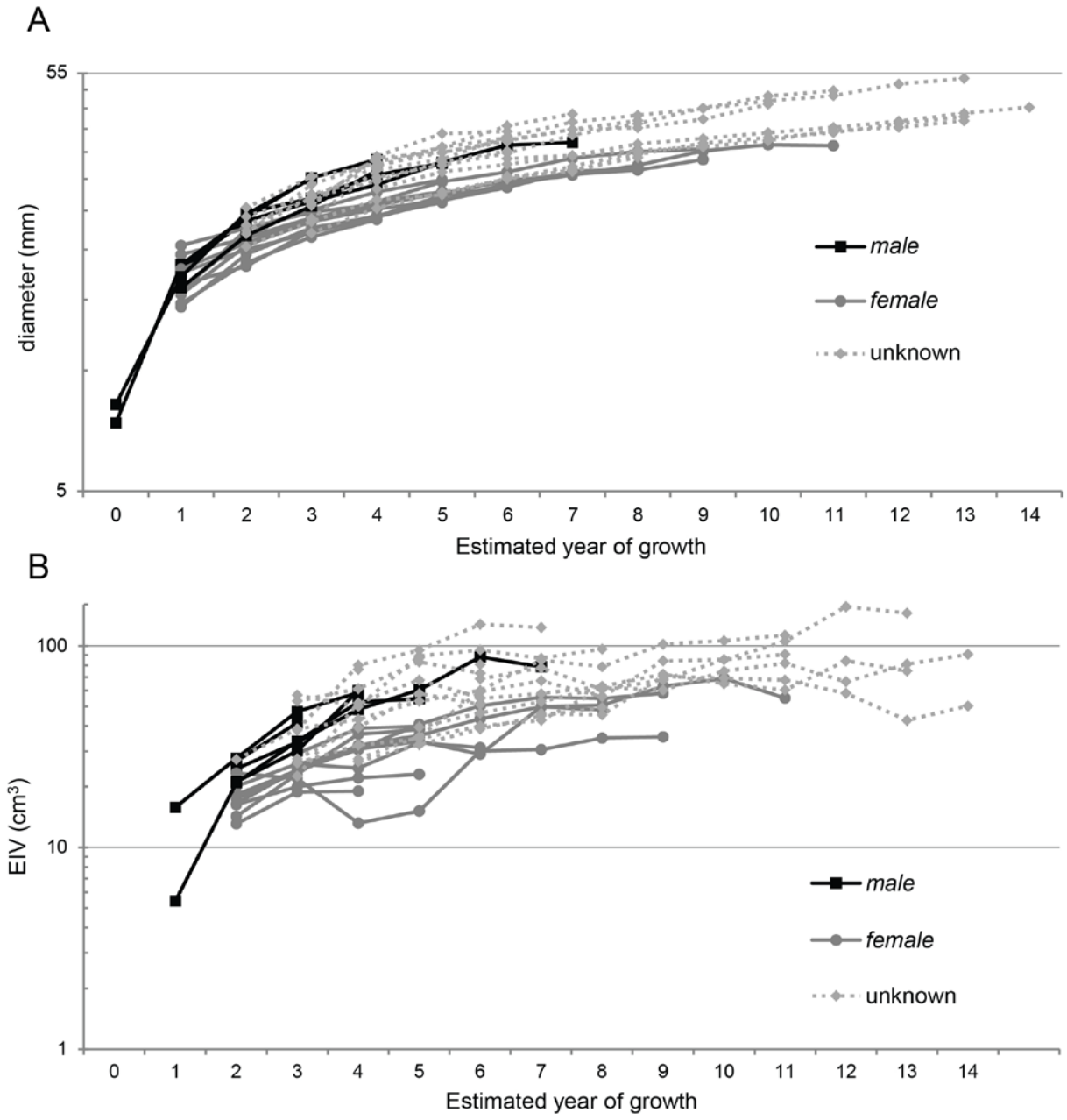
A
55
5
diameter (mm)
male
female
unknown
0 1 2 3 4 5 6 7 8 9 10 11 12 13 14
Estimated year of growth
B
100
10
1
EIV (cm3)
male
female
unknown
0 1 2 3 4 5 6 7 8 9 10 11 12 13 14
Estimated year of growth

Figure 5.4. Sampling scheme for isotope analysis of annual growth increments.
Stable isotope records reported in this study represent serial analyses of annual dentin growth increments, each sampled evenly across an entire year from one year-boundary to the next. Annual increments of growth in CT scans (A) guided planning of samples (B) that were traced onto tusk surfaces (C) for sampling using a manually controlled milling station. Tusk displayed here is TA-3.

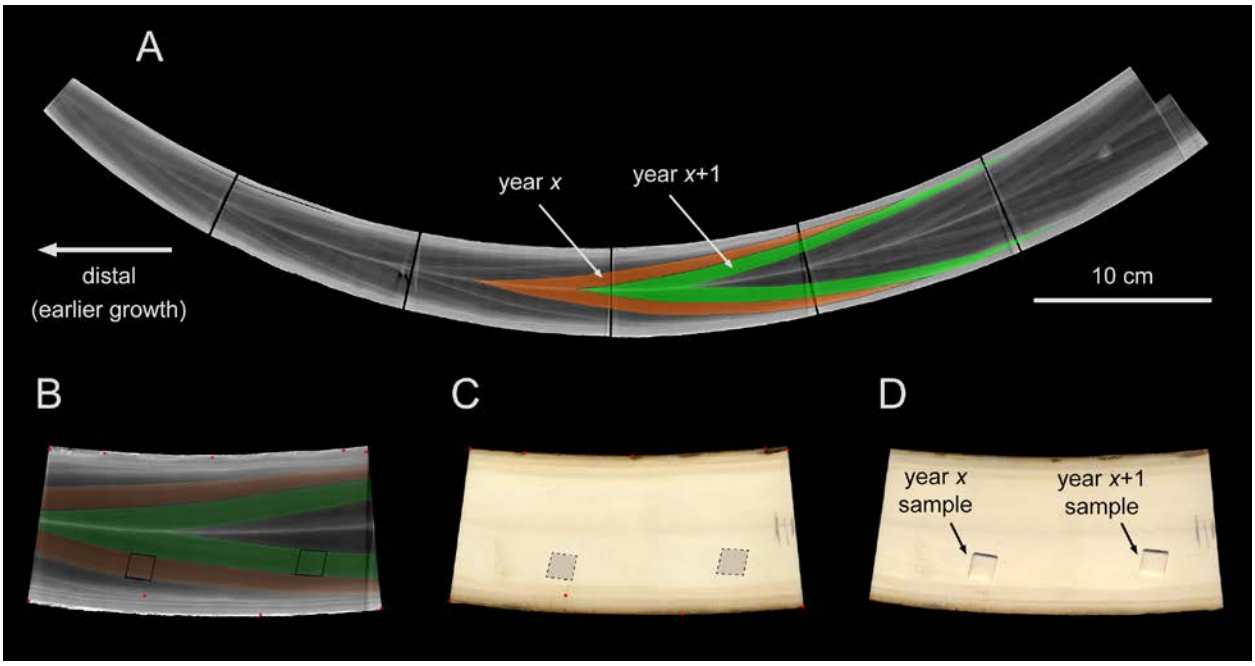

Figure 5.5. Dentin collagen pretreatment test results.
A block sample of dentin from a mastodon premaxillary tusk ("Loc. 8") from the Ziegler Reservoir fossil site assemblage was split into two pieces that each represent approximately equivalent growth intervals. After demineralization with 0.5 M HCl, one was treated with chloroform-methanol (C:M = 2:1) to remove lipids (see *Chapter 2* – Fisher et al., 2014: *Methods*) and the other was not. A powder sample approximately representing the same growth interval as the block samples was divided into six subsamples. Three of these were for demineralized using the procedure described above (*Methods: Isotope analyses*) that does not include a 'defatting' step. The other three were treated with C:M for 5 minutes and rinsed 5 times with ultrapure (double-deionized) water prior to demineralization. The original powder sample and two block samples are equivalent to the precision afforded by the sampling method (see *Chapter 2* – Fisher et al., 2014; Rountrey et al., 2009). The powder sample was mixed thoroughly (sample was suspended in ultrapure water and vortexed for 1 minute) prior to being divided into six equal samples to ensure sample consistency. (A) Atomic ratio of carbon:nitrogen (C:N) plotted for each sample. Samples not treated with C:M have higher average C:N for blocks and powders, a probable indication of trace lipids in dentin samples. (B) Carbon and nitrogen isotope values for all test samples. Error bars are set to machine precision (± 0.12 ‰) for carbon and nitrogen in the University of Michigan Stable Isotope Lab. Samples that were not 'defatted' have slightly lower average $\delta^{13}C$ and slightly higher $\delta^{15}N$ than those that were treated with C:M. One defatted powder sample and one block sample not treated with C:M have anomalous measurements. Including anomalous results, samples treated with C:M have more scatter (higher standard deviations) for $\delta^{15}N$ and less scatter for $\delta^{13}C$. Data are presented in Table 5.2.

A

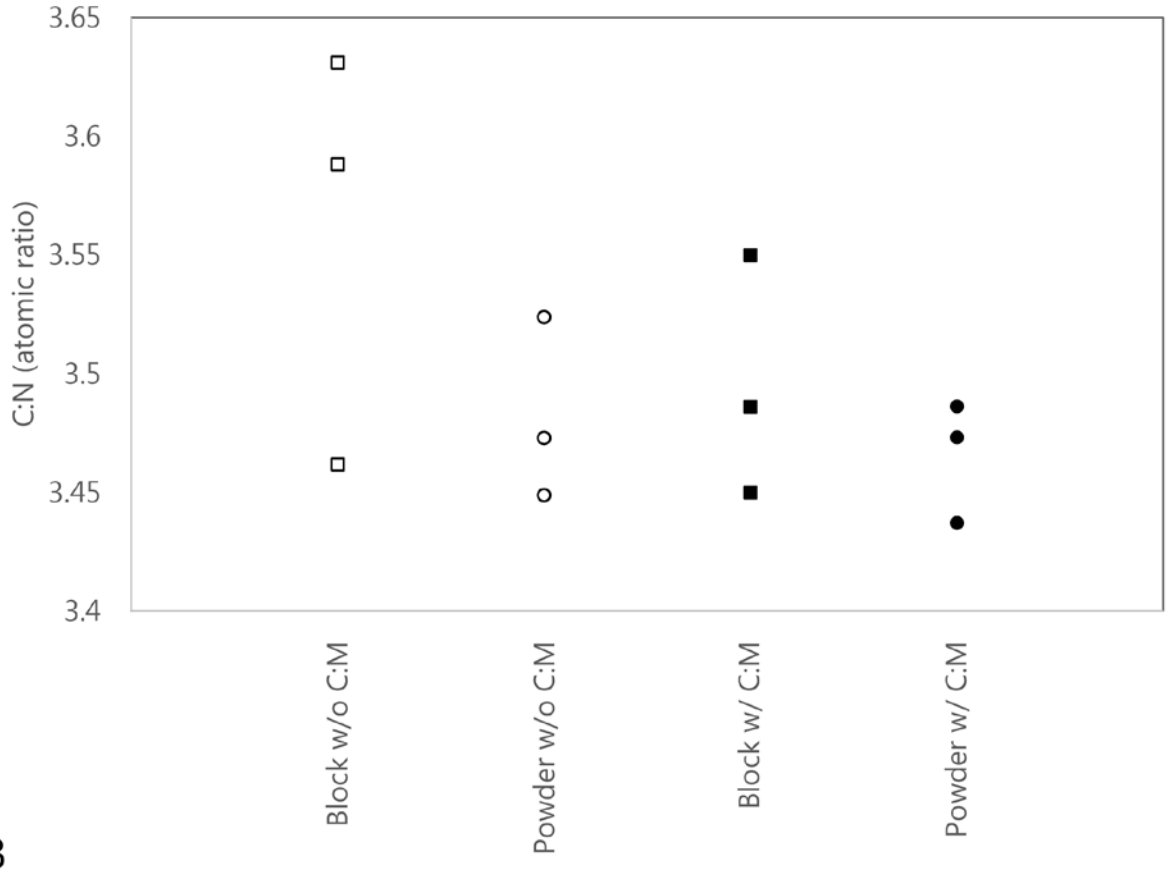
3.65
3.6
3.55
3.5
3.45
3.4
C:N (atomic ratio)
Block w/o C:M
Powder w/o C:M
Block w/ C:M
Powder w/ C:M

B

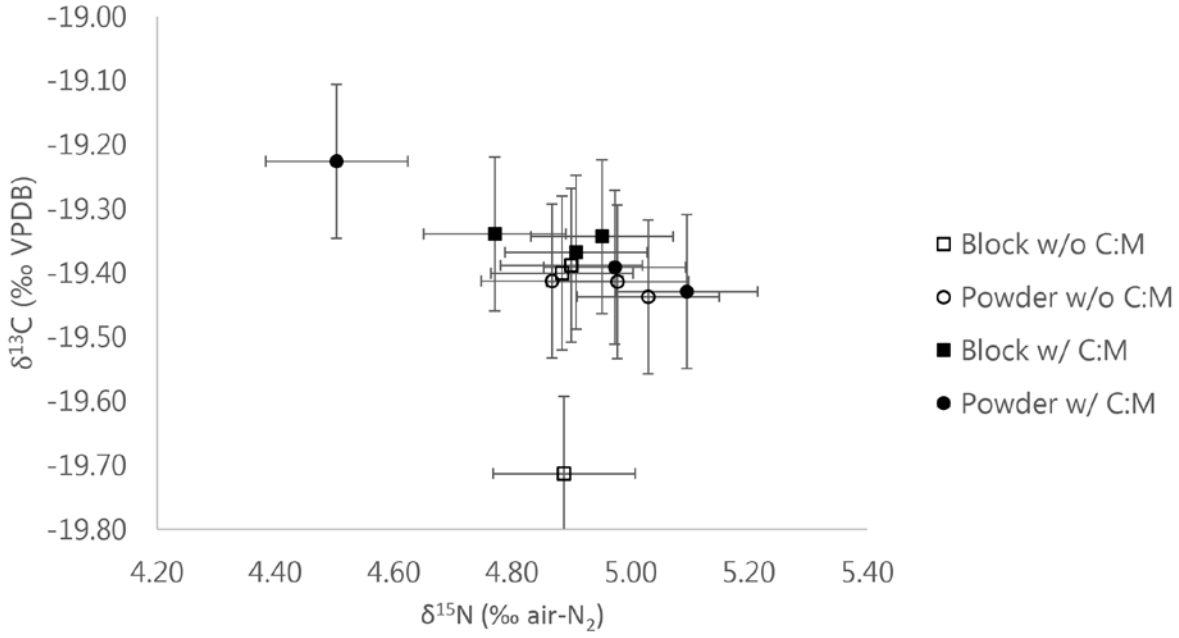
-19.00
-19.10
-19.20
-19.30
-19.40
-19.50
-19.60
-19.70
-19.80
δ13C (‰ VPDB)
4.20
4.40
4.60
4.80
5.00
5.20
5.40
δ15N (‰ air-N2)
Block w/o C:M
Powder w/o C:M
Block w/ C:M
Powder w/ C:M

Figure 5.6. Possible neonatal features in fully preserved tusk tips.
A set of low-density growth lines may indicate the time of birth in microCT growth records of some tusks included in this study. The feature is marked with arrows in the magnified inset that shows the tip of the tusk in finer detail. Traces of enamel indicate that this tusk contains some of the earliest dentin formed. A piece of enamel, showing as a small bright rectangle laying along the outer surface of the dentin, can be seen top-center in the inset. The tusk shown here is 2003-857.

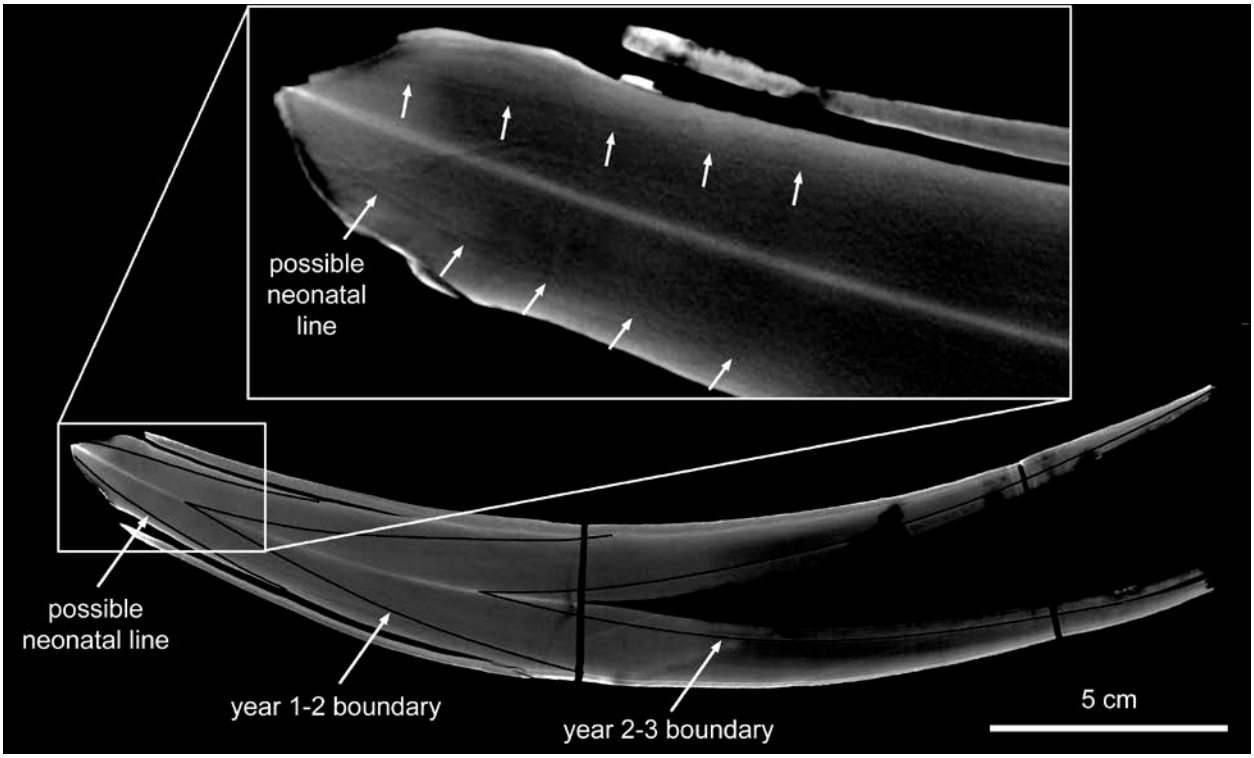

Figure 5.7. Temporal distribution of minimum $\delta^{15}N$ for each tusk analyzed.
Minimum $\delta^{15}N$ for each tusk analyzed is plotted against its radiocarbon date. Two tusks analyzed for nitrogen isotope composition were too old for reliable radiocarbon dating and are displayed at the bottom of the plot indicating their apparent antiquity (~ >40,000 years BP). Error bars show the confidence intervals for reliable AMS ^{14}C dates. The last glacial maximum (LGM) is designated as the interval from 19 – 26.5 k ^{14}C years BP (Clark et al., 2009). The approximate time of mammoth extirpation is indicated as 10 k years BP. Two of the tusks have dates very close to that time. Geographic region for each specimen is marked next to its data point (key included). Excluding tusks from Chukotka (the remainder of which are almost entirely from Taimyr), minimum $\delta^{15}N$ shows a slight trend to lower values throughout the ~ 30 ka interval. Chukotka specimens fall along this same trend except during the LGM when their minimum $\delta^{15}N$ values are about 2 – 3 ‰ higher than expected.

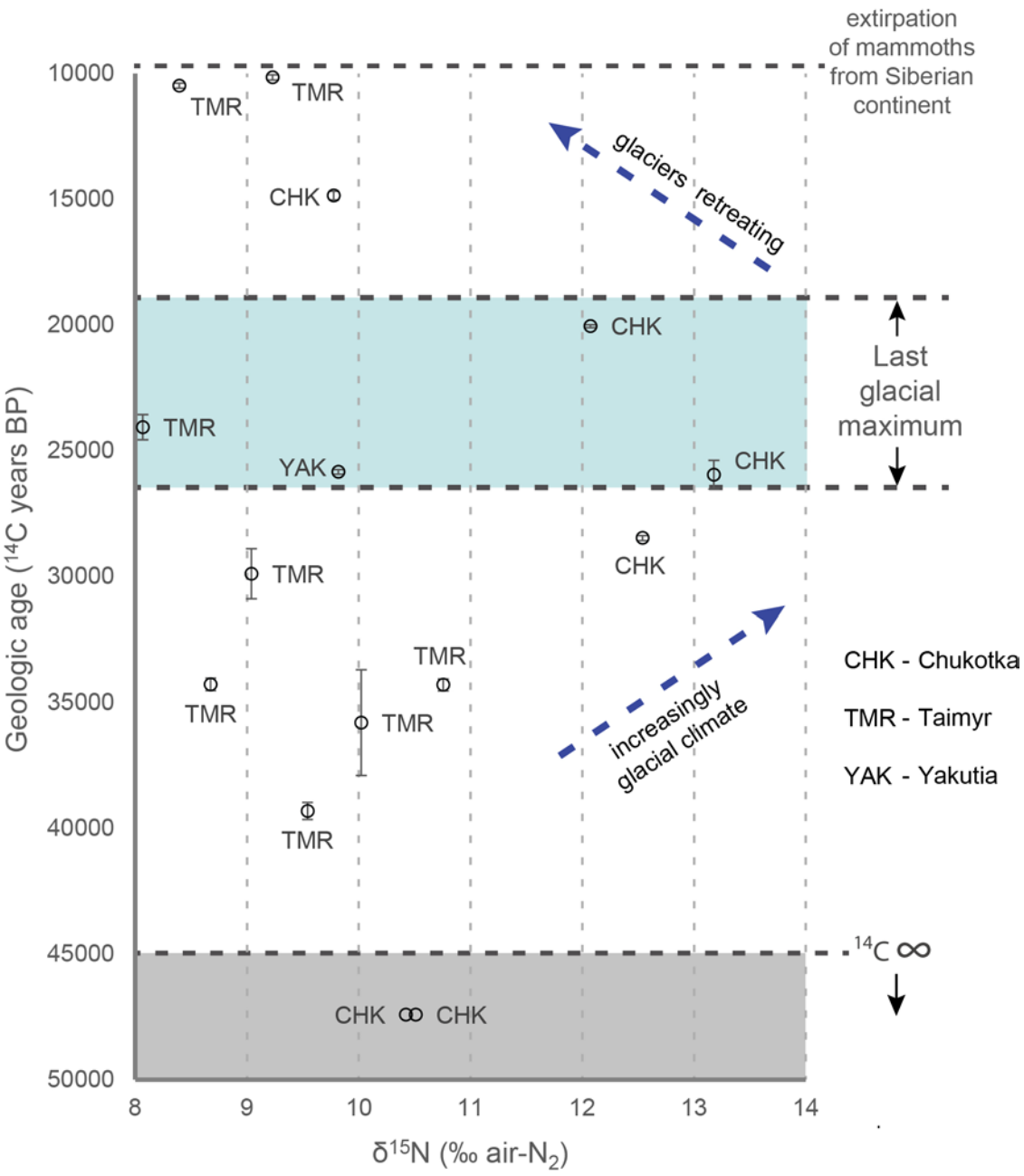
extirpation of mammoths from Siberian continent
glaciers retreating
Last glacial maximum
increasingly glacial climate
CHK - Chukotka
TMR - Taimyr
YAK - Yakutia
$^{14}C\ \infty$
Geologic age (^{14}C years BP)
$\delta^{15}N$ (‰ air-N_2)
10000
15000
20000
25000
30000
35000
40000
45000
50000
8
9
10
11
12
13
14
TMR
CHK
YAK

Figure 5.8. TA-3 isotope and growth records.
Serial records of (A) $\delta^{15}N$, (B) $\delta^{13}C$ [no data], and (C) EIV (see Figures 5.2, 2.3) of specimen TA-3 are plotted for comparison. To maintain a consistent format for easy comparison between records of different tusks, the $\delta^{13}C$ plot is included even though no data is available for this tusk, and years 1 – 13 are displayed even though none of the tusks contain that entire interval of growth. Vertical axes for isotope records are similarly inclusive spanning 8 ‰ in both the $\delta^{15}N$ and $\delta^{13}C$ charts, even though maximum within-tusk variation is significantly less than that. EIVs are plotted on a log scale to better represent their geometric increase. Interpreted weaning age is marked with an arrow on the $\delta^{15}N$ plot. Precise EIV calculations could not be made for the early portion of this record when weaning apparently occurred, but they do display a small decrease in year 9 coincident with a slight increase in $\delta^{15}N$.

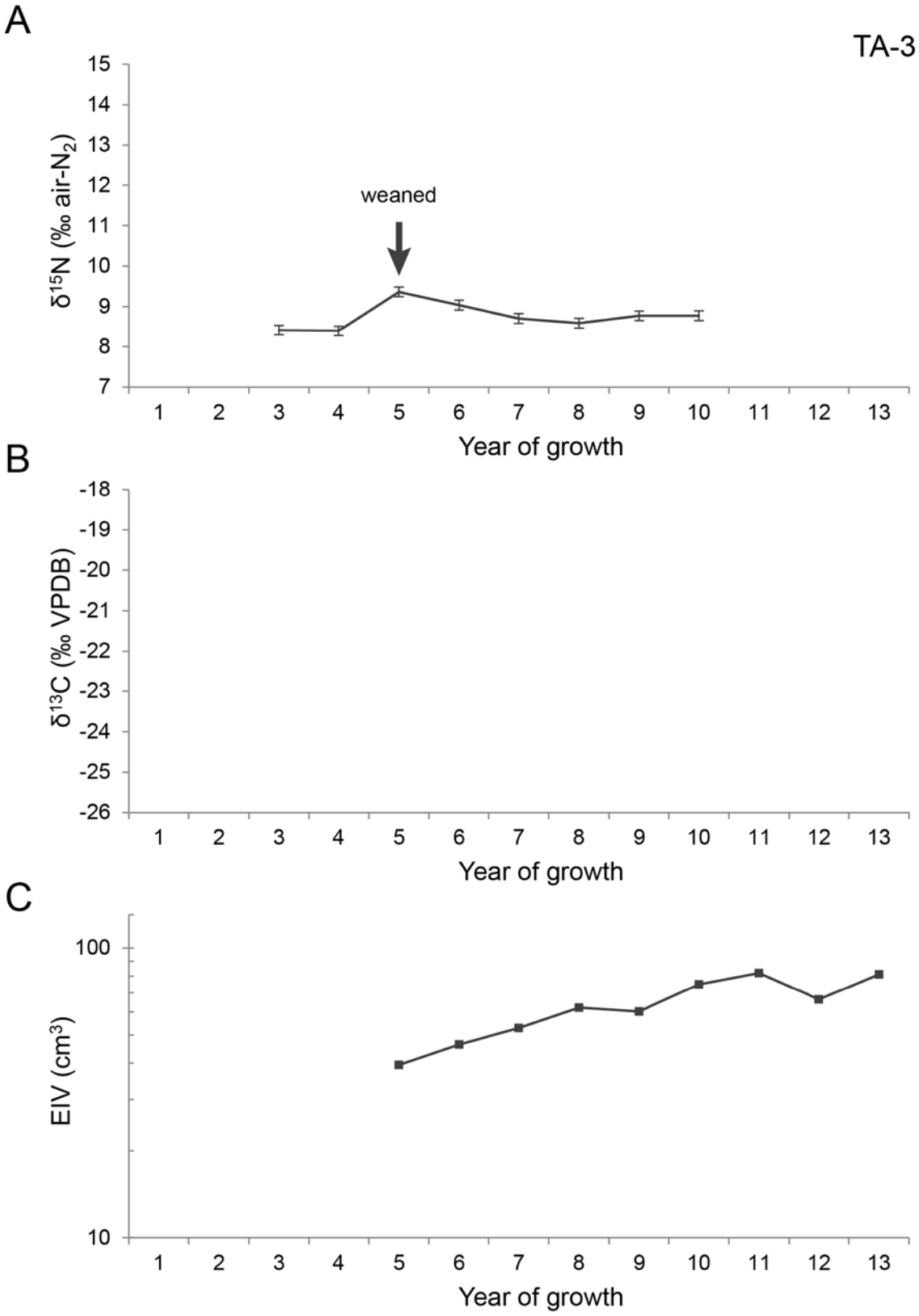
A
TA-3
15
14
13
12
11
10
9
8
7
δ15N (‰ air-N2)
weaned
1
2
3
4
5
6
7
8
9
10
11
12
13
Year of growth
B
-18
-19
-20
-21
-22
-23
-24
-25
-26
δ13C (‰ VPDB)
1
2
3
4
5
6
7
8
9
10
11
12
13
Year of growth
C
100
10
EIV (cm3)
1
2
3
4
5
6
7
8
9
10
11
12
13
Year of growth

Figure 5.9. 2000-245 isotope and growth records.
Serial records of (A) $\delta^{15}N$, (B) $\delta^{13}C$, and (C) EIV (see Figures 5.2, 2.3) of specimen 2000-245 are plotted for comparison. To maintain a consistent format for easy comparison between records of different tusks, years 1 – 13 are displayed even though none of the tusks contain that entire interval of growth. Vertical axes for isotope records are similarly inclusive spanning 8 ‰ in both the $\delta^{15}N$ and $\delta^{13}C$ charts, even though maximum within-tusk variation is significantly less than that. EIVs are plotted on a log scale to better represent their geometric increase. Interpreted weaning age is marked with an arrow on the $\delta^{15}N$ plot, where there is an abrupt spike following a sustained decrease. When available, carbon records do not show a consistent relationship to nitrogen, EIV fluctuations, or interpreted weaning ages. The sample for year 4 was omitted due to a high C:N value. The EIV record displays a slight decrease in year 8 coincident with evidence for weaning in the $\delta^{15}N$ record. Years 1 and 4 are missing from the $\delta^{13}C$ due to abnormally high carbon weight percent for those samples (see Table 5.3).

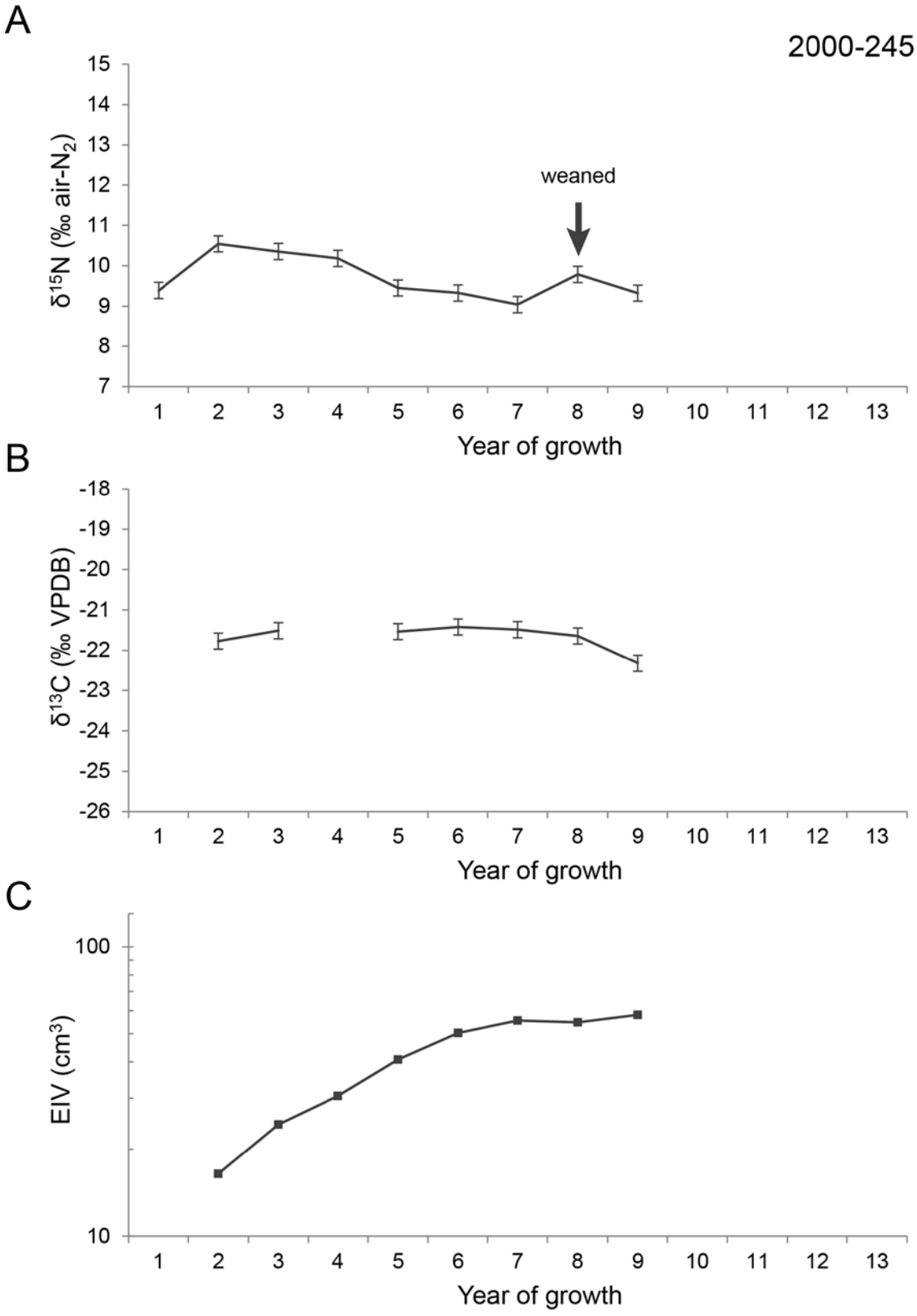
A
2000-245
15
14
13
12
11
10
9
8
7
δ15N (‰ air-N2)
weaned
1
2
3
4
5
6
7
8
9
10
11
12
13
Year of growth
B
-18
-19
-20
-21
-22
-23
-24
-25
-26
δ13C (‰ VPDB)
1
2
3
4
5
6
7
8
9
10
11
12
13
Year of growth
C
100
10
EIV (cm3)
1
2
3
4
5
6
7
8
9
10
11
12
13
Year of growth

Figure 5.10. 2000-246 isotope and growth records.
Serial records of (A) $\delta^{15}N$, (B) $\delta^{13}C$ [no data], and (C) EIV (see Figures 5.2, 2.3) of specimen 2000-246 are plotted for comparison. To maintain a consistent format for easy comparison between records of different tusks, the $\delta^{13}C$ plot is included even though no data is available for this tusk, and years 1 – 13 are displayed even though none of the tusks contain that entire interval of growth. Vertical axes for isotope records are similarly inclusive spanning 8 % in both the $\delta^{15}N$ and $\delta^{13}C$ charts, even though maximum within-tusk variation is significantly less than that. EIVs are plotted on a log scale to better represent their geometric increase. Interpreted weaning age is marked with an arrow on the $\delta^{15}N$ plot. In this nearly flat $\delta^{15}N$ profile, year 5 has the first increase that is too big to be accommodated by analytical error alone. Evidence for weaning in this tusk is weak, but consistent year-to-year $\delta^{15}N$ values are inconsistent with continued nursing. High resolution sampling could help resolve this estimate. The EIV record displays a slight decrease in year 5 coincident with evidence for weaning in the $\delta^{15}N$ record.

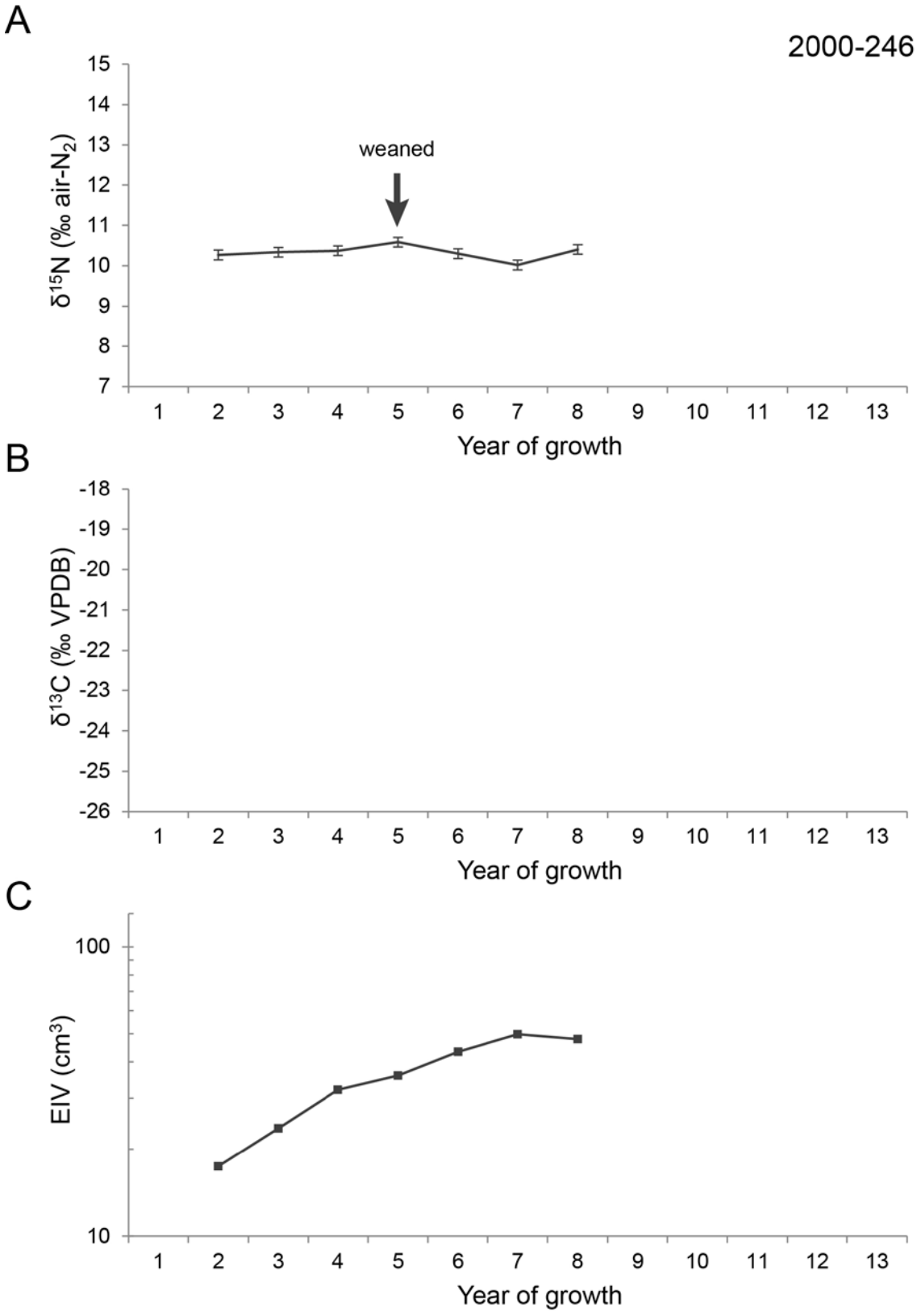
A
2000-246
weaned
$\delta^{15}N$ (‰ air-N_2)
15
14
13
12
11
10
9
8
7
1 2 3 4 5 6 7 8 9 10 11 12 13
Year of growth
B
$\delta^{13}C$ (‰ VPDB)
-18
-19
-20
-21
-22
-23
-24
-25
-26
1 2 3 4 5 6 7 8 9 10 11 12 13
Year of growth
C
EIV (cm^3)
100
10
1 2 3 4 5 6 7 8 9 10 11 12 13
Year of growth

Figure 5.11. 2000-286 isotope and growth records.
Serial records of (A) $\delta^{15}N$, (B) $\delta^{13}C$ [no data], and (C) EIV (see Figures 5.2, 2.3) of specimen 2000-286 are plotted for comparison. To maintain a consistent format for easy comparison between records of different tusks, the $\delta^{13}C$ plot is included even though no data is available for this tusk, and years 1 – 13 are displayed even though none of the tusks contain that entire interval of growth. Vertical axes for isotope records are similarly inclusive spanning 8 ‰ in both the $\delta^{15}N$ and $\delta^{13}C$ charts, even though maximum within-tusk variation is significantly less than that. EIVs are plotted on a log scale to better represent their geometric increase. Interpreted weaning age is marked with an arrow on the $\delta^{15}N$ plot. This nearly flat $\delta^{15}N$ profile does not contain an increase outside the range of analytical error, but year 4 has the first measured increase. In that same year, the EIV profile displays a slight increase, which could considered a contraindication of weaning. Evidence for weaning in this tusk is inconclusive, but may have occurred in year 4. Year 7 has a lower than expected EIV based on the growth trend, but is not accompanied by a significant increase in $\delta^{15}N$. The lack of any sustained decrease is inconsistent with weaning being delayed to year 7. Year-to-year consistency in $\delta^{15}N$ suggests that weaning may have occurred very early in this individual, possibly even as early as year 2 or 3. A relatively deep pulp cavity and rapidly increasing diameter identify this as a male tusk. However, among male tusks it displays one of the lowest EIV growth trajectories. Its death before the end of year 8 may have resulted from long-term deficiencies, which, given its late ^{14}C date, could be seen as evidence for climate stress right at the end of the Pleistocene. Alternatively, considering the lack of evidence for prolonged nursing, this could be an animal had long-term negative consequences from being weaned too early. For this study, I estimate weaning age at 4 years. This is the earliest estimate of all tusks included, but 2 other post-LGM tusks display more clear records of relatively early weaning.

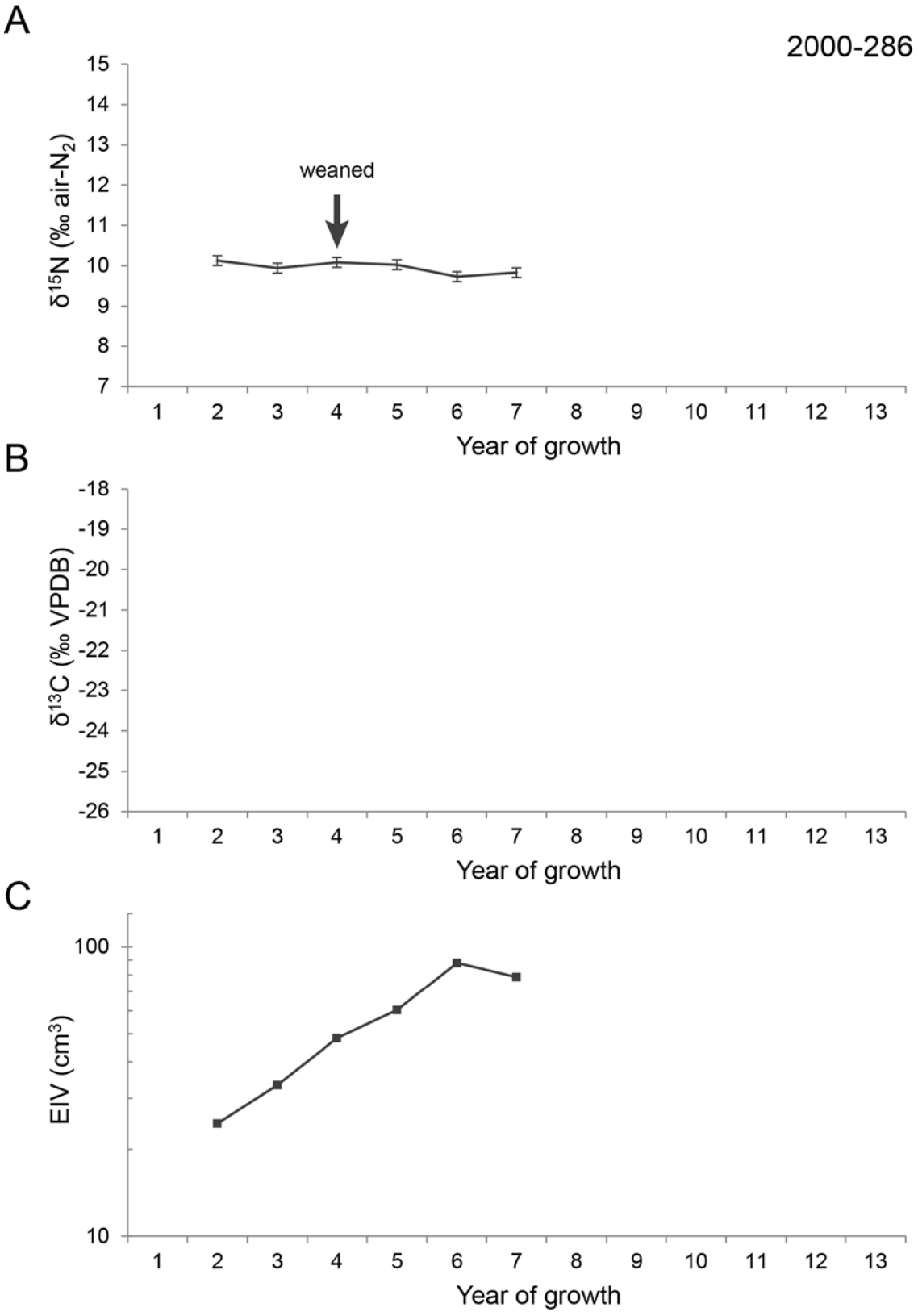
A
2000-286
15
14
13
12
11
10
9
8
7
δ15N (‰ air-N2)
weaned
1 2 3 4 5 6 7 8 9 10 11 12 13
Year of growth
B
-18
-19
-20
-21
-22
-23
-24
-25
-26
δ13C (‰ VPDB)
1 2 3 4 5 6 7 8 9 10 11 12 13
Year of growth
C
100
10
EIV (cm3)
1 2 3 4 5 6 7 8 9 10 11 12 13
Year of growth

Figure 5.12. 2000-305 isotope and growth records.
Serial records of (A) $\delta^{15}N$, (B) $\delta^{13}C$, and (C) EIV (see Figures 5.2, 2.3) of specimen 2000-305 are plotted for comparison. To maintain a consistent format for easy comparison between records of different tusks, years 1 – 13 are displayed even though none of the tusks contain that entire interval of growth. Vertical axes for isotope records are similarly inclusive spanning 8 % in both the $\delta^{15}N$ and $\delta^{13}C$ charts, even though maximum within-tusk variation is significantly less than that. EIVs are plotted on a log scale to better represent their geometric increase. Interpreted weaning age is marked with an arrow on the $\delta^{15}N$ plot, where there is an abrupt spike following a sustained and tapering decrease. When available, carbon records do not show a consistent relationship to nitrogen, EIV fluctuations, or interpreted weaning ages. In this record, the carbon record closely tracks the nitrogen record and also includes a spike in year 7. Since $\delta^{13}C$ records are quite variable in analyzed specimens, it is unclear if this increase in $\delta^{13}C$ can be attributed to weaning, but it does match the a priori expectation for the effect of removing the carbon-light milk fat from the calf's diet. The EIV record displays a slight decrease in year 7 coincident with evidence for weaning in the $\delta^{15}N$ record.

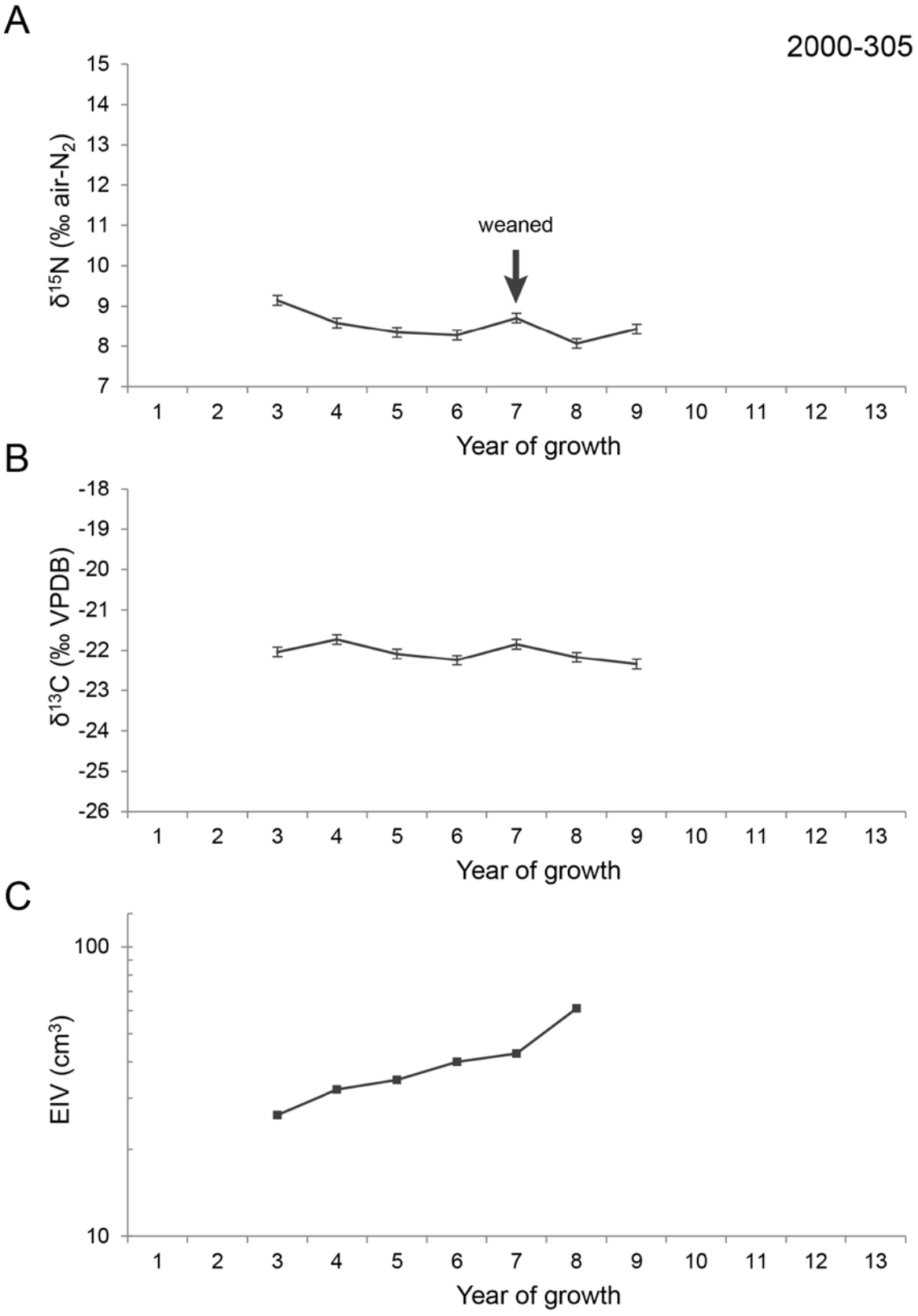
A
2000-305
15
14
13
12
11
10
9
8
7
δ15N (‰ air-N2)
weaned
1 2 3 4 5 6 7 8 9 10 11 12 13
Year of growth
B
-18
-19
-20
-21
-22
-23
-24
-25
-26
δ13C (‰ VPDB)
1 2 3 4 5 6 7 8 9 10 11 12 13
Year of growth
C
100
10
EIV (cm3)
1 2 3 4 5 6 7 8 9 10 11 12 13
Year of growth

Figure 5.13. 2007-002 isotope and growth records.
Serial records of (A) $\delta^{15}N$, (B) $\delta^{13}C$ [no data], and (C) EIV (see Figures 5.2, 2.3) of specimen 2007-002 are plotted for comparison. To maintain a consistent format for easy comparison between records of different tusks, the $\delta^{13}C$ plot is included even though no data is available for this tusk, and years 1 – 13 are displayed even though none of the tusks contain that entire interval of growth. Vertical axes for isotope records are similarly inclusive spanning 8 ‰ in both the $\delta^{15}N$ and $\delta^{13}C$ charts, even though maximum within-tusk variation is significantly less than that. EIVs are plotted on a log scale to better represent their geometric increase. Interpreted weaning age is marked with an arrow on the $\delta^{15}N$ plot, where there is an abrupt increase following a sustained and tapering decrease. The EIV record displays a significant decrease in year 4 coincident with evidence for weaning in the $\delta^{15}N$ record.

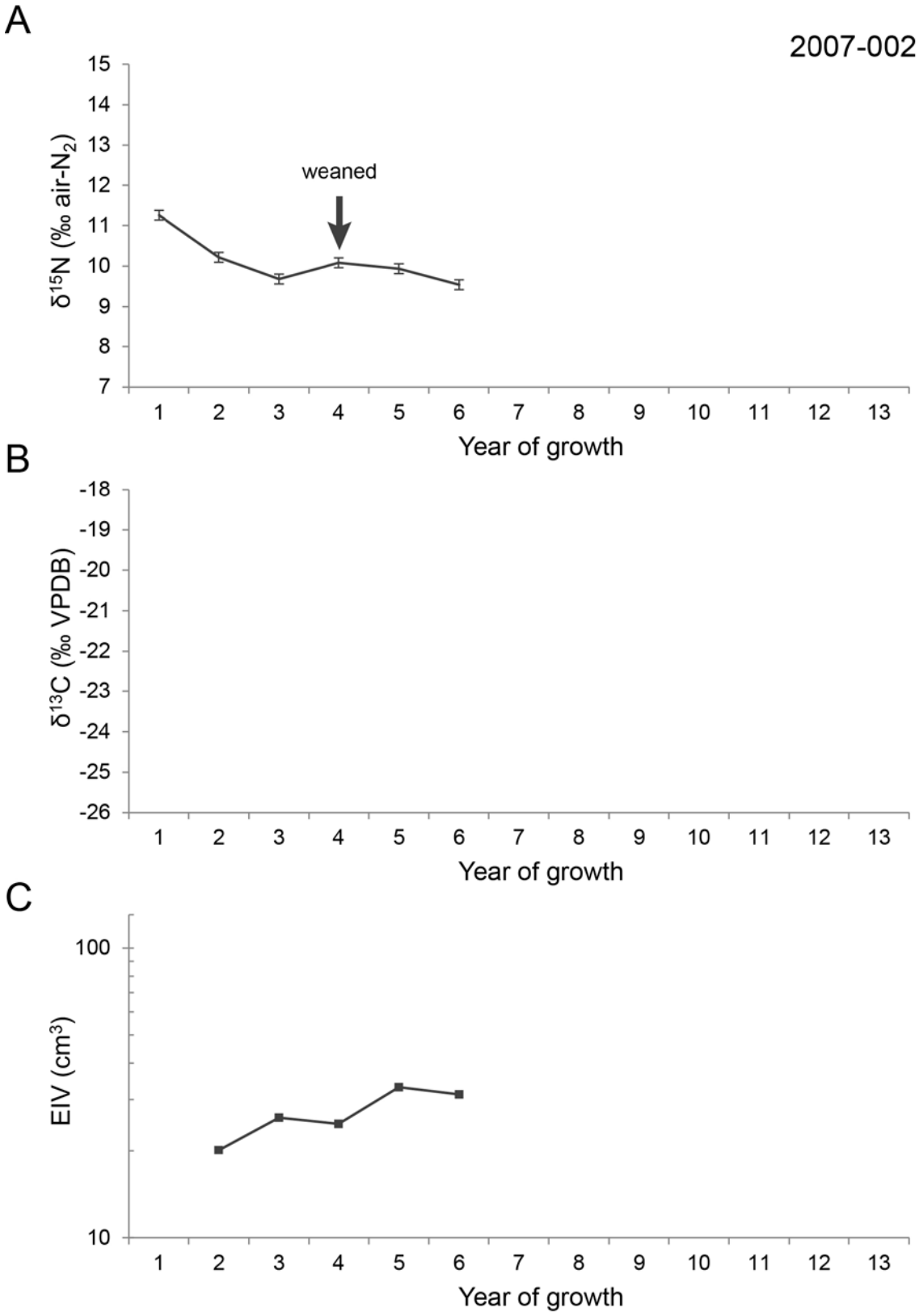
A
2007-002
15
14
13
12
11
10
9
8
7
δ15N (‰ air-N2)
weaned
1 2 3 4 5 6 7 8 9 10 11 12 13
Year of growth
B
-18
-19
-20
-21
-22
-23
-24
-25
-26
δ13C (‰ VPDB)
1 2 3 4 5 6 7 8 9 10 11 12 13
Year of growth
C
100
10
EIV (cm3)
1 2 3 4 5 6 7 8 9 10 11 12 13
Year of growth

Figure 5.14. 2007-005 isotope and growth records.
Serial records of (A) $\delta^{15}N$, (B) $\delta^{13}C$, and (C) EIV (see Figures 5.2, 2.3) of specimen 2007-005 are plotted for comparison. To maintain a consistent format for easy comparison between records of different tusks, years 1 – 13 are displayed even though none of the tusks contain that entire interval of growth. Vertical axes for isotope records are similarly inclusive spanning 8 % in both the $\delta^{15}N$ and $\delta^{13}C$ charts, even though maximum within-tusk variation is significantly less than that. EIVs are plotted on a log scale to better represent their geometric increase. Interpreted weaning age is marked with an arrow on the $\delta^{15}N$ plot, where there is an abrupt spike following a sustained decrease. When available, carbon records do not show a consistent relationship to nitrogen, EIV fluctuations, or interpreted weaning ages. In this record, carbon displays almost no variation over the sampled interval. The EIV record displays a significant decrease in year 8 coincident with evidence for weaning in the $\delta^{15}N$ record.

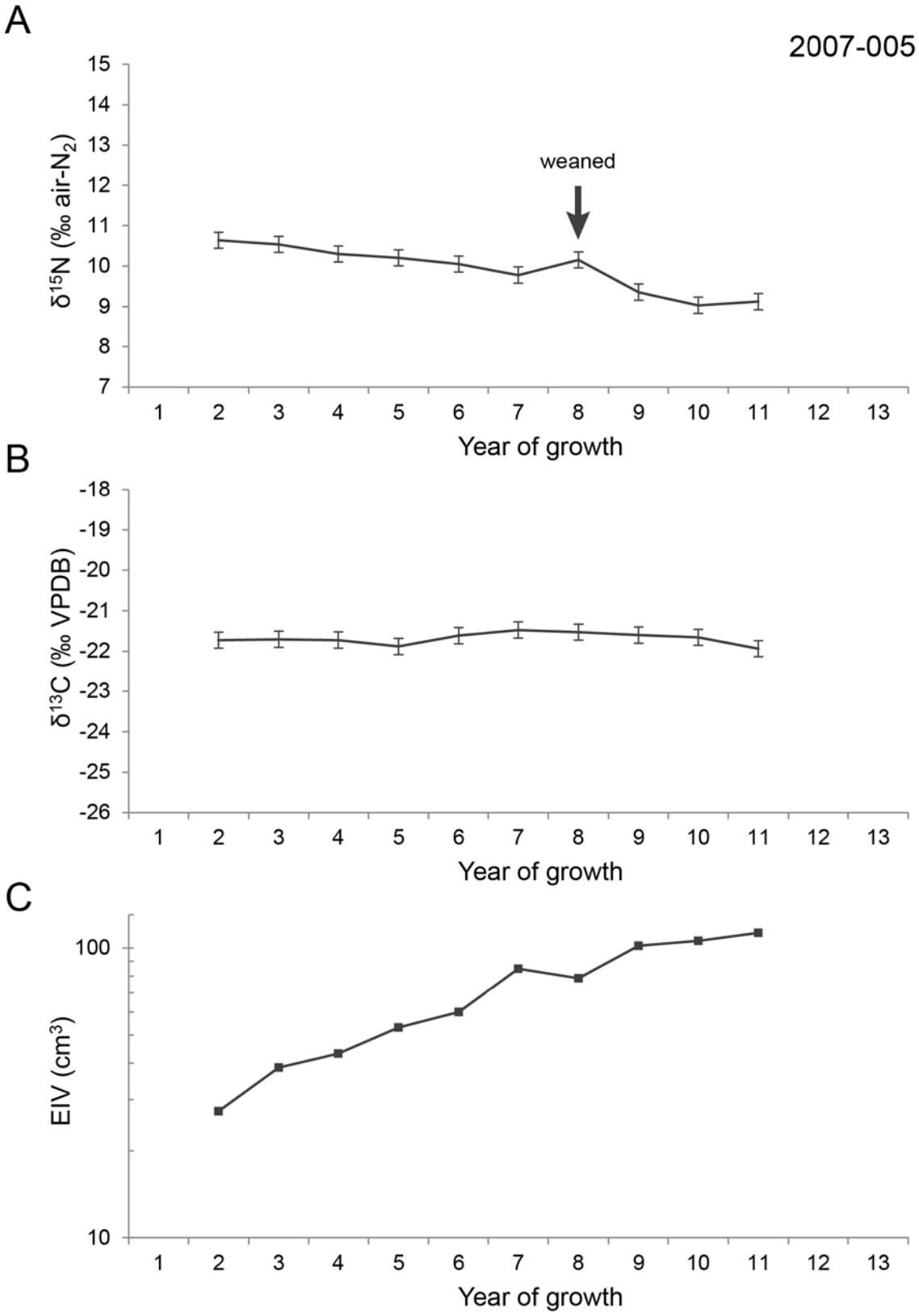
A
2007-005
weaned
δ15N (‰ air-N2)
15
14
13
12
11
10
9
8
7
1 2 3 4 5 6 7 8 9 10 11 12 13
Year of growth
B
δ13C (‰ VPDB)
-18
-19
-20
-21
-22
-23
-24
-25
-26
1 2 3 4 5 6 7 8 9 10 11 12 13
Year of growth
C
EIV (cm3)
100
10
1 2 3 4 5 6 7 8 9 10 11 12 13
Year of growth

Figure 5.15. 2009-001 isotope and growth records.
Serial records of (A) $\delta^{15}N$, (B) $\delta^{13}C$ [no data], and (C) EIV (see Figures 5.2, 2.3) of specimen 2009-001 are plotted for comparison. To maintain a consistent format for easy comparison between records of different tusks, the $\delta^{13}C$ plot is included even though no data is available for this tusk, and years 1 – 13 are displayed even though none of the tusks contain that entire interval of growth. Vertical axes for isotope records are similarly inclusive spanning 8 ‰ in both the $\delta^{15}N$ and $\delta^{13}C$ charts, even though maximum within-tusk variation is significantly less than that. EIVs are plotted on a log scale to better represent their geometric increase. Interpreted weaning age is marked with an arrow on the $\delta^{15}N$ plot, where the record first increases in year 6 following a decline in year 5. There is an even greater increase in year 7. Due to the annual-scale sampling resolution, this is consistent with the calf being weaned late enough in year 6 that the resulting increase in $\delta^{15}N$ was mostly offset by low values associated with advanced stage of nursing. Based on the consistency with other patterns and the minimal evidence for weaning prior to year 5 anywhere in our sample, it is likely that weaning did not occur prior to the sampled years of growth. In this case, the EIV record does not display any significant perturbations from its increasing trend.

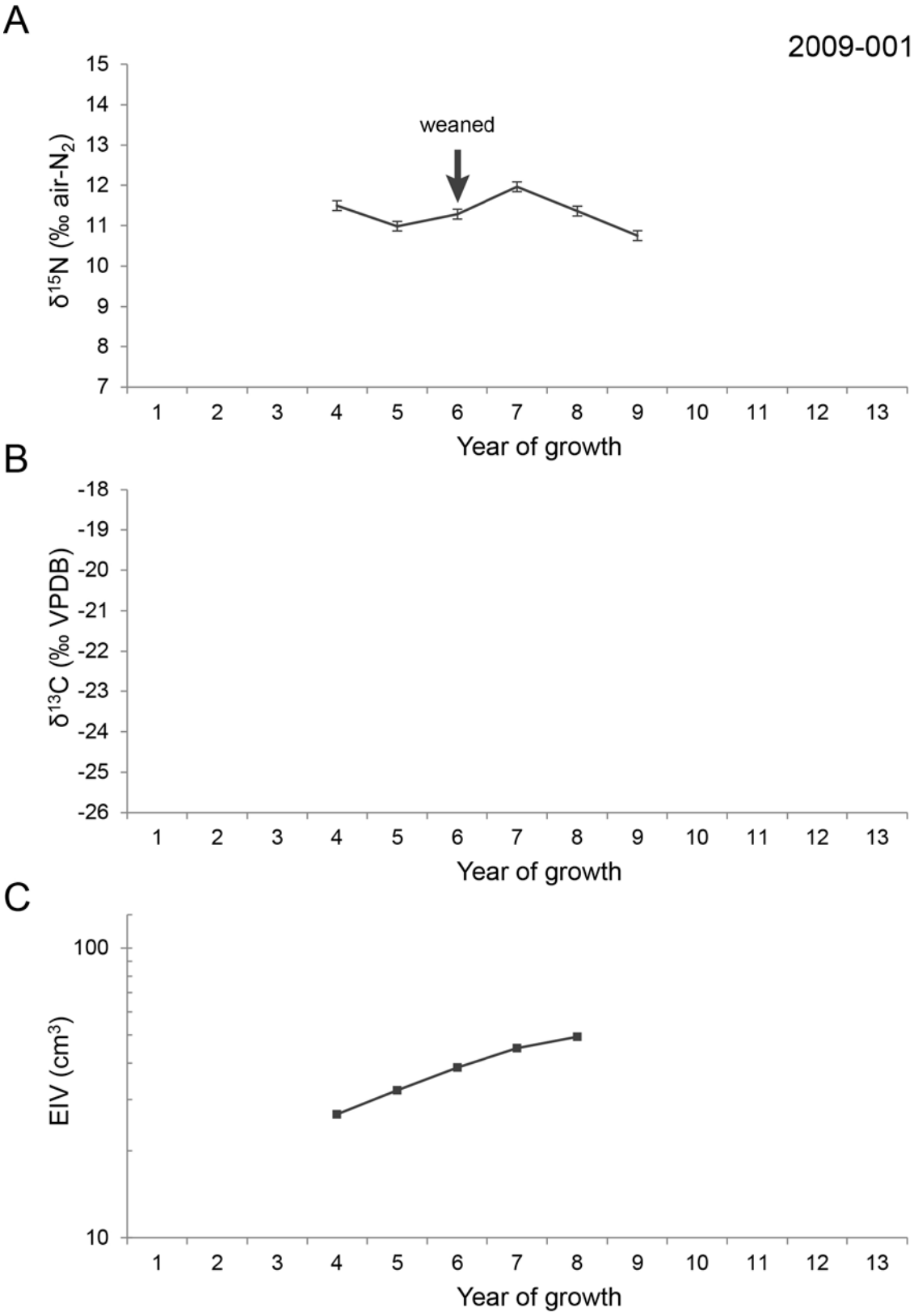
A
2009-001
weaned
δ15N (‰ air-N2)
15
14
13
12
11
10
9
8
7
1 2 3 4 5 6 7 8 9 10 11 12 13
Year of growth
B
δ13C (‰ VPDB)
-18
-19
-20
-21
-22
-23
-24
-25
-26
1 2 3 4 5 6 7 8 9 10 11 12 13
Year of growth
C
EIV (cm3)
100
10
1 2 3 4 5 6 7 8 9 10 11 12 13
Year of growth

Figure 5.16. ZCHM-19 isotope and growth records.
Serial records of (A) $\delta^{15}N$, (B) $\delta^{13}C$ [no data], and (C) EIV (see Figures 5.2, 2.3) of specimen ZCHM-19 are plotted for comparison. To maintain a consistent format for easy comparison between records of different tusks, the $\delta^{13}C$ plot is included even though no data is available for this tusk, and years 1 – 13 are displayed even though none of the tusks contain that entire interval of growth. Vertical axes for isotope records are similarly inclusive spanning 8 ‰ in both the $\delta^{15}N$ and $\delta^{13}C$ charts, even though maximum within-tusk variation is significantly less than that. EIVs are plotted on a log scale to better represent their geometric increase. The sample for year 8 had unusually high nitrogen and carbon yields and was omitted as unreliable. The measured value for that sample showed a dramatic increase from the previous year and was initially considered to mark weaning. Samples could be rerun in light of machine issues during this and other analyses. Missing data prevents a weaning age estimate based on the preserved record in this tusk. However, with the record starting at year 6 and sign of the decrease in $\delta^{15}N$ associated with the normal gradual reduction in nursing, it would be difficult to rule out weaning prior to the beginning of the record. The EIV record for this tusk is variable but does not show any consistent relationship to changes in $\delta^{15}N$. The sample for year 8 had unusually high weight percent of both $\delta^{15}N$ and $\delta^{13}C$ and was not plotted here (see Table 5.3).

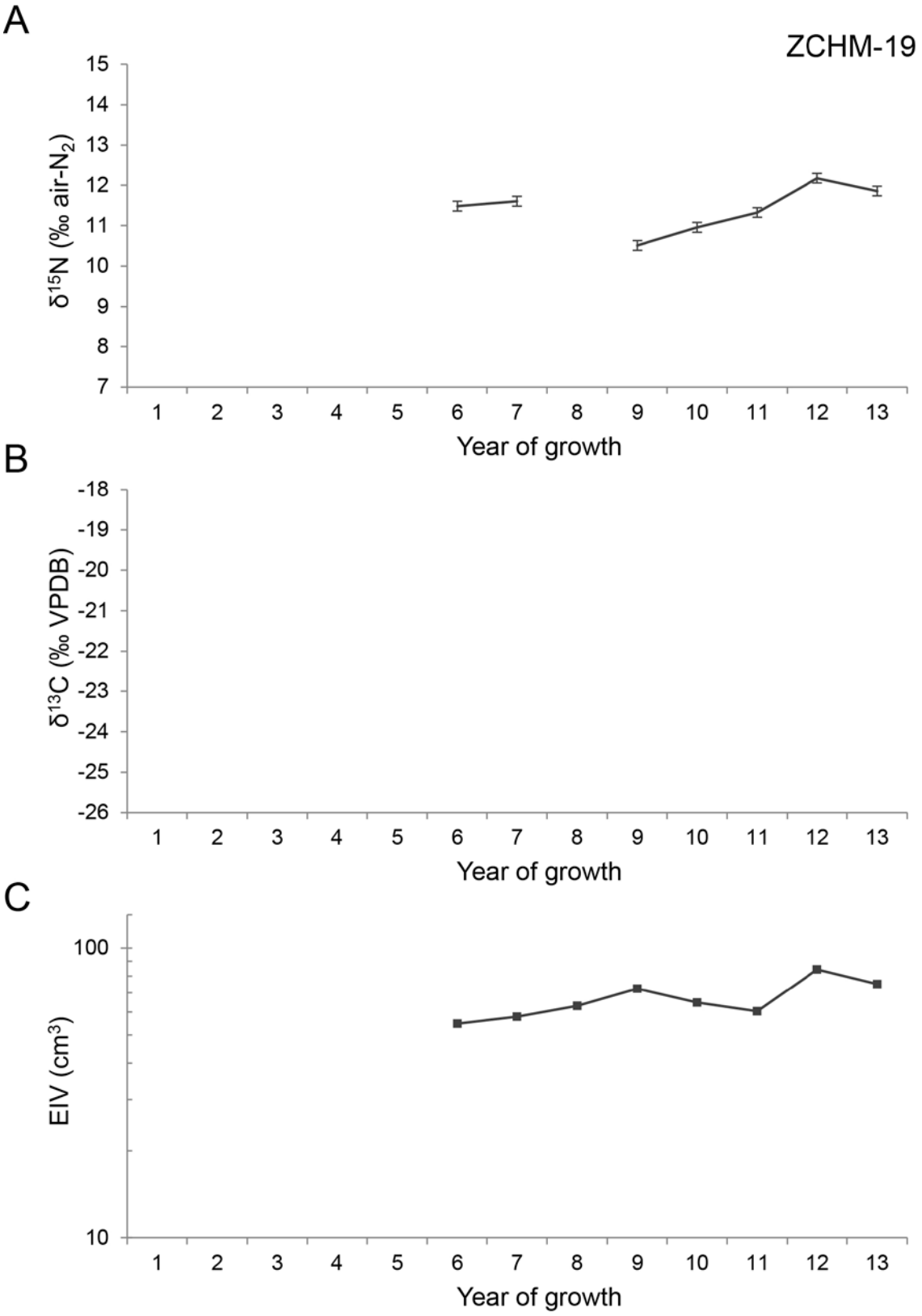
A
ZCHM-19
15
14
13
12
11
10
9
8
7
δ15N (‰ air-N2)
1 2 3 4 5 6 7 8 9 10 11 12 13
Year of growth
B
-18
-19
-20
-21
-22
-23
-24
-25
-26
δ13C (‰ VPDB)
1 2 3 4 5 6 7 8 9 10 11 12 13
Year of growth
C
100
10
EIV (cm3)
1 2 3 4 5 6 7 8 9 10 11 12 13
Year of growth

Figure 5.17. ZCHM-20 isotope and growth records.
Serial records of (A) δ^{15}N, (B) δ^{13}C [no data], and (C) EIV (see Figures 5.2, 2.3) of specimen ZCHM-20 are plotted for comparison. To maintain a consistent format for easy comparison between records of different tusks, the δ^{13}C plot is included even though no data is available for this tusk, and years 1 – 13 are displayed even though none of the tusks contain that entire interval of growth. Vertical axes for isotope records are similarly inclusive spanning 8 ‰ in both the δ^{15}N and δ^{13}C charts, even though maximum within-tusk variation is significantly less than that. EIVs are plotted on a log scale to better represent their geometric increase. Interpreted weaning age is marked with an arrow on the δ^{15}N plot, where the record first increases in year 7 following a sustained and tapering decline through year 6. This increase continues through year 8 suggesting it took some time for this individual to recover from the loss of milk supplementation. As one of the most complete records in our sample, this tusk clearly displays the expected nursing pattern in δ^{15}N followed by a substantial increase we interpret here as evidence that it was weaned. Although the EIV record does not corroborate a year 7 weaning with its own independent decrease, it does contain a significant drop in year 6 just prior to increased δ^{15}N values.

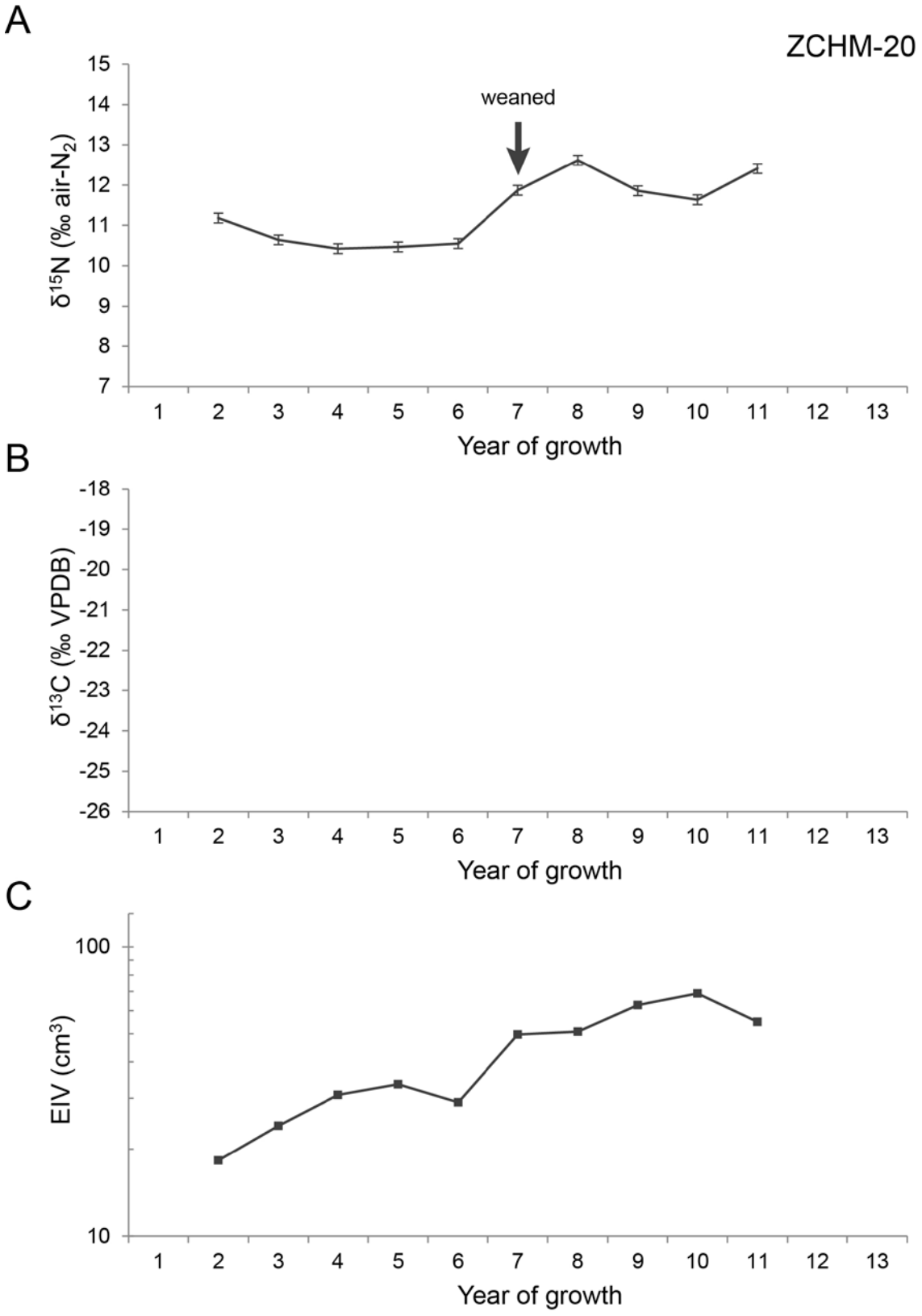
A
ZCHM-20
weaned
$\delta^{15}N$ (‰ air-N_2)
15
14
13
12
11
10
9
8
7
1 2 3 4 5 6 7 8 9 10 11 12 13
Year of growth
B
$\delta^{13}C$ (‰ VPDB)
-18
-19
-20
-21
-22
-23
-24
-25
-26
1 2 3 4 5 6 7 8 9 10 11 12 13
Year of growth
C
EIV (cm^3)
100
10
1 2 3 4 5 6 7 8 9 10 11 12 13
Year of growth

Figure 5.18. ZCHM-22 isotope and growth records.
Serial records of (A) $\delta^{15}N$, (B) $\delta^{13}C$ [no data], and (C) EIV (see Figures 5.2, 2.3) of specimen ZCHM-22 are plotted for comparison. To maintain a consistent format for easy comparison between records of different tusks, the $\delta^{13}C$ plot is included even though no data is available for this tusk, and years 1 – 13 are displayed even though none of the tusks contain that entire interval of growth. Vertical axes for isotope records are similarly inclusive spanning 8 ‰ in both the $\delta^{15}N$ and $\delta^{13}C$ charts, even though maximum within-tusk variation is significantly less than that. EIVs are plotted on a log scale to better represent their geometric increase. The growth record for this tusk terminates just before the year 4-5 boundary. Other than a year 3 brief pause in the decreasing $\delta^{15}N$ trend, the record contains nothing that might indicate weaning, and it is likely that it was not yet weaned when it died.

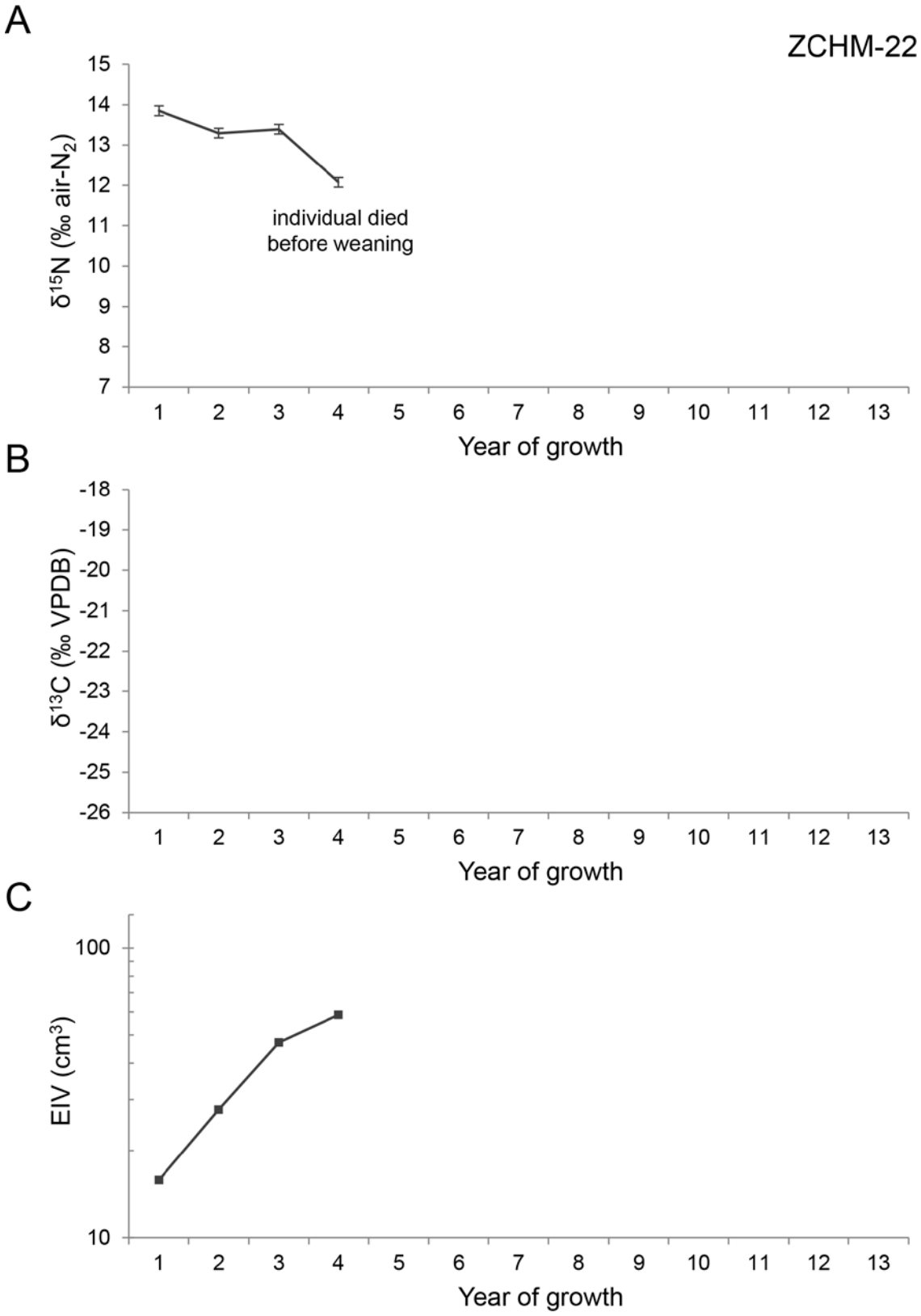
A
ZCHM-22
15
14
13
12
11
10
9
8
7
δ15N (‰ air-N2)
individual died
before weaning
1 2 3 4 5 6 7 8 9 10 11 12 13
Year of growth
B
-18
-19
-20
-21
-22
-23
-24
-25
-26
δ13C (‰ VPDB)
1 2 3 4 5 6 7 8 9 10 11 12 13
Year of growth
C
100
10
EIV (cm3)
1 2 3 4 5 6 7 8 9 10 11 12 13
Year of growth

Figure 5.19. ZCHM-24 isotope and growth records.
Serial records of (A) δ^{15}N, (B) δ^{13}C, and (C) EIV (see Figures 5.2, 2.3) of specimen ZHCM-24 are plotted for comparison. To maintain a consistent format for easy comparison between records of different tusks, years 1 – 13 are displayed even though none of the tusks contain that entire interval of growth. Vertical axes for isotope records are similarly inclusive spanning 8 ‰ in both the δ^{15}N and δ^{13}C charts, even though maximum within-tusk variation is significantly less than that. EIVs are plotted on a log scale to better represent their geometric increase. Interpreted weaning age is marked with an arrow on the δ^{15}N plot, where the record displays the first increase greater than can be accounted for by analytical error. When available, carbon records do not show a consistent relationship to nitrogen, EIV fluctuations, or interpreted weaning ages. The carbon record for this tusk does not contain much variation and shows no change coincident with weaning age as interpreted from nitrogen results. Obscure CT increments in this tusk complicated measurement of annual features for EIV calculations and the resulting EIV record is unusual. It displays some fluctuations, but nothing that corroborates year 6 as weaning age. However, the almost exclusively increasing trend starting with year 3 is inconsistent with a drawn out period of nursing.

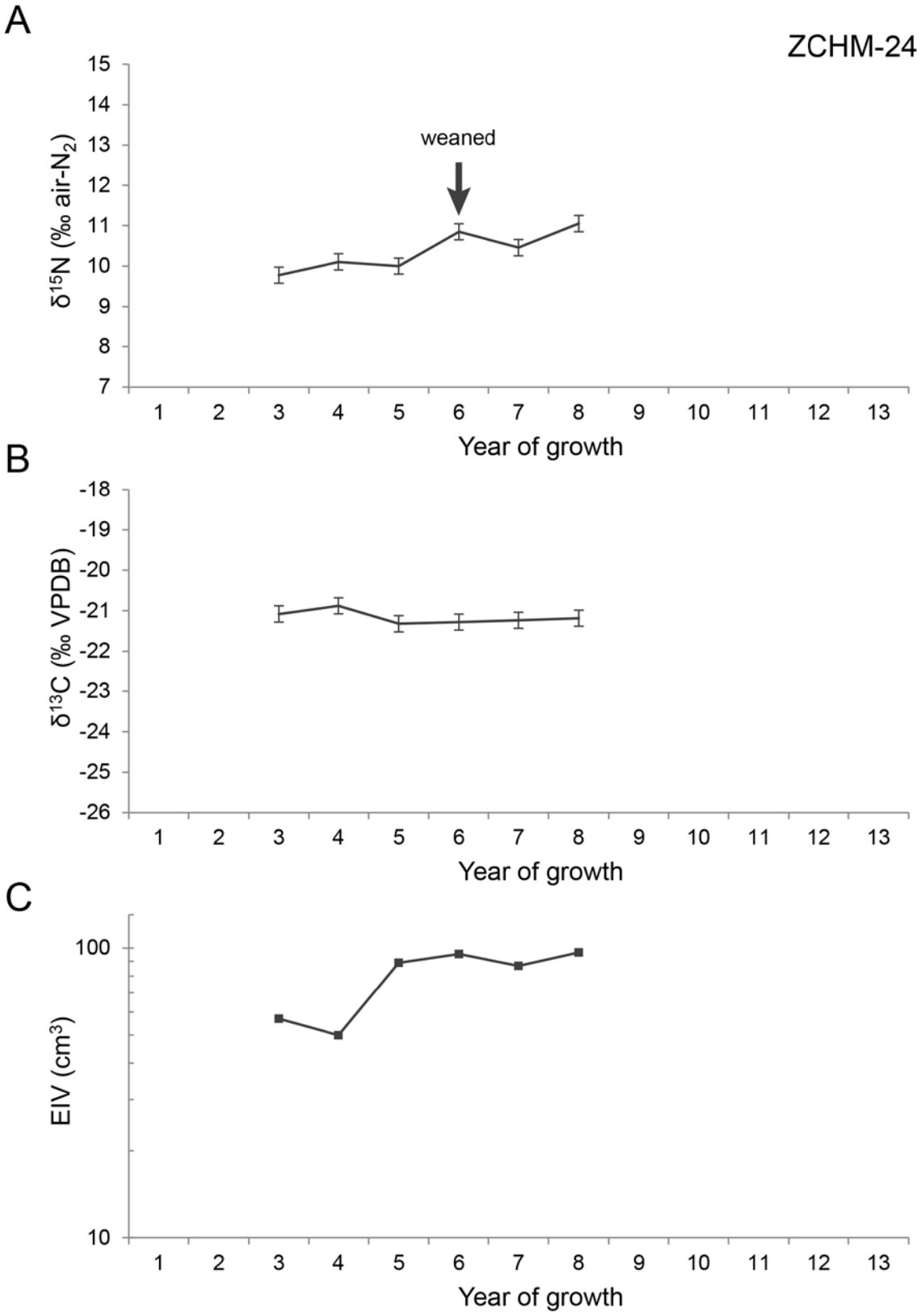
A
ZCHM-24
weaned
δ15N (‰ air-N2)
15
14
13
12
11
10
9
8
7
1 2 3 4 5 6 7 8 9 10 11 12 13
Year of growth
B
δ13C (‰ VPDB)
-18
-19
-20
-21
-22
-23
-24
-25
-26
1 2 3 4 5 6 7 8 9 10 11 12 13
Year of growth
C
EIV (cm3)
100
10
1 2 3 4 5 6 7 8 9 10 11 12 13
Year of growth

Figure 5.20. ZCHM-26 isotope and growth records.
Serial records of (A) $\delta^{15}N$, (B) $\delta^{13}C$, and (C) EIV (see Figures 5.2, 2.3) of specimen ZHCM-26 are plotted for comparison. To maintain a consistent format for easy comparison between records of different tusks, years 1 – 13 are displayed even though none of the tusks contain that entire interval of growth. Vertical axes for isotope records are similarly inclusive spanning 8 ‰ in both the $\delta^{15}N$ and $\delta^{13}C$ charts, even though maximum within-tusk variation is significantly less than that. EIVs are plotted on a log scale to better represent their geometric increase. Weaning age cannot be estimated for this tusk based on missing data. Further analyses to obtain a record of year 6 may enable an estimate of weaning age, if it is significantly higher than year 5 or significantly lower than year 7. A partial year 8 analyzed with higher resolution sampling to see if nitrogen is enriched compared to the same portion of the previous year. When available, carbon records do not show a consistent relationship to nitrogen, EIV fluctuations, or interpreted weaning ages. In this case, the missing year 6 analysis confounds interpretation of the carbon results. There is a decrease in year 6 of the EIV record, but without a corresponding increase in $\delta^{15}N$, this evidence is inconclusive. Year 5 was missed in the sampling process.

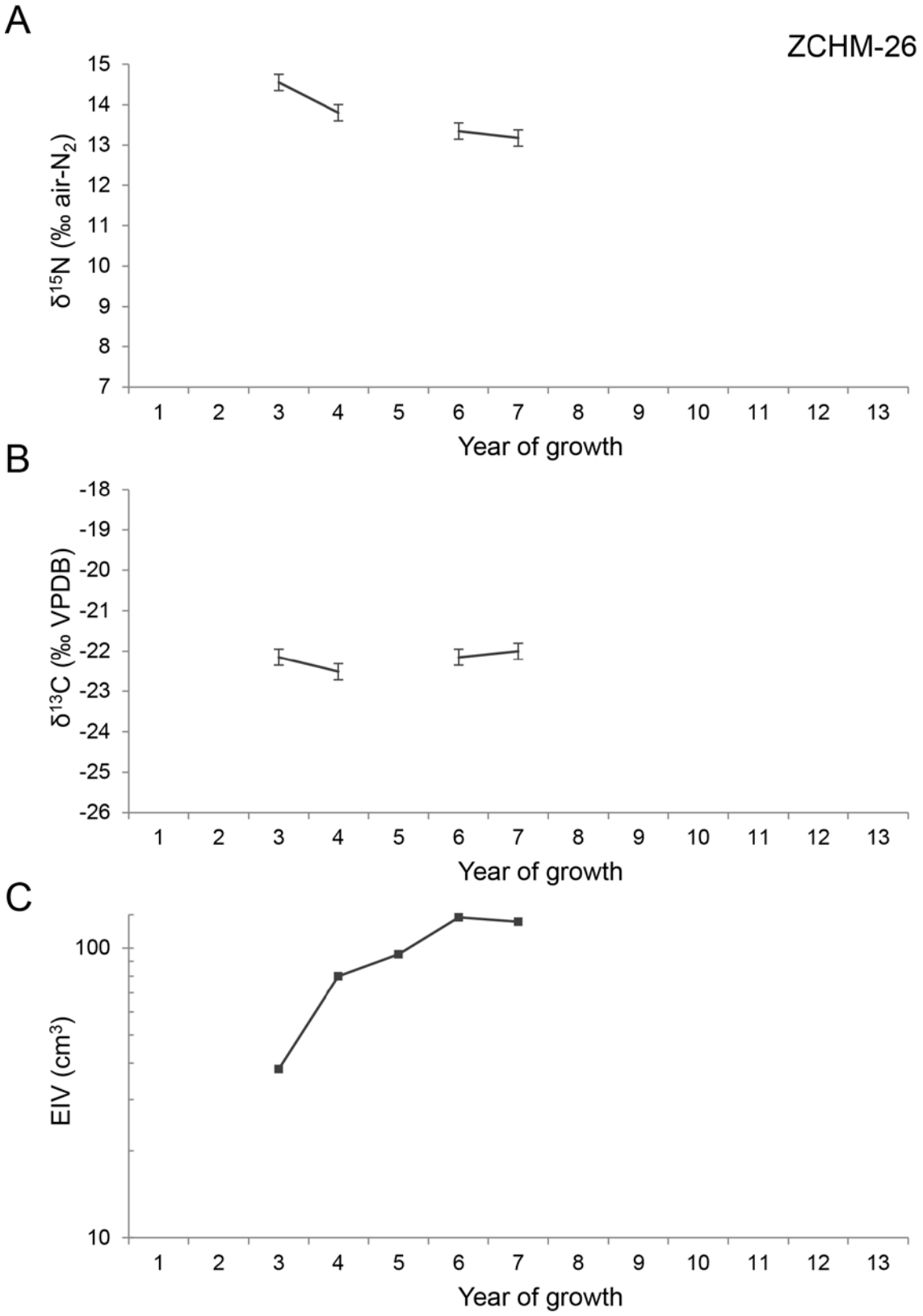
A
ZCHM-26
15
14
13
12
11
10
9
8
7
δ15N (‰ air-N2)
1 2 3 4 5 6 7 8 9 10 11 12 13
Year of growth
B
-18
-19
-20
-21
-22
-23
-24
-25
-26
δ13C (‰ VPDB)
1 2 3 4 5 6 7 8 9 10 11 12 13
Year of growth
C
100
10
EIV (cm3)
1 2 3 4 5 6 7 8 9 10 11 12 13
Year of growth

Figure 5.21. ZCHM-51 isotope and growth records.
Serial records of (A) $\delta^{15}N$, (B) $\delta^{13}C$, and (C) EIV (see Figures 5.2, 2.3) of specimen ZHCM-51 are plotted for comparison. To maintain a consistent format for easy comparison between records of different tusks, years 1 – 13 are displayed even though none of the tusks contain that entire interval of growth. Vertical axes for isotope records are similarly inclusive spanning 8 ‰ in both the $\delta^{15}N$ and $\delta^{13}C$ charts, even though maximum within-tusk variation is significantly less than that. EIVs are plotted on a log scale to better represent their geometric increase. Proposed weaning age for this tusk is marked with an arrow on the $\delta^{15}N$ chart, where the record increases for the first time at year 10. With no indication of a decreasing trend leading up to this increase, interpretation of this increase as a sign of weaning is somewhat problematic. When available, carbon records do not show a consistent relationship to nitrogen, EIV fluctuations, or interpreted weaning ages. In this case, $\delta^{13}C$ decreases in years 8 and 9, but it is not clear that this is relevant for estimating weaning age. Although year 10 is the latest estimated weaning age in the sample analyzed in this study, it is not totally inconsistent with estimates of late weaning in other tusks from the period just prior to the last glacial maximum. The EIV record does not corroborate a year 10 weaning. In fact, significantly decreased EIVs in year 8 and 9 may be considered evidence for slightly earlier weaning (even more in line with other records with similar ^{14}C dates), but the evidence is fairly inconclusive. Year 10 is included as its weaning age in this analysis. The alternative treatment given current data and methods would be to drop its estimate from the dataset, but this would not greatly affect the overall pattern.

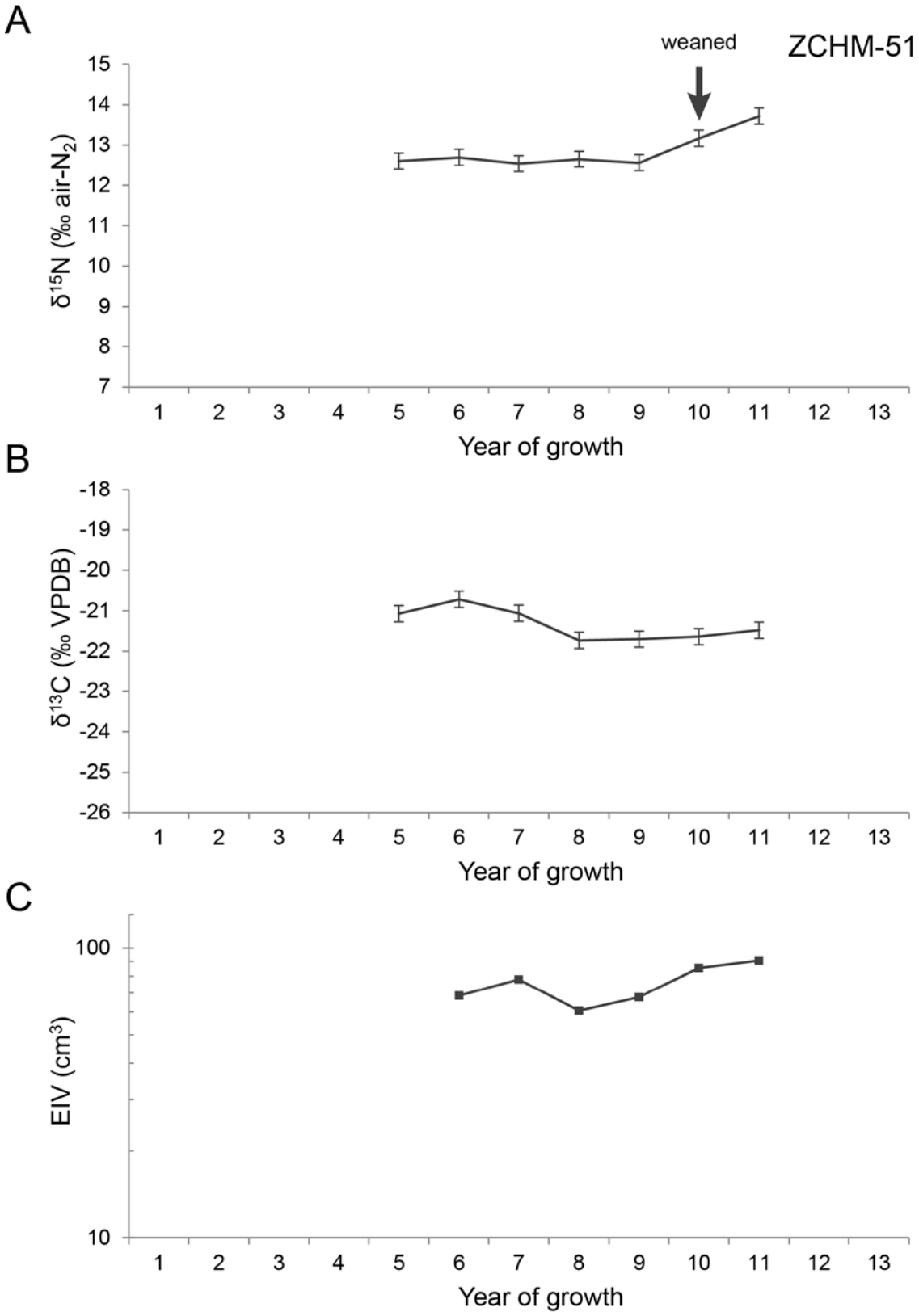
A
weaned
ZCHM-51
15
14
13
12
11
10
9
8
7
δ15N (‰ air-N2)
1 2 3 4 5 6 7 8 9 10 11 12 13
Year of growth
B
-18
-19
-20
-21
-22
-23
-24
-25
-26
δ13C (‰ VPDB)
1 2 3 4 5 6 7 8 9 10 11 12 13
Year of growth
C
100
10
EIV (cm3)
1 2 3 4 5 6 7 8 9 10 11 12 13
Year of growth

Figure 5.22. AM-6 isotope and growth records.
Serial records of (A) $\delta^{15}N$, (B) $\delta^{13}C$, and (C) EIV (see Figures 5.2, 2.3) of specimen AM-6 are plotted for comparison. To maintain a consistent format for easy comparison between records of different tusks, years 1 – 13 are displayed even though none of the tusks contain that entire interval of growth. Vertical axes for isotope records are similarly inclusive spanning 8 ‰ in both the $\delta^{15}N$ and $\delta^{13}C$ charts, even though maximum within-tusk variation is significantly less than that. EIVs are plotted on a log scale to better represent their geometric increase. Proposed weaning age for this tusk is marked with an arrow on the $\delta^{15}N$ chart, where the record increases for the first time in year 5 following decreases in years 3 and 4. When available, carbon records in this study do not show a consistent relationship to nitrogen, EIV fluctuations, or interpreted weaning ages. In this case, $\delta^{13}C$ results look a lot like the expected nitrogen record with a tapering decrease in the first years followed by a spike. Taken at face value, this pattern could in this specimen be the carbon equivalent to the expected $\delta^{15}N$ pattern. Decreasing levels could be due to reduced trophic enrichment (which occurs in $\delta^{13}C$, though to a lesser degree than $\delta^{15}N$). But this ignores the contribution of carbon-light milk fat which should result in lower calf $\delta^{13}C$, when nursing is providing a greater contribution to its diet. The increase in $\delta^{13}C$ does also occur coincident with the $\delta^{15}N$ increase interpreted as an effect of weaning in one other tusk sampled. The EIV record shows an increase in year 5 that is contrary to expectations if increased $\delta^{15}N$ is a result of nutritional difficulty. However, in specimen is the heavily worn and broken-off tip of a larger tusk. EIVs were calculated from diameters that were necessarily rough estimates over most of length of the tusk fragment.

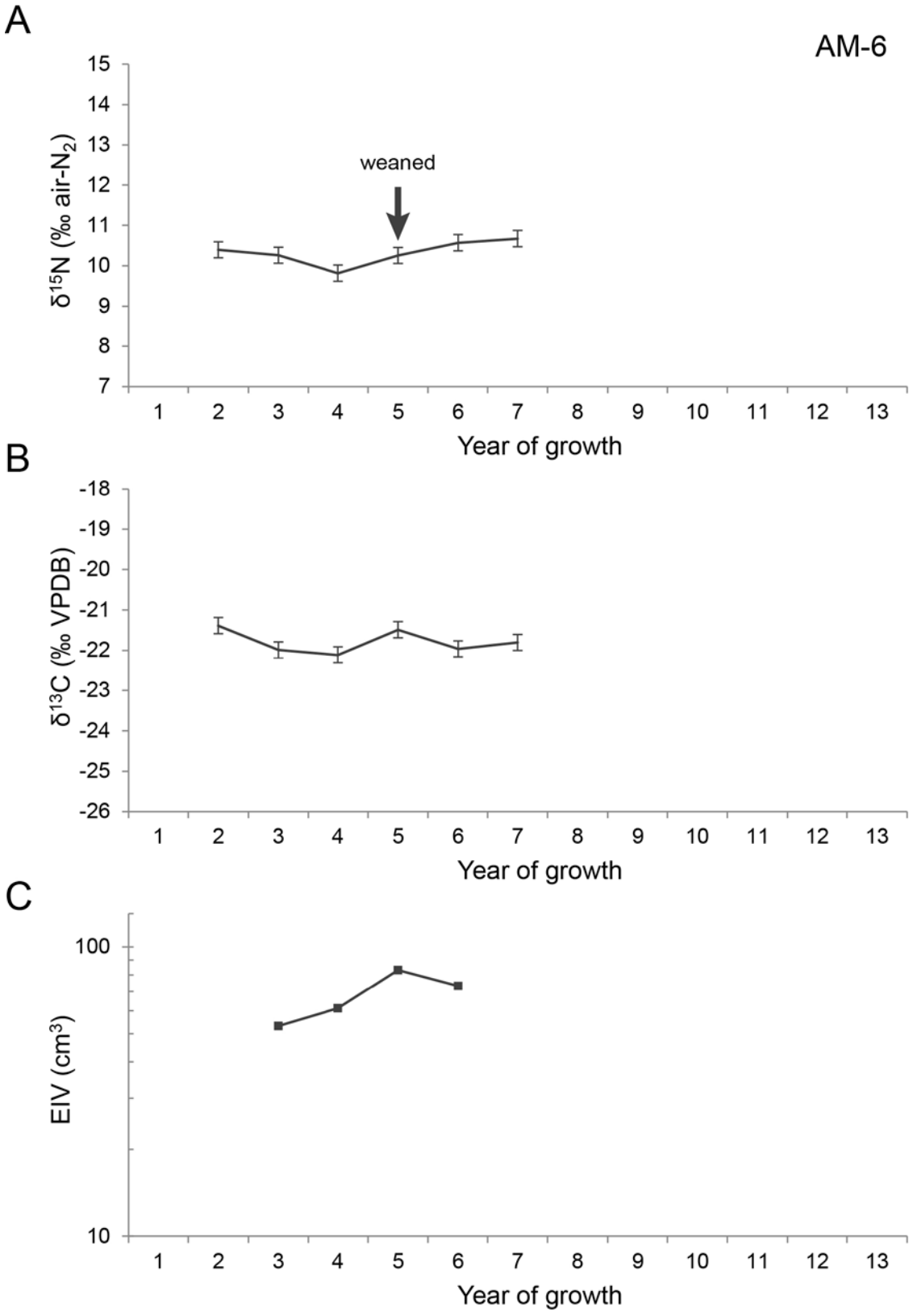
A
AM-6
15
14
13
12
11
10
9
8
7
δ15N (‰ air-N2)
weaned
1
2
3
4
5
6
7
8
9
10
11
12
13
Year of growth
B
-18
-19
-20
-21
-22
-23
-24
-25
-26
δ13C (‰ VPDB)
1
2
3
4
5
6
7
8
9
10
11
12
13
Year of growth
C
100
10
EIV (cm3)
1
2
3
4
5
6
7
8
9
10
11
12
13
Year of growth

Figure 5.23. Temporal distribution of estimated weaning ages.
Estimated weaning age for each tusk analyzed is plotted against its radiocarbon date. One tusks with a confident weaning age estimate was too old for reliable radiocarbon dating and is displayed at the bottom of the plot indicating its apparent antiquity (>37,200 years BP). Error bars show the confidence intervals for reliable AMS ^{14}C dates. The last glacial maximum (LGM) is designated as the interval from 19 – 26.5 k ^{14}C years BP (Clark et al., 2009). The approximate time of mammoth extirpation is indicated as 10 k years BP. Two of the tusks have dates very close to that time. Geographic region for each specimen is marked next to its data point (key included). Excluding the one tusk from Yakutia, estimated weaning ages are higher during the LGM than they are both preceding and following the LGM. There is even some indication of weaning age increasing leading into the LGM and then decreasing after. The estimate of earliest weaning is also the youngest specime geologically.

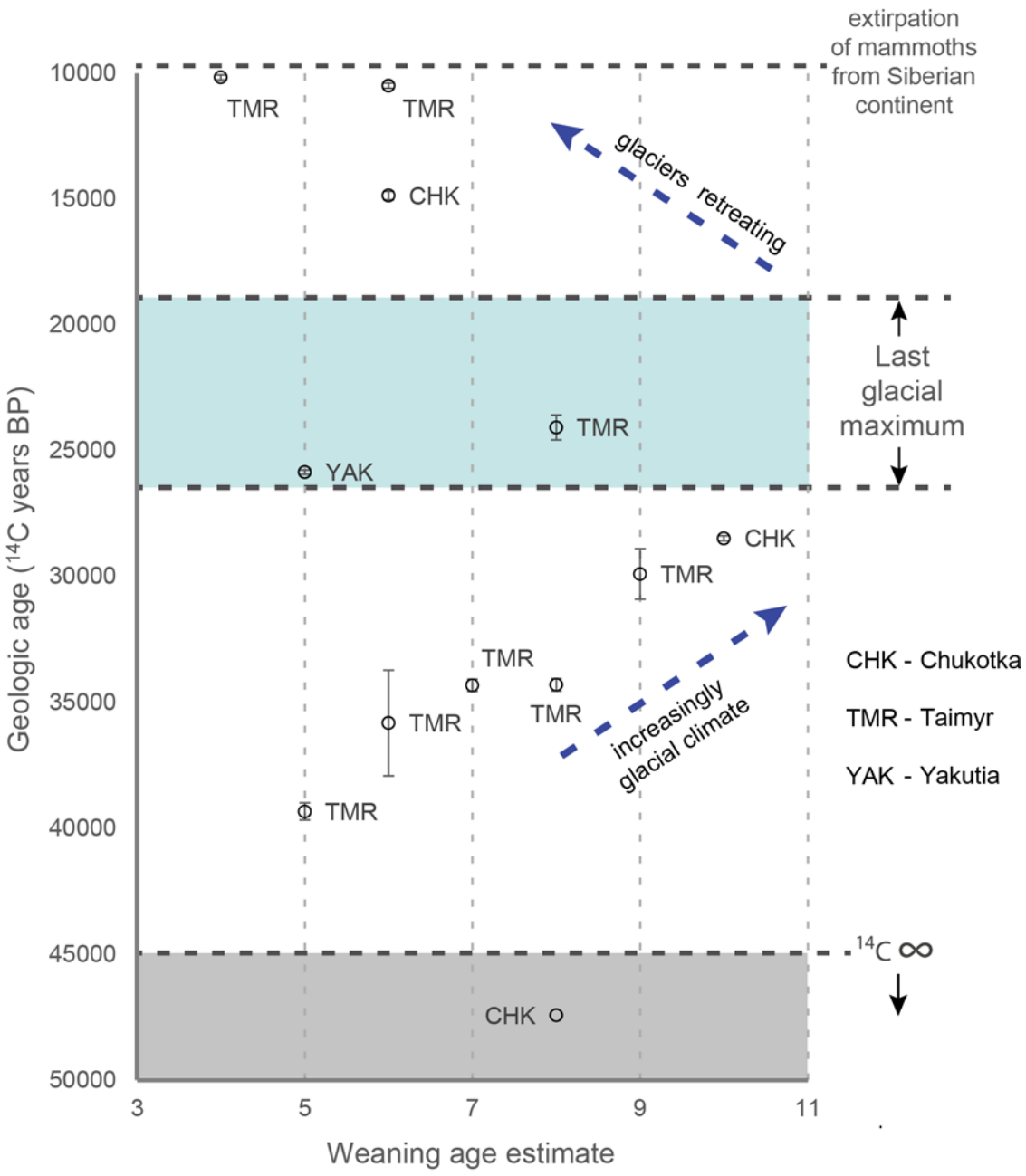
extirpation of mammoths from Siberian continent
10000
15000
20000
25000
30000
35000
40000
45000
50000
Geologic age (^{14}C years BP)
TMR
TMR
CHK
glaciers retreating
Last glacial maximum
TMR
YAK
CHK
TMR
TMR
TMR
TMR
TMR
increasingly glacial climate
CHK - Chukotka
TMR - Taimyr
YAK - Yakutia
^{14}C ∞
CHK
3
5
7
9
11
Weaning age estimate

Figure 5.24. Temporal distribution of 4-year growth volumes for *males* and *females*. Total volume of growth over a 4-year interval are plotted against radiocarbon dates separately for *females* (A) and *males* (B). In *females*, the interval compared is from the 5th to the 8th year of growth. The interval for comparison in *males* is year 3 to year 6. Tusks included in these plots are only ones containing the entire compared interval and reliable radiocarbon dates. Error bars show the confidence intervals for reliable AMS ^{14}C dates. The last glacial maximum (LGM) is designated as the interval from 19 – 26.5 k ^{14}C years BP (Clark et al., 2009). The approximate time of mammoth extirpation is indicated as 10 k years BP. Two of the tusks (one of each sex) have dates very close to that time. Geographic region for each specimen is marked next to its data point (key included). Females display a weak positive trend in growth volume, but all tusks are from the Taimyr region. Males show no clear trend, but have higher growth volumes in Yakutia and Chukotka than in Taimyr, even during the LGM. Sample sizes in these comparisons are especially small since they are divided between males and females.

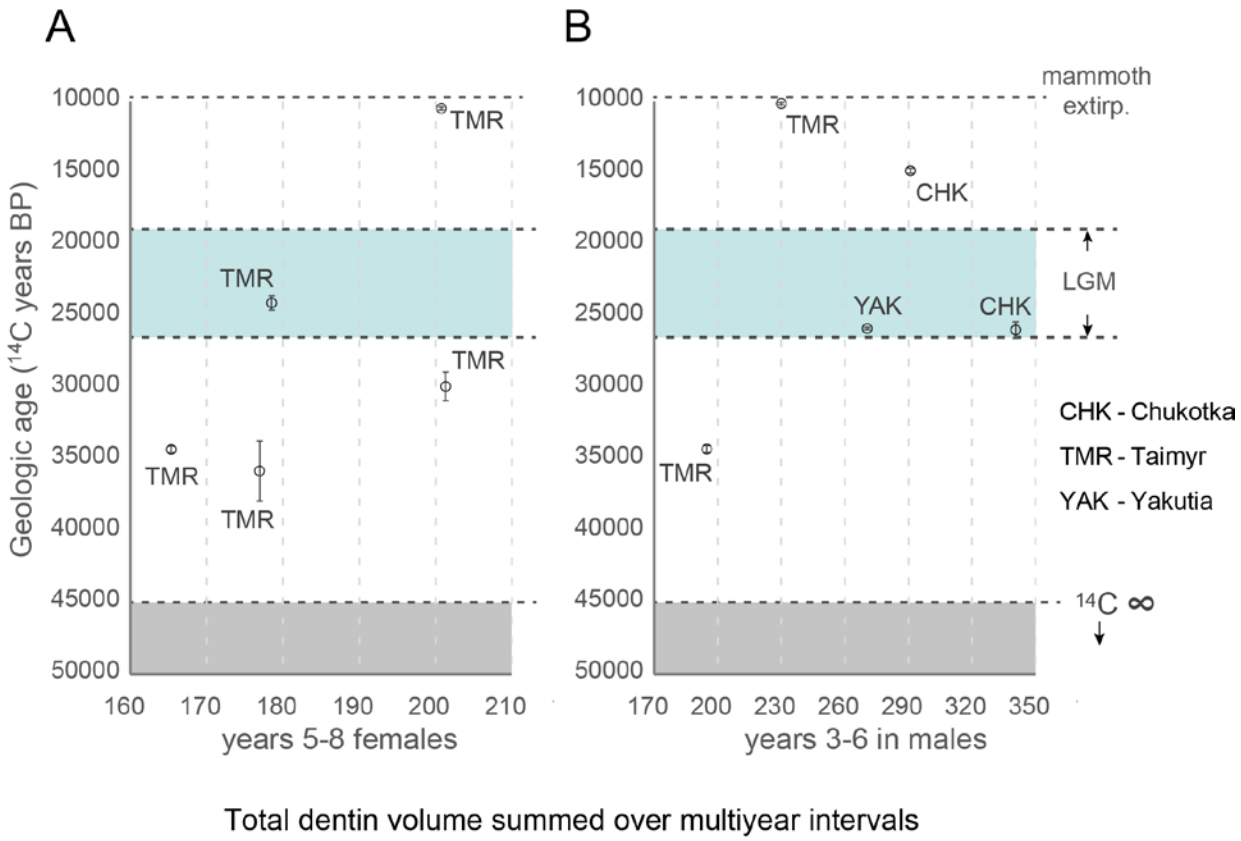

References

Allentoft, M. E., Heller, R., Oskam, C. L., Lorenzen, E. D., Hale, M. L., Gilbert, M. T. P., Jacomb, C., Holdaway, R. N., Bunce, M. 2014. Extinct New Zealand megafauna were not in decline before human colonization. Proceedings of the National Academy of Sciences 111(13): 4922-4927.

Alroy, J. 2001. A multispecies overkill simulation of the end-Pleistocene megafaunal mass extinction. Science 292(5523):1893-1896.

Bateson, P., Barker, D., Clutton-Brock, T., Deb, D., D'Udine, B., Foley, R. A., Gluckman, P., Godfrey, K., Kirkwood, T., Lahr, M. M., McNamara, J., Metcalfe, N. B., Monaghan, P., Spencer, H. G., Sultan, S. E. 2004. Developmental plasticity and human health. Nature 430:419-421.

Bengtson, J. L., Laws, R. M. 1985. Trends in Crabeater Seal Age at Maturity: An Insight into Antarctic Marine Interactions. In: Siegfried, W. R., Condy, P. R., Laws, R. M. (Eds.) Antarctic Nutrient Cycles and Food Webs. Springer-Verlag, Berlin, Germany, pp. 669-675.

Breslawski, R. P., Byers, D. A. 2014. Holocene bison diminution on the Snake River Plain, Idaho, USA. The Holocene 24(7): 864-875.

Brook, B. W., Bowman, D. M. 2004. The uncertain blitzkrieg of Pleistocene megafauna. Journal of Biogeography 31(4):517-523.

Burney, D. A., Flannery, T. F. 2005. Fifty millennia of catastrophic extinctions after human contact. TRENDS in Ecology and Evolution 20(7):395-401.

Carrick, R., Csordas, S. E., Ingham, S. E. 1962. Studies on the southern elephant seal, *Mirounga leonina* (L.). IV. Breeding and development. Wildlife Research 7(2): 161-197.

Cherney, M., Fisher, D., Hren, M. 2014. Comparing stable isotope compositions of hair in a mother-calf pair of elephants (*Loxodonta africana*) during nursing and weaning. Journal of Vertebrate Paleontology, Program and Abstracts 2014, p. 108.

Chowdhury, A. A. 1978. Effect of maternal nutrition on fertility in rural Bangladesh. In: Mosely, W. (Ed.), Nutrition and human reproduction. Plenum Press, New York, pp. 401-410.

Ciccioli, N. H., Wettemann, R. P., Spicer, L. J., Lents, C. A., White, F. J., Keisler, D. H. 2003. Influence of body condition at calving and postpartum nutrition on endocrine function and reproductive performance of primiparous beef cows. Journal of Animal Science 81(12):3107-3120.

Clark, P. U., Dyke, A. S., Shakun, J. D., Carlson, A. E., Clark, J., Wohlfarth, B., Mitrovica, J. X., Hostetler, S. W., McCabe, A. M. 2009. The last glacial maximum. Science 325(5941):710-714.

Coltman, D. W., O'Donoghue, P., Jorgenson, J. T., Hogg, J. T., Strobeck, C., Festa-Bianchet, M. 2003. Undesirable evolutionary consequences of trophy hunting. Nature 426(6967): 655-658.

Cooper et al., 2015

Delgado, H. L., Lechtig, A., Martorell, R., Brineman, E., Klein, R. E. 1978. Nutrition, lactation, and postpartum amenorrhea. American Journal of Clinical Nutrition 31(2):322-327.

Delgado, H. L., Martorell, R., Klein, R. E. 1982. Nutrition, lactation, and birth interval components in rural Guatemala. The American journal of clinical nutrition 35(6):1468-1476.

Delvoye, P., Robyn, C. 1980. Breast-feeding and post partum amenorrhea in Central Africa. Journal of Tropical Pediatrics and Environmental Child Health 26(5):184-189.

DeNiro, M. J. 1985. Postmortem preservation and alteration of in vivo bone collagen isotope ratios in relation to palaeodietary reconstruction. Nature 317:806-809.

DeNiro, M. J., Epstein, S. 1981. Influence of diet on the distribution of nitrogen isotopes in animals. Geochimica et Cosmochimica Acta 45(3):341-351.

Douglas-Hamilton, I., Douglas-Hamilton, O. 1975. Among the elephants. The Viking Press, New York, USA.

Dreimanis, A. 1968. Extinction of mastodons in eastern North America: testing a new climatic-environmental hypothesis. The Ohio Journal of Science 68(6):257-272.

Dupras, T. L., Schwarcz, H. P., Fairgrieve, S. I. 2001. Infant feeding and weaning practices in Roman Egypt. American Journal of Physical Anthropology 115(3):204-212.

El Adli, J., Fisher, D., Cherney, M., Labarca, R., Lacombat, F. 2015. First analysis of tusk growth rate and season of death of a South American gomphothere. Journal of Vertebrate Paleontology, Program and Abstracts, 2014, p. 120.

Faith, J. T. 2011. Late Pleistocene climate change, nutrient cycling, and the megafaunal extinctions in North America. Quaternary Science Reviews 30(13):1675-1680.

Faith, J. T. 2014. Late Pleistocene and Holocene mammal extinctions on continental Africa. Earth-Science Reviews 128, 105-121.

Fisher, D. C. 1996. Extinction of proboscideans in North America. In: Shoshani, J., Tassy, P. (Eds.), The Proboscidea: Evolution and Palaeoecology of Elephants and Their Relatives. Oxford University Press, Oxford, pp. 296–315.

Fisher, D. C. 2001. Season of death, growth rates, and life history of North American mammoths. In: West, D. (Ed.), Proceedings of the First International Conference on Mammoth Site Studies: 11-13 March 1998 (pp. 121-135).

Fisher, D. C., 2008. Taphonomy and paleobiology of the Hyde Park mastodon. In: Allmon, W. D., Nester, P. L. (Eds.), Mastodon Paleobiology, Taphonomy, and Paleoenvironment in the Late Pleistocene of New York State: Studies on the Hyde Park, Chemung, and North Java Sites. Palaeontographica Americana 61, 197–290.

Fisher, D.C., 2009. Paleobiology and extinction of proboscideans in the Great Lakes region of North America. In: Haynes, G. (Ed.), American Megafaunal Extinctions at the End of the Pleistocene. Springer, Dordrecht, pp. 55–75.

Fisher, D. C., Cherney, M. D., Newton, C., Graham, R. W., Rountrey, A. N., Calamari, Z. T., Stuckey, R. K., Lucking, C. 2014(a). Taxonomy and tusk growth analyses of Ziegler Reservoir proboscideans. Quaternary Research 82(3):518-532.

Fisher, D. C., Shirley, E. A., Whalen, C. D., Calamari, Z. T., Rountrey, A. N., Tikhonov, A. N., Buigues, B., Lacombat, F., Grigoriev, S., Lazarev, P. A. 2014(b). X-ray computed tomography of two mammoth calf mummies. Journal of Paleontology 88(4):664-675.

Fogel, M. L., Tuross, N., Owsley, D. W. 1989. Nitrogen isotope tracers of human lactation in modern and archaeological populations. Carnegie Institution of Washington Yearbook 1989:111-117.

Fuller, B. T., Fuller, J. L., Harris, D. A., Hedges, R. E. M. 2006. Detection of breastfeeding and weaning in modern human infants with carbon and nitrogen stable isotope ratios. American Journal of Physical Anthropology 129:279-293.

Gannes, L. Z., Del Rio, C. M., Koch, P. 1998. Natural abundance variations in stable isotopes and their potential uses in animal physiological ecology. Comparative biochemistry and physiology Part A: Molecular & integrative physiology 119(3):725-737.

Geist, V. 1989. Environmentally guided phenotype plasticity in mammals and some of its consequences to theoretical and applied biology. In: Bruton, M. N. (Ed.), Alternative life-history styles of animals. Springer, Netherlands, pp. 153-176.

Gohman, S. C. L. 2009. Vegetation change and the extinction of the woolly mammoth (*Mammuthus primigenius*) in eastern Siberia. Unpublished thesis, University of Minnesota, ix+226 pp.

Gohman, S. C. L., Fox, D. L., Fisher, D. C., Vartanyan, S. L., Tikhonov, A. N., Mol, D., Buigues, B. 2010. Paleodietary and paleoenvironmental implications of carbon and nitrogen isotopic variations in late Pleistocene and Holocene tusks of *Mammuthus primigenius* from northern Eurasia. In: Lazarev, P., Boeskorov, G.,

Maschenko, E. (Eds.), Proceedings of the 4th International Mammoth Conference, Yakutsk 8, pp. 177-187.
Gomendio, M. 1991. Parent/offspring conflict and maternal investment in rhesus macaques. Animal Behaviour 42(6):993-1005.
Graham, R. W., Lundelius, E. L. 1984. Coevolutionary disequilibrium and Pleistocene extinctions. In: Martin, P. S., Klein, R. G. (Eds.), Quaternary extinctions: a prehistoric revolution. The University of Arizona Press, Tucson, Arizona, pp. 223-249.
Grayson, D. K. 1984(a). Nineteenth century explanations of Pleistocene extinctions: A review and analysis. In: Martin, P. S., Klein, R. G. (Eds.), Quaternary extinctions: a prehistoric revolution. The University of Arizona Press, Tucson, Arizona, pp. 5-39.
Grayson, D. K. 1984(b). Explaining Pleistocene extinctions: thoughts on the structure of a debate. In: Martin, P. S., Klein, R. G. (Eds.), Quaternary extinctions: a prehistoric revolution. The University of Arizona Press, Tucson, Arizona, pp. 807-823.
Grayson, D. K., Meltzer, D. J. 2003. A requiem for North American overkill. Journal of Archaeological Science 30(5):585-593.
Grund, B. S., Surovell, T. A., Lyons, S. K. 2012. Range sizes and shifts of North American Pleistocene mammals are not consistent with a climatic explanation for extinction. World Archaeology 44(1):43-55.
Guthrie, R. D. 2003. Rapid body size decline in Alaskan Pleistocene horses before extinction. Nature 426(6963):169-171.
Heaton, T. H., Vogel, J. C., von La Chevallerie, G., Collett, G. 1986. Climatic influence on the isotopic composition of bone nitrogen. Nature 322:822-823.
Hennart, P. H., Vis, H. L. 1980. Breast-feeding and post partum amenorrhea in Central Africa. Journal of Tropical Pediatrics and Environmental Child Health 26(5):177-83.
Hill, M. E., Hill, M. G., Widga, C. C. 2008. Late Quaternary Bison diminution on the Great Plains of North America: evaluating the role of human hunting versus climate change. Quaternary Science Reviews 27(17):1752-1771.
Hobson, K. A., Alisauskas, R. T., Clark, R. G. 1993. Stable-nitrogen isotope enrichment in avian tissues due to fasting and nutritional stress: implications for isotopic analyses of diet. Condor 95(2):388-394.
Hobson, K. A., Sease, J. L. 1998. Stable isotope analyses of tooth annuli reveal temporal dietary records: an example using Steller sea lions. Marine Mammal Science 14(1):116-129.
Howie, P. W., McNeilly, A. S. 1982. Effect of breast-feeding patterns on human birth intervals. Journal of reproduction and fertility 65(2):545-557.

Iacumin, P., Nikolaev, V., Ramigni, M. 2000. C and N stable isotope measurements on Eurasian fossil mammals, 40 000 to 10 000 years BP: herbivore physiologies and palaeoenvironmental reconstruction. Palaeogeography, Palaeoclimatology, Palaeoecology 163(1):33-47.

Jennings, S., Greenstreet, S., Reynolds, J. 1999. Structural change in an exploited fish community: a consequence of differential fishing effects on species with contrasting life histories. Journal of Animal Ecology 68(3):617-627.

Johnson, C. 2013. What happened to the Megafauna? Wildlife Australia 50(3):18.

Johnson, C. N., Bradshaw, C. J., Cooper, A., Gillespie, R., Brook, B. W. 2013. Rapid megafaunal extinction following human arrival throughout the New World. Quaternary International 308:273-277.

Jones, T. L., Porcasi, J. F., Erlandson, J. M., Dallas, H., Wake, T. A., Schwaderer, R. 2008. The protracted Holocene extinction of California's flightless sea duck (*Chendytes lawi*) and its implications for the Pleistocene overkill hypothesis. Proceedings of the National Academy of Sciences 105(11):4105-4108.

Koch, P. L., Barnosky, A. D. 2006. Late Quaternary extinctions: state of the debate. Annual Review of Ecology, Evolution, and Systematics 37:215-250.

Koch, P. L., Fisher, D. C., Dettman, D. 1989. Oxygen isotope variation in the tusks of extinct proboscideans: a measure of season of death and seasonality. Geology 17(6):515-519.

Konner, M., Worthman, C. 1980. Nursing frequency, gonadal function, and birth spacing among! Kung hunter-gatherers. Science 207(4432):788-791.

Kurz, K. M., Habicht, J. P., Rasmussen, K. M., Schwager, S. J. 1993. Effects of maternal nutritional status and maternal energy supplementation on length of postpartum amenorrhea among Guatemalan women. The American journal of clinical nutrition 58(5):636-642.

Langman, V. A., Roberts, T. J., Black, J., Maloiy, G. M., Heglund, N. C., Weber, J. M., Kram, R., Taylor, C. R. 1995. Moving cheaply: energetics of walking in the African elephant. The Journal of Experimental Biology 198(3):629-632.

Lee, P. C. 1987. Nutrition, fertility and maternal investment in primates. Journal of Zoology 213(3):409-422.

Lee, P. C., Majluf, P., Gordon, I. J. 1991. Growth, weaning and maternal investment from a comparative perspective. Journal of Zoology 225(1):99-114.

Lee, P. C., Bussière, L. F., Webber, C. E., Poole, J. H., Moss, C. J. 2013. Enduring consequences of early experiences: 40 year effects on survival and success among African elephants (*Loxodonta africana*). Biology letters 9(2):20130011.

Lee, P. C., Moss, C. J. 1986. Early maternal investment in male and female African elephant calves. Behavioral Ecology and Sociobiology 18(5):353-361.
Leshchinskiy, S. V. 2009. Mineral deficiency, enzootic diseases and extinction of mammoth of Northern Eurasia. In: Doklady Biological Sciences 424(1), MAIK Nauka/Interperiodica, pp. 72-74.
Lima-Ribeiro, M. S., Diniz-Filho, J. A. F. 2013. American megafaunal extinctions and human arrival: improved evaluation using a meta-analytical approach. Quaternary International 299:38-52.
Lindstedt, S. L., Boyce, M. S. 1985. Seasonality, fasting endurance, and body size in mammals. American Naturalist 125(6):873-878.
Lister, A. M., Sher, A. V. 1995. Ice cores and mammoth extinction. Nature 378:23-24.
Little, M. A., Galvin, K., Mugambi, M. 1983. Cross-sectional growth of nomadic Turkana pastoralists. Human Biology 55(4):811-830.
Lopes dos Santos, R. A., De Deckker, P., Hopmans, E. C., Magee, J. W., Mets, A., Damsté, J. S. S., Schouten, S. 2013. Abrupt vegetation change after the Late Quaternary megafaunal extinction in southeastern Australia. Nature Geoscience 6(8):627-631.
Loudon, A. S., McNeilly, A. S., Milne, J. A. 1983. Nutrition and lactational control of fertility in red deer. Nature 320:145-147.
Lyman, R. L. 1987. On the analysis of vertebrate mortality profiles: sample size, mortality type, and hunting pressure. American Antiquity 52(1):125-142.
Lyons, S. K., Smith, F. A., Brown, J. H. 2004. Of mice, mastodons and men: human-mediated extinctions on four continents. Evolutionary Ecology Research 6(3):339-358.
Martin, P. S. 1973. The discovery of America. Science 179(4077):969-974.
Martínez, G., Gutiérrez, M. A., Tonni, E. P. 2013. Paleoenvironments and faunal extinctions: Analysis of the archaeological assemblages at the Paso Otero locality (Argentina) during the Late Pleistocene–Early Holocene. Quaternary International 299:53-63.
McDade, T. W. 2001. Parent-offspring conflict and the cultural ecology of breast-feeding. Human Nature 12(1):9-25.
McNeilly, A. S. 1994. Suckling and the control of gonadotropin secretion. The Physiology of Reproduction 2:1179-1212.
McNeilly, A. S. 1997. Lactation and fertility. Journal of Mammary Gland Biology and Neoplasia 2(3):291-298.
Migliano, A. B., Vinicius, L., Lahr, M. M. 2007. Life history trade-offs explain the evolution of human pygmies. Proceedings of the National Academy of Sciences 104(51):20216-20219.

Minagawa, M., Wada, E. 1984. Stepwise enrichment of ^{15}N along food chains: further evidence and the relation between $\delta^{15}N$ and animal age. Geochimica et Cosmochimica Acta 48(5):1135-1140.

Mosimann, J. E., Martin, P. S. 1975. Simulating overkill by Paleoindians: did man hunt the giant mammals of the New World to extinction? Mathematical models show that the hypothesis is feasible. American Scientist 63(3):304-313.

Nelson, D. E., Angerbjörn, A., Lidén, K., Turk, I. 1998. Stable isotopes and the metabolism of the European cave bear. Oecologia 116(1-2):177-181.

den Ouden, N., Reumer, J. W. F., van den Hoek Ostende, L. W. 2012. Did mammoth end up a lilliput? Temporal body size trends in Late Pleistocene Mammoths, *Mammuthus primigenius* (Blumenbach, 1799) inferred from dental data. Quaternary International 255:53-58.

Palkopoulou, E., Dalén, L., Lister, A. M., Vartanyan, S., Sablin, M., Sher, A., Edmark, V. N., Brandström, M. D., Germonpré, M., Barnes, I., Thomas, J. A. 2013. Holarctic genetic structure and range dynamics in the woolly mammoth. Proceedings of the Royal Society of London B: Biological Sciences 280(1770):20131910.

Prescott, G. W., Williams, D. R., Balmford, A., Green, R. E., Manica, A. 2012. Quantitative global analysis of the role of climate and people in explaining late Quaternary megafaunal extinctions. Proceedings of the National Academy of Sciences 109(12):4527-4531.

Proaktor, G., Coulson, T., Milner-Gulland, E. J. 2007. Evolutionary responses to harvesting in ungulates. Journal of Animal Ecology 76(4):669-678.

Raubenheimer, E. J., Van Heerden, W. F. P., Van Niekerk, P. J., De Vos, V., Turner, M. J. 1995. Morphology of the deciduous tusk (tush) of the African elephant (*Loxodonta africana*). Archives of oral biology 40(6):571-576.

Raubenheimer, E. J. 2000. Early development of the tush and the tusk of the African elephant (*Loxodonta africana*). Archives of oral biology 45(11):983-986.

Richards, M. P., Mays, S., Fuller, B. T. 2002. Stable carbon and nitrogen isotope values of bone and teeth reflect weaning age at the Medieval Wharram Percy site, Yorkshire, UK. American Journal of Physical Anthropology 119(3):205-210.

Ripple, W. J., Van Valkenburgh, B. 2010. Linking top-down forces to the Pleistocene megafaunal extinctions. BioScience 60(7):516-526.

Robbins, C. T., Felicetti, L. A., Sponheimer, M. 2005. The effect of dietary protein quality on nitrogen isotope discrimination in mammals and birds. Oecologia 144(4):534-540.

Roberts, R. G., Flannery, T. F., Ayliffe, L. K., Yoshida, H., Olley, J. M., Prideaux, G. J., Laslett, G. M., Baynes, A., Smith, M. A., Jones, R., Smith, B. L. 2001. New ages for the last

Australian megafauna: continent-wide extinction about 46,000 years ago. Science 292(5523):1888-1892.
Rountrey, A.N., 2009. Life Histories of Juvenile Woolly Mammoths from Siberia: Stable Isotope and Elemental Analyses of Tooth Dentin. Unpublished dissertation, University of Michigan, xiii+331 pp.
Rountrey, A.N., Fisher, D.C., Vartanyan, S., Fox, D.L., 2007. Carbon and nitrogen isotope analyses of a juvenile woolly mammoth tusk: Evidence of weaning. Quaternary International 169-170, 166–173.
Rountrey, A.N., Fisher, D.C., Tikhonov, A.N., Kosintsev, P.A., Lazarev, P.A., Boeskorov, G., Buigues, B., 2012. Early tooth development, gestation, and season of birth in mammoths. Quaternary International 255, 196–205.
Rutter, L. M., Randel, R. D. 1984. Postpartum nutrient intake and body condition: effect on pituitary function and onset of estrus in beef cattle. Journal of Animal Science 58(2):265-274.
Sandom, C., Faurby, S., Sandel, B., Svenning, J. C. 2014. Global late Quaternary megafauna extinctions linked to humans, not climate change. Proceedings of the Royal Society of London B: Biological Sciences 281(1787):20133254.
Schoeninger, M. J., DeNiro, M. J. 1984. Nitrogen and carbon isotopic composition of bone collagen from marine and terrestrial animals. Geochimica et Cosmochimica Acta 48(4):625-639.
Schweger, C., Froese, D., White, J. M., Westgate, J. A. 2011. Pre-glacial and interglacial pollen records over the last 3 Ma from northwest Canada: Why do Holocene forests differ from those of previous interglaciations? Quaternary Science Reviews 30(17):2124-2133.
Shanley, D. P., Kirkwood, T. B. 2000. Calorie restriction and aging: a life-history analysis. Evolution 54(3):740-750.
Sheridan, J. A., Bickford, D. 2011. Shrinking body size as an ecological response to climate change. Nature Climate Change 1(8):401-406.
Sikes, S. K. 1971. Natural history of the African elephant. Weidenfeld and Nicolson, London, pp. 397.
Smith, E. F. 1991. The influence of nutrition and postpartum mating on weaning and subsequent play behaviour of hooded rats. Animal Behaviour 41(3):513-524.
Smith, K.M., Fisher, D.C., 2011. Sexual dimorphism of structures showing indeterminate growth: tusks of American mastodons (*Mammut americanum*). Paleobiology 37, 175–194.
Steadman, D. W., Martin, P. S., MacPhee, R. D., Jull, A. J. T., McDonald, H. G., Woods, C. A., Iturralde-Vinent, M., Hodgins, G. W. 2005. Asynchronous extinction of late

Quaternary sloths on continents and islands. Proceedings of the National Academy of Sciences of the United States of America 102(33):11763-11768.
Taylor, C. R., Schmidt-Nielsen, K., Raab, J. L. 1970. Scaling of energetic cost of running to body size in mammals. American Journal of Physiology 219(4):1104-1107.
Tikhonov, A., Vartanyan, S. 2001. Populations of woolly mammoth in North-East Siberia – dwarfing in isolation or last stage of extinction? The World of Elephants. Consiglio Nazionale delle Ricerche-Roma, Rome p. 519.
Trivers, R. L. 1974. Parent-offspring conflict. American zoologist 14(1):249-264.
Tucker, V. A. 1970. Energetic cost of locomotion in animals. Comparative Biochemistry and Physiology 34(4):841-846.
Usmani, R. H., Dailey, R. A., Inskeep, E. K. 1990. Effects of limited suckling and varying prepartum nutrition on postpartum reproductive traits of milked buffaloes. Journal of dairy science 73(6):1564-1570.
Van der Spuy, Z. M. 1985. Nutrition and reproduction. Clinics in obstetrics and gynaecology 12(3):579-604.
Walker, R., Gurven, M., Hill, K., Migliano, A., Chagnon, N., De Souza, R., Djurovic, G., Hames, R., Hurtado, A. M., Kaplan, H., Kramer, K., Oliver, W. J., Valeggia, C., Yamauchi, T. 2006. Growth Rates and Life Histories in Twenty-Two Small-Scale Societies. American Journal of Human Biology 18:295-311.
Webb, S. D. (1984). Ten million years of mammal extinctions in North America. In: Martin, P. S., Klein, R. G. (Eds.), Quaternary extinctions: a prehistoric revolution. The University of Arizona Press, Tucson, Arizona, pp. 189-210.
Wheeler, J. P., Purchase, C. F., Macdonald, P. D. M., Fill, R., Jacks, L., Wang, H., Ye, C. 2009. Temporal changes in maturation, mean length-at-age, and condition of spring-spawning Atlantic herring (*Clupea harengus*) in Newfoundland waters. ICES Journal of Marine Science: Journal du Conseil fsp117.
Wood, S.N. 2006. Generalized Additive Models: An Introduction with R. Chapman and Hall/CRC Press.
Wroe, S., Field, J. 2006. A review of the evidence for a human role in the extinction of Australian megafauna and an alternative interpretation. Quaternary Science Reviews 25(21):2692-2703.
Wroe, S., Field, J. H., Archer, M., Grayson, D. K., Price, G. J., Louys, J., Faith, J. T., Webb, G. E., Davidson, I., Mooney, S. D. 2013. Climate change frames debate over the extinction of megafauna in Sahul (Pleistocene Australia-New Guinea). Proceedings of the National Academy of Sciences 110(22):8777-8781.
York, A. E., Thomason, J. R., Sinclair, E. H., Hobson, K. A. 2008. Stable carbon and nitrogen isotope values in teeth of Steller sea lions: age of weaning and the impact of the

1975-1976 regime shift in the North Pacific Ocean.Canadian Journal of Zoology 86(1):33-44.

Chapter 6

Conclusion

My research exploring the causal mechanisms behind the late Pleistocene extinctions has been driven by more than mere curiosity or fascination concerning the history of life on Earth, and the roles our species may have played in that history. The scientific approaches to discovery and knowledge provide tools for communally building objective insights into the history and workings of nature. Paleontological understandings establish big-picture perspectives on how life has changed through time and how our behaviors can impact these processes. This knowledge enhances our ability to mitigate our own impact on the world that we inhabit and share with so many other forms of life. These studies aim to help advance our mechanistic understanding of the late Pleistocene extinctions in part to make us better equipped to predict and limit the potential future consequences of our activity.

Through multiple generations of scientific investigation, paleontologists have been unable to establish a consensus on how the late Pleistocene megafaunal extinctions occurred. Correlations between the timing of extinctions and potential causal

events have not been able to provide unequivocal conclusions. One problem is that such temporal observations are generally consistent with multiple hypothetical models. Another problem is that establishing a meaningful correlation between time of extinction and a particular mechanism is complicated when extinction may not have been the result of an acute cause, but rather a consequence of long-term interactions. If extinction was a drawn-out process, how would we determine when the process began?

If we cannot determine when the process started, how can we establish meaningful correlations with potential mechanisms? Rather than rely on temporal correlations, we may be able determine causes of these extinctions by looking at 'fingerprints' left behind in the fossil record by the culprit. I do not claim to have determined unequivocally through my studies the mechanism behind these extinctions, but I have fleshed out one aspect of an approach that had been previously proposed by my adviser and other academic predecessors to have potential for providing unambiguous answers to scientific questions pertaining to these events.

Life-history reconstructions provide a perspective that cannot be obtained from other types of data measured from fossil materials. Tusk growth records can be used to study timing of various ontogenetic milestones, patterns in growth rate, birth rates,

seasons of death, and other details of fossil proboscidean life histories (e.g., Fisher 1996, 2001, 2008, 2009; Fisher and Fox, 2003; Rountrey et al., 2007). Each of these parameters tells us something about a population's environment, since it represents a net product of adaptive responses. Life-history analyses provide a way to test opposing predictions of competing extinction hypotheses. Climate-related explanations for the late Pleistocene extinctions predict very different life-history expectations than hunting-based hypotheses (Fisher 1996, 2009), since the first would lead to deceleration of life-histories (e.g., Bengtson and Laws, 1985; Lee and Moss, 1986; Little et al., 1983; Geist, 1989) and the second would encourage acceleration (e.g., Carrick et al., 1962; Geist, 1989; Jennings et al., 1999; Proaktor et al., 2007; Wheeler et al., 2009).

My work adds methods and interpretive frameworks to the growing toolbox for interpreting proboscidean tusk growth records. CT scans consistently reveal subannual variations in X-ray attenuation of fossil tusk dentin that enable 3D characterizations of annual growth increments over the duration of tusk formation. Specific patterns of seasonal variation in CT scans differ between tusks from northern Siberia and those from ZR, but within each group, there is a high degree of uniformity, even in individuals separated by thousands of years. Further work is required to determine the cause of

variation in CT scans. Even without understanding fully the physiological processes that cause variations in radiodensity of dentin, we can measure annual growth increments visible in CT scans and use CT imagery to guide serial sampling for compositional analyses.

In three years of bimonthly sampling from zoo elephants, I have been able to sample new growth in individual tail hairs (mother) and tail hair clumps (calf). To my knowledge this had never previously been attempted. Our procedure provides a simple way to monitor serial changes in hair composition in elephants. Difficulties encountered in the process could be avoided in future experiments by selection of hairs located more distally on the tail and by more frequent sampling during warm months when hairs grow faster and are more prone to abrasion and breakage.

Discovery of a spike in $\delta^{15}N$ that appears to be a symptom of weaning in Siberian woolly mammoths provides a clear signal that could be explored in other records. It is unclear whether procedures used to measure cortisol in elephant tail hair could be used to collect information from fossil proboscidean materials, but the stability of this steroid hormone paired with the pristine preservation of arctic specimens that sometimes include frozen soft tissue of fossil mammoths makes it an intriguing possibility.

Projects described in the preceding chapters expand our understanding of mammoth and mastodon paleobiology, proboscidean nursing physiology, and the late Pleistocene extinctions. Specimens from the Ziegler Reservoir fossil site provide the first extensive look at growth records from mastodon mandibular tusks and for proboscideans from the Sangamon interglacial (*Chapter 2*, *Chapter 3*). Serial analyses of hair, milk, and diet from a mother African elephant and her calf document an isotopic signature of nursing in proboscideans and contribute other previously unobserved patterns in elephant tail hair growth and composition (*Chapter 4*). Evidence of changes in growth rates and weaning ages in Siberian woolly mammoths over the last 30 ka of the Pleistocene suggests that vegetational changes due to warming conditions were not responsible for their extinction (*Chapter 5*). These data provide a basis for further investigations into the causes of the late Pleistocene megafaunal extinctions.

References

Bengtson, J. L., Laws, R. M. 1985. Trends in Crabeater Seal Age at Maturity: An Insight into Antarctic Marine Interactions. In: Siegfried, W. R., Condy, P. R., Laws, R. M. (Eds.) Antarctic Nutrient Cycles and Food Webs. Springer-Verlag, Berlin, Germany, pp. 669-675.

Carrick, R., Csordas, S. E., Ingham, S. E. 1962. Studies on the southern elephant seal, *Mirounga leonina* (L.). IV. Breeding and development. Wildlife Research 7(2): 161-197.

Fisher, D. C. 1996. Extinction of proboscideans in North America. In: Shoshani, J., Tassy, P. (Eds.), The Proboscidea: Evolution and Palaeoecology of Elephants and Their Relatives. Oxford University Press, Oxford, pp. 296–315.

Fisher, D. C. 2001. Season of death, growth rates, and life history of North American mammoths. In: West, D. (Ed.), Proceedings of the First International Conference on Mammoth Site Studies: 11-13 March 1998 (pp. 121-135).

Fisher, D. C., 2008. Taphonomy and paleobiology of the Hyde Park mastodon. In: Allmon, W. D., Nester, P. L. (Eds.), Mastodon Paleobiology, Taphonomy, and Paleoenvironment in the Late Pleistocene of New York State: Studies on the Hyde Park, Chemung, and North Java Sites. Palaeontographica Americana 61, 197–290.

Fisher, D.C., 2009. Paleobiology and extinction of proboscideans in the Great Lakes region of North America. In: Haynes, G. (Ed.), American Megafaunal Extinctions at the End of the Pleistocene. Springer, Dordrecht, pp. 55–75.

Fisher, D.C., Fox, D.L., 2003. Season of death and terminal growth histories of Hiscock mastodons. In: Laub, R.S. (Ed.), The Hiscock Site: Late Pleistocene and Holocene Paleoecology and Archaeology of Western New York State. Bulletin of the Buffalo Society of Natural Sciences 37, 83–101.

Geist, V. 1989. Environmentally guided phenotype plasticity in mammals and some of its consequences to theoretical and applied biology. In: Bruton, M. N. (Ed.), Alternative life-history styles of animals. Springer, Netherlands, pp. 153-176.

Jennings, S., Greenstreet, S., Reynolds, J. 1999. Structural change in an exploited fish community: a consequence of differential fishing effects on species with contrasting life histories. Journal of Animal Ecology 68(3):617-627.

Lee, P. C., Moss, C. J. 1986. Early maternal investment in male and female African elephant calves. Behavioral Ecology and Sociobiology 18(5):353-361.

Little, M. A., Galvin, K., Mugambi, M. 1983. Cross-sectional growth of nomadic Turkana pastoralists. Human Biology 55(4):811-830.

Proaktor, G., Coulson, T., Milner-Gulland, E. J. 2007. Evolutionary responses to harvesting in ungulates. Journal of Animal Ecology 76(4):669-678.

Rountrey, A.N., Fisher, D.C., Vartanyan, S., Fox, D.L., 2007. Carbon and nitrogen isotope analyses of a juvenile woolly mammoth tusk: Evidence of weaning. Quaternary International 169-170, 166–173.